# New synthetic pathways towards cyaphido complexes

Inaugural-Dissertation

to obtain the academic degree

Doctor rerum naturalium (Dr. rer. nat.)
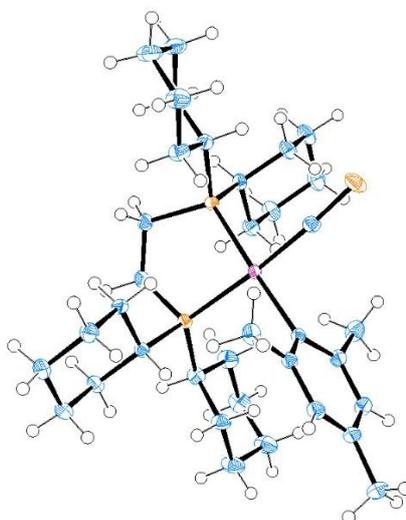
submitted to the Department of Biology, Chemistry, Pharmacy

of Freie Universität Berlin

by

Tim Görlich

from Bruckmühl, Germany

2023

This dissertation was carried out within the time period of Mai 2018 until April 2022 at the Institute of Chemistry and Biochemistry of Freie Universität Berlin under the supervision of Professor Dr. Christian Müller.

1st reviewer: Prof. Dr. Christian Müller

2nd reviewer: Prof. Dr. Sebastian Hasenstab-Riedel

Date of defense: 28 April 2023

Declaration

I herewith confirm that I have prepared this dissertation without the help of any impermissible resources. All citations are marked as such. The present thesis has neither been accepted in any previous doctorate degree procedure nor has it been evaluated as insufficient.

Berlin, 24 January 2023

_____

Tim Görlich

Dedicated to my father

Dr. Siegfried Görlich.

Acknowledgment

List of publications

Tim Görlich, Daniel S. Frost, Nico Boback, Nathan T. Coles, Birger Dittrich, Peter Müller, William D. Jones, and Christian Müller, **Photochemical C(sp)–C(sp^2) Bond Activation in Phosphaalkynes: A New Route to Reactive Terminal Cyaphido Complexes L$_n$M–C≡P**, *J. Am. Chem. Soc.* **2021**, *143*, 46, 19365-19373.

Tim Görlich, Peter Coburger, Eric S. Yang, Jose Goicoechea, Hansjörg Grützmacher, and Christian Müller, **The Chemistry of the Cyaphide Ion**, *Angew. Chem. Int. Ed.* **2023**, accepted for publication.

Abstract

The elusive cyaphide anion (C≡P⁻), the higher analog of the common cyanide anion (C≡N⁻), has been subject of studies since the late nineteenth century, however notable achievements in this field have only been made since the nineties. The cyaphide ion has been mostly established and investigated as cyaphido ligand in few transition metal complexes. Nevertheless, the gained information is still limited and, until recently, only one reliable synthetic strategy towards highly sterically shielded cyaphido complexes, which cannot undergo follow-up reactions on the cyaphido moiety, was developed.

In this work, the history of the cyaphide anion and all literature known preparations are reviewed. Furthermore, new theoretical insights to the cyaphide ion are presented and complemented with additional calculations. Moreover, several novel cyaphido complexes synthesized by two innovative preparation protocols are demonstrated. The first method takes advantage of a light induced C(sp^2)-C(sp) cleavage reaction in a platinum(0) coordinated arylphosphaalkyne to generate the cyaphido ligand (Scheme I, a). The particularly for this photolysis reaction designed precursors are optimized by means of applied phosphaalkynes with specific substitution pattern and diphosphine ligands in regards of their σ-donation capability and bite angles. The resulting cyaphido platinum(II) complexes of the type [(P,P)Pt(η^1-C≡P)(Ar)] are characterized by nuclear magnetic resonance and infrared spectroscopy, single-crystal X-ray diffraction analysis and investigated towards consecutive reactions on the cyaphido moiety, especially by means of [3+2] cycloaddition reactions with organic azides to yield the corresponding triazaphospholato complexes. The second method introduces the well-known trimethylsilylphosphaalkyne as cyaphide anion transfer reagent by fluorodesilylation to build new cyaphido gold(I) complexes (Scheme I, b). This strategy has the potential to get applied to other metals soon.
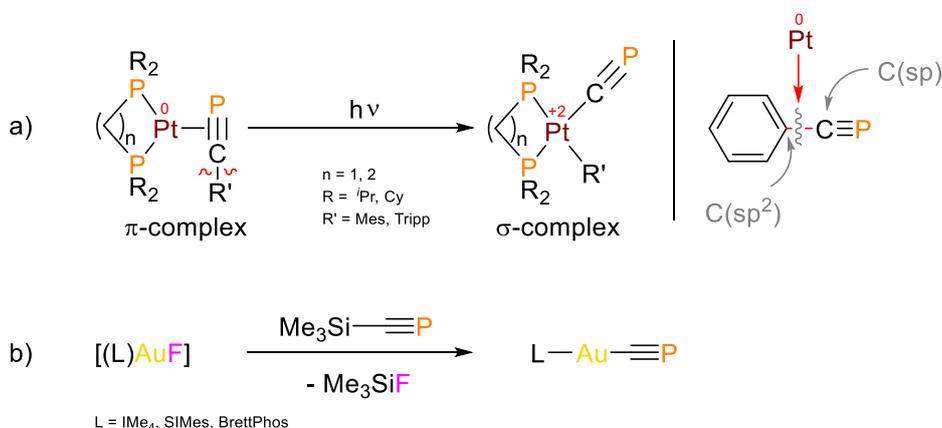
Scheme I. Light induced C(sp^2)-C(sp) cleavage reaction in arylphosphaalkynes (a) and generation of cyaphido gold (I) complexes by fluorodesilylation of trimethylsilylphosphaalkyne (b).

Kurzfassung

Das schwer fassbare Cyaphid-Anion (C≡P⁻), das höhere Analogon des wohlbekannten Cyanid-Anions (C≡N⁻), ist seit dem späten neunzehnten Jahrhundert Gegenstand von Studien, wobei jedoch erst in den neunziger Jahren nennenswerte Erfolge auf diesem Gebiet erzielt wurden. Das Cyaphid-Ion wurde hauptsächlich als Cyaphido-Ligand in wenigen Übergangsmetallkomplexen etabliert und untersucht. Dennoch sind die gewonnenen Informationen noch immer begrenzt, und bis vor kurzem wurde nur eine zuverlässige Synthesestrategie für sterisch abgeschirmte Cyaphido-Komplexe entwickelt, die keine Folgereaktion an der Cyaphidogruppe eingehen können.

In dieser Arbeit wird die Geschichte des Cyaphid-Anions und alle literaturbekannten Synthesen dargelegt. Außerdem werden neue theoretische Erkenntnisse über das Cyaphid-Ion vorgestellt und durch zusätzliche Berechnungen ergänzt. Darüber hinaus werden mehrere neuartige Cyaphido-Komplexe dargestellt, die durch zwei innovative Herstellungsprotokolle synthetisiert wurden. Die erste Methode nutzt eine lichtinduzierte C(sp^2)-C(sp)-Spaltungsreaktion eines Platin(0)-koordinierten Arylphosphaalkins zur Erzeugung des Cyaphidoliganden (Schema I, a). Die speziell für diese Photolysereaktion konzipierten Vorstufen werden durch den Einsatz von Phosphaalkinen mit spezifischem Substitutionsmuster und Diphosphinliganden hinsichtlich ihrer σ-Donator-Fähigkeit und Bisswinkel optimiert. Die resultierenden Cyaphidoplatin(II)-Komplexe des Typs [(P,P)Pt(η^1-C≡P)(Ar)] werden durch kernmagnetische Resonanz- und Infrarotspektroskopie sowie durch Röntgeneinkristallbeugungsanalyse charakterisiert und auf Folgereaktionen an der Cyaphido-Gruppe untersucht, insbesondere durch [3+2]-Cycloadditionsreaktionen mit organischen Aziden, um die entsprechenden Triazaphospholato-Komplexe zu erhalten. Bei der zweiten Methode wird das bekannte ((Trimethyl)silylphosphaalkin als Cyaphid-Anionentransferreagenz durch Fluordesilylierung eingeführt, um neue Cyaphidogold(I)-Komplexe zu bilden (Schema I, b). Diese Strategie könnte bald auch auf andere Metalle angewendet werden.
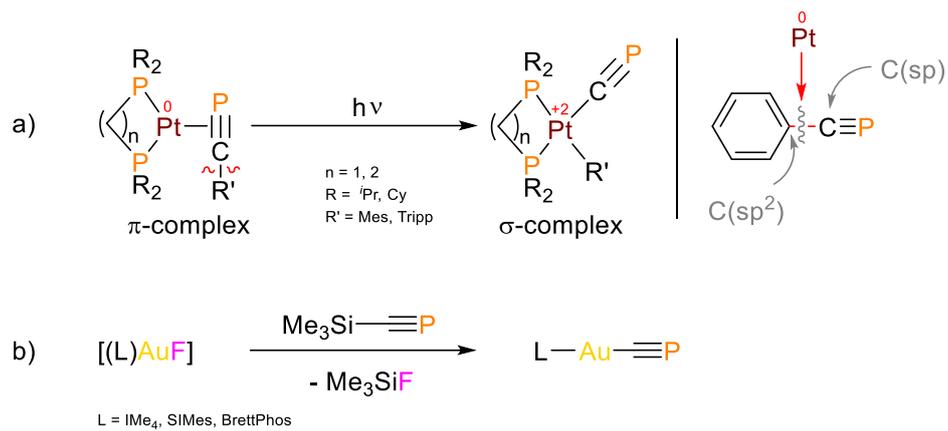
Schema I. Lichtinduzierte C(sp^2)-C(sp)-Spaltungsreaktion von Arylphosphaalkinen (a) und Erzeugung von Cyaphidogold(I)-Komplexen durch Fluordesilylierung von Trimethylsilylphosphaalkin (b).

Table of content

1 Introduction

1.1 Low-coordinate phosphorus compounds

Since the preparation of triphenylphosphine[1] ($\lambda^3\sigma^3$) by MICHAELIS in 1882 and the preparation of pentaphenylphosphorus[2], the first $\lambda^5\sigma^5$ carbophosphorus compound, by WITTIG and RIEBER in 1948 the organophosphorus chemistry evolved rapidly,[3] leading to various "classical" phosphorus compounds with equal number of valency (λ) and coordination (σ).[4-5] In contrast, low-coordinate phosphorus compounds possess a lower coordination as valency number by formation of π_{PX}-bonds. Generally, it is considered that GIER isolated the first low-coordinate carbophosphorus compound, the unstable, unsubstituted phosphaalkyne HC≡P ($\lambda^3\sigma^1$),[6] while BURG and MAHLER synthesized the first diphosphene, the neutral phosphinidene-phosphorane CF$_3$P=PMe$_3$ ($\lambda^3\sigma^2$),[7] both in 1961 (Figure 2). These events mark the entry point to the access of a wide range of different types of low-coordinate phosphorus compounds. A selection of well-established species of carbophosphorus compounds are phosphaalkenes,[8-9] phosphaalkynes,[10-13] phosphinines,[14-17] triazaphospholes,[18] phospholides[19] and phosphinidenes[20-21] (Figure 1).

$\lambda^3\sigma^2$ $\lambda^3\sigma^1$ $\lambda^3\sigma^2$ $\lambda^3\sigma^2$ $\lambda^2\sigma^2$ $\lambda^1\sigma^1$

phosphaalkene   phosphaalkyne   phosphinine   triazaphosphole   phospholide   phosphinidene
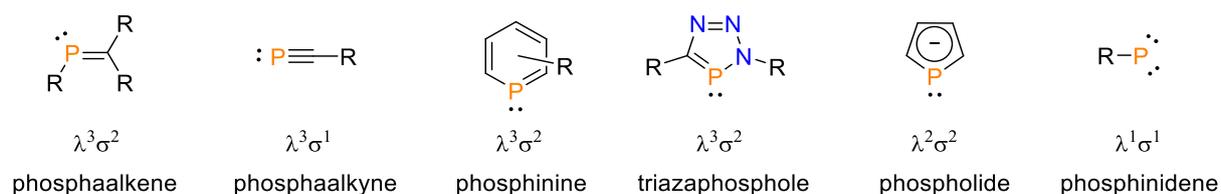
Figure 1. Selected types of low-coordinate phosphorus compounds with λ- and σ-nomenclature.

Before disscussing the main aspects of this work, the generation of phosphaalkynes and cyaphido complexes, the following brief summary highlights selected major milestones of the low-coordinate phosphorus chemistry development (Figure 2).

In 1964 DIMROTH and HOFFMAN reported on trivalent phosphacyanines ($\lambda^3\sigma^1$),[22] which evince a partial P-C double bond in the crystal structure.[23] The next ground breaking result was the synthesis of 2,4,6-triphenylphosphinine ($\lambda^3\sigma^2$), the first aromatic structure containing a low-coordinate phosphorus, achieved by MÄRKL in 1966,[24] which established a common pathway to novel heterocycles bearing a formally sp^2-hybridized phosphorus atom. In 1971 ASHE III succeeded in the synthesis of the unsubstituted phosphinine.[25] Even many four-coordinated phosphazene were already known at the time, the first extremely hydrolysis and light sensitive trivalent derivative, an iminophosphine ($\lambda^3\sigma^2$), was found by NIECKE and FLICK in 1973.[26] Three years later, BECKER isolated the first stable trivalent carbophosphene, a phosphaalkene ($\lambda^3\sigma^2$), by reaction of pivaloyl chloride with substituted disilylphosphines.[27] In 1977 SCHMIDPETER synthesized the first triazaphosphole ($\lambda^3\sigma^2$) by reductive elimination of acylhydrazine with phosphorus pentachloride.[28] In the early 80s, YOSHIFUJI reported on the first stable P=P

double bond ($\lambda^3\sigma^2$),[29] BECKER demonstrated the first kinetically stabilized phosphaalkyne ($\lambda^3\sigma^1$),[30] APPEL isolated the first stable bis methylene phosphorane ($\lambda^5\sigma^3$)[31] and COWLEY prepared the first metallo- $\lambda^4\sigma^2$ phosphorus compound[32] with an M=P linkage. In 1991 MATHEY succeeded in the first synthesis of a biphosphinine by performing a Negishi coupling on two protected phosphinines.[33] A further milestone of carbophosphorus compounds was presented by JUN and ANGELICI in 1994, when they detected the novel cyaphido (C≡P⁻) ligand ($\lambda^3\sigma^1$) in the coordination sphere of a platinum atom. Although the cyaphido complex itself could not be isolated, it was successfully trapped as diplatinum complex.[34] One year later, CUMMINS and SCHROCK independently synthesized the first two terminal metallophosphyne M≡P complexes ($\lambda^3\sigma^1$) of molybdenum and tungsten.[35-36] In 2006 GRÜTZMACHER crystalized the first stable cyaphido complex ($\lambda^3\sigma^1$),[37] which was a crucial step for the further advance of the cyaphido chemistry.
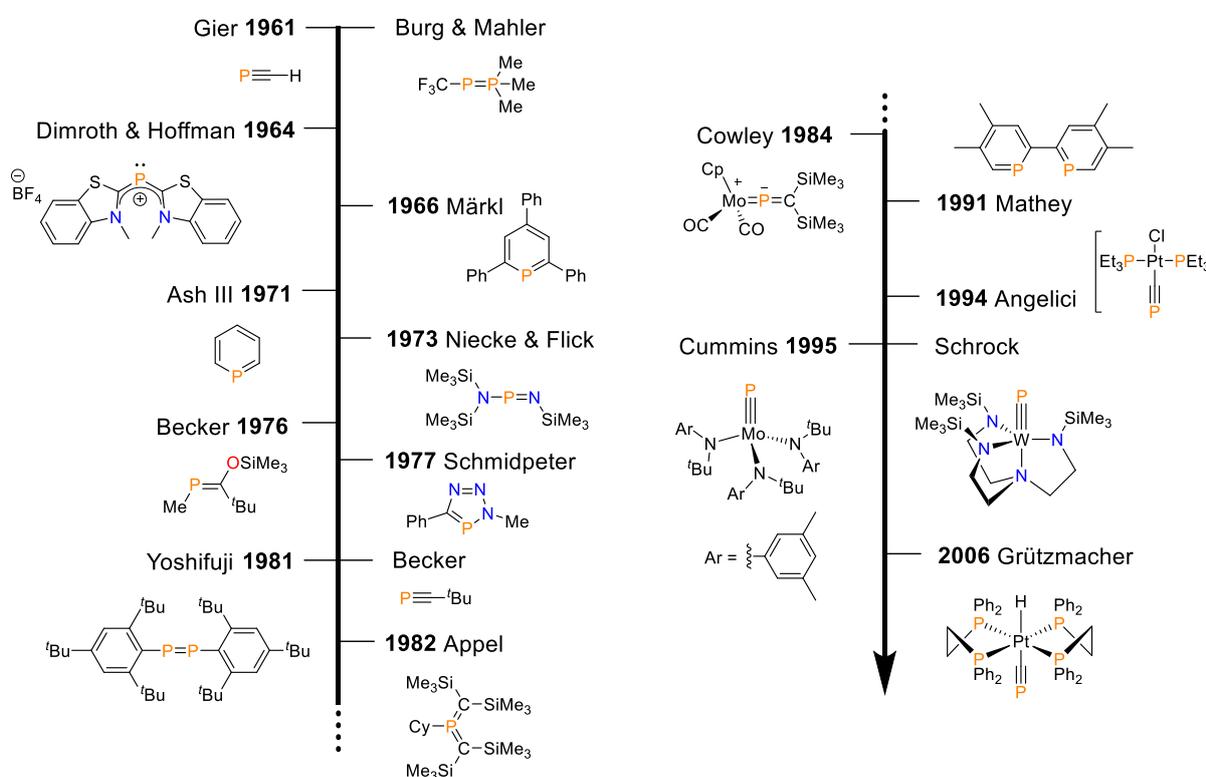
Figure 2. Timeline developments of meaningful low-coordinate phosphorus compounds.

Those examples of low-coordinate phosphorus compounds convincingly render the connection between phosphorus and carbon. Even though phosphorus is the higher homolog of nitrogen and therefore shares its characteristics and reactivity to a certain level, it resembles more silicon[38-40] and complies mostly with carbon.[41] This diagonal relationship can be explained by the similar electronegativity (2.55 C, 2.19 P; Pauling scale; Figure 3a) and van der Waals radii (1.70 Å C, 1.80 Å P), which lead to strong covalent P-C bonds (bond-dissociation energy 605 (C-C), 507.5 kJ·mol⁻¹ (P-C)).[42] Furthermore, the carbanion (C⁻) is valence isoelectronic to phosphorus (P), whereas carbon (C) is valence isoelectronic to a cationic phosphorus (P⁺;

Figure 3b). Consequently, a formal CH fragment is isolobal to a trivalent phosphorus atom with a lone pair (Figure 3c).[41] These analogy not only explains the quantity of "classical" phosphorus, but also the numerous findings of low-coordinate phosphorus compounds, e.g. the similarity between phosphaalkene and alkene (calc. π-bond strength 43 kcal·mol^{-1} (P=C), 65 kcal·mol^{-1} (C=C)).[43]
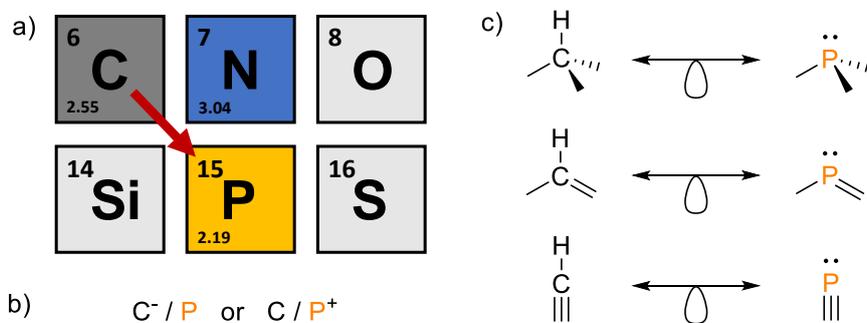
Figure 3. Diagonal relationship (a), valence isoelectronicity (b) and isolobal analogy (c) of carbon and phosphorus.

Note!

Parts of this introduction (chapter 1.2, 1.4) were also used for a minireview[44], which is accepted for publication in Angewandte Chemie (cf. list of publications).

1.2   History of the C≡P triple bond

The chemistry of low-coordinate phosphorus compounds has come a long way from its origins, which was largely driven by chemical curiosity. Nowadays, phosphinines, phosphaalkenes, phosphaalkynes and phosphaketenes are common representatives of this class of compounds, and widely used in a myriad of applications including as ligands in homogenous catalysis, precursors to phosphorus-containing materials, or as building blocks to previously inaccessible and more advanced phosphorus-containing molecules.[8, 10-11, 14, 16-17, 43, 45-49]

The humble beginnings of phosphaalkynes and cyaphide are deeply interwoven. Both species represent a significant part of this work and therefore, the shared history around the development of the C≡P triple bond with the main focus on the cyaphide ion will be outlined. While phosphaalkynes became rapidly accessible after their discovery, the cyaphide (C≡P$^-$) anion, the phosphorus analog of the cyanide anion (C≡N$^-$), has a long history from its initial discovery to its manageable use in the laboratory. Interestingly, the first entries for its synthesis date back to 1894. SHOBER and SPANUTIUS claimed the synthesis of Na(C≡P) in a two-step reaction (Scheme 1). In their description, the reduction of PH_3 by elemental sodium forms $NaPH_2$ or related species (Na_2PH, Na_3P) and the further treatment with CO gas yields Na(CP) and H_2O. They postulated that the highly unstable Na(C≡P) immediately reacts with water. Therefore, they analyzed the decomposition products and considered the formation of sodium formate (HCOONa) and phosphine (PH_3) as an indirect proof for their theory.[50] In 2011 (117 years later!), GRÜTZMACHER and co-workers reinvestigated the synthesis of $NaPH_2$ with CO gas using modern analytical technics.[51] They determined that the more stable sodium 2-phosphaethynolate Na(OC≡P) was formed instead of Na(C≡P) (Scheme 1). The corresponding Li analog (Li(OC≡P)) was reported by BECKER in 1992.[52] Even though SHOBER and SPANUTIUS did not synthesize Na(C≡P), they did, however, isolate the first species containing a carbon–phosphorus triple bond. It is interesting to note that in the 128 years since SHOBER and SPANUTIUS first claimed the synthesis of NaCP no binary cyaphide salt has been reported.

Shober & Spanutius (original claim, 1894)

$NaPH_2$ + CO $\longrightarrow$ NaC≡P + H_2O

Na(C≡P) + 2 H_2O $\longrightarrow$ Na(HCOO) + PH_3

Grützmacher *et al.* (2011)

$NaPH_2$ $\xrightarrow{\text{CO}_{excess}}$ Na(O-C≡P) + Na(O-CH=PH)$_{traces}$

Na(O$^-$C≡P) + x H_2O $\longrightarrow$ PH_3 + Na(H_2PO_2) + CO + Na(HCO_3)
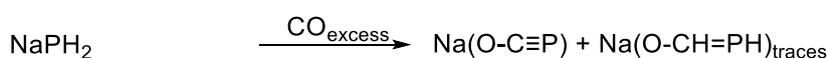
Scheme 1. Proposed (Shober & Spanutius) and found (Grützmacher *et al.*) reaction of $NaPH_2$ with CO.

In 1930, HERZBERG was able to observe the vibrational spectrum of the C≡P radical by setting an electric discharge in a chamber filled with a mixture of argon and phosphorus vapor. The tap grease as well as the sealing wax might have led to an intake of carbon in the electric arc, which further formed C≡P radicals and potentially (C≡P)$_2$, a theoretical analog of cyanogen. In accordance with this observation, a control experiment with argon and a small trace of nitrogen revealed the typical bands for C≡N. Consequently, HERZBERG was the first who succeeded in the "synthesis" of a cyaphide species, albeit without isolation.[53]

The major synthetic breakthrough was finally achieved in 1961. GIER, who also tried to reproduce the synthesis of Na(C≡P), demonstrated the synthesis and isolation of hydrogen cyaphide (HC≡P), also called methinophosphide, methylidynephosphane, phosphaethyne, or phosphaacetylene, by passing PH$_3$ gas through a rotating arc between two graphite electrodes sealed in a water-cooled copper reactor. The gaseous products (hydrogen cyaphide, acetylene, phosphine, ethylene) were first captured inside cooling traps ($T = -196$ °C) and then separated by gas-chromatography. HC≡P is an extremely reactive, pyrophoric, colorless gas, which tends to polymerize even at temperatures of $T = -130$ °C. In contrast to the former syntheses, GIER was able to fully characterize this species by elemental analysis, mass spectrometry and infrared spectroscopy. Moreover, the reaction of HC≡P with anhydrous HCl gave further proof of its existence as CH$_3$PCl$_2$ was formed as the product.[6] In isolating HCP, GIER was able to demonstrate the accessibility of a chemical compound with a carbon-phosphorus triple bond, thus demonstrating that Pitzer's double bond rule was not applicable for phosphorus.[54-55] Further evidence for the existence of HC≡P was reported by NIXON and co-workers who recorded the *in-situ* microwave spectrum of HCP generated by a hydrogen halide elimination reaction from dichlorophosphines performed under flash vacuum pyrolysis.[56-58] These experiments also paved the way for the synthesis of numerous phosphaalkynes later.[10-11, 46]

In the following decades the physical properties of HC≡P were closely investigated and microwave characterizations were performed.[59] Intriguingly, astronomers were able to detect traces of C≡P radicals and later even HC≡P in the outer space near the carbon star envelop of IRC +10216.[60-61] Theoretical calculations for a possible C≡P$^-$ anion were also performed, before it was finally confirmed by experimental figures.[62]

In 1992, the group of ANGELICI reported on the first example of a coordination compound bearing a terminal cyaphide ligand (cyaphido, C≡P$^-$). Even though the Pt complex itself could not be isolated, further characterization of a subsequent compound unequivocally proved the successful synthesis of a cyaphido ligand in the coordination sphere of Pt(II).[63]

1.3 Phosphaalkynes

1.3.1 History and introduction

Phosphaalkynes or carbophosphynes are $\lambda^3\sigma^1$ phosphorus compounds bearing a C≡P triple bond and refute the classical double bond rule, which denies the existence of $(p\text{-}p)\pi$ multiple bonds between carbon and higher main-group elements, due to the expected instability caused by the unfavorable overlap of the C_{2p}-P_{3p} orbitals.[64-65] As discussed in the previous chapter (1.2), hydrogen cyaphide HC≡P, also called phosphaacetylene, methinophosphide, phosphaethyne or methylidynephosphane, was the first synthesized, characterized and for further syntheses used phosphaalkyne.[6, 66-68] Based on the hydrogen halide elimination by flash pyrolysis several additional thermally and kinetically instable phosphaalkynes were synthesized (Figure 4).[57, 67, 69-71] A major breakthrough was the preparation of *tert*-butylphosphaalkyne (*tert*-butylphosphaacentylene), the first kinetically stable phosphaalkyne, by BECKER *et al.* in 1981.[30] As stable building block it granted access to a wide range of follow-up reactions until today.[72-74] Surprisingly, the similar trimethylsilylphosphaalkyne (TMS-C≡P) is semi-stable and has to be stored as toluene solution at low temperature to avoid the slow decomposition at room temperature.[75-77] The phenylphosphaalkyne (PhC≡P) is even less stable ($\tau_{1/2}$ = 7 min at T = 0 °C) and only suitable for *in situ* reactions.[45] In the following decades a lot of stable phosphaalkynes have been synthesized,[11] among them the very stable and nowadays even commercial available adamantylphosphaalkyne,[78] the highly stable 2,4,6-*tert*-butylphenylphosphaalkyne (Mes*C≡P) and tritylphosphaalkyne (triphenylmethylphospha-alkyne, Ph$_3$CC≡P).[79-80] Further representatives of the class are listed and discussed in several reviews.[10-13, 43, 81-87] Besides the numerous synthesized alkyl- and aryl- derivatives, few amino-[88-95] and phosphonio-[96-97] functionalized phosphaalkynes have been prepared. Moreover, the 2-phosphaethynolate anion (P≡C-O$^-$, cf. chapter 1.2) recently became an important reagent since GRÜTZMACHER and co-workers introduced an optimized synthesis in 2011.[49, 51, 98] Even higher chalcogen homologs of the 2-phosphaethynolate anion (S, Se) are accessible.[99-102] A less well established class are the diphosphaalkynes. Until now, only two examples have been isolated. The first diphosphaalkyne, a 1,3-bis(phosphaethinyl)adamantan, was probably synthesized by VEEK in 1997, though it was unstable and never published.[103] The first entry for a diphosphaalkyne in the literature was made with the 9,10-bis(phosphaethinyl)triptycen by BRYM and JONES in 2003,[104] followed by 1,4-diphosphaethinylbicyclo[2.2.2]octane as second.[105] So far, isophosphaalkynes (phosphaisocyanides) are the most elusive class of phosphaalkynes. Although ANGELICI and WEBER had already initial successes by the synthesis of semi-bridging isophosphaalkyne ligands in the coordination sphere of platinum and iron in the early 90s,[106-107] all selective trials to obtain a free isophosphaalkyne failed. Typically, most attempts yield a regular phosphaalkyne instead of an isophosphaalkyne caused by an intramolecular 1,2-P-C shift.[108-109]
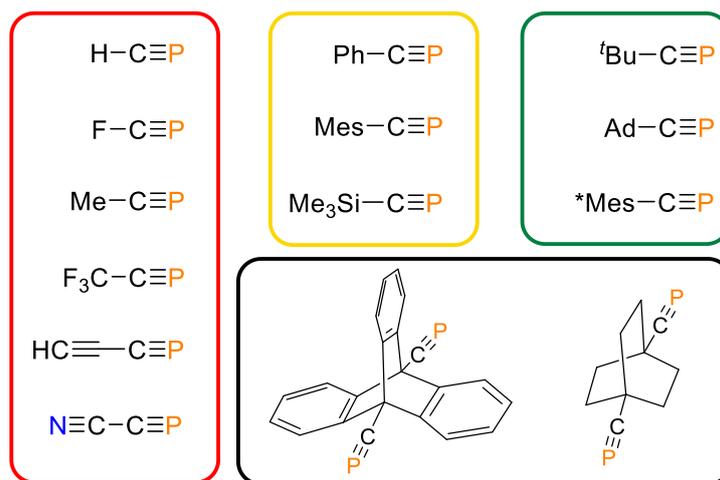
Figure 4. Overview of selected unstable (red), semi-stable (yellow), stable (green) phosphaalkynes and the only two isolable diphosphaalkynes (black).

1.3.2 Characteristics and coordination chemistry of phosphaalkynes

Phosphaalkynes (R-C≡P) are the phosphorus analogs of alkynes (R-C≡C-H) and share multiple characteristics with them.[110] Phosphaalkynes are fully linear (180°) and have a perfect cylindrical shape with $C_{\infty v}$ symmetry (e.g. H-C≡P) if not broken by the substituent (C_{3v} for Me-C≡P).[111] The electronegativity difference between carbon (2.55) and phosphorus (2.19) effects an uneven charge distribution leading to a polarized C≡P bond in the phosphaalkynes causing varying degrees of dipole moments depending on the combined substituent.[111-114] The C≡P triple bond consists of a single $2p_\sigma$-$3p_\sigma$ and two $2p_\pi$-$3p_\pi$ bonds with a typical bond length of around 1.54 Å.[115] Astonishingly, different substituents only have a very limited influence on the C≡P bond length and most species can be described as λ^3-phosphaalkynes.[114, 116] Calculations for several phosphaalkyne species revealed that the highest occupied molecular orbital (HOMO) is always represented by the C≡P-π-orbital, whereas the lone pair of the phosphorus is lower in energy.[115, 117] An electron-density distribution (EDD) determination of *tert*-butylphosphaalkyne shows the location of the lone pair much closer to the phosphorus atom in comparison to the phosphaalkene analog.[112] A further comparison of *tert*-butylphosphaalkyne with its alkyne analog by calculation revealed that the frontier molecular orbitals (MOs) are almost similar. While the HOMO possesses a comparable energy level, the lowest occupied molecular orbital (LUMO) of the phosphaalkyne is 1.67 eV lower in energy, resulting in smaller HOMO-LUMO gap making it a better electron-acceptor.[117] Molecular electrostatic potential (MEP) analysis of different phosphaalkynes show two minima. The lower one (e.g. -17.1 kcal·mol^{-1} for HC≡P; -25.2 kcal·mol^{-1} for acetylene) is located on both sides perpendicular to the symmetry axis of the C≡P bond midpoint, while the other minimum (-5.4 kcal·mol^{-1} for HC≡P), near the terminal phosphorus atom, represents the lone pair (Figure 5a). The side-on reaction with electrophiles is highly favored, due to the large differences in

the electrostatic potentials, while the end-on reaction is mostly suppressed but inevitably not unattainable.[115] Generally, the chemistry of phosphaalkynes is predominated by side-on reactions in contrast with the chemistry of nitriles, which favor the reaction over the lone pair of the nitrogen atom. This behavior can be illustrated by an orbital correlation diagram for the first two ionization potentials of a set of phosphaalkynes and nitriles which shows a much higher π-n separation for the phosphaalkynes (Figure 5b).[118] Calculated comparisons between C-N and C-P multiple bond strengths suggest that nitrogen favors C≡N triple bonds while phosphorus prefers C=P double bonds. This outcome explains the stability of nitriles and the tendency of phosphaalkyne to dimerize (head to tail)[115] unless prevented by sterically demanding substituents.[119] Being an electron-acceptor, phosphaalkynes react with electrophiles.[117] Due to the polarization along the C≡P bond with the more pronounced localized negative charge on the carbon atom, it is the preferred reactive site for incoming electrophiles,[112] as demonstrated for the stepwise addition of HCl to Ph-C≡P.[120] Investigations of JAYASURIYA indicate a substantial impact of the substituent on the phosphaalkyne. The substitution with an aromatic ring system, demonstrated by calculations on phenylphosphaalkyne, results in a reduction of the π-electron density in the ring system accompanied with an increase of the π-electron density in the C≡P bond. In consequence, the C≡P group has a deactivating effect on the phenyl ring towards electrophilic attacks.[111] Strong electron-withdrawing groups (EWG) such as -F, -CF$_3$ and HC≡C- have two effects. Firstly, they annul the negative potential region near the phosphorus atom initially induced by the lone pair. Secondly, they reduce the overall π-electron density of the C≡P triple bond region, reducing the ability to react with incoming electrophiles.[111] Electron-releasing groups (ERG), like -CH=CH$_2$, -CH$_3$, -NH$_2$ and -OH, increase the negative charge of the C≡P triple bond region, therefore have an activating effect on the C≡P group towards electrophilic agents.[114]
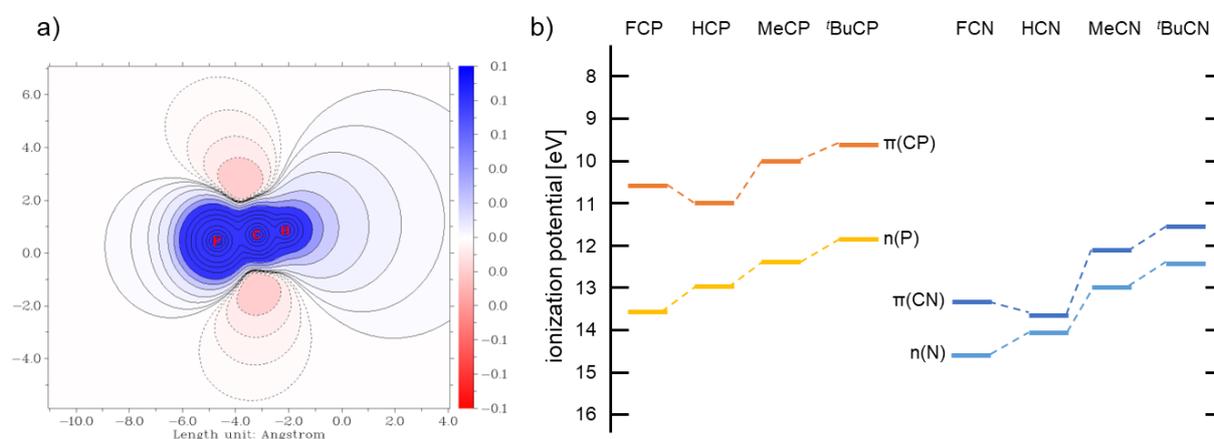
Figure 5. Molecular electrostatic potential (MEP) of HC≡P (dashed contours are negative potential) (a)[115] and orbital correlation diagram for the first two ionization potentials of RCP (left) and RCN (right)(b)[118].

Acting as a Lewis base, phosphaalkynes coordinate with Lewis acidic metal centers, mostly with early and late transition metals, offering a wide range of coordination modes (Figure 6).[12,

[81] The typical coordination mode is side-on (**b**) via the π-system of the C≡P tiple bond analog alkynes and ethenes. However, the reaction is in favor for the phosphaalkyne due to the low lying electron accepting π* orbital.[117] This fact can be vividly demonstrated by the reaction of *tert*-butylphosphaalkyne with [Pt(PPh$_3$)$_2$(η^2-C$_2$H$_4$)] resulting in the liberation of ethene under the formation of [Pt(PPh$_3$)$_2$(η^2-^{t}BuC≡P)].[121] Additionally, the ability to accept electrons from the metal core can also promote cyclodimerization reactions of the phosphaalkyne in the transition metal sphere leading to 1,3-diphosphacyclobutadiene, which η^4-coordinates to the metal (**f**).[117, 122-127] Phosphaalkynes normally favor the η^2-type ligation, due to the HOMO represented at the C≡P-π-orbital and not at the energetically low-lying phosphorus lone pair (typically HOMO-2 or lower). Therefore, there is a wide variety of such complexes differ by the central transition metal, the applied phosphaalkyne and co-ligands.[121, 128-134] In 2016 SCHEER *et al.* reported on the successful synthesis of the first homoleptic phosphaalkyne complexes bearing two η^2-coordinated phosphaalkynes without additional ligands on silver(I).[135] Recently, GOICOECHEA and co-workers even succeeded in the preparation of a η^2-tris(phosphaalkyne)tungsten complex.[136] By increasing both the steric demand of the substituents of the phosphaalkynes and of the metal center η^1-coordination products (**a**) can be achieved. Several end-on complexes mainly with electron-rich and bulky phosphonic Mo(0), W(0), Re(I), Fe(II) and Ru(II) have been realized.[137-144] Interestingly, the insertion of a phosphaalkyne into a metal-H bond leads to an 1,3-H-shift to the carbon of the phosphaalkyne, resulting in an η^1-phosphalkene complex with reverse polarity of the P=C bond represented by a nucleophilic phosphorus atom.[145] An additional binding mode can be initiated by the η^2-coordination of a phosphaalkyne to a transition metal. The coordination to the metal center positively affects the donor ability of the phosphorus lone pair which can subsequently bind to another metal atom.[115, 118] This combination of side-on and end-on complexes (**c**) is known for either the same or different combinations of metals.[134, 146-147] Another option is the η^2-coordination of the same phosphaalkyne to two metal centers in a bridged fashion (**d**).[139, 148] Often this is accompanied by a further coordination on a third metal over the phosphorus lone pair (**e**), occupying all possible vacancies.[149-153] Consequently, phosphaalkynes can donate 2, 4 or 6 electrons (e$^-$) leading to side-on, end-on or bridged coordination modes.
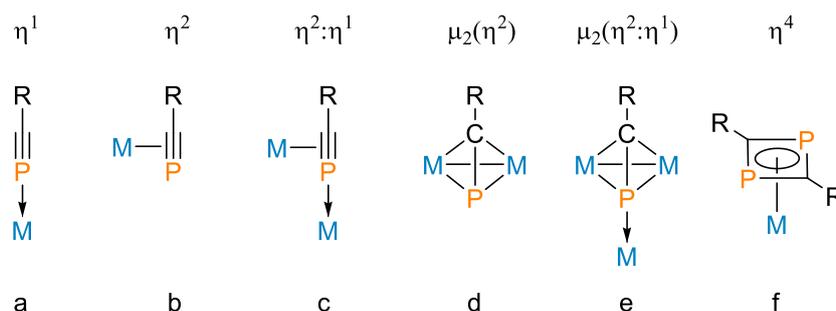
Figure 6. Phosphaalkyne coordination modes (a-f).

1.3.3 Synthesis of phosphaalkynes

Since the discovery of H-C≡P, via conversion of PH_3 at a graphite electrode,[6] a numerous variety of substituted phosphaalkynes have been synthesized. General, the *β*-elimination is the predominant method to generate the C≡P triple bond.[11] In the beginning, most of the small kinetical labile phosphaalkynes were produced by flash vacuum pyrolysis of halogen phosphines at high temperatures (T = 900-1100 °C) by elimination of HCl, which has to be absorbed by bases (KOH, K_2CO_3 etc.) to prevent undesired reverse reactions (Scheme 2a).[57, 66, 68-70, 154] An improved method is the elimination of chlorotrimethylsilane from chloro-[(trimethylsilyl)methyl]phosphine derivatives at elevated temperatures (Scheme 2b). Due to the stability of the Si-Cl bond, no base additives are necessary to trap released HCl.[75, 120] An adapted and nowadays highly relevant route can be performed under much milder conditions (room temperature) by addition of silver trifluoromethanesulfonate and the moderate strong base 1,4-diazabicyclo[2.2.2]octane (DABCO) to obtain the silyl-substituted phosphaalkynes Me_3Si-C≡P, Ph_3Si-C≡P and the tritylphosphaalkyne Ph_3C-C≡P in multi-gram scale (Scheme 2c).[37, 77, 80] The most common method to various kinetically stable phosphaalkynes is the elimination of hexamethyldisiloxane from suitable substituted phosphaalkenes at raised temperatures or by treating with a catalytic amount of base (Scheme 2d).[30, 78-79, 155] The necessary phosphaalkenes are usually generated from the appropriate carboxylic acid chlorides and tris(trimethylsilyl)phosphane or its more reactive lithium derivative. So far, this route is also the most suitable for the preparation of diphosphaalkynes.[104-105]
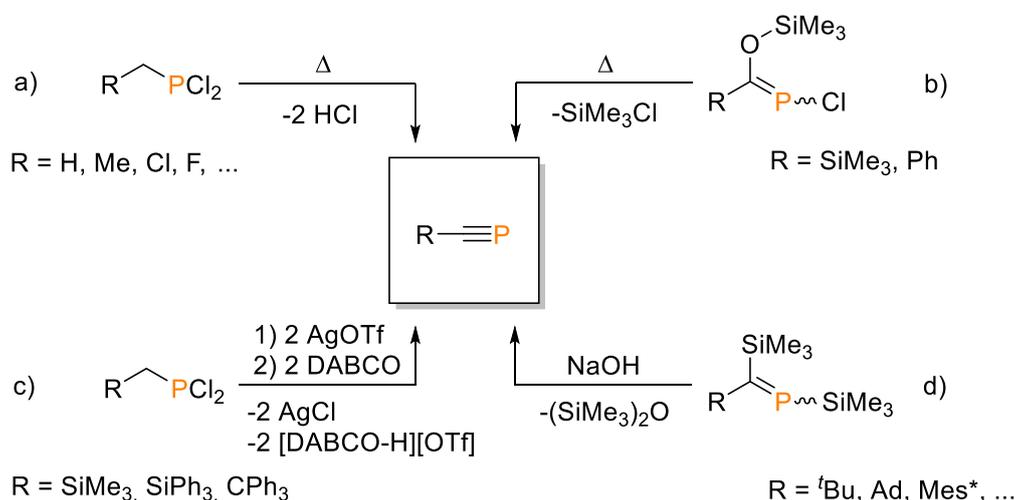
Scheme 2. Common synthetic pathways of labile and sterically stabilized phosphaalkynes.

Further less common methods for the synthesis of phosphaalkynes are well described in the specialized literature[10, 12, 83, 85-86] and are not discussed here. Instead, a selection of recent methods, not yet covered by phosphaalkyne review articles, will be briefly presented.

Today sodium phosphaethynolate became an important building block due to its stability, simple accessibility and extensive reactivity. It can be primarily synthesized by addition of a

suitable carbon source like CO to NaPH$_2$ under high pressure ($p \approx 110$ bar). The sodium phosphide can also be generated *in situ* by deprotonation of phosphine gas (PH$_3$) with NaO^{t}Bu (Scheme 3a,b).[49, 51, 156] Most kinetical labile phosphaalkynes used to be mainly synthesized by flash vacuum pyrolysis of halogen phosphines of the type R-PCl$_2$ in low yields and the isolation is challenging. A more reliable method is the vacuum-gas-solid reaction of dichloromethylphosphines (R-CCl$_2$-PH$_2$) with K$_2$CO$_3$. The dichloromethylphosphines can be generated by reduction of phosphonate with AlHCl$_2$.[157] A improved synthesis protocol uses the strong, non-nucleophilic base 1,8-Diazabicyclo[5.4.0]undec-7-ene (DBU) for the final elimination of the *α*-dichlorophosphines to obtain the sensitive, labile phosphaalkynes at low temperature ($T = -40$ °C; Scheme 3c).[158] Recently, a further procedure for the controlled thermal liberation of unstable phosphaalkynes was developed. The chlorine atom of dibenzo-7-chlorophosphanorbornadiene can be substituted with an appropriate Wittig reagent to get a suitable precursor, which can be simply stored and later used for a controlled release of kinetically labile phosphaalkynes. Upon thermolysis the dibenzo-7-phosphanorbornadienes release the desired phosphaalkyne, together with anthracene and triphenylphosphine (Scheme 3d).[159-160] Nitrogen-substituted phosphaalkynes are still rare. A new one-step synthesis from CsF, tris(trimethylsilyl)phosphine and supermesityl isocyanate give access to the stable, nitrogen-substituted 2,4,6-(*tert*-butyl)phenylphosphaalkyne (Scheme 3e).[161] Lately, a new method based on salt metathesis was established. It was found that the addition of the novel [Mg(^{Dipp}NacNac)(CP)(dioxane)] (Dipp = 2,6-di(isopropyl)phenyl, ^{Dipp}NacNac = CH{C(CH$_3$)N-(Dipp)}$_2$) to chlorotrimethylsilane *in situ* generates the well-known trimethylsilylphosphaalkyne (Me$_3$SiC≡P) by C≡P$^-$ transfer and formation of MgCl$_2$ as driving force (Scheme 3f).[162] So far, this synthesis was just used as proof of concept, but it has the potential to become an alternative synthesis strategy to the firmly established elimination protocols. The method offers the ability to create novel phosphaalkynes, which were not accessible before. In addition, potential halogen precursors are readily commercially available.

a) $2\ NaPH_2 + 2\ CO$ $\xrightarrow[\text{110 bar, 80 °C}]{\text{DME}}$ $Na(DME)_2(O\!\!=\!\!\equiv\!\!P)$ + [structure: H, ξ, P, H–C–$ONa(DME)$]

b) $PH_3 + 3\ NaO^tBu +$ [structure: EtO–C(=O)–OEt] $\xrightarrow[\text{dioxane}]{\text{DME}}$ $Na(dioxane)_x(O\!\!=\!\!\equiv\!\!P) + 3\ NaO^tBu + 3\ {}^tBuOH$

c) [structure: Cl, R, Cl, P(=O)(–O^iPr)(–O^iPr)] $\xrightarrow[\text{Et}_2\text{O, -78 °C}]{AlHCl_2}$ [structure: Cl, R, Cl, P(H)(H)] $\xrightarrow[\text{Et}_2\text{O, -40 °C}]{DBU}$ $R\!\!=\!\!\equiv\!\!P$

   R = Me, Et, Pr, Bu,
   n-pentyl, Cy, ...

d) [structure: PPh_3, P, R, anthracene-bridged structure] $\xrightarrow[\substack{-PPh_3 \\ -\text{anthracene}}]{\Delta}$ $R\!\!=\!\!\equiv\!\!P$

   R = H, Me, Et, ^iPr, ^sBu

e) $^*Mes\!-\!N\!=\!C\!=\!O$ $\xrightarrow[\substack{-Me_3SiF \\ -(Me_3Si)_2O}]{\substack{CsF \\ P(SiMe_3)_3}}$ [structure: Cs, $^*Mes$, $N\!-\!C\!\equiv\!P$]

f) $Me_3Si\!-\!Cl$ $\xrightarrow[\text{toluene}]{\text{[Mg structure with Dipp, N, diox, C≡P]}}$ $Me_3Si\!\!=\!\!\equiv\!\!P$

Scheme 3. Selection of novel phosphaalkyne syntheses.

1.3.4 Reactivity of phosphaalkynes

The carbon-phosphorus triple bond mimics the carbon-carbon triple bond (cf. chapter 1.3.2) and shows in many aspects similar reactivities. The HOMO is located at the C≡P bond and has π-symmetry, whereas the phosphorus lone pair is usually represented by the HOMO-1.[118] In contrast to acetylenes the triple bond of phosphaalkynes is positive polarized at the phosphorus atom, leading to selective protonation of the carbon atom and not of the phosphorus lone pair.[163] Consequently, the chemistry of phosphaalkynes is strongly marked by various addition and cycloaddition reactions, some of the most relevant reaction types will be illustrated in this section.

The 1,2-addtion reaction can be mainly carried out with halogen compounds and organolithium derivatives. Typically, this reaction is executed with HCl leading to a stepwise saturation of P≡C triple bond, whereby the hydrogen atoms exclusively attach to the carbon atom while the chlorine atoms ending up at the phosphorus atom (Scheme 4a).[120] The addition of MeLi

initially yields the lithiated phosphaalkene which can be subsequently hydrolyzed (Scheme 4b).[164]

a) $Ph\!\!-\!\!\!\equiv\!\!P$ $\xrightarrow{\text{HCl (1 eq)}}$ $\underset{Ph}{\overset{H}{}}C\!\!=\!\!P\overset{Cl}{}$

b) $^t Bu\!\!-\!\!\!\equiv\!\!P$ $\xrightarrow[\text{2) H}_2\text{O}]{\text{1) MeLi (1 eq)}}$ $\underset{^t Bu}{\overset{H}{}}C\!\!=\!\!P\!\!\leadsto\!\!Me$
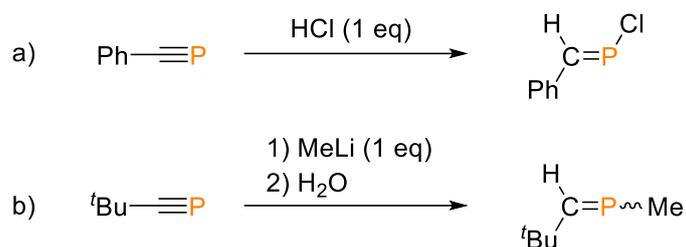
Scheme 4. 1,2-addtion reaction on phosphaalkyne with HCl (a) and MeLi (b).

Phosphaalkynes can undergo all kind of cycloaddition reactions. Usually, [2+1], [3+2] and [4+2] cycloadditions are the predominated variants which cleanly convert the $\lambda^3\sigma^1$-phosphorus atom into a $\lambda^3\sigma^2$-phosphorus atom. The [2+1] cycloaddition reaction gives access to three-membered ring systems containing a C=P fragment. Most of those ring systems will be built by the addition of carbenes, silylenes or germylenes (Scheme 5a).[165-167] Recently, the group of three-membered ring systems was expanded with phosphaaluminirenes.[168] Heteromolecular [2+2] cycloadditions are very rarely described in the literature. Most [2+2]-cycloadditions take place between small, reactive phosphaalkynes of the same kind, leading to dimerization and oligomerization, which will be discussed later. One example of a heteromolecular [2+2] cycloaddition is the reaction of *tert*-butylphosphaalkyne with a stannylidene forming a stannacyclobutene (Scheme 5b).[169] However, it can be discussed if the formation of the stannacyclobutene is in reality an initial [2+1]-cycloaddition with a subsequent insertion of a further stannylene as it was found for the stepwise silylene addition.[170] A wide range of [3+2] cycloaddition reactions are known for phosphaalkynes. Those 1,3-dipolar reactions are well-established for diazo and azide compounds (Scheme 5c).[155, 171] The [3+2] cycloaddition reactions pf phosphaalkynes with azides ("click" reaction)[172] proceed selectively due to the polarization along the C≡P bond in contrast to acetylenes which react unselective upon addition of copper or ruthenium catalysts.[173-176] Further 1,3-dipolar reactions with phosphaalkynes are still in development. Recently, a novel selective copper-catalyzed [3+2]-cycloaddition reaction between isocyanoacetates and phosphaalkynes for the preparation of 1,3-azaphospoles was described.[177] Beside of that phosphaalkynes can also undergo multifarious [4+2] cycloaddition reactions. The most prominent are Diels-Alder reactions with 1,3-dienes or even 1,3-heterodienes. Despite the versatile possibilities, there are limitations given by the stability of the phosphaalkynes due to the high thermal activation barrier of those reactions. The preparation of phosphinines by addition of phosphaalkynes to pyrone, cyclopentadienes or cyclohexadienes are well documented (Scheme 5d).[11, 178-179]
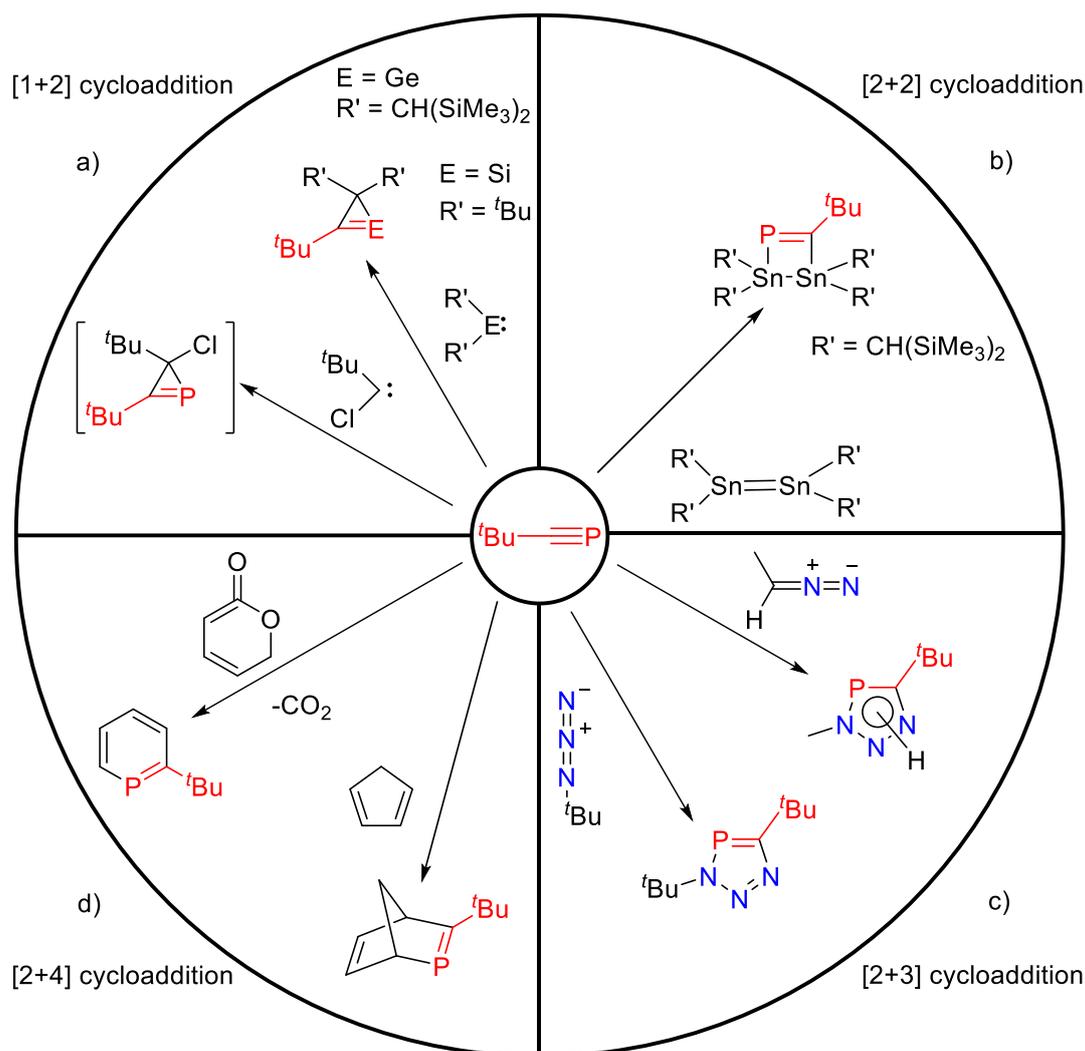
Scheme 5. Selection of confirmed cycloaddition reactions on *tert*-butylphosphaalkyne.

As mentioned before [2+2] cycloaddition reactions of phosphaalkynes are often monomolecular between phosphaalkynes with small substituents (H, F, Me, Ph etc.) of the same type, leading to oligomeric species. Those reactions are thermally induced and yield product mixtures of different oligomers and polymers, which are challenging to separate and characterize.[81] However, it was possible to isolate tetramers for larger and more kinetically stable phosphaalkynes like *tert*-butylphosphaalkyne.[180] Computational investigations have proven that the formation of phosphaalkyne dimers, trimers, tetramers and higher oligomers are theoretically thermodynamically favored.[76] Along other tetramers and oligomers,[82] even a hexamer of *tert*-butylphosphaalkyne was successfully isolated and crystallographically characterized.[181] Transition and main group metals are capable to initiate an controlled oligomerization leading to a more straight-forward synthesis of phosphaalkyne oligomers (Figure 7).[81] It was possible to prepare the elusive diphosphatetrahedrane, the head to head dimer of *tert*-butylphosphaalkyne, with the help of a nickel catalyst.[182] Besides catalytic oligomerization reactions, side-on coordination of mainly cyclodimers or cyclotrimers to the metal and sandwich complexes are possible.[81, 125, 183] Apart from the most typical cycloaddition

reaction, many more specialized variants and consecutive reactions were found, such as an elegant way for the preparation of functionalized phosphinines by an iron- or copper-catalyzed [2+2+2] cycloaddition reaction of diynes with phosphaalkynes.[184-185]
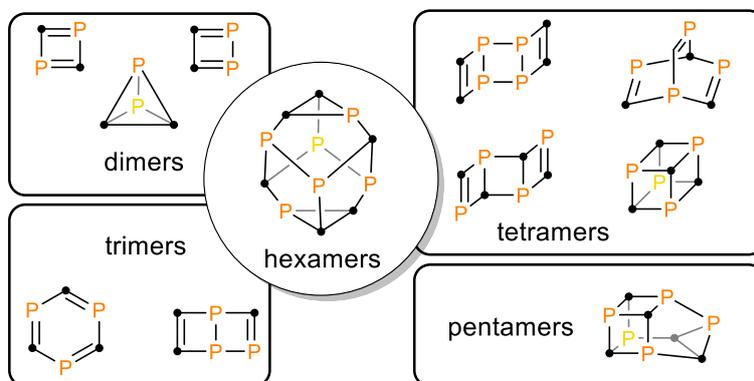
Figure 7. Reported phosphaalkyne oligomers synthesized with metal catalysts, mostly with ^{t}BuCP. Some of the shown oligomers are only stable when coordinated on metals. The ▪ symbol represents a C-R unit for clarity.

1.4 The cyaphido ligand and its complexes

1.4.1 Theoretical studies and spectroscopic properties

Since the discovery of HC≡P by GIER in 1961[6] the chemistry of the C≡P triple bond developed rapidly, resulting in numerous unstable phosphaalkynes, all of which exhibited a tendency to polymerize. With the synthesis of ^{t}Bu-C≡P in 1985, BECKER and co-workers set the starting point for the continuous development of thermally stable phosphaalkynes.[186-187] The increased steric shielding of the C≡P triple bond by the ^{t}Bu group allowed for the synthesis of a variety of transition-metal complexes with phosphaalkyne ligands.[43] Nevertheless, the generation and stabilization of a terminal C≡P$^-$ ligand on a transition metal remained a challenge until 2006.[37] Until recently, the generation of the cyaphido ligand could only be carried out starting from a phosphaalkyne in the coordination sphere of a metal (cf. chapter 1.4.2). Hence, the history of the C≡P$^-$ anion is deeply linked with the chemistry of phosphaalkynes. Most analytical and theoretical studies on C≡P triple bonds focus on phosphaalkynes whereas the C≡P$^-$ anion or radical have only partly been covered.[188-192] The investigation of the C≡P triple bond in HC≡P comprises mainly the reactivity of this species and various spectroscopic techniques such as vibrational-rotational spectroscopy,[193] Raman spectroscopy,[194] microwave spectroscopy[195-196] and NMR spectroscopy[116] as well as DFT calculations[113] and led to an evaluation of the bonding properties and estimations of the gas-phase acidities.[197]

This section will exclusively discuss the main results concerning HC≡P and C≡P$^-$ as an anion, ligand and radical. Hydrogen cyaphide is a linear molecule and the phosphorus analog of hydrocyanic acid (hydrogen cyanide). In contrast to HC≡N it is pyrophoric, highly reactive and polymerizes even at low temperatures. Generally, the C≡P triple bond is polarized as $C^{\delta-}$ - $P^{\delta+}$, however, it is much less polarized than the C≡N triple bond, due to the decreased electronegativity of phosphorus compared with nitrogen.[113] Based on microwave spectroscopy the dipole moment was determined as μ(HC≡P) = 0.390(5) D (μ(HC≡N) = 3.00 D), while the H-C and C≡P bond distances were found to be 1.0670 Å and 1.5402 Å, respectively (HC≡N: 1.063 Å, 1.155 Å).[195, 198] Solid HC≡P shows three main vibrations in its infrared spectrum at $\tilde{v}$(C-H stretch) = 3120, $\tilde{v}$(C-P stretch) = 1265 and $\tilde{v}$(H-CP bend) = 671 cm^{-1} (HC≡N: $\tilde{v}$ = 3180, 2120, 830 cm^{-1}).[6] NMR spectroscopy of HC≡P reveals one signal at δ(^{31}P) = -32.0 ppm (d, $^2J_{P,H}$ = 43.9 Hz) and δ(^{13}C) = +154 ppm (dd, $^1J_{C,H}$ = 211, $^1J_{C,P}$ = 54.0 Hz).[199] Calculations of the gas-phase acidity (ΔG^0_{acid}) confirmed that HC≡P is a weaker Brønsted acid than HC≡N. However, the opposite result was found for the corresponding methyl derivatives (CH$_3$C≡N < CH$_3$C≡P).[197]

Based on calculations, the dipole moment of the C≡P$^-$ anion is strongly increased to 2.42 D compared to C≡N$^-$ (0.63 D),[200-201] whereby most of the negative charge is located on the carbon atom (-0.83 C, -0.17 P) in contrast to the cyanide anion (-0.4 C, -0.6 N).[202] Overall, the

C≡P bond is polarized ($C^{\delta-}$ - $P^{\delta+}$) with a high negative charge on the carbon atom, whereas the positive charge on the phosphorus atom decreases upon coordination to a metal center.[113] Electron localization function (ELT) calculations provide insight into the distribution of the valence electrons. The 10 VE of C≡P⁻ are separated between the carbon atom V(C) = 2.66, the phosphorus atom V(P) = 4.22 and the corresponding bond V(C,P) = 2.91 (C≡N⁻: V(C) = 2.86, V(N) = 3.39, V(C,N) = 3.54). The C≡P bond length in the C≡P⁻ anion is calculated to be 1.598 Å long (C≡N⁻ = 1.180 Å due to the smaller covalent radius of nitrogen), in contrast to about 1.54 Å (exp.) for phosphaalkynes and 1.56 Å (exp.) for transition metal complexes containing terminal cyaphido ligands. The calculated harmonic vibrational stretching wavelength of C≡P⁻ is $\tilde{\nu}$ = 1198 cm⁻¹ (C≡N⁻: $\tilde{\nu}$ = 2108 cm⁻¹), while ΔH^0 for the formation of C≡P⁻ was found to be higher in comparison to C≡N⁻, which confirmed that the cyaphide anion is less stable than the ubiquitous cyanide congener.[62, 113, 197]

The information about the reactivity and coordination of C≡P⁻ is very limited. Until now, the primary coordination to metals is realized through the carbon atom. Additional coordination and reactions occur first via the π system (side-on mode) before the phosphorus lone pair gets involved via σ coordination (end-on) as third reaction side.[203-204] The C≡P ligand acts similar as a free phosphaalkyne after the first coordination through the carbon to a metal complex (cf. chapter 1.3.2) and contrary to the C≡N. The cyanido ligand strongly favors the η^1 coordination (end-on) to Lewis acids. This reaction is driven by σ-donation from the nitrogen lone pair, which represent the HOMO of the C≡N⁻ ion.[205-206] Recent computational investigations of cyaphido transition metal complexes of the type M-(η^2-C≡P) reveal a large contribution of the metal π back-bonding into the cyaphido π^* antibonding orbital, giving an explanation for the excellent π acceptor properties of the η^2 coordinated cyaphido ligand in agreement with the results of the experiments.[203] Consequently, cyaphido transition metal complexes of the type M-(η^1-C≡P) prefer to react with Lewis basic metals, whereas complexes of the type M-(η^2-C≡P) can most likely only react with Lewis acids.

1.4.2   Synthesis of cyaphido complexes

1.4.2.1   Generation of C≡P⁻ from a bridging μ-C=PR ligand

By 1991 several alkyl and aryl stabilized phosphaalkynes had been synthesized, and their behavior as ligands towards transition metal complexes had highlighted some significant differences when compared to metal nitriles complexes. Expect for two examples, in which the phosphaalkyne is end-on η^1-bonded via the phosphorus atom to the metal center,[137, 144] all other reports showed a preference for a side-on η^2-coordination via the P≡C triple bond.[46] This is in line with theoretical calculations and demonstrates the preferred side-on coordination mode via the π-system. Another coordination mode was found by ANGELICI, who reported on

a homo-bimetallic Pt-complex with a :C=PR ligand (isocyaphide). In fact, the X-ray analysis revealed a semibridging μ_2-C=PR ligand coordinated over the carbon atom between two Pt centers. Shortly afterwards, WEBER and co-workers demonstrated the synthesis of a diiron complex also bearing a :C=PR ligand coordinating in the same manner.[106-107] In 1992 ANGELICI *et al.* showed the crucial further development of this chemistry. Treatment of the phosphavinyl platinum complexes *trans*-[(X)(PEt$_3$)$_2$Pt[C(P=R)X]] (**1.1a**,**b**; X = Cl, Br; R = 2,4,6-tri-*tert*-butylphenyl) with 1 eq of [Pt(PEt$_3$)$_4$] gave the air-stable diplatinum complexes [(X)(PEt$_3$)Pt(μ_2-C=PR)Pt(PEt$_3$)$_2$(X)] (**1.3a**,**b**), bearing the μ_2-bridging isocyaphide ligand (Scheme 6). Addition of [Pt(PEt$_3$)$_4$] to the Pd-analog **1.1c** astonishingly gave two independent compounds, *trans*-[(X)(PEt$_3$)$_2$Pd(R)] (**1.5a**,**b**), and the first ever reported terminal cyaphido complexes *trans*-[(X)(PEt$_3$)$_2$Pt(C≡P)] (**1.4a**,**b**). Even though **1.4a**,**b** were surprisingly stable in nonpolar organic solvents, all attempts at separating **1.4a**,**b** from **1.5a**,**b** failed. However, the compounds could be analyzed by means of ^{31}P{^{1}H} NMR spectroscopy, showing a triplet resonance at δ = 68 ppm for the cyaphide phosphorus nucleus with a $J_{P,P}$ coupling of 9.2 Hz and an additional $J_{P,Pt}$ coupling of 303 Hz. Furthermore, **1.4a**,**b** were successfully trapped by reaction with a second equivalent of [Pt(PEt$_3$)$_4$] yielding the cyaphido bridging complexes [(X)(PEt$_3$)$_2$Pt(μ-C≡P)Pt(PEt$_3$)$_2$] (**1.6a**,**b**), which could be fully characterized by means of NMR spectroscopy, elemental analysis and single crystal X-ray diffraction to unambiguously verify the proposed structure (Figure 8).
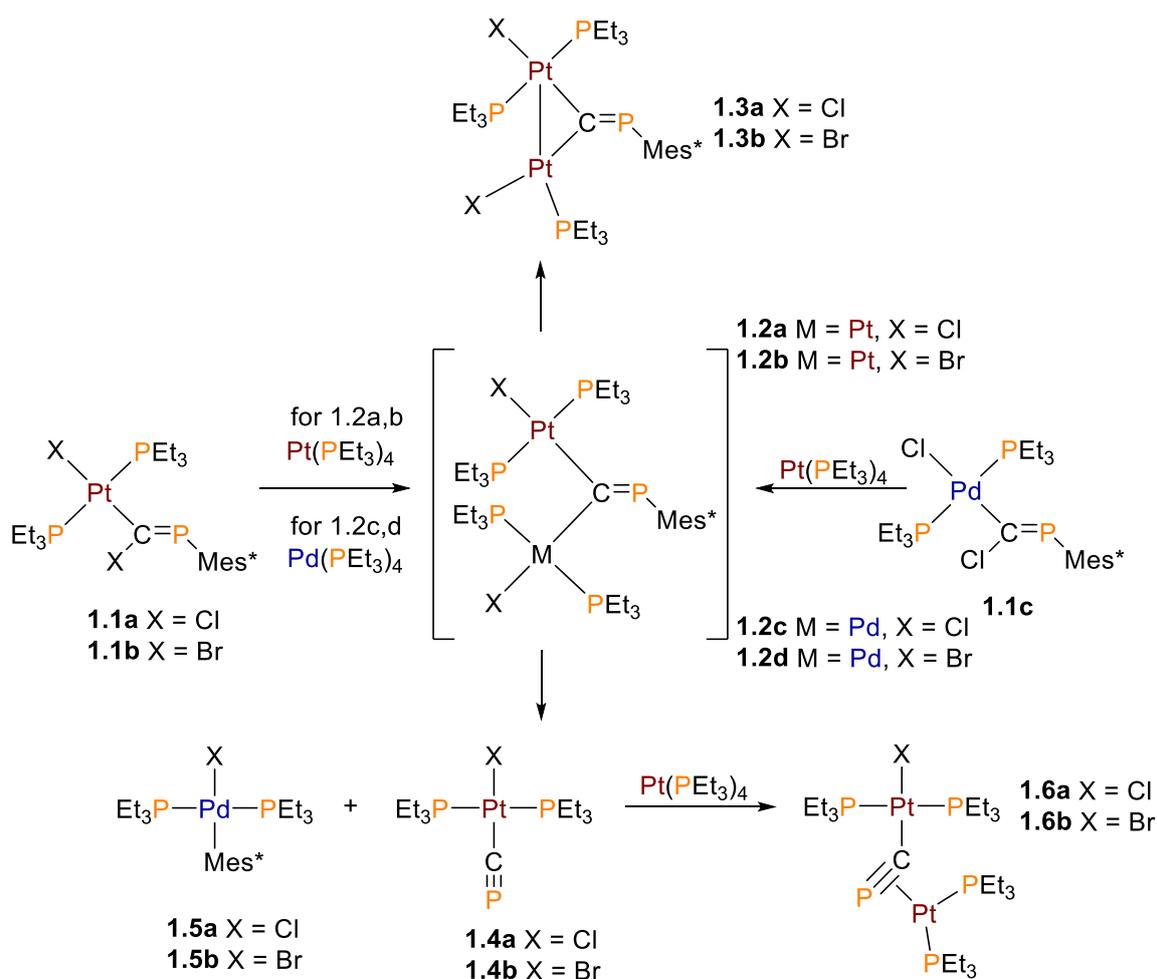
Scheme 6. Reaction pathways for the synthesis of the diplatinum complexes **1.3a,b** and the cyaphido bridged complexes [(X)(PEt₃)₂Pt(μ-C≡P)Pt(PEt₃)₂] (**1.6a,b**); Mes* = 2,4,6-tri-*tert*-butylphenyl.
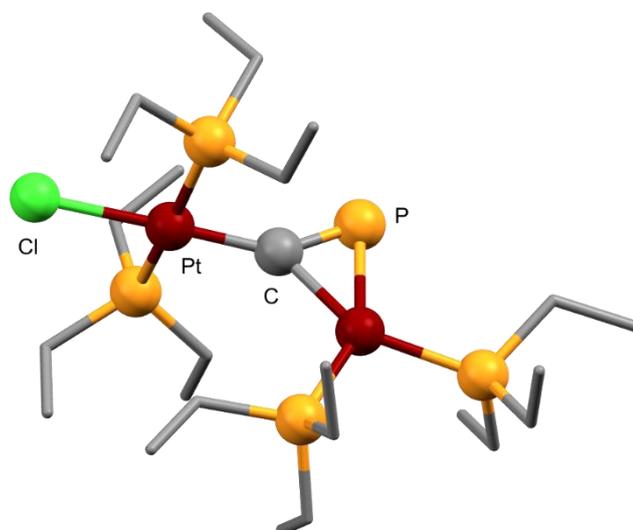
Figure 8. Ball and stick model of the molecular structure of **1.6a** in the crystal. Hydrogens omitted and carbon atoms of the PEt₃ ligands reduced for clarity.

Despite the fact that no intermediates were observed in the ^{31}P NMR spectrum during the course of the reaction, ANGELICI assumed the formation of the mixed Pt-Pd complexes **1.2c,d** after the initial oxidative addition of the C-X bond of **1.1a,b** to the [Pd(PEt₃)₄]. The subsequent

transfer reaction of the aryl substituent (R) from the phosphorus atom of the isocyaphido ligand, accompanied by the scission of the bridging carbon atom from the Pd center afforded the two independent products **1.4a,b** and **1.5a,b**. To affirm this theory the same reaction was performed starting from **1.1c** and Pt(PEt$_3$)$_4$, which indeed afforded the same products. Although complex **1.6a,b** does not contain a "pure" terminal cyaphido ligand due to the additional side-on coordination of a [Pt(PEt$_3$)$_2$] complex, DFT calculations still suggest the presence of a P≡C triple bond.[113] The resonance of the phosphorus atom of the bridging cyaphido ligand appears as a doublet of doublet of triplets at δ = 107.0 ppm in the ^{31}P{^{1}H} NMR spectrum. The triplet arises from the two PEt$_3$ co-ligands at the [(X)Pt(II)(C≡P)] core, whereas the two doublets are caused by the two magnetically non-equivalent PEt$_3$ co-ligands at the π-coordinated Pt(0) fragment. Two additional ^{195}Pt satellites are observed with a coupling constant of $^2J_{Pt(\eta1-CP),P}$ = 255 Hz and $^1J_{Pt(\eta2-CP),P}$ = 58 Hz. The X-ray crystal structure determination of **1.6a,b** clearly revealed that the two Pt centers are not connected to one another. The C≡P bond length of 1.666(6) Å in **1.6a** is longer than the average C≡P distance of an uncoordinated phosphaalkyne (1.54 Å) and the calculated C≡P bond length of the terminal cyaphido ligand (1.566 Å) in the non-isolated complex **1.4a**. However, the Pt-C≡P bond-angle of 144.0(3)° in **1.6a** significantly deviates from linearity.[34, 63]

1.4.2.2   Generation of C≡P⁻ by elimination of Me$_3$Si-O-SiMe$_3$

Twelve years later, in 2004, WILLNER and co-workers reported on the first successful isolation of a Lewis-pair, consisting of the cyaphide anion and the Lewis acid B(CF$_3$)$_3$. The synthesis of this compound followed the typical elimination route used for the preparation of phosphaalkynes[11] (**Scheme 7**). Interestingly, the resulting borate anion [(CF$_3$)$_3$B(C≡P)]⁻ was even stable in wet acetonitrile and was isolated as colorless tetraphenyl phosphonium salt (**1.7**) with a melting point of T = 125 °C. The C≡P moiety of **1.7** showed a resonance at δ = 202.3 ppm in the ^{13}C NMR spectrum and the associated ^{31}P NMR signal at δ = 39.6 ppm. The Raman spectrum showed a C≡P⁻ stretching band at $\tilde{\nu}$ = 1468 cm^{-1}, while the crystallographic characterization revealed a C≡P distance of 1.563(10) Å.[207]
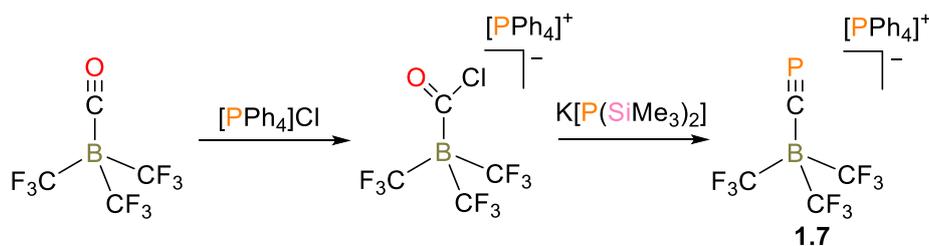
Scheme 7. Brief reaction sequence for the isolation of [PPh$_4$][(CF$_3$)$_3$BCP].

1.4.2.3   Generation of C≡P⁻ by deprotection of R₃Si-subsituted phosphaalkynes

A milestone in the chemistry of the cyaphide anion was achieved by GRÜTZMACHER and co-workers. They developed the strategy to generate the desired cyaphido ligand in the coordination sphere of a metal center by using a kinetically stabilized phosphaalkyne that contains an adequate leaving group. Treatment of triphenylmethyl phosphaalkyne or its corresponding complexes [MH(dppe)$_2$(η^1-P≡C-CPh$_3$)]OTf (M = Fe, Ru, dppe = 1,2-bis(diphenylphosphino)ethane) with nucleophiles was initially not fruitful. However, they continued this approach with the higher homolog Ph$_3$SiC≡P (δ(^{31}P) = 111, δ(^{13}C) = 193.3 ppm (d, $J_{C,P}$ = 16.4 Hz)), as -SiR$_3$-groups are generally prone to nucleophilic attack. Even though Ph$_3$SiC≡P can neither be isolated nor is it kinetically and thermodynamically stable (t$_{1/2}$ ≈ 1 d at T = 23 °C), it can be isolated as an η^1-coordinated ligand in the complex [RuH(dppe)$_2$(η^1-P≡C-SiPh$_3$)]OTf (**1.8a**, Scheme 8). This was proven by means of NMR spectroscopy (δ(^{31}P) = 143.8 (d, $^2J_{P,P}$ = 27.8 Hz), δ(^{13}C) = 175.1 ppm ($J_{C,P}$ = 71.4 Hz)), as well as by single crystal X-ray diffraction (P≡C bond length 1.530(3) Å). Applying various nucleophiles (fluorides, hydroxides, alkoxides) resulted in undesired side reactions. In 2006, the persistent work finally paid off, as the addition of a slight excess of sodium phenoxide resulted in the preparation of the "first 'true' M-C≡P complex" [RuH(C≡P)(dppe)$_2$] (**1.8b**) – a terminal metal cyaphido complex. In this way a convenient route to access cyaphido complexes was at once finally established. The NMR spectra of **1.8b** revealed a broad signal at δ(^{31}P) = 143.8 ppm with coupling to the hydride (d, $^3J_{P,H}$ = 19.5 Hz). The quaternary carbon atom of the cyaphido moiety was detected in a ^{13}C^{1}H HMQC experiment and reveal a resonance at δ(^{13}C) = 287.1 ppm ($^1J_{P,C}$ ≈ 90 Hz). [RuH(C≡P)(dppe)$_2$] is only moderately air-sensitive in the solid state. Crystal structure determination revealed the 180° rotation of the C≡P ligand upon cleaving off the Ph$_3$Si$^+$ group in the initial P-coordinated starting complex (Figure 9). The C≡P distance was found to be 1.573(2) Å, which is longer than in uncoordinated phosphaalkynes but much shorter than in side-on coordinated phosphaalkyne complexes. The Raman and infrared spectra displayed an intense band at $\tilde{v}$ = 1229 cm^{-1} for the C≡P stretch vibration.[37]
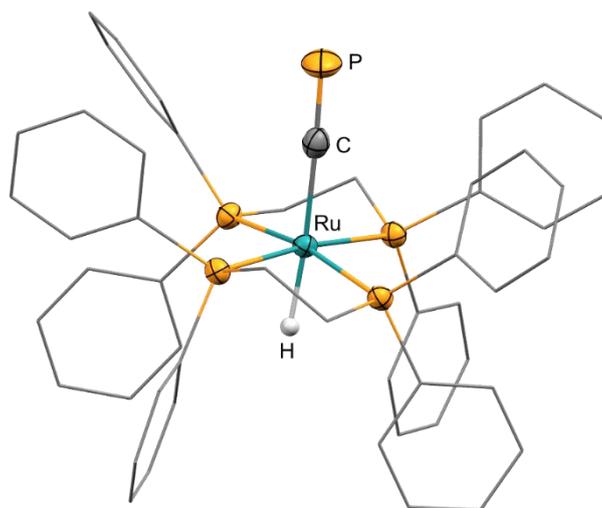
Figure 9. Molecular structure of **1.8b** in the crystal. Anisotropic displacement ellipsoids are shown at 50% probability level. Hydrogens omitted and carbon atoms of the dppe ligands reduced for clarity.

While the observation of a possible P-metalated phosphoniocarbene intermediate in the ^{31}P NMR spectrum indicated an initial attack of the phenoxide at the phosphorus atom, DFT calculations suggested that a further transition state is too high in energy to be a reasonable mechanism for the formation of C≡P and elimination of Ph₃SiOPh (Scheme 8). Instead, a direct nucleophilic attack of the phenolate at the silicon was proposed, leading to a penta-coordinate silicon species as an intermediate. Direct elimination of Ph₃SiOPh would result in the complex [Ru]-P≡C, the formation of which is thermodynamically unfavorable. The weak overlap between suitable P-centered orbitals and Ru *d*-orbitals prevent a Ru-P *σ*-bond with respect to a more favorable Ru-C bond. Thus, a rearrangement to the more favored η^2-bonded intermediate takes place, followed by rotation of the C≡P⁻ moiety under formation of the final cyaphido complex [RuH(C≡P)(dppe)₂].[208] Even though this approach did not lead to initially attempted preparation of a bimetallic cyaphido complex (M-CP-M) yet, it was certainly the starting point and inspiration for the preparation of various, unique cyaphido complexes.
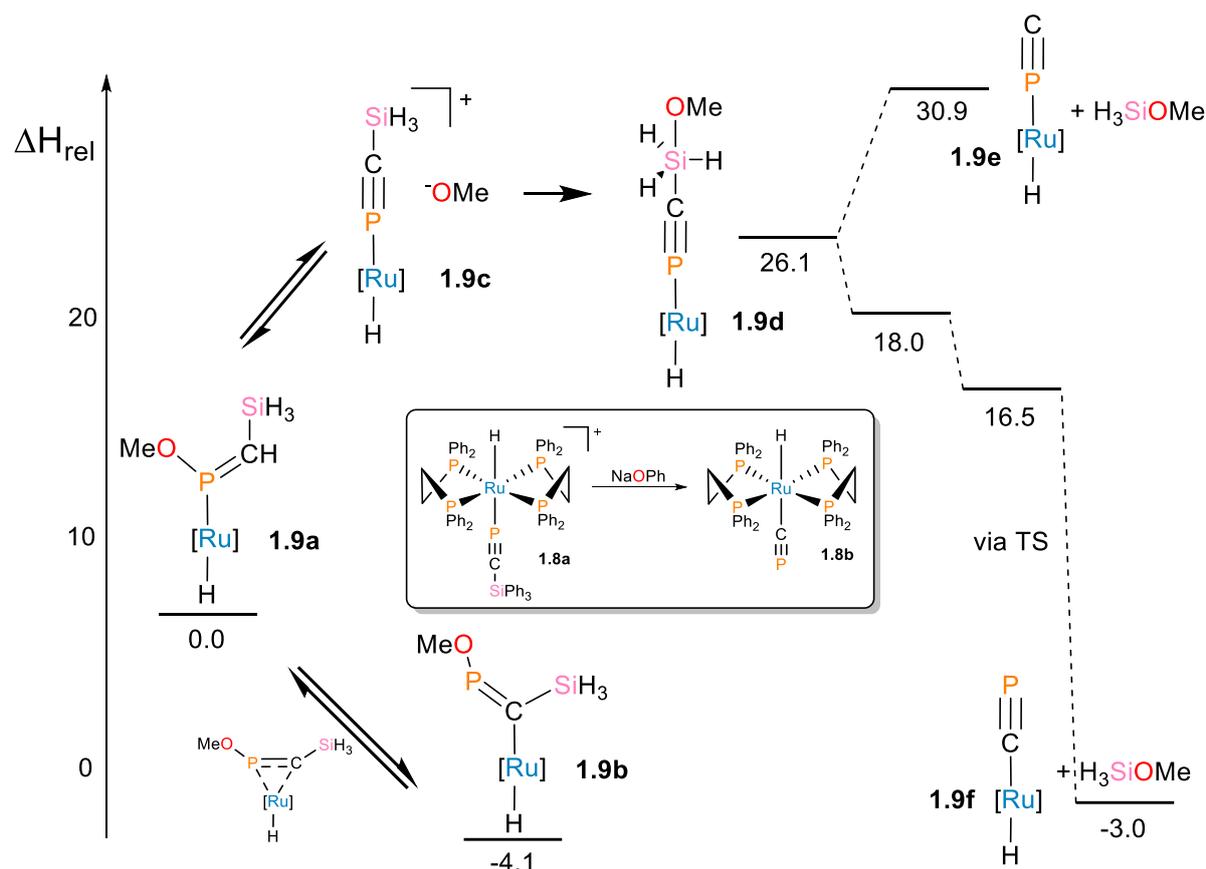
Scheme 8. Synthesis of [RuH(C≡P)(dppe)₂] (**1.8b**) (middle) and proposed mechanism via ion pair generation; all Ph groups replaced with H to simplify the calculation.

Six years later, RUSSELL *et al.* investigated the coordination chemistry of trimethylsilylphosphaalkynes (Me₃SiC≡P) towards selected transition metal complexes and synthesized, *inter alia*, the bis(phosphaalkyne) complex [Mo(η^1-P≡CSiMe₃)₂(dppe)₂]. However, following the desilylation protocol reported by Grützmacher, did not lead to a cyaphido complex. Instead, addition of tetrabutylammonium difluorotriphenylsilicate (TBAT) as fluoride source showed evidence for the formation of a mixed phosphaalkyne-cyaphido complex of the type [Mo(η^1-P≡CSiMe₃)(C≡P)(dppe)₂] (**1.10**, Figure 10). Two low-field shifted multiplets at δ = 197.8 and δ = 183.0 ppm were recorded in the ³¹P NMR spectrum, whereas signals consistent with the formation of PH₃SiF (remnant from TBAT) and Me₃SiF (expected leaving group) could be detected in the ¹⁹F spectrum. Unfortunately, it was not possible to verify the identity of the product by further characterization techniques.[139]

1.19b R = C CC$_6$H$_4$(NO$_2$)-*p*
1.20b R = CCCO$_2$Et
1.21 R = Me
1.29a R = Br
1.29b R = Cl
1.29c R = I
1.30 R = none, OTf counter anion

1.8b R = H
1.11b R = CCCO$_2$Me
1.12b R = CCC$_6$H$_4$(OMe)-*p*
1.15b R = CCC$_6$H$_4$Me-p
1.16b R = CCC$_6$H$_5$
1.17b R = CCC$_6$H$_4$F-p
1.18b R = CCC$_6$H$_4$(CO$_2$Me)-p

C≡C

1.10

1.14
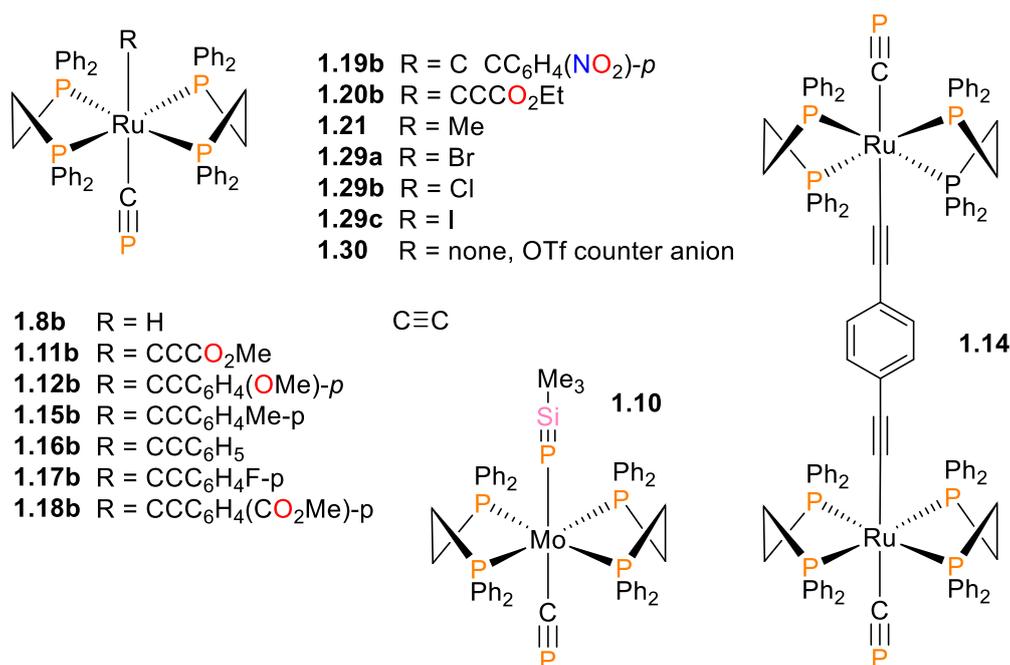
Figure 10. Overview of cyaphido complexes of the type [(dppe)$_2$M(CP)(L)] (M = Ru, Mo).

With the aim to analyze the electronic properties of cyaphido-containing coordination compounds, CROSSLEY and co-workers synthesized two new cyaphido complexes in 2014, in which the C≡P$^-$ ligand was incorporated into a conjugated *π*-system. Using two ruthenium alkynyl complexes as starting point for their approach, the *in situ* conversion to the respective triflate salts and subsequent addition of Me$_3$SiC≡P afforded [Ru(dppe)$_2$($η^1$-P≡CSiMe$_3$)-(C≡CR)][OTf] (R = CO$_2$Me (**1.11a**), *p*-C$_6$H$_4$OMe (**1.12a**)). Both compounds showed quintet resonances (**1.11a**: *δ* = 108.4 ($^2J_{P,P}$ = 35 Hz), **1.12a**: *δ* = 113.1 ppm ($^2J_{P,P}$ = 34)) in the ^{31}P{^{1}H} NMR spectrum and a doublet (**1.11a**: *δ* = 192.4 ($^1J_{P,C}$ = 89.9 Hz), **1.12a**: *δ* = 188.2 ppm ($^1J_{P,C}$ = 88.7)) in the ^{13}C{^{1}H} spectrum for the C≡P moiety of the coordinated phosphaalkyne group. The C≡P distance for **1.11a** was found to be 1.528(11) Å by single crystal X-ray diffraction. Further treatment of **1.11a** and **1.12a** with KO*t*Bu resulted in the desilylation and rearrangement process (180° rotation of the C≡P group), yielding the cyaphido complexes **1.11b** and **1.12b**, respectively (Figure 10, Figure 11).
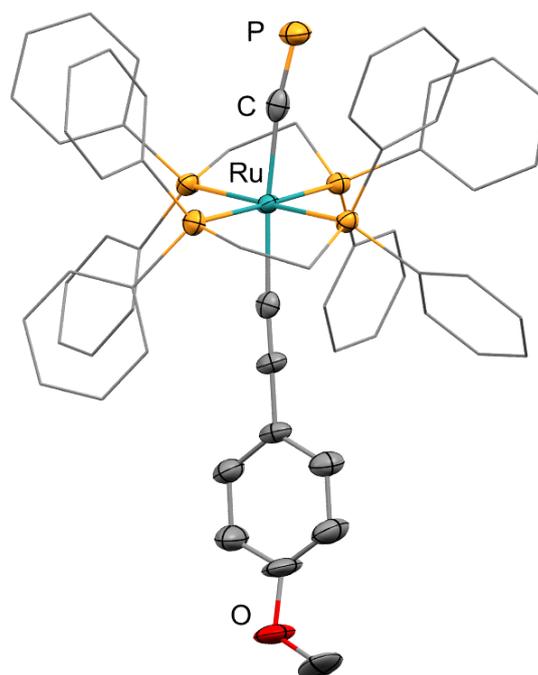
Figure 11. Molecular structure of **1.11b** in the crystal. Anisotropic displacement ellipsoids are shown at 50% probability level. Hydrogens omitted and carbon atoms of the dppe ligands reduced for clarity.

In contrast to the synthesis developed by GRÜTZMACHER, who observed an intermediate generated by the reversible attack of phenolate at the phosphorus atom, Crossley *et al.* could not find any evidence for such a species, even when conducting *in situ* NMR measurements at $T = -78$ °C. Crossley and co-workers concluded that the decreased electrophilicity of the phosphorus atom in **1.11a**/**1.12a** combined with the less sterically shielded leaving group provoked a direct nucleophilic attack at the SiMe$_3$ moiety, leading to a significantly shortened reaction time. Both cyaphido complexes **1.11b** and **1.12b** show substantially high field shifted NMR resonances (**1.11b**: $\delta(^{31}P\{^1H\}) = 161.5$ (s), $\delta(^{13}C\{^1H\}) = 279.1$ (m); **1.12b** $\delta(^{31}P\{^1H\}) = 159.5$ (m), $\delta(^{13}C\{^1H\}) = 281.9$ (m) ppm) compared to the phosphaalkyne analogs. The Raman and infrared spectra displayed the typical, yet slightly stronger C≡P bond due to competition with the *trans*-alkynyl ligand (back donation from the metal into the π^* orbital). The C≡P stretching vibrations were observed at $\tilde{\nu} = 1255$ cm^{-1} for **1.11b** and 1261 cm^{-1} for **1.12b**. The X-ray diffraction study of [Ru(dppe)$_2$(η^1-P≡CSiMe$_3$)-(C≡C-*p*-C$_6$H$_4$OMe)][OTf] (**1.12b**) verified a shorter C≡P bond length of 1.544(4) Å compared to **1.8b** (1.573(2)), which is also consistent with decreased π-backdonation from ruthenium to the cyaphide ligand (when compared to **1.8b**). The linearity of the conjugated π-system is slightly distorted (Ru-C≡C 174.4(3)°, Ru-C≡P 172.3(2)°). Additional computational calculations of the frontier orbitals revealed broad consensus with typical bis(alkynyl) complexes. In both cases the HOMO and HOMO−1 consist of the out-of-phase mixing of the Ru (d$_{xy}$, d$_{xz}$), C≡C (π) and C≡P (π) orbitals, with a considerable contribution from the cyaphide moiety (**1.11b**: 50% π(C≡P) for both orbitals; **1.12b**: 24% π(C≡P) HOMO, π(C≡P) 43% HOMO−1). The HOMO−LUMO gap (ΔE **1.11b** 3.45 eV, **1.12b**

3.70 eV) of both complexes is notably distinct. The LUMOs are dominated by the dppe ligands, the $\pi^*_{C\equiv P}$ do not contribute perceptibly to anti-bonding orbitals until LUMO+18/19. The lone-pair of the cyaphido ligand lies about 1.6 eV below the HOMO (**1.11b**: HOMO-6, **1.12b**: HOMO-7) and possesses about 75% s- and 25% p-orbital character, with the typical polarization ($C^{\delta-}$ - $P^{\delta+}$). A combined UV-Vis spectroscopy and TD-DFT study described a strong, absorption around $\lambda \approx 250$ nm induced by LLCT (ligand-to-ligand charge transfer) between the π-CP/CC and dppe π^* orbitals for both compounds. A second band at about $\lambda \approx 300$ nm was observed for **1.12b**. Other less pronounced absorptions arise mainly from ILCT (intra-ligand charge transfer) between different π and π^* transitions.[209]

In continuation of their work, CROSSLEY and co-workers reported a bimetallic complex bearing two conjugated C≡P moieties in 2018. The reaction of [{Ru(dppe)$_2$}$_2${μ-(C≡C)$_2$C$_6$H$_4$-p}Cl$_2$] with two equivalents of AgOTf and Me$_3$SiC≡P afforded the corresponding linear bisethynylbenzene-bridged bimetallic complex with two terminal phosphaalkyne groups attached. This compound showed a resonance at $\delta = 111.4$ ppm ($J_{P,P} = 34$ Hz) in the ^{31}P{^{1}H} NMR spectrum. Sequential treatment with KOtBu cleaved the trimethylsilyl groups and gave the new complex **1.14** with two terminal cyaphido ligands. NMR spectroscopy revealed a doublet at $\delta(^{31}$P{^{1}H}) = 159.7 ppm ($^3J_{P,P} = 48.3$ Hz) and $\delta(^{13}$C{^{1}H}) = 281.8 ppm ($^1J_{C,P} = 92.0$ Hz) for the C≡P moiety. The C≡P stretching mode was recorded at $\tilde{\nu} = 1247$ cm^{-1} in the corresponding IR spectrum. Calculations of the frontier orbitals gave the relative energies for the HOMO-1 (-4.53 eV), HOMO (-4.17 eV) and LUMO (-0.93 eV) with about 14% contribution from $\pi_{C\equiv P}$ for the HOMO (ca. 25% for HOMO-1/-2) showing some degree of conjugation. The lone-pairs of the terminal cyaphido ligands are strongly stabilized and represented by the HOMO-14 and HOMO-15 with an amount of about 75% s- and 25% p-orbital character. The observed UV and calculated electronic spectra confirmed a dominance of the LLCT and MLCT (metal-to-ligand charge transfer) transitions. The LLCT transitions are directed from the bis-ethynylbenzene bridge and cyaphido ligands into the dppe scaffold resulting in absorption bands at $\lambda = 370$ and 250 nm. Further detected ILCT transition within the π-system are negligible. Cyclic voltammetry studies revealed two distinct irreversible oxidations. Apparently, the reduced stability for the mixed valence state prevented reversibility, but indicated an electron-acceptor character of the cyaphido ligand, as expected.[210]

Building on the initial idea of linking the conjugated π-systems of acetylido and cyaphido ligands by transition-metal centers, CROSSLEY and co-workers published a series of *trans*-cyaphido-alkynyl complexes in 2019. Starting from the ruthenium-alkynyl precursors *trans*-[Ru(dppe)$_2$(C≡CR)Cl] (R = C$_6$H$_4$Me-p **1.15a**, C$_6$H$_5$ **1.16a**, C$_6$H$_4$F-p **1.17a**, C$_6$H$_4$(CO$_2$Me)-p **1.18a**, C$_6$H$_4$(NO$_2$)-p **1.19a**, CO$_2$Et **1.20a**) substitution of Cl by Me$_3$SiC≡P using AgOTf, AgPF$_6$ or TlOTf afforded the corresponding *trans*-[Ru(dppe)$_2$(η^1-P≡SiMe$_3$)(C≡CR)]$^+$ salts, which exhibited a characteristic resonance at approximately $\delta(^{31}$P) = 110 ppm for the η^1-

phosphaalkyne ligand. The respective cyaphido complexes (**1.15b** - **1.20b**) were obtained by addition of KO*t*Bu. Notably, the purity and yield were affected by the counterion (triflate > hexafluorophosphate salts) and traces of silver ions apparently promoted the formation of a phosphacarbon-free complex of unknown identity. However, this issue was avoided by using TlOTf instead, leading to a fast, clean reaction under ambient conditions. In accordance with the previously conducted reactions (cf. **1.11b**,**1.12b**) no reversible intermediate of the type [RuH(dppe)$_2${C(SiMe$_3$)=P(O*t*Bu)}] could be observed, even at low temperatures (*T* = -78 °C). The NMR and UV spectroscopic data, as well as a selection of structural information for complexes **1.17b** and **1.18b** are depicted in the summary Table 1 (in the end of the introduction). Generally, the complexes **1.15b** - **1.20b** show an NMR resonance at $\delta(^{31}P_{(CP)})$ = 160 - 170 ppm and $\delta(13C_{(CP)}) \approx$ 280 ppm, while the infrared spectra display typical values ($\tilde{v}$ = 1238 - 1257 cm^{-1}) for the C≡P stretching mode. The C≡P bond length becomes longer upon conversion from η^1-phosphaalkyne to the cyaphido ligand, which is in line with an expected π-back donation from the metal center into the ligand ($\pi_{Ru} \rightarrow \pi^*_{CP}$). Further evaluation of a series of substituted phenylacetylenes revealed a general trend that correlates with the donor/acceptor properties of the terminal alkynyl substituents. The chemical shifts of the C≡P moiety (δP) slightly increase with increased electron-withdrawing character of the *trans*-substituent, while δC follows the opposite trend. This behavior is in line with computational calculations showing extensive out-of-phase mixing of the Ru (d$_{xy}$, d$_{xz}$), C≡C (π) and C≡P (π) in the HOMO and HOMO-1 resulting in a certain amount of metal-mediated conjugation. Consequently, these complexes can be considered as analogs of classical *trans*-bis-acetylides. A closer inspection of the frontier orbitals illustrates two situations for the energetically low-lying orbitals. In complexes **1.15b**, **1.16b**, and **1.17b** the main contribution belongs to the Ru(dppe)$_2$ moiety, while the more electron-withdrawing alkynyls of compounds **1.18b** and **1.19b** induce a domination of the C$_6$H$_4$R moieties. In all cases the π^* system of the cyaphido ligand contributes significantly only to LUMOs of high energy (> LUMO+17) around 5 eV above the HOMO. Thus, the electronic spectra are mainly designated as LLCT and MLCT transitions from the HOMO/HOMO-1 to the chelating dppe ligands. They reveal an intense band at λ = 300 nm for **1.15b**, **1.16b**, **1.17b** and λ = 350 nm for **1.18b** and **1.19b**. Additionally, minor contributions from ILCT is observed from the arene/alkynyl section into the cyaphido across all complexes, which further diminished with increasing electron-withdrawing character of the *trans*-alkynyl substituents. Cyclic voltammetric experiments confirmed the electron-accepting properties of the cyaphido ligand as the anodic oxidation potentials increased compared to the chlorido analogs. The irreversible oxidation event increases towards anionic potentials with the electron-withdrawing capacity of the remote substituent at the phenylacetylene ligand. However, the irreversible oxidation always lead to an uncharacterized, cyaphido-free species.[211]

Targeting follow-up reactions at the cyaphido ligand (cf. 1.4.3), CROSSLEY *et al.* synthesized a modified ruthenium cyaphido complex with the intention of generating an accessible cyaphido moiety. Starting from the literature-known complex [Ru(dppe)$_2$Me$_2$][212], CH$_3^+$ elimination with TlOTf afforded [Ru(dppe)$_2$Me][OTf]. Subsequent addition of Me$_3$SiC≡P gave *trans*-[Ru(dppe)$_2$(Me)(η^1-P≡CSiMe$_3$)][OTf] which exhibited a characteristic NMR resonances at δ(^{31}P{^{1}H}) = 121.3 ppm (qnt, $^2J_{P,P}$ = 28 Hz) and δ(^{13}C{^{1}H}) = 185.1 ppm (d, $^1J_{C,P}$ = 69 Hz) for the phosphaalkyne ligand. Elimination of the trimethylsilyl group with phenolate generated the corresponding neutral cyaphido complex *trans*-[Ru(dppe)$_2$(Me)(C≡P)] (**1.21**), which showed strongly downfield shifted NMR signals at δ(^{31}P{^{1}H}) = 177.9 (br) ppm and δ(^{13}C{^{1}H}) = 294.3 ppm (br) for the cyaphido ligand. The molecular structure was confirmed by single crystal X-ray diffraction, albeit with major uncertainty for the C≡P bond length due to a disorder across two sites of the carbon atom, resulting in mismatching distances (C≡P 1.392(8) Å; Ru-C 2.186(8) Å) and angles (P-C-Ru 165.5(5)°) for the C≡P$^-$ ligand compared with other known ruthenium cyaphido complex.

1.4.2.4 Generation of C≡P$^-$ by reductive C-O bond cleavage in OC≡P$^-$

In 2017 MEYER and co-workers demonstrated the synthesis of an exceptional diuranium cyaphido complex, which was obtained by direct generation of a cyaphide anion through reductive C-O bond cleavage of the phosphaethynolate anion. The reaction of Na(OC≡P) with U(III) chelate complex **1.13a** and the consecutive addition of [2.2.2]cryptand in DME resulted in the paramagnetic dinuclear cyaphido complex [Na(2.2.2-crypt)]-[{((^{Ad,Me}ArO)$_3$N)U(DME)}(μ-O){((^{Ad,Me}ArO)$_3$N-U(CP)}] (**1.13d**, Scheme 9). The phosphorus resonance of the C≡P moiety was found at δ(^{31}P) = 265.8 (s) ppm. The X-ray structure determination revealed a typical C≡P bond length of 1.523(8) Å and a U-C distance of 2.570(7) Å. The U-C-P angle was found to be nearly linear (177.5(4)°) (Figure 12).
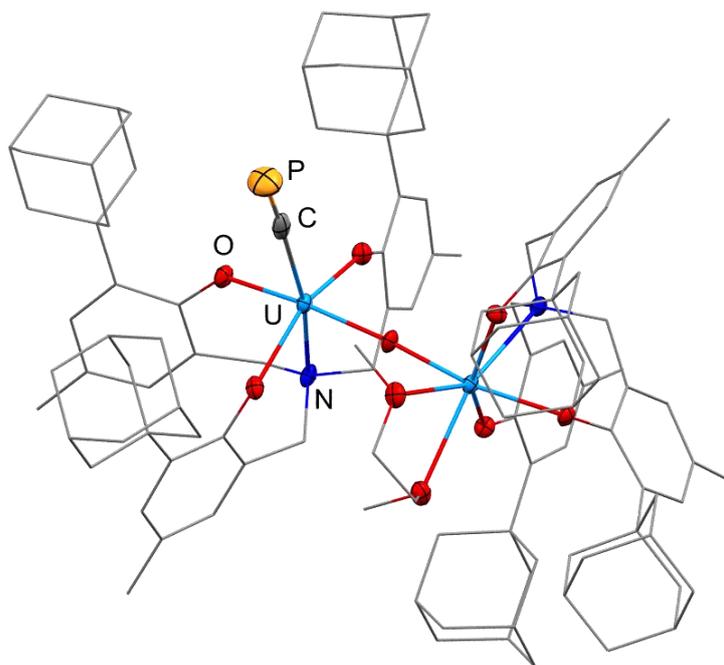
Figure 12. Molecular structure of **1.13d** in the crystal. Anisotropic displacement ellipsoids are shown at 50% probability level. Hydrogens, co-crystalized toluene and [Na(2.2.2-crypt)] species omitted. Most carbon atoms reduced for clarity.

Additional computational studies were performed to determine the oxidative addition mechanism. In a first one-electron transfer step OC≡P⁻ coordinates to the U(III) center via the oxygen atom, resulting in the mononuclear U(IV) intermediate **1.13b**. Due to the exceptional oxophilicity and reducing power of U(III), a second equivalent of **1.13a** coordinates to the oxygen atom affording the key intermediate **1.13c** with a (OCP)³⁻ entity sandwiched between two U(IV) centers. This specific arrangement of the OCP group, η^2-coordination via O and C atom to one U center and the μ-oxo bridging to the second one, facilitated O–C bond cleavage (activation barrier 4.4 kcal mol⁻¹) and generated of the μ-oxo-bridging diuranium(IV/IV) complex bearing a C≡P⁻ moiety.[213]
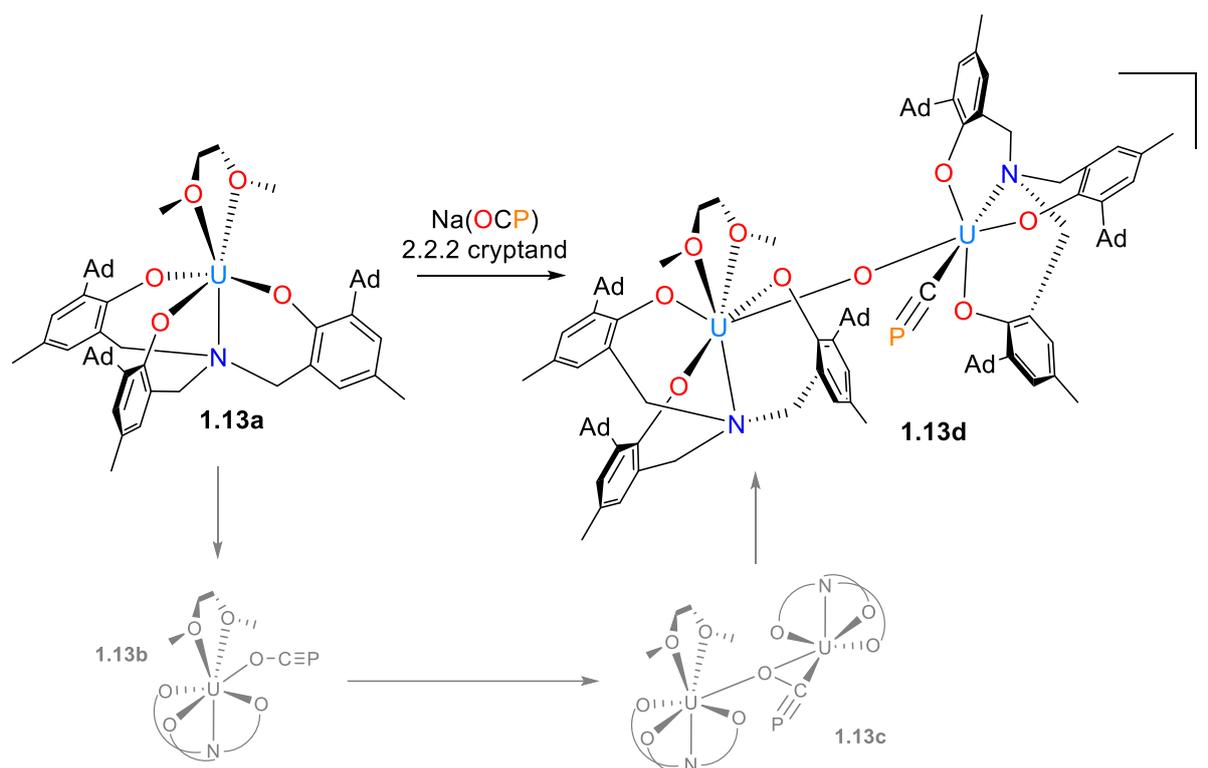
Scheme 9. [Na(2.2.2-crypt)]-[{((^{Ad,Me}ArO)$_3$N)U(IV)(DME)}(μ-O){((^{Ad,Me}ArO)$_3$N-U(IV)(CP)}] (**1.13d**) and proposed pathway.

1.4.2.5 Generation of C≡P⁻ by reductive C-O bond cleavage in R$_3$Si-OC≡P

Building on the observation that a cyaphido ligand can be generated by reductive C−O bond cleavage of the phosphaethynolate anion in the coordination sphere of a strong oxophilic U(III) center, GOICOECHEA and co-workers investigated the possibility to generate the cyaphide ion, from reduction of a R-O-C≡P precursor. In 2021, the group succeeded in accessing Grignard-type reagents **1.22a**–**d**, which can be used to transfer the cyaphide ligand to other metal centers. (Figure 13).

1.22a R = dioxane
1.22b R = THF
1.22c R = IMes (abnormal)
1.22d R = I^{i}Pr
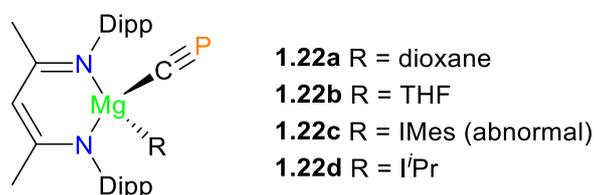
Figure 13. Cyaphide transfer reagents 1.22a-d.

In situ silylation of [Na(dioxane)$_x$]PCO with ^{i}Pr$_3$SiOTf, resulted in the formation of the literature-known kinetic product ^{i}Pr$_3$SiOCP.[214] Subsequent reduction with Jones' magnesium(I) reagent[215-216] [Mg(^{Dipp}NacNac)]$_2$ (Dipp = 1,3-diisopropylphenyl, NacNac = β-diketiminate ligand) afforded an equimolar mixture of the Grignard reagent [Mg(^{Dipp}NacNac)(C≡P)(dioxane)] (**1.22a**) and the by-product Mg(^{Dipp}NacNac)(OSi^{i}Pr$_3$)(dioxane)] (**1.23**). Computational studies

suggested an exergonic mechanism (ΔG = 52.2 kcal mol^{-1}) with a moderate energy barrier of ΔG = 12.5 kcal mol^{-1}. Initially, the ^{i}Pr$_3$SiOC≡P symmetrically coordinates via the phosphorus atom to the dimagnesium core of Jones' reagent forming a metalla-phosphaalkene intermediate. This species subsequently initiates the Mg–Mg bond cleavage, which finally leads to a stabilized intermediate. The terminal and side-on bound P=C-O entity undergoes a transition state consisting of a four-membered ring (Scheme 10, **TS2**), caused by the strong oxophilicity of magnesium. This leads to the cleavage of the C–O bond of the phosphaethynolate ion and formation of the two independent Mg monomers. Substantial steric protection is essential, as the slightly less sterically shielded [Mg(^{Mes}NacNac)]$_2$ compound produces a reaction mixture containing cyaphide-based oligomers. The NMR shifts for the C≡P moiety of [Mg(^{Dipp}NacNac)(CP)(dioxane)] were found at δ(^{31}P{^{1}H}) = 177.2 (s), δ(^{13}C{^{1}H}) = 271.0 (d, $^1J_{C,P}$ = 34 Hz) ppm. Crystallographic characterization revealed a tetrahedral structure with a linear arrangement of the Mg-C≡P moiety (177.37(15)°) (Figure 14). The molecular structure of **1.22a** further showed typical distances of 2.118(2) Å and 1.553(2) Å for the Mg–C and C≡P bond, respectively. Due to the instability of the isolated compound, the C≡P stretching vibration ($\tilde{\nu}$ = 1327 cm^{-1}) was determined by means of calculations. The similar solubility of **1.22a** and **1.23** prevented separation, and **1.22a** was found to decompose *in vacuo*. Use of dioxane-free Na(OC≡P) in the reaction affords a solvent-free analog of **1.22a** with unknown identity and a singlet resonance in the ^{31}P{^{1}H} NMR spectrum at δ = 246.7 ppm (this is believed to be a cyclic trimer as observed for [Mg(^{Mes}NacNac)(CN)]$_3$).[215] However, due to rapid decomposition in the solid state, the isolation of this species was unsuccessful.
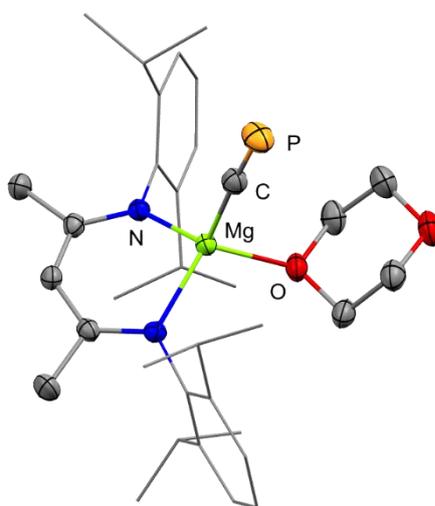
Figure 14. Molecular structure of **1.22a** in the crystal. Anisotropic displacement ellipsoids are shown at 50% probability level. Hydrogens omitted and Dipp groups reduced for clarity.

Addition of the NHCs IMes or I^{i}Pr (IMes =1,3-dimesitylimidazol-2-ylidene; I^{i}Pr = 1,3-diisopropylimidazol-2-ylidene) to a crude mixture of **1.22a** and **1.23** successfully exchanged dioxane and afforded the stable carbene adducts [Mg(^{Dipp}NacNac)(CP)(IMes)] (**1.22c**) and

[Mg(DippNacNac)(CP)(I^{i}Pr)] (**1.22d**), which could be isolated and found to be stable in the solid state. Both compounds showed similar chemical shifts in their ^{31}P{^{1}H} NMR spectra (δ = 162.9 ppm (**1.22c**), 174.9 ppm (**1.22d**)) and their molecular structures were unambiguously verified by means of single crystal X-ray diffraction. However, while I^{i}Pr carbene coordinates as expected, the IMes carbene showed "abnormal" coordination in the solid state. The infrared C≡P stretching vibrations for both compounds matched with the calculated values (IMes: $\tilde{v}$ = 1316 cm^{-1} (calc.: $\tilde{v}$ = 1311 cm^{-1}), I^{i}Pr: $\tilde{v}$ = 1325 cm^{-1} (calc.: $\tilde{v}$ = 1325 cm^{-1})) and nicely illustrated the accuracy for the calculated value of **1.22a**.[162]
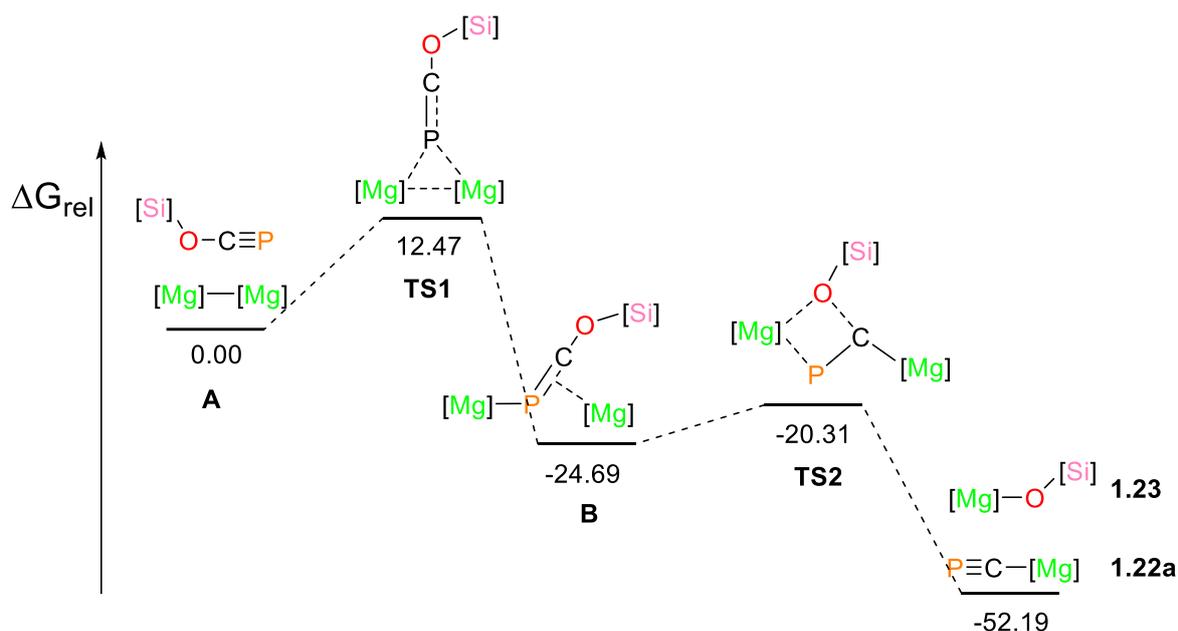
Scheme 10. Mechanism for the formation of **1.22a**; ΔG in kcal mol^{-1}.

1.4.3 Reactivity of the cyaphido-ligand

1.4.3.1 Reaction with transition metal complexes

Since the first cyaphido complexes (**1.6a**, **1.8b**) were prepared, many attempts have been made to functionalize the C≡P$^-$ ligand. The reactivity of the C≡P$^-$ ligand is expected to be dominated by the π-system, similar to the situation in phosphaalkyne complexes. Nevertheless, investigations on coordination compounds containing η^2-coordinated phosphaalkynes showed that the metal fragment enhances the coordination ability of the phosphorus lone pair.[151, 188] On the other hand, calculations have shown that the lone pair of the phosphorus atom in cyaphido complexes is energetically stabilized with respect to the π-system, which would prevent an additional coordination via the lone pair. In 1999, the group of ANGELICI demonstrated a possibility to react the cyaphido ligand in **1.6a** with an additional, coordinatively unsaturated transition metal complex. In (Cl)(PEt$_3$)$_2$Pt(μ-C≡P)Pt(PEt$_3$)$_2$ (**1.6a**) the C≡P triple bond is already occupied and sterically blocked for further coordination on the

opposite site. Addition of either [Pt(Cl)$_2$(PEt$_3$)]$_2$ or W(CO)$_5$(thf) to **1.6a** affords the first examples of the trinuclear cyaphido complexes Cl(Et$_3$P)$_2$Pt[μ-η^1,η^1,η^2-C≡P{Pt(PEt$_3$)(Cl)$_2$}]Pt(PEt$_3$)$_2$ (**1.24**) and Cl(Et$_3$P)$_2$Pt[μ-η^1,η^1,η^2-C≡P{W(CO)$_5$}]Pt(PEt$_3$)$_2$ (**1.25**), respectively (Scheme 11). While **1.24** could not be isolated due to it propensity to decompose under vacuum, compound **1.25** could be characterized crystallographically (Figure 15).
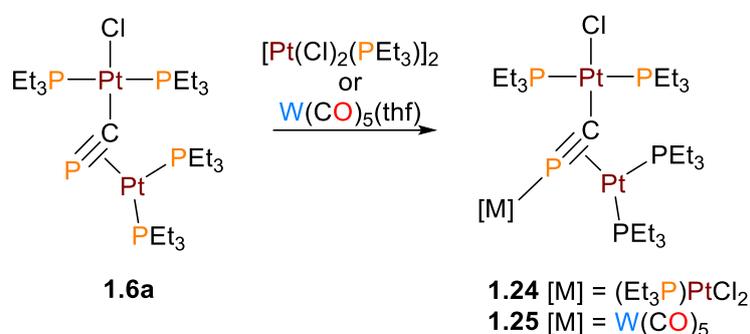
Scheme 11. Reaction of **1.6a** with transition metal complexes.
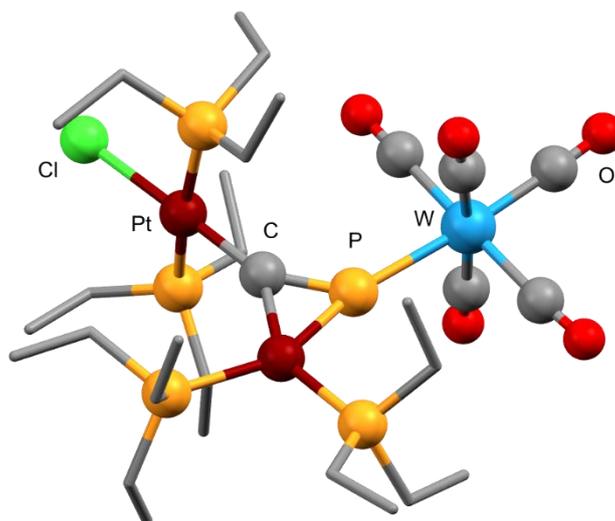
Figure 15. Ball and stick model of the molecular structure of **1.25** in the crystal. Hydrogens omitted and carbon atoms of the PEt$_3$ ligands reduced for clarity.

The phosphorus atom of the C≡P-moiety in **1.24** (δ(^{31}P) = 111.2 ppm) only showed a minor downfield shift of δ = 4 ppm with respect to **1.6a** (δ(^{31}P) = 107.0 ppm) in the ^{31}P NMR spectrum, whereas the signal in **1.25** (δ(^{31}P) = 41.4 ppm) is strongly upfield shifted by δ = 66 ppm. The molecular structure of **1.25** in the crystal reveals distorted square planar coordination environments for both the Pt(0) and Pt(II) centers. The C-P distance of 1.663(9) Å is identical to that of **1.6a**, and in line with typical C-P double-bond distances.[217] The bent geometry of the Pt–C≡P moiety (Pt-C-P angle 145.2(6)°, W-P-C 136.1(3)°) indicates a formal sp^2 hybridization of the phosphorus and carbon atoms, consistent with Pt(II)-character of the metal center (Figure 15).

1.4.3.2   Reaction with organic electrophiles

Another functionalization of the C≡P⁻ ligand was achieved by reaction of **1.6a** with excess MeI, yielding the methyl isocyaphido complex (Cl)(Et₃P)Pt(μ-C=PMe)Pt(PEt₃)₂(I) (**1.26c**; Scheme 12). In this case, MeI methylates the phosphorus atom of the cyaphido ligand resulting in the formation of an isocyaphido (C≡P-R) ligand. The reaction also results in the substitution of one of the PEt₃ co-ligands by iodide. This type of reaction is well known for terminal cyanido complexes.[206] The alkylation reaction was attempted for a series of different alkyl and aryl halides, however it was only feasible for benzyl bromide (**1.27**) and isopropyl iodide (**1.28**). The reaction with benzyl bromide successfully yielded the bridging isocyaphido complexes **1.27** in solution, however the isolation was not possible. In the case of isopropyl iodide, the desired complexed could be observed by ³¹P NMR spectroscopy but quickly decomposed before the reaction was completed. Nevertheless, the ³¹P NMR spectroscopic data showed an increased downfield shift going from methyl, benzyl to isopropyl (δ(ppm) = 155.4 (**1.26c**), 172.1 (**1.27**), 200.3 (**1.28**)). The proposed mechanism for the formation of **1.26c** starts with the initial methylation of the phosphorus atom of the C≡P⁻ ligand, forming the cationic isocyaphido intermediate **1.26a** (Scheme 12). The subsequent attack of the iodide on the side-on coordinated Pt-fragment afforded the bridging isocyaphido intermediate **1.26b**. The unobserved intermediate undergoes a consecutive rearrangement under formation of a Pt-Pt bond and loss of one PEt₃ ligand, yielding the final product **1.26c**, which contains a semibridging isocyaphido ligand. The isocyaphido intermediate **1.26c** could be trapped and isolated either as a BPh₄ or OTf salt by addition of NaBPh₄ and MeI or MeOTf to **1.6a**, respectively and showed a signal in the ³¹P NMR spectrum at δ = 34.7 ppm.[204]

1.26c R = Me, X = I   (for MeI)
1.27   R = Bn, X = Br (for BnBr)
1.28   R = ^{i}Pr, X = I   (for ^{i}PrI)
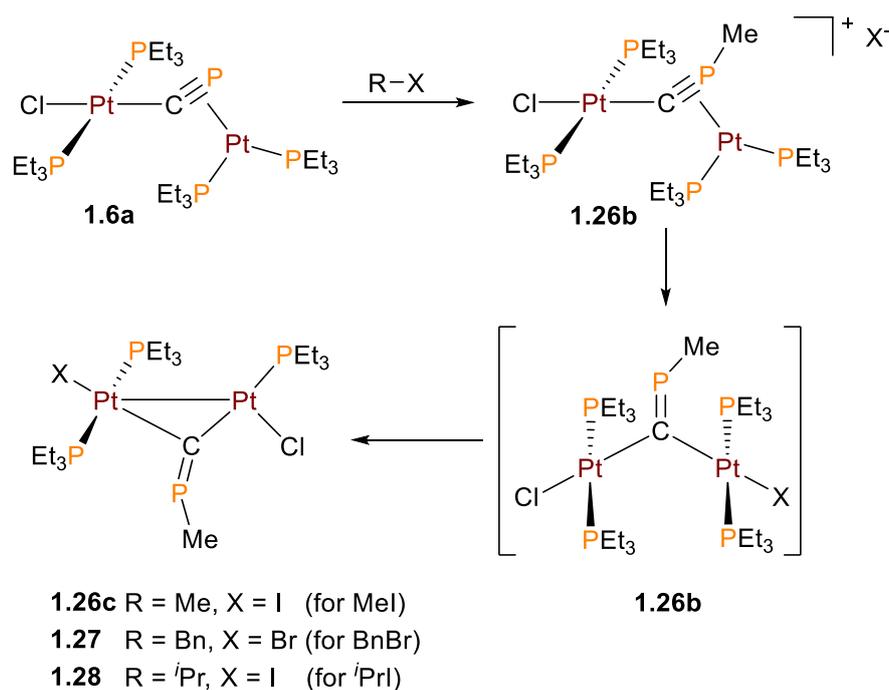
Scheme 12. Proposed mechanism for the methylation/alkylation of **6a**.

1.4.3.3 Reactivity at the metal center

A further attempt to coordinatively engage the cyaphido ligand was undertaken by CROSSLEY and co-workers in 2019. In an attempt to coordinate $ZnBr_2(PPh_3)_2$ to the phosphorus atom of the cyaphido ligand of *trans*-[Ru(dppe)$_2$(Me)(C≡P)] (**1.21**) both compounds were reacted in a 1:1 ratio. Surprisingly, an unexpected substitution of CH_3^- for Br^- occurred, yielding *trans*-[Ru(dppe)$_2$(Br)(C≡P)] (**1.29a**), which was characterized by means of single crystal X-ray diffraction. Bond angles and bond lengths are similar to those observed for **1.21** and typical for *trans*-[Ru(dppe)$_2$(alkyl)(C≡P)] complexes. The only notable exception is the Ru-C≡P bond distance, which is shortened by around 0.150 Å. Further investigation revealed that $ZnBr_2$ containing 5 mol% PPh_3 should be used for optimal reaction conditions. Applying $ZnCl_2$ or ZnI_2 resulted in the formation of compounds **1.29b** and **1.29c**. The NMR spectroscopic data showed significant shifts for the C≡P$^-$ ligand in the halide complexes **1.29a** compared to the methyl precursor **1.21**. While the ^{31}P resonance was upfield shifted by δ = 46 ppm, a downfield shift of δ = 28 ppm was observed for the ^{13}C signal of the C≡P-carbon atom. The mechanism of the zinc halide-mediated halogen/methyl exchange at a transition metal center is unclear. Importantly, halide complexes of this type are inaccessible by conventional routes, because [Ru(dppe)$_2$(Cl)]$^+$ does not react with P≡CSiMe$_3$. These halide cyaphido complexes are predestined for metathesis reactions. Indeed, treating **1.29a** with Me$_2$Mg resulted in the slow formation of the original complex **1.21**. However, the analogous reaction with LiC≡CPh only occurred in presence of TlOTf, yielding the *trans*-phenylethynyl cyaphido complex **1.16b**, which showed an upfield shift of the ^{31}P NMR signal of δ = 16 ppm for the C≡P$^-$ ligand with respect to **1.21**. Concerning the mechanism, the formation of the discrete 5-coordinated intermediate **1.30** was expected. This compound was isolated and its formation further verified by addition of TlOTf to **1.29a**. The spectroscopic examinations clearly identified the compound as the salt [Ru(dppe)$_2$(C≡P)][OTf] (**1.30**), which showed resonances at δ(^{31}P) = 154 ppm (q, $J_{P,P}$ = 7 Hz) for the phosphorus atom of the cyaphido ligand as well as at δ(^{31}P) = 52.1 ppm (d, $J_{P,P}$ = 7 Hz) for the co-ligand dppe. The same reaction was achieved by adding [AgPF$_6$] to **1.29a**, resulting in the analogous PF$_6^-$ salt. The crystallographic characterization of **1.30** revealed the presence of a square-pyramidal arrangement around the metal center with angles and distances similar to **1.29a**, but with less perturbation along the dppe co-ligands resalting in a more ideal square shape. (Figure 16). It turned out that the vacant coordination site is accessible for a carbonyl ligand by simply passing CO gas through a solution of **1.30** in dichloromethane.
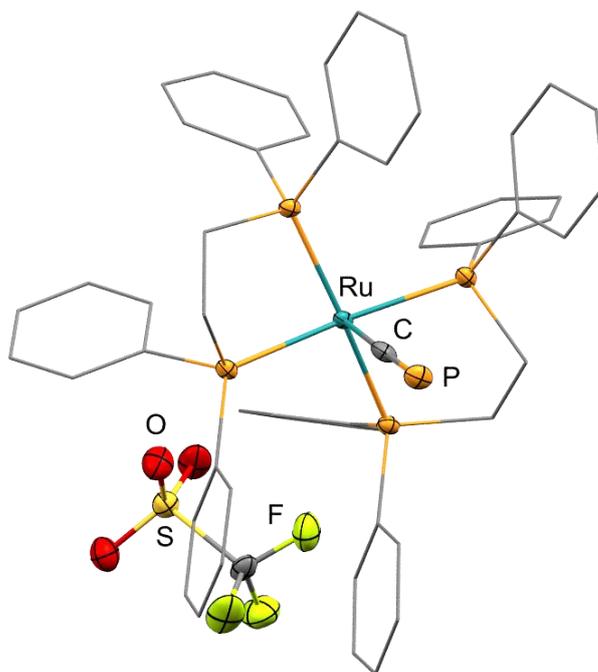
Figure 16. Molecular structure of **1.31** in the crystal. Anisotropic displacement ellipsoids are shown at 50% probability level. Hydrogens and co-crystalized toluene omitted. Carbon atoms of the dppe ligands reduced for clarity.

The product [Ru(dppe)$_2$(CO)(C≡P)][OTf] (**1.31**) was characterized by means of X-ray crystallography (C≡P distance of 1.53(2) Å), NMR and IR spectroscopy. The cyaphido ligand shows a resonance at δ(^{31}P) = 181 ppm (q, $^3J_{P,P}$ = 10 Hz), while the C≡P stretching vibration was detected at $\tilde{v}$ = 1261 cm^{-1}. A comparison with the complex *trans*-[Ru(dppe)$_2$(CO)(C≡CR)][218] indicated that the C≡P$^-$ ligand acts as an alkynyl analog with slightly enhanced acceptor properties.[219]

1.4.3.4   Transfer of the C≡P$^-$ ligand

As described in section 1.4.2.5, GOICOECHEA and co-workers recently reported on the synthesis of [Mg(^{Dipp}NacNac)(C≡P)(dioxane)] (**1.22a**). The highly polarized Mg-C≡P bond should offer the capability to undergo salt metathesis reactions allowing transfer of the cyaphido group. This possibility was first investigated by reacting **1.22a** with chlorotrimethylsilane. Indeed, quantitative C≡P$^-$ transfer took place, resulting in the formation of the known phosphaalkyne Me$_3$SiC≡P. A similar reaction was observed for the NHC compounds **1.22c** and **1.22d**. In the next step this metathesis reaction was successfully demonstrated for the main-group metal compound [Ge(^{Dipp}NacNac)Cl]. However, in this case the product [Ge(^{Dipp}NacNac)(C≡P)] (**1.32**) exhibited a tendency to decompose and could not be isolated (Figure 17).

1.32 M = Ge
1.33 M = Sn

1.34

1.35
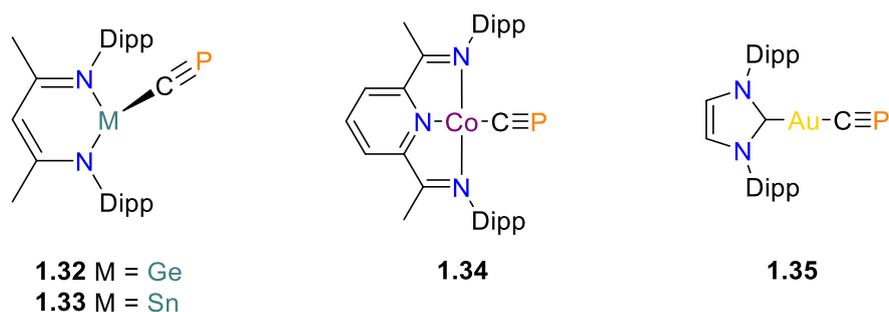
Figure 17. New cyaphido complexes by C≡P⁻ transfer via [Mg(DippNacNac)(C≡P)(dioxane)] (**1.32**, **1.33**, **1.34**, **1.35**).

In contrast, the same reaction with the Sn analog afforded [Sn(DippNacNac)(C≡P)] (**1.33**), which was isolated by fractional crystallization. Spectroscopic investigation revealed a ³¹P{¹H} resonance at δ = 122.4 ppm ($^2J_{P,Sn}$ = 69.8 Hz), while no carbon signal could be found for the cyaphido group, presumably due to broadening by the presence of Sn. The infrared spectrum revealed a C≡P stretching mode in accordance with computational calculations ($\tilde{\nu}$ = 1327 cm⁻¹) at an unusual high wave number of $\tilde{\nu}$ = 1321 cm⁻¹. Single crystal X-ray diffraction analysis of **1.33** revealed a comparable C-P distance of 1.542(4) Å with respect to compounds **1.22a**–**c** (Figure 18). The Sn-C≡P moiety is linear (179.16°) and the Sn–C bond is, as expected, rather long (2.216(4) Å).
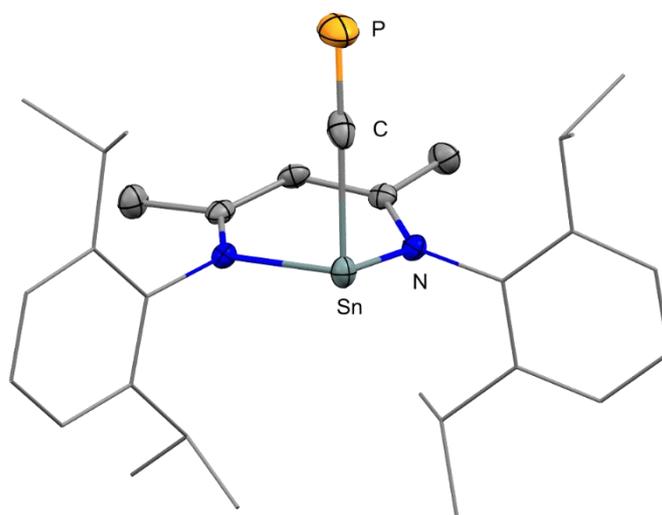
Figure 18. Molecular structure of **1.33** in the crystal. Anisotropic displacement ellipsoids are shown at 50% probability level. Hydrogens omitted and Dipp groups reduced for clarity.

Next, this intermetallic cyaphide transfer was successfully applied towards the two transition metal complexes [(DippPDI)CoCl] (DippPDI = 2,6-{2,6-^{i}Pr₂C₆H₃NCMe}₂C₅H₃N) and [Au(IDipp)Cl] (IDipp = 1,3-bis(2,6-diisopropylphenyl)imidazol-2-ylidene). Interestingly, [(DippPDI)Co(C≡P)] (**1.34**), is the first example of a 3d metal cyaphido complex. The C≡P⁻ ligand showed a single resonance in the ³¹P{¹H} NMR spectrum at δ = 345.4 ppm and a stretching vibration at $\tilde{\nu}$ = 1306 cm⁻¹ in the corresponding IR spectrum. Moreover, the molecular structure of **1.34** was undoubtedly confirmed by means single-crystal X-ray diffraction (Figure 19).
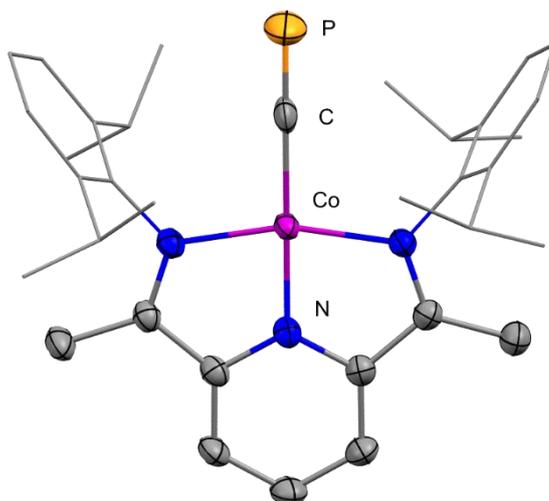
**Figure 19.** Molecular structure of **1.34** in the crystal. Anisotropic displacement ellipsoids are shown at 50% probability level. Hydrogens omitted and Dipp groups reduced for clarity.

The Au(I) complex [Au(IDipp)(C≡P)] (**1.35**) showed a singlet resonance in the $^{31}P\{^{1}H\}$ spectrum, that appeared substantially upfield shifted at δ = 84.1 ppm, compared to **1.34**. The $^{13}C\{^{1}H\}$ signal for the C≡P^{-} ligand was observed at δ = 247.7 ppm ($^{1}J_{C,P}$ = 6.1 Hz). The high stretching vibration of $\tilde{\nu}$ = 1342 cm^{-1} in the infrared spectrum is clearly influenced by the coupling to the *trans*-Au-C$_{carbene}$ stretch mode, induced by the linearity of the gold center (C-Au-C = 178.2(2)°, Au-C-P = 178.0(5)°). The C≡P bond length of 1.552(6) Å is within the usual range, while an Au-C≡P distance of 1.972(6) Å was found. Interestingly, the Au-C$_{carbene}$ distance of 2.034(6) Å is slightly elongated in comparison with [(IDipp)AuCl] (1.942(3) Å) and more in line with [Au(IDipp)(C≡CPh)] (2.018(7) Å), and [Au(IDipp)(C≡N)] (1.985(15) Å), respectively.[220] This indicates a similar σ-donor ability of C≡P^{-} and C≡CPh^{-}. Even though this seems to be a facile reaction, it most likely marks a revolutionary step in the synthetic history of cyaphido compounds. This has already been demonstrated with the access to the very first main group metal and 3*d* transition metal cyaphido complex, and the first examples of trigonal pyramidal, square planar and linear cyaphido metal complexes.[162]

1.4.3.5   Recent formation of a trimetallic cyaphido complex

Based on the remarkable linear Au(I) cyaphido complex, [Au(IDipp)(C≡P)] (**1.35**), YANG and GOICOECHEA demonstrated consecutive coordination reactions to obtain hetero-, bi- and tri-metallic transition metal complexes, sharing a joint cyaphido ligand. The first attempts were aimed to mimic the common bridging mode η^{1}:η^{1}-cyanido complex ([M]-C≡N-[M]). A good accessibility of the phosphorus lone pair of the **1.35** was expected due to the minimized steric protection of the cyaphido ligand. Even though first dummy reactions between the Lewis acid B(C$_{6}$F$_{5}$)$_{3}$ and the isostructural Au(I) cyanido complex [Au(IDipp)(C≡N)] were successful, no coordination of unsaturated electrophiles to the Au(I) cyaphido complex **1.35** could be

accomplished. Calculations of the frontier orbitals of **1.35** indicated an increased electrophilicity due to the relatively low-lying π^* orbitals, while the phosphorus lone pair is energetically too far below the HOMO to be an efficient electron donor for incoming Lewis acids. Therefore, the umpolung reaction with the two electron-rich, nucleophilic late transition metal complexes [{Ni(^{Me}I^{i}Pr)$_2$}$_2$(μ_2-COD)] and [Rh(Cp*)(PMe$_3$)$_2$] were investigated. Indeed, the Ni(0) carbene complex reacts with **1.35** at room temperature by liberating the COD ligand and coordination, yielding the heterobimetallic complex [Au(IDipp)(μ_2-C≡P)Ni(^{Me}I^{i}Pr)$_2$] (**1.36**) (Figure 20). A single resonance of δ = 246.0 ppm in the ^{31}P{^{1}H} NMR spectrum and a doublet at δ = 280.3 ppm (d, $^1J_{C,P}$ = 105 Hz) in the ^{13}C{^{1}H} spectrum for the μ_2-cyaphido ligand was recorded. The Raman spectroscopically assigned C≡P stretch vibration is drastically reduced ($\tilde{v}$ = 1125 cm^{-1} (**1.36**) vs $\tilde{v}$ = 1350 cm^{-1} (**1.35**)), indicating a weakened C≡P bond strength. This is confirmed by the molecular structure gained by X-ray diffraction, which shows a bond length of 1.642(4) Å compared to 1.552(6) Å for **1.35**. The solid-state structure also verifies the η^1:η^2-coordination of the bridging cyaphido ligand with a bent Au-C-P bond angle of 146.3(2)° (178.0(4)° (**1.35**)). Additional DFT calculations certify a 29.3 kcal·mol^{-1} energy gain of the η^1:η^2-cyanido mode over the theoretically also possible linear η^1:η^1-isomer. Another reaction with the Rh(I) Lewis base complex [Rh(Cp*)(PMe$_3$)$_2$] at T = 80 °C overnight yielded in displacement of one trimethylphosphine and side-on coordination to the cyaphido ligand of **1.35**, observed by ^{31}P{^{1}H} spectroscopy. The two coupling resonances in the ^{31}P{^{1}H} spectrum at δ = 94.7 ppm (dd, $^1J_{P,Rh}$ = 34 Hz, $^2J_{P,P}$ = 6 Hz) for the cyaphido phosphorus and δ = -5.0 ppm (dd, $^1J_{P,Rh}$ = 209 Hz, $^2J_{P,P}$ = 5 Hz) for the trimethylphosphino ligand prove the formation of [Au(IDipp)(μ_2-C≡P)Rh(Cp*)(PMe$_3$)] (**1.37**) (Figure 20). The C≡P bond stretching vibration of $\tilde{v}$ = 1175 cm^{-1}, identified by Raman spectroscopy, is in line with the one found for **1.36** ($\tilde{v}$ = 1125 cm^{-1}). The η^1:η^2-coordination was confirmed by X-ray diffraction, revealing a Au-C-P bond angle of 151.4(2)° and a bond length of 1.631(4) Å for the cyaphido group.
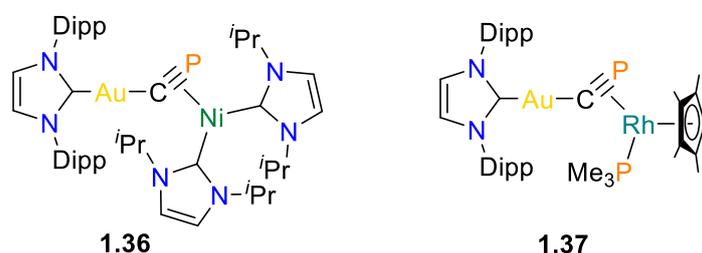
Figure 20. Heterobimetallic cyaphido complexes by addition of electron-rich transition metals to [Au(IDipp)(C≡P)] (**1.35**).

The molecular structures of **1.36** and **1.37** in their single crystals indicated that further reactions of the cyaphido phosphorus with electrophiles are possible. Addition of **1.37** to [W(CO)$_5$(THF)] yields the red heterotrimetallic complex [Au(IDipp)(μ_2-C≡P){Rh(Cp*)(PMe$_3$)}{W(CO)$_5$}] (**1.38**). The analog reaction with **1.36** only provides unidentified product mixtures. The ^{31}P{^{1}H} NMR

spectrum of **1.38** confirms the successful coordination of tungsten by showing a doublet of doublets with ^{183}W satellites (δ = 48.5 ppm, dd, $^1J_{P,W}$ = 175 Hz, $^1J_{P,Rh}$ = 62 Hz, $^2J_{P,P}$ = 13 Hz) for the μ_3-cyaphido ligand and another set of doublets (δ = -3.9 ppm, dd, $^1J_{P,Rh}$ = 194 Hz, $^2J_{P,P}$ = 13 Hz) for the trimethylphosphino ligand in addition. The Raman spectrum reveals a C≡P stretching vibration of $\tilde{v}$ = 1186 cm^{-1}, nearly identical with the precursor **1.37** ($\tilde{v}$ = 1175 cm^{-1}). The X-ray analysis of the molecular structure shows the expected bonding of the cyaphido group to the three metal centers in a η^1:η^2:η^1 (σ + π + σ) coordination mode (Figure 21). The cyaphido bond length was determined to 1.605(4) Å. The observed contraction over **1.37** (1.631(4) Å) is in accordance with the detected slightly increase of the C≡P bond stretching vibration. The strengthening of the bond is also reflected in the increase of the ^{31}P-^{103}Rh coupling constant ($^1J_{P,Rh}$ = 34 to 62 Hz). A computationally fragment-based analysis for **1.36**, **1.37** and **1.38** was accomplished to get a deeper insight into the orbital contributions of each M-(η^2-CP). In all cases the largest contribution to the M-(η^2-CP) bond is the π-back-donation from the side-on coordinating metal core (Ni/Rh) into the cyaphido π^* antibonding orbital. The only other major coordination arises from the σ donation of the cyaphido π bonding orbital into Ni/Rh. Consequently, the side-on η^2-cyaphido ligand acts mainly as π acceptor. Those first examples of multi-metallic transition metal complexes nicely demonstrated the excellent bridging properties of the cyaphido ligand and proved further perspectives of consecutive coordination at the cyaphido moiety.[203]
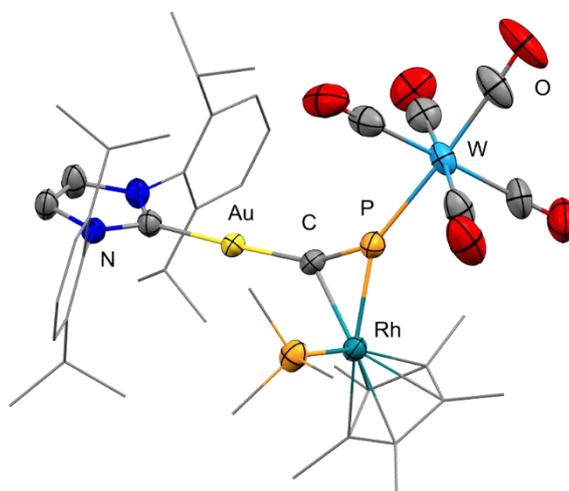
Figure 21. Molecular structure of **1.38** in the crystal. Anisotropic displacement ellipsoids are shown at 50% probability level. Hydrogens omitted and carbon atoms of the ligands partly reduced for clarity.

Table 1. Summary of the key figures of the cyapido ligand in different metal complexes. [a] decomposition of the product, [b] disorder in the crystallographic structure of C≡P, [c] solvent free, [d] calculated, [e] major product, [f] minor product.

cpd	core metal	$\delta\ ^{31}P_{(C\equiv P)}$ [ppm]	$\delta\ ^{13}C_{(C\equiv P)}$ [ppm]	$\tilde{v}_{(C\equiv P)}$ [cm^{-1}]	C≡P [Å]	M-CP [Å]	M-C-P [°]
1.4a	Pt	68.0	-	-	-	-	-
1.6a	Pt	107.0	-	-	1.666(6)	1.950(6)	144.0(3)
1.7	B	39.6	202.3	1468	1.563(10)[a]	-	-
1.8b	Ru	143.8	287.1	1229	1.573(2)	2.057(2)	177.9(1)
1.10	Mo	197.8 183.0	-	-	-	-	-
1.11b	Ru	161.5	279.1	1255	1.57(1)	2.05(1)	171.9(7)
1.12b	Ru	159.5	281.9	1261	1.544(4)	2.065(4)	172.3(2)
1.13d	U	265.8	-	-	1.523(8)	2.579(7)	177.5(4)
1.15b	Ru	159.8	281.8	1247	-	-	-
1.16b	Ru	160.6	281.8	1248	-	-	-
1.17b	Ru	161.7	281.5	1239	1.493(3)	2.118(3)	177.8(2)
1.18b	Ru	165.3	280.8	1245	1.549(19)	2.076(9)[b]	172.8(6)
1.19b	Ru	170.0	279.5	1242	-	-	-
1.20b	Ru	168.3	278.7	1257	-	-	-
1.21	Ru	177.9	294.3	1217	1.392(8)	2.186(8)	165.5(5)
1.22a	Mg	177.2 246.7[c]	271.0	1327[d]	1.553(2)	2.118(2)	177.37(15)
1.22b	Mg	175.0	271.4	-	1.501(4)	2.160(4)	178.5(3)
1.22c	Mg	162.9	-	1316	1.550(2)	2.166(2)	176.3(1)
1.22d	Mg	173.3[e] 167.7[f]	-	1325	1.531(3)	2.144(3)	176.8(2)
1.24	Pt	111.2	-	-	-	-	-
1.25	Pt	41.4	-	-	1.663(9)	1.952(9)	145.2(6)
1.29a	Ru	135.4	-	1249	1.544(10)	1.901(9)	175.8(5)
1.29b	Ru	132	265.5	1250	1.638(17)	1.687(16)[b]	177.4(10)
1.29c	Ru	140	-	-	-	-	-
1.30	Ru	154	265	1242	1.572(4)	1.904(4)	178.9(2)
1.31	Ru	181.3	249	1261	1.53(2)	2.06(2)	176.0(13)
1.32	Ge	106.4	-	-	-	-	-
1.33	Sn	122.4	-	1321	1.542(4)	2.216(4)	179.2(2)
1.34	Co	345.4	-	1306	1.506(4)	1.926(4)	178.3(3)
1.35	Au	84.1	247.7	1342	1.552(6)	1.972(6)	178.0(5)
1.36	Au	246.0	280.3	1125	1.642(4)	1.992(4)	146.3(2)
1.37	Au	94.7	-	1175	1.631(4)	1.975(4)	151.4(2)
1.38	Au	48.5	-	1186	1.605(4)	1.992(4)	155.4(3)

1.5 Motivation of this work

Since the discovery of Prussian Blue by DIESBACH in 1706, the cyanide ion plays an important role in the field of inorganic and material chemistry.[221] The inorganic C≡N⁻ ion as well as its organic complements, nitriles (R-C≡N) and isonitriles (R-N≡C), are still highly relevant ligands in coordination chemistry.[222-228] In the past simple alkali metal cyanides were momentous for the gold mining.[229-230] Today, designated Prussian Blue analogs (PBAs) are of special importance due to their stimulus-responsive magnetic properties.[231-233] The organic derivatives are meaningful in the production of nylon and other polymers.[234-235] Being the analog of the industrial important C≡N⁻, the valence isoelectronic cyaphide anion (C≡P⁻) is an exceptional candidate to enrich the coordination chemistry of tomorrow. At the current state, only a few examples of cyaphido metal complexes have been reported (cf. chapter 1.4.2) and the obtained knowledge is very limited.

It is to mention that the introduction (cf. chapter 1.4) contains several recent breakthroughs in the field of cyaphido complexes. At the time, when this study started (May 2018) most of the presented results were unknown/unpublished. Since the discovery of the first cyaphido complex *trans*-[(Cl)(PEt₃)₂Pt(C≡P)] by ANGELICI in 1992 and the fist follow-up reactions in 1999, no substantial cyaphido complexes were synthesized until the stable [RuH(C≡P)(dppe)₂] by GRÜTZMACHER in 2006. Two similar Ruthenium complexes were synthesized by CROSSLEY, using Grützmacher's method in 2014 and one bizarre uranium complex by MEYER by reductive C-O bond cleavage in OC≡P⁻ in 2017. All further contributions are from 2018 or later.

In this respect, the cyaphido ligand itself and the corresponding cyaphido complexes are barely explored and deserves extensive investigations towards stability, reactivity, properties of the cyaphido ligand and possible coordination modes. Furthermore, the structural information is mainly limited to Ruthenium and bridged bimetallic platinum complexes.

The goal of this work was the development of a novel reliable pathway towards cyaphido complexes. Ideally, leading to a variety of similar cyaphido compounds to examine the impact of small changes in the system. Gathering structural information of the molecule in the crystal to validate the products and the effect on the C≡P tripe bond upon coordination to the metal center. Furthermore, the possibilities and limitations of the follow-up chemistry were explored, including addition, cycloaddition, and coordination reactions. Finally, first substitution experiments of the cyaphido ligand were inspected to evaluate the possibility of a C≡P⁻ transfer in the future.

2 Results and discussion

2.1 Synthesis of cyaphido platinum complexes by light induced arylphosphaalkyne cleavage

2.1.1 Introduction

Until 2018, four different methods for the preparation of cyaphido complexes were known. First, the not entirely comprehensible cleavage of a bimetallic complex bearing a bridging μ-C=PR ligand (cf. chapter 1.4.2.1), which leads to a non-isolable cyaphido Pt(II) complex (Scheme 13a).[34, 63] The cleavage process is not clearly defined, but current knowledge suggest a reductive elimination from the carbon of the μ-C=PR group (μ-isophosphaalkyne), followed by an elimination of the aromatic substituent R from the phosphorus atom and oxidative addition at the palladium atom. The initial driving force for this reaction is unidentified. However, the instability of the intermediate can be explained by the instable metal-metal bond between palladium and platinum. In addition, the temporarily formed η^1-isophosphaalkyne is an unfavored species and prefers to transform the better stabilized regular phosphaalkyne as mentioned in chapter 1.3.1. The cleaved aromatic substituent R cannot undergo the typical 1,2-P-C shift to recombine with the C≡P group, because of the already fully occupied quaternary carbon atom. Instead, it occupies the free coordination site of the platinum atom. The second method utilize the typical $(SiMe_3)_2O$ elimination route by addition of $E(P(SiMe_3)_2)$ (E = alkali metal) to an acid chloride substituted boron compound (Scheme 13b, cf. chapter 1.4.2.2).[207] Third is the desilylation of a η^1-silylphosphaalkyne ruthenium complex with a suitable oxygen base to obtain a cyaphido complex (Scheme 13c, cf. chapter 1.4.2.3).[37] Lastly, is the addition of NaOC≡P to a uranium complex and reductive cleavage of the C-O bond in NaOC≡P by another equivalent of this complex bearing an extremely oxophilic uranium(III) center (Scheme 13d, cf. chapter 1.4.2.4).[213]

a)

$$[\, X\!-\!Pt(L)(L)\cdots C\!=\!P(R)\cdots Pd(L)(L)\!-\!X \,] \longrightarrow$$

X = halogen
L = phosphine
R = aryl-

$$L\!-\!Pt\!-\!L \;(C\!\equiv\!P) \quad + \quad L\!-\!Pd\!-\!L \;(R)$$

b)

$$O\!=\!C(Cl)R \xrightarrow[-\,KCl]{K[P(SiMe_3)_2]} O\!=\!C(P(SiMe_3)_2)R \xrightarrow[-\,O(SiMe_3)_2]{[1,3]\text{-}SiMe_3\ shift} P\!\equiv\!C\!-\!R$$

R = B(CF$_3$)$_3$ with cation

c)

$$[SiR_3\!-\!C\!\equiv\!P\!-\![Ru]\!-\!H]^{+} \xrightarrow[\substack{*\ \text{suitable base to cleave -SiR}_3 \\ (OH^-\ \text{for clarity})}]{^-OH^{*}} \xrightarrow{} \xrightarrow{-\,R_3SiOH} [\,C\!\equiv\!P\!-\![Ru]\!-\!H\,] \xrightarrow{} P\!\equiv\!C\!-\![Ru]\!-\!H$$

R = aryl-, alkyl-

d)

$$[U]^{+3} \xrightarrow[-\,[Na][2.2.2\ cryptand]]{\substack{Na(O\!\equiv\!P) \\ 2.2.2\ cryptand}} \big[[U]^{+4}\!-\!O\!-\!C\!\equiv\!P\big]^{-} \xrightarrow{+\,[U]^{+3}} \big[[U]^{+4}\!-\!O(\!-\![U]^{+4})\!-\!C\!\equiv\!P\big]^{-} \xrightarrow[cleavage]{C\!-\!O\ bond} \big[[U]^{+4}\!-\!O\!-\![U]^{+4}\!-\!C\!\equiv\!P\big]^{-}$$
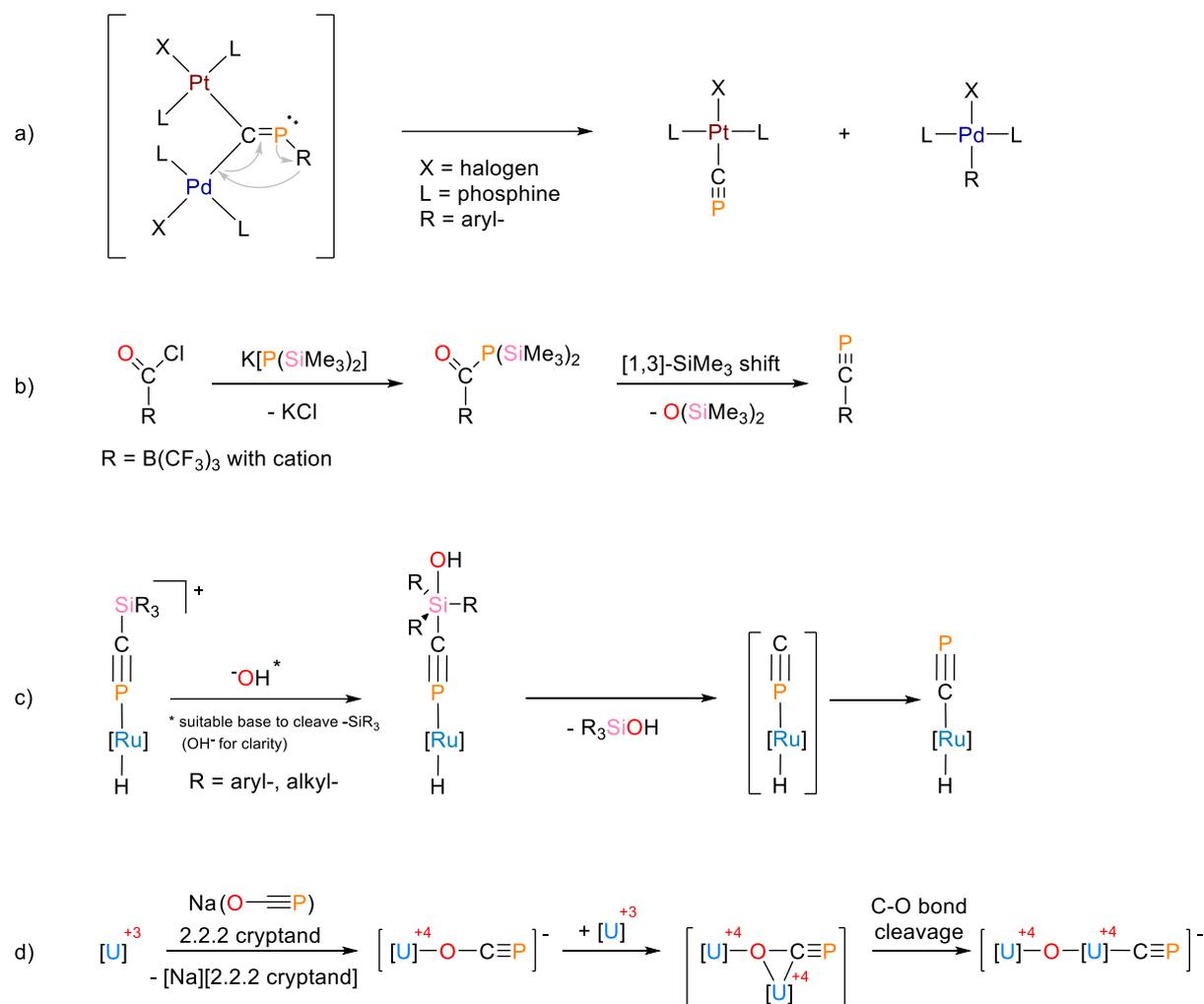
Scheme 13. The four schematic reaction procedures to create cyaphido compounds (or Lewis adduct (b)) known until 2018.

Methods **a** and **b** have in common that the C≡P group will be generated directly on the core atom. Both routes are highly specialized reactions and appear unusable for a general procedure to receive cyaphido complexes. Methods **c** and **d** comprise the coordination of a C≡P containing molecule (phosphaalkyne or 2-phosphaethynolate anion) and consecutive cleavage of the supplementary part to obtain the cyaphido ligand. In route **d**, a strong oxophilic metal is needed to split the C-O bond. The reaction scope is very limited, since this reaction has not been demonstrated to work with another metal than uranium. In contrast, method **c** is a promising candidate to become a more general synthetic route towards cyaphido complexes, because of the controllable cleavage of the organic substituent in the silylphosphaalkyne. This was already demonstrated by the adapted synthesis of advanced cyaphido ruthenium complexes by CROSSLEY and co-workers and first attempts of RUSSEL *et al.* towards a similar molybdenum complex.[139, 209] However, a considerable drawback of this method is the demand for large steric ligands on the metal center to achieve the initial η^1-coordination of the silylphosphaalkyne, which are also necessary to cleave the silyl group of the phosphaalkyne by a base without attacking the metal center. In consequence, the created cyaphido ligand will

be highly protected by the bulky substituents of the metal and hardly accessible for follow-up reactions. Another preparation method, avoiding strong steric shielding is required to get easy access to cyaphido complexes and to maintain the ability to study consecutive reactions on the cyaphido moiety.

Since the first successful C-CN bond activation in benzonitrile with Ni(0) in 1971,[236-237] numerous examples for the metal-mediated activation of C-C bonds in nitriles (R-C≡N) leading to cyanido complexes have been found.[238] Most of those activations have been demonstrated on nickel complexes,[239-244] but there are also examples for Mo,[245] Fe,[246] Co,[247] Rh,[248] Pd,[249-250] Pt[251] and Cu[252-253]. Since 2000, JONES and co-workers intensively investigated the reversible thermal cleavage of the C(sp)-C(sp^2) bond in benzonitrile[254] (Scheme 14a) and a selection of other nitriles with Ni(0).[255-262] One year later, this concept was successfully transferred to the C(sp)-C(sp^2) bond cleavage in diphenylacetylene (tolane) by photolysis of a Pt(0) complex (Scheme 14b),[263] and later expanded to other acetylenes to gain deeper insights into the system.[264-267] Furthermore, the bond cleavage of C-Si[268] and C-CN[269] was examined. Based on JONES' results, the valence isoelectricity between phosphaalkynes and nitriles as well as the fact that phosphaalkynes act even more like acetylenes than nitriles, it is reasonable to apply a similar strategy for the synthesis of cyaphido complexes.
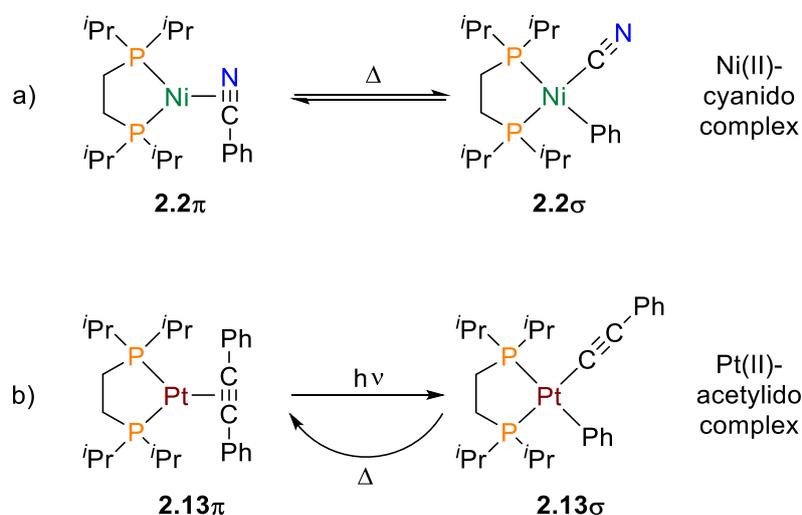
Scheme 14. Thermal synthesis of the Ni(II)cyanido complex **2.2σ** and photolytic generation of Pt(II)acetylido complex **2.13σ**.

The development of a suitable reaction pathway towards cyaphido complexes started with a critical inspection of the literature for cleavage reactions of nitriles and diphenylacetylene. All Ni(0) complexes were prepared by addition of two equivalents nitrile to the nickel dimer [(dippe)NiH]$_2$ (**2.1**, dippe = 1,2-bis(diisopropylphosphino)ethane), which act as a source for the [Ni(dippe)] fragment, yielding the corresponding η^2-nitrile complex (Scheme 15). The [(dippe)Ni(η^2-NCPh)] (**2.2π**) complex, generated by the aromatic benzonitrile, partly transforms into the [(dippe)Ni(η^1-CN)(Ph)] (**2.2σ**) complex at room temperate. This reaction results in an

equilibrium between **2.2π** and **2.2σ**, which is influenced by variation of the temperature. Elevated temperatures shift the equilibrium in favor for **2.2σ**. The equilibrium constant K_{eq} of around one was determined to be at T = 91 °C in THF.[254] The reaction also depends on the used solvent. In THF the formation of **2.2σ** is thermodynamically slightly downhill, while in toluene it is uphill (T = 300 K).
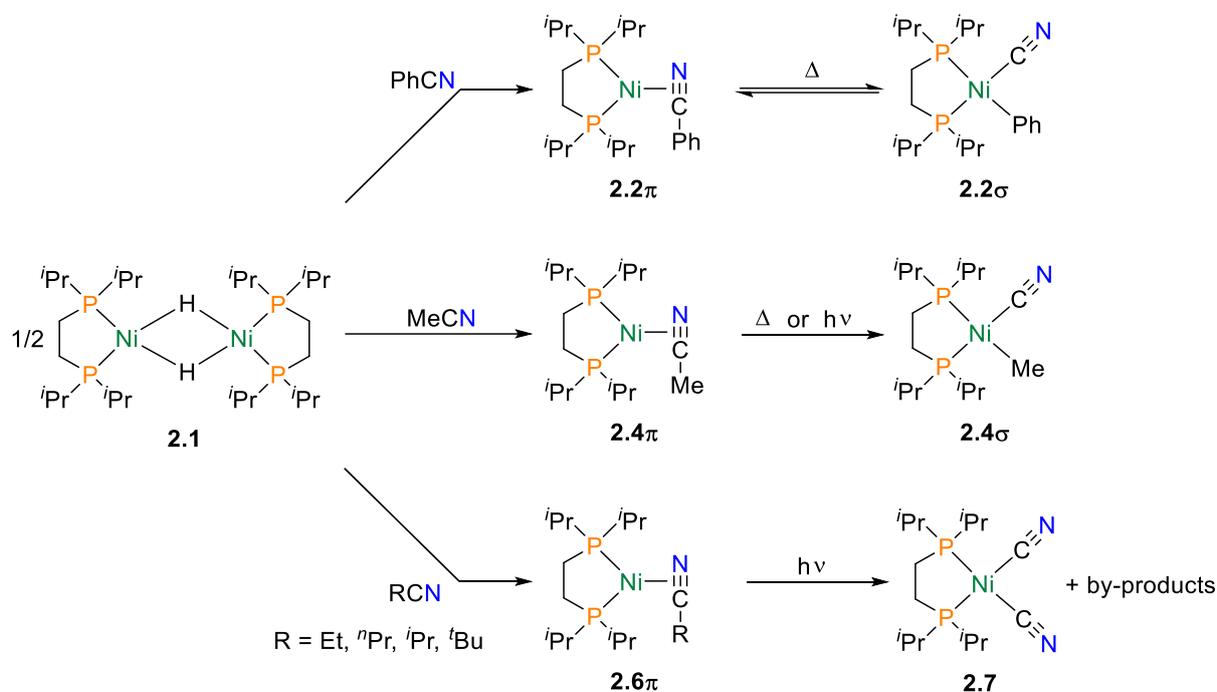
Scheme 15. Activation and cleavage of the C-CN bond of nitriles in [(dippe)Ni(nitrile)] complexes.

Additional computational studies describe the energy barriers and the transition states for the cleavage of benzonitrile (Scheme 16). To simplify the calculations the [Ni(dmpe)] (dmpe = 1,2-bis(dimethylphosphino)ethane) fragment was used, which provides in average 1-2 kcal·mol^{-1} more stable complexes than their dippe counterparts. The first transition state (**2.3-TS1**) is 30.2 kcal·mol^{-1} higher in energy than the η^2-benzonitrile complex (**2.3π**). In **2.3-TS1**, the nickel center is mainly coordinated to the nitrile carbon and weakly bonded to the nitrogen and the aryl-carbon atoms. A temporary species during the transformation is the η^2-arene complex (**2.3-S1**), 18.1 kcal·mol^{-1} lower in energy and in which the nickel is coordinated to the C_{ipso}=C_{ortho} double bond of the benzonitrile. Several transition states in which the nickel alternately coordinates to different aryl carbons on the way from **2.3-S1** to **2.3-TS2** (ΔE = 17.1 kcal·mol^{-1}) are not displayed in Scheme 16 for clarity. In transition state **2.3-TS2**, the nickel binds to the nitrile carbon and the *ipso*-aryl-carbon atom. Compound **2.3σ**, 30.1 kcal·mol^{-1} lower in energy, is finally formed after the cleavage of the remaining C-CN bond in the benzonitrile, giving a total energy difference of only 0.9 kcal·mol^{-1} between **2.3π** and **2.3σ**.[258] The small energy difference and the moderate energy barrier might be responsible for the observed equilibrium.
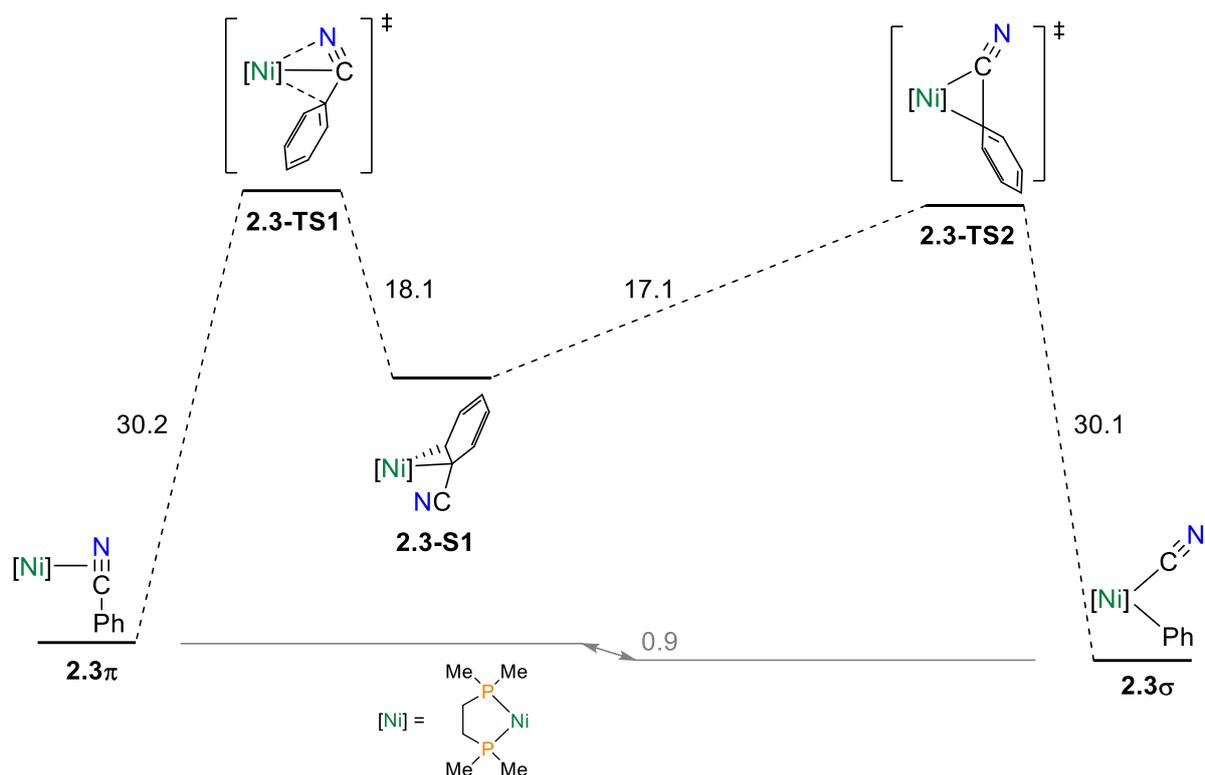
Scheme 16. Energetics of the C-CN bond cleavage in benzonitrile. Free energies in kcal·mol^{-1} relative to the total energies of the fragments ([Ni(dmpe)] and PhCN).

Expanding the scope of nitriles showed some astonishing results. While all nitriles (RCN, R = Me, Et, ^{n}Pr, ^{i}Pr, ^{t}Bu, ^{c}Pr, ^{c}Bu, adamantyl) successful reacted with [(dippe)NiH]$_2$ (**2.1**) to form the expected [(dippe)Ni(η^2-NCR)] complexes, only some of them undergo C-CN cleavage to their respective [(dippe)Ni(CN)(R)] complex. The acetonitrile derivative (**2.4π**) converts already at room temperature slowly to the corresponding σ-complex (**2.4σ**, Scheme 15), although better yields are received on heating to T = 80 °C. Surprisingly, there is no equilibrium between the π-complex and the σ-complex for acetonitrile in contrast to the benzonitrile derivative. Furthermore, the activation and cleavage can also be carried out by photolysis (λ > 300 nm). The adamantyl complex remains stable against thermal and photochemical activation, the remaining η^2-nitrile complexes could be only activated by photolysis. While cyclopropyl- and cyclobutylnitrile yielded the typical σ-complexes, ethyl-, propyl-, isopropyl- and *tert*-butylnitrile gave mainly [(dippe)Ni(CN)$_2$] (**2.7**), the corresponding [(dippe)Ni(alkyene)] complex and various by-products.[257] The reaction of [(dippe)Ni(η^2-NCMe)] (**2.4π**) was further investigated by computational studies by using the [Ni(dmpe)] fragment with acetonitrile as a model for the Ni(0) complex (Scheme 17). The first transition state (**2.5-TS1**) is 30.7 kcal·mol^{-1} higher in energy than the π-complex (**2.5π**). At this state the nickel is primary coordinated to the nitrile carbon and weaker to the nitrogen and methyl carbon, leading to the species **2.5-S1**. This stable, high energy species can be considered as an η^3-H,C,C-acetonitrile complex with agnostic C-H interaction to the metal center. The next transition state (**2.5-TS2**) lies only 2.2 kcal·mol^{-1} higher in energy, leads to the C-CN bond cleavage and finally to the

30.1 kcal·mol^{-1} lower in energy square-planar Ni(II) σ-complex (**2.5σ**). Consequently, the total energy difference between the π-complexes (**2.5π**) and σ-complexes (**2.5σ**) is 2.1 kcal·mol^{-1}. The overall transformation process is very similar to the one found for the benzonitrile derivative. Molecule orbital analysis of the bent acetonitrile, as it appears in structure **2.5π**, reveal that HOMO and HOMO-1 are mostly π nitrile bonding orbitals, whereas the LUMO is represented by the π* nitrile antibonding orbital. The HOMO of the [Ni(dmpe)] fragment is predominately located at the $3d_{x2-y2}$ orbital, while the LUMO is primarily the Ni *sp* hybrid orbital directed towards the incoming acetonitrile ligand. Thus, complex **2.5π**. possesses strong bonding interactions from the back-donating HOMO of the nickel fragment into the LUMO of the acetonitrile. This results in square-planar geometry for **2.5π** which is more in accordance with a d^8 rather than a d^{10} electron configuration of the nickel. It is essential for the explanation of the C-CN cleavage and the formation of the oxidative product (**2.5σ**) to examine the bonding situation in **2.5-TS2**. The back-donation from the nickel fragment HOMO into the acetonitrile LUMO favors the formation of the Ni-CH$_3$ σ bond and the cleavage of the C-CN bond, due to its σ antibonding character towards the C-CN bond and the agnostic C-H interaction. Therefore, the transition state **2.5-TS2** is exactly in between the tetrahedral d^{10} Ni(0) acetonitrile complex and the square-planar d^8 Ni(II) methyl cyanido product.[259]
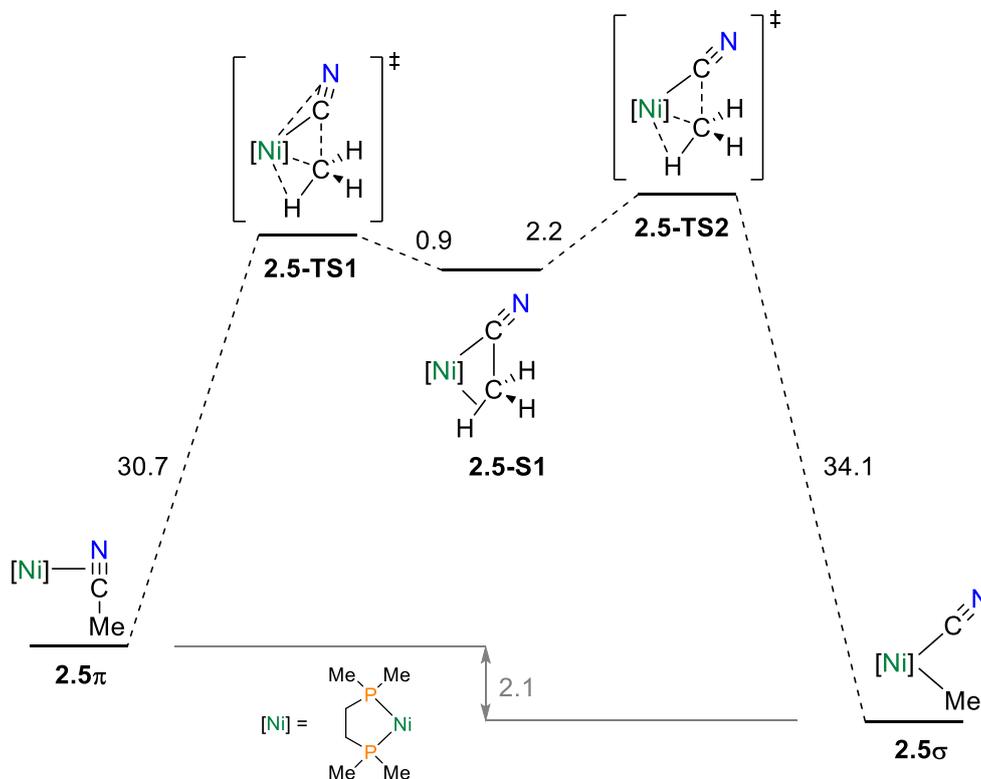
Scheme 17. Energetics of the C-CN bond cleavage in acetonitrile. Free energies in kcal·mol^{-1} relative to the total energies of the fragments ([Ni(dmpe)] and MeCN).

Adopting the benzonitrile activation concept to the Pt derivative primarily led to C-H activation (**2.10**, β-H elimination on the benzene ring) instead of the intended C-CN activation (**2.9σ**) in

the nitrile by heating to $T = 140\ °C$ for 1 h (Scheme 18). The low yield of **2.9** indicated that the product **2.10** is kinetically favored. Prolonged heating of the C-H activation product **2.10** showed additional β-CN elimination (**2.11**) and successive C-H activation to the stable cyanido complex (**2.12**).[269]
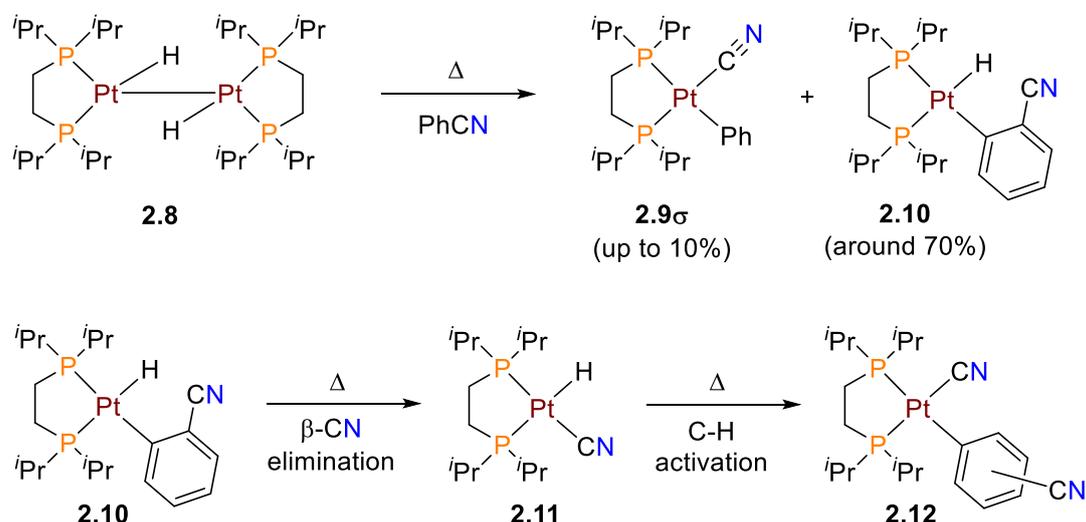
**Scheme 18.** Reaction of [(dippe)PtH] with benzonitrile and follow-up reaction of **2.10** by prolonged heating.

As mentioned before, the quantitative C-C cleavage could be achieved by the photolysis of the diphenylacetylene derivative (Scheme 14).[263] In addition, a series of the type [(dtbpe)Pt(R^{1}C≡CR^2)] (dtbpe = 1,2-bis(di-*tert*-butylphosphino)ethane, $R^1 = R^2$ = phenyl, 3,5-xylyl, *p*-F-phenyl, C_6F_5; R^1 = *p*-F-phenyl, R^2 = *p*-tolyl) was synthesized to analyze the impact of EWGs and EDGs on the activation process.[265] First, there was no significant difference between the dippe and dtbpe substituted diphenylacetylene platinum complexes in respect to the thermodynamical uphill oxidative addition of the C(sp^2)-C(sp) bond cleavage. The cleavage was carried out by irradiation ($\lambda > 300$ nm) in C_6D_6 for 4 h. The absorption of compound **2.14π** tails into the near UV to around $\lambda \approx 360$ nm. The reverse reaction, C-C reductive coupling, could be fully achieved by heating to $T = 80\ °C$ and has an energy barrier of around 32 kcal·mol^{-1}. The d^{10} Pt^0 complex **2.14π** shows a disordered square-planar geometry. The elongated C≡C triple bond and bending of the C≡C-Ph moiety indicates a strong π back-donation. The d^8 Pt(II) complex **2.14σ** has a regular square-planar geometry. To evaluate the influence of the acetylene substrate, the stability of three modified σ-complexes were determined (Scheme 19) and compared to the diphenylacetylene derivative. The electron-donating bis(3,5-dimethylphenyl)acetylene and the moderate electron-withdrawing bis(perfluorophenyl)-acetylene had no significant effect on the stability, while the strong electron-withdrawing bis(perfluorophenyl)acetylene successfully stabilized the σ-complex with an increased energy barrier of around 47 kcal·mol^{-1}. The large difference in the stabilization effect of bis(perfluorophenyl)acetylene can be explained by the presence of two *ortho*-fluorines, which increase the strength of the Pt-aryl bond in **2.17σ**.[270] It was not possible to

overcome the thermodynamical uphill pathway for the C-C cleavage reaction by ligand modification. Surprisingly, a mixed hetero-substituted acetylene with an EWG on one and an EDG on the other end did not lead to a selective C-C cleavage on one site of the acetylene.[265] Furthermore, it is expected that EWGs on the chelating diphosphine ligand would generally accelerate the elimination whereas EDGs would induce the opposite effect.[271]
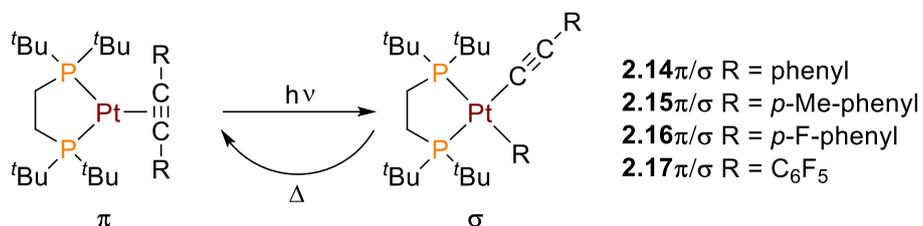
**Scheme 19.** Structures of modified [(dtbpe)Pt(acetylene)] complexes.

Investigations with asymmetric acetylene derivatives of the type [L_2Pt(PhC≡CR)] (R = Me, CF_3, ^tBu; L = dippe, dtbpe) were performed to examine the possibility of C(sp^3)-C(sp) bond activation. However, in no case C(sp^3)-C(sp) cleavage took place. Remarkably, only the electron-deficient trifluoromethylphenylacetylene ligand provided C(sp^2)-C(sp) cleavage. Irradiation of [(dtbpe)Pt(PhC≡CR)] (R = Me, ^tBu) in C_6D_6 yielded [(dtbpe)Pt(D)(C_6D_5)] by elimination of the acetylene from platinum and C-H (here C-D) activation of the solvent.[266] Further examinations of symmetrical complexes of the type [(dtbpe)Pt(RC≡CR)] (R = Me, CF_3, ^tBu) either showed C-H activation or no reaction at all. The analog 2,4-hexadiyne complex bearing C(sp)-C(sp) and C(sp^3)-C(sp) bonds only showed C-H activation of the solvent. In contrast, the [(dippe)Pt(PhC≡CC≡CPh)] complex (**2.18π**, Scheme 20) featuring C(sp)-C(sp) and C(sp^2)-C(sp) bonds exclusively undergoes the regular C(sp^2)-C(sp) cleavage. Accordingly, the C-C activation for such platinum systems is strictly limited to C(sp^2)-C(sp) bonds.[267]
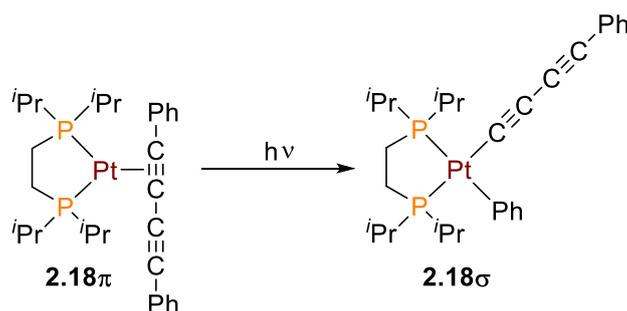
Scheme 20. C(sp^2)-C(sp) cleavage in [(dippe)Pt(PhC≡CC≡CPh)] by photolysis.

A similar C(sp^2)-C(sp) cleavage process in the 2,2'-dibromotolane ligand of a (diphosphine)Pt(0) complex was reported by WEIGAND and co-workers. The synthesized [(dppbe)Pt(η^2-2,2'-dibromotolane)] complex (**2.19π**; dppbe = 1,2-bis(diphenylphosphino)-benzene) has a distorted square-planar geometry. The elongated C≡C bond of the η^2-tolane and the bent C-Ph units suggest a strong π back-donation from the platinum center and

convergence to a C=C double bond. Irradiation with UV light of the solid **2.19π** led to the C(sp^2)-C(sp) cleavage in the tolane (diphenylacetylene) and consecutive intramolecular oxidative addition (Scheme 21). The uphill platinum insertion reaction into the aryl-alkynyl C-C bond is highly selective and thermal reversible.


2.19π   **2.19σ**
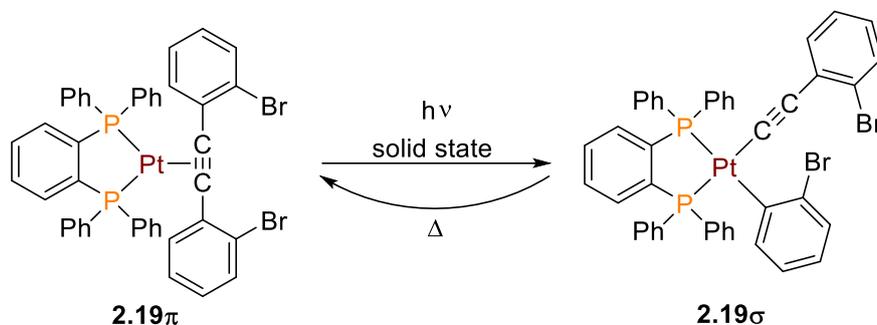
Scheme 21. UV light induced C(sp^2)-C(sp) cleavage in the 2,2'-dibromotolane ligand and thermal back reaction.

Computational investigations confirm that the tolane acts as 2e⁻ donor with a strong σ-bonding from the alkyne π into the platinum 6s orbital. The π back-donation from the platinum $5d_{x2-y2}$ into the antibonding alkyne π^* orbital led to a weakening of the C≡C triple bond. The UV light irradiation causes an intense MLCT from the platinum $5d_{x2-y2}$ into the antibonding alkyne π^* orbital and promotes the C(sp^2)-C(sp) cleavage, followed by the platinum insertion and rearrangement to the σ-complex **2.19σ**. The C(sp^2)-C(sp) cleavage heavily depends on the electronic nature of the tolane ligands and the spatial orientation of the phenyl groups. The wide dihedral angle suppresses the phenyl-conjugation and can be achieved by *ortho*-substitution. Generally, the C-C cleavage can be tuned by addition of EWGs to the phenyl groups, causing more intense MLCT. Further modification of this system demonstrated that the Pt(0) π-complex is always thermodynamically favored and lower in energy than the Pt(II) σ-complex. However, the activation barrier for the C-C cleavage can be lowered by EDGs, whereas EWGs stabilize the σ-complex at the expense of an increased activation barrier (Scheme 22).[272-275]
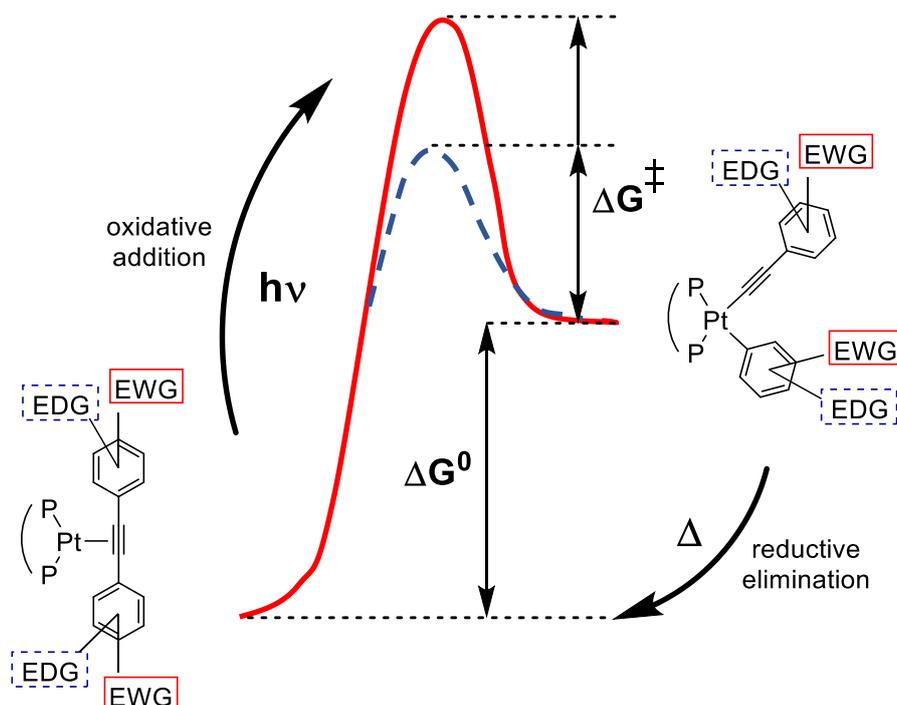
Scheme 22. Energetics of the photochemical oxidative C(sp^2)-C(sp) bond cleavage and the thermal reductive elimination.[274]

Based on this knowledge, a novel synthetic route towards cyaphido complexes with moderate steric demand was envisaged. The key factors for a possible successful transfer of the C(sp^2)-C(sp) bond cleavage concept are the valence isoelectricity between benzonitrile and aryl-phosphaalkynes (Scheme 23a), the similarity in the reactivity of acetylenes and phosphaalkynes, and the tendency of phosphaalkynes for η^2-/π-coordination on metals. To realize the cleavage between the aromatic sp^2-carbon atom and the phosphaalkyne sp-carbon atom a stable phosphaalkyne transition metal complex must be synthesized, first. Therefore, a suitable Ni and Pt(0) precursor, a phosphine and a kinetically stabilized phosphaalkyne is required (Scheme 23b). Ni- and Pt-bis(cyclooctadiene) were chosen as metal(0) precursor, due to its easy substitution of the cyclooctadienes. Furthermore, electron-donating chelating diphosphines were selected to get a *cis*-configuration for the complex and to enhance the electron density in the metal. The arylphosphaalkyne should be *ortho*-substituted to avoid potential *ß*-H-elimination reactions. As entry to the study the [(dippe)Ni(MesCP)] and [(dippe)Pt(MesCP)] should be synthesized (Scheme 23c). Later, additional modification to the carbon chain length of the diphosphine and different substituents on the phosphaalkyne aryl group should be evaluated to tune the C(sp^2)-C(sp) bond cleavage process.
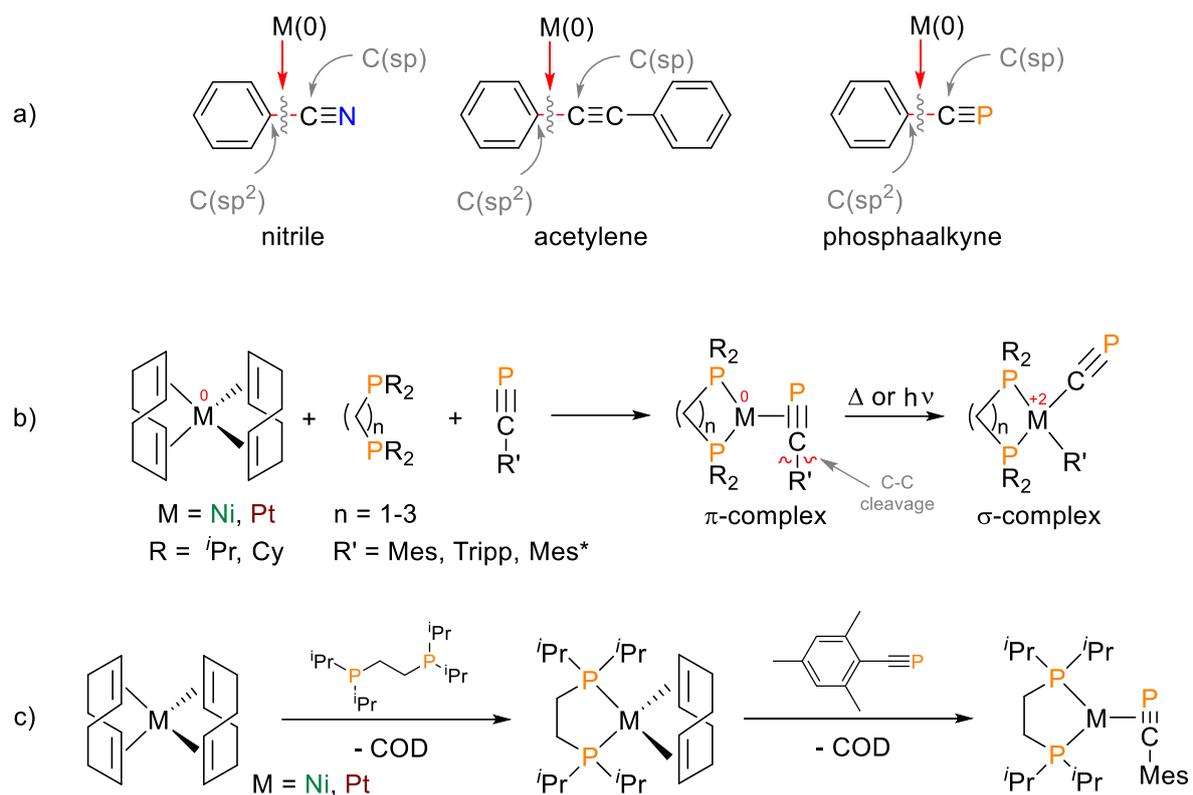
Scheme 23. Cleavage concept (a), planned synthetic approach (b) and first attempt (c) for the preparation of a cyaphido complex.

2.1.2 Preparation of starting materials

2.1.2.1 Transition metal precursors

The light and temperature sensitive bis(cycloocta-1,5-diene)nickel(0) and the bis(cycloocta-1,5-diene)platinum(0) serve as starting compounds for the preparation of the phosphaalkyne complexes. The yellow $[Ni(COD)_2]$ was first synthesized by WILKE *et al.* in 1966.[276] The common synthesis is the reduction of $[Ni(acac)_2]$ with triethylaluminum or diisobutylaluminum hydride in excess of 1,5-cyclooctadiene (COD).[277] However, today $[Ni(COD)_2]$ is widely commercially available. The colorless $[Pt(COD)_2]$ was first synthesized in1967 by MÜLLER and GÖSER by photolysis of $[(COD)Pt(^iPr)_2]$ in the presence of COD. Later, $[Pt(COD)_2]$ was also generated by evaporation of elemental platinum into a COD atmosphere. Even though there was demand for $[Pt(COD)_2]$ as universal Pt(0) source for synthetic chemistry, the synthesis procedures were either too complicated or suffered from low yields. That changed with the more convenient synthesis by STONES *et al.* by reduction of $[(COD)PtCl_2]$ with Li_2COT (COT = cycloocta-1,3,5,7-tetraene) in excess of COD, resulting moderate yields of around 40% to 60%.[278-279] This method is still broadly used today, due to the balance of effort, costs and yields. However, it is common knowledge that the published yields are highly overestimated and there are further methods for the synthesis of $[Pt(COD)_2]$ with higher yields or less effort. First of all, the synthesis of $[Pt(COD)_2]$ can also be achieved more reliably by transformation of tris(2-norbornene)platinum by heating in excess of COD.[279] Secondly, the elimination of chloride in $[(COD)PtCl_2]$ can also be performed with different reducing agents like colbaltocene, samarium(II) iodide,[280-281] or by potassium formate in combination with 18-crown-6 or $[(bpy)Ni(COD)]$.[282-283] Especially the last two methods are promising, due to their simple execution but suffer from the high prices of the starting materials. The $[Pt(COD)_2]$ for this work was produced by a slightly modified synthetic route of STONE (Scheme 24),[279] due to the already existing knowledge for it. In the first step, an acetic acid aqueous solution of potassium tetrachloroplatinate(II) (**1**) was heated together with COD to $T = 90$ °C for 1 h. The pale-yellow suspension was chilled to $T = 0$ °C, filtrated and the dichloro(1,5-cyclooctadiene)-platinum(II) (**2**) was isolated as colorless powder in nearly quantitative yields.[284] The freshly synthesized (1,3,5,7-cyclooctatetraene)dilithium[285] (**3**) ether solution from elemental lithium and COT[286-288] was added to the suspension of **2** in COD at $T = -30$ °C. After work up, the crude product was purified by column chromatography with alumina and crystallization from toluene solution. Colorless flakes of bis(cycloocta-1,5-diene)platinum(0) (**4**) could be isolated with a typical yield of around 30%. **4** must be stored under inert conditions in the absence of light and temperatures below $T = -20$ °C to avoid decomposition to elemental platinum and COD.[279]
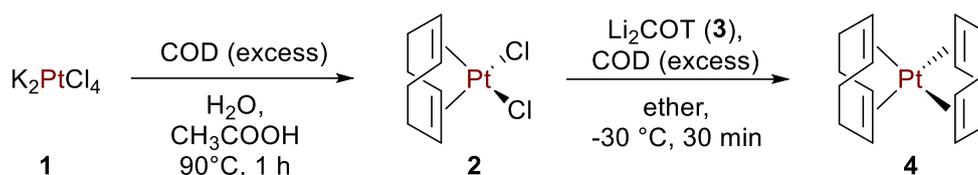
Scheme 24. Synthesis of [Pt(COD)$_2$] (**4**) starting from the platinum salt **1**.

2.1.2.2 Chelating phosphine ligands

Since the discovery of the coordination chemistry by WERNER in 1983, the chemical importance of the coordination ligands has been demonstrated by their effect on electricity and valence orbital interaction on the metal center.[289] In short, the reactivity of a metal in a complex strongly depends on its coordinated ligands.[290] Phosphines attained a substantial position in the coordination chemistry,[291] due to their ability to act as both σ-donor and π-acceptor.[292] They can ideally interact with the *d* orbitals of transition metals and consequently stabilize the complex.[293] Polydentate phosphines usually possess an even better stabilization effect.[294] The first bidentate phosphines were synthesized by ISSLEIB and MÜLLER in 1959.[295] Until today, many di- and polydentate phosphines has been realized, nevertheless it is still a field of active development.[296] The binding situation of phosphines is well explored and also appropriate for the polydentate phosphines. The phosphorus atom of the phosphine donates electron density to the transition metal center by applying a σ-bond, while the metal establishes a π-back bonding to the phosphine.[293] The ability to act as σ-donor and π-acceptor is significantly dependent on the substitution. Generally, EDGs enhance the σ-donor and inhibit the π-acceptor ability, while EWGs show exactly the opposite tendency (Figure 22).[292]

σ-donor ability

Ni(CO)$_3$X: P(CH)$_3$ = P(OCH$_3$)$_3$ > PH(CH$_3$)$_2$ > PH$_2$(CH$_3$) > PH$_3$ > PCl$_3$ > PF$_3$

π-acceptor ability

Ni(CO)$_3$X: PF$_3$ > PCl$_3$ >> P(OCH$_3$)$_3$ > PH$_3$ > PH$_2$(CH$_3$) > PH(CH$_3$)$_2$ > P(CH)$_3$
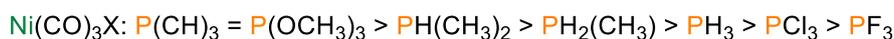
Figure 22. σ-donor and π-acceptor ability of a selection of phosphine ligands.

However, the donor and acceptor properties of bidentate phosphines, in particular the influence of the bite angle (P-M-P angle), are less intensely investigated yet. Bidentate phosphines are commonly used to create a rigid steric environment with well-defined positions (*cis*, *trans*) and electron-donating properties to affect the binding (conformation) and reactivity of the metal center towards further ligand coordination. The P-M-P angle is affected by the backbone of bidentate phosphines and tend to be smaller than in monodentate phosphines. A computational study towards the impact of bidentate phosphines on tetrahedral nickel complexes of the type [(R$_2$P(CH$_2$)$_n$PR$_2$)Ni(CO)$_2$] and [(R$_2$P(CH$_2$)$_n$PR$_2$)NiH$_2$] (n = 1-3, R = H, Me,

Et, ^{i}Pr, ^{t}Bu, Ph, OMe, CF$_3$, F) revealed the electronic and general consequences of this geometric difference.[297] The analysis of the carbonyl complexes showed a distorted tetrahedral structure for all bidentate phosphines complex compared to the [(PMe$_3$)Ni(CO)$_2$]. The P-Ni-P angle decreased from 110° for [(PMe$_3$)Ni(CO)$_2$] by around 12° for each CH$_2$ group removed from the phosphine backbone in [(R$_2$P(CH$_2$)$_n$PR$_2$)Ni(CO)$_2$] (n = 1-3). Depending on the specific substituents the figures are 98-103° (n = 3), 88-91° (n = 2) and 75-78° (n = 1). The P-Ni-P angle of a specific backbone chain length is affected by steric effects of the substituents. Thus, the measured angle was largest for *tert*-butyl groups and smallest for fluorine. Interestingly, the Ni-P distance of the backbone was 0.03 Å longer in the case of only one CH$_2$ group, whereas was identical for two and three groups. The poorer orbital overlap, caused by the small P-Ni-P angle for a single CH$_2$ group backbone, is responsible for the shortened Ni-P distance. A further point of the study was the investigation of the substituent effect in bidentate phosphines according to the calculated Tolman's electronic substituent parameter[298], showing essentially identical values for bidentate and unidentate phosphine complexes. Consequently, the substituents possess the same relative effect on the donor-acceptor properties and Tolman's tables are still valid even for bidentate phosphines. Furthermore, it was noted that the length of the CH$_2$ backbone has a notable effect on the symmetric carbonyl stretching vibration. For instance, addition of one methylene unit to the backbone decreases the CO wavenumber by around $\tilde{\nu}$ = 4 cm^{-1}, which is equal to exchanging all phosphorus substituents from their methyl to ethyl derivatives. Consequently, bidentate phosphines become more electron donating with increased backbone chain size, leading to P-M-P angle broadening, which reflects the typically called bite angle effect (Figure 23).[299-301] The bite angle influences the donation of the metal fragment to other ligands by affecting the geometry of the complex together with the orbital energy of the d$_{xy}$ metal-ligand hybrid orbital in the P-Ni-P plane. Bonding analysis of [(R$_2$P(CH$_2$)$_n$PR$_2$)NiH$_2$] showed that the nickel-based frontier orbitals of the L$_2$Ni fragment interacts with the hydrogen atoms over a filled d (hybrid) orbital with π symmetry and an empty p (hybrid) orbital with σ symmetry. The d orbital lies energetically below the p orbital. Both orbitals increase in energy if the coordinated phosphine becomes more electron rich, leading to a decrease of σ donation from H$_2$ to Ni and an increase of π back-bonding from Ni to H$_2$. For EDGs, the Ni to H$_2$ π back-donation is dominating, while for EWGs, it is the σ donation from H$_2$ to Ni. Interestingly, nickel dihydrogen complexes with electron-withdrawing bidentate phosphines showed lower H$_2$ dissociation energies than their electron-donating counterparts.[297]
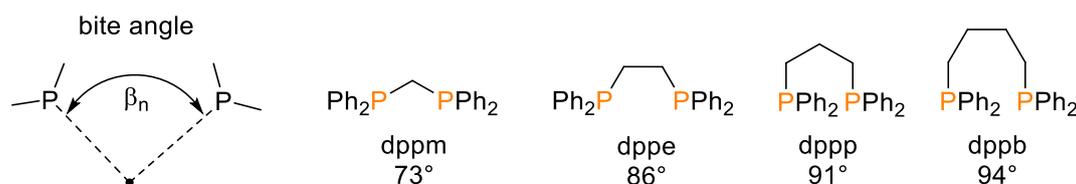
Figure 23. Bite angle sketch and four typical diphosphines with their common bite angle.

Besides the electron donating and accepting properties and the steric demand of the substituents, the bite angle, the angle occurred between the coordinated phosphorus atoms of the diphosphine and the metal center (P-M-P), can substantially affect the characteristics of the metal core and consequently the reactivity of the complex. Generally, altering the bite angle of a bidentate ligand shows two effects.[302] First, the substituents of a bidentate ligand with a wider bite angle exert more steric repulsion on the other ligands and the metal core (Figure 24a). Second, a fixed bite angle forces the metal center towards a designated geometry by influencing the electronic or orbital interaction of the metal. For instance, the ideal bite angle for a tetrahedral Ni(0) would be 109.5°, whereas it would be 90° for a square planar Ni(II) complex (Figure 24b). This concept of the "natural bite angle" was introduced by WHITEKER and CASEY in 1990 and is defined "as the preferred chelation angle determined only by ligand backbone constraints and not by metal valence angles".[303] The bite angle size can be adjusted by the diphosphine (carbon) backbone size (bridge length), the number of the methylene units. This bite angle effect was the first time utilized by IWAMOTO and YUGUCHI for the study of a catalytical co-dimerization of butadiene and ethene.[304] However, an useful bridge length is typically between one to three methylene groups. Reaching a linker size of C_4, like in dppb (1,4-bis(diphenylphosphino)butane), has a reduced propensity for chelation and increased tendency for bridging bimetallic structures, due to the increased flexibility of the diphosphine ligand.[305] The bite angle effect leads to mainly four observed consequences. An adjusted bite angle can influence the equilibrium between two species by changing the preferred geometry (Figure 24c). It can also affect the product selectivity in catalytic reactions like increased selectivity for linear hydroformylation products for larger bite angle ligands.[302] The most prominent example is the effect on the reductive elimination rates. Wide bite angle bidentate ligands increasing the rate of the reductive elimination step by enforcing the zero valent metal oxidation state with their predefined wide angle over higher metal valences which are typical for square planar complexes with around 90° bond angles.[302, 306] Bite angle ligands clearly also have an effect on oxidative addition reactions on the metal center. However, the general trend is a less plausible and depending on many additional factors. Overall, the electron-donating nature of the P substituents of the diphosphines is more dominant than the bite angle on oxidative addition. Computational studies verified that mono-ligated species like [Pt(PH$_2$CH$_2$PH$_2$)] have lower energy barriers for oxidative addition than its ethenyl [Pt(PH$_2$(CH$_2$)$_2$PH$_2$)] or monodentate analog [Pt(PH$_3$)$_2$], due to reduced steric factors and the

pre-bent complex geometry which facilitate the bonding of the incoming substrate.[307] Consequently, the necessary strain in pushing the already coordinated ligands closer together upon oxidative addition of incoming substrate is reduced with smaller bite angles. Astonishingly, this is a purely steric and not an orbital effect.[301, 308-310]
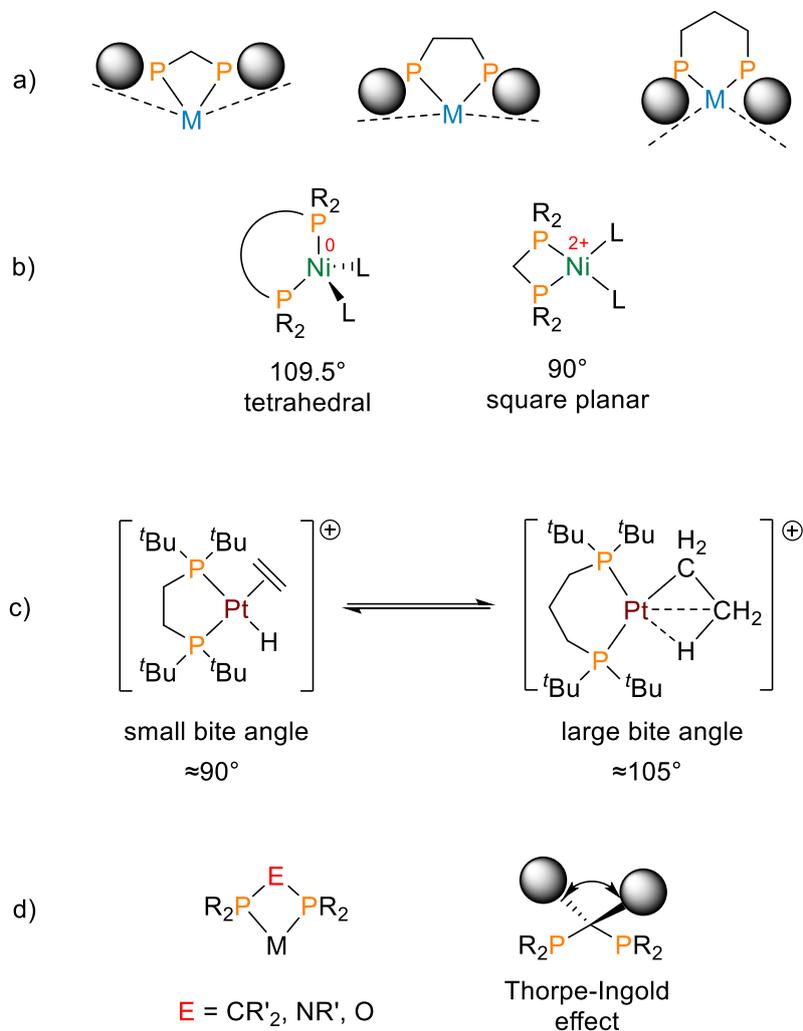
Figure 24. Steric effects in relation of the bite angle (a), idealized bite angle for Ni(0) and Ni(II) complexes (b), effect of the bite angle towards an equilibrium (c), Thorpe-Ingold effect (gem-dimethyl or angle compression effect; d).

A further way to adjust the bite angle of a diphosphine ligand, especially of those with a single atom linker, is the exchange of the linking unit (E, Figure 24d). For instance, replacing the CH_2 moiety with an amine (N-R) usually leads to a smaller bite angle.[311] Alternatively, the protons of the methylene backbone group can be substituted with more steric demanding groups to widen the angle between the geminal substituents on the backbone (Thorpe-Ingold effect[312-313]), leading to a compression of the other angles and improvement of the chelating effect.[314] The same effect can be achieved by large substituents on the diphosphine phosphorus atoms.[315] Computational analysis showed that decreasing the bite angle of a diphosphine ligand would enhance the reactivity due to a rise of the HOMO energy in the L_2M fragment (Figure 25).[316-318] Finally, it is possible to generate hetero-polydentate chelating ligands

(hybrid ligands) with electronically differentiated donors. Usually, one of the donors is weaker bonded than the others and can readily dissociate. These hemilabile polydentate ligands[319] are useful for catalytic reactions to offer temporary vacancies for incoming substrates, especially for polymerizations.[320] Taking all these information[299-303, 305-311, 314-326] into account it is reasonable to consider alkyne substituted (σ-donating) diphosphines with C_2 or C_3 backbone for the synthesis of the phosphaalkyne complexes to stabilize the zero valent Ni(0) or Pt(0) metal center. However, diphosphines with a methylene backbone would certainly better suitable for the generation of the cyaphido complexes, due to their stabilizing effect for square planar Ni(II) complexes.[299, 326]
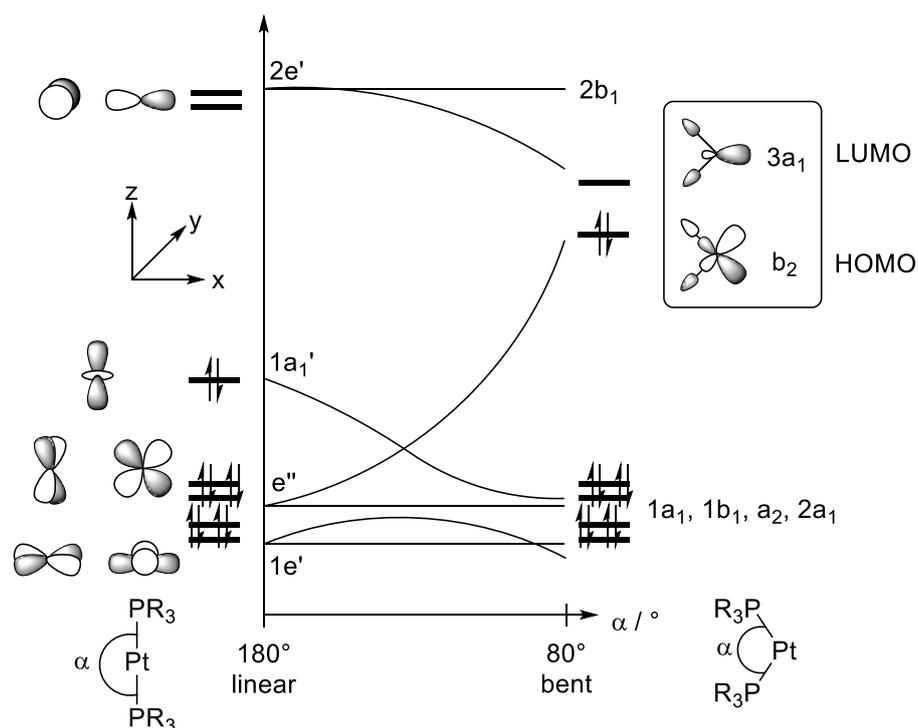

Figure 25. Walsh diagram for a 14-electron d^{10} platinum fragment in dependency of the bite angle (linear to bent).[326]

A broad selection of different diphosphines were used for the preparation of the phosphaalkyne complex to analyze their stability and possible C-CP bond activation (Table 2, Figure 26).

Table 2. Overview of used chelating (di)phosphines. Compounds marked with * were ordered from chemical suppliers.

compound	abbreviation	number
1,2-bis(dicyclohexylphosphino)ethane*	dcpe	**30**
1,2-bis(diphenylphosphino)ethane*	dppe	**31**
1,3-bis(diisopropylphosphino)propane*	dippp	**32**
1,3-bis(dicyclohexylphosphino)propane*	dcpp	**33**
1,3-bis(diphenylphosphino)propane*	dppp	**34**
bis(diphenylphosphino)ferrocene*	dppf	**35**
bis(di-*tert*-butylphosphino)methane	dtbpm	**15**
bis(dicyclopentylphosphino)methane	dcppm	**24**

bis(dicyclohexylphosphino)methane	dcpm	**21**
1,2-bis(diisopropylphosphino)ethane	dippe	**8**
(diisopropylphosphinodimethylamino)ethane	dippdmae	**29**

dtbpm (**15**)   dcpm (**21**)   dcppm (**24**)

dippe (**8**)   dcpe (**30**)   dippdmae (**29**)

dppe (**31**)   dippp (**32**)   dcpp (**33**)

dppp (**34**)   dppf (**35**)
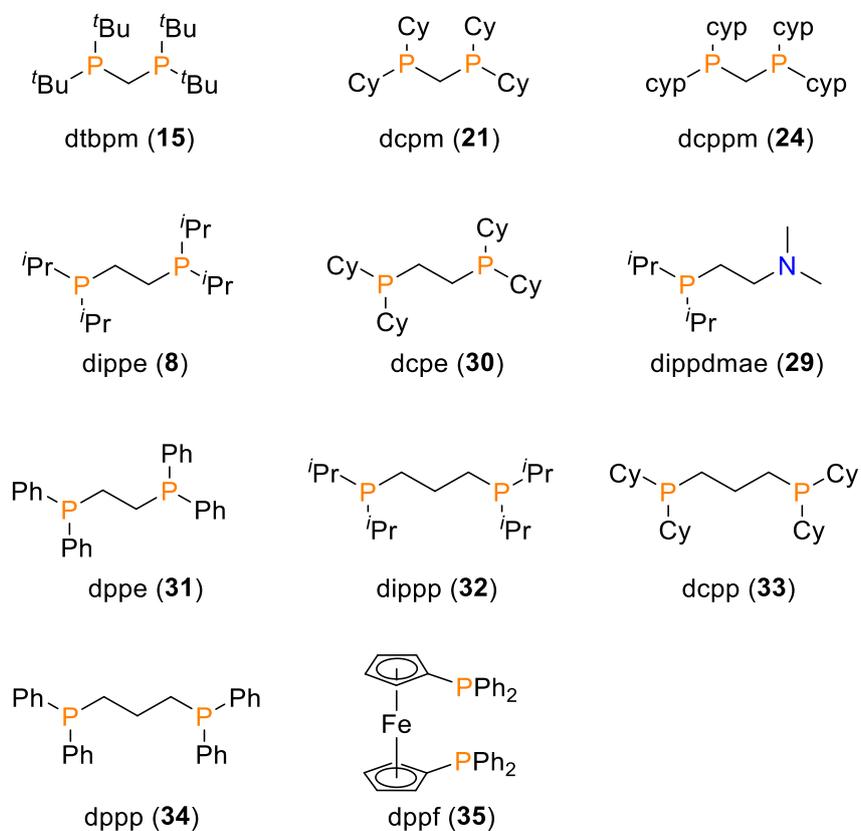
Figure 26. Overview of used chelating (di)phosphines.

2.1.2.2.1 Synthesis of 1,2-bis(diisopropylphosphino)ethane

1,2-bis(diisopropylphosphino)ethane represents a chelating diphosphine ligand with moderate steric demand and good σ-donor abilities due to its isopropyl groups. Furthermore, the C_2 backbone should stabilize the resulting phosphaalkyne complex but also reduce the steric strain good enough to allow the oxidative C-CP cleavage. Hence, this ligand was taken as starting point of the study.

1,2-bis(diisopropylphosphino)ethane (**8**) was prepared by adopting a literature synthesis for 1,2-bis(diethylphosphino)ethane (Scheme 25).[327-328] First, 2-bromopropane (**5**) was converted to the corresponding Grignard reagent **6**, which was added dropwise to a solution of 1,2-bis(dichlorophosphino)ethane (**7**). After work up and fractional distillation the product **8** could be obtained as colorless, air sensitive oil with a yield of 69%. It was stored as a 0.2 M THF solution at T = -20 °C.
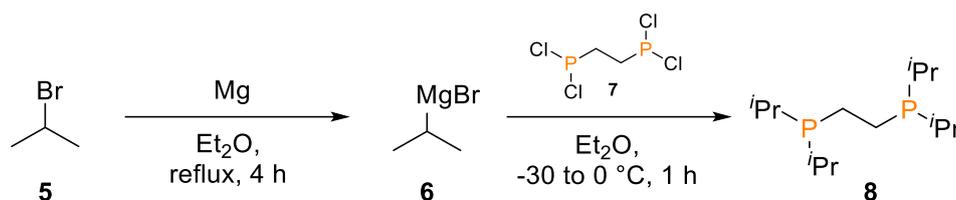
**Scheme 25.** Synthesis of 1,2-bis(diisopropylphosphino)ethane (**8**).

2.1.2.2.2 Synthesis of bis(di-*tert*-butylphosphino)methane

The bis(di-*tert*-butylphosphino)methane (**15**) ligand is one of the most steric demanding common chelate ligands. The *tert*-butyl groups and the short methylene bridge results in a small bite angle, which stabilizes mostly square planar complexes with transition metals of oxidation state +II. The dtbpm ligand was synthesized by two different literature known pathways. The first route, established by KARSCH, is a one-step direct synthesis with low yields due to the formation of several by-products.[329-330] The second method by HOFMANN is a more flexible five-step synthesis with moderate yields with the option to also synthesize asymmetric variants.[315, 331-333]

The direct preparation of dtbpm (**15**) by KARSCH is possible by four consecutive substitution reactions of bis(dichlorophosphino)methane (**9**) with *tert*-butyllithium (Scheme 26). However, the product **15** could not be isolated in sufficient purity, due to the presence of several non-separable by-products.[334] Two of the cyclic by-products (**15a**, **15b**) could be identified by $^{31}P\{^1H\}$ NMR spectroscopy (Figure 27).[329]
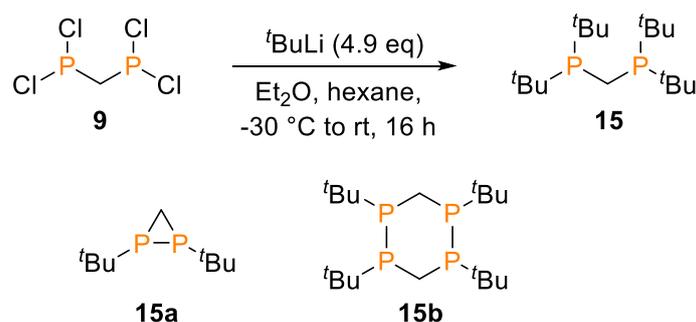

Scheme 26. Direct synthesis of bis(di-*tert*-butylphosphino)methane (**15**) and typical cycloaddition by-products (**15a**, **15b**).
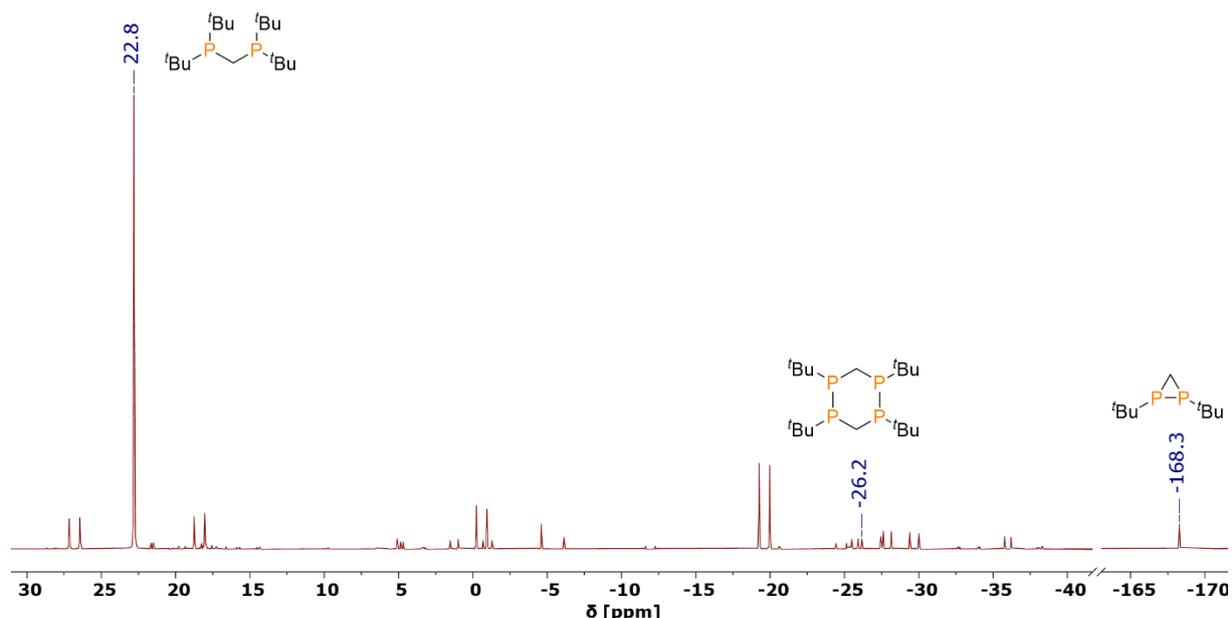
Figure 27. $^{31}P\{^1H\}$ NMR spectrum of dtbpm (**15**) synthesized by the method of KARSCH.

The more flexible five-step synthesis by HOFMANN includes a Grignard reaction, followed by a methylation, lithiation and final substitution to assemble the two independent phosphines (**12**, **14**) to the diphosphine (**15**, Scheme 27).[315] The product **15** was isolated in 65% yield from **14** with negligible impurities (Figure 28) and stored as 0.2 M THF solution at T = -20 °C. Attempting the unfavorable coordinating complex Ni(dtbpm)$_2$ (cf. 2.1.2.2.6 for explanation) by mixing **15** to Ni(COD)$_2$ only yielded the oxidized species **15a**, which could be obtained and characterized by single crystal X-ray diffraction (Figure 29).[334]
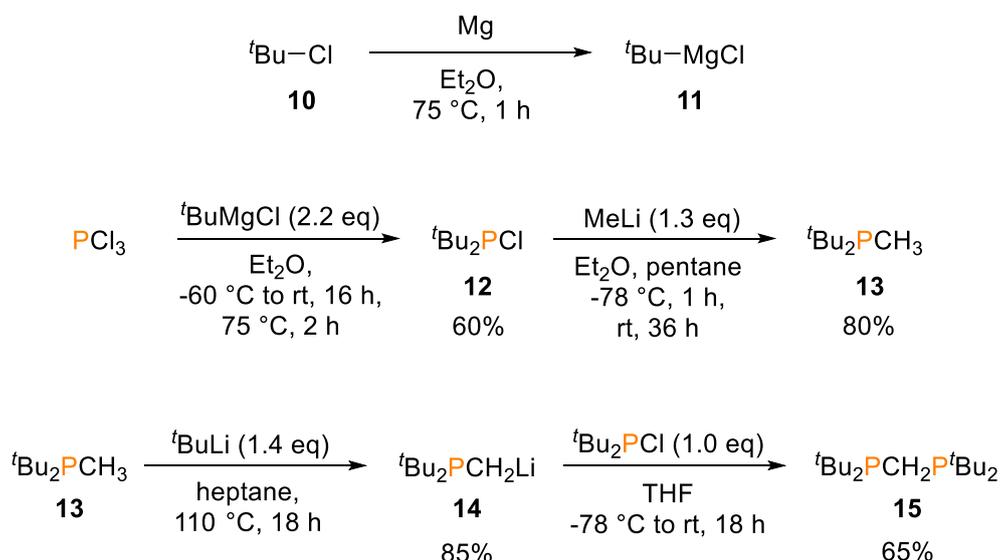
Scheme 27. Five-step synthesis of bis(di-*tert*-butylphosphino)methane (**15**).
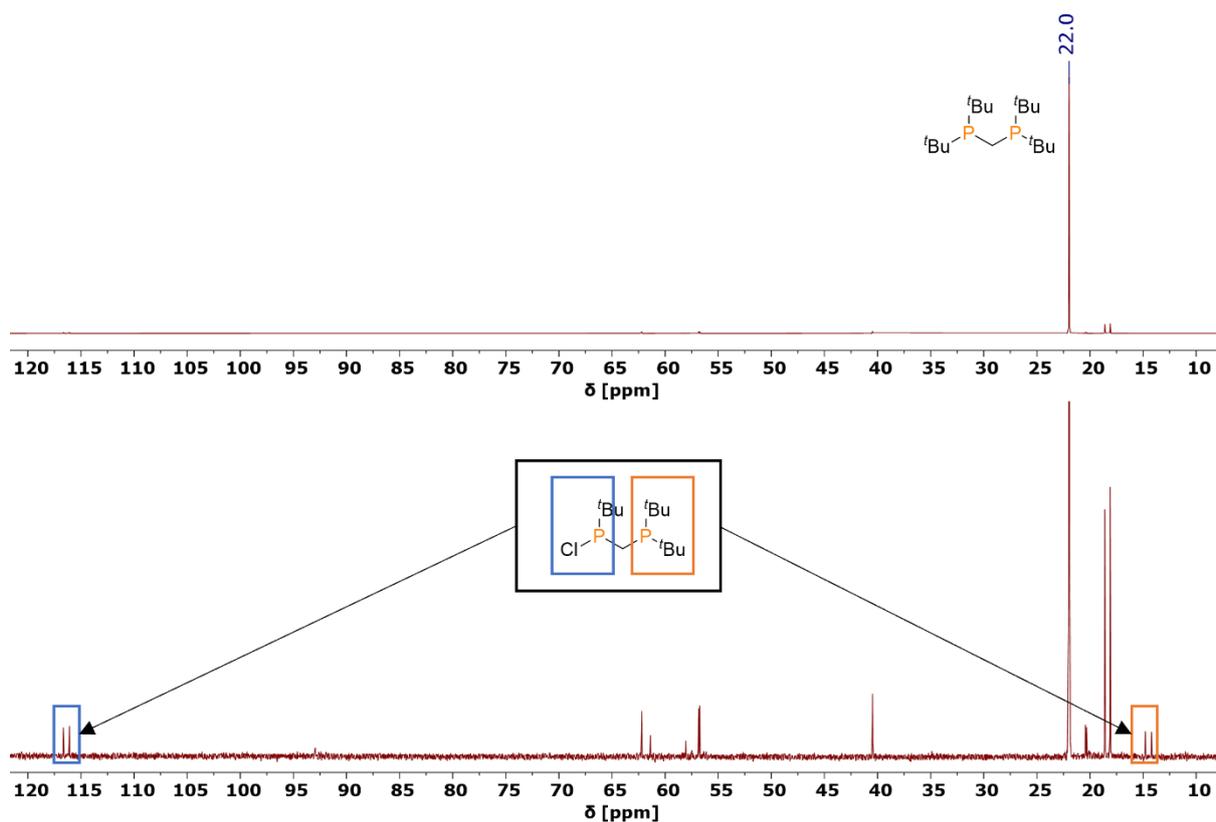
Figure 28. ^{31}P{^{1}H} NMR spectrum of dtbpm (**15**, top) synthesized by the method of HOFMANN and its scaled up spectrum (bottom) to identify the impurities.
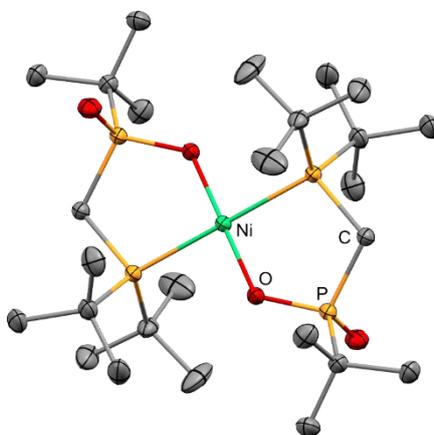

Figure 29. Molecular structure of **15a** in the crystal. Anisotropic displacement ellipsoids are shown at 50% probability level. Hydrogens and co-crystalized 1,4-dioxane omitted for clarity.

2.1.2.2.3 Synthesis of bis(dicyclohexylphosphino)methane

Dcpe (**21**) is the cyclohexyl substituted analog of dtbpe (**15**). The cyclohexyl groups can undergo a ring flip to the two possible chair conformers,[335] which allows a decrease of the steric demand compared to *tert*-butyl groups. Thus, a marginal larger bite angle is expected by keeping similar σ-donor properties. The synthesis proceeded analogously to the flexible synthetic pathway for dtbpm (**15**, Scheme 28).[315] The dcpe (**21**) was obtained in 59% yield

with traces of one by-product (Figure 30), which is in accordance with the result for dtbpe (**15**). **21** was stored as 0.2 M THF solution at T = -20 °C. During the course of the study the molecular structure in the crystal of the fully oxidized version of dcpe **21a** was obtained (Figure 31).[334] The oxidation occurred during the crystallization and was not recognized by NMR experiments.

$$Cy-Cl \xrightarrow[\text{75 °C, 3.5 h}]{\text{Mg} \atop \text{Et}_2\text{O,}} Cy-MgCl$$

16   **17**

$$PCl_3 \xrightarrow[\substack{\text{Et}_2\text{O,} \\ \text{-60 °C to rt, 16 h,} \\ \text{75 °C, 2 h}}]{\text{CyMgCl (2.4 eq)}} Cy_2PCl \xrightarrow[\substack{\text{pentane} \\ \text{-78 °C, 2 h,} \\ \text{rt, 16 h}}]{\text{MeLi (1.2 eq)}} Cy_2PCH_3$$

                 18   **19**
                 43%   93%

$$Cy_2PCH_3 \xrightarrow[\substack{\text{heptane,} \\ \text{110 °C, 18 h}}]{^t\text{BuLi (1.3 eq)}} Cy_2PCH_2Li \xrightarrow[\substack{\text{THF} \\ \text{-78 °C to rt, 16 h}}]{Cy_2PCl \text{ (1.0 eq)}} Cy_2PCH_2PCy_2$$

19   **20**   **21**
                 95%   59%
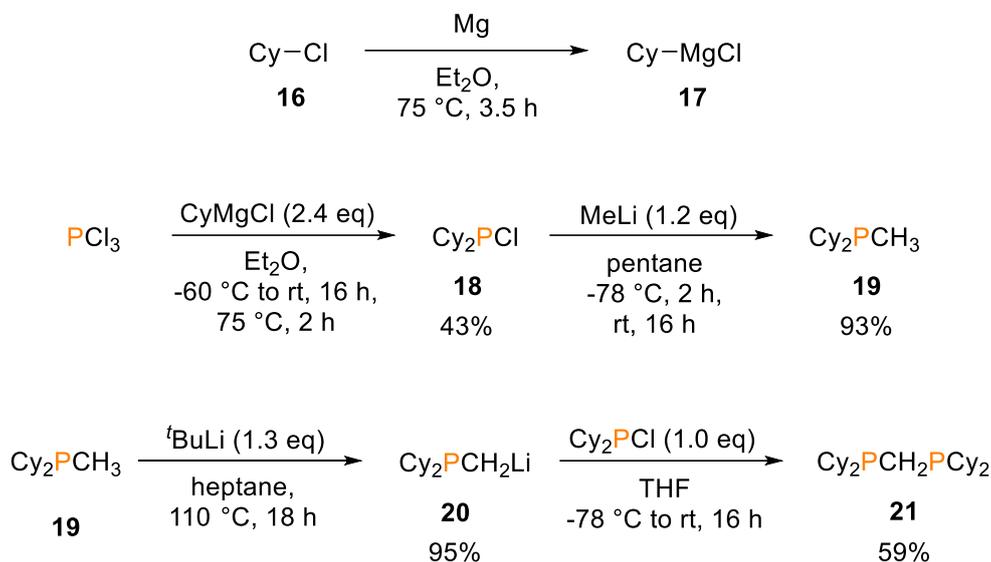
Scheme 28. Five-step synthesis of bis(dicyclohexylphosphino)methane (**21**).
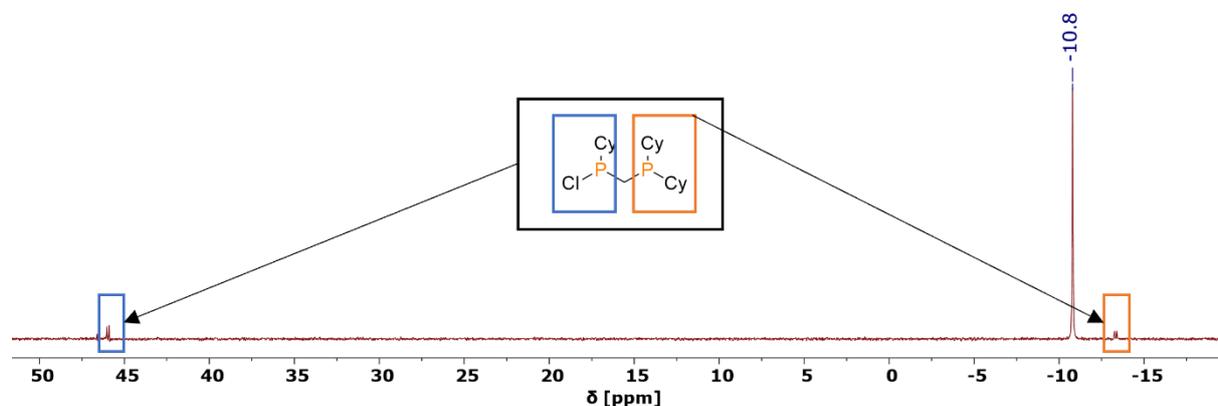
Figure 30. ^{31}P{^{1}H} NMR spectrum of dcpm (**21**) synthesized by the method of Hofmann.
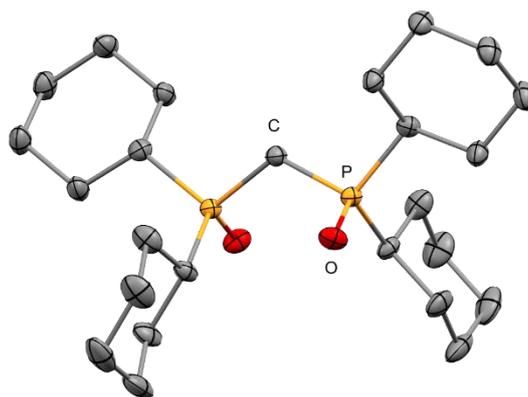
Figure 31. Molecular structure of **21a** in the crystal. Anisotropic displacement ellipsoids are shown at 50% probability level. Hydrogens and co-crystalized water omitted for clarity.

### 2.1.2.2.4 Synthesis of bis(dicyclopentylphosphino)methane

In addition to dcpe (**21**), the less bulky bis(dicyclopentylphosphino)methane (**24**) was synthesized by a Grignard reaction (Scheme 29). Even though, dcppm (**24**) was successfully produced, the isolation by distillation and recrystallisation was not sufficient. Several unidentified by-products were found by ^{31}P{^{1}H} NMR spectroscopy (Figure 32). When **24** was later used for follow-up reaction, undesired side reaction could not be excluded due to the number of by-products.[334]
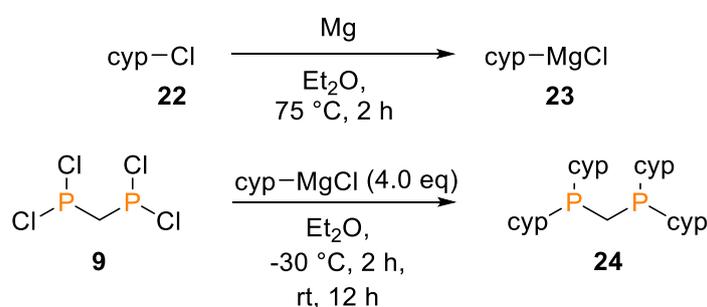
**Scheme 29.** Grignard reaction for the synthesis of bis(dicyclopentylphosphino)methane (**24**).
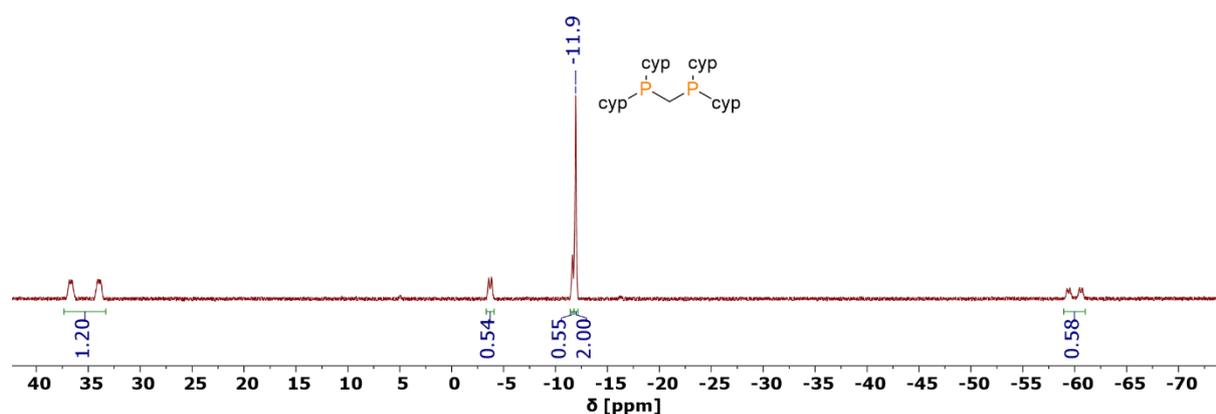
Figure 32. Quantitative ^{31}P NMR spectrum of dcppm (**24**) to evaluate the amount of by-products.

2.1.2.2.5 Synthesis of (diisopropylphosphinodimethylamino)ethane

The (diisopropylphosphinodimethylamino)ethane ligand (**29**, dippdmae) is the hemilabile analog of 1,2-bis(diisopropylphosphino)ethane (**8**). The phosphine part offers the same steric demand and σ-donor properties, while the dimethylamine group can be easily detached from the transition metal center to permit temporary coordination of a substrate to promote possible catalytic reactions. Dippdmae (**29**) was prepared[336] according to the procedure of WERNER.[337]

For the preparation of **29**, two additional reactions are necessary to get the direct precursors **26** and **28** (Scheme 30). First, chlorodiisopropylphosphine (**27**) was hydrogenated with lithium aluminum hydride, yielding the diisopropylphosphine (**28**).[338-339] To obtain the second precursor **26** the hydrochloride was absorbed from 2-chloro-*N,N*-dimethylethylamine hydrochloride by addition of potassium hydroxide.[340] The released 2-chloro-*N,N*-dimethylethylamine (**26**) was caught and temporally stored with an cooling trap, to avoid the formation of the undesired intramolecular cyclisation product (**26a**), which presumable reacts to miscellaneous oligomers.[341-343] In the final reaction, **28** was first lithiated with *n*-butyllithium and then coupled to **26** by substitution. Distillation of the crude product yielded an air and temperature sensitive colorless high viscous gel (51%), which was stored at T = -20 °C.
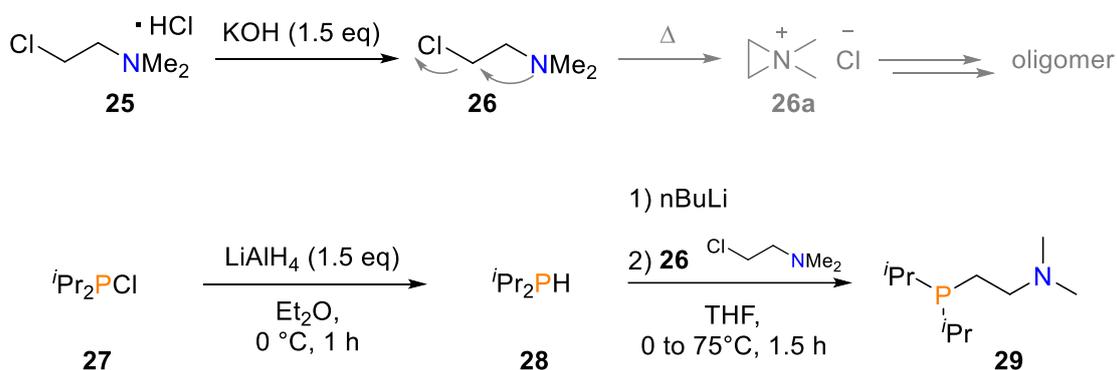

Scheme 30. Reaction steps for the synthesis of (diisopropylphosphinodimethylamino)ethane (**29**).

2.1.2.2.6 Reactivity towards bis(cyclooca-1,5-diene)-nickel(0) and -platinum(0)

In the next step, a selection of the chelating (di)phosphines were reacted with the intended (COD)$_2$Ni(0) and (COD)$_2$Pt(0) precursors to evaluate their reactivity, to detect potential side reaction and to gather helpful ^{31}P NMR shifts for the expected (COD)M(L) and M(L$_2$) (M = Ni, Pt; L = **8**, **15**, **21**, **24**, **29**, **30**) products, which might occur as undesired by-product or intermediate in the later scheduled reaction of the phosphaalkyne complexes. To prove the reactivity of the chelating (di)phosphine ligands towards (COD)$_2$Ni(0) and (COD)$_2$Pt(0), two equivalents of the appropriate ligand were added to a suspension of the metal precursor in THF (for C$_1$ bridged ligands) or toluene (for C$_1$ bridged ligands) and stirred at room temperature overnight (Scheme 31). After recording the ^{31}P{^{1}H} NMR spectrum, the reaction mixture was

heated (THF: T = 75 °C, toluene: T = 110 °C) for several hours before recording another NMR sample.
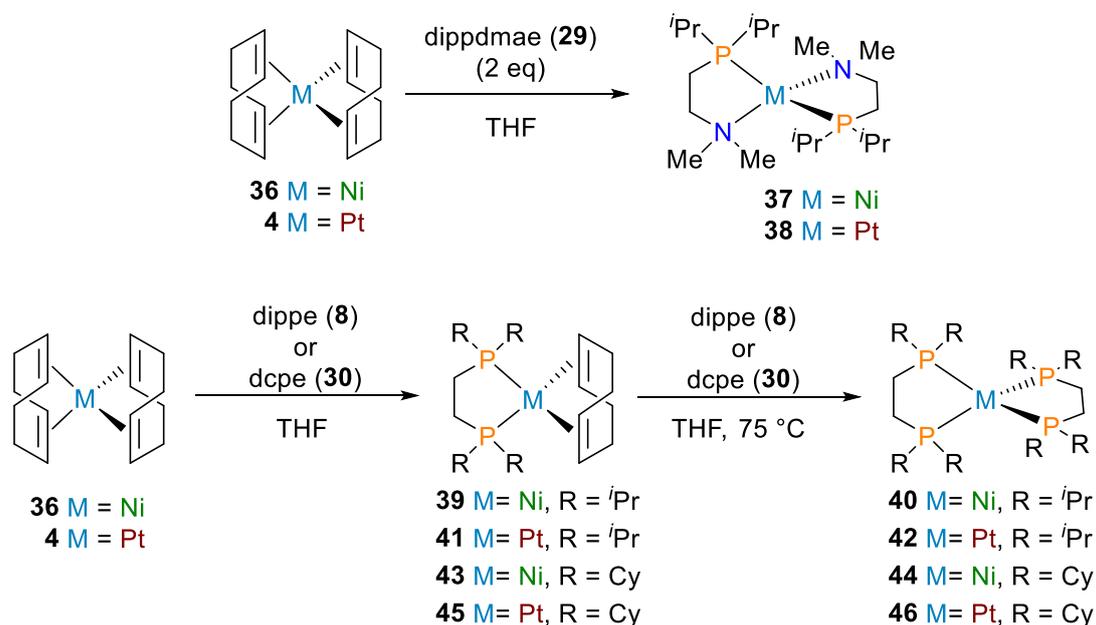
Scheme 31. Results for the successful coordination of the selected (di)phosphine ligands with Ni(COD)$_2$ or Pt(COD)$_2$.

Many conclusions could be drawn by combining literature facts with the observed ^{31}P{^{1}H} NMR spectra.[325, 344-347] Based on the spectra the ligand consumption could be monitored and on the basis of the platinum satellites, a successful coordination of the phosphorus atoms to the platinum center could be proven. The results are summarized in Table 3.

Table 3. Observed ^{31}P{^{1}H} NMR shifts [ppm], ^{195}Pt satellites [Hz] in the brackets for the free ligand (L) and the corresponding transition metal (M) complexes. T_{max} gives the maximum applied temperature. ^{a} reactions referring to the last entry/obtained product in the line are accessible at rt; ^{b} heating led to decomposition of the observed product; ^{c} products are not unequivocal verified to be correct, ^{d} literature value δ(^{31}P) = 78.7 ppm ($^1J_{P,Pt}$ = 3244 Hz) for (dippe)Pt(COD) (**41**).[345]

L (2 eq)	(COD)$_2$M(0) precursor	L ^{31}P{^{1}H} shift	(COD)M(L) ^{31}P{^{1}H} shift	M(L)$_2$ ^{31}P{^{1}H} shift	T_{max} [°C]
dippdmae (**29**)	Ni	0.3	-	45.9^c	75^a
dippdmae (**29**)	Pt	0.3	-	54.3 (4238)^c	75^a
dippe (**8**)	Ni	8.9	69.1	52.9	75
dippe (**8**)	Pt	8.9	-^{d}	42.1 (3583)	75^a
dcpe (**30**)	Ni	0.9	59.0	42.8	75
dcpe (**30**)	Pt	0.9	69.1 (2990)	30.3 (3592)	75^a
dtbpm (**15**)	Ni	22.0	43.3	-	75
dtbpm (**15**)	Pt	22.0	47.4 (2494)^b	-	110^a
dcpm (**21**)	Ni	-10.8	-	-	75
dcpm (**21**)	Pt	-10.8	-	-	110
dcppm (**24**)	Ni	-11.9	-	-	110

Besides the $^{31}P\{^1H\}$ shifts for some of the expected products, the evaluation of the results provides further insides into the influence of the (di)phosphine steric hindrance on the complex formation. As expected, the ligand dippdmae (**29**) possesses the lowest steric demand due to the NMe$_2$ group and cleanly reacted to the di-chelate product M(dippdmae)$_2$ for both Ni and Pt. However, it should be pointed out that the structure is not verified by additional measurements. The effect of the increased bulkiness of the diphosphino ligand can be clearly monitored for dippe (**8**) and dcpe (**30**). In both cases, the ligands reacted with Ni(COD)$_2$ to the (COD)Ni(L) complex, but additional heating is necessary to get the Ni(L)$_2$ complex. In contrast, the larger platinum core of Pt(COD)$_2$ reacted already at room temperature to the corresponding Pt(L)$_2$ complex and in the case of dippe (**8**) the intermediate (COD)Pt(dippe) could not even be observed. Astonishingly, the diphosphine ligands bearing a methylene backbone are not able to form a stable M(L)$_2$ (M = Ni, Pt) complex. It is assumed, that the steric demand of the ligands is too large to form a tetragonal transition metal(0) complex. Only in the case of dtbpm (**15**), the mono-substituted species (COD)M(dtbpm) could be observed (Scheme 32). The literature known [Pt(dtbpm)]$_2$ dimer (**49**) was not found.[348-349]
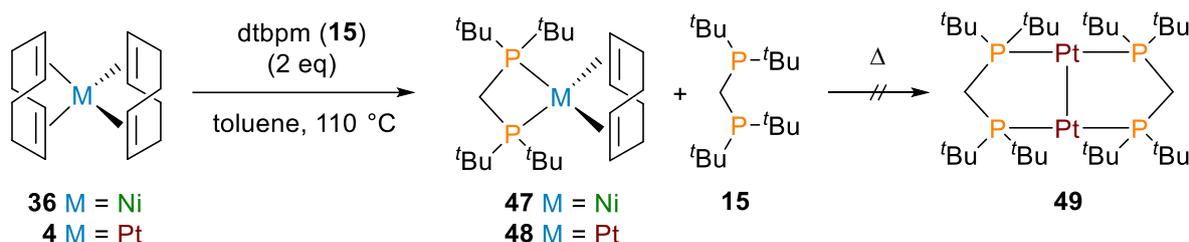

Scheme 32. Reaction of Ni(COD)$_2$ or Pt(COD)$_2$ with the methylene backbone ligand dtbpm (**15**).

2.1.2.3 Phosphaalkynes

To achieve a light induced cleavage of the phosphaalkyne C-CP bond, the phosphaalkyne must meet certain criteria (cf. 2.1.1). Most importantly it requires an aromatic sp^2-carbon atom next to the sp-carbon atom of the C≡P group. In addition, *ortho* substitution is recommended to avoid possible ß-H-elimination reactions, especially in the case of platinum complexes. The best kind of substitution, EDGs or EWGs, is not clear yet. EDGs would probably favor the cleavage process by lowering the oxidation barrier. However, EWGs might stabilize the generated cyaphido complex by increasing this barrier. Therefore, the literature known mesitylphosphaalkyne (**68**, Figure 33) was selected for first attempts to get a standard, which can be extended in both directions along the electronegativity of the substituents (compare **76**, **92**). In addition, silylphosphaalkynes should also be evaluated for possible Si-CP cleavage, via the thermal and photochemical silicon-carbon activation on Pt(0)-alkyne complexes found by MÜLLER, LACHICOTTE and JONES.[268] Optionally, the synthesis of di-, or triphosphaalkynes was considered as building block for the generation of cyaphido complexes bearing multiple

cyaphido groups. Figure 33 shows the selection of the planned phosphaalkynes. However, the fluorinated phosphaalkyne **92** could not be isolated and the polyphosphaalkynes **97** and **105** could not be synthesized. Table 7, at the end of chapter 2.1.2.3.7, provides a list of all used phosphaalkynes together with their ^{31}P NMR chemical shifts.
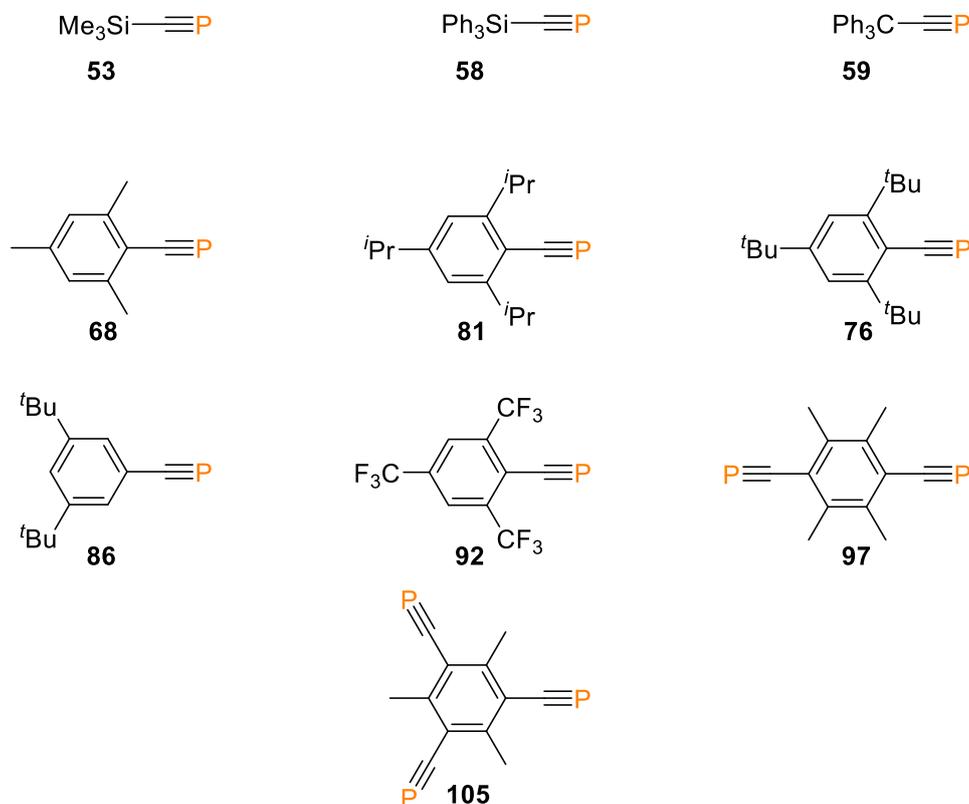
Figure 33. Planned selection of phosphaalkynes for the synthesis of phosphaalkyne/cyaphido complexes. The phosphaalkynes **53**, **58**, **59**, **68**, **81** and **76** are literature known compounds.

2.1.2.3.1 Synthesis of trimethylsilylphosphaalkyne

Trimethylsilylphosphaalkyne (**53**) was first synthesized by APPLE and WESTERHAUS in 1981.[75] A more convenient and reliable synthesis was introduced by RUSSEL and co-workers in 2010.[77] The later synthesis was used to obtain **53** in reasonable yields. Starting from (chloromethyl)trimethylsilane (**50**, Scheme 33) a Grignard reaction with phosphorus trichloride gave the precursor **52**. In the final step, a formal double elimination of HCl from the dichlorophosphine **52** with DABCO yielded the phosphaalkyne **53**. The silver cations of the AgOTf act as chloride scavenger, which is crucial for the reaction, since the chloride anions of the liberated HCl would undergo a nucleophilic attack of the silyl group. Generally, the AgOTf assists the elimination process by drastically shorting the reaction time. **53** is volatile *in vacuo* and was separated from the reaction mixture by collecting it as toluene solution with a cooling trap. Isolated **53** is unstable at room temperature and usually stored as toluene solution at low temperatures (T = -80 °C).
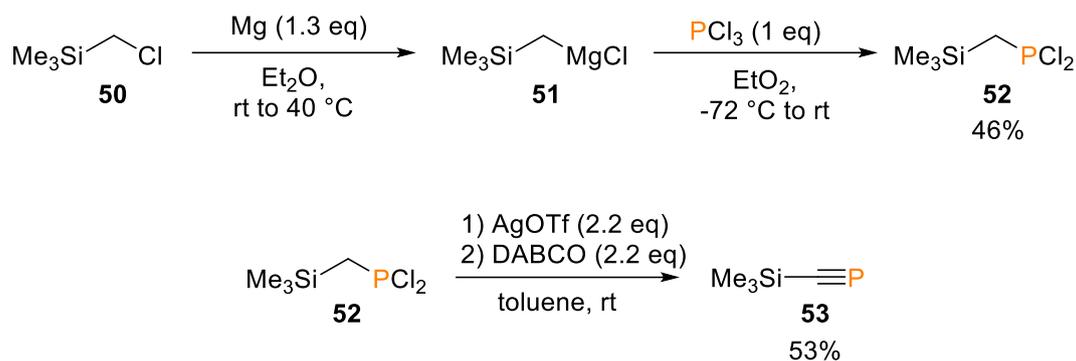
Scheme 33. Reaction sequence for the formation of trimethylsilylphosphaalkyne (**53**).

The literature known triphenylsilylphosphaalkyne[37] (**58**) was synthesized analogously to **53**, however the reaction sequence starts with a Grignard reaction from the trichloro(chloromethyl)silane (Scheme 34). Isolation of the solid product **58** results in fast decomposition. As **53** it should be stored as toluene solution at low temperatures.
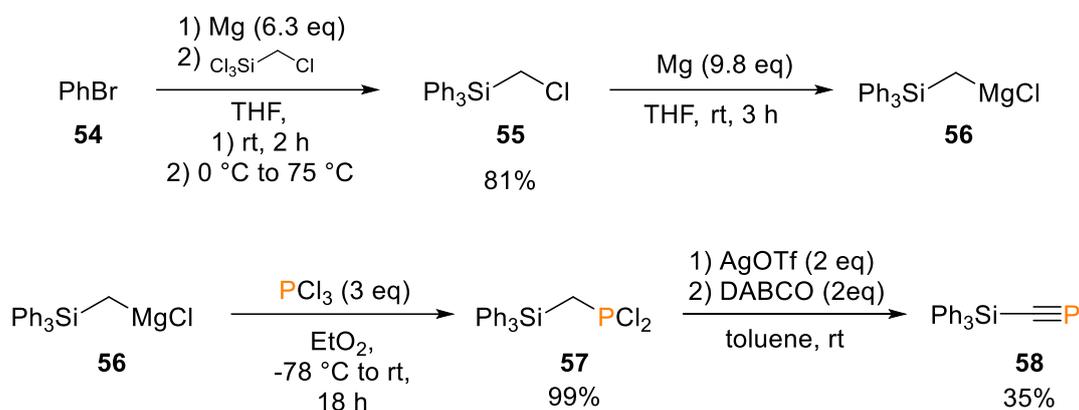

Scheme 34. Reaction sequence for the formation of triphenylsilylphosphaalkyne (**58**).

The tritylphosphaalkyne[80] (**59**, Figure 33) was provided by the group of GRÜTZMACHER. The preparation is analogously to **58**, except for the final step. The HCl elimination in (2,2,2-triphenylethyl)phosphonous dichloride[350] is carried out with an excess of DABCO (10 eq) in acetonitrile at $T = 75$ °C without the addition of AgOTf in 4 h. Based on the gained knowledge of similar reactions, a significant decrease of the reaction time even under milder reaction condition is expected by applying AgOTf, however this was not evaluated by GRÜTZMACHER and co-workers. **59** can be isolated as colorless solid in around 40% yields and is surprisingly stable towards oxidation even in solution.

2.1.2.3.2 Synthesis of supermesitylphosphaalkyne

Supermesitylphosphaalkyne[79] (**76**) was prepared according to the literature following the typical hexamethyldisiloxane elimination route (1.3.3, Scheme 2d). In the first step, 1,3,5-tri-*tert*-butylbenzene (supermesitylene, **72**, Scheme 35) was brominated to **73**. The bromine atom

was exchanged with lithium by addition of *n*-butyllithium and consequently substituted with CO_2 by addition of dry ice. Hydrogenation of the 2,4,6-tri-*tert*-butylbenzoate intermediate yielded the carboxylic acid **74**, which was converted to the acid chloride **75** by addition of thionyl chloride. Treating the precursor **75** with $LiP(SiMe_3)_2$ resulted the supermesitylphosphaalkyne (**76**), which was isolated in moderate yields by column chromatography. **76** is kinetically stable and can be stored as a solid at room temperature. Similar to tritylphosphaalkyne (**58**), supermesitylphosphaalkyne can be even handled under air for a limited time.
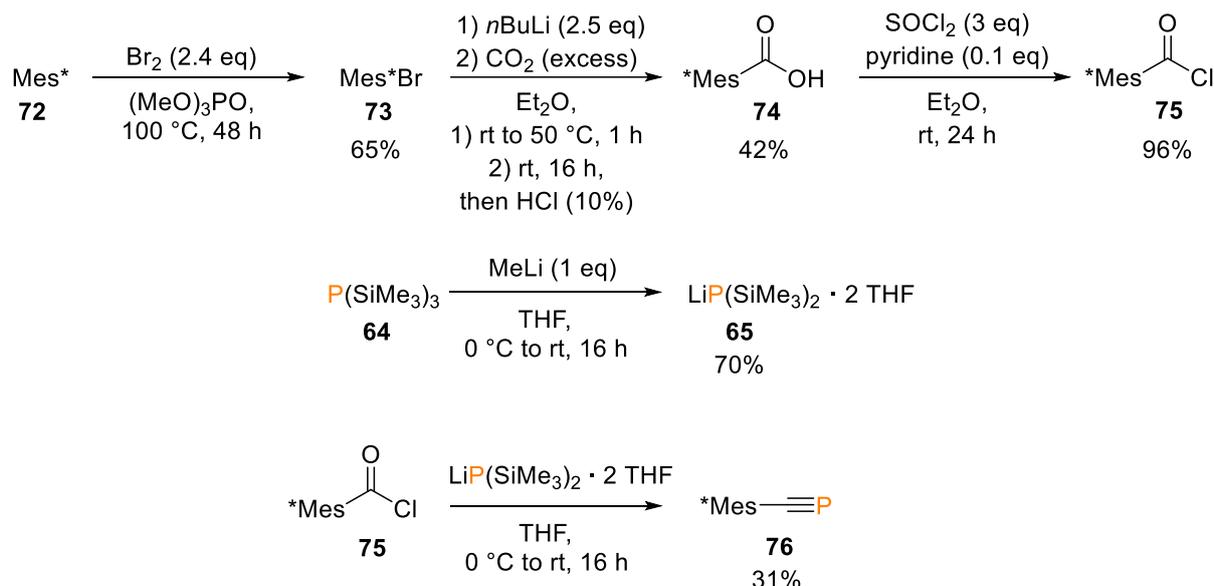

Scheme 35. Reaction sequence for the formation of supermesitylphosphaalkyne (**76**).

2.1.2.3.3 Synthesis of mesitylphosphaalkyne

A nearly identical reaction route should also lead to the mesitylphosphaalkyne[351] (**68**, Scheme 36). The mesityl acid chloride (**63**) was prepared analogously to the reaction sequence for supermesitylphosphaalkyne (**76**). The low yield for the chlorination of the carboxylic acid **62** is unusual and the reason unclear. In the next step, $P(SiMe_3)_2$ or $LiP(SiMe_3)_2$ was added to the acid chloride **63**. Surprisingly, the reaction did not lead directly to the desired phosphaalkyne **68**, as it worked for the supermesityl derivative. Instead the reaction stopped at the stage of the (*E,Z*)-[mesityl(trimethylsiloxy)methylene]trimethylsilylphosphine (**66**), as it is described for the adamantylphosphaalkyne.[78] Generally, both reactions work similarly, however $LiP(SiMe_3)_2$ reacted much faster and provides higher yields according to ^{31}P NMR spectroscopy. Typically, the ratio between *E*-isomer ($\delta(^{31}P)$ = 126.3 ppm) and the *Z*-isomer ($\delta(^{31}P)$ = 122.4 ppm) is around 3:2. Theoretically, this intermediate can be converted to the phosphaalkyne **68** by catalysis with NaOH,[351] as it is demonstrated for *tert*-butyl- and adamantylphosphaalkyne.[30, 78] However, in case of **68** it is described as not reproducible. In fact, several attempts to get **68** by this method failed. Instead, the procedure reported by REGITZ and co-workers using

aluminum trichloride was applied, because it is outlined as "absolutely reliable".[351] Unexpectedly, the isolation of (E/Z)-**66** by bulb-to-bulb distillation did not work as described and mostly resulted in decomposition of the starting material. In the end, the reaction with aluminum trichloride was performed with the crude product of (E/Z)-**66**. However, even several attempts did not provide any product signals according to the $^{31}P\{^1H\}$ NMR spectrum, thus another method for the synthesis of mesitylphosphaalkyne (**68**) was established.
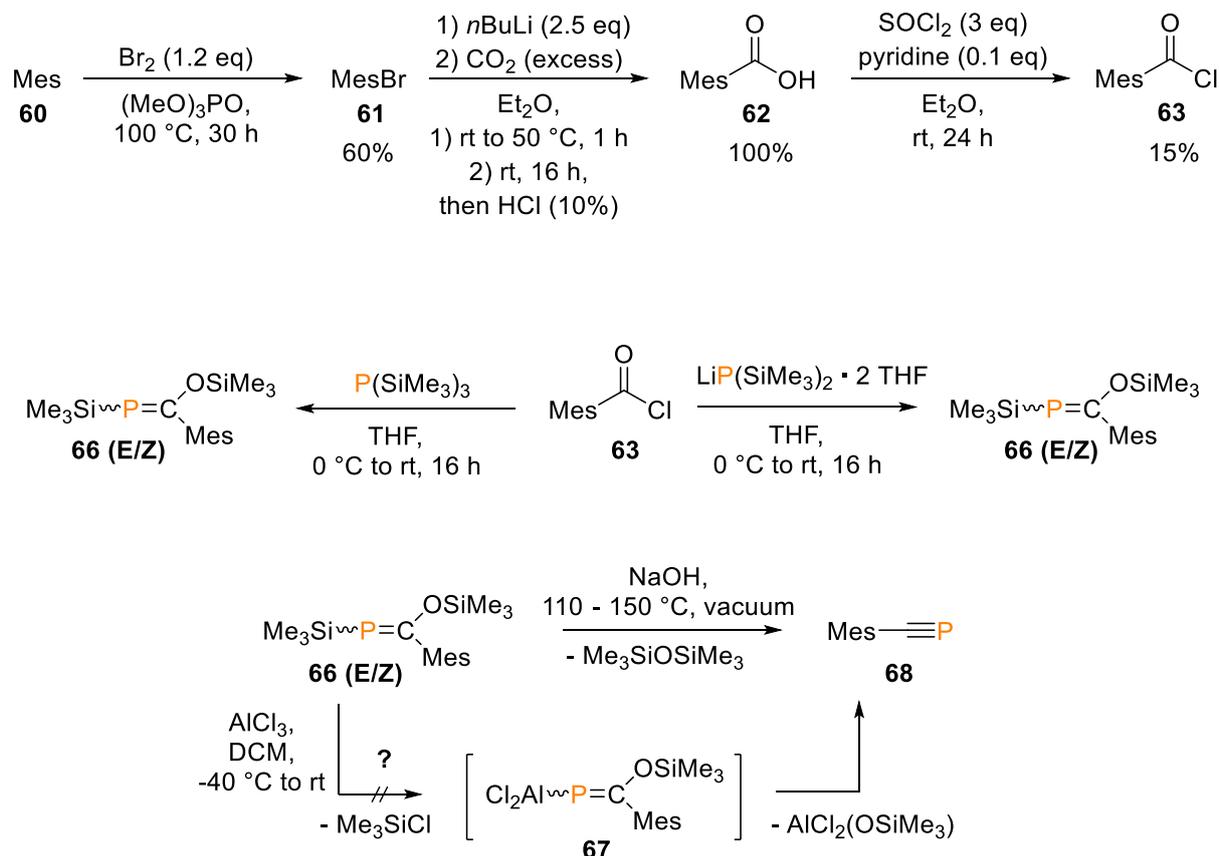
**Scheme 36.** Literature known reaction sequence towards mesitylphosphaalkyne (**68**).

Inspired by the ease of the synthesis of trimethylsilylphosphaalkyne (**53**) by RUSSEL via Grignard reaction and HCl elimination (Scheme 33),[77] a similar approach was started. First, mesitylene (**60**) was chloromethylated via Blanc reaction[352] to the (chloromethyl)mesitylene (**69**, Scheme 38).[353] Multiple chloromethylations of the mesitylene was observed. Overnight reaction at room temperature mainly yielded the di-substituted product, 1,3-di(chloromethyl)mesitylene, together with **69** and even traces of 1,3,5-tri(chloromethyl)mesitylene (**98**). Although the products could clearly be distinguished by thin-layer chromatography with pure hexane, the separation of the mono- and di-substituted products by column chromatography failed. Adjusting the reaction temperature and time resulted in up to 95% yield of **69** and only traces of the di-substituted by-product, which could be removed by quick recrystallization from pentane by temporary cooling with liquid nitrogen. In the first attempt, the dichloro((mesityl)methyl)phosphine (**71**) should be received by Grignard

reaction as demonstrated for the dichloro((trimethylsilyl)methyl)phosphine (**52**). This reaction was unsuccessful even at low temperatures (T = -72 °C), which generally improved the selectivity. However, a literature known synthesis for benzyldichlorophosphine (Scheme 37) showed a highly increase selectivity by transmetalation of the Grignard compound to the organozinc compound.[354] This effect can be explained by the decreased electronegativity difference between the metal and the carbon ($\Delta EN(MgC)$ = 1.24, $\Delta EN(ZnC)$ = 0.90).[355]

$$Ph\diagup MgCl \xrightarrow[\text{EtO}_2, \, 0\,°C]{\text{ZnCl}_2} Ph\diagup ZnBr \xrightarrow[\text{EtO}_2, \, 40\,°C]{\text{PCl}_3} Ph\diagup PCl_2$$
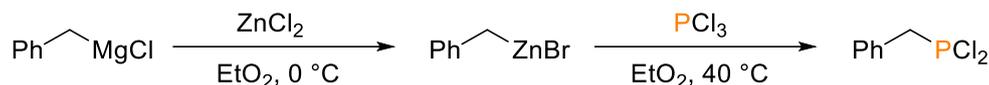
Scheme 37. Synthesis of benzyldichlorophosphine by transmetalation of the Grignard compound to the more selective organozinc compound.

Contrary to the literature, the transmetalation step can be omitted if the elemental zinc has an active surface (free of an oxidized layer). The activation of zinc was realized by sonication in an ultrasonic bath for several hours.[356] Dropwise addition of (chloromethyl)mesitylene (**69**) to the zinc suspension at T = 10 °C mostly gave the organozinc compound **70**. Next to the mesitylmethyl chloride (**70**, MesCH$_2$-ZnCl), additional di(mesitylmethyl) zinc ((Mes-CH$_2$)$_2$-Zn), traces of the homo-coupling product Mes-CH$_2$CH$_2$-Mes and the DME-zinc complex [ZnCl$_2$(DME)]$_2$[357] were found, even under optimized conditions. While the presence of (Mes-CH$_2$)$_2$-Zn can be neglected because it should react the same way as **70**, the unreactive homo-coupling product must be avoided by evading higher reaction temperatures. In the next step, the organozinc compound **70** was added dropwise to an excess of phosphorus trichloride to avoid multiple substitution reactions on the phosphorus atom. Finally, HCl was eliminated from **71** by addition of AgOTf and the base DABCO at room temperature within an hour. Filtration of the resulting brownish suspension through diatomaceous earth and purification by column chromatography with pentane as eluent resulted the mesitylphosphaalkyne (**68**), typically in yields higher than 50%. **68** is a light and moderately temperature sensitive colorless oil and should be stored at T = -20 °C in the absence of light. The decomposition can be minimized by dissolving in toluene. Nevertheless, light of short wavelengths will inevitably lead to polymerization/decomposition under formation of black particles. The particles are insoluble in typical laboratory solvents, cannot be removed by filtration thought diatomaceous earth and were not further characterized. Generally, the elimination step also works without the AgOTf as additive, however a large excess of DABCO is needed for a complete reaction in reasonable time. With an excess of twelve equivalents of DABCO the reaction took six days to complete at room temperature. That was not practical due to the extended time, the struggle to fully remove the excess of DABCO and the drastically reduced yield of **68**, probably caused by the already proceeding decomposition.
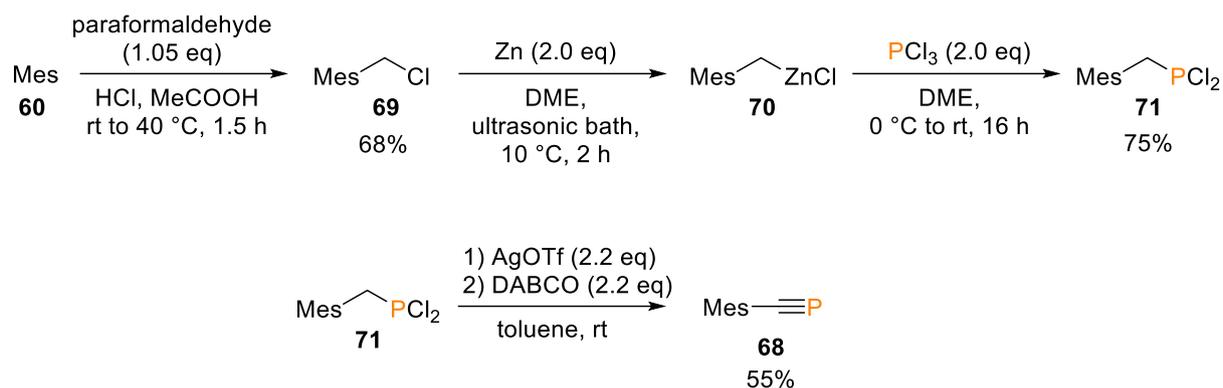
Scheme 38. Reaction sequence for the formation of mesitylphosphaalkyne (**68**).

Although mesitylphosphaalkyne (**68**) is literature known, there was no molecular structure in a single crystal published. With a melting point of $T = 10.5\,°C$, it could be crystallized from an acetonitrile solution (0.25 M) at $T = -30\,°C$. The bond length and angles of the molecular structure in the crystal (Figure 34) are nearly identical to supermesitylphosphaalkyne, which was only crystallized and characterized for comparison reasons. The C≡P bond length is 1.545 Å (1.549 Å for Mes*CP) and the C-C-P angle is 180° as expected.
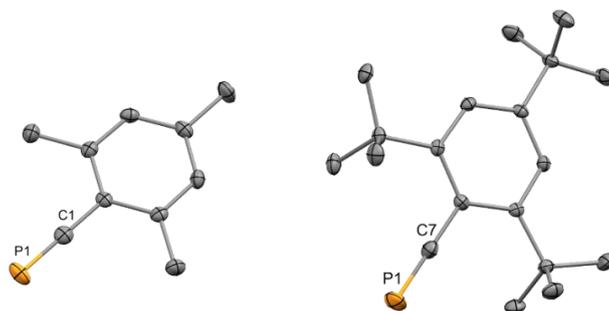
Figure 34. Molecular structure of **68** (left) and **76** (right) in the crystal. Anisotropic displacement ellipsoids are shown at 50% probability level. Hydrogens omitted for clarity.

68 should be suitable for reaction in most common solvents. It was successfully applied in reactions with pentane, benzene, toluene, diethyl ether, DME, diglyme, THF, dioxane, DCM and acetonitrile as solvent, therefore, it should be 'stable' within its general properties in alkanes, arenes, ethers, organohalides and nitriles. Its 'stability' was experimental qualified for a selection of representative solvent species by ^{1}H and ^{31}P{^{1}H} NMR measurements at room temperature for one week. The NMR chemical shifts are only marginal affected by the solvent. The results are summarized in Table 4.

Table 4. ^{1}H (400 MHz) and ^{31}P{^{1}H} (162 MHz) NMR signals for MesCP (**68**) in different solvents. All signals are singlets and given in ppm.

solvent	^{1}H (Ar-H)	^{1}H (*ortho*-CH$_3$)	^{1}H (*para*-CH$_3$)	^{31}P{^{1}H} (C≡P)
benzene	6.57	2.40	1.98	2.02
THF	6.88	2.44	2.25	0.45
DCM	6.87	2.46	2.27	1.44
MeCN	6.90	2.43	2.25	1.34

2.1.2.3.4 Synthesis of 2,4,6-tri(isopropyl)phenylphosphaalkyne

Several examples have demonstrated that mesitylphosphaalkyne (**68**) and supermesitylphosphaalkyne (**76**) show different reactivities and coordination behavior toward metal complexes. For instance, two molecules of **68** undergo a cycloaddition reaction and coordination on [W(CO)$_5$THF], while **76** exclusively builds a π-coordination complex. [126, 133-134] Certainly, this behavior is caused by the enormous steric demand of **76**, which can even lead to the usually unfavorable σ-coordination via the lone pair of the phosphorus atom.[143] With respect to the steric demand and the effect of the electron donation properties, it would be useful to complete the substitution row from Me to ^{t}Bu with a ^{i}Pr derivative. Therefore, the 2,4,6-tri(isopropyl)phenylphosphaalkyne (**81**, Scheme 39) was synthesized. At the date this reaction was carried out, the alternative reaction route for **81** found in the literature was not published.[185] Hence, this reaction is an adaption of the reaction sequence for **68** with optimized reaction conditions. **78** was synthesized from 1,3,5-triisopropylbenzene by Blanc reaction. This time multiple chloromethylations were not observed therefore an excess of paraformaldehyde and elevated temperatures could be used. The organozinc compound **79** was only formed at higher reaction temperatures with a small share of 1,3,5-triisopropyl-2-methylbenzene and the homo-coupling compound 1,2-bis(2,4,6-triisopropylphenyl)ethane as by-product. The dichlorophosphine species **80** was again generated by addition of **79** to phosphorus trichloride. Based on prior investigations, the final elimination step of two HCl with AgOTf and DABCO needed elevated temperature and a small reaction scale, to yield reasonable amount of **81**. After filtration of the reaction mixture, the isolated crude product was purified by column chromatography and subsequent fractional distillation. **81** is highly light sensitive and was stored at T = -20 °C in the darkness, to avoid precipitation of a green solid within several minutes.
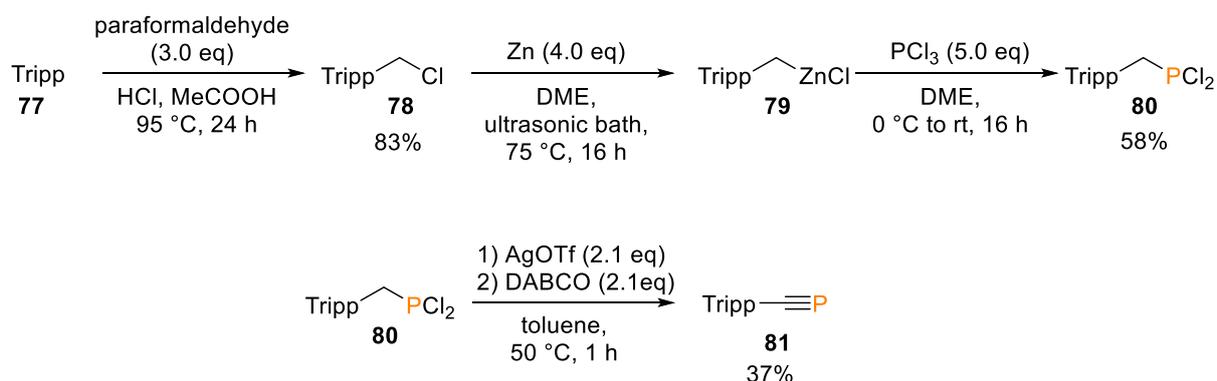
Scheme 39. Reaction sequence for the formation of 2,4,6-tri(isopropyl)phenylphosphaalkyne (**81**).

During the optimization for the reaction conditions of **81**,[358] the influence of temperature, concentration and strength of the base as well as the polarity of the solvent was analyzed to identify the elimination mechanism (E1 vs E2). The interrelationship between E1 and E2 mechanism and their competing S$_N$1 and S$_N$2 reactions were extensively studied by INGOLD

and HUGHES.[359] Four parameters have the most impact on the two elimination types. The base concentration and strength generally favor bimolecular reaction, leading to an enhancement of E2. Increasing the solvent polarity favors unimolecular reactions by stabilization of the cation intermediate. Elevated temperature improves both reactions, however E1 can exclusively be improved by the reaction temperature. As a result, exclusive temperature dependence should be an indication for E1, whereas additional dependence of the base strength should point out an E2 mechanism. Table 5 summarizes the performed reactions.

Table 5. Reaction conditions for the investigation of the elimination step for the synthesis of **81**. Except of the reaction at $T = 50$ °C (1 h) the reaction time was 16 h. The reactions were performed with 50 mg of **80** or less in the case of AgOTf additive.

	KHMDS (2 eq)	LDA (2 eq)	DBU (2 eq)	DABCO (10 eq)	DABCO, AgOTf (2.1 eq)
50 °C					toluene
20 °C	toluene, MeCN	toluene	toluene	MeCN	MeCN
-20 °C			MeCN		toluene

The products were not isolated and the validation mainly conducted via ^{31}P NMR spectroscopy. The strongest non-nucleophilic bases KHMDS and LDA did not yield any product, however, DBU and DABCO did. The reaction with DBU, a base of moderate strength, also showed several by-products. The selectivity could not be improved by lowering the reaction temperature and the use of acetonitrile as solvent to stabilize the expected protonated DBU species. Instead, no product formation was observed and even more by-products were found. DABCO showed the best selectivity with two resonances in the ^{31}P spectrum, one for the product **81** ($\delta = 3.8$ ppm) and another at $\delta = 28$ ppm. Under the assumption that the signal at $\delta(^{31}P) = 28$ ppm corresponds to an intermediate, the reaction mixture was heated to $T = 75$ °C for 2 h. The signal at $\delta(^{31}P) = 28$ ppm stayed unchanged, whereas the product signal completely vanished and many unspecific signals occurred. Presumably, **81** is not stable at higher temperatures in the presence of chloride ions and excess of DABCO. An addition of AgOTf seemed to prevent this. Certainly, the selectivity increases with declining basicity, indicating a E1 mechanism by excluding E2. To verify this assumption, the temperature dependency was analyzed. At $T = 50$ °C 53% of crude product **81** could be isolated, whereas a reaction at $T = -20$ °C only yielded 14% of **81** after 16 h. Additional ^{1}H NMR data showed that in both cases 1,3,5-triisopropyl-2-methylbenzene emerged as primary by-product (15% at $T = 50$ °C, 30% at $T = -20$ °C). It is for sure, that increased temperatures improve both, yield and selectivity. Finally, the impact of the polarity was evaluated by the usage of acetonitrile instead of toluene as solvent. Normally a polar solvent should stabilize the ionic intermediate (carbocation) of an E1 mechanism, even though polar solvents are generally unfavorable for eliminations. The reaction with acetonitrile at room temperature did not yield any significant

amount of **81** according to the ^{31}P NMR data. However, the isolated yield could not be specified due to substantial elemental silver residue in the sample. The silver could not completely be removed by filtration, probably due to complexation of the silver with the acetonitrile. Even though most facts suggest an E1 mechanism, the negative impact of the basicity is inconclusive, because in principle it should not affect the E1 mechanism, and cannot be explained.

2.1.2.3.5 Synthesis of 3,5-di-(*tert*-butyl)phenylphosphaalkyne

The 3,5-di-(*tert*-butyl)phenylphosphaalkyne (**86**, Mdtbp-CP, Figure 33) with ^{t}Bu groups in *meta* position should provide decent electron donating properties, while being less sterically demanding than typical arylphosphaalkynes. Furthermore, it would show if steric protection of the *ortho* position is needed to obtain a stable arylphosphaalkyne and if it is necessary to avoid *ß*-H-elimination during the C-CP activation process. For the synthesis of **86**, 1,3-di-tert-butyl-5-methylbenzene (**82**) was selected over 1,3-di-tert-butylbenzene as starting material due to the much lower price and its predefined *meta* positioning of the ^{t}Bu groups. Both synthetic pathways, the zinc route and the hexamethyldisiloxane elimination were considered (Scheme 40).
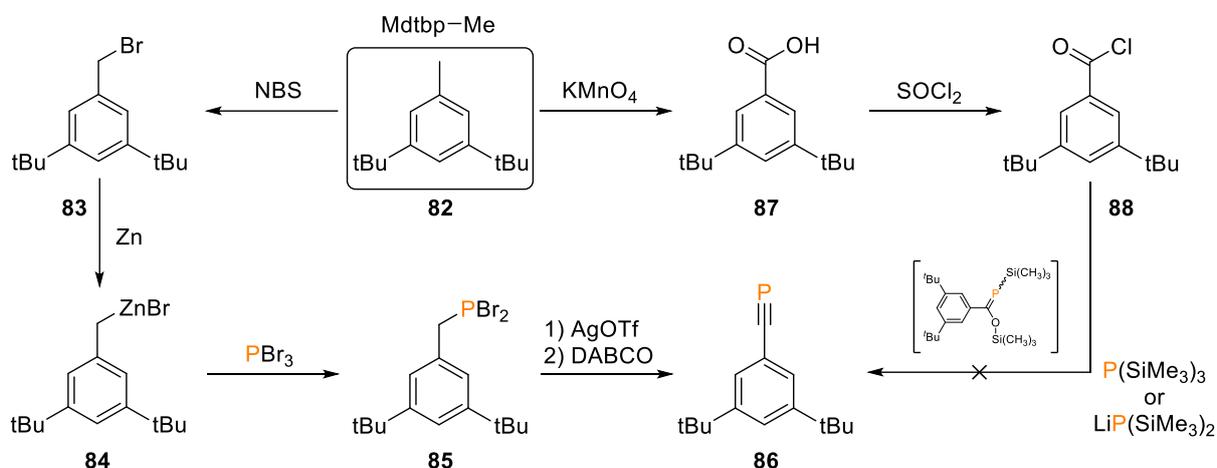
Scheme 40. Planned reaction pathways for the synthesis of **86**.

Except for the oxidation to the carboxylic acid **87**[360-362], the hexamethyldisiloxane elimination route proceeded analogously to the sequence for supermesitylphosphaalkyne (**76**). The final elimination step to receive **86**, however, did not work no matter if P(SiMe$_3$)$_3$ or LiP(SiMe$_3$)$_2$ was used. In the ^{31}P{^{1}H} NMR spectrum a resonance at δ = 123 ppm was found, indicating the generation of [((3,5-di-*tert*-butyl)phenyl)(trimethylsiloxy)methylene]trimethylsilylphosphine as observed in the analog reaction of Mes-CP (**68**). All attempts of basic catalysis to eliminate the hexamethyldisiloxane failed. Thus, it was impossible to obtain **86** by this route.

To follow the zinc route (Scheme 41), **82** was first brominated,[363-365] then the organozinc compound was formed and reacted with phosphorus tribromide to receive **85**. The phosphorus tribromide was used instead of phosphorus trichloride to avoid a mixed halogen product. The 3,5-di-(*tert*-butyl)phenylphosphaalkyne (**86**) could be obtained by double HBr elimination from **85** by addition of AgOTf and DABCO and purification by column chromatography in low yields. **86** is a colorless, probably temperature sensitive product and was stored in the absence of light at T = -20 °C.
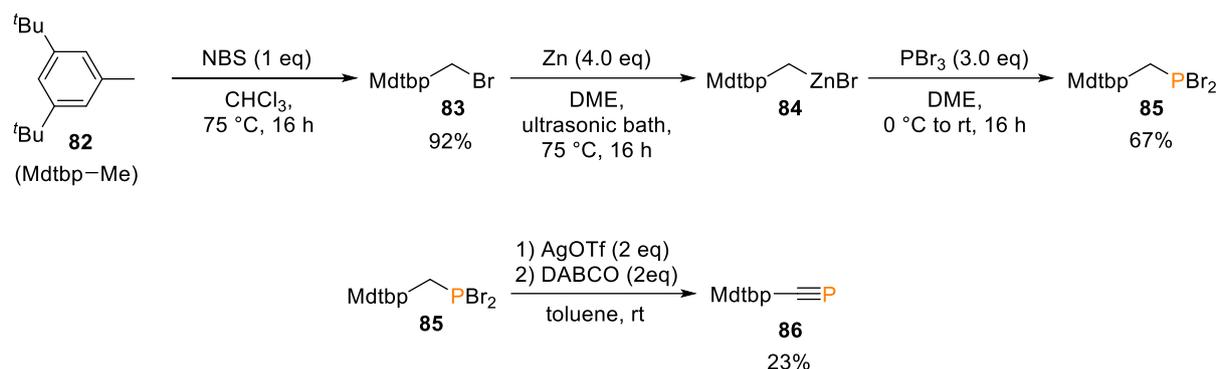
Scheme 41. Reaction sequence for the formation of 3,5-di-(*tert*-butyl)phenylphosphaalkyne (**86**).

2.1.2.3.6 Synthesis of 2,4,6-tris(trifluoromethyl)phenylphosphaalkyne

The 2,4,6-tris(trifluoromethyl)phenylphosphaalkyne (**92**, Ttfmp-CP, Scheme 42) should be synthesized originating from 1,3,5-tris(trifluoromethyl)benzene (**89**) by following the hexamethyldisiloxane elimination route. First, **89** was lithiated with *n*BuLi and then substituted with CO_2 sublimated from dry ice yielding the carboxylic acid **91**.[366] Several attempts with $P(SiMe_3)_3$ and the more reactive $LiP(SiMe_3)_2$ were made to transform **91** to **92** (Table 6).

Table 6. Reaction conditions to transform **91** to **92**.

#	reagent	solvent	conditions
1	$P(SiMe_3)_3$	THF	1) 23 °C, 18 h; 2) 64 °C, 2 h
2	$LiP(SiMe_3)_2$	THF	1) 23 °C, 18 h; 2) 64 °C, 2 h
3	$P(SiMe_3)_3$	toluene	70 °C, 18 h
4	$LiP(SiMe_3)_2$	toluene	1) 70 °C, 18 h; 2) 100 °C, 2 h
5	$LiP(SiMe_3)_2$	toluene	-15 °C, 20 min

Only for the addition of $LiP(SiMe_3)_2$ at low temperatures (#5, Table 6) a new selective resonance at $\delta(^{31}P)$ = 94.5 ppm occurred, which nearly matches with the calculated shift of $\delta(^{31}P)$ = 108.5 ppm The NMR calculation were carried out by Eric Yang of the Goicoechea group at def2-mSVP level of theory, for details see the experimental part. However, all attempts of isolation were unsuccessful. It is presumed that **92** is unstable and decomposes at higher temperatures. Furthermore, it might be volatile and was accidentally removed *in vacuo*. Later

attempts to collect the potential **92** in a cooling trap failed, but might have been afflicted by the overall small reaction scale.
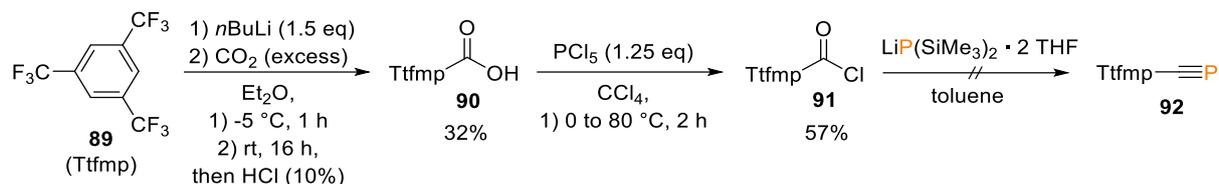
Scheme 42. Reaction sequence for the formation of 2,4,6-tris(trifluoromethyl)phenylphosphaalkyne (**92**).

2.1.2.3.7 Attempted synthesis of di-, triphosphaalkynes

Succeeding with the aryl-mono-phosphaalkynes, the possibility for the synthesis of polyphosphaalkynes was considered to later expand the scope for the preparation of potential polycyaphido complexes. First, the diphosphaalkyne **97** (1,4-bis(phosphaethynyl)durene) should be prepared, starting from 1,2,4,5-tetramethylbenzene (**93**, durene, Scheme 43) following the zinc route, successfully applied to arylphosphaalkynes. The methyl groups in *ortho* (and *meta*) position should be adequate to stabilize the resulting diphosphaalkyne as previously shown for MesCP (**68**). Again, the Blanc reaction successfully provides the chloromethylated product **94**, showing two singlet resonances at $\delta = 4.28$ ppm for the methylene bridges and at $\delta = 1.99$ ppm for the four methyl groups in the ^{1}H NMR spectrum. After addition of **94** to the activated Zn powder, only the signal of the methylene bridges shifted to $\delta(^1\text{H}) = 3.06$ ppm, which is in line with the previously synthesized organozinc compounds and matches the expectations for **95**. However, several reactions with phosphorus trichloride and tribromide failed. Thus, another method described by KNOCHEL *et al.* to avoid aggregation of organozinc compounds was applied but furnished the same result.[367] A classical Grignard reaction was also ineffective. All products were titrated against an iodine-THF solution but were not able to discolor the solution, which indicated the absence of any Grignard compound. The formation of a polymerization product is not plausible, due to the sharp ^{1}H NMR signals. Instead the formation of the homo-coupling product, the methylated [2.2]paracyclophane (**95a**, Scheme 43), is more likely and the ^{1}H signals matches with the only published spectrum for **95a**.[368] Even this reaction did not lead to the synthesis of a diphosphaalkyne, it might be a much shorter and better yielding route towards [2.2]paracyclophanes compared to the published six-step, low yielding route.
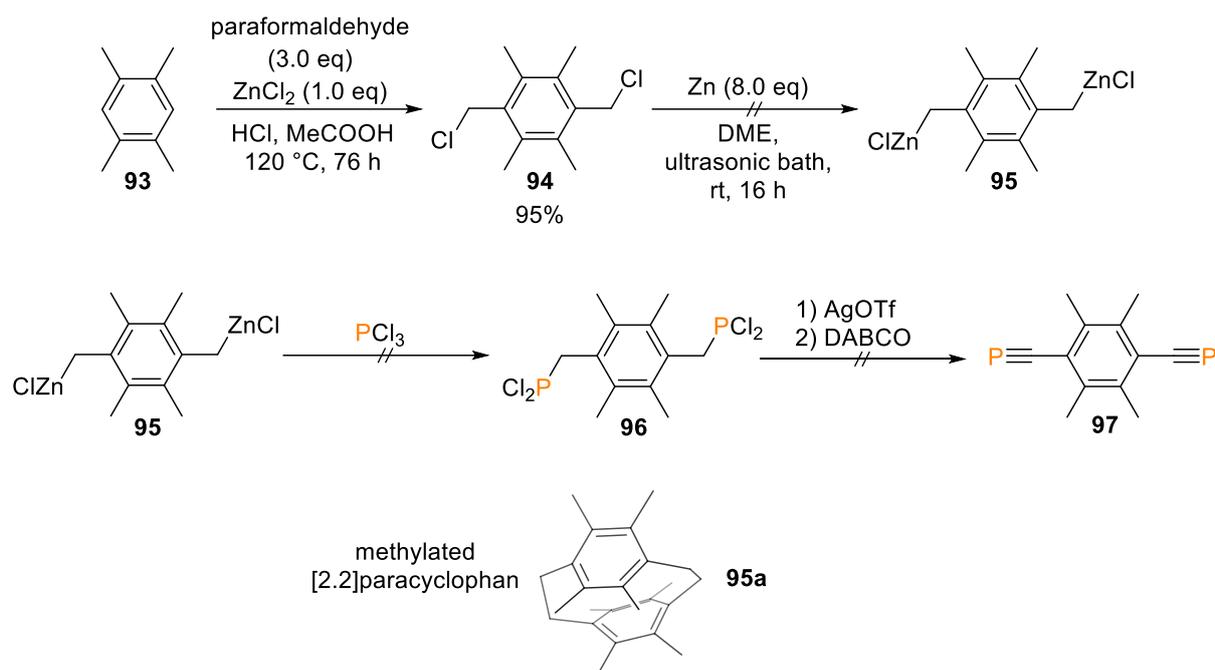
Scheme 43. Planned reaction sequence for the synthesis of 1,4-bis(phosphaethynyl)durene (**97**) and proposed product **95a** from reaction of **94** with elemental zinc.

A further attempt towards the triphosphaalkyne **105** (1,3,5-tris(phosphaethynyl)mesitylene) started from mesitylene (**60**, **Scheme 44**). Already previously seeing the tendency of multiple chloromethylation on **60**, the conversion to **98** by applying the Blanc protocol was straightforward and could be confirmed by single crystal diffraction (Figure 35). A aliquot portion of **98** was converted to the iodide analog **99** via Finkelstein reaction.[369] Both **98** and **99** were reacted with activated zinc or magnesium to obtain the corresponding organometallic compound. The reaction mixture was directly added to the phosphorus trichloride without purification or analysis. However, only in the reaction of **103** with PCl₃, promising ^{31}P NMR resonances at $\delta = 183.0$ and 182.9 ppm, which match the calculated value of $\delta(^{31}P) = 184.5$ ppm, could be monitored. The attempted isolation of the compounds, showing those signals, by column chromatography was unsuccessful.
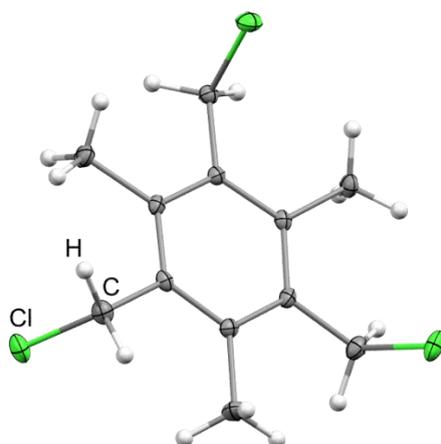
Figure 35. Molecular structure of **98** in the crystal is already literature known but was remeasured to prove the precursor identity for the intended synthesis of **97**. Anisotropic displacement ellipsoids are shown at 50% probability level. Hydrogens omitted for clarity.

Overall, the synthesis of polyphosphaalkynes by the zinc route failed at the step of the generation of the organozinc compound, even under harsh reaction conditions. Consequently, the hexamethyldisiloxane elimination route from the carboxylic acid stays the means of choice for the preparation of diphosphaalkynes as demonstrated by CAMERON[104-105] with two isolated diphosphaalkynes and CROSSLEY[370-371] with temporary *in situ* generated diphosphaalkynes.
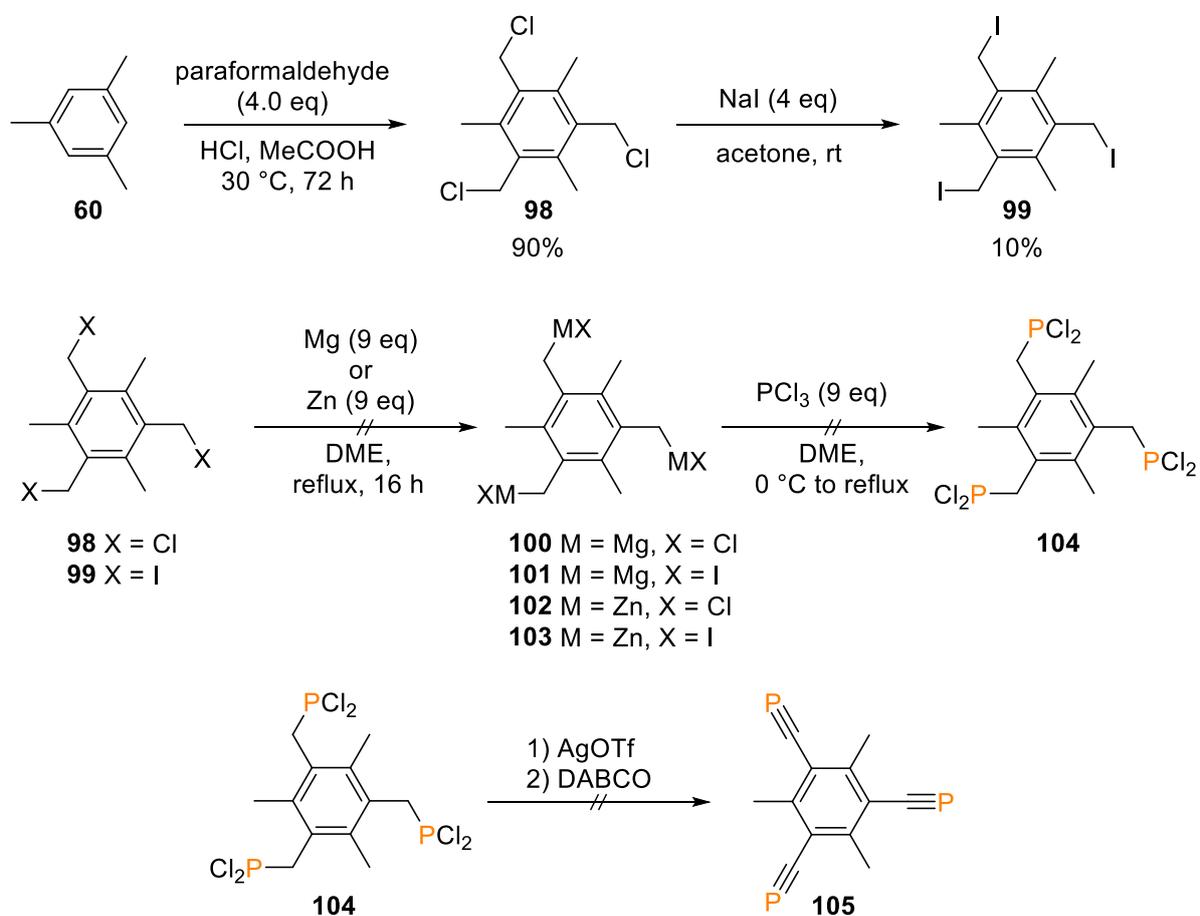
Scheme 44. Planned reaction sequence for the synthesis of the 1,3,5-tris(phosphaethynyl)mesitylene (**105**).

Table 7. NMR ^{31}P signals of phosphaalkynes used for the synthesis of phosphaalkyne complexes.

number	compound	^{31}P NMR [ppm]
53	Me$_3$SiC≡P	96.2
58	Ph$_3$SiC≡P	112.4
59	Ph$_3$CC≡P	-49.2
68	MesC≡P	1.5
81	TrippC≡P	3.8
86	MtbpC≡P	-36.3
76	Mes*C≡P	34.5

2.1.2.3.8 Electronic structure assay

For a deeper insight, all scheduled phosphaalkynes were analyzed by means of quantum chemistry, especially in terms of their electronic properties. To get some reliable references the well-studied HCP, MeCP and PhCP were included in the calculations. The geometry optimizations were realized with the PBEh-3c method, which offered a good correlation of bond distances and angles compared to the corresponding structurally characterized phosphaalkynes. The found bond lengths of the phosphaalkynes C≡P triple bonds are summarized in comparison with their associated literature values in Table 8. The calculated values for HCP and MeCP are a bit overestimated, whereas the larger arylphosphaalkynes are very close to the experimental data.

Table 8. Calculated C≡P distances of the synthesized and scheduled phosphaalkynes (PBEh-3c method) with their associated literature values. ^{a} value for all CP bonds in the molecule, ^{e} experimental values, $^{e'}$ experimental value of **58** σ-coordinated to a Ru complex, ^{c} calculated value. MdtbpCP (**86**) = 3,5-di-(*tert*-butyl)phenylphosphaalkyne, TtfmpCP (**92**) = 2,4,6-tris(trifluoromethyl)phenylphosphaalkyne, durene(CP)$_2$ (**97**) = 1,2-bis(phosphaethynyl)-durene, Mes^t(CP)$_3$ (**105**) = 1,3,5-tris(phosphaethynyl)mesitylene.

molecule	C≡P bond length [Å]	literature value [Å]
HCP	1.529	1.542^e [195]
MeCP	1.535	1.544^e [58]
PhCP	1.539	1.516^c [111]
MesCP (68)	1.541	1.545^e [372]
TrippCP (81)	1.543	-
Mes*CP (76)	1.544	1.516^e [164]
MdtbpCP (86)	1.539	-
TtfmpCP (92)	1.533	-
Me$_3$SiCP (53)	1.540	1.525^c [116]
Ph$_3$SiCP (58)	1.539	1.530$^{e'}$ [37]
TritylCP (59)	1.536	1.538^e [80]
durene(CP)$_2$ (97)	1.541^a	-
Mes^t(CP)$_3$ (105)	1.540^a	-

The molecular orbitals were calculated for the optimized structures using the B3LYP functional with the def2-TZVP basis set and the def2/J auxiliary basis set. First, the energetic levels of the HOMOs and LUMOs of HCP, MeCP, PhCP and MesCP (**68**) are evaluated towards the

influence of the aromatic benzene ring for a subsequent comparison to their nitrile and acetylene analogs (Figure 36). The HOMO energies continuously raise from HCP to MesCP with a bigger step of 1.87 eV between MeCP and PhCP. The LUMO energies do not show a clear trend but are decreased for the aryl systems. The HOMO-LUMO gaps shrink from HCP to MesCP in correlation with the raised HOMO levels, making the arylphosphaalkynes to a better π-donor and slightly better π-acceptor. The lone pair at the phosphorus atom is always significantly below the HOMO with the tendency to slightly rise in energy along the series from HCP to MesCP, while the energy gap between the lone pair and HOMO increases from 1.98 eV for HCP to 2.98 eV for MesCP, making the arylphosphaalkynes also a better σ-donor. Due to the much higher energy level of the HOMO, a reaction via the π-system will always be highly preferable over a σ-bonding.
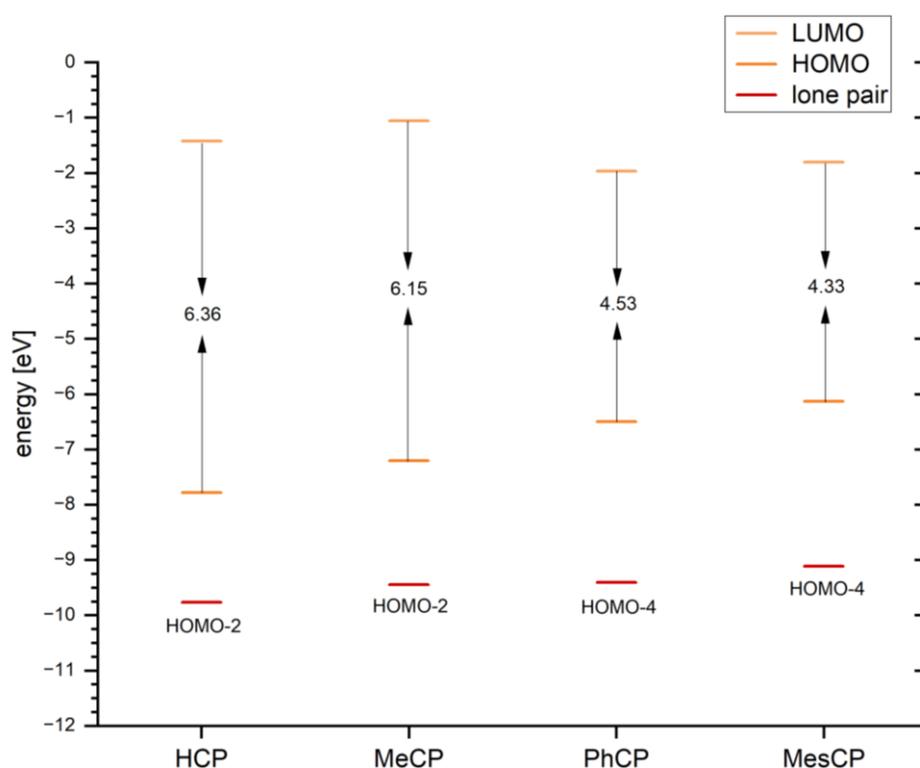
Figure 36. Calculated HOMO and LUMO energy levels as well as the phosphorus lone pairs for selected phosphaalkynes.

To analyze the differences between the C≡CH, C≡N and C≡P groups, phenylacetylene, benzonitrile and phenylphosphaalkyne were compared. These molecules are fast to be calculated, possess an aromatic benzene ring such as the relevant arylphosphaalkynes for the scheduled activation and all atoms share one joint plane, which makes those systems convenient to visualize in a 2D picture. The Laplacian of the electron density is depicted for all three molecules in Figure 37, illustrating negative charge density between all bonds, which is in line with the covalent character of the bonds.[373] The natural charge of the molecules was evaluated by a natural population analysis (NPA), showing a negative charge between -0.14

and -0.21 for all carbons of the phenyl ring of the three molecules. The charge distribution between the C≡CH, C≡N and C≡P group differ significantly. The carbon atom bound to the phenyl group of the C≡CH unit is nearly neutral (-0.02), whereas the carbon atom of the C≡N unit is positively (0.32) and the carbon atom of C≡P unit is strongly negatively (-0.51) polarized. In consequence, the outer carbon atom (-0.24) of the phenylacetylene and the nitrogen atom (-0.38) of the benzonitrile is negatively charged, whereas the phosphorus atom (0.51) of the phenylphosphaalkyne is positively polarized. These results are typical and in accordance with the electronegativity of nitrogen and phosphorus. The natural bond orbital (NBO) analysis displays a triple bond for each of the three molecules (C≡CH, C≡N, C≡P) with a population of six electrons. All three different triple bonds consist of one σ-bond from sp^x-hybrid orbitals and two regular π-bonds. In the case of phenylphosphaalkyne the bonds are spitted in nearly equal parts between the two carbon atoms. The occupancy of the triple bond of benzonitrile is slightly in favor of the nitrogen atom, which have a share of 57% of the σ-bond and 55% of both π-bonds. The electrons of the nitrogen lone pair are composed of nearly half of the s and the p orbitals of the nitrogen. The C≡P triple bond in the phenylphosphaalkyne is dominated by the carbon with a share of 65% of the σ-bond and 55% of both π-bonds. The σ-bond consists of a $0.81(sp^{0.85})_c + 0.59\ (sp^{2.91})_P$ hybrid composition from carbon and phosphorus, whereas the phosphorus lone pair has mostly s character (76%) and hardly p share (24%).
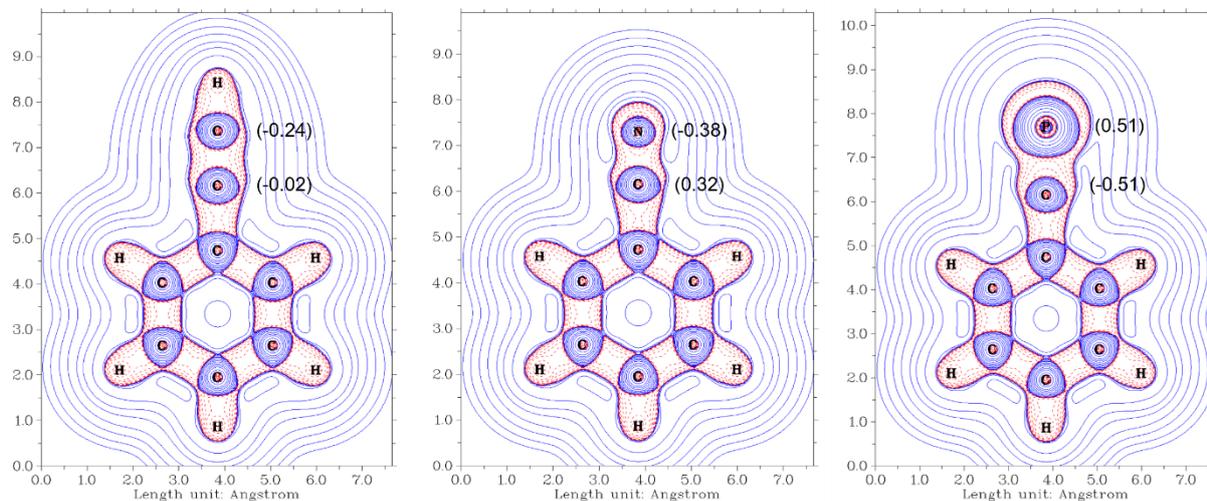

Figure 37. Contour plot of the Laplacian of the electron density in phenylacetylene (left), benzonitrile (middle), phenylphosphaalkyne (right). Positive contour lines are blue and negative contour dashed lines are red. In parentheses are the values for the atomic partial charges received from the natural population analysis (NPA).

The charge transfer and a possible stabilization within each of the three molecules was analyzed by second order perturbation theory analysis. In all three molecules, a stabilization of around 21 kcal·mol^{-1} was found for the aromatic C-C bonds within the phenyl ring. The C≡C triple bond of the phenylacetylene participates with 12.4 kcal/mol to the aromatic system. The C≡N bond of benzonitrile provide an additional stabilization of 7.9 kcal·mol^{-1} to the aromatic system and 9.5 kcal·mol^{-1} to the C_{ipso}-CN bond by the lone pair. The phenylphosphaalkyne

benefits from the 14.0 kcal·mol^{-1} stabilization provided by the CP bond to the aromatic system and 13.6 kcal·mol^{-1} from the lone pair into the C_{ipso}-CP bond. Overall, the electron density is well-distributed in all three molecules, although it is visibly increased at the nitrogen side of the C≡N bond in benzonitrile and decreased in similar fashion at the phosphorus atom of phenylphosphaalkyne (Figure 38), which is in accordance with the previously discussed charges at the nitrogen and phosphorus atom. The electron localization function (ELF) plots illustrate the localization of the electron pairs between atoms, displaying the location of the bonds in the three molecules and the lone pairs at the nitrogen and phosphorus atom (Figure 39). As visible from the plot, the lone pair and the triple bond is more diffuse in the case of the phosphorus atom compared to nitrogen atom.
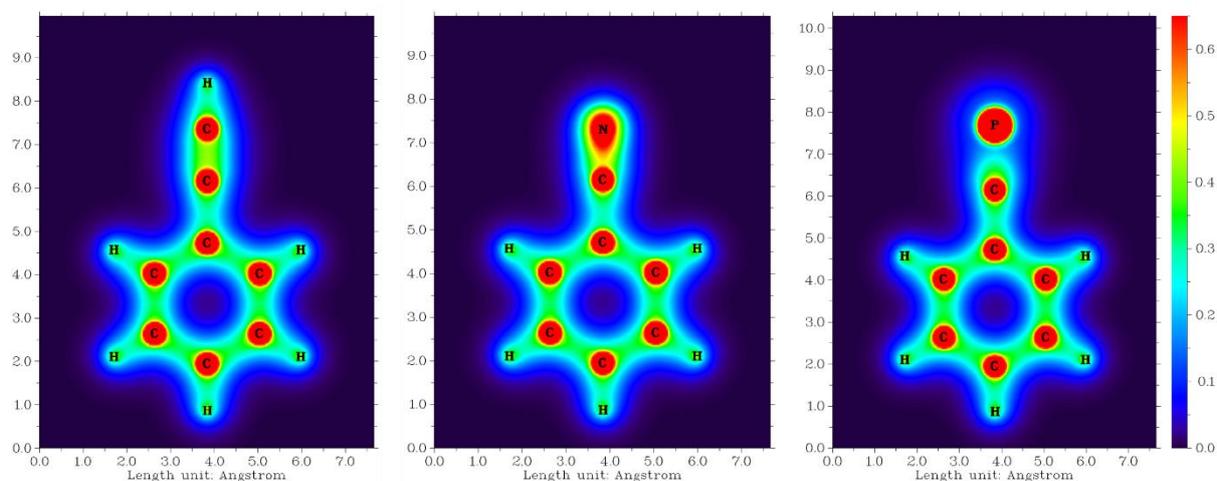

Figure 38. Color filled map of the electron density of phenylacetylene (left), benzonitrile (middle), phenylphosphaalkyne (right).
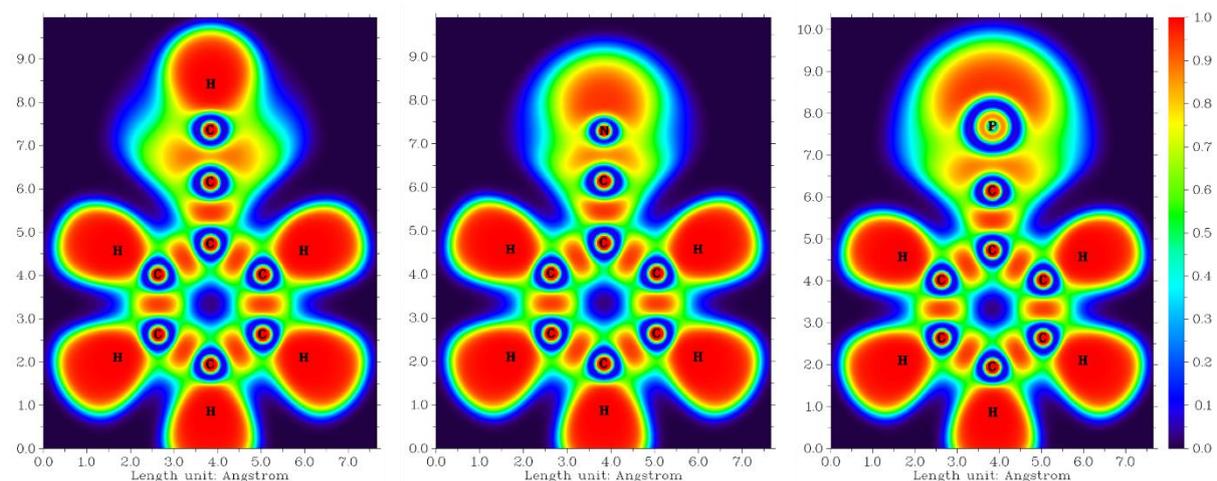

Figure 39. Color filled map of the electron localization function (ELF) of phenylacetylene (left), benzonitrile (middle), phenylphosphaalkyne (right).

Complementary to the bonding situation, the HOMO and LUMO energy levels of all scheduled phosphaalkynes including their acetylene and nitrile derivatives were calculated (Figure 40). Along the whole series the HOMOs of the phosphaalkynes and acetylenes have a similar

energy level, slightly in favor of the phosphaalkynes. Their HOMOs lie noticeable higher in energy than the HOMOs of the nitriles. The energy gap between the phosphaalkyne and nitrile HOMOs is roughly 0.5 to 1.3 eV, except for Ph_3Si derivatives. The energy levels of the LUMOs are decreasing in energy from acetylene, over nitriles to the phosphaalkynes. For the very similar row of Mes, Tripp, Mes* and Mdtbp the energy gaps are approximately 0.5 eV, the other derivatives do not show a clear trend. The HOMOs and LUMOs of the Ttfmp derivatives are the lowest in energy of this series, due to the electron withdrawing *ortho-* and *para*-CF_3 groups. Astonishingly, the HOMO-LUMO energy gaps are nearly identical for the acetylene and nitrile derivatives, whereas the gaps for the phosphaalkynes are significant smaller (Figure 41). The largest energy gap was determined for the Me_3Si and the lowest for the durene derivatives.
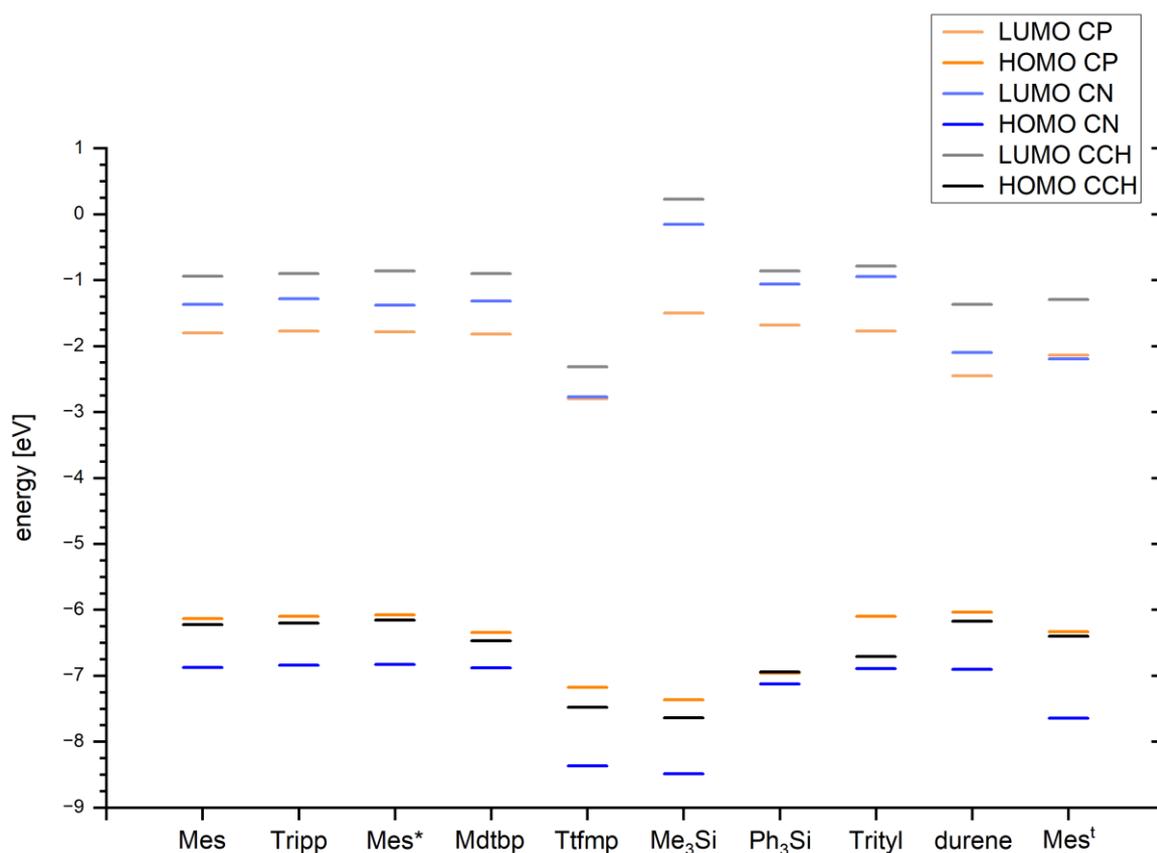

Figure 40. Calculated HOMO and LUMO energy levels for all scheduled phosphaalkynes and their acetylene and nitrile derivatives. The durene derivatives possess two *trans*-units and the Mes[t] derivative three CP units in 1,3,5 position on a regular mesitylene (unit = CCH/CN/CP).
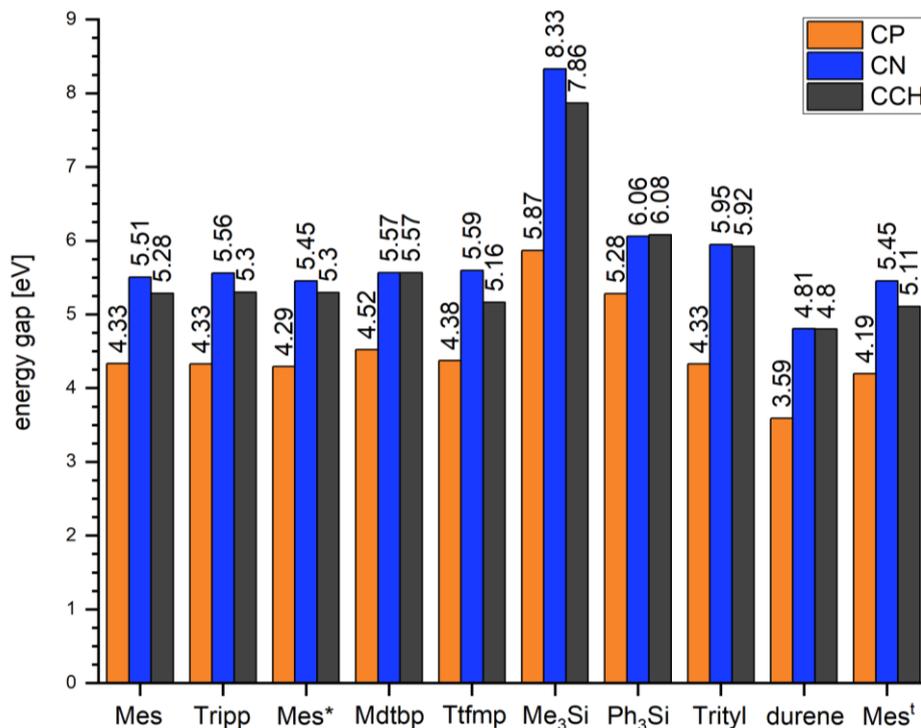
Figure 41. HOMO-LUMO energy gaps of all scheduled phosphaalkynes and their acetylene and nitrile derivatives. The durene derivatives possess two *trans*-units and the Mes^t derivative three units in 1,3,5 position on a regular mesitylene (unit = CCH/CN/CP).

The HOMOs and LUMOs molecular orbitals as well as the lone pair of all presented phosphaalkynes have very similar shape, especially at the C≡P group. As a representative, TrippCP (**81**) is illustrated in Figure 42. The pronounced phosphorus lone pair is represented by the HOMO-12 around 3.4 eV below the HOMO. The HOMO has an energy level of -6.1 eV with a bonding π-orbital at the C≡P unit, whereas the LUMO (-1.8 eV) is around 4.3 eV higher in energy with an antibonding π^*-orbital at the C≡P unit.

LUMO

HOMO
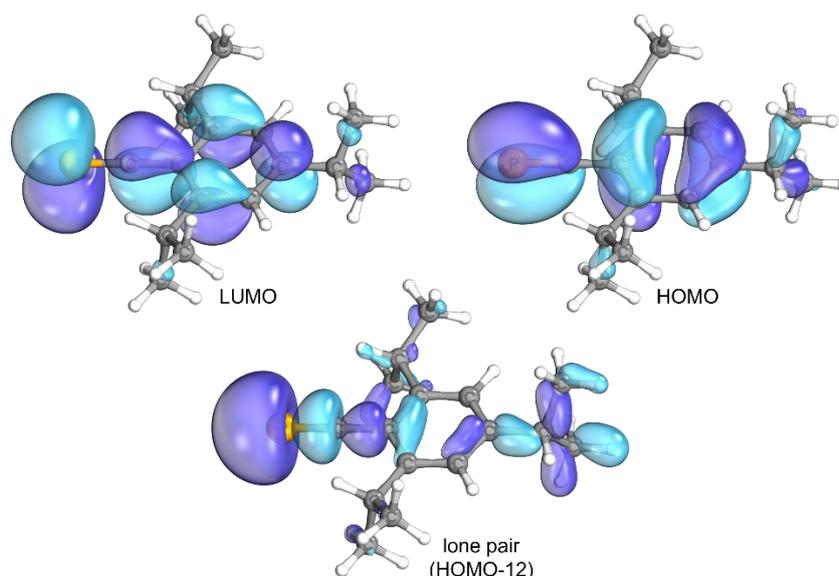
lone pair
(HOMO-12)

Figure 42. Optimized structure and frontier molecular orbitals as well as the molecular orbital of the phosphorus lone pair of TrippCP (**81**).

## 2.1.2.3.9 Reactivity tests of the isolated phosphaalkynes

As described in chapter 1.3.4 phosphaalkynes are predestined for cycloaddition reactions and cyclizations on metals due to the polarization of the C≡P triple bond. A common reaction type is the pericyclic [4+2] cycloaddition with pyrones to generate a phosphinine (Scheme 45), which was found by RÖSCH und REGITZ for the reaction of 2-pyrone with *tert*-butylphosphaalkyne.[178] The functionalization of phosphinines via the pyrone route is limited to the substitution pattern of the reagents. However, MÜLLER and co-workers demonstrated a method to functionalize specific phosphinines after their preparation.[374-375]
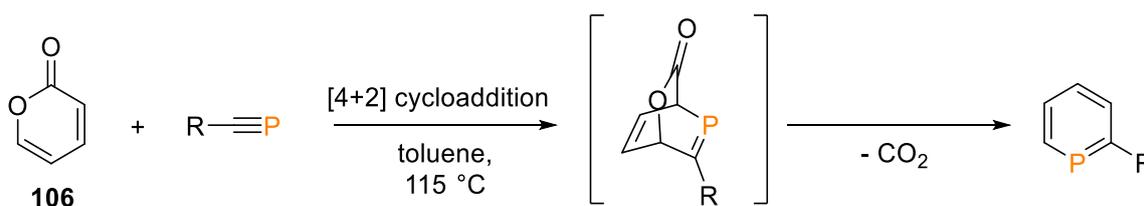
**Scheme 45.** General synthesis of a phosphinine by the pyrone route.

Due to the large steric demand of the ^{t}Bu groups supermesitylphosphaalkyne (**76**) did not react with 2-pyrone even at elevated temperatures. In contrast, mesitylphosphaalkyne (**68**) could barely react with 2-pyrone or 3-bromo-2-pyrone in toluene at around $T \approx 100\,°C$ to the corresponding phosphinine (Scheme 46) in low yields of around 10%. The ^{31}P{^{1}H} NMR spectra displayed one signal at $\delta = 208.9$ ppm for **110** and two signals for the two possible isomers of **111** ($\delta = 208.4$ ppm) and **111a** ($\delta = 221.8$ ppm). It was not possible to separate the two isomers, though the phosphorus signals of them could be distinguished by a ^{1}H^{31}P-HMBC experiment. An exclusive qualitative proof for the reaction of the triphenylsilylphosphaalkyne

(**58**) with **108** showed only one $^{31}P\{^1H\}$ signal at $\delta = 239.6$ ppm for **112**, which can typically be isolated by column chromatography.


108 $R^1 = H$ **58** $R^2 = SiPh_3$
109 $R^1 = Br$ **68** $R^2 = Mes$

110 $R^1 = H$, $R^2 = Mes$
111 $R^1 = Br$, $R^2 = Mes$
112 $R^1 = H$, $R^2 = SiPh_3$

111a

[4+2] cycloaddition
toluene,
100°C - 130 °C,
16 h
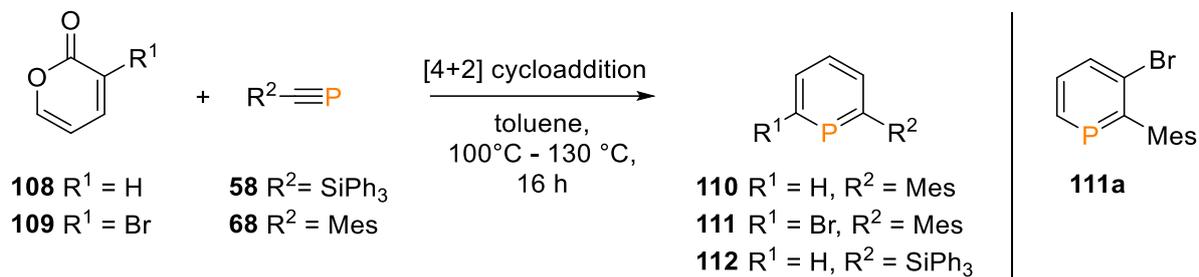
Scheme 46. Synthesized phosphinines by the pyrone route.

A Young NMR tube scale reaction of **58** with the dipyrone **113** was performed to investigate if **58** will react equally to the trimethylsilylphosphaalkyne (**53**), which yielded three different compounds, the trimethylsilyl analogs of the pyrone substituted phosphinine **114**, the diphosphinine **115** and the trimer **116** (Scheme 47). The trimer **116** was formed by a cascade reaction sequence involving product **114**. The detailed mechanistic background of the four consecutive reactions was analyzed by means of NMR spectroscopy and DFT calculations.[376-377] Due to the increased steric demand of **58** a more selective reaction towards the diphosphine **115** was expected. However, only the product **114** with a singlet at $\delta = 237.4$ ppm could be observed in the $^{31}P\{^1H\}$ NMR spectrum, next to several unknown impurities with a resonance at around $\delta = 20$ ppm. The formation of **116** can be excluded because of the lack of any P-P couplings in the spectrum.


excess
Ph$_3$Si—≡P
58
toluene,
130 °C,16 h

113

114   **115**   **116**
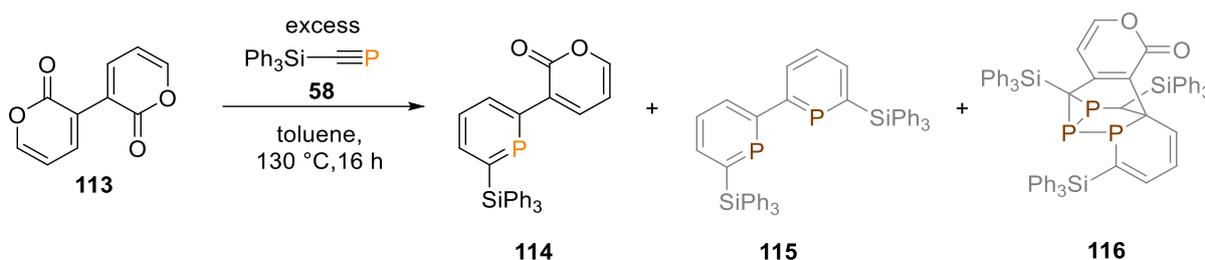
Scheme 47. Investigated reaction of the dipyrone **113** with the phosphaalkyne **58**. The assumed grey compounds found for the analog reaction with Me$_3$Si-CP (**53**) were not formed in this reaction.

As demonstrated by REGITZ *et al.*, phosphaalkynes can react in regioselective [3+1] cycloaddition reactions to the 3H-1,2,3,4-triazaphosphole (Scheme 48).[378] The selectivity is caused by the polarization of the C≡P triple bond of the phosphaalkyne.[18] The steric demand of the substituents influence the reaction time, but has almost no effect on the selectivity.[171]


[3+2] cycloaddition
toluene, rt
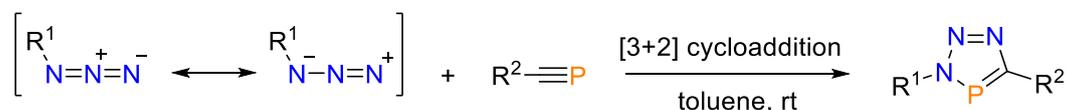
Scheme 48. Regioselective cycloaddition reaction to triazaphospholes.

For reference reasons several triazaphospholes were synthesized as reliable source of ^{31}P{^{1}H} NMR data and a selection of those are depicted in Figure 43.

Bn$-$N$_3$ Mes$-$N$_3$ Dipp$-$N$_3$

117   **118**   **119**

120   **121**   **122**

177.3   182.8   179.4

123   **124**   **125**

187.5   172.1   178.4

Mdtbp =   Tripp =   Dipp =
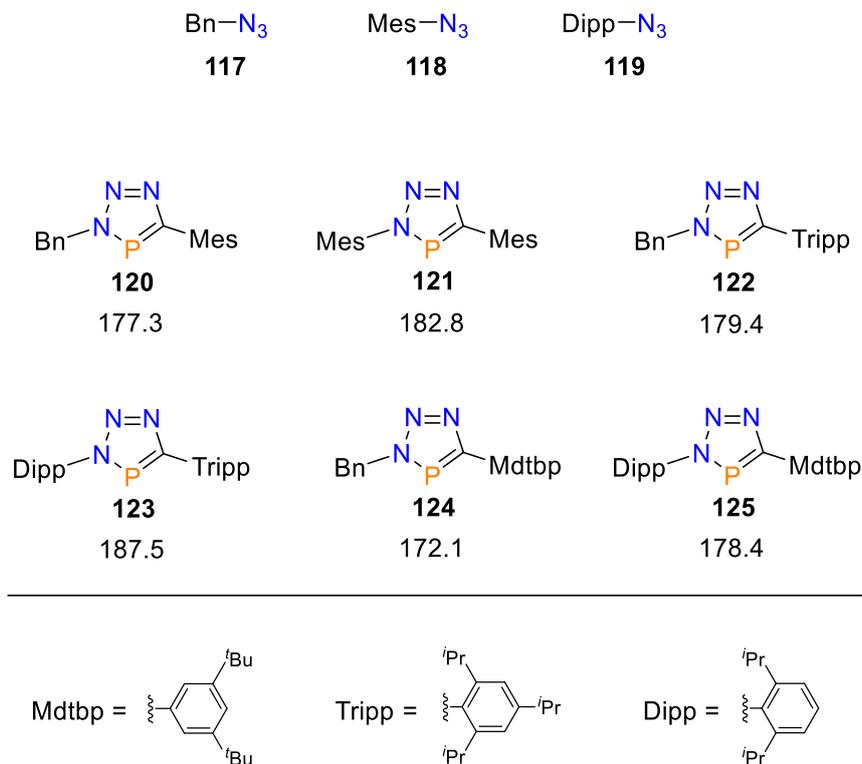
Figure 43. Selection of synthesized phosphaalkynes with ^{31}P{^{1}H} NMR signals below.

Another interesting cyclization reaction of phosphaalkynes demonstrated by IONKIN and co-workers yields triphospholes and tetraphospholes.[379-380] Based on the hexamethyldisiloxane elimination route, supermesitylphosphaalkyne (**76**) is *in situ* generated by reaction of 2,4,6-tri-*tert*-butylbenzoyl chloride (**75**) with cesium (bis(trimethylsilyl)phosphide as phosphorus source, which is *in situ* generated by an excess of CsF to P(SiMe$_3$)$_3$. The formed supermesitylphosphaalkyne (**76**) cyclizes in the ongoing reaction to the triphospholes **129** and tetraphospholes **130** with significant number of by-products (Scheme 49). The mechanism is not verified yet, but it is presumed that **129** is formed by an [2+1] cycloaddition reaction of two molecules of **76** with **126** under loss of the trimethylsilyl groups caused by the high affinity of silicon towards fluorine atoms and the favorable aromatization. The mechanism for the formation of **130** is not assisted by any observation and exclusively speculative. The most plausible would be an [2+1] cycloaddition reaction between **76** and an *in situ* generated phosphorus analog of cesium azide (Cs-P=P≡P) or cesium pentaphosphacyclopentadienide.[381]
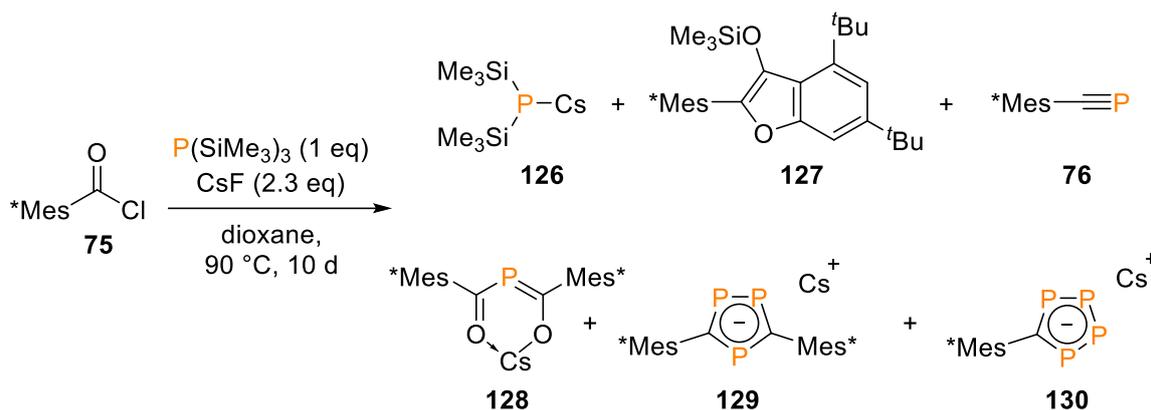
Scheme 49. Literature synthesis of 3,5-bis-(2,4,6-tri-*tert*-butyl-phenyl)-4*H*-[1,2,4]triphosphole (**129**) and 5-(2,4,6-tri-*tert*-butyl-phenyl)-1*H*-[1,2,3,4]tetraphosphole (**130**) with by-products.

This reaction sequence was adapted towards the mesityl derivatives by using carboxylic acid **63**. Due to the stepwise formation of the different reaction products during the course of the reaction, it should be proven if MesCP (**68**) could be identified and isolated from the reaction mixture at a certain time. In addition, the mesityl analog of triphospholes **129** and tetraphospholes **130** should be synthesized. Surprisingly, the reaction progression for mesityl was much slower then given for the supermesityl in the literature. Starting from the carboxylic acid **63** it took 25 days for the complete conversion of all P(SiMe₃)₃ instead of around 5 to 10 days mentioned for **75**. At no point of the reaction MesCP (**68**) could be identified, however the direct precursors (*E,Z*)-[mesityl(trimethylsiloxy)methylene]trimethylsilylphosphine (**66**, Scheme 36) were already observed after around one day (Figure 44). Directly starting from MesCP (**68**) to by-pass the hexamethyldisiloxane elimination significantly accelerated the reaction by shortening the reaction time to 5 days (Scheme 50). Furthermore, the reaction is more selective towards the triphospholes **131**. Nevertheless, both reactions yielded some by-products which did not fit the literature observations and could not be identified.
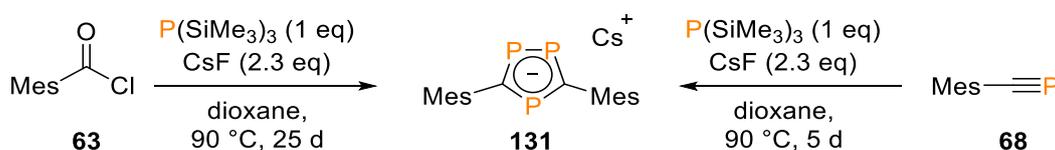

Scheme 50. Formation of 3,5-bis-(2,4,6-tri-*tert*-butyl-phenyl)-4*H*-[1,2,4]triphosphole (**131**) by hexamethyldisiloxane elimination route (left) and shorted reaction my starting from the phosphaalkyne **68** (right).
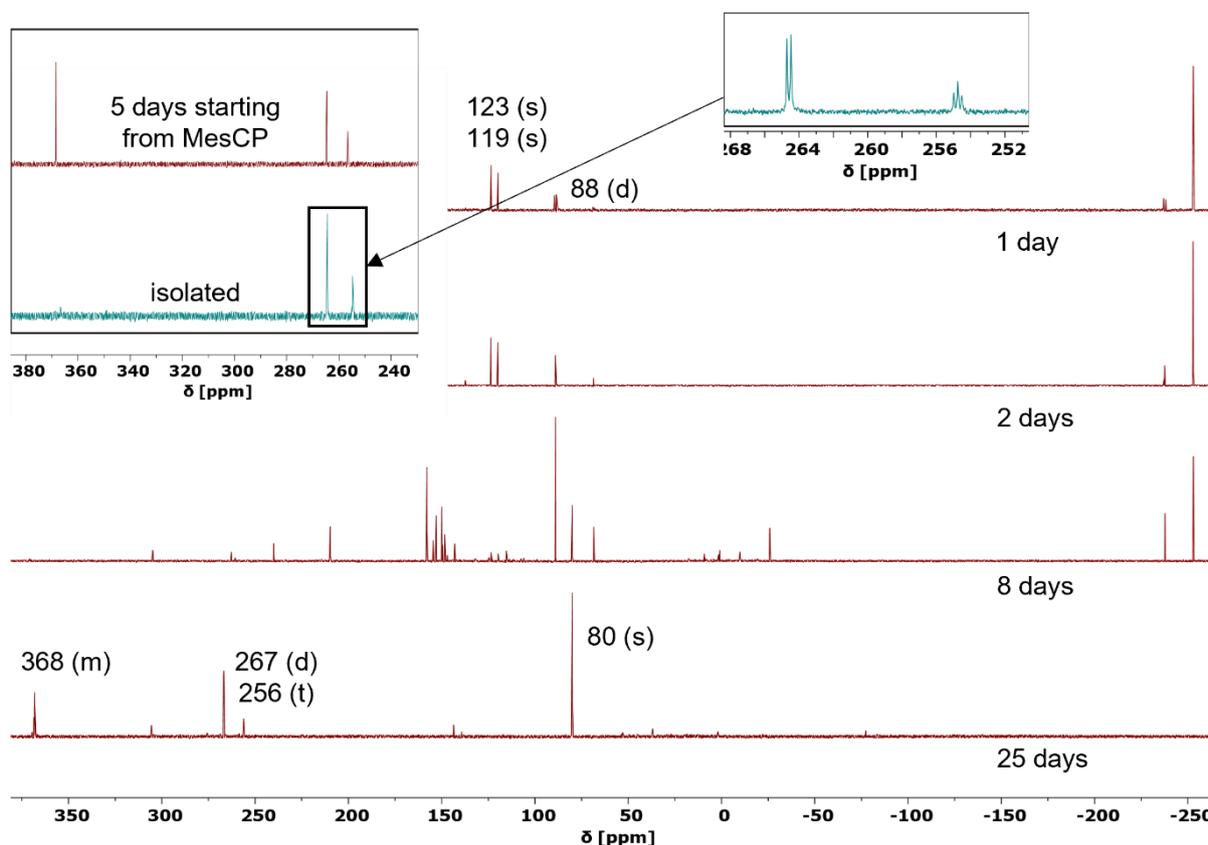
Figure 44. Reaction progress of 2,4,6-trimethylbenzoyl chloride (**63)** with CsF and P(SiMe$_3$)$_3$ monitored by ^{31}P{^{1}H} NMR and the alternative approach starting from MesCP (**68**) instead of **63**.

Even though **131** could be successfully isolated by this reaction the same molecule **133** with sodium as cation can be much faster synthesized by addition of MesCP (**68**) to the sodium pentaphosphacyclopentadienide (**132**, Scheme 51).[382]
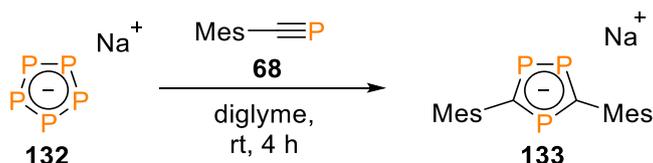

Scheme 51. Synthesis of the triphosphole **133** starting from sodium pentaphosphacyclopentadienide (**132**).

SCHEER *et al.* demonstrated the different reaction behavior of MesCP (**68**) and Mes*CP (**76**) with the tungsten complex [W(CO)$_5$(thf)] (**134**). Two units of **68** cyclize, as most small phosphaalkynes do, in the coordination sphere of the tungsten to **136** and three by-products,[126] whereas two bulky supermesitylphosphaalkynes (**76**) form a π-coordination complex **135** (Scheme 52).[134] This reaction was revisited with the new TrippCP (**81**), whose steric demand is in between the other two phosphaalkynes. The reaction of **81** with **134** selectively yielded the cyclization product **137**, which showed a singlet at $\delta = 69.1$ ppm in the ^{31}P NMR spectrum.

Scheme 52. Different reaction behavior of [W(CO)$_5$(thf)] depending on the steric demand of the used arylphosphaalkyne. The reactions were carried out in THF starting at room temperature and heated to T = 65 °C. The [W] symbolize a [W(CO)$_5$] fragment.[126, 134]

Another cyclodimerization can be achieved on the iron(0) precursor **138**, which can be formed from pentacarbonyl iron(0) and an excess of cyclooctene (coe) under low temperatures and UV irradiation (λ_{max} = 365 nm).[383] The addition of *tert*-butylphosphaalkyne to **138** results in the formation of the literature known iron complex **139** (Scheme 53).[384] The same reaction could be carried out with MesCP (**68**). Surprisingly, the resulting complex **140** (δ(^{31}P) = 76.9 (s) ppm) was not published but an entry for its molecular structure in the crystal can be found in the CCDC database and matches with the synthesized sample. In contrast to the reaction with [W(CO)$_5$(thf)], the addition of TrippCP (**81**) did not yield the Tripp derivative **141**. Instead, five independent ^{31}P signals between δ = 100 and 175 ppm were observed. None of them could be isolated by sublimation, therefore uncontrolled decomposition of the dimerization product is assumed.

Scheme 53. Phosphaalkyne cyclodimerization on the tricarbonylbis(cyclooctene)iron(0) complex (**138**).[384]

2.1.3 Preparation of phosphaalkyne complexes (π-complexes)

[(dippe)Ni(MesCP)] (**142**) and [(dippe)Pt(MesCP)] (**143**) were selected as an entry point in search of suitable phosphaalkyne complexes of the type [(L)M(R)] (L = chelating (di)phosphine, two phosphines; M = Ni, Pt; R = phosphaalkyne), in the following mostly called π-complex, for the intended C-CP cleavage reaction. According to the ^{31}P and ^{1}H NMR results, both complexes were synthesized nearly quantitatively by addition of bis(diisopropyl-phosphino)ethane (dippe, **8**) and mesitylphosphaalkyne (MesCP, **68**) to a toluene suspension or a THF solution of Ni(COD)$_2$ (**36**) or Pt(COD)$_2$ (**4**) at room temperature. **143** could also be synthesized by starting from tetrakis(triphenylphosphine)platinum(0), although the yield is very low and the released triphenylphosphine could only be removed by sublimation under the formation of other impurities (Scheme 54).
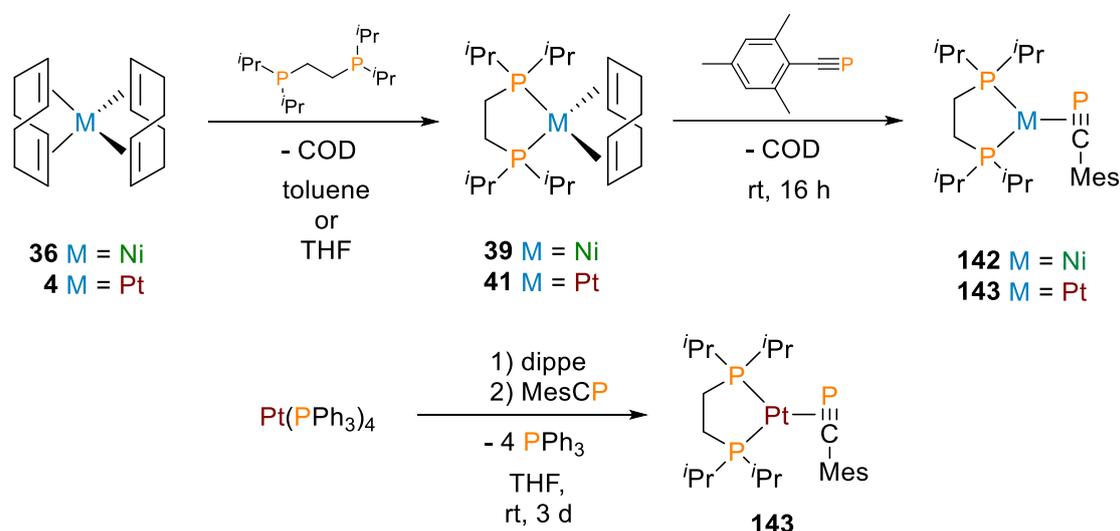

Scheme 54. Preparation of [(dippe)Ni(MesCP)] (**142**) and [(dippe)Pt(MesCP)] (**143**) starting from Ni/Pt(COD)$_2$ (top) and synthesis of **143** starting from tetrakis(triphenylphosphine)platinum(0) (bottom).

The ^{31}P{^{1}H} spectrum of **142** shows three low field shifted signals compared to the free ligands (Figure 45). The doublet at δ = 171.7 ppm belongs to the phosphaalkyne phosphorus atoms which is in agreement with the predicted shift of the theoretical [(dmpe)Ni(MesCP)] (**C1**, dmpe = 1,2-bis(dimethylphosphino)ethane) complex calculated by ERIC YANG (cf. 4.1 and 5.1). The phosphaalkyne phosphorus of **142** couples with a coupling constant of $^{2}J_{P,P}$ = 16.6 Hz to one of the diphosphine phosphorus atom at δ = 70.9 ppm, which is most likely in *trans* position to the phosphaalkyne phosphorus atom. As a doublet of doublets, it also couples to the other dippe (*cis*-)phosphorus atom at δ = 81.5 ppm with a coupling constant of $^{2}J_{P,P}$ = 34.0 Hz. An explanation for the ^{31}P assignment will be later given for the platinum analog **143**. Figure 46 shows a comparison of the ^{1}H spectra of dippe (**8**, blue), MesCP (**68**, green) and [(dippe)Ni(MesCP)] (**142**, red) with assignment of their hydrocarbon groups. The three well-separated signals of the MesCP ligand can be easily detected, while the signals of the dippe ligand are more complicated to identify, due to linking with each other by ^{1}H^{1}H and ^{1}H^{31}P

couplings and the loss of their previous molecular symmetry. All carbon atoms could be assigned by the $^{13}C\{^1H\}$ NMR measurement. The isopropyl group signals are in the area at around δ = 19 - 26 ppm, the aromatic carbons are between δ = 128 - 150 ppm. The quaternary carbon of the C≡P moiety appears as a doublet of doublets of doublets, which is highly deep field shifted to δ = 231.8 ppm with respective coupling constants of $J_{C,P}$ = 80.1, 32.5 and 4.7 Hz to the phosphorus atoms.
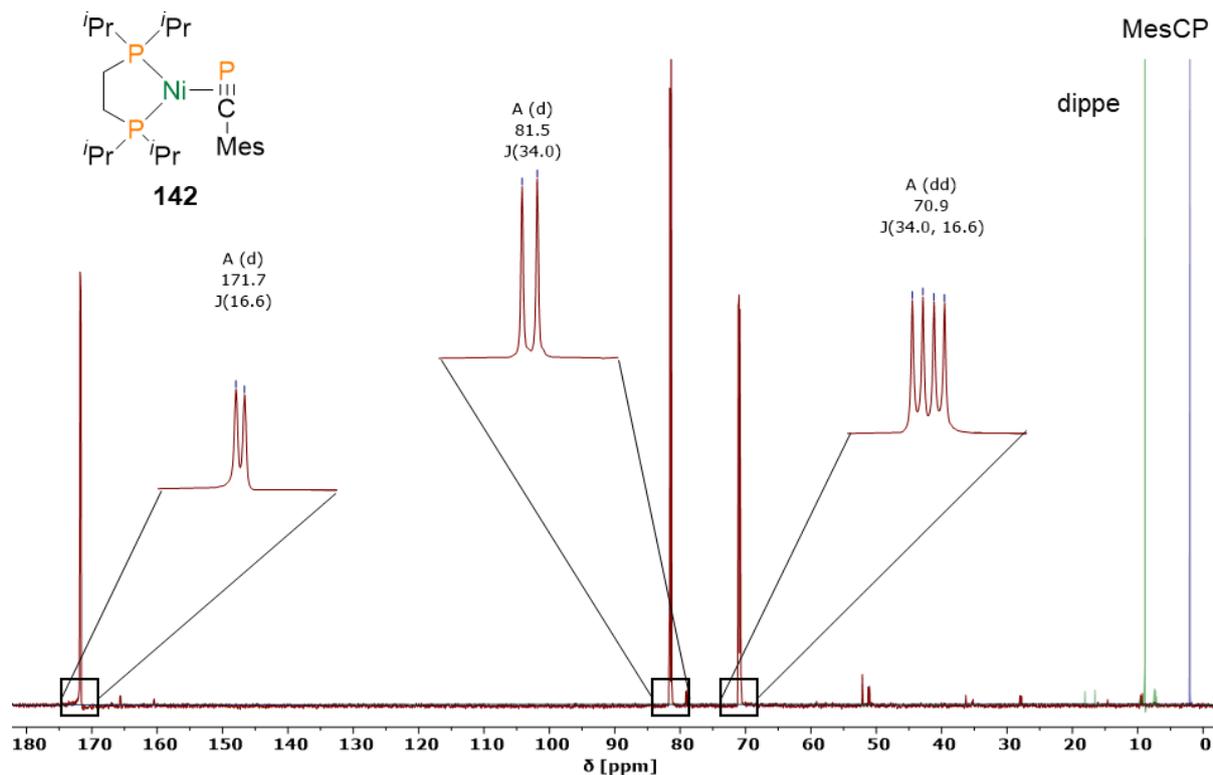
Figure 45. $^{31}P\{^1H\}$ NMR spectrum of [(dippe)Ni(MesCP)] (**142**) in benzene-d_6 with magnifications of the resonances. Both ligands, dippe (**8**, green) and MesCP (**68**, blue), given as reference.
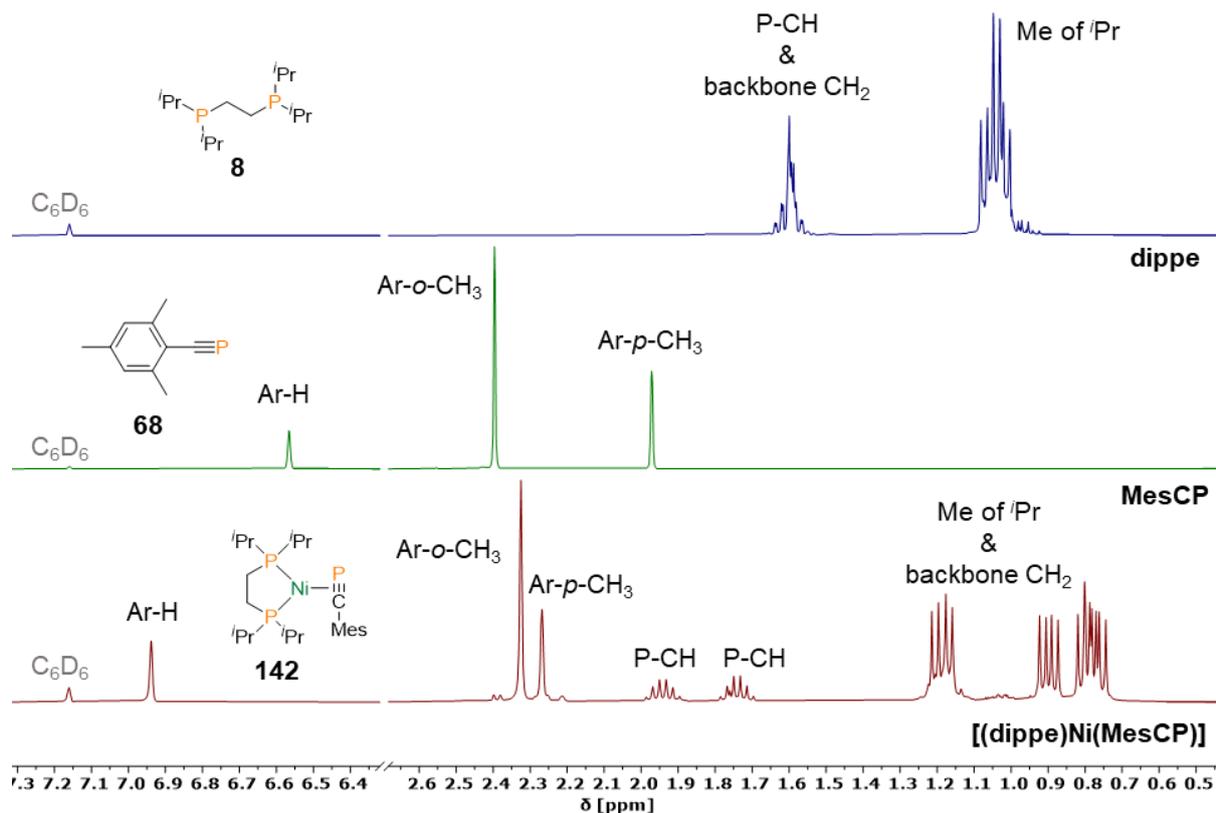
Figure 46. ^{1}H NMR spectra of dippe (**8**, blue), MesCP (**68**, green) and [(dippe)Ni(MesCP)] (**142**, red) in benzene-d[6] to visualize the changed shifts of specific hydrocarbon groups after ligand coordination.

A comparison of the molecular structure of **142** with the nitrile complex[254] **2.2π** (chapter 2.1.1, Scheme 14) prepared by JONES' *et al.* revealed the same expected square-planar coordination (Figure 47). Due to the π-back donation for the nickel center into the antibonding π* orbital of the C≡P triple bond, the C≡P triple bond is elongated (1.6453(19) Å), and its bond length is closer to a C=P double bond (typically 1.67 Å)[217] instead of a C≡P triple bond (typically 1.55 Å)[113]. The mesityl group of the coordinated mesitylphosphaalkyne is strongly bent (142.88(14)°) away from the complex center in contrast to the linear configuration in free mesitylphosphaalkyne. The bending of the aryl group in **142** is also significant larger than in **2.2π** (136.1(4)°), due to the increased steric demand of the methyl groups in the *ortho* position.
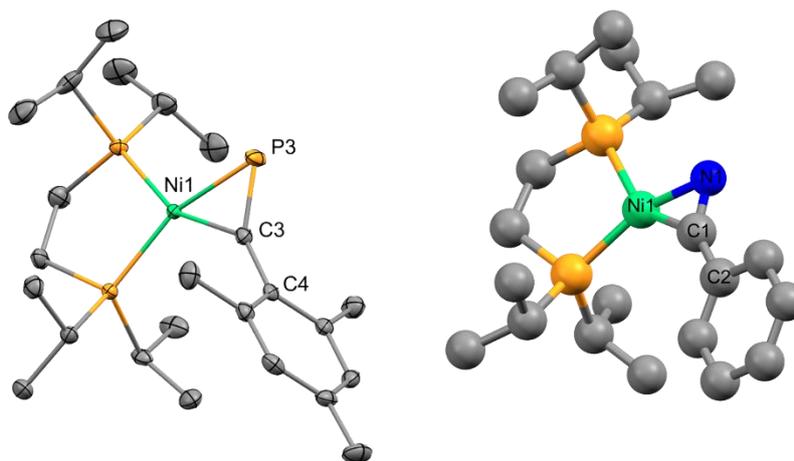
Figure 47. Molecular structure of **142** in the crystal (left). Anisotropic displacement ellipsoids are shown at 50% probability level. Hydrogens omitted for clarity. Selected bond lengths (Å) and angles (°): C3-P3: 1.6453(19), P3-C3-C4: 142.88(14). Molecular structure of **2.2π** in the crystal (right), shown as ball-stick model. Hydrogens omitted for clarity. Selected bond lengths (Å) and angles (°): C1-N1: 1.225(6), N1-C1-C2: 136.1(4).

The platinum π-complex **143** revealed a similar ^{31}P{^{1}H} spectrum as the nickel complex **142** with three main signals, one at $\delta = 139.4$ ppm for the phosphaalkyne moiety and two at $\delta = 82.0$ and 73.1 ppm for the dippe unit. The C≡P phosphorus signal of **143** closely matches the predicted chemical shift of [(dmpe)Pt(MesCP)] (**C7**) at $\delta(^{31}$P$) = 146.8$ ppm. In contrast to the nickel derivative **142**, all resonances appeared as doublet of doublets this time, meaning that the phosphaalkyne phosphorus atom couples to both dippe phosphorus atoms and those also couple to each other. Furthermore, each resonance shows two additional resonances for the platinum satellites, due to the ^{31}P^{195}Pt coupling. The correct assignment of these satellites, depicted in Figure 48, can be verified by several parameters. First, the satellites possess an specific intensity, which should be around 1/5 of the main signal, due to the natural abundance of ^{195}Pt of around 34% and the typical magnetic field strength of the used 400 MHz NMR device.[385] Second, the satellites must bear the same coupling constants and pattern as the main signal. Third, the distance of both satellites from the centered main signal must be identical. The phosphorus-platinum coupling constant for the phosphaalkyne moiety is $^1J_{P,Pt} = 230$ Hz. The coupling of the diphosphine is substantially higher with over $^1J_{P,Pt} = 3000$ Hz, the bigger coupling constant of $^1J_{P,Pt} = 3210$ Hz probably belongs to the phosphorus atom in *trans* position to the phosphaalkyne phosphorus atom.[385] The ^{31}P^{195}Pt coupling were also reversely confirmed by the ^{31}P satellites found for the platinum signal at $\delta = -4611$ ppm in the ^{195}Pt{^{1}H} spectrum (Figure 49). The *cis*/*trans* assignment of the phosphorus signals in a platinum complex can be achieved by the $^1J_{Pt,P}$ and the $^2J_{P,P}$ coupling constants. The $^1J_{Pt,P}$ coupling constant is mostly depending on the oxidation state of the platinum, the molecular configuration and the involved ligand types. Generally, the $^1J_{Pt,P}$ coupling constant of a phosphorus nuclei decreases with the σ-donor ability of the ligand (e.g., Ph⁻ > Me⁻ > PEt₃) in *trans* position to it.[386-395] Additionally, in almost all cases, the $^2J_{P,P}$ coupling

constant in phosphorus containing metal complexes (P-M-P) is larger for phosphorus ligands in *trans* vs. *cis* position to each other.[396-400] Based on the theoretical information and in agreement with experimental literature data[401], the *cis* dippe phosphorus atom was assigned to the signal at $\delta(^{31}P\{^1H\})$ = 82.0 ppm ($^2J_{P,P}$ = 37.3, 15.7 Hz) whereas the *trans* phosphorus atom to the signal at $\delta(^{31}P\{^1H\})$ = 73.1 ppm ($^2J_{P,P}$ = 37.4, 28.8 Hz) relative to the phosphaalkyne phosphorus atom. The ^1H NMR spectrum of **143** shows a better separation of the hydrocarbon group signals than **142**, but was further improved by ^{31}P decoupling to identify all groups (Figure 50). The $^{13}C\{^1H\}$ NMR is very similar to that of **142** with the quaternary carbon of the C≡P moiety at nearly the same shift (δ = 232.7 ppm (ddd, J = 83.1, 59.1, 8.7 Hz)), however the second and third order doublets exhibit higher coupling constants. The molecule **143** shows a square-planar geometry (Figure 51). The C≡P distance is 1.653(3) Å, which is negligible longer than found for the nickel complex (1.6453(19) Å). The C-CP bond, which should later be cleaved, is a bit shorter in **143** than in **142** (140.9(4) Å vs. 142.88(14) Å). Due to the increased valence orbital size of the platinum compared to the nickel complex, the general bond lengths to the surrounding atoms are increased by around 0.110 Å to the dippe phosphorus atoms, 0.179 Å to the phosphorus atom and 0.081 Å to the carbon atom of the C≡P unit. The bite angle of the nickel derivative **142** is about 3.6° wider, whereas the opposite angle is around 3.3° narrower (Figure 52) than in **143**.
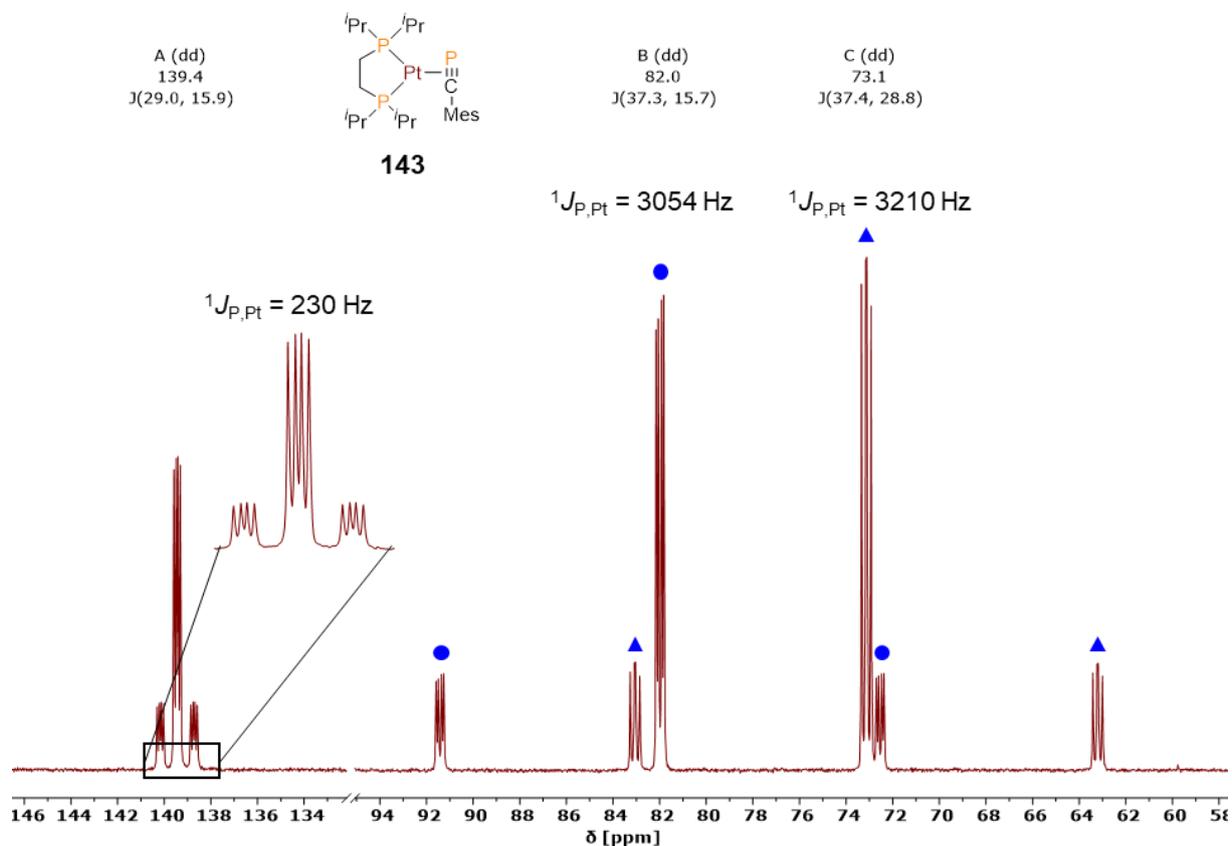

Figure 48. $^{31}P\{^1H\}$ NMR spectrum of [(dippe)Pt(MesCP)] (**143**) in tetrahydrofuran-d_8 with magnification of the MesCP phosphorus signal to highlight the ^{195}Pt satellites of the C≡P phosphorus. The blue dots and triangles assign the ^{195}Pt satellites of the two dippe phosphorus signals.
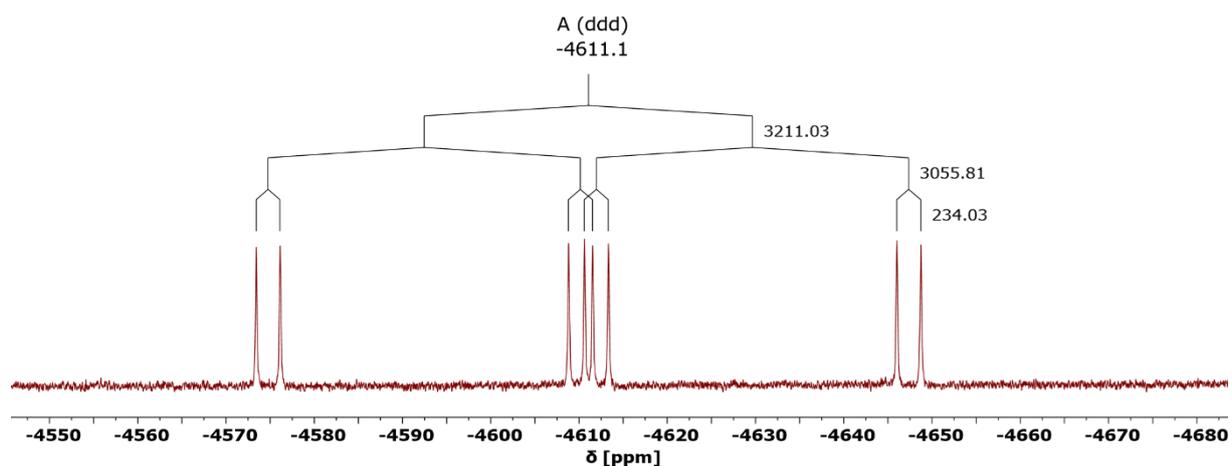
Figure 49. ^{31}Pt{^{1}H} NMR spectrum of [(dippe)Pt(MesCP)] (**143**) in tetrahydrofuran-d$_8$ with illustrated ^{31}P coupling tree.
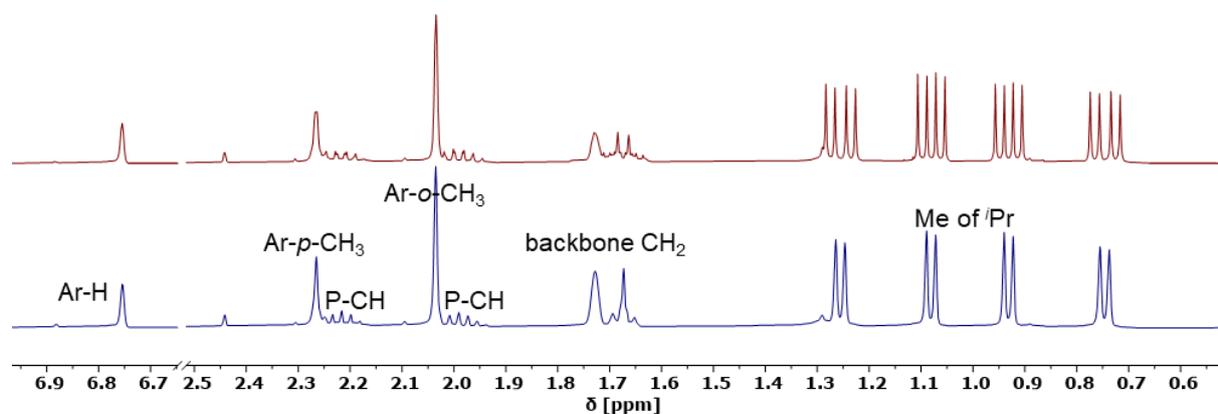
Figure 50. Stacked ^{1}H (top) and ^{1}H{^{31}P} (bottom) NMR spectra of [(dippe)Pt(MesCP)] (**143**) in tetrahydrofuran-d$_8$ to assign the hydrocarbon groups and to visualize the reduced coupling complexity by suppressing the ^{1}H^{31}P coupling.
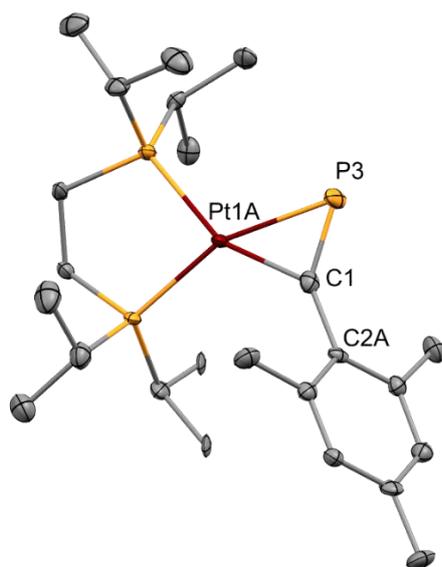
Figure 51. Molecular structure of **143** in the crystal. Anisotropic displacement ellipsoids are shown at 50% probability level. Hydrogens omitted for clarity. Selected bond lengths (Å) and angles (°): C1-P3: 1.653(3), P3-C1-C2A: 140.9(4).
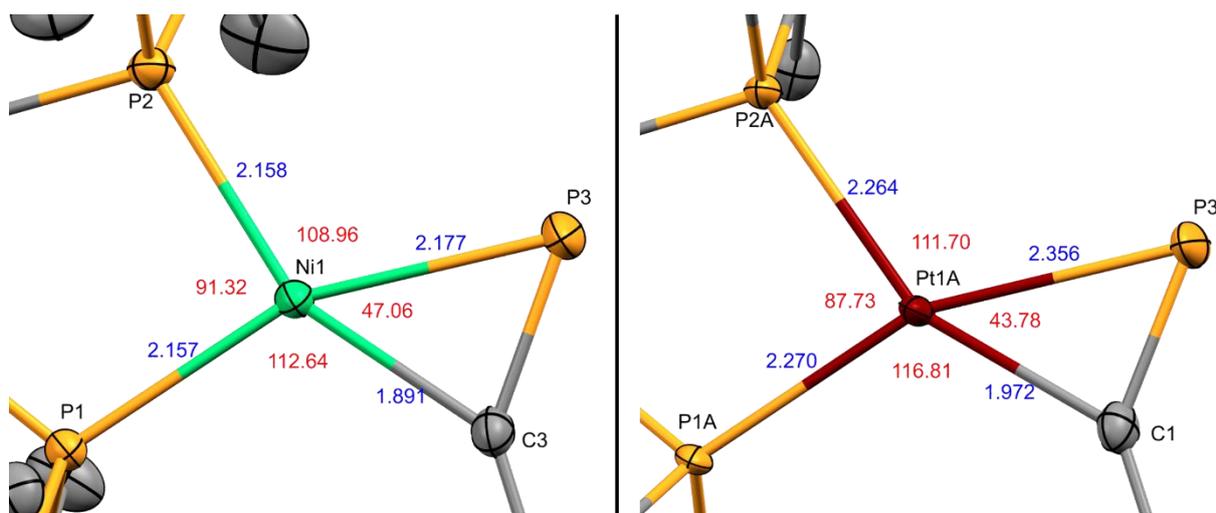
Figure 52. Metal core with surrounding atoms of the molecular structure of **142** and **143** in the crystal. Anisotropic displacement ellipsoids are shown at 50% probability level. Selected bond lengths (Å) in blue and angles (°) in red.

After succeeding in the synthesis and isolation of [(dippe)Ni(MesCP)] (**142**) and [(dippe)Pt(MesCP)] (**143**), a broad selection of π-complexes were prepared, based on the different combination of (di)phosphines and phosphaalkynes. Main subject of the study was the influence of the bite angle as a function of the size (methy, ethyl or propyl) of the diphosphine backbone and, within each backbone size, the impact of the steric demand of the phosphaalkyne as well as the effect of the bulk and electronic properties of phosphine substituents. In addition, it should be clarified if chelating phosphines are necessary for the C-CP cleavage process and if the hemilabile (diisopropylphosphinodimethylamino)ethane ligand (**29**, dippdmae) might offers the possibility of catalytical cycloaddition reactions of the

phosphaalkynes on the metal complex towards triphosphabenzene derivatives (Scheme 55). Furthermore, the option of a Si-CP bond cleavage in silylphosphaalkyne should be investigated.
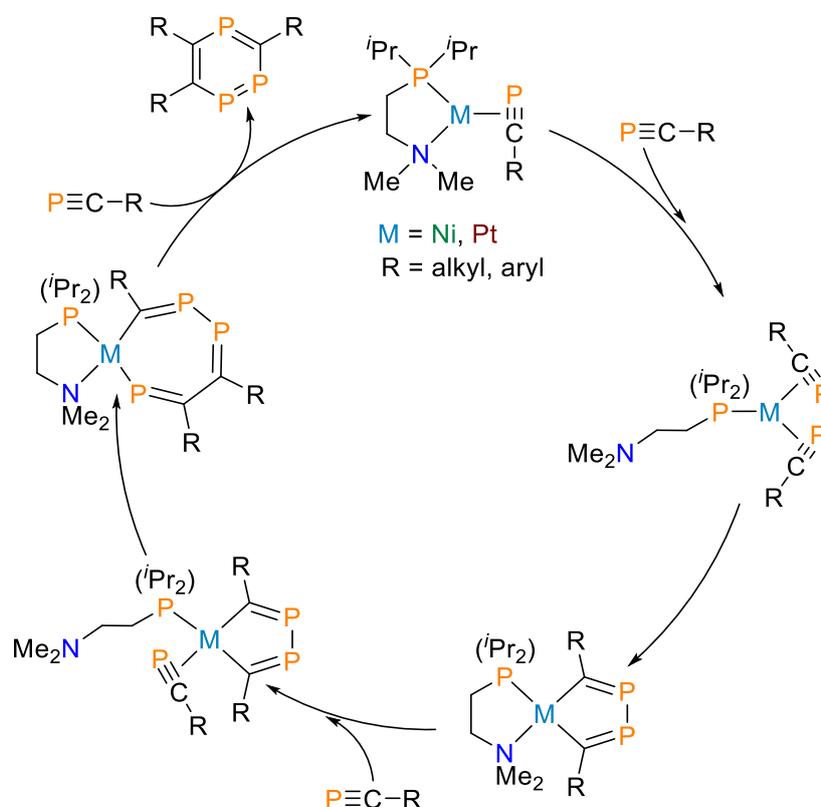
Scheme 55. Possible catalytic cyclotrimerization of phosphaalkyne in the presence of dippdmae-metal-phosphaalkyne complex. Adopted scheme of cyclotrimerization of alkynes in the coordination sphere of nickel.[255]

Figure 53 gives an overview over the targeted π-complexes. Most representatives of the C$_2$ (**142** - **162**) and C$_3$ (**172** - **175**) backbone fraction, with exception of the silylphosphaalkyne based π-complexes (**154** - **157**), could be realized and were partly or fully characterized, depending on their success towards the C-CP cleavage process. The preparation of the C$_1$ backbone derivatives (**163** - **171**) were primarily limited by the instability of insufficient sterically shielded phosphaalkynes. Furthermore, their reactions were less selective, which made it more challenging to receive pure samples in reasonable yields. Table 9 presents the summary of all π-complexes with their corresponding ^{31}P$\{^1$H$\}$ NMR figures, as the most relevant method for their characterization and comparison. All showed π-complexes were checked towards their C-CP cleavage ability by heating to $T = 75\,°C$ in THF or $T = 100\,°C$ in toluene and irradiation with ultraviolet light ($\lambda_{max} = 365$ nm) or violet light ($\lambda_{max} = 405$ nm). Some samples were also examined for possible chemical activation by addition of Lewis acids. The results of those studies will be discussed in the next chapters (cf. 2.1.4.2, 2.1.5.1.1). This chapter exclusively focuses on π-complexes either as selected representative of their class or their success in the activation process. It should be already mentioned that all nickel based π-complexes as well as non-chelating and C$_3$ backbone phosphine-based complexes showed

no C-CP cleavage or other positive response to the activation process. Generally, all nickel based π-complexes are colored yellow, whereas the platinum complexes are mostly dark yellow to orange, with exception of the red C_1 derivatives.
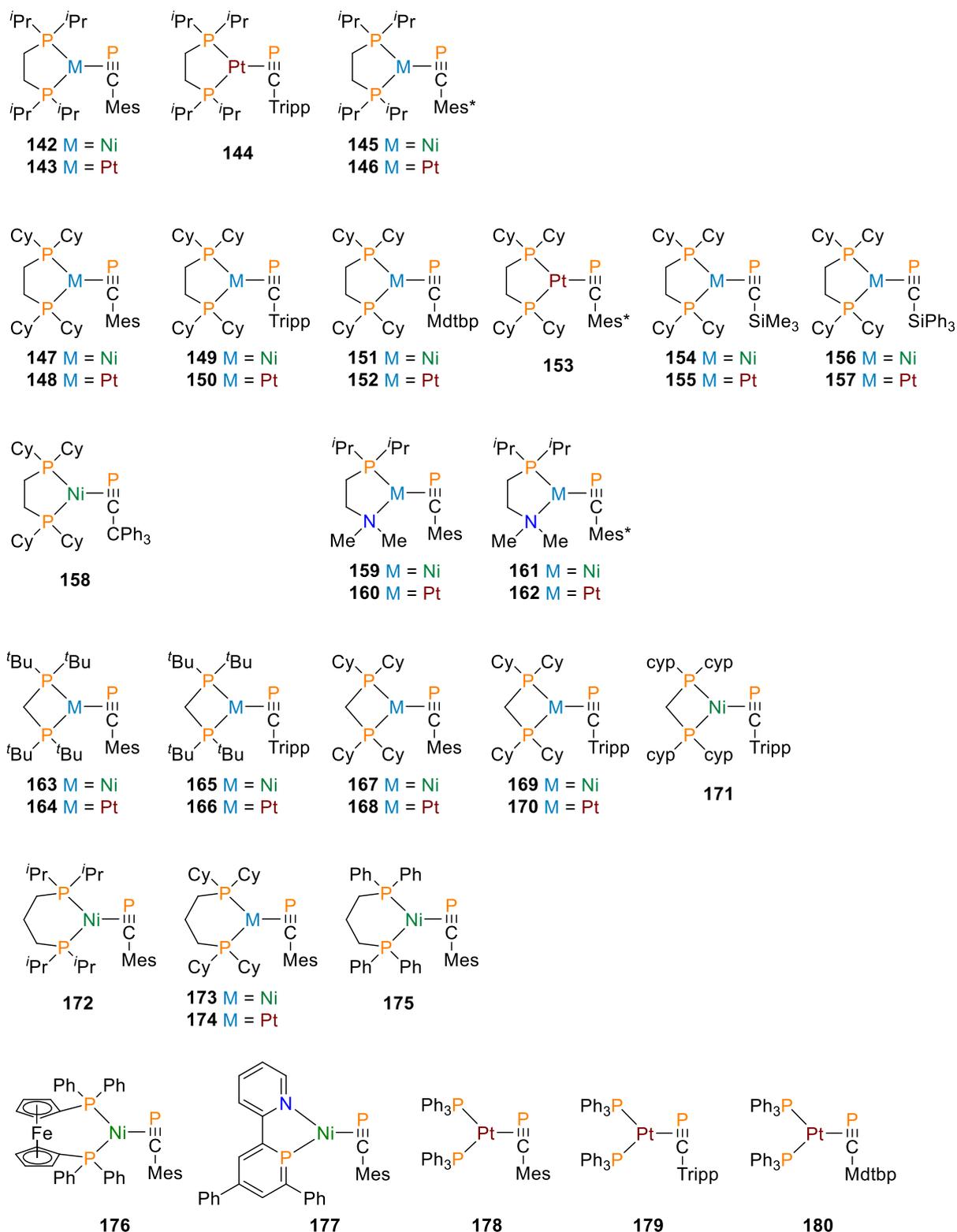
Figure 53. Scheduled phosphaalkyne complexes by addition of phosphine and phosphaalkyne to Ni(COD)$_2$ or Pt(COD)$_2$.

Table 9. Overview over the $^{31}P\{^1H\}$ NMR signals of the synthesized π-complexes. Values in parentheses were not found and are calculated. Red values are unreliable. [a] not all ^{31}P signals found, [b] decomposition, [c] two signals found for dippdmae due to two isomers, [d] synthesis failure most likely related to impurities in the dcppm ligand, [e] C-C≡P activation by UV ($λ_{max}$ = 365 nm) or violet light ($λ_{max}$ = 405 nm).

π-compound	nr	$^{31}P\{^1H\}$ P1 [ppm]	$J_{P,P}$ P1 [Hz]	$J_{P,Pt}$ P1 [Hz]	$^{31}P\{^1H\}$ P2 [ppm]	$J_{P,P}$ P2 [Hz]	$J_{P,Pt}$ P2 [Hz]	$^{31}P\{^1H\}$ P3 [ppm]	$J_{P,P}$ P3 [Hz]	$J_{P,Pt}$ P3 [Hz]	$^{195}Pt\{^1H\}$ Pt1 [ppm]	hv[e]
[(dippe)Ni(MesCP)]	**142**	172.6	16.4		82.2	33.9		71.8	33.9, 16.5			no
[(dippe)Pt(MesCP)]	**143**	140.5	29.2, 15.7	234	82.9	37.2, 15.7	3056	74.0	37.1, 29.1	3211	-4611	yes
[(dippe)Pt(TrippCP)]	**144**	145.8	28.7, 17.2	229	79.5	36.5, 16.7	3044	70.7	36.5, 28.2	3213		yes
[(dippe)Ni(Mes*CP)]	**145**	156.3	14.8		80.1	37.8		60.5	37.8, 14.8			no
[(dippe)Pt(Mes*CP)]	**146**	126.5	28.8, 18.7	167	78.0	39.0, 18.7	3036	65.5	39.0, 28.8	3283	-4576	no
[(dcpe)Ni(MesCP)]	**147**	169.6	16.9		70.4	35.6		62.2	35.6, 16.6			no
[(dcpe)Pt(MesCP)]	**148**	140.0	29.5, 15.6	230	71.7	37.8, 14.5	3056	65.8	37.7, 29.4	3205	-4582	yes
[(dcpe)Ni(TrippCP)]	**149**	171.1	16.8		67.1	32.6		59.6	32.6, 15.8			no
[(dcpe)Pt(TrippCP)]	**150**	149.9	29.1, 17.5	217	69.2	35.4, 16.7	3046	64.2	35.4, 29.1	3212	-4578	yes
[(dcpe)Ni(MdtbpCP)][a]	**151**	(177.2)			58.9	39.6		50.6	39.6, 14.6			no
[(dcpe)Pt(MdtbpCP)]	**152**	137.3	31.0, 19.7	204	69.6	33.4, 19.4	2937	64.3	31.8	3178		yes
[(dcpe)Pt(Mes*CP)]	**153**	128.0	28.8, 18.8	166	67.4	39.3, 18.4	3045	58.9	39.2, 28.1	3278		no
[(dcpe)Ni(Me₃SiCP)]	**154**	-	-	-	-	-	-	-	-	-	-	-
[(dcpe)Pt(Me₃SiCP)]	**155**	-	-	-	-	-	-	-	-	-	-	-
[(dcpe)Ni(Ph₃SiCP)][a]	**156**	(322.7)			75.4	29.3		66.0	29.3, 18.5			no
[(dcpe)Pt(Ph₃SiCP)]	**157**	287.9	30.9	129	72.5	33.3, 6.7	3264	65.2	31.8	3221		no

Compound	No.											
[(dcpe)Ni(TritylCP)]	**158**	148.9	15.0		71.9	27.8, 11.5		56.4	27.9, 16.9			no
[(dippdmae)Ni(MesCP)][b]	**159**	165.7			39.2							dcp.
[(dippdmae)Pt(MesCP)][c]	**160**	112.3	18.5	195	32.6	24.7, 20.4	3556	30.6	24.6, 16.7	3362		dcp.
[(dippdmae)Ni(Mes*CP)]	**161**	157.4	11.2		57.7	11.0						dcp.
[(dippdmae)Pt(Mes*CP)][b]	**162**	101.3		118	63.1	6.5	3878					dcp.
[(dtbpm)Ni(MesCP)]	**163**	-	-	-	-	-	-	-	-	-	-	-
[(dtbpm)Pt(MesCP)]	**164**	-	-	-	-	-	-	-	-	-	-	-
[(dtbpm)Ni(TrippCP)]	**165**	195.9	21.3		48.3	89.3		41.3	89.1, 21.4			no
[(dtbpm)Pt(TrippCP)]	**166**	155.8	33.7, 16.7	220	29.4	58.6, 33.3	2626	25.1	58.7, 16.3	2683		yes
[(dcpm)Ni(MesCP)]	**167**	192.3	20.4		22.0	49.1		16.9	50.3, 21.7			no
[(dcpm)Pt(MesCP)]	**168**	-	-	-	-	-	-	-	-	-	-	-
[(dcpm)Ni(TrippCP)]	**169**	199.4	21.3		21.1	48.1		16.1	48.6, 20.8			no
[(dcpm)Pt(TrippCP)]	**170**	163.8	36.1, 17.7	224	1.4	17.1, 9.3	2543	-0.4	35.7, 9.7	2654	-3991	yes
[(dcppm)Ni(TrippCP)][d]	**171**	-	-	-	-	-	-	-	-	-	-	-
[(dippp)Ni(MesCP)]	**172**	164.9	13.2, 6.2		30.4	5.6		28.7	13.0			no
[(dcpp)Ni(MesCP)]	**173**	164.9	13.8, 5.7		22.4	4.7		22.2	13.2			no
[(dcpp)Pt(MesCP)]	**174**	126.0	24.8, 17.3	221	19.4	23.8	3305	17.9	15.6	3119		no
[(dppp)Ni(MesCP)]	**175**	151.4			19.2			18.0				no
[(dppf)Ni(MesCP)]	**176**	149.7	15.2		28.9	15.6, 4.8		27.4	4.8			no
[(P,N)Ni(MesCP)]	**177**	231.1			184.7							no

[(PPh₃)₂Pt(MesCP)]	**178**	96.9	23.9, 12.1	165	29.2	23.4	3700	25.1	23.1, 11.7	3454	no
[(PPh₃)₂Pt(TrippCP)]	**179**	105.9	24.0, 13.4	145	29.0	23.7	3725	23.4	23.7, 12.3	3424	no
[(PPh₃)₂Pt(MdtbpCP)]	**180**	111.6	26.3, 14.5	108	32.6	24.8	3566	25.7	23.7, 13.1	3362	no

It is worth to mention that the following discussion does not follow the chronological order of the experiments performed in the laboratory. These started mostly with the C_2-π-complexes and based on the gained knowledge it could be estimated at an early stage whether the pursuit of a certain ligand combination makes sense for the project or not. If not stated otherwise, the preparation of the π-complexes follows the general synthesis starting from Ni(COD)$_2$ or Pt(COD)$_2$ and addition of the phosphine and phosphaalkyne (Scheme 54).

The option for silylphosphaalkyne complexes was evaluated by using Me$_3$SiCP (**58**) and the bulkier Ph$_3$SiCP (**59**). The attempt of getting the [(dcpe)Ni(Me$_3$SiCP)] complex (**154**) led to an instant black solution upon addition of **58** to the mixture of [Ni(COD)] (**36**) and dcpe (**30**). Four ^{31}P{^{1}H} resonances were found at δ = 161.7 (t), 94.1 (t), 79.1 (s) and 20.6 (s) ppm. The two low-field shifted signals couple to each other with a $J_{P,P}$ = 21 Hz constant, indicating the formation of a symmetrical compound taking three phosphorus atoms into consideration. According to the integration in the ^{31}P spectrum, the two singlets are independent compounds and a possible [(dcpe)Ni(Me$_3$SiCP)] complex represented by the signals at δ = 161.7, 94.1, 79.1 ppm, similar to results for other π-complexes, can be excluded. In addition, computational ^{31}P NMR predictions for [(dmpe)Ni(Me$_3$SiCP)] (**C2**) suggest the shift of the C≡P phosphorus at δ = 300.9 ppm. Heating the reaction mixture only converted the signal at δ(^{31}P{^{1}H}) = 20.6 to 169.1 ppm. Irradiation of the solution by a mercury high-pressure lamp (λ_{max} = 365 nm) equipped with a band-pass filter for λ = 300 - 400 nm did not show any effect. The formation of [(COD)Ni(dcpe)] (**43**) and [Ni(dcpe)$_2$] (**44**) could be excluded (cf. chapter 2.1.2.2.6). The analog reaction towards the platinum complex **155** resulted in a red solution, which slowly turned black. The ^{31}P{^{1}H} spectrum was dominated by unreacted Me$_3$SiCP (**58**). Heating the reaction mixture to T = 50 °C showed three independent singlets at δ(^{31}P{^{1}H}) = 169.1, 60.0 and 45.1 ppm but without any platinum couplings. Crystals, not suitable for single crystal diffraction, were isolated and characterized by NMR. The ^{31}P{^{1}H} spectrum contains one singlet at δ = 64.5 ppm with platinum satellites ($J_{P,Pt}$ = 3542 Hz) and the ^{1}H confirms only the presence of cyclohexyl groups. [(COD)Pt(dcpe)] (**45**) and [Pt(dcpe)$_2$] (**46**) could be excluded, instead the structures **181** or **182** (Scheme 56), similar to the literature known complexes [Pt(dppe)(SiHMe$_2$)$_2$] and [Pt(dppe)(μ-SiMe$_2$)]$_2$, were assumed.[402] However, no ^{29}Si signal could be found and the identity of the compound remained unknown. It is noteworthy that RUSSELL *et al.* synthesized the Me$_3$SiCP based platinum complex **2.20** and the palladium dimer **2.21** (Scheme 56).[139] The dimer **2.21** is stabilized by dppe, whereas **2.20** with its PPh$_3$ ligands decomposed rapidly at room temperature to multiple products, which might include a pentametallic cluster like for the analogous palladium reaction. Similar reaction pathways are also conceivable for the presented π-complex reaction.
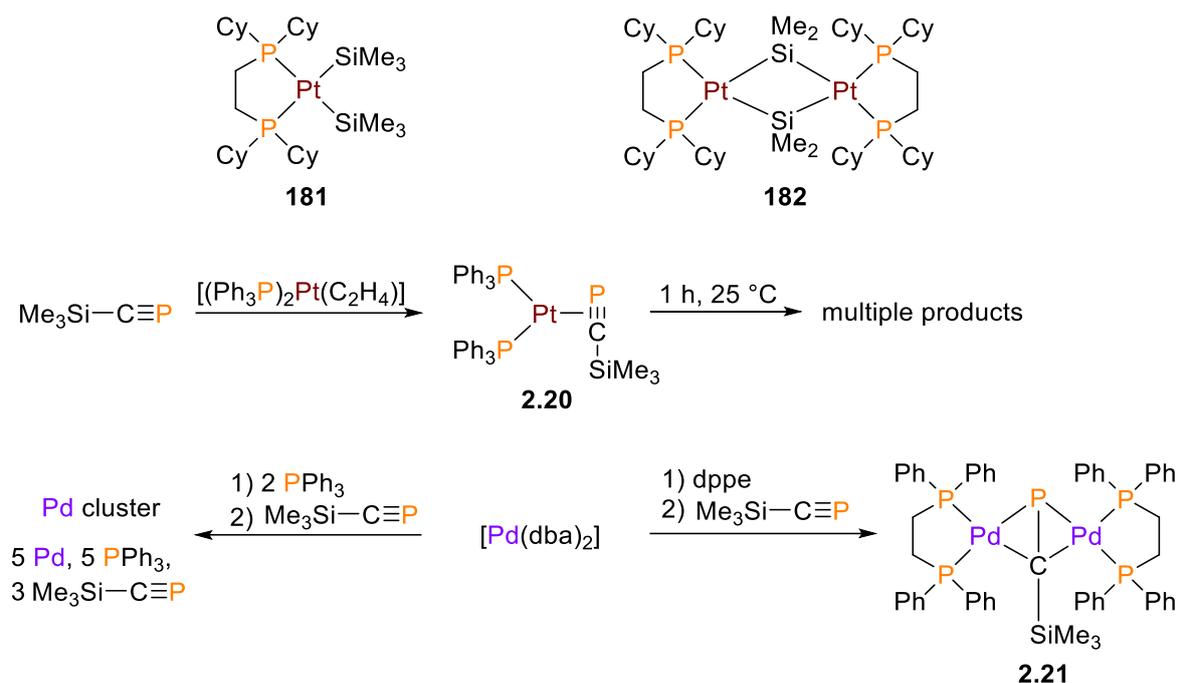
Scheme 56. Possible outcomes (**181**, **182**) by attempting the preparation of [(dcpe)Pt(Me₃SiCP)] (**155**) and performed reactions of Me₃Si-CP with Pt(0) or Pd(0) precursors by Russell and co-workers.[139]

The synthesis of [(dcpe)Ni(Ph₃SiCP)] (**156**) yielded exclusively four $^{31}P\{^1H\}$ NMR signals for two independent compounds (Figure 54). Interestingly, the fist compound (cf. signals C and D) shows a similar shift, pattern and coupling constant as the two triplets found in the attempt of synthesize complex [(dcpe)Ni(Me₃SiCP)] (**154**). This compound (signals C, D) was removed from the reaction mixture by precipitation from pentane but decomposed during this step. The signals A ($\delta(^{31}P\{^1H\})$) = 75.4 ppm, (dd, $J_{P,P}$ = 29.7, 6.4 Hz) and B ($\delta(^{31}P\{^1H\})$ = 66.0 ppm, (dd, $J_{P,P}$ = 29.4, 18.8 Hz) of the remaining compound reflect the typical shifts and coupling constants of π-complexes bearing a dcpe ligand and belong most likely to the desired product **156**, which should have a similar ^{31}P shift for the C≡P moiety (δ = 322.7 ppm) as calculated model complex [(dmpe)Ni(Ph₃SiCP)] (**C3**). Unfortunately, that was not recognized at this time due to a lack of comparable dcpe complexes and shifts beyond δ = 300 ppm were not recorded. Nevertheless, the isolated compound was exposed to an array of violet light LEDs (λ = 405 nm) for several hours without showing any change in the $^{31}P\{^1H\}$ spectrum. Thus, an activation of the C-CP bond can be excluded. In the analog reaction with platinum, the π-complex [(dcpe)Pt(Ph₃SiCP)] (**157**) was obtained ($\delta(^{31}P\{^1H\})$ = 287.9 (calc. 267.5 for [(dcpe)Pt(Ph₃SiCP)] (**C5**)), 72.5, 65.2 ppm) in combination with an unknown by-product at $\delta(^{31}P\{^1H\})$ = 68.0 ppm (Figure 55). Even though the chemical shift of the by-product fits with the [(COD)Pt(dcpe)] (**45**), the ^{195}Pt satellites did not match. Irradiation with violet light (λ_{max} = 405 nm) did not show any effect, hence no further studies on silylphosphaalkyne complex were performed.

The similar [(dcpe)Ni(TritylCP)] complex (**158**) could also be synthesized and shows a less deep-field-shifted phosphaalkyne moiety of $\delta(^{31}P\{^1H\}) = 148.9$ ppm (145.7 ppm calc. for [(dmpe)Ni(TritylCP)] (**C4**)), whereas the dcpe phosphorus atoms possess similar shifts of $\delta(^{31}P\{^1H\}) = 71.9$ and 56.4 ppm. **158** did not react under UV ($\lambda_{max} = 365$ nm) or violet light ($\lambda_{max} = 405$ nm) irradiation. However, the $^{31}P\{^1H\}$ spectrum revealed an additional set of signals for a second species in addition to [(COD)Ni(dcpe)] (**43**) and [Ni(dcpe)$_2$] (**44**, Figure 56). Taking into account the ^{31}P NMR shifts of compound **2.21** (Scheme 56) reported by RUSSELL and co-workers,[139] and the excess of dcpe ligand, the formation of the [{(dcpe)Ni}$_2$(μ_2-TritylCP)] dimer complex is assumed but has not been verified.
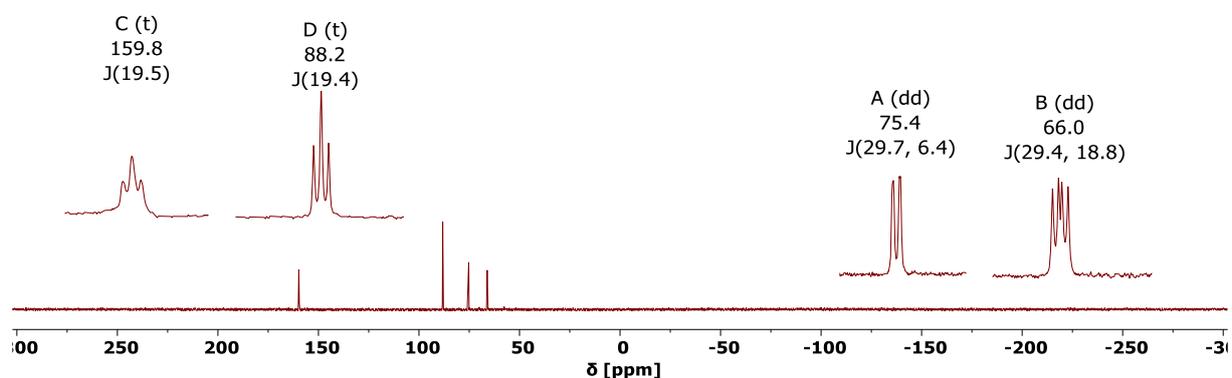
Figure 54. $^{31}P\{^1H\}$ NMR spectrum of the reaction mixture of [(dcpe)Ni(Ph$_3$SiCP)] (**156**) in toluene with magnification of the phosphorus signals of the two compounds (1: A, B; 2: C, D).
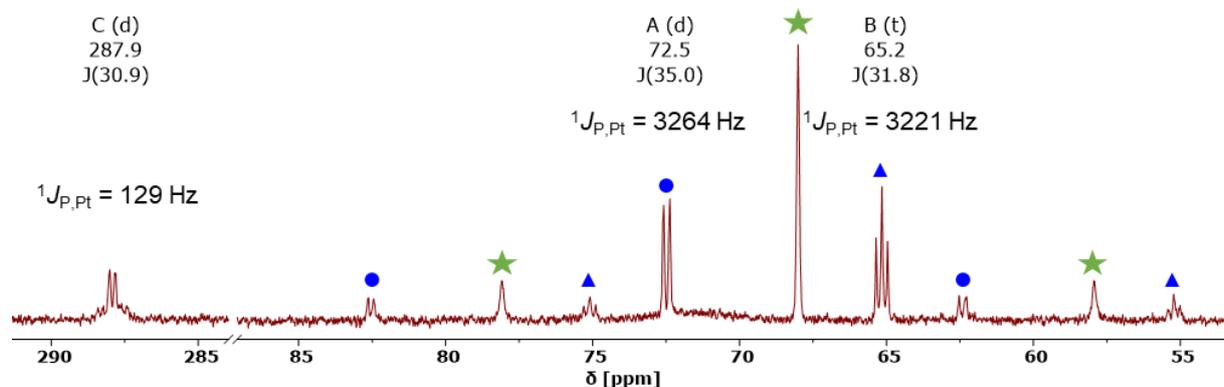
Figure 55. $^{31}P\{^1H\}$ NMR spectrum of [(dcpe)Pt(Ph$_3$SiCP)] (**157**) in tetrahydrofuran. The blue dots and triangles assign the ^{195}Pt satellites of the two dcpe phosphorus signals of the compound **157**, whereas the green stars mark the corresponding ^{195}Pt satellites of an unknown by-product.
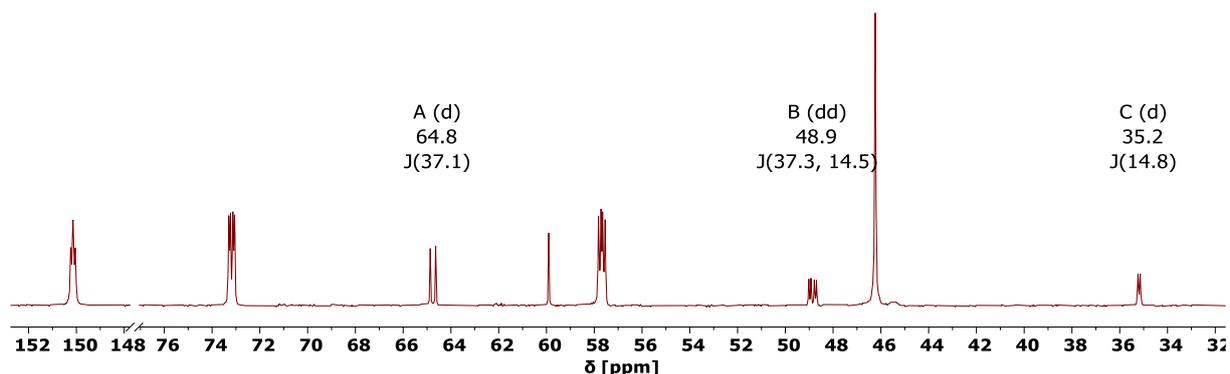
Figure 56. $^{31}P\{^1H\}$ NMR spectrum of [(dcpe)Pt(TritylCP)] (**157**) in tetrahydrofuran-d_8. The signals A, B and C are from a additional compound, presumably [{(dcpe)Ni}$_2$(μ_2-TritylCP)].

The dippdmae π-complexes **159** - **162** are more sensitive than their dippe or dcpe counterparts and easily react with most impurities within the reaction mixture making it challenging to isolate them. Interestingly, the two $^{31}P\{^1H\}$ signals for [(dippdmae)Ni(MesCP)] (**159**) appear at δ = 165.7 and 39.2 ppm are broad multiplets, whereas the signals of [(dippdmae)Ni(Mes*CP)] (**161**) are sharp doublets at δ = 157.4 and 57.7 ppm. The $^{31}P\{^1H\}$ spectrum of the [(dippdmae)Pt(MesCP)] complex (**160**) suggests the assumption of two isomers in the case of the less bulky MesCP (**68**), orientating the phosphorus atom of the dippdmea either *cis* or *trans* to the phosphorus atom of the MesCP (Figure 57). The signal at $\delta(^{31}P\{^1H\})$ = 32.6 ppm with the larger $^{31}P^{195}Pt$ coupling constant should be the π-complex with the phosphorus atom in *trans* position. The bulkier supermesitylphosphaalkyne complex **162** showed, likewise to the nickel derivative, only a set of two sharp resonances. Addition of an excess of the appropriate phosphaalkyne to these complexes did not result in the catalytical formation of a triphosphabenzene. Longer heating or irradiation with UV light (λ_{max} = 365 nm) led to decomposition, especially with an excess of phosphaalkyne or impurities. Potentially, less steric demanding phosphaalkynes might show positive results, but are generally unstable and impractical for handling.
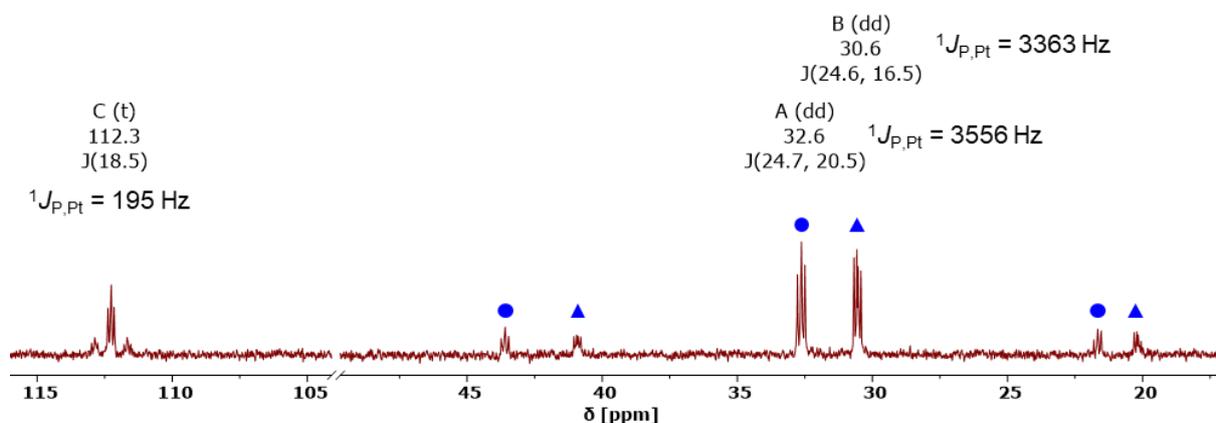

Figure 57. $^{31}P\{^1H\}$ NMR spectrum of [(dippdmae)Pt(MesCP)] (**160**) in tetrahydrofuran-d_8. The blue dots and triangles assign the ^{195}Pt satellites of the dippdmae phosphorus signals.

The non-chelating π-complexes **178** - **180** were synthesized by addition of the appropriate phosphaalkyne to ethylenebis(triphenylphosphine)platinum(0) (**183**, Scheme 57). The $^{31}P\{^1H\}$ spectra of these complexes reveal three signals, a doublet of doublets at approximately $\delta \approx 100$ ppm for the phosphaalkyne, a triplet at about $\delta \approx 30$ ppm and a doublet of doublets at about $\delta \approx 25$ ppm. The $^{31}P^{195}Pt$ coupling constants of the phosphaalkyne and phosphine phosphorus atoms are larger than the correlating derivatives with chelating diphosphines. Compound **180** slowly decomposed or reacted to non-specified compounds and, a potential C-H activation, as observed by JONES *et al.* for benzonitrile might be implicated (cf. chapter 2.1.1, Scheme 18).[269] The molecular structures of **178** - **180** were not determined, however a square-planar coordination environment around the metal center in compliance with the chelating derivatives is expected, as found for the diphenylacetylene counterpart.[403-405] No photochemical activation was observed for the non-chelating π-complexes **178** - **180**.
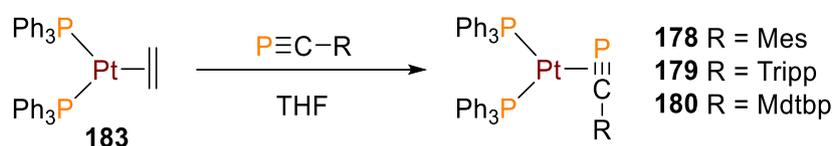
Scheme 57. Preparation of arylphosphaalkyne-bis(triphenylphosphino)planitum complexes.

All examined C_3 π-complexes with mesitylphosphaalkyne are stable. Their ^{31}P chemical shifts are given in **Table 9**. Even the platinum derivative **174** did not react by irradiation with UV (λ_{max} = 365 nm) or violet light (λ_{max} = 405 nm). The molecular structure of [(dcpp)Ni(MesCP)] (**173**) revealed an increased bite angle of around 10° and slightly increased nickel bond distances of 0.014 Å on average against the C_2 backbone derivative [(dippe)Ni(MesCP)] (**142**, Figure 58).
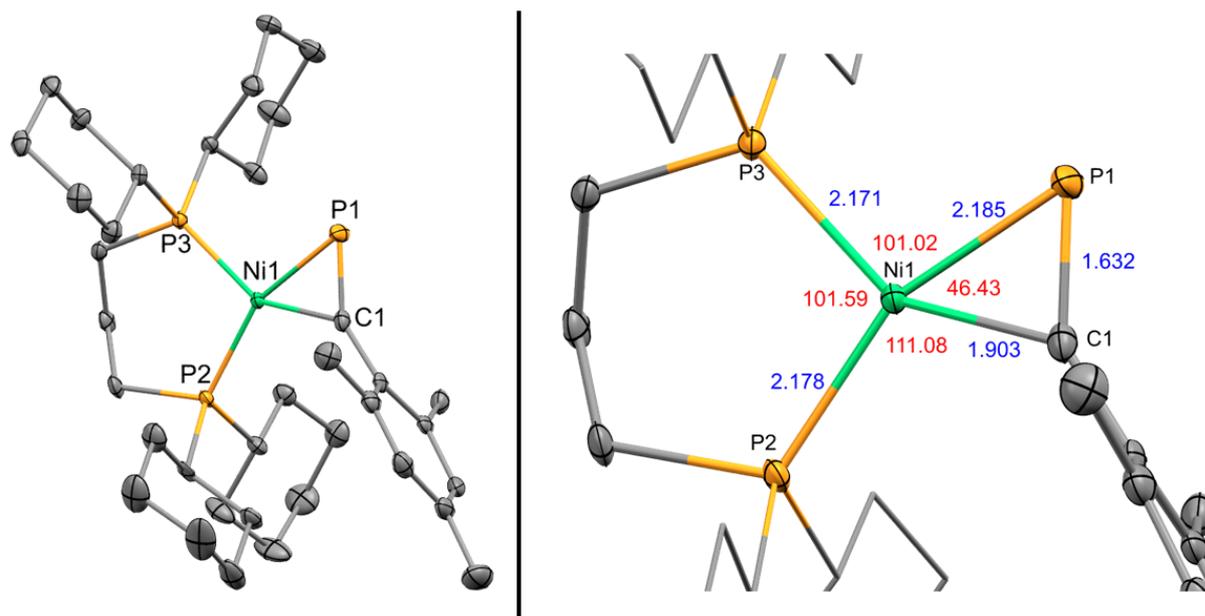
Figure 58. Molecular structure of [(dcpp)Ni(MesCP)] (**173**) in the crystal. Anisotropic displacement ellipsoids are shown at 50% probability level. Hydrogens omitted for clarity. Selected bond lengths (Å) in blue and angles (°) in red.

The synthesis of the C_1 π-complexes differs a bit from the other π-complexes. For the best results, it is important to add dtbpm (**15**) or dcpm (**21**) at low temperatures (T = -30 °C) under vigorous stirring and allow the reaction mixture to warm to room temperature or, even better, heat to around T = 35 °C. After stirring the red solution for 3 h, the phosphaalkyne was added dropwise at T = -30 °C under vigorous stirring until the reaction solution turned bright red or golden, before allowing to warm up to room temperature and stir for additional 16 h. There are two reasons for that. Firstly, the reaction yields unknown by-products if performed at room temperature. Secondly, the formation of the intermediate [(P,P)M(COD)] and the final phosphaalkyne complex [(P,P)M(R-C≡P)] takes much more time than for the other π-complexes with larger bite angles. Those effects are more prominent for the sterically more demanding dtbpm (**15**) ligand. Too fast addition of the C_1-diphosphine ligands might lead to intermolecular reactions and the formation of metal dimers or even clusters (cf. chapter 2.1.2.2.6, Scheme 32), but that was never investigated. The choice of the phosphaalkyne also influences the formation and/or stability of the generated π-complex. In general, all MesCP C_1 π-complexes seemed to be unstable, especially in the case of dtbpm (**15**). Directly after applying MesCP to the reaction mixture of [(dtbpm)M(COD)], promising ^{31}P{^{1}H} resonances of a potential [(dtbpm)M(MesCP)] complex were observed, but these resonances disappeared in the further course of the reaction. In the end, only the [(dcpm)Ni(MesCP)] (**167**) could be monitored without doubt. In contrast, all TrippCP derivatives could be detected by means of ^{31}P{^{1}H} NMR spectroscopy. The most relevant representative, [(dcpm)Pt(TrippCP)] (**170**), was successfully isolated and fully characterized. The ^{31}P{^{1}H} spectra of the C_1 π-complexes revealed the typical signal pattern, however, the gap between the phosphaalkyne and the two

phosphine signals is the largest in the row of the synthesized arylphosphaalkyne π-complexes with δ = 178 ppm for [(dcpm)Ni(TrippCP)] (**169**) and δ = 162 ppm for the platinum derivative **170**. The nickel π-complexes [(dtbpm)Ni(TrippCP)] (**165**), [(dcpm)Ni(MesCP)] (**167**) and [(dcpm)Ni(TrippCP)] (**169**) did not react if exposed to violet light (λ_{max} = 405 nm), whereas the platinum complexes slowly converted into a new species, which will be discussed in detail in the next chapter (2.1.4.2). The $^{31}P\{^1H\}$ spectra of [(dtbpm)Pt(TrippCP)] (**166**) and [(dcpm)Pt(TrippCP)] (**170**) are depicted in Figure 59. The smaller $P^{31}Pt^{195}$ coupling constants of around $^1J_{P,Pt} \approx 2600$ Hz for the phosphine signals of both complexes are conspicuous against the typical values of more than $^1J_{P,Pt}$ = 3000 Hz. The $^{13}C\{^1H\}$ signal of the C≡P units was found in the typical area of around $\delta \approx 225$ ppm (**166**: 224.5 ppm, **170**: 221.5 ppm), although the $^{195}Pt\{^1H\}$ signal of δ = -3991 ppm, measured for **170**, is downfield shifted compared to the values at around $\delta \approx -4500$ ppm found for the C$_2$ platinum π-complexes. The noticeable shift in the ^{195}Pt NMR, together with the significant change of the $^{195}Pt^{31}P$ couplings, indicates the impact of the narrow bite angle, which also impairs the orbital overlap between the phosphine phosphorus atom and the platinum atom.[301, 406-408] The molecular structure of **170** in the crystal has a square-planar geometry. The methylene carbon C17 lies in the plane of the platinum bonded phosphorus atoms. The platinum bond lengths are slightly elongated compared to the C$_2$ π-complexes **143** (Figure 60), whereas the C≡P distance is unchanged. The bite angle of **170** is substantial decreased by 14°, whereas the corresponding angle (P1-Pt1-C1) is identical. Consequently, the two wider angles between the diphosphine phosphorus atoms and C≡P moiety are further enlarged. The aryl group of **170** (P1-C1-C2: 147.5(2)°) is less bent from the ideal 180° than in **143** (140.9(4)°), even though it is bulkier (Tripp vs Mes).
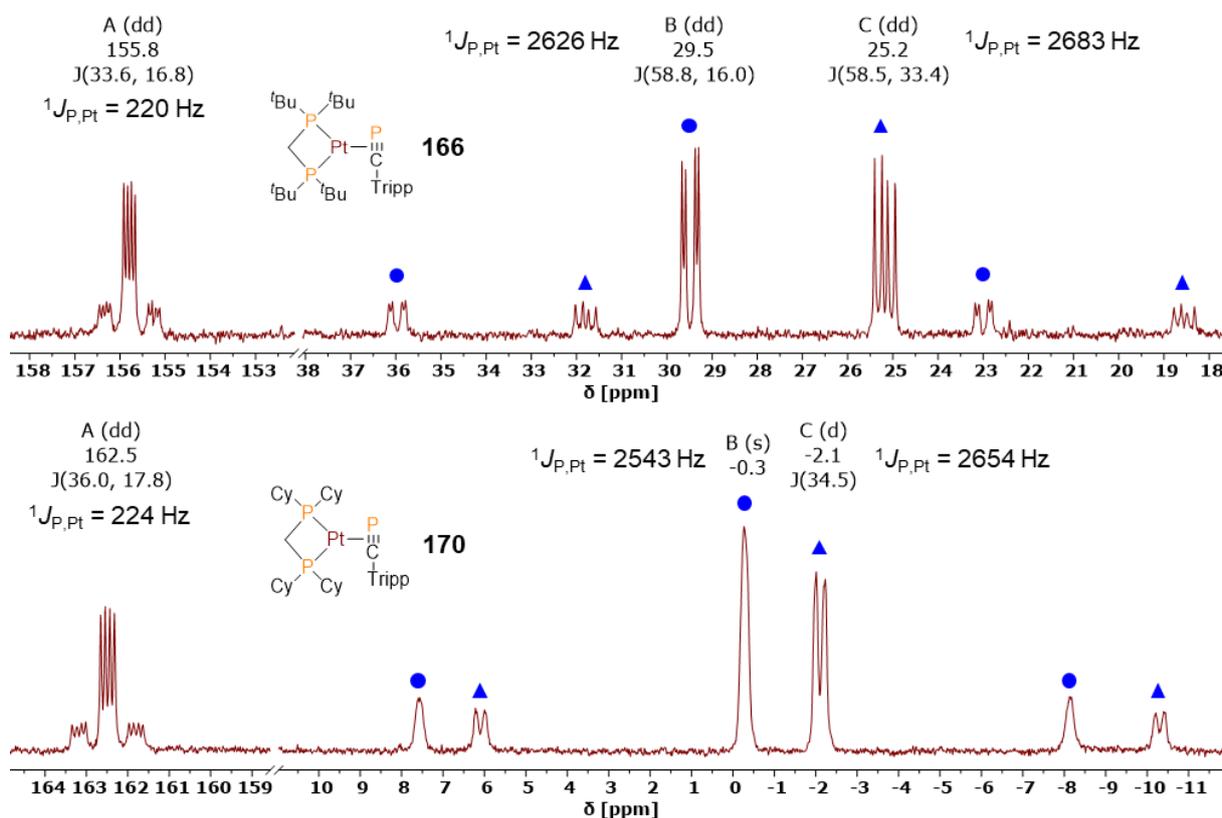
Figure 59. $^{31}P\{^1H\}$ NMR spectrum of [(dtbpm)Pt(TrippCP)] (**166**, top) and [(dcpm)Pt(TrippCP)] (**170**, bottom) in tetrahydrofuran-d_8. The blue dots and triangles assign the ^{195}Pt satellites of the dtbpm (top) and dcpm (bottom) phosphorus signals.
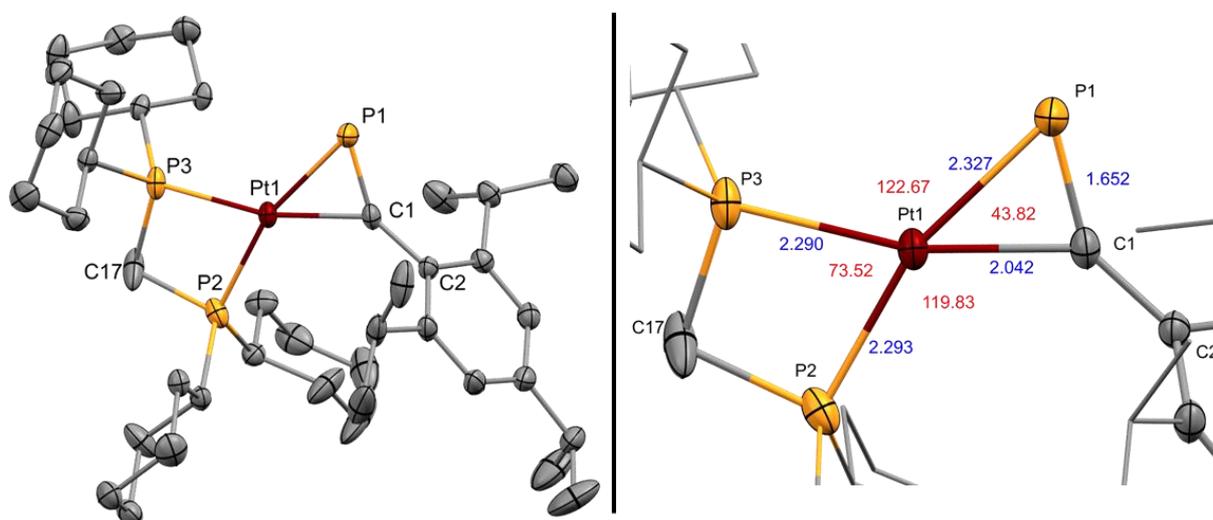
Figure 60. Molecular structure of [(dcpm)Pt(TrippCP)] (**170**) in the crystal. Anisotropic displacement ellipsoids are shown at 50% probability level. Hydrogens omitted for clarity. Selected bond lengths (Å) in blue and angles (°) in red.

The most relevant compounds for the study were the C_2 arylphosphaalkyne complexes. They are stable and could be isolated almost purely and in quantitative yields. Even though the stoichiometry of the ligands needs to be very accurate (1 eq) to avoid the formation of

undesired by-products, the generated π-complex are remarkable stable at room temperature. Supplementary addition of chelating diphosphines did not yield the corresponding [M(P,P)$_2$] dimer by liberating the phosphaalkyne. The lightweight nickel π-complex [(dippe)Ni(MesCP)] (**142**) could be purified by sublimation. The sublimation of the heavier [(dippe)Ni(Mes*CP)] (**145**) and platinum based complexes like [(dippe)Pt(MesCP)] (**143**) already resulted in product mixtures and decomposition products. All platinum derivatives, with the exception of the supermesitylphosphaalkyne complexes [(dippe)Pt(Mes*CP)] (**146**) and [(dcpe)Pt(Mes*CP)] (**153**), reacted upon irradiation with UV (λ_{max} = 365 nm) or violet light (λ_{max} = 405 nm), for details see chapter 2.1.4.2. None of the nickel π-complexes reacted by photolysis. The ^{31}P{^{1}H} spectra of the C$_2$ π-complexes show three signals with typical pattern. The phosphorus atom of C≡P unit has a shift range between δ = 126 and 172 ppm. The shifts of the nickel complexes are in average δ = 30 ppm higher (deeper downfield shifted) in comparison to their platinum analogs. The diphosphine signals are between δ = 59 and 83 ppm with the same value for the analog nickel and platinum complexes within the uncertainty of measurement. The platinum complexes possess supplementary ^{195}Pt satellites with values of between $^1J_{P,Pt}$ = 166 and 230 Hz for the C≡P unit, around $^1J_{P,Pt} \approx$ 3000 Hz for the deeper downfield shifted phosphorus atom of the diphosphine group and around $^1J_{P,Pt} \approx$ 3200 Hz for the second phosphorus atom. The ^{31}P shift for the C≡P units of [(dcpe)Ni(MesCP)] (**147**, exp. 169.6, calc. 183.8 for **C1**) and [(dcpe)Pt(MesCP)] (**148**, exp. 140.0, calc. 146.8 for **C7**) was computationally calculated as reference point for further predictions and is in reasonable agreement with the found values, taking in account that the cyclohexyl groups were replaced with methyl groups to reduce the calculation time. A spin simulation of the platinum complex **148** is in excellent agreement with the measure spectrum (Figure 61).
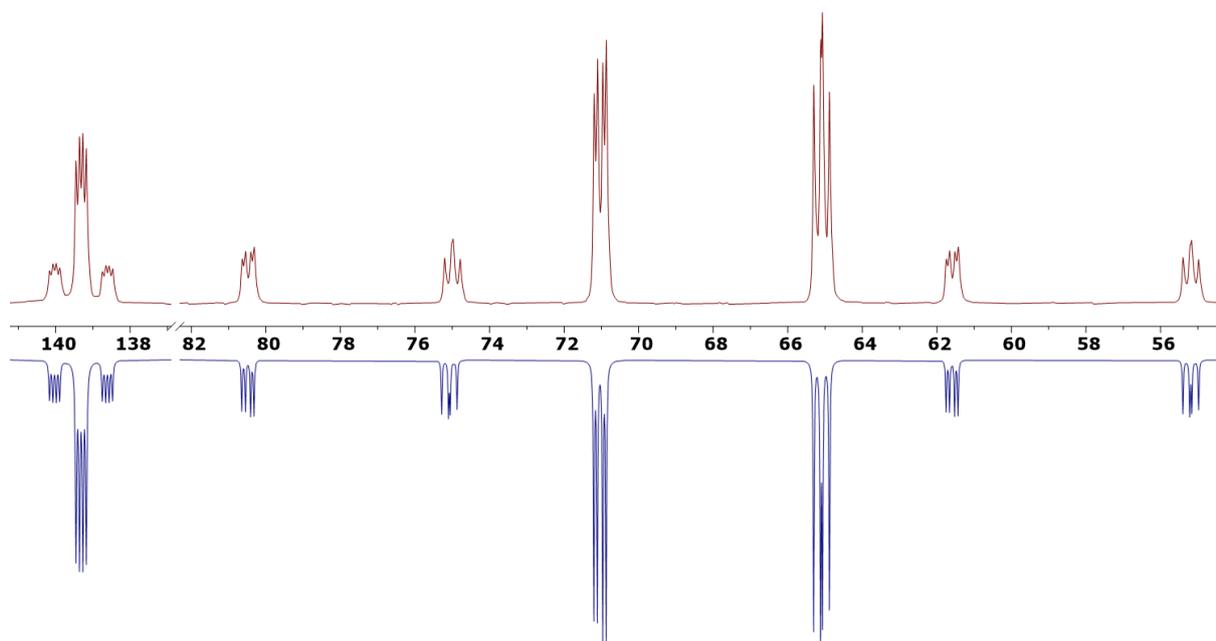
Figure 61. Measured (top) and simulated (bottom) $^{31}P\{^1H\}$ NMR spectrum of [(dcpe)Pt(MesCP)] (**148**). Scale in ppm.

Figure 62 lists the $^{31}P\{^1H\}$ spectra of all platinum C_2 π-complexes to visualize some $^{31}P\{^1H\}$ NMR tendencies. All dippe signals appear at a deeper low-field shift than the dcpe signals. Furthermore, the signal gap between the two phosphorus signals of the diphosphine is larger. Interestingly, there is a significant difference in the shifts of the C≡P phosphorus atom. Taking the MesCP complexes **143** and **148** as reference, the signals of the analogous Mes*CP complexes **146** and **153** are less high-field shifted, whereas the signals of the TrippCP complexes **144** and **150** are clearly more low-field shifted, leading to a significant larger shift gap $\Delta\delta$ (Figure 62) between the C≡P phosphorus and the next diphosphine signal. The NMR chemical shift is depending on the shielding of the atomic nucleus by the electrons (magnetic susceptibility; cf. Shoolery's rule).[409] Inversely, the chemical shift also represents the electronic situation of an atomic nucleus. Already anticipating the results of the π-complex activation, the best outcomes were achieved by π-complex with the largest shift gap $\Delta\delta$ within a class; namely the TrippCP complexes **144** and **150**.
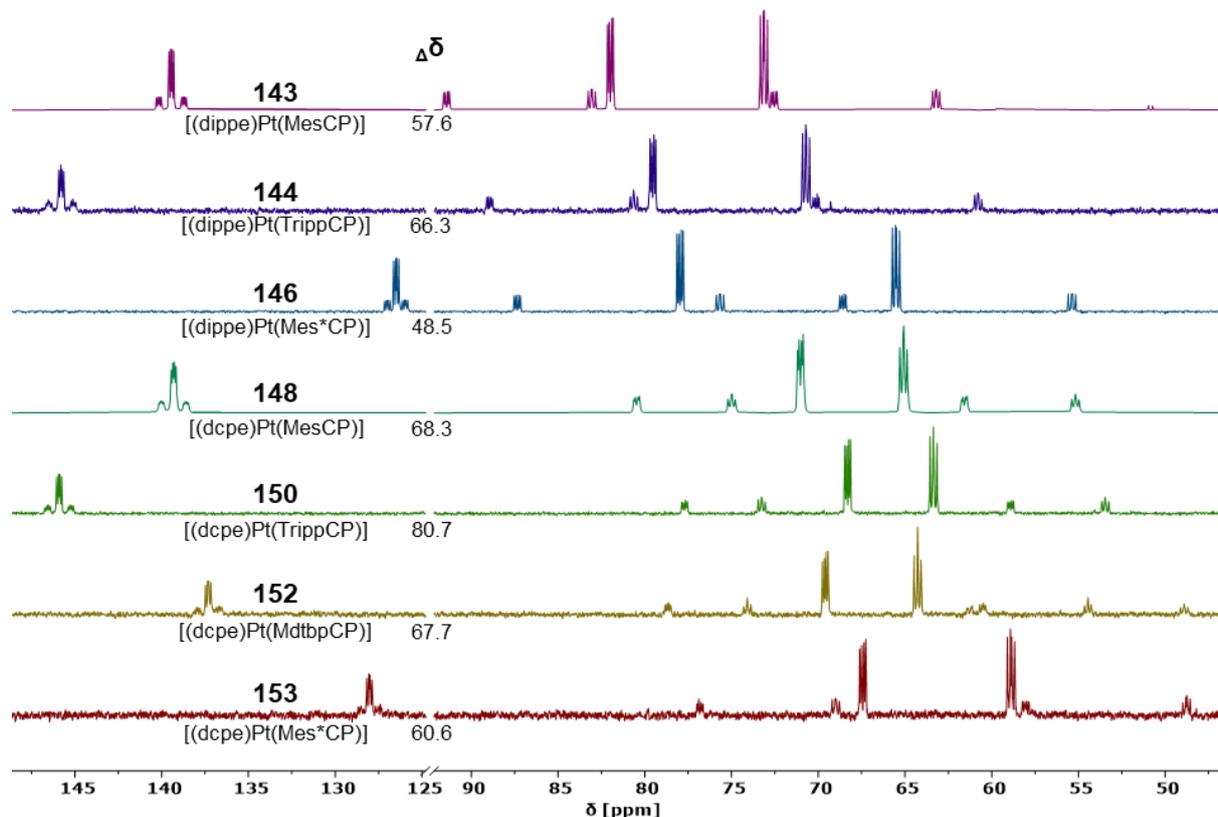
Figure 62. $^{31}P\{^{1}H\}$ NMR spectra of the synthesized C_2 arylphosphaalkyne platinum complexes. The $\Delta\delta$ [ppm] value is the shift difference between the C≡P phosphorus signal an the highest shifted (left) phosphorus of the diphosphine.

The molecular structure of the C_2 π-complexes in the crystal shows a slightly twisted square-planar geometry. Taking [(dcpe)Pt(MesCP)] (**148**) as example, the twist is induced by the dcpe ligand with one bridging carbon (C15) above and the other (C14) below the (Figure 63) imaginative plane spanned by the three phosphorus atoms. The bond length and angles including the platinum core as well as the C≡P distance comply with those found for [(dippe)Pt(MesCP)] (**143**, cf. Figure 52). The Mes group is marginal less bent with an P3-C41-C23 angle of 145.7(8)° against 140.9(4)°.
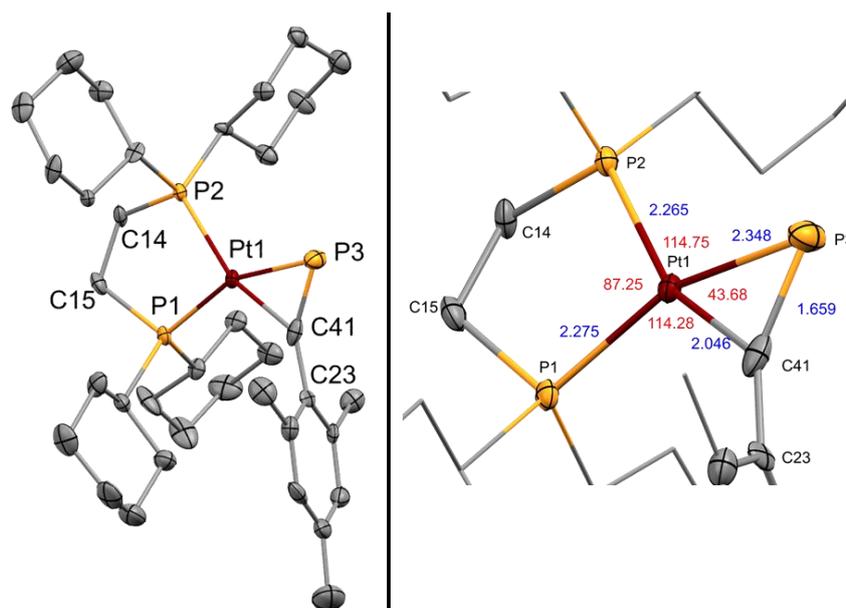
Figure 63. Molecular structure of [(dcpe)Pt(MesCP)] (**148**) in the crystal. Anisotropic displacement ellipsoids are shown at 50% probability level. Hydrogens omitted for clarity. Selected bond lengths (Å) in blue and angles (°) in red.

The molecular structures of [(dippe)Ni(Mes*CP)] (**145**) and [(dippe)Pt(Mes*CP)] (**146**) are analogously to the previous discussed molecular structures of [(dippe)Ni(MesCP)] (**142**) and [(dippe)Pt(Mes*CP)] (**143**) with slightly wider bond angles for the nickel complex for the P1-Ni1-P2 and the opposite angle (Figure 64). Surprisingly, the Mes* group is in both cases (**145**: 150.9(1)°, **146**: 149.5(5)°) even less bent, closer to ideal 180°, than found for the analog mesityl complexes. However, the *ipso* carbon of the supermesityl ring of both complexes **145** and **146** is bent around 15° out of aromatic plane. This effect is in correlation with the steric demand of the groups in *ortho* position. A comparison of the platinum structures **143**, **170** and **146** bearing the MesCP, TrippCP and Mes*CP revealed an increase of this out of plane bending trend from around 1, over 7 to 15°.
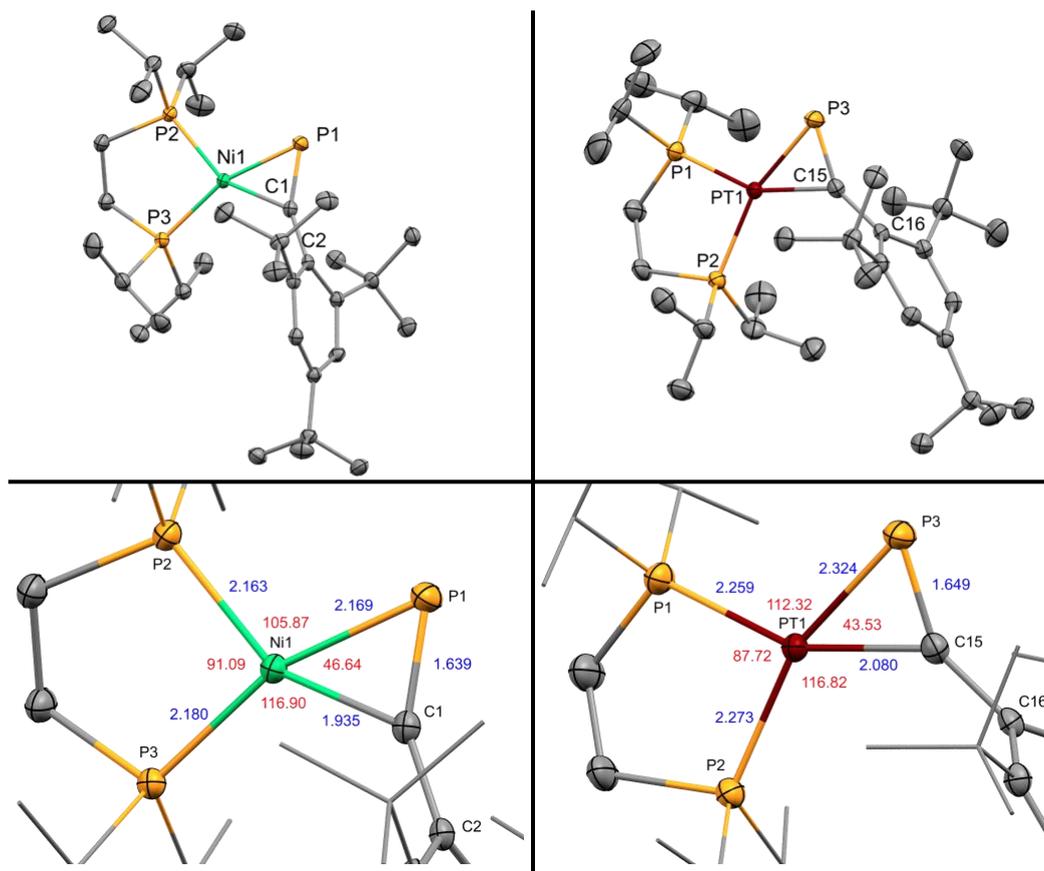
Figure 64. Molecular structure of [(dippe)Ni(Mes*CP)] (**145**, left) and [(dippe)Pt(Mes*CP)] (**146**, right) in the crystal. Anisotropic displacement ellipsoids are shown at 50% probability level. Hydrogens omitted for clarity. Selected bond lengths (Å) in blue and angles (°) in red.

To complete the row of d^{10} metals, the two palladium complexes [(dippe)Pd(MesCP)] (**184**) and [(dcpe)Pd(MesCP)] (**185**) were synthesized (Scheme 58). The preparation was realized with tetrakis(triphenylphosphine)palladium(0) (Pd(PPh$_3$)$_4$) or tris(dibenzylideneacetone)-dipalladium(0) (Pd$_2$(dba)$_3$) instead of Pd(COD)$_2$. Even though Pd(COD)$_2$ can be synthesized by the same method as its platinum derivative, the whole preparation including the isolation must take place at low temperatures not exceeding T = -25 °C.[278-279] The reported yields are low and the compound itself highly sensitive, therefore other Pd(0) precursor were more reasonable for a prove of concept reaction. The major drawback of starting the synthesis with Pd(PPh$_3$)$_4$ or Pd$_2$(dba)$_3$ is the product isolation. The liberated triphenylphosphine has a similar solubility as the product **184**, which could not be separated by column chromatography or sublimation due to its highly sensitive nature. The same issue applies to the isolation attempt of **185**, although the dibenzylideneacetone could be mostly removed by washing **185** with hot hexane if accepting very low yields (> 15%). Both palladium complexes **184** and **185** did not react upon heating to T = 65 °C in THF but decompose upon irradiation with UV (λ_{max} = 365 nm) or violet light (λ_{max} = 405 nm) within several hours. Due to the lack of any evidence for C-CP cleavage capability and the general higher sensitivity of the palladium complexes, no further investigations were conducted.
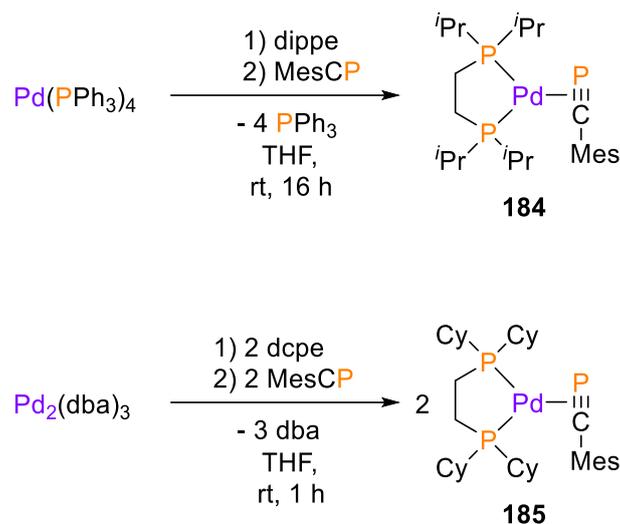
Scheme 58. Preparation of [(dippe)Pd(MesCP)] (**184**) and [(dcpe)Pd(MesCP)] (**185**).

The ^{31}P NMR studies revealed a similar pattern as for the nickel and platinum complexes. The palladium complexes possess the lowest shift for the C≡P moiety with δ = 97.2 ppm for **184** and δ = 97.2 for **185**, which is in line with the predicted value of around δ = 108 ppm for the hypothetical [(dmpe)Pd(MesCP)] (**C6**) complex. The ^{31}P NMR signals of the dippe and dcpe groups are approximately δ = 10 ppm less downfield shifted than for the Pt analogs (Figure 65). The ^{1}H spectra follow this tendency with less low-field shifted signals such as illustrated for the ^{1}H{^{31}P} spectrum of [(dippe)Pd(MesCP)] (**184**) in Figure 66.
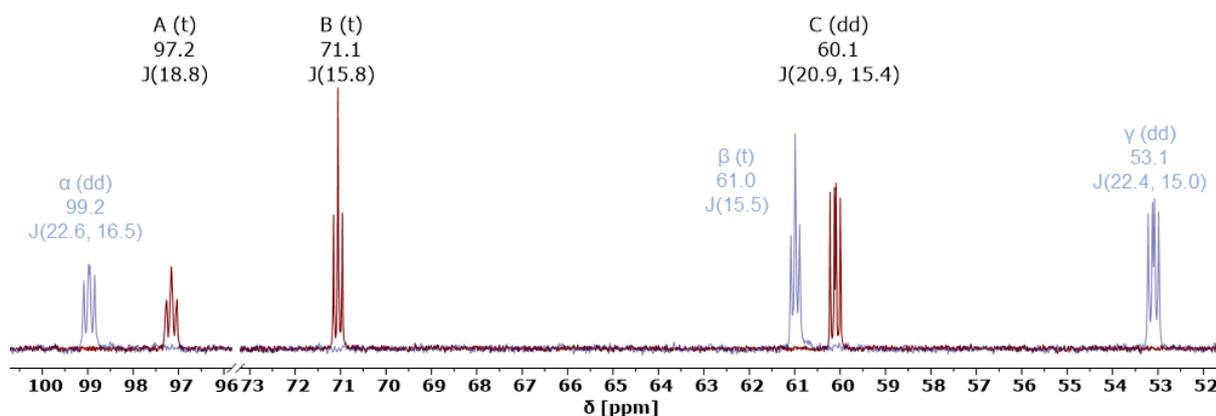
Figure 65. ^{31}P{^{1}H} NMR spectra of [(dippe)Pd(MesCP)] (**184**, red) and [(dcpe)Pd(MesCP)] (**185**, blue) in tetrahydrofuran-d$_8$.
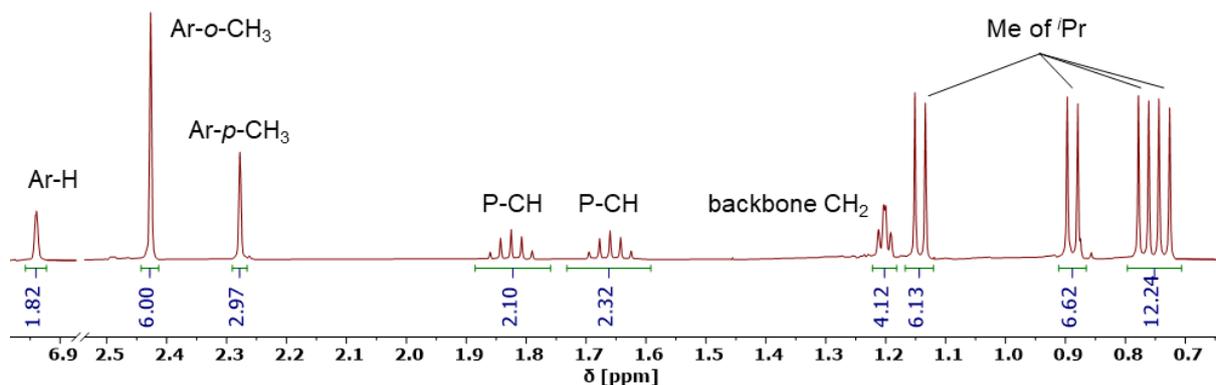
Figure 66. $^1H\{^{31}P\}$ NMR spectrum of [(dippe)Pd(MesCP)] (**184**) in benzen-d_6.

The approach to transfer this concept to d^9 transition metals by applying either dippe together with MesCP or dcpe with TrippCP to the commercially available [Rh(COD)$_2$]BF$_4$ or [Ir(COD)$_2$]BF$_4$ only let to decomposition and the formation of double chelate complexes of the kind [(P,P)$_2$Rh/Ir]BF$_4$. The connectivity structure could be proven by the single crystal X-ray diffraction analysis of [Ir(dcpe)$_2$]BF$_4$ (Figure 67). The d^9 transition metals for the C-CP slitting were not investigated further, however, it is assumed that rhodium precursor, like [Rh(dippe)(μ-K · THF)]$_2$, with the metal in the formal oxidation state of -I are potentially suitable for the cleavage reaction as it was already demonstrated for the C-CN cleavage by JONES and co-workers.[248]
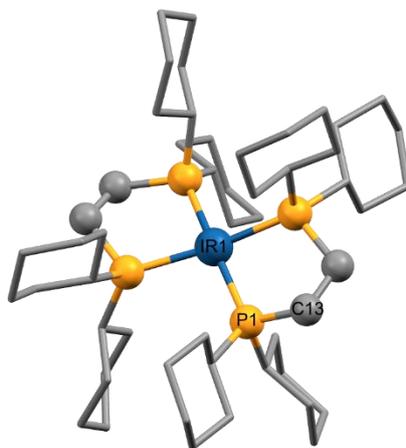
Figure 67. Connectivity structure of [Ir(dcpe)$_2$]BF$_4$ in the crystal, shown as ball-stick model. Hydrogens, four co-crystalized toluenes and BF$_4^-$ anion omitted for clarity.

2.1.4   Preparation of cyaphido complexes (σ-complexes)

2.1.4.1   Coordination Modes

For a deeper understanding of the chemistry of cyaphido ligand, DFT calculations were performed to gain insight into the frontier molecular orbitals of the cyaphido ligand with respect to the well-established cyanido ligand.[410] The MO scheme (Figure 68) reveals similar energy levels for the HOMOs, indicating that the cyaphido and cyanido ligand possess similar σ-donor strengths. In contrast, the degenerate LUMO and LUMO+1 of C≡P$^-$ is energetically stabilized by 3 eV. In addition, the degenerate HOMO−1 and HOMO−2 are destabilized by 0.6 eV in the cyaphide anion. Since these two orbital sets correspond to π^* and π orbitals, cyaphido has slightly better π-donor and much stronger π-acceptor properties than cyanide.
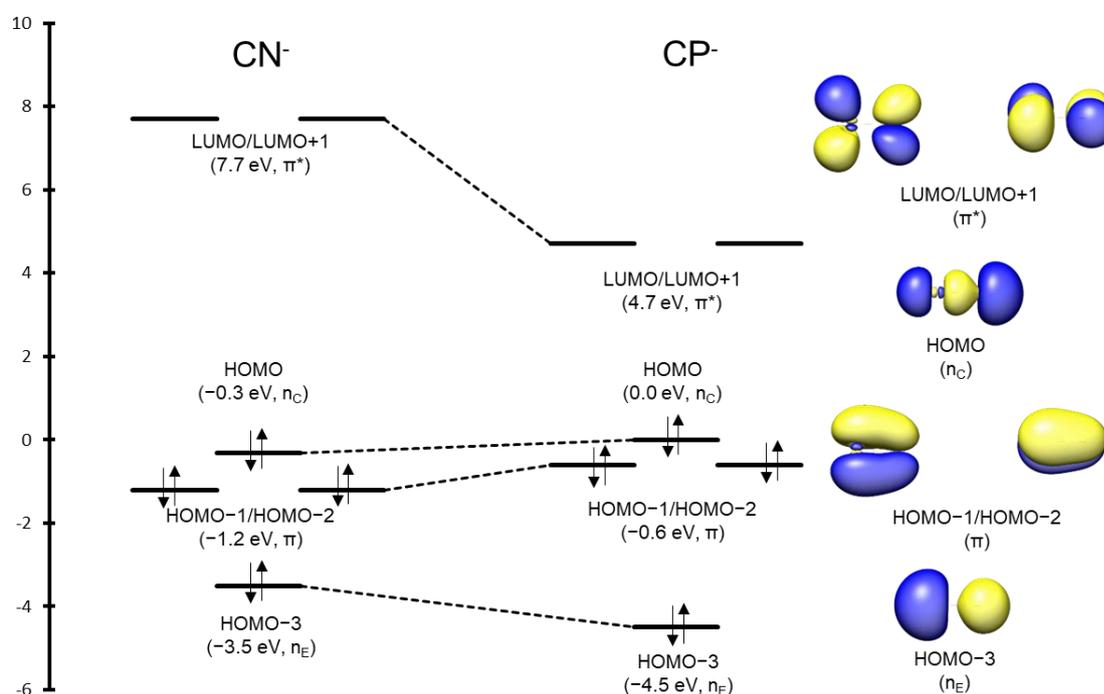
Figure 68. MO Scheme for CN$^-$ and CP$^-$ (left) and selected MOs of CP$^-$ (right).

Calculations of the CO-stretching vibrations, $\tilde{v}_{CO}$, of generic nickelates [Ni(CO)$_3$CE]$^-$ (E = N, P) were performed (Figure 69). The lower CO-stretching vibrations of the η^1-cyaphido complex are provoked by stronger electron back-donation into the π^*(CO) orbitals with respect to the cyanido complex, which refers to a higher electron density at the metal center and the slightly better net-donor characteristics of C≡P$^-$. The C≡P bond length of [Ni(CO)$_3$CP]$^-$ was calculated to be 1.582 Å, whereas the C≡N distance of the cyaphido analog was assigned to be 1.607 Å long. Interestingly, a second minimum structure for [Ni(CO)$_3$CP]$^-$ was found, where the cyaphide anion is coordinated in a side-on fashion ([Ni(CO)$_3${η^2-CP}]$^-$, Figure 69). While this isomer is higher in energy than for the σ-coordinated nickelate (ΔE = 20.9 kcal·mol^{-1}), the calculated $\tilde{v}_{CO}$ values are similar. This finding hints to the strong π-donor abilities of the

cyaphide anion. The π-coordination led to an elongation of the C≡P bond distance (1.622 Å) in [Ni(CO)$_3$\{η^2-CP\}]$^-$.

$$\tilde{\nu}_{CO}= \quad \text{1962, 2025 cm}^{-1} \qquad \text{1957, 2017 cm}^{-1} \qquad \text{1957, 1968, 2019 cm}^{-1}$$
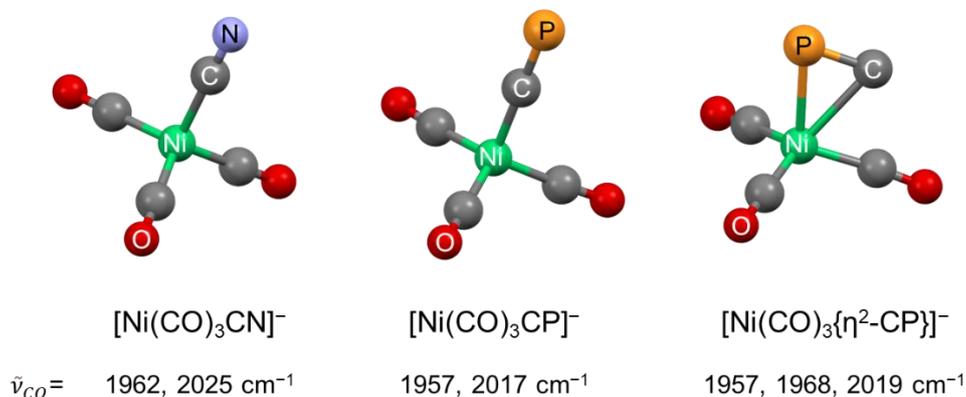
Figure 69. Calculated structures of generic nickelates [Ni(CO)$_3$CE]- (E = N, P) and the wavenumbers of the CO-stretching vibrations.

The π-coordination mode represents the minimum energy structure of the homobimetallic complex [(Ag(NH$_3$)$_2$\{μ-η^1:η^2-CP\}]$^+$. While the analogous cyanido complex [(Ag(NH$_3$)$_2$\{μ-η^1-CN\}]$^+$ shows a linear bridging mode of the central cyanide ligand, the cyaphido ligand binds one silver atom via the carbon atom (σ-coordination, Ag-C 2.001 Å) and the second silver atom is bound via the π-system (Ag-C 2.138 Å, Ag-P 2.651 Å, Figure 70). EDA-NOCV calculations show that the cyaphido ligand in this complex acts simultaneously as a π-donating (25.3 kcal·mol^{-1}) and π-accepting ligand (12.8 kcal·mol^{-1}). This is in accordance with the rather small energy gap between the HOMO−1/HOMO−2 and the LUMO/LUMO+1 orbitals in C≡P$^-$ (5.3 eV, Figure 68).
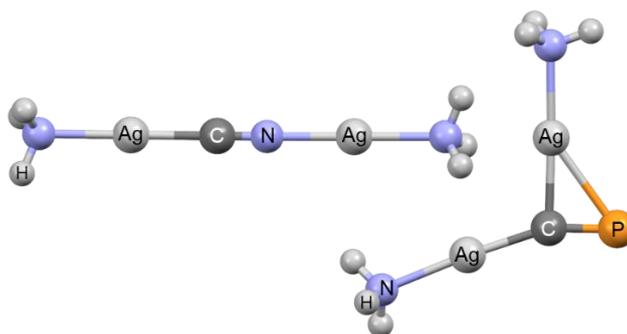
Figure 70. Structure of the calculated homobimetallic complexes [(Ag(NH$_3$)$_2$\{μ-η^1:η^1-CN\}]$^+$ (left) and [(Ag(NH$_3$)$_2$\{μ-η^1:η^2-CP\}]$^+$ (right).

When the two [Ag(NH$_3$)]$^+$ fragments in those complexes are formally replaced by sterically demanding metal fragments, namely a [Ru^{II}(NH$_3$)$_5$]$^{2+}$ and a [Ru^{III}(NH$_3$)$_5$]$^{3+}$ fragment, dinuclear paramagnetic complexes are obtained, which were analyzed towards the influence of the bridging ligand (CN or CP) on the electronic ground state structures. The bridged cyanido complex [Ru^{II}(NH$_3$)$_5$-CN-Ru^{III}(NH$_3$)$_5$]$^{4+}$ retains its linear M-CN-M structure (Figure 71). In the analogous cyaphido complex, the C≡P$^-$ ligands now also adopts a σ-bridging mode, however

in a zig-zag fashion (Ru-C-P 158.0°, C-P-Ru 144.0°, C-P 1.664 Å). Not only do the structures of these two complexes deviate from each other, their electronic structures also show some profound differences: In the cyanido complex, the spin-population is exclusively located on the formal Ru(III)-fragment, which coordinates to the nitrogen atom of the cyanido ligand. In contrast, the spin-population in the cyaphido complex is rather evenly distributed over the whole molecule (Ru: 0.4 each, CP$^-$: 0.2). Therefore, the cyanido complex can be described as a Ru(II)-Ru(III) complex, whereas the corresponding cyaphido complex is best described as a mixed-valent complex where each ruthenium center formally has an oxidation state of +2.5.
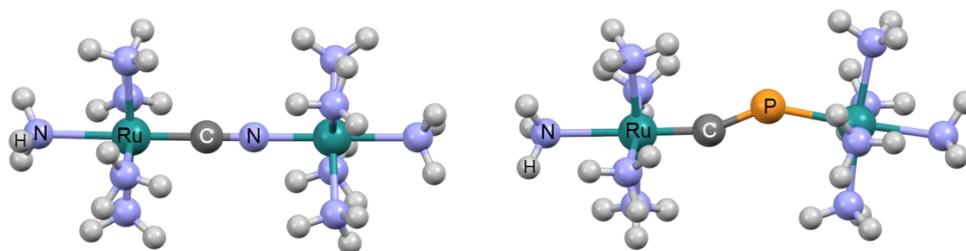
Figure 71. Structure of the calculated homobimetallic complexes [Ru^{II}(NH$_3$)$_5$-CN-Ru^{III}(NH$_3$)$_5$]$^{4+}$ (left) and [Ru^{II}(NH$_3$)$_5$-CP-Ru^{III}(NH$_3$)$_5$]$^{4+}$ (right).

In summary, these calculations show that the cyaphide anion is not only a fundamental curiosity, but also has the potential to access metal complexes with markedly different properties than their corresponding cyanido complexes. Particularly, in dinuclear complexes in which the first metal center is terminally coordinated to carbon of the cyaphido ligand, resulting a metallaphosphaalkyne [M]-C≡P, and the second metal center [M'] might coordinate in a side-on η^2-fashion to the C≡P triple bond, due to the energetically low-lying π^*-orbitals of the C≡P ligand. If this η^1,η^2-mode is denied by steric interactions, a trans bent [M]-C≡P-[M'] unit might be feasible.[44]

2.1.4.2 Attempts to synthesize cyaphido complexes

All stable π-complexes of the selected compounds **142** - **180** (cf. 2.1.3, Figure 53) were examined towards the described potential C-CP cleavage reaction by thermal or primarily photolytic activation (cf. 2.1.1). Selected complexes were also subject of a chemical activation process with boron-based Lewis acids, which will be discussed later. As mentioned in chapter 2.1.3, the light induced intramolecular cleavage reaction could exclusively be observed for specific platinum complexes. In the following, C-CP cleavage complexes bearing an end-on, η^1 bonded cyaphido ligand will simply called σ-complex to keep the unified nomenclature, introduced with the side-on, η^2 bonded phosphaalkyne π-complexes.

The first positive result was found when [(dippe)Pt(MesCP)] (**143**) was irradiated with UV light of a high-pressure mercury lamp (100 W) with λ_{max} = 365 nm in toluene and later in THF for

12 h. The ^{31}P{^{1}H} NMR spectrum shows three additional high-field shifted signals with changed ^{31}P^{31}P and ^{31}P^{195}Pt coupling constants for the C-CP cleavage product [(dippe)Pt(CP)(Mes)] (**143σ**, Figure 72). The doublet of doublets at $δ$ = 97.8 ppm belongs to the phosphorus atom of the newly generated cyaphido ligand, which is about $δ$ = 40 ppm upfield shifted in comparison with the phosphaalkyne phosphorus atom in **143**. This high-field shift was expected, due to the enhanced shielding of the phosphorus nucleus and is in line with the predicted shift of $δ(^{31}$P) = 85.8 ppm for the C≡P phosphorus atom of the envisaged [(dmpe)Pt(CP)(Mes)] (**C7σ**) complex. The ^{31}P^{195}Pt coupling constant of the cyaphido ligand in **143σ** is significantly increased in comparison to **143** from $^1J_{P,Pt}$ = 234 Hz to $^2J_{P,Pt}$ = 340 Hz, even though the coupling is increased from ^1J to ^2J, presumably due to the improved alignment of the C≡P moiety near to linearity towards the Pt center along the Pt-C≡P axis. The ^{31}P{^{1}H} NMR signals of the two phosphorus atoms of the dippe ligand are $δ$ = 16 ppm upfield shifted to $δ$ = 67.3 and 56.2 ppm and appear as a doublet. Both signals show drastically decreased ^{31}P^{195}Pt coupling constant values over the π-complex precursor. Presumably, the ^{31}P *cis*- and *trans*-signals of the dippe ligand are still identically arranged as found in the signal order of the π-complex ^{31}P NMR spectrum. The *cis* phosphorus atom with $^1J_{P,Pt}$ = 1653 Hz of **143σ** is more low-field shifted than the *trans* phosphorus atom with $^1J_{P,Pt}$ = 2169 Hz. Both coupling constants are in good agreement with the theoretical background, which was previously discussed for the π-complex **143**. Moreover, the *cis* phosphorus atom of **143σ**, which is in *trans* position to mesityl group, matches the typical $^1J_{P,Pt}$ coupling constant of around 1700 Hz, which is found for dppe phosphorus atom in *trans* position to a phenyl group.[411] Furthermore, the ^{195}Pt^{31}P coupling constant of the *trans* phosphorus atom can be used as probe to estimate the σ-donor strength of the cyaphido ligand. In agreement with the calculations for the nickel carbonyl complex (cf. 2.1.4.1), which anticipated a slightly higher σ-donor strength for CP$^-$ than CN$^-$ in metal complexes, a comparison between **143σ** ($^1J_{P,Pt}$ = 2169 Hz) and JONES' cyanido complex, [(dippe)Pt(Ph)(CN)] (**2.9σ**, $^1J_{P,Pt}$ = 2744 Hz),[269] validate the stronger σ-donor ability to the cyaphido. The ^{31}P^{31}P coupling constants of the σ-complex **143σ** are generally smaller compared to the π-complex **143**. Interestingly, the conversion after twelve hours of irradiation is only about 20% according to a quantitative ^{31}P NMR measurement and cannot be increased by additional reaction time, which indicates an equilibrium between **143** and **143σ** during the photolysis. Indeed, the slow back reaction to **143** could be observed by monitoring a sample at room temperature over several days by means of NMR spectroscopy. The back reaction rate is diminished with decreased concentration of **143σ**. A freshly prepared 20 mol% sample of **143σ** in THF could be completely converted back to **143** by heating to T = 60 °C for 1 h. Consequently, the competing back reaction is thermally induced, however additional factors cannot be excluded. To conclude, the photolytic oxidative addition towards **143σ** competes with the thermal reductive elimination back reaction to **143**. Even though these two inverse

reactions appear as a chemical equilibrium at first glance, they are not. Instead, both reactions are independent from each other, until irradiation with a continuous beam of light is set. The constant irradiation establishes the classical chemical equilibrium situation, which is influenced by temperature, pressure and the concentration of the substances. Obviously, the last two parameters are difficult to change in a laboratory environment but the temperature as well as the intensity of the light can be modified in the favor of **143σ**. Before addressing these parameters, the impact of dcpe on the reactions was studied.
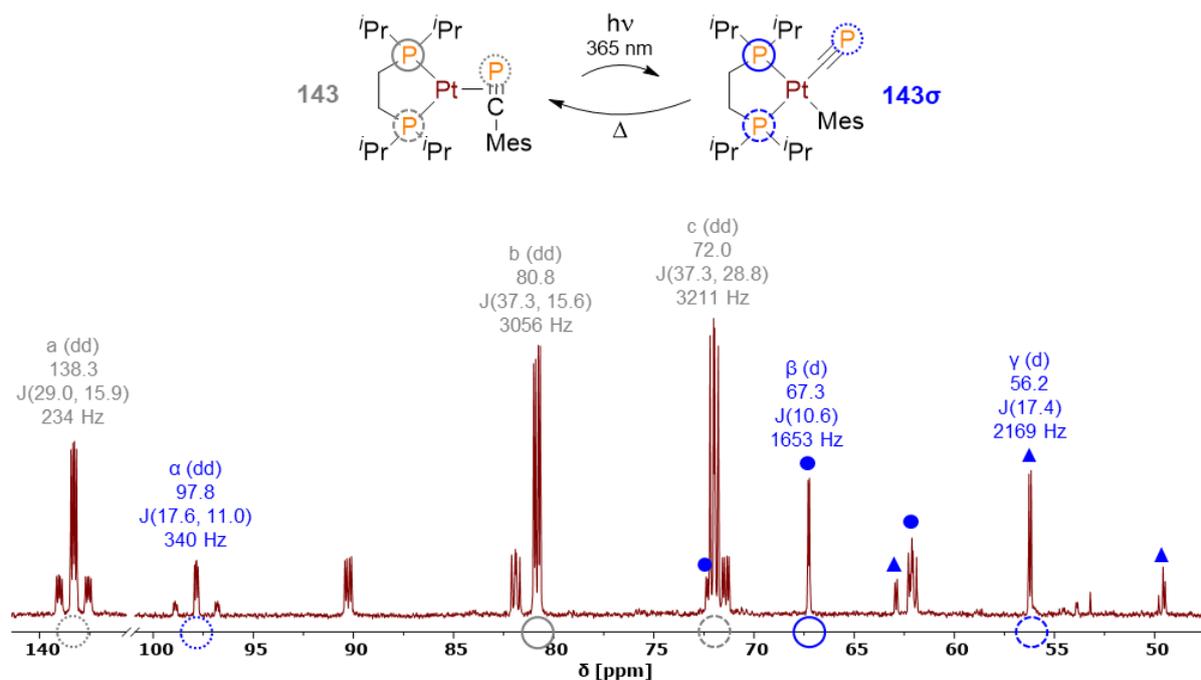
Figure 72. $^{31}P\{^1H\}$ NMR spectrum of a 5:1 mixture of [(dippe)Pt(MesCP)] (**143**, grey) and [(dippe)Pt(CP)(Mes)] (**143σ**, blue) in tetrahydrofuran-d_8. The labels show the multiplet type, chemical shift [ppm], $^{31}P^{31}P$ coupling constants [Hz] and the ^{195}Pt satellites [Hz]. Cycles tag the corresponding phosphorus nuclei.

The replacement of isopropyl by cyclohexyl group should increase the electron density at the metal center, which should favor the oxidative addition according to previous considerations (cf. 2.1.1). Indeed, the same irradiation experiment (UV, high-pressure mercury lamp, λ_{max} = 365 nm, 100 W) of [(dcpe)Pt(MesCP)] (**148**) in THF for 12 h, resulted in the formation of about 30 mol% [(dcpe)Pt(CP)(Mes)] (**148σ**). That is an improvement of 50% over the analogous dippe complex under the same conditions. The $^{31}P\{^1H\}$ spectrum reveals a new set of signals for the σ-complex (Figure 73). The C≡P moiety is represented by a doublet of doublets at δ = 97.0 ppm in the $^{31}P\{^1H\}$ NMR spectrum with an increased $^{31}P^{195}Pt$ coupling constant of $^2J_{P,Pt}$ = 338 Hz. The two doublets at δ = 60.7 and 49.7 ppm of the dcpe ligand showcase a decreased $^{31}P^{195}Pt$ coupling constant compared to the initial π-complex. These findings are in good agreement with the previous results found for [(dippe)Pt(CP)(Mes)] (**143σ**).
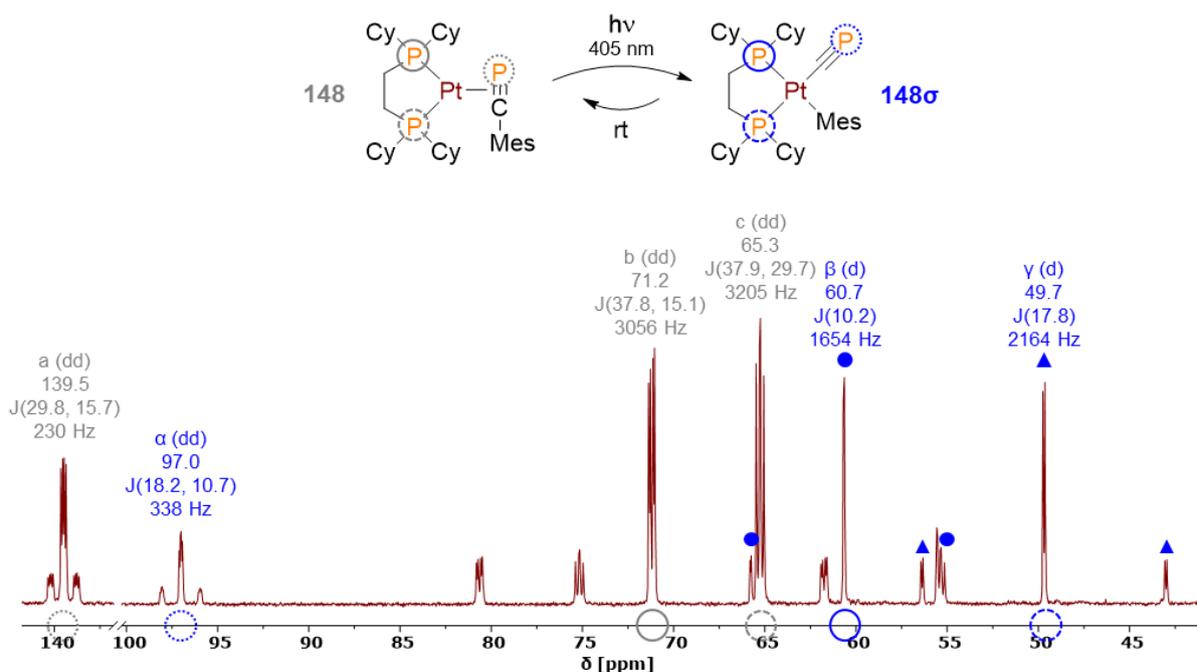
Figure 73. $^{31}P\{^1H\}$ NMR spectrum of a 5:2 mixture of [(dcpe)Pt(MesCP)] (**148**, grey) and [(dcpe)Pt(CP)(Mes)] (**148σ**, blue) in tetrahydrofuran-d_8. The labels show the multiplet type, chemical shift [ppm], $^{31}P^{31}P$ coupling constants [Hz] and the ^{195}Pt satellites [Hz]. Cycles tag the corresponding phosphorus nuclei.

Prolonged irradiation time did not provide more product **148σ**, analogously to **143σ**. The maximum conversion was already reached after 8 h of photolysis. Extended irradiation over several days resulted in decomposition of both compounds **148** and **148σ**. Irradiation with a high-pressure mercury lamp for more than one day resulted in an accumulation of broad resonances in the area of the dcpe signals in the $^{31}P\{^1H\}$ NMR spectrum. Moreover, the appearance of a new singlet with ^{195}Pt satellites was observed, indicating the formation of Pt(dcpe)$_2$. Furthermore, all resonances of the ^1H NMR spectrum were significantly broadened. The same effect was also found for the system **143**/**143σ**. Presumably, the emitted high energy light ($\lambda < 250$ nm) of the high-pressure mercury lamp has a negative impact on the platinum complexes, especially on the C≡P tripe bond. In addition, the mercury lamp also produces an enormous amount of thermal energy, which considerably heats the exposed sample even at distances over one meter. To limit the negative effect of short and long wavelength light, two parallel connected band-pass filter ($\lambda = 340 - 480$ nm, 300 - 400 nm) were used to cover the whole irradiation sample, mainly allowing the light of $\lambda = 300 - 480$ nm to pass. Consequently, the irradiation damage could be highly reduced, whereas the conversion to **148σ** was improved to 39% for an exposure period of 8 h. In addition, cooling was applied by dipping the sample into a half shell Dewar vessel filled with dry ice and ethanol (absorption above $\lambda > 220$ nm) to maintain around $T = 0$ °C during the irradiation process. An improvement of 4%-points, resulting in a total conversion of 43%, was verified over a series of three independent samples. These samples were analyzed towards the thermally induced reductive elimination to **148**, which was found to be significantly slower than the reverse reaction of **143σ**. Astonishingly, no

kinetic relation could be made, because all three independent samples possessed a non-comparable reaction rate. The reverse reaction at room temperature was completed for all three samples within two weeks. Potentially, platinum nanoparticles, which might get released during the initial formation of the π-complex, have a tremendous impact on the reductive elimination rate. Pure samples, proven by elementary analysis, offered dramatically reduced elimination rates, resulting in incomplete reverse reactions even after heating to $T = 60\ °C$ for one week. No kinetical studies were performed, due to this disparity. Interestingly, the transformation from **148** to **148σ** by UV light ($\lambda_{max} = 365$ nm) proceeds even faster in the solid phase, however the transformation ratio is the same and the total amount of compound is restricted by the exposed surface of the solid, due to the limited penetration ability of the light. In solution, there is a correlation between the solubility of the π-complex and the product ratio formed by photolysis. High solubility results in faster transformation and higher product ratios. The best results were found for THF as solvent, followed by toluene, benzene and fluorobenzene. The limited solubility in pentane and hexane resulted in highly extended reaction time and low σ-complex yields. Acetonitrile and benzonitrile were not able to dissolve the π-complex in relevant concentrations. The best solubility for the proved solvents was found for DCM. However, a longer residence time of a mixture of **148** and **148σ** in DCM led to decomposition and formation of $[(dcpe)PtCl_2]$. The σ-complex **148σ** is slightly less soluble in toluene than the π-complex **148**. This aspect was used to grow single crystals for X-ray measurement by storing a saturated toluene solution of 43% **148σ** at $T = -30\ °C$ for two days. The thin colorless needles were picked at low temperatures to avoid potential thermal back reaction in the solid state, which might crack any formed single crystals. Nevertheless, it was not possible to receive reliable crystal data suitable for a publication by this method, however, several measurements on different crystals confirmed the correct connectivity structure (Figure 74). Noteworthy, storing a saturated toluene sample with 43 mol% **148σ** at $T = -30\ °C$ for two months only resulted in precipitation of a colorless solid. Separate ^{31}P NMR analysis of the liquid and the solid phase revealed a **148σ** proportion of 30% in the liquid and unchanged 43% in the solid. Meaning the back reaction still proceeded at $T = -30\ °C$ even though with drastically decreased reaction rate, at least in the liquid phase.
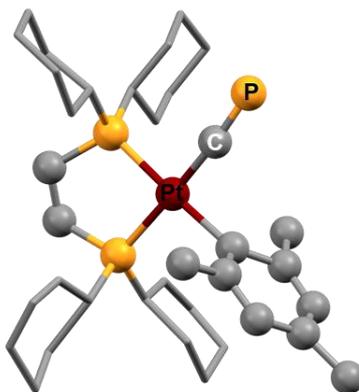
Figure 74. Connectivity structure of [(dcpe)Pt(CP)(Mes)] (**148σ**) as ball and stick model.

Recognizing the improved transformation results by reducing high energy light ($\lambda < 300$ nm) and heat, additional photolysis experiments were performed with different UV light ($\lambda_{max} = 365$ nm) sources. Irradiation of an NMR sample of **148** in a UV light photoreactor at room temperature resulted in 13% of **148σ** in 1.5 h. Extended exposure time did not yield more product. Another photolysis attempt was done with a 1.5 m long UV light luminescent tube ("blacklight") labeled with 50 Watt. Irradiation at room temperature for 5 h gave 9% conversion and 16% after 22 h, which also was the upper limit by this method. The same setup with one additional luminescent tube resulted in 20% (5 h) and 21% (22 h) conversion. Based on these outcomes, it can be presumed that the wavelength of the light is the major contributor for the absolute conversion yield whereas the light intensity primary influences the conversion rate and has a minor impact on the yield. Therefore, a UV-Vis spectrum of **148** was recorded (Figure 75) and a UV-Vis spectrum of the complex [(dmpe)Pt(MesCP)] (**C7**, dmpe = 1,2-bis(dimethyl-phosphino)ethane) was simulated (Figure 76) to identify the optimal light absorption wavelength. For the prediction of the vertical electronic excitations by the *ab initio* unparametrized STEOM-DLPNO−CCSD method (cf. experimental section for details), the cyclohexyl groups of the dcpe ligand were replaced by methyl groups to reduce the calculation time. The recorded absorption reveals two maxima at around $\lambda \approx 230$ and 275 nm and a flat absorption shoulder roughly at $\lambda \approx 400$ nm. These absorption bands are in good agreement with the calculated spectrum for the approximated compound model [(dmpe)Pt(MesCP)] (**C7**) with maxima at $\lambda = 238.7$, 275.7 and 403.6 nm. The best results for the light induced activation of photoactive compounds are usually achieved by irradiation with the longest possible absorption wavelength, which is typically the absorption shoulder. The analysis of the absorption band at $\lambda = 403.6$ nm classifies the MLCT ($d_{x2-y2} \rightarrow \pi^*_{CP}$) as major contributor for this transition in [(dmpe)Pt(MesCP)], which is in line with the findings of WEIGAND, GONZÁLEZ and co-workers for their observed photochemical cleavage in Pt(0)-diphenylacetylene complexes (cf. 2.1.1). Based on the excellent correlation between the measured and calculated absorption spectrum a similar transition situation is anticipated for the lowest singlet excitations in [(dcpe)Pt(MesCP)] **148**. Therefore, irradiation of **148** with this specific

wavelength should maximize the electronic excitation for the photochemical bond C(sp)-C(sp^2) activation.
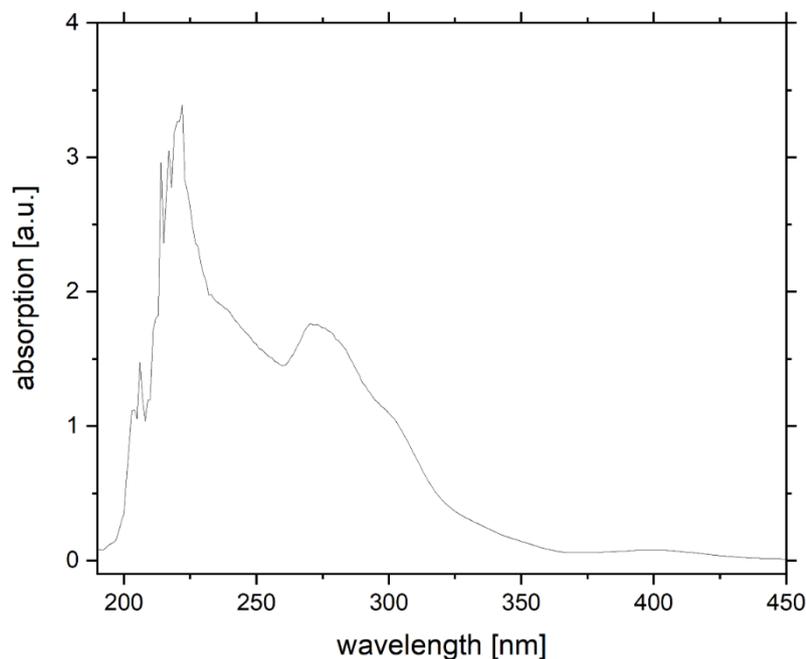
Figure 75. UV-Vis spectrum of [(dcpe)Pt(MesCP)] (**148**) in THF.
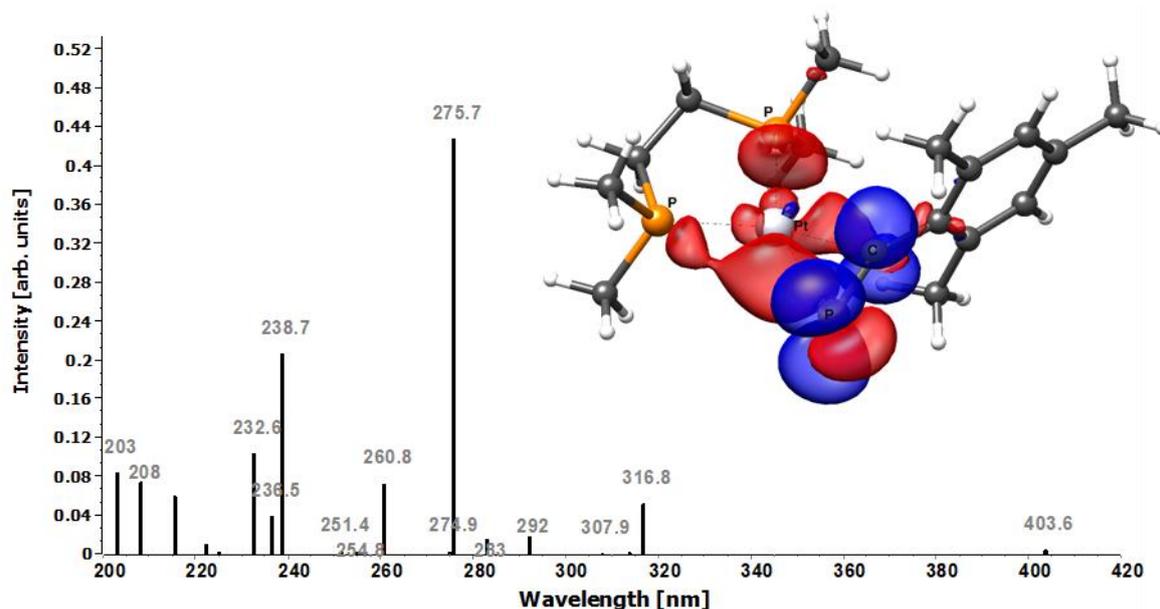
Figure 76. UV-Vis Spectrum and density difference plot (isosurface value 0.003) for the MLCT transition (from red to blue) at λ = 403.6 nm obtained from the DLPNO-STEOM-CCSD calculation for [(dmpe)Pt(MesCP)] (**C7**).

To ensure the optimal photolytic conditions for the photochemical C-CP cleavage and oxidative addition process, a "blacklight LED array" (violet light) with 15 W of λ_{max} = 405 nm was used as light source. Besides the optimized light wavelength, the LED array emits nearly no heat to the sample, which should minimize the induced antagonistic thermal reductive elimination reaction. The irradiation of **148** in THF with one "blacklight LED array" yielded a maximum of 79% of the cyaphido complex **148σ** after 5 h. That doubles the product yield by cutting the

reaction time for 38% (3 h) compared to the conventional activation by the UV mercury high-pressure lamp (λ_{max} = 365 nm, 100 W) including the band-pass filter (λ = 300 - 480 nm). Setting up a second LED array reduced the total reaction time to 2.5 h, while maintaining the maximum conversion of 79%. Supplementary cooling to T = 0 °C increased the product yield to 85% and further decreased the reaction time to 2 h. The highest monitored transformation ratio was achieved at T = -20 °C after an exposure time of 4 h, yielding 90% of **148σ**. The irradiation setup was further tweaked by installing two additional LED arrays, giving a total amount of four LED arrays placed in a square manner around the sample (Figure 77).

Figure 77. The UV mercury high-pressure lamp (100 W, λ_{max} = 365 nm) irradiating three NMR samples (left) and the setup of four violet light ("blacklight") LED arrays (4x 15 W, λ_{max} = 405 nm) irradiating one NMR samples in the middle (right).

A sample of **148**, irradiated via the setup of four LED arrays, was monitored by ^{31}P NMR spectroscopy every 30 min until reaching the maximum conversion to **148σ**. For the first measurement a completeness of 49% was observed. The second reading after 1 h gave 75% of **148σ**. After 1.5 and 2 h the same value of 80% was determined. Putting these outcomes into relation to the measured reaction time for the irradiation with one and two LED arrays, the assumption can be made that the conversion of **148** to **148σ** correlates linearly with the light intensity and the maximum was reached by the LED setup after around one hour and 15 minutes. Further irradiations of the π-complex were made without supporting cooling since the complexity of continuous cooling solution is disproportionate with the additional product yield obtained. Furthermore, all gained product yields on top of the regular yield received at room temperature decreased rapidly by warming the irradiated sample to room temperature. The increased *in situ* yields of **148σ** allowed for further compound characterizations. The infrared spectrum of a solid sample of **148**/**148σ** (2:8) revealed the vibrational mode of the cyaphido ligand with the stretching vibration of $\tilde{v}$ = 1259 cm^{-1}, which is in line with the IR data found for the cyaphido ligand in [(dppe)Ru(CP)(H)] (**1.8b**, $\tilde{v}$ = 1229 cm^{-1}, cf. 1.4.2.3). The slightly raised value found for **148σ** compared to **1.8b** indicates a diminished π-back donation from the metal

into the π^*-orbitals of the C≡P unit and reflects the HSAB concept statement that Pt(II) is harder than Ru(II). The ^{195}Pt{^{1}H} resonances of **148σ** verify the ^{31}P^{195}Pt coupling constants found in the ^{31}P{^{1}H} NMR spectrum (Figure 78). The ^{195}Pt signal of **148σ** is δ = 120 ppm less high-field shifted than in **148**.
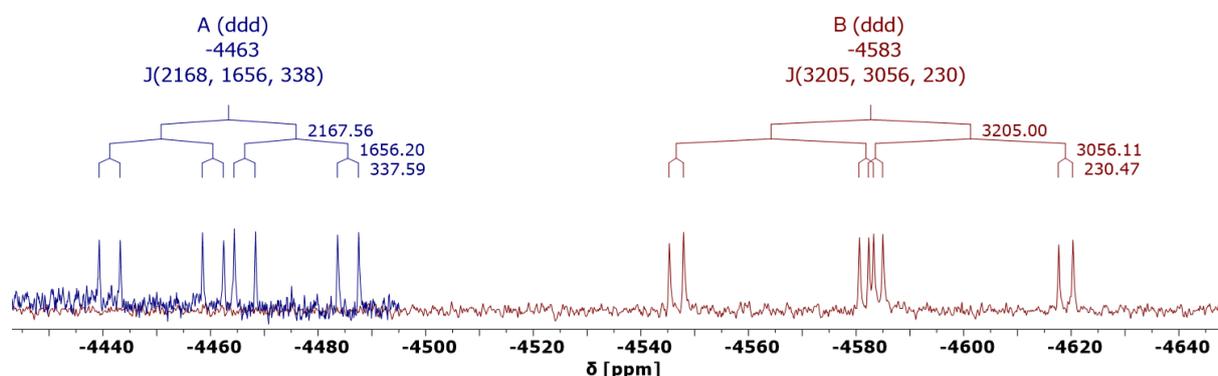

Figure 78. Superimposed ^{195}Pt{^{1}H} NMR spectra of [(dcpe)Pt(CP)(Mes)] (**148σ**, blue) and [(dcpe)Pt(CP)(Mes)] (**148**, red).

The significantly improved yield of **148σ** (80%) made it easier to obtain single crystals from saturated reaction solutions by cooling or evaporation. Several crystallizations finally resulted in a single crystal of **148σ** in excellent quality, which ultimately confirmed the previously found connectivity structure and existence of the C≡P ligand within the molecule (Figure 79). The metal center of **148σ** showed a square-planar geometry, as expected for a platinum in the oxidation state +II. In comparison to the π-complex [(dcpe)Pt(MesCP)] (**148**, Figure 63), the bond length between the platinum and the diphosphine ligand slightly increased from 2.265(2) Å to 2.2939(6) Å for the phosphorus atom in *cis* position and from 2.275(3) Å to 2.3154(5) Å for the phosphorus atom in *trans* position to the C≡P ligand. The cyaphido C≡P distance is 1.563(2) Å, shorter than the 1.573(2) Å found in the archetype [(dppe)$_2$Ru(CP)(H)] (**1.8b**, Figure 80). The Pt1-C1-P1 angle in **148σ** is 176.6(1)°, which is close to the expected linearity for a σ-coordinated triple bond unit and in good agreement with the Pt1-C1-N1 angle of 174.6(4)° found in the cyanido complex [(dippe)Pt(CN)(Ph)] (**2.9σ**, Figure 80) reported by JONES and co-workers. In the direct comparison with the slightly twisted π-complexes **143**, **148** and **146**, the angles around the Pt(II) center in **148σ** are closer to the ideal 90° angles of a square-planar structure, as a direct result of the C-CP cleavage. The splitting of the coordinated phosphaalkyne ligand into the two independent units Mes and C≡P allows for an optimized structure geometry with less tension. Generally, the Pt-C and Pt-P bond length of the similar Pt(II) structures **148σ** and **2.9σ** are akin, except for the *trans* influenced Pt-P bond across the CP or rather CN ligand.
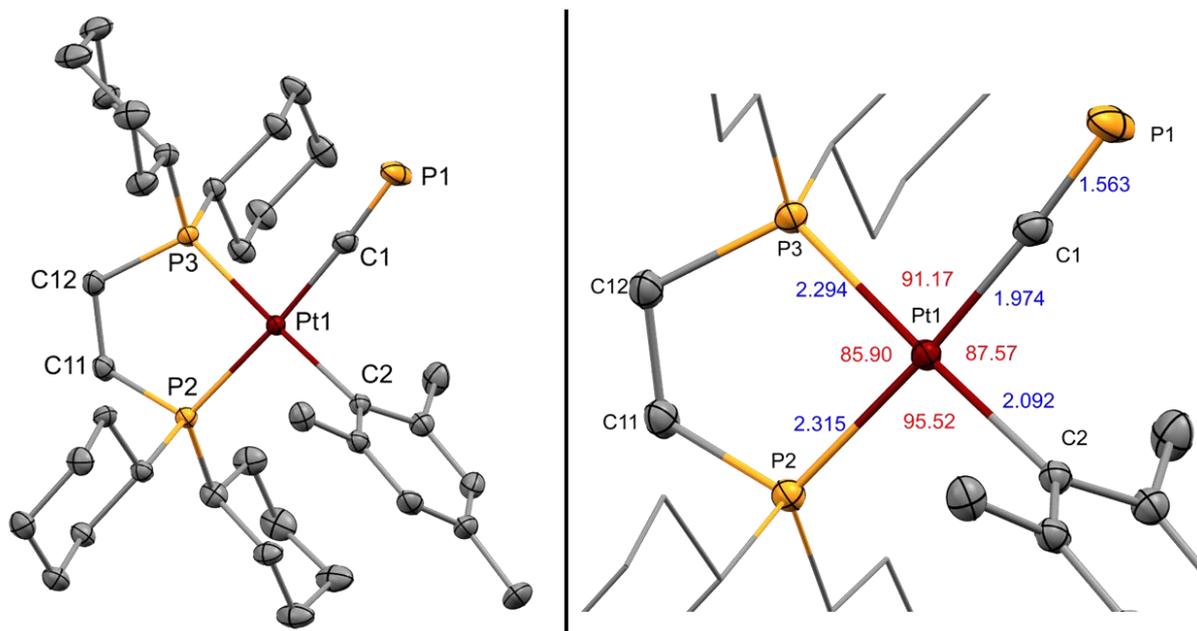
Figure 79. Molecular structure of [(dcpe)Pt(CP)(Mes)] (**148σ**) in the crystal. Anisotropic displacement ellipsoids are shown at 50% probability level. Hydrogens omitted for clarity. Selected bond lengths (Å) in blue and angles (°) in red.
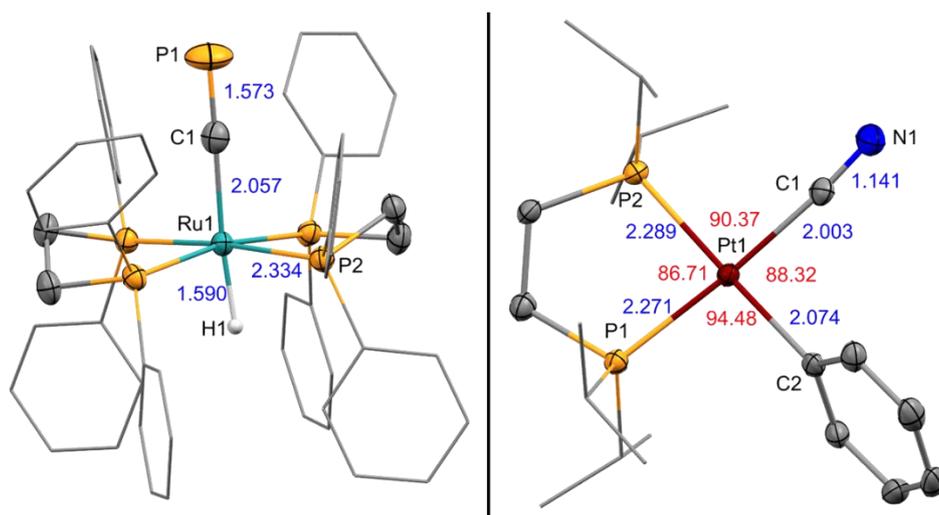

Figure 80. Molecular structure of GRÜTZMACHER's [(dppe)₂Ru(CP)(H)] (**1.8b**) and JONES' [(dippe)Pt(CN)(Ph)] (**2.9σ**) in the crystal. Anisotropic displacement ellipsoids are shown at 50% probability level. Hydrogens omitted, cyclohexyl and isopropyl as wireframe for clarity. For comparison, the infrared wavelengths of C≡P in **1.8b** and C≡N in **2.9σ** are $\tilde{v}$ = 1229 cm⁻¹ and 2278 cm⁻¹, respectively.

With the gained information regarding the activation of **148**, the irradiation process of the *π*-complex **143** was revisited. The UV-Vis spectrum of **143** shows an absorption shoulder at around $\lambda \approx 400$ nm, in line with the DLPNO-STEOM-CCSD calculation giving the highest vertical electronic excitations at 398.3 nm, which is very similar to **148**. The transition is mainly caused by MLCT ($d_{x2-y2} \to \pi^*_{CP}$) and LLCT ($\pi_{Mes} \to \pi^*_{CP}$). Nevertheless, the ³¹P NMR yield for the formation of the *σ*-complex **143σ** could only be improved from 20% (26% with band-pass filters) to 31% by switching the light source from the mercury high-pressure lamp (λ_{max} = 365 nm) to the full four "blacklight LED arrays" setup (λ_{max} = 405 nm). Consequently,

the increased electron density on the metal center, caused by the cyclohexyl groups, has a significant impact on the activation and oxidative addition reaction.

As a next step after the successful diphosphine ligand modification, the influence of the substitution pattern of the arylphosphaalkyne was studied. Attaching EWGs on the aryl moiety should normally rise the activation barrier of the C-CP cleavage process, whereas EDGs should lower the activation barrier (cf. 2.1.1, Scheme 22), as described by WEIGAND, GONZÁLEZ and co-workers. Increasing the barrier should hamper the thermodynamical reductive elimination, whereas the decrease of the barrier could make the initiation of the oxidative addition easier. Overall, EWG-substituted compounds and *ortho*-derivatives possess the strongest MLCT ($d_{x2-y2} \rightarrow \pi^*_{CP}$) and were most efficient in WEIGAND's tolane $C(sp^2)$-$C(sp)$ cleavage investigations. This supposed activation barrier concept should be analyzed for the arylphosphaalkyne platinum complexes by comparing the effect of Mes*CP (**76**) and TtfmpCP (**92**) substituted π-complexes against the MesCP (**68**) derivative as standard for the light induced activation process. The advantage for the *ortho*-substituted arylphosphaalkynes should be studied in contrast to a *meta*-substituted CP (**86**) for their corresponding π-complexes. Unfortunately, TtfmpCP (**92**) could not be isolated and hence not used to build any π-complexes. Interestingly, none of the analyzed Mes*CP π-complexes, [(dippe)Pt(Mes*CP)] (**146**) and [(dcpe)Pt(Mes*CP)] (**153**), showed any reactivity upon irradiation by UV (λ_{max} = 365 nm) or violet light (λ_{max} = 405 nm). Considering this fact as well as the success with the MesCP π-complexes (**143**, **148**), the TrippCP analogs were synthesized because their steric demand and electronic properties are right in between the two other species (**68**, **76**).

The irradiation of [(dcpe)Pt(TrippCP)] (**150**) in THF with violet light (4x 15 W, λ_{max} = 405 nm) generates the corresponding σ-complex [(dcpe)Pt(CP)(Tripp)] (**150σ**, Scheme 59). Astonishingly, the transformation to the σ-complex is more effective but slightly slower than for the previous systems (**143**, **148**) and continues up to full completeness. The thermal back reaction at room temperature is significantly slower than for [(dcpe)Pt(CP)(Mes)] (**148σ**). These findings contradict the prognosticated lower activation barrier, expecting a faster transition in both directions. Instead, the opposite, a higher activation barrier, seems plausible.
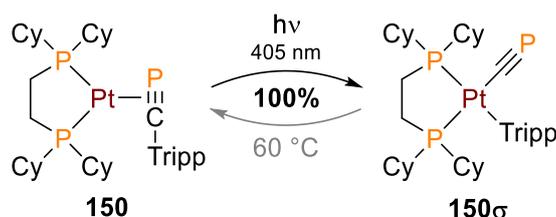

Scheme 59. Photolysis of [(dcpe)Pt(TrippCP)] (**150**) and thermal back reaction of [(dcpe)Pt(CP)(Tripp)] (**150σ**).

The ^{31}P{^{1}H} NMR spectrum of **150σ** reveals a high-field shift of the C≡P moiety of around δ = 40 ppm against the π-complex **150**, in line with the findings for **143σ** and **148σ**. The C≡P

ligand signal appears as doublet of doublets at δ = 108.3 ppm ($^3J_{P,P}$ = 17.8, 10.7 Hz) with additional ^{195}Pt satellites ($^2J_{P,Pt}$ = 331 Hz, Figure 81). The dcpe ligand only shows a ^{31}P^{31}P coupling to the cyaphido ligand. The two phosphorus doublets with ^{195}Pt satellites ($^1J_{P,Pt}$ = 1647, 2145 Hz) are located at $\delta(^{31}$P{^{1}H}) = 60.2 and 47.9 ppm, which is in excellent agreement with the results of **148σ**. The ^{31}P^{31}P spin interactions were simulated to verify the couplings in **150σ** and is depicted in Figure 81. The ^{195}Pt satellites were confirmed by the ^{195}Pt^{31}P coupling constants in the ^{195}Pt{^{1}H} spectrum of **150σ**, showing a doublet of doublets of doublets at δ = -4393 ppm (δ = -4578 ppm for the π-complex **150**). As already noted, the activation process of **150**, as well as the thermal back reaction from **150** to **150σ**, is slower than for the MesCP analogs **148**/**148σ**. Figure 82 shows extracts of an ^{31}P{^{1}H} NMR study on the reversible oxidative addition and reductive elimination processes. The yellow spectrum showcases the situation after photolysis with violet light (4x 15 W, λ_{max} = 405 nm) for 1.5 h. At this state, the reaction solution contains about 72% of **150σ** and required around an additional 1.5 h to reach completeness (green). As for the previous irradiation reaction, the last percentage points the maximum conversion takes most of the overall reaction time. The thermal back reaction is generally slower than for **148σ**, but behaves the same way, proceeding fast at the beginning at high concentration of **150σ** and drastically slowing down for reduced quantity of **150σ** in the mixture. After 18 h, already 31% of **150** was formed (turquoise). Five days later, around 40% of **150** was measured (blue). After two weeks, 63% of the σ-complex was converted to the π-complex **150** (purple). At this point, the back reaction almost came to a halt, showing around 65% of **150** after one month. The monitoring at room temperature was stopped and the reaction mixture of **150**/**150σ** was heated to T = 60 °C for 1 h, going through the back reaction without any evidence for by-products or decomposition (rose), even in the ^{1}H NMR spectrum.
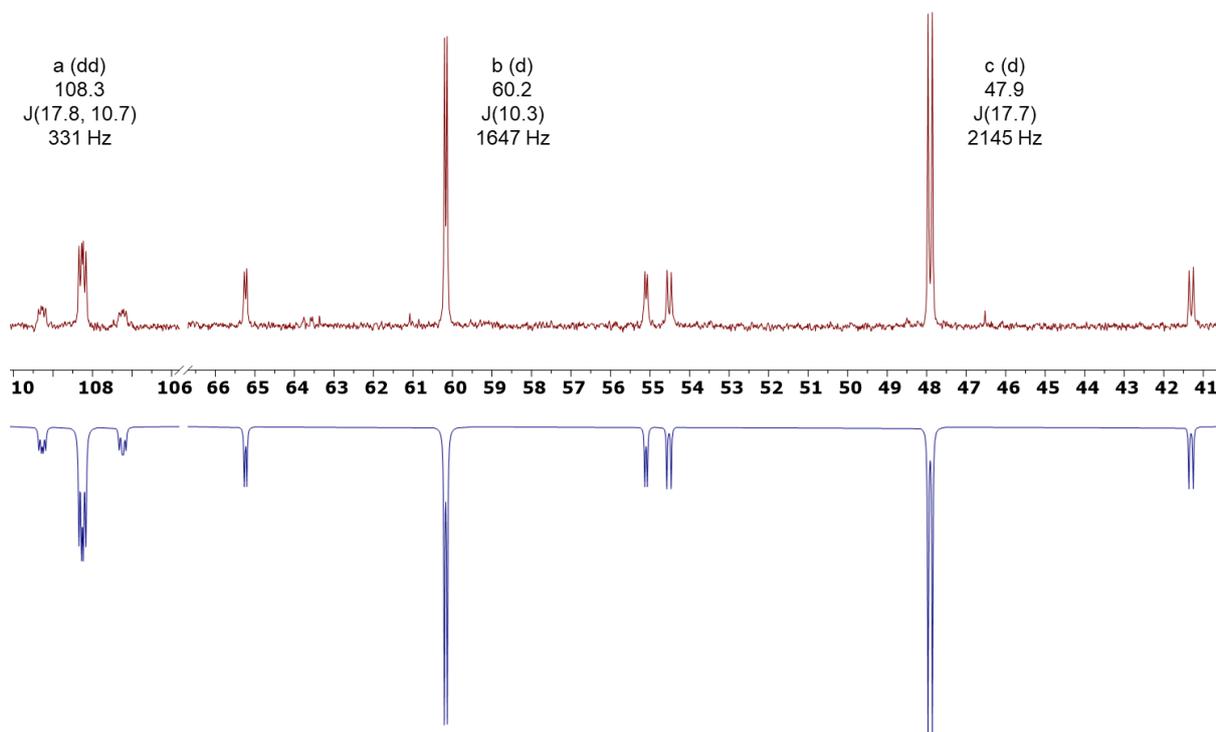
Figure 81. Measured (top) and simulated (bottom) ^{31}P{^{1}H} NMR spectrum of [(dcpe)Pt(CP)(Tripp)] (**150σ**). Scale in ppm.
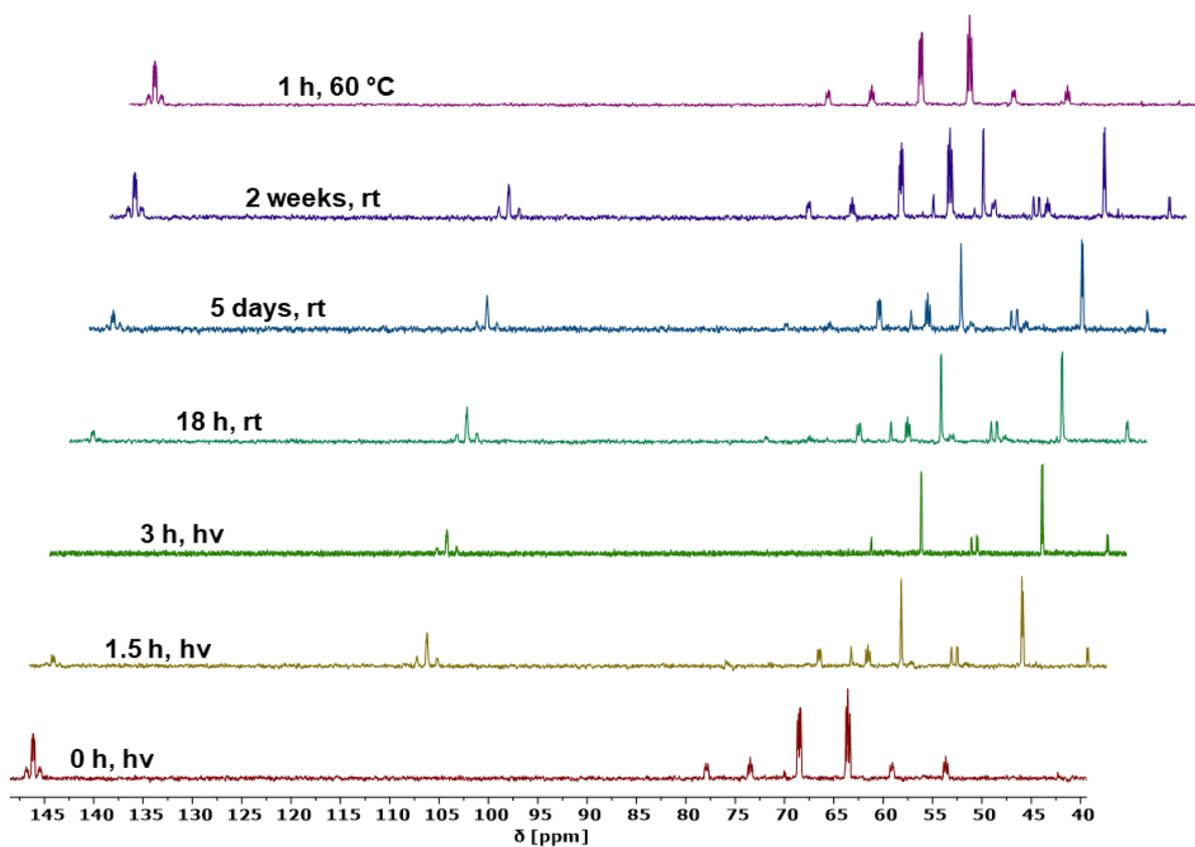
Figure 82. ^{31}P{^{1}H} NMR monitored photolysis of [(dcpe)Pt(TrippCP)] (**150**) to [(dcpe)Pt(CP)(Tripp)] (**150σ**) and thermal back reaction from **150σ** to **150** in THF.

Crystals of **150σ**, suitable for single crystal diffraction analysis could be obtained by slow evaporation of a concentrated THF solution within 16 h (Figure 83). The square-planar geometry of **150σ** was confirmed and matches the molecular structure, bond lengths and angles of **148σ**. The Tripp unit is partly disordered, but with no impact on the area of interest at the Pt(II) center and the C≡P ligand. The cyaphido C≡P distance is 1.556(6) Å long and the Pt1-C1-P1 angle is 174.3(4)°. The *cis* P2-Pt1 distance of the dcpe ligand is shorter (2.288(2) Å) than the *trans* P3-Pt1 distance (2.315(1) Å), like in **148σ**. The shorter C≡P bond length in **150σ** against **1.8b** is in line with the measured stretching vibration of $\tilde{\nu}$ = 1260 cm^{-1} for the C≡P unit in the infrared spectrum compared to $\tilde{\nu}$ = 1229 cm^{-1} for **1.8b**. Both, the shorter C≡P distance as well as the higher infrared stretching vibration, as result of the shorter bond length, indicate a weaker π-back donation of the Pt(II) center into the C≡P π*-orbitals compared to the Ru(II) center in **1.8b**. The angles around the Pt(II) center in **150σ** are in excellent agreement with the results of **148σ**. Overall, the increased steric demand of the Tripp group does not impact the bond length nor angles of the core structure.
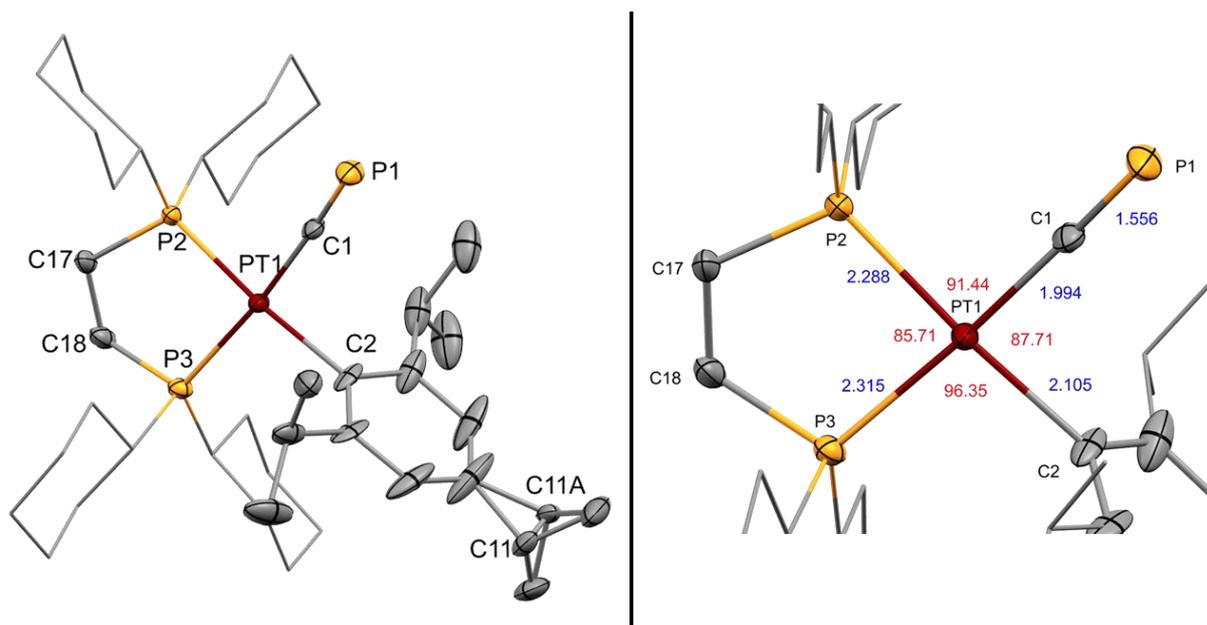
Figure 83. Molecular structure of [(dcpe)Pt(CP)(Tripp)] (**150σ**) in the crystal. Anisotropic displacement ellipsoids are shown at 50% probability level. Hydrogens omitted and cyclohexyl as wireframe for clarity. The *para*-isopropyl group of Tripp is modeled with two independent carbons (C11, C11A), due to disorder in the molecular structure. Selected bond lengths (Å) in blue and angles (°) in red.

In order to further analyze the influence of the Tripp group, the isolated [(dippe)Pt(TrippCP)] (**144**) π-complex was irradiated in THF by the violet light setup (λ_{max} = 405 nm) for 4.5 h, giving a conversion of 83% to the σ-complex **144σ** (Figure 84). Additional irradiation for 5 h under constant conditions did not change the product ratio. The resulting cyaphido complex **144σ** possesses the typical ^{31}P{^{1}H} parameters, similar to the already discussed σ-complex **150σ**, and is depicted in Figure 84. The rate of the still at room temperature slowly proceeding back reaction was not studied. The experiment confirms the effectiveness of the TrippCP for the

light induced C-CP cleavage reaction, showing a 2.7-fold improved conversion rate of **144** over the MesCP analog **143**. However, it again confirms the impact of the diphosphine ligand, demonstrating better conversion rates for the dcpe substituted over the dippe complexes, as already presented in the comparison of **148** with **143**. Accordingly, the conversion rate of the π-complex to the σ-complex is strongly influenced by the substitution of the aromatic ring of the arylphosphaalkyne and the electron donor ability of the diphosphine ligand.
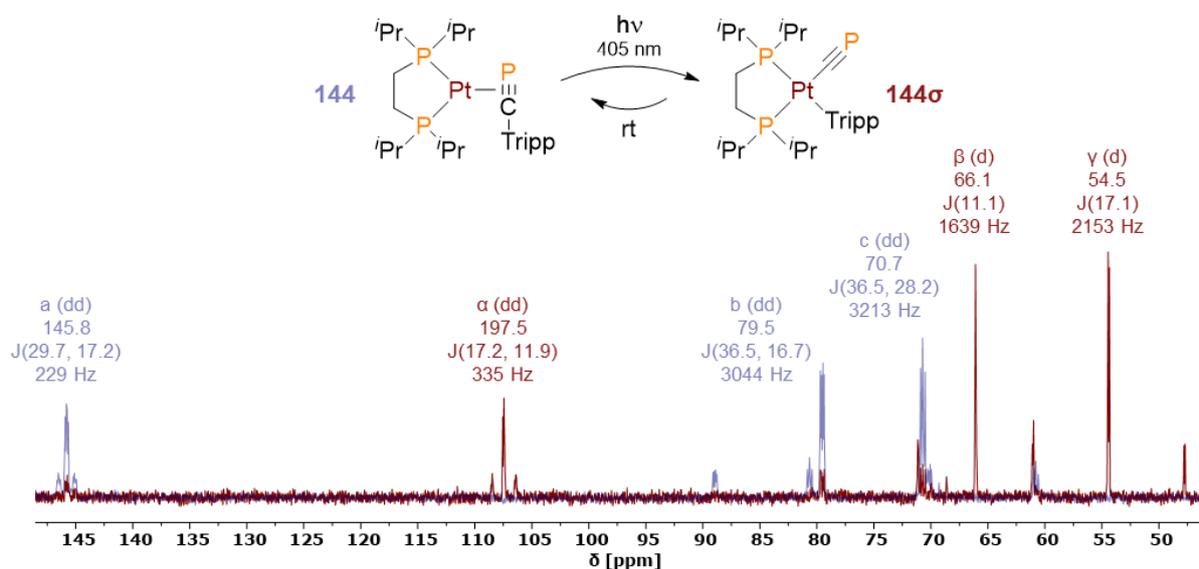
Figure 84. Superimposed ^{31}Pt{^{1}H} NMR spectra of [(dippe)Pt(TrippCP)] (**144**, blue) and a 83:17 mixture of **144** and [(dippe)Pt(CP)(Tripp)] (**144σ**, red).

A THF sample of [(dcpe)Pt(MdtbpCP)] (**152**) was irradiated by the violet light setup (λ_{max} = 405 nm) for 20 h to investigate the effect of the changed substitution pattern on the aromatic ring of the arylphosphaalkyne ligand. The conversion rate to **152σ** is very slow in relation to all previously studied σ-complexes. Irradiation of **152** for 1 h led to a turnover of around 3%. Extended photolysis gave higher product yields but also showed significant formation of by-products in the ^{31}P{^{1}H} NMR spectra (Figure 85). The various by-products were not analyzed, due to an overall decrease of all ^{31}P{^{1}H} signal intensities, indicating serious decomposition reactions. The experiment was stopped after 20 h, resulting a product quantity of around 67% (**152σ**). The ^{31}P{^{1}H} cyaphido resonance at δ = 90.2 ppm is more downfield shifted than for all other investigated σ-complexes. All other ^{31}P{^{1}H} parameters are nearly identical to the other C$_2$ σ-complexes. Overall, the highly prolonged reaction time of **152** bearing ^{t}Bu groups in the *meta* position of the arylphosphaalkyne is evidence for its poor effectiveness in the photolysis reaction. This result agrees with the assertion of WEIGAND and GONZÁLEZ that *ortho* substituted arylalkynes bear more intensive MLCT ($d_{x2-y2} \rightarrow \pi^*_{alkyne}$), which is the core feature for the light induced activation (cf. 2.1.1). In addition, the observed decomposition might be caused by an β-elimination process with follow-up reactions similar to the findings of JONES *et al.* for the benzonitrile complex (cf. 2.1.1, Scheme 18).
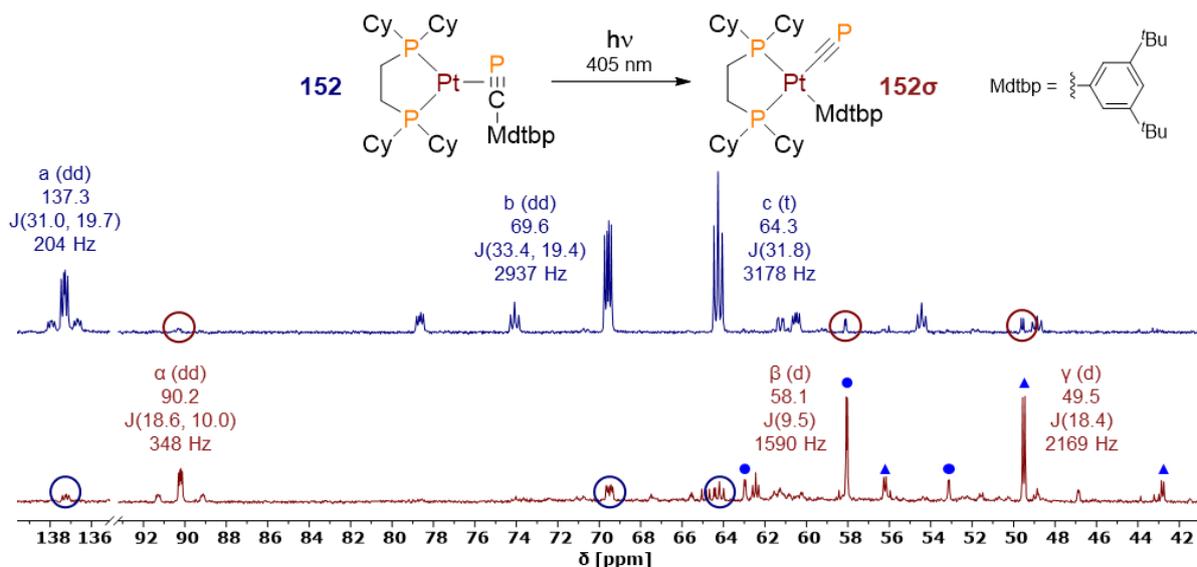
Figure 85. Resulting ^{31}Pt{^{1}H} NMR spectra of a mixture of [(dcpe)Pt(MdtbpCP)] (**152**) and [(dcpe)Pt(CP)(Mdtbp)] (**152σ**) after irradiation of **152** in THF with violet light (λ_{max} = 405 nm) for 1 h (blue) and 20 h (red). First traces of **152σ** after 1 h are highlighted with red cycles. Remnants of **152** after 20 h are marked with blue cycles. The dcpe ^{195}Pt satellites of **152σ** are tagged with blue dots and triangles.

Until now, only the effect of the ligand substitution was studied for [(dcpe)Pt(TrippCP)] **148**, which is showing the best result for the light induced C-CP splitting. In the next step, the impact of the bite angle was analyzed through photolysis of the methylene bridged (C$_1$) π-complexes [(dtbpm)Pt(TrippCP)] (**166**) and [(dcpm)Pt(TrippCP)] (**170**). Generally, a smaller bite angle should favor the oxidative addition and stabilize the cyaphido complex, whereas the reductive elimination should be inhibited (cf. 2.1.2.2). Irradiation of **166** in THF by the violet light setup (λ_{max} = 405 nm) at room temperature for 48 h gave around 75% of [(dtbpm)Pt(CP)(Tripp)] (**166σ**) in the NMR sample (Figure 86). Against the expectations for the oxidative addition, prolonged photolysis did not overcome this product maximum. However, no back reaction (reductive elimination) to **166** was observed at room temperature. After heating to T = 60 °C for 2 h, 5% of **166σ** remained in the THF solution, while forming corresponding quantities of **166**. The ^{31}P{^{1}H} characteristics of the C$_1$ σ-complex **166σ** are similar to the C$_2$ derivatives. The C≡P signal is located at δ = 104.9 ppm with ^{195}Pt satellites of $^2J_{P,Pt}$ = 360 Hz. The dbtpm resonances are high-field shifted to δ = -7.6 and -11.1 ppm and the ^{31}P^{195}Pt coupling constants are decreased to $^1J_{P,Pt}$ = 1333 and 1761 Hz compared to **166**.
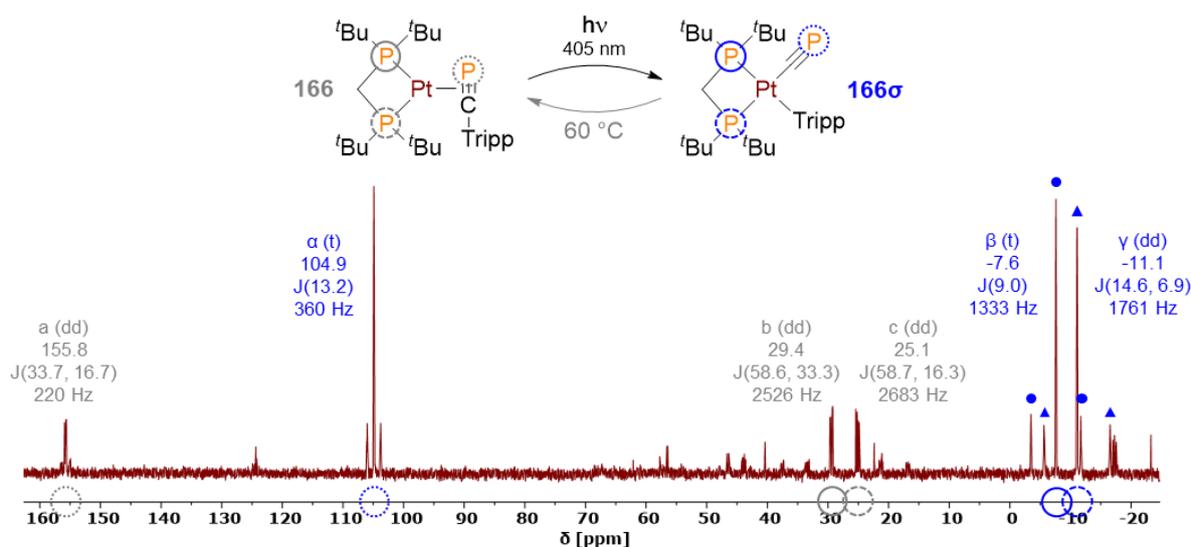
Figure 86. Resulting ^{31}Pt{^{1}H} NMR spectra of a 1:3 mixture of [(dtbpm)Pt(TrippCP)] (**166**) and [(dtbpm)Pt(CP)(Tripp)] (**166σ**) after irradiation of **166** in THF with violet light (λ_{max} = 405 nm) for 48 h. The dtbpm ^{195}Pt satellites of **166σ** are marked with blue dots and triangles. Cycles tag the corresponding phosphorus nuclei.

The [(dcpm)Pt(TrippCP)] (**170**) complex reacted almost quantitatively upon photolysis, resulting in 97% conversion to [(dcpm)Pt(CP)(Tripp)] (**170σ**). No back reaction was observed, neither at room temperature for 5 days nor at T = 60 °C for 2 h. Prolonged heating (T = 60 °C) for 24 h diminished the concentration of **170σ** to 60%. Repeated irradiation granted again a maximum of 97% of **170σ**. However, numerous repetitions of this cycle increased the proliferation of unidentified decomposition products. As for all other cyaphido complexes the ^{31}P{^{1}H} signals are upfield shifted and the ^{31}P^{195}Pt coupling constants are increased for the C≡P unit and decreased for the diphosphine ligand in comparison to the π-complex. The specific signals of **170σ** and **170** are depict in Figure 87.
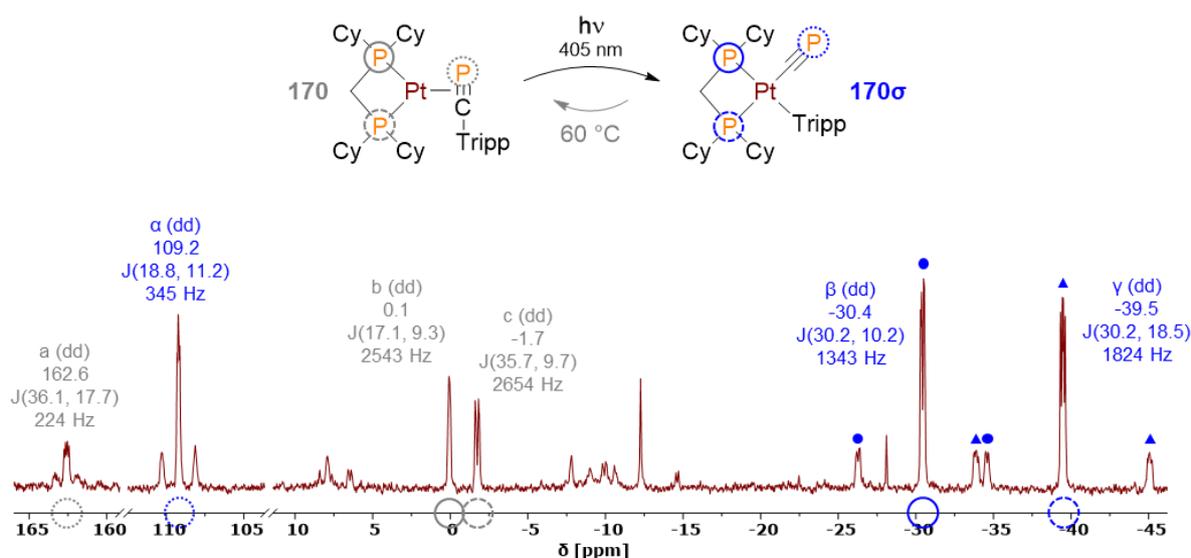
Figure 87. Resulting ^{31}Pt{^{1}H} NMR spectra of a 1:3 mixture of [(dcpm)Pt(TrippCP)] (**170**) and [(dcpm)Pt(CP)(Tripp)] (**170σ**) after irradiation of **170** in THF with violet light (λ_{max} = 405 nm) for 48 h. The dtbpm ^{195}Pt satellites of **170σ** are marked with blue dots and triangles. Cycles tag the corresponding phosphorus nuclei.

In contrast to the C_2 analog **150σ** ($\delta(^{195}Pt\{^1H\})$ = -4393), the $^{195}Pt\{^1H\}$ signal is downfield shifted to δ = -3792 ppm (Figure 88). The $^{195}Pt^{31}P$ couplings confirm the detected ^{195}Pt satellites in the $^{31}P\{^1H\}$ spectrum.
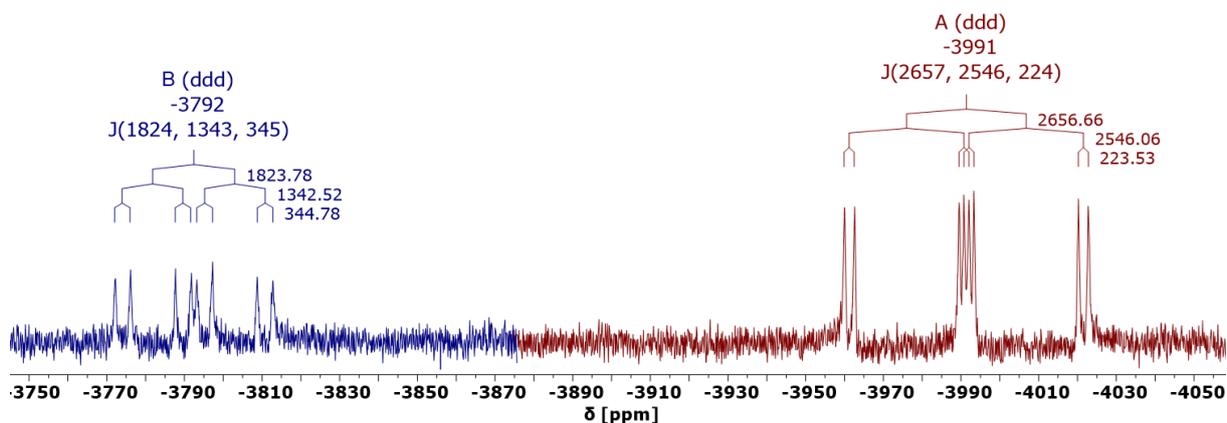
Figure 88. Superimposed $^{195}Pt\{^1H\}$ NMR spectra of [(dcpm)Pt(TrippCP)] (**170**, red) and [(dcpm)Pt(CP)(Tripp)] (**170σ**, blue).

Both molecular structures, **166σ** and **170σ**, confirmed the assumption of an inhibited reductive elimination for a narrow bite angle. Further studies for the C_1 σ-complexes were limited to the **170/170σ** system, due to its much slower back reaction and better σ-complex yields.

Evaporation of a concentrated benzene solution of **170σ** over 16 h yielded crystals, suitable for single crystal diffraction analysis. Interestingly, a not resolved large residual electron density peak near the platinum core was found but could be assigned as the platinum center of a second complex with almost identical conformation, indicating a whole-molecule disorder. The high quality of the diffraction data allowed, in combination with the concept of "archetype structures"[412] and molecule-in-cluster calculations[413], to identify the second structure as [(dcpm)Pt(H)(Tripp)] with an occupancy of 2.5%. The square-planar geometry of the molecular structure of **170σ** is depicted in Figure 89. The bond distances are unremarkable and nearly identical to the C_2 analog **150σ** with exception of the marginal extended Pt1-P2 bond. As expected, the bond angles around the platinum core differ from **150σ**. The P2-Pt1-P3 angle is with 73.20(1)° akin with its π-complex **170** and significantly smaller than 85.71° in **150σ**. In consequence, all other angles around the platinum core are wider. The highest increase of 6.18° over **150σ** can be found for the angle P2-Pt1-C1. The opposite angle (P3-Pt1-C11) is 3.26° larger and the C1-Pt1-C11 angle is only 1.9° wider. The measured C≡P stretching vibration of $\tilde{\nu}$ = 1262 cm^{-1} by infrared spectroscopy and the determined C≡P bond distance of 1.555(1) Å is in excellent correlation to the previously found values for the other cyaphido complexes.
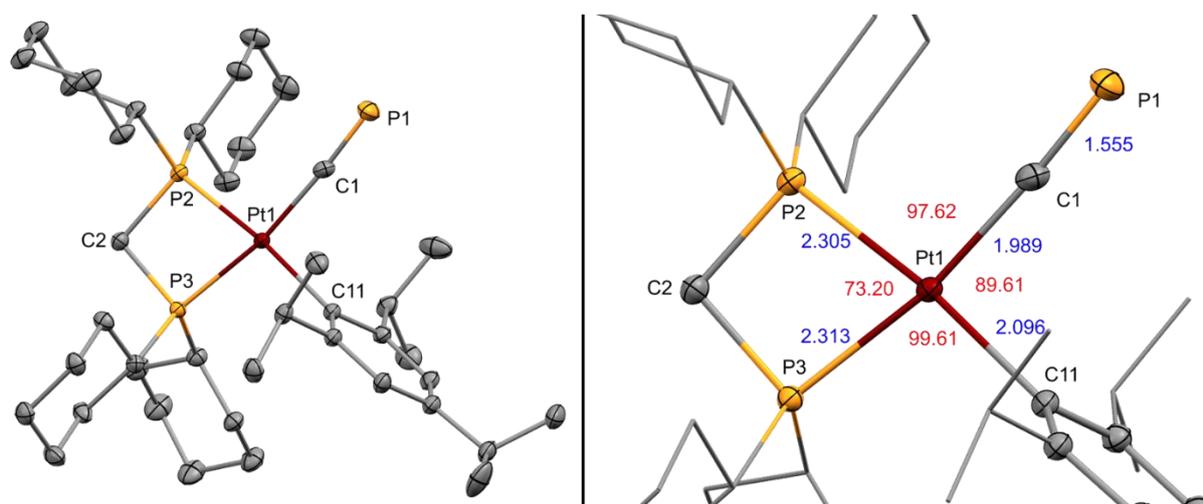
Figure 89. Molecular structure of [(dcpe)Pt(CP)(Tripp)] (**170σ**) in the crystal. Anisotropic displacement ellipsoids are shown at 50% probability level. Hydrogens and co-crystalized benzene omitted for clarity. Selected bond lengths (Å) in blue and angles (°) in red.

The UV-Vis spectra of **150** and **170** were recorded to analyze the absorption bands (Figure 90), that might give a hint for the much slower light induced activation and oxidative addition reaction in **170** compared to the C_2 bridged analog **150**. The absorption spectrum of **150** is similar to the recorded spectrum of **148** (Figure 75), showing two maxima at around $\lambda \approx 225$ and 275 nm although the second maximum at $\lambda = 275$ nm is less intense. Both spectra (**148**, **150**) show the for the activation process important, absorption shoulder at around $\lambda \approx 400$ nm. In contrast, the UV-Vis spectrum of **170** has additional maxima ($\lambda = 240 - 270$ nm) between the two peaks at $\lambda = 220$ and 285 nm and the absorption shoulder at around $\lambda \approx 400$ nm is less prominent. The full absorption area from $\lambda = 200$ to 425 nm is similar for both.
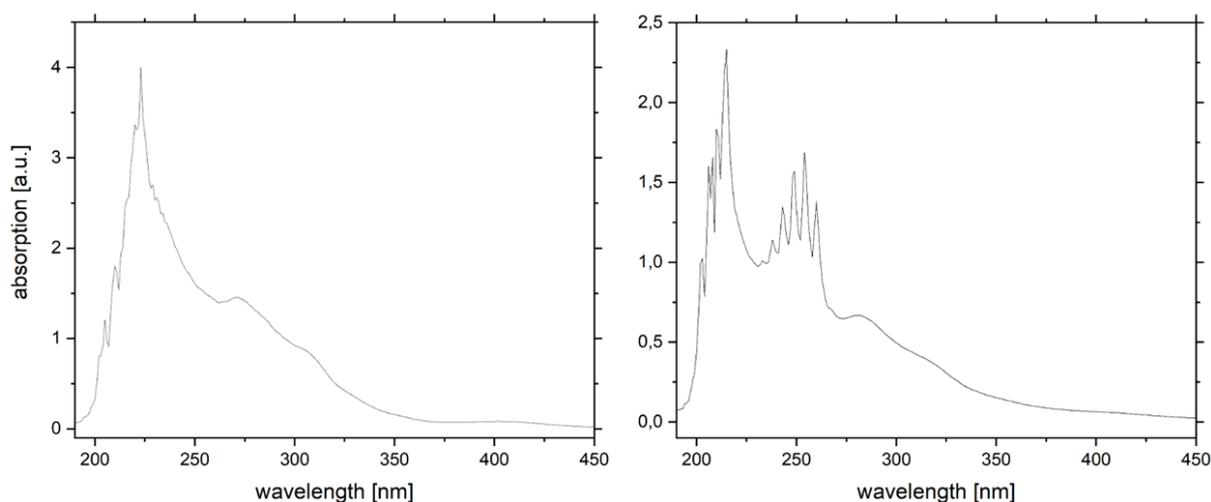
Figure 90. UV-Vis spectrum of [(dcpe)Pt(TrippCP)] (**150**, left) and [(dcpm)Pt(TrippCP)] (**170**, right) in THF.

To get deeper insights into the absorption at $\lambda = 400$ nm for the π-complex **170**, the vertical electronic excitations for the simplified C_1 model complex [(dmpm)Pt(MesCP)] (**C9**, dmpm = bis(dimethylphosphino)methane) was predicted by the *ab initio* unparametrized STEOM-DLPNO-CCSD method (Figure 91). The calculated spectrum is similar to the spectrum of the

C_2 model complex [(dmpe)Pt(MesCP)] (**C7**, Figure 76), but shows more absorption bands in the area from $\lambda = 220$ to 260 nm. The most intense bands are at $\lambda = 213.3$ and 277.6 nm. The longest wavelength absorption can be found at $\lambda = 399.5$ nm, which represents the, for the activation process important, absorption shoulder. The main contributors of this band are a MLCT ($d_{x2-y2} \rightarrow \pi^*_{CP}$) and LLCT ($\pi_{Mes} \rightarrow \pi^*_{CP}$), which are illustrated via a density difference plot in Figure 91.
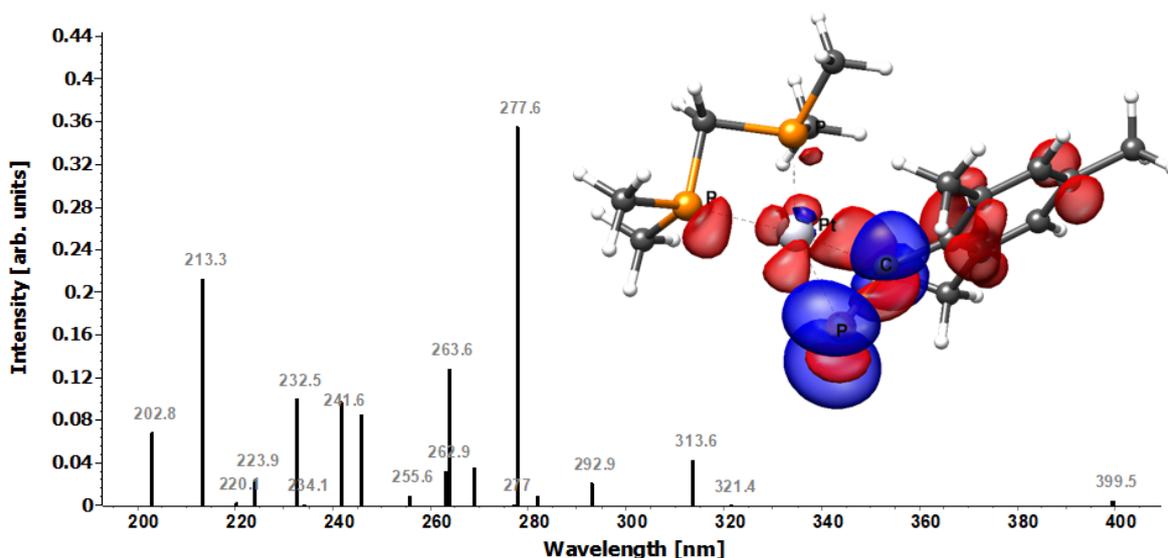
Figure 91. UV-Vis Spectrum and density difference plot (isosurface value 0.003) for the MLCT transition (from red to blue) at $\lambda = 399.5$ nm obtained from the DLPNO-STEOM-CCSD calculation for [(dmpm)Pt(MesCP)] (**C9**).

Even though the calculated spectrum of the model complex [(dmpm)Pt(MesCP)] (**C9**) matches the recorded spectrum of **170** well, the previous experiments showed an enormous impact of the substituents on the light induced activation of the π-complex and the stabilization of the resulting cyaphido complex. Therefore, the UV-Vis spectrum and the transitions of actual complex **170** with all its ligands was calculated. However, the calculation method had to be changed to the less accurate TD-DFT with ωB97xD-D3/def2-TZVP level of theory due to computation power restraints. The relation between the two calculation methods was affirmed for the model compounds [(dmpm)Pt(MesCP)] (**C9**), [(dmpe)Pt(MesCP)] (**C7**) and the simplest synthesized complex [(dippe)Pt(MesCP)] (**143**). The results and the deviation values for the lowest energy singlet excitations are depicted in Table 10. In all cases, independent of the calculation method, the MLCT ($d_{x2-y2} \rightarrow \pi^*_{CP}$) is the main contributor of the lowest energy singlet excitation. The LLCT ($\pi_{Mes} \rightarrow \pi^*_{CP}$) occasionally also shows a significant contribution but depending on the calculation method. The deviation of the lowest energy singlet excitation between the two methods is always about $\lambda \approx 31$ nm with the TD-DFT studies showing the higher energies. According to the experimental UV-Vis data for [(dippe)Pt(MesCP)] (**143**, Figure 92), the DLPNO-STEOM-CCSD calculations are more accurate. Taking this into account, the lowest energy singlet excitations for [(dcpm)Pt(TrippCP)] (**170**) is expected at around $\lambda \approx 415$ nm, based on the calculated value of $\lambda = 383.6$ nm with the TD-DFT method.

Table 10. Lowest energy singlet excitations (S$_1$) of **C9**, **C7**, **143** and **170** calculated by STEOM-DLPNO-CCSD and TD-DFT method.

	STEOM-DLPNO-CCSD		TD-DFT$_{\omega B97xD-D3/def2-TZVP}$		$\Delta E_{(STEOM-DLPNO-CCSD - TD-DFT)}$ [nm]
	E [nm]	assignment	E [nm]	assignment	
C9	399.5	MLCT (d$_{x2-y2}$ → π^*_{CP}) LLCT (π_{Mes} → π^*_{CP})	370.1	MLCT (d$_{x2-y2}$ → π^*_{CP})	29.4
C7	403.6	MLCT (d$_{x2-y2}$ → π^*_{CP})	373.6	MLCT (d$_{x2-y2}$ → π^*_{CP}) LLCT (π_{Mes} → π^*_{CP})	30.0
143	398.3	MLCT (d$_{x2-y2}$ → π^*_{CP}) LLCT (π_{Mes} → π^*_{CP})	365.8	MLCT (d$_{x2-y2}$ → π^*_{CP})	32.5
170	-		-	383.6	MLCT (d$_{x2-y2}$ → π^*_{CP})	-
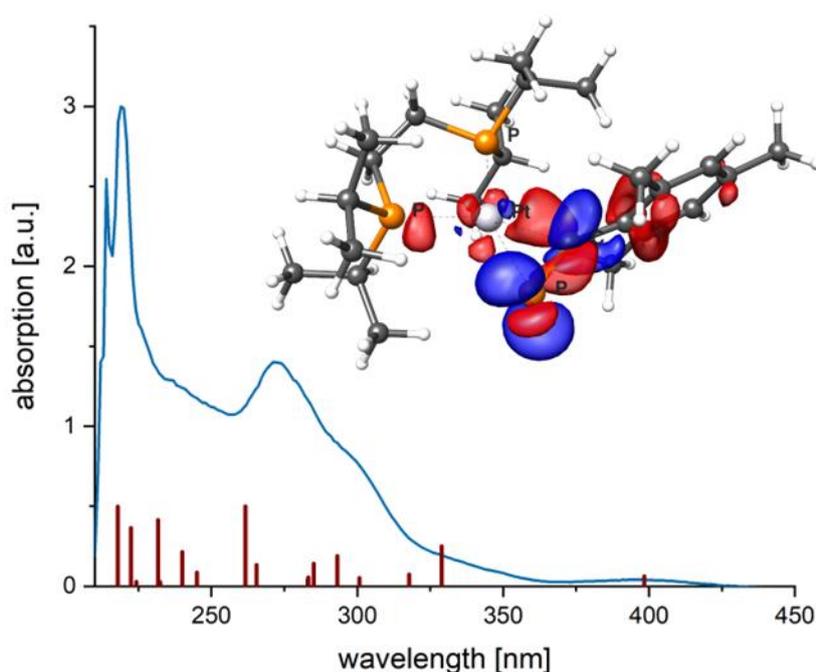
Figure 92. Experimental UV-Vis spectrum (blue) and theoretical vertical excitations (red) calculated with the DLPNO-STEOM-CCSD method for [(dippe)Pt(MesCP)] (**143**). Density difference plot (isosurface value 0.003) for the transition at λ = 398.3 nm for **143** with MLCT (d$_{x2-y2}$ → π^*_{CP}) and LLCT (π_{Mes} → π^*_{CP}) as main contribution. The transition occurs from red to blue.

Overall, the less accurately calculated UV-Vis spectrum of **170** (Figure 93) is in better agreement with the experimental data than the more accurately calculated UV-Vis spectrum of the model complex [(dmpm)Pt(MesCP)] (**C9**), demonstrating the influence of the substitutions in addition to the bite angle. The DLPNO-STEOM-CCSD calculation would indisputably also furnish the best results for **170** but is too time intensive. Assuming the lowest energy singlet excitation for **170** at around $\lambda \approx 415$ nm and even thought the light source ("blacklight") is labeled with λ_{max} = 405 nm and appeared strong violet (λ_{violet} = 380 - 430 nm) and not blue (λ_{blue} = 430 - 490 nm) to the eye, it might be possible that the light emission at higher wavelength (λ > 410 nm) is less intense. That could explain the much slower reaction

time of **170** to **170σ** in comparison to **143**, which has its lowest absorption band at $\lambda = 398.3$ nm.
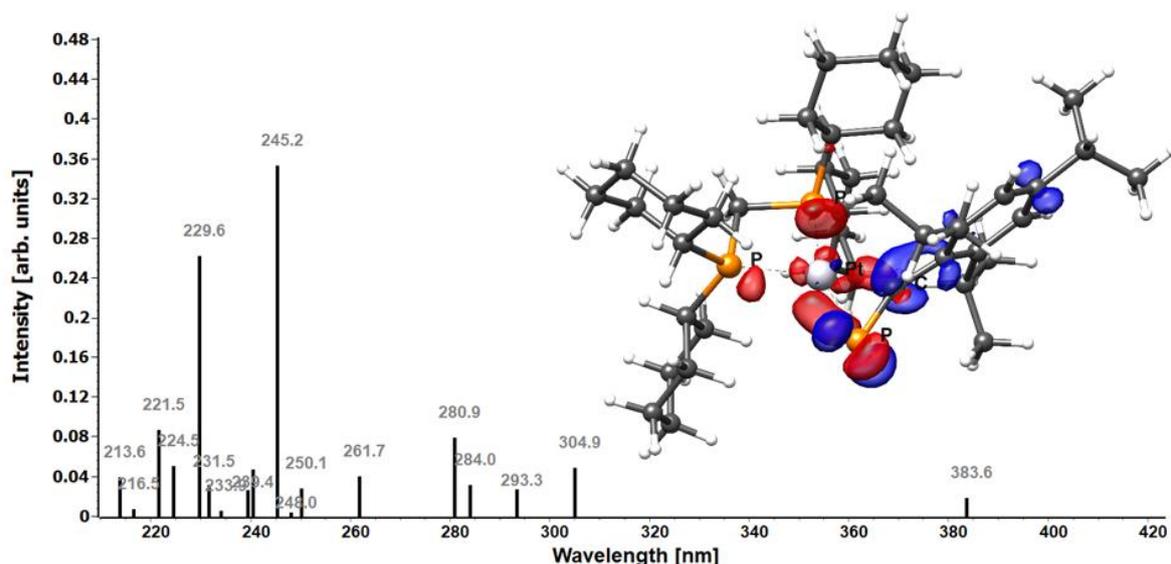

Figure 93. UV-Vis Spectrum and density difference plot (isosurface value 0.003) for the MLCT transition (from red to blue) at $\lambda = 383.6$ nm obtained from the TD-DFT calculations at the ωB97xD-D3/def2-TZVP level of theory for [(dcpm)Pt(TrippCP)] (**170**).

All conducted cyaphido complex syntheses suggest, that the overall C-CP activation process in the platinum based π-complexes is thermodynamically uphill, as it was already described first by JONES et al.[265] and later by WEIGAND, GONZÁLEZ and co-workers[274] for the tolane C(sp^2)-C(sp) cleavage in platinum complexes (cf. 2.1.1). Consequently, thermal back reaction (reductive elimination) is hampered by the activation barrier. In order to estimate the energy of this barrier DFT calculations at the ωB97xD-D3/def2-TZVP level of theory were conducted for the C_1-bridged model complex [(dmpm)Pt(CP)(Mes)] (**C9σ**). The gas phase Gibbs free energy (ΔG^0) and the activation barrier ($\Delta G^{\ddagger}$) for the reaction **C9σ → C9** are illustrated in Figure 94. The energetic profile of the reductive elimination is exergonic ($\Delta G < 0$) with $\Delta G^0 = -25.82$ kcal·mol^{-1}. However, an energy of 29.15 kcal·mol^{-1} must be expended to overcome the transition state (**C9-TS**) at the highest point of the activation barrier. This finding confirms experimental observations, that the formal Pt(0) π-complexes are overall thermodynamically more stable than the corresponding Pt(II) σ-complexes. Similar results gained from the calculation on the C_2-bridged model complex [(dmpe)Pt(MesCP)] (**C7**) underline this outcome.
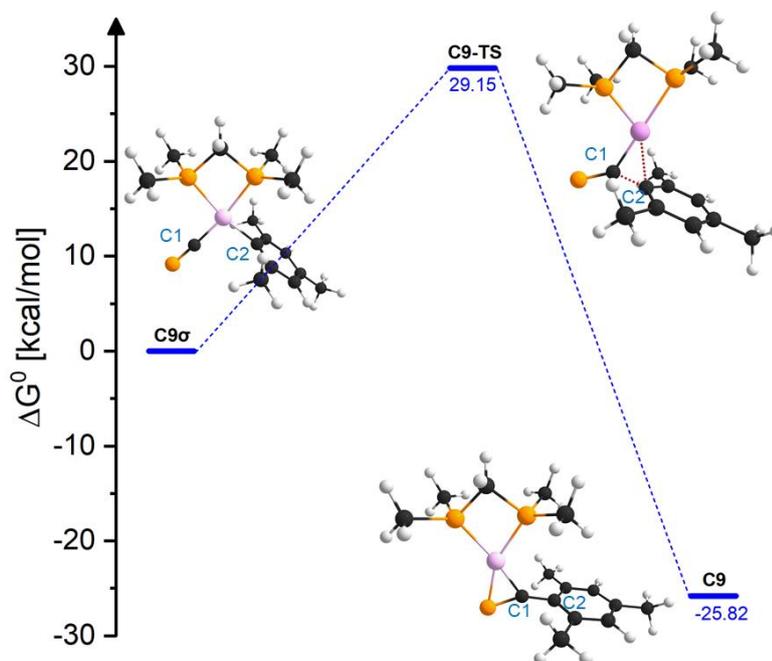
Figure 94. Energy diagram with Gibbs free energies and activation barrier of the thermal reductive elimination from **C9σ** to **C9**. Relative free Gibbs energies are given in kcal·mol⁻¹ with respect to the σ-complex **C9σ** (0 kcal·mol⁻¹). The new bond is built between the C1-C2 carbon, whereas the Pt1-C2 bond is erased. Distance C1-C2 [Å]: **C9σ** 2.912, **C9-TS** 1.491, **C9** 1.456.

The electronic structure of **170σ** was analyzed by means of DFT calculation (ωB97xD-D3/def2-TZVP). The geometry, bond lengths and angles of the computational model matches with crystallographic data of **170σ**. The frontier molecular orbitals of the Pt(II)-cyaphido complex **170σ** (Figure 95) significant differ from the Ru-cyaphido complexes described by CROSSLEY and co-workers (cf. 1.4.2.3). The phosphorus atom of the cyaphido ligand is a major component of the LUMO (0.81 eV). The HOMO-1 (-7.96 eV) and HOMO-3 (-8.34 eV) shows a high contribution of $\pi_{C\equiv P}$, whereas the HOMO (-7.69 eV) has barely interactions with the cyaphido ligand. The HOMO-LUMO gap is 8.50 eV. The lone pair of the terminal phosphorus atom contributes significantly to the HOMO-6 (-9.33 eV) with a stabilization of 1.64 eV in respect to the HOMO, which is much less than for the typical L_nRu-C≡P complexes. Similar shapes and values were also found for the frontier molecular orbitals of the C_2 structure **143σ**. These electronic properties are relevant for potential consecutive reactions at the C≡P ligand. The computational study suggests mainly two reaction types, nucleophilic additions (A_N) at the phosphorus atom and electrophilic additions (A_E) at the C≡P-π-system or the phosphorus lone pair, which include cycloaddition reactions. In contrast to the archetype [(dippe)₄Ru(CP)(X)] complexes, the C≡P moiety in the Pt(II)-cyaphido complexes are readily accessible as they are evident from the molecular structures in the crystals of **148σ**, **150σ** and **170σ** (cf. Figure 79, Figure 83, Figure 89). Therefore, these types of Pt(II)-cyaphido complexes are predestined to undergo follow-up reactions.
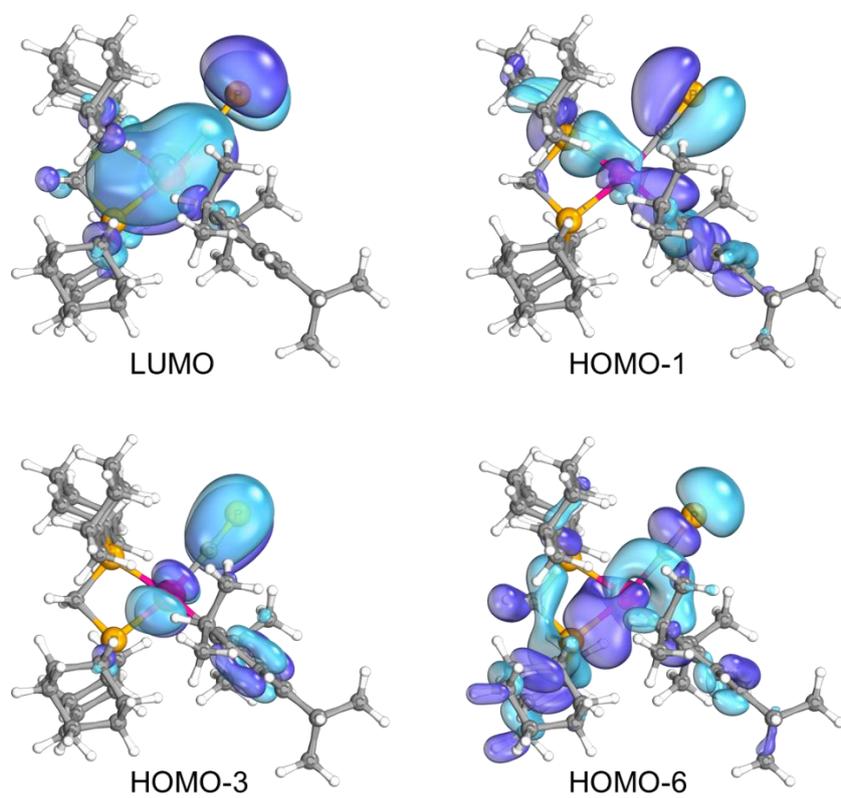
**Figure 95.** Selected frontier molecular orbitals of **170σ**.

2.1.5 Consecutive reactions

2.1.5.1 Consecutive reaction on the π-complex phosphorus

2.1.5.1.1 Lewis-acid assisted cleavage

###### 2.1.5.1.1.1 Introduction to the Lewis-acid promoted reactions

Several examples demonstrated, that the use of Lewis acids can increase the selectivity, reaction rates and extend the transition-metal catalyst's lifetimes for hydrocyanation reactions by coordination to the nitrogen lone pair.[414-415] Furthermore, a dramatically increase of the reaction rates of alkyne arylcyanations was found for boron and aluminum based Lewis acids.[416-417] JONES, GARCÍA and co-workers studied the effect of Lewis-acid promoted selectivity and reaction rates for the C-CN cleavage reactions in their Ni(0)-π-nitrile systems with surprisingly disparate outcomes depending on the specific system.[256-257, 259, 262, 418] Using BPh$_3$ on the nickel allyl cyanide **2.22π** successfully accelerated the C-CN cleavage, suppressed the undesired C-H cleavage (Scheme 60) and is irreversible.[256] The coordination of BPh$_3$ to the nitrogen lone pair of the nitrile probably diminishes the electron density from the cyanido antibonding orbitals, leading to a stronger C≡N bond, which is reflected in the increase of the C≡N stretching vibration by $\tilde{\nu} = 54$ cm^{-1} in the infrared spectrum upon coordination of the Lewis acid. Astonishingly, the formed Lewis acid adduct **2.25** shows a σ-π allyl interconversion with **2.26** being thermodynamically favored. In contrast to the allyl nitrile, the analogous crotononitrile adduct **2.24** did not undergo the C-CN cleavage reaction even at elevated temperatures, which might indicated a stronger π-coordination due to the increased electron accepting properties of the Lewis acid-coordinated olefin.[256]
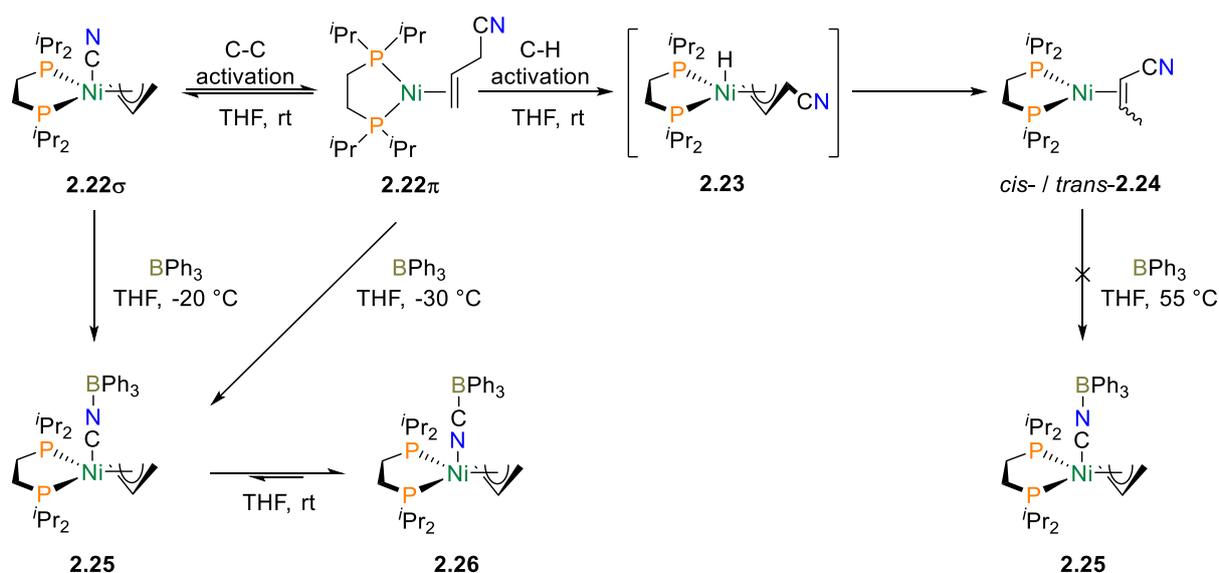
Scheme 60. Lewis acid promoted C-CN cleavage in nickel allyl cyanide **2.22π** and the Lewis-acid inhibited acetonitrile complex [(dippe)Ni(η^2-MeCN-BPh$_3$)] (**2.27**).

A suppression of the C-CN cleavage process upon coordination of the Lewis acid ZnCl$_2$ or BEt$_3$ was also observed for the allyl cyanide complex [(dppf)Ni(η^3-allyl-CN-LA)] (**2.27π**, **2.28π**,

LA = Lewis acid, Scheme 61), even though the oxidative addition to [(dppf)Ni(η^3-allyl)(CN-LA)] (**2.27σ**, **2.28σ**) was still possible.[418] Lewis-acid inhibitions of the oxidative addition in favor for an accelerated reductive elimination were previously reported for palladium-phosphine complexes.[419] The coordination of the Lewis acid to the cyanido induces a positive charge at the nitrogen and carbon atom, therefore making the carbon more susceptible to nucleophilic attacks. The oxidative addition in the acetonitrile complex [(dippe)Ni(η^2-MeCN-BEt$_3$)] (**2.29π**) was also strongly inhibited by the Lewis acid and did not show any C-CN cleavage product by heating to T = 100 °C, however, irradiation with UV light (λ_{max} = 365 nm) still resulted in the formation of **2.29σ**.[259]

2.27π LA = ZnCl$_2$
2.28π LA = BEt$_3$

2.27σ LA = ZnCl$_2$
2.28σ LA = BEt$_3$

2.29π

2.29σ
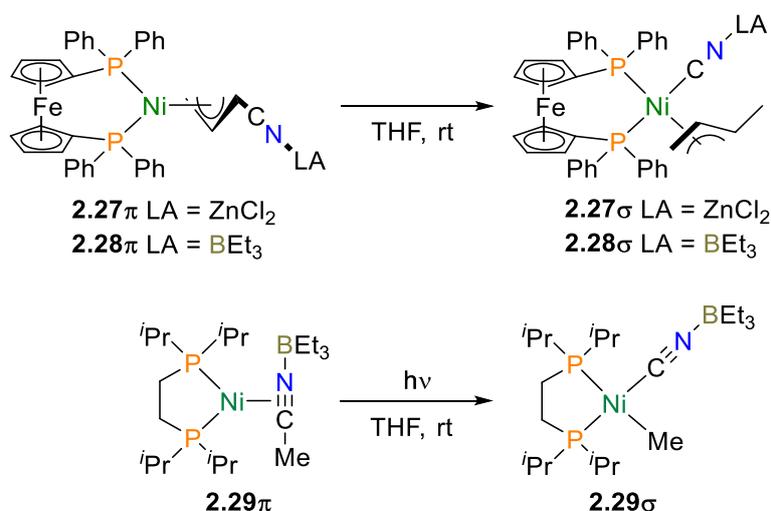
Scheme 61. Strongly Lewis-acid inhibited C-CN cleavage reaction of [(dppf)Ni(η^3-allyl-CN-LA)] (top) and the only thermally Lewis-acid inhibited C-CN cleavage reaction of [(dippe)Ni(η^2-MeCN-BEt$_3$)] (bottom).

Overall, the coordination of Lewis acids to the nitrogen atom of a Ni-π-nitrile complex renders ambivalent results. Sometimes, the Lewis acid strongly assisted the C-CN cleavage, whereas in other cases, it induces limited suppression to the oxidative addition or even promotion of the reductive elimination. Further studies were carried out for the benzonitrile complex [(dippe)Ni(PhCN)] (**2.2π**) with the Lewis acids BPh$_3$ and BF$_3$.[262] Both Lewis acids yielded the corresponding C-CN cleavage products. The reaction rate is affected by the type as well as the amount of Lewis acid used. Adding a mixture of BPh$_3$ and BF$_3$ to **2.2π** first resulted in the quick formation of [(dippe)Ni(Ph)(CN-BF$_3$)] and subsequent slow transformation into [(dippe)Ni(Ph)(CN-BPh$_3$)] (**2.30σ**). This proves that BF$_3$ is less acidic than BPh$_3$ and gives the kinetically controlled adduct, whereas the thermodynamically more stable adduct is obtained with BPh$_3$. The reaction rate for both Lewis acids is heavily dependent on the used equivalents in respect of **2.2π**. An excess of Lewis acid (eq > 1) strongly inhibits the C-CN cleavage and generation of the Lewis-acid σ-complex, whereas eq < 1 accelerates this reaction up to 100 times. The mechanism for the formation of **2.30σ** was examined to get an in-depth explanation for this behavior (Scheme 62). The crucial point in the Lewis-acid acceleration or inhibition is

the equilibrium between **2.2π** and **2.30π**, which depends on the stoichiometry of BPh$_3$. An excess of BPh$_3$ strongly shifts the equilibrium to the favor of **2.30π**. Calculations revealed that **2.30π** is lower in energy than **2.2π**, thus more stabilized. Consequently, more energy is needed to overcome the energy barrier to undergo the C-CN cleavage reaction, which significantly slows down the reaction rate. However, **2.2π** is also in equilibrium with the less stable **2.2π$_{arene}$**, which is crucial for the formation of the regular σ-complex **2.2σ** (cf. 2.1.1, **2.3-S1** in Scheme 16). Low temperature NMR studies suggest that small quantities of BPh$_3$, dissociated from **2.30π**, coordinate to **2.2π$_{arene}$** and form the much more stabilized **2.30π$_{arene}$**, which quickly converts to **2.30σ** upon warming. In consequence, the coordination of BPh$_3$ to **2.2π$_{arene}$** is the rate-determining step in the formation of **2.30σ** and key to accelerate the C-CN cleavage reaction.[262]
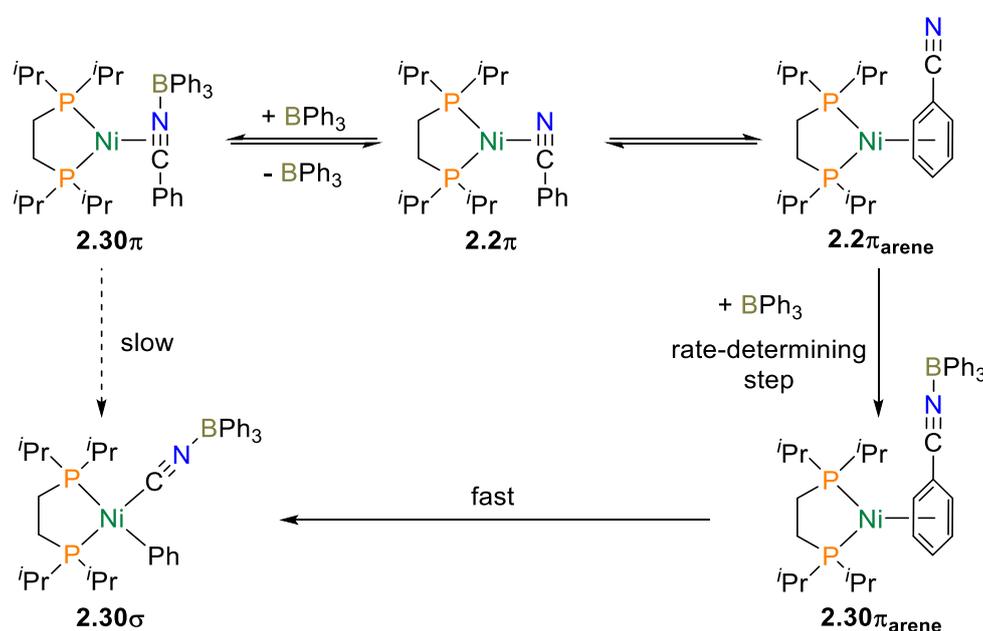
Scheme 62. Proposed mechanism for the formation of [(dippe)Ni(Ph)(CN-BPh$_3$)] (**2.30σ**) by JONES and co-workers.

Besides nickel complexes, JONES *et al.* also analyzed palladium complexes towards the ability of Lewis-acid assisted activation.[249] The precursor complex [dippe)Pd(μ-H)]$_2$ (**2.32**, Scheme 63) was *in situ* generated by mixing [(dippe)PdCl$_2$] (**2.31**) with 2 eq of potassium triethylborohydride and subsequently treated with acetonitrile to obtain the π-complex [(dippe)Pd(MeCN-BEt$_3$)] (**2.33π**), which could not be isolated as a solid. Heating of the reaction mixture to receive [(dippe)Pd(Me)(CN-BEt$_3$)] (**2.33σ**) also led to decomposition, whereas UV irradiation (λ_{max} = 365 nm) generated the unstable and quickly decomposing **2.33σ**, which prevent the characterization. However, the system could be stabilized by exchanging BEt$_3$ with the bulkier BPh$_3$ in the π-complex (**2.33π** → **2.34π**). The resulting [(dippe)Pd(MeCN-BPh$_3$)] (**2.34π**) could be transformed to the corresponding σ-complex **2.34σ** by heating or by photolysis. The best ratio was obtained by heating and resulted in a 1:1 mixture of **2.34π** and **2.34σ**. Contrary to the observation on the analog synthesis with Ni (cf. **2.29π** in Scheme 61),

the Lewis acid BPh_3 favors the C-CN cleavage reaction in acetonitrile within the palladium system. The best result was achieved by addition of benzonitrile to the precursor **2.32**, which instantly resulted in the exclusive formation of the C-CN cleavage product [(dippe)Pd(Ph)(CN-BEt_3)] (**2.35σ**) instead of the π-complex [(dippe)Pd(PhCN-BEt_3)] (**2.35π**).[249] As for nickel, the Lewis-acid assisted cleavage reaction is highly dependent on the acidity and the steric demand of the Lewis acid as well as the electronic and steric properties of the nitrile. Overall, a prediction for the occurrence of a Lewis-acid promotion or inhibition remains challenging.
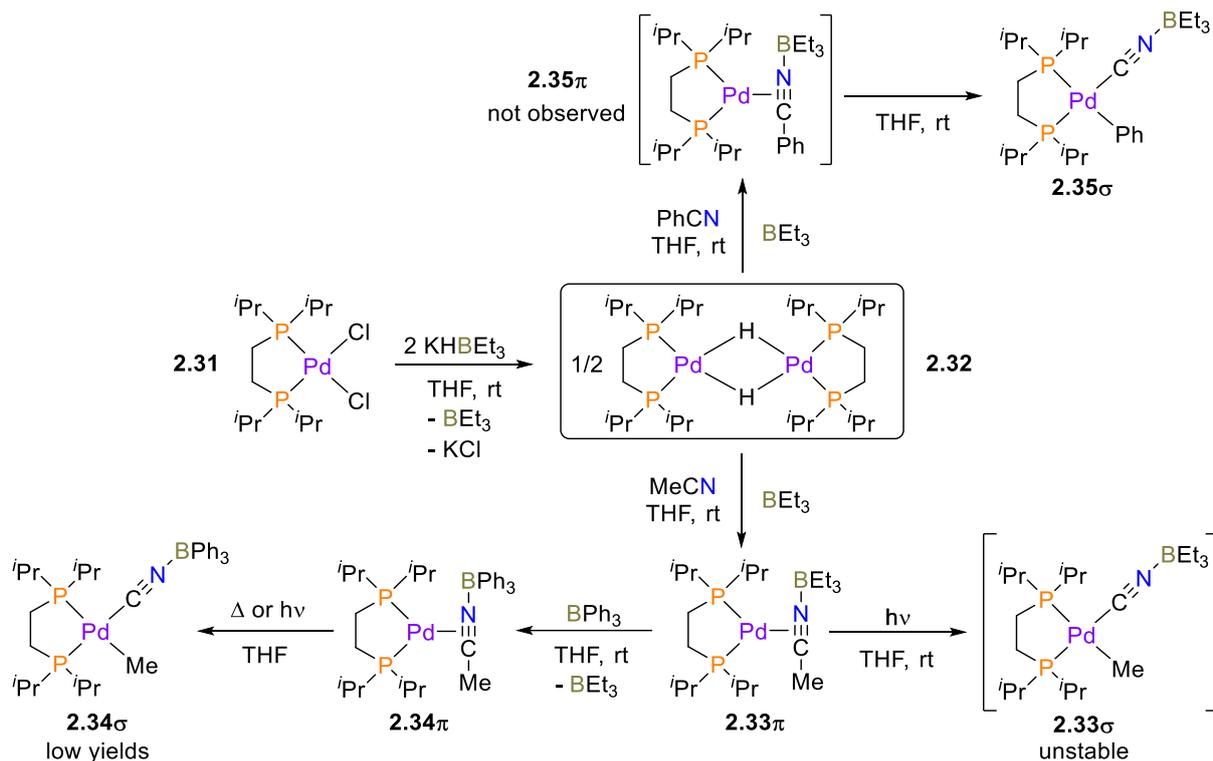
Scheme 63. Lewis-acid assisted C-CN cleavage reaction in palladium complexes.

2.1.5.1.1.2 Lewis-acid boron adducts

Based on that background, the addition of Lewis acids on a selection of synthesized π-complexes was analyzed with the intention to find a chemical activation for the C-CP cleavage, mainly for nickel based π-complexes. In demand for a suitable Lewis acid $ZnCl_2$, BEt_3, BPh_3 and $B(C_6F_5)_3$ were screened towards their coordination on [(dippe)Ni(MesCP)] (**142**). Only for the toluene solution of **142** with tris(pentafluorophenyl)borane an instant color change from yellow to strong red and shifts of the ^{31}P signals appeared. All other Lewis acids did not show any activity, even after heating the mixture. In addition to that, the effect of triphenylborane towards [(dcpe)Ni(MesCP)] (**147**) and [(dcpe)Pt(MesCP)] (**148**) in toluene was investigated by means of heating or irradiation ($\lambda_{max} = 365$ nm) of the solution. However, none of these mixtures showed any reactivity. Consequently, the Lewis acid tris(pentafluorophenyl)borane was exclusively used for further studies. Tris(pentafluorophenyl)borane did not react with free

MesCP (**68**) or TrippCP (**81**). It turned out that tris(pentafluorophenyl)borane acts surprisingly different towards the various π- and σ-complexes, which will be pointed out for the compounds **142**, **147**, **148**, **149**, **150**, **153**, **169** and **185**. Generally, the Lewis acid coordination reactions were carried out by mixing separately prepared toluene solutions of the respective metal precursor complex and $B(C_6F_5)_3$. The order of the addition is arbitrary and does not influence the reaction outcome. The molecular structure of the final Lewis-acid adducts could not be determined, however, the possibility of the boron η^1-coordination on the phosphaalkyne phosphorus atom leading either to a π-complex of the fashion $[(P,P)M(aryl\text{-}C{\equiv}P\text{-}B(C_6F_5)_3]$ or the formation of a σ-complex adduct, $[(P,P)M(aryl)(C{\equiv}P\text{-}B(C_6F_5)_3]$, will be discussed at the end of this chapter and in chapter 2.1.5.1.1.3. For reference reasons the ^{11}B (δ = 58.7 ppm) and ^{19}F (δ = -128.98, -142.19, -160.37 ppm) NMR of $B(C_6F_5)_3$ were measured. Figure 96 shows all successfully conducted reactions between the π-complex and $B(C_6F_5)_3$ and assign a compound number to the outcome.
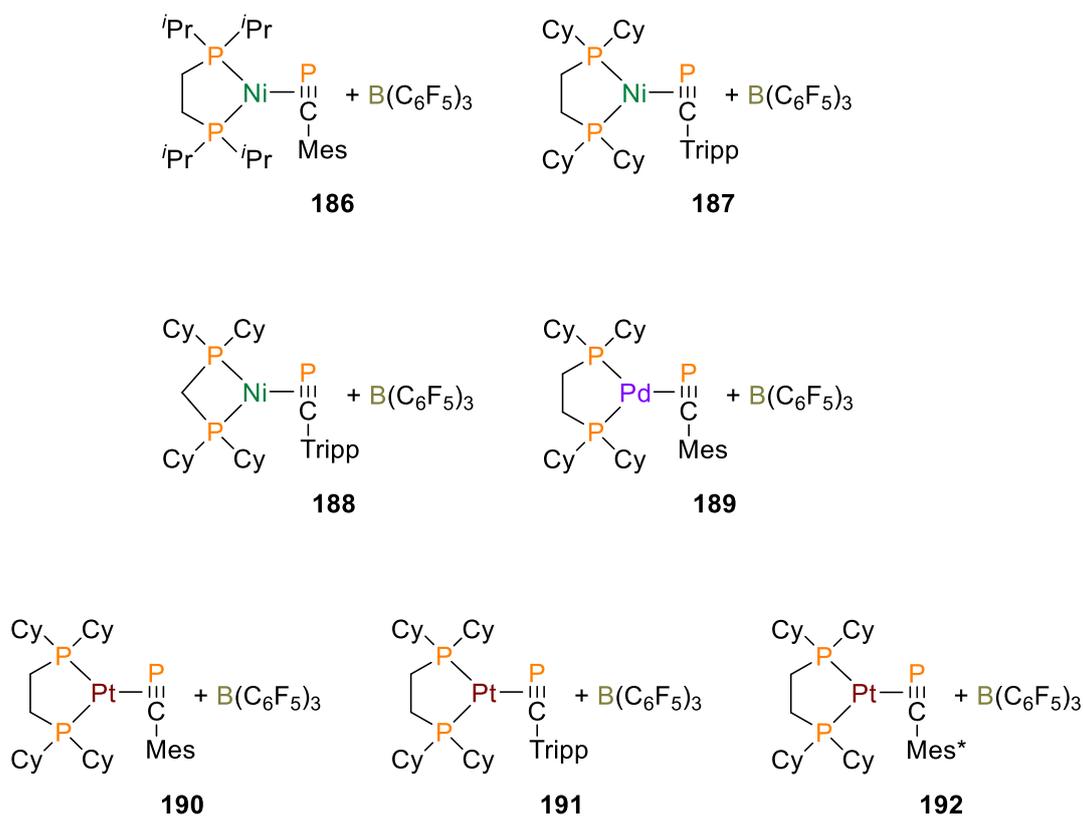
Figure 96. Not specified boron adducts by addition of $B(C_6F_5)_3$ to different π-complexes.

Upon addition of 0.5 eq of $B(C_6F_5)_3$ to [(dippe)Ni(MesCP)] (**142**) the $^{31}Pt\{^1H\}$ signal of the phosphaalkyne phosphorus atom shifted δ = 43.8 ppm upfield and showed an additional splitting to a doublet of doublets with a conspicuous large $^{31}P^{31}P$ coupling constant of $J_{P,P}$ = 119.1 Hz (Figure 97). The dippe phosphorus atoms experience only a marginal downfield shift below δ = 3.0 ppm and a decrease of the $^{31}P^{31}P$ dippe coupling constant by half (from $J_{P,P}$ = 16.5 Hz to 8.3 Hz). The ^{11}B NMR showes only one broad signal at around

$\delta \approx$ -12 ppm, while the ^{19}F signals are broadened and slightly shifted to δ = -130.62, -135.05 and -165.66 ppm. Overall, the NMR spectroscopy results appeared inconclusive. All three NMR spectra, ^{31}P{^{1}H}, ^{11}B and ^{19}F, showed only one single species, however two different compounds, the starting material **142** and a boron adduct are expected in the ^{31}P{^{1}H} spectrum, due to the addition of only 0.5 eq B(C$_6$F$_5$)$_3$. Furthermore, the signal of the alleged phosphaalkyne phosphorus atom did show neither additional ^{11}B couplings nor the typical boron signal broadening. The ^{1}H spectrum also did not provide clarity.
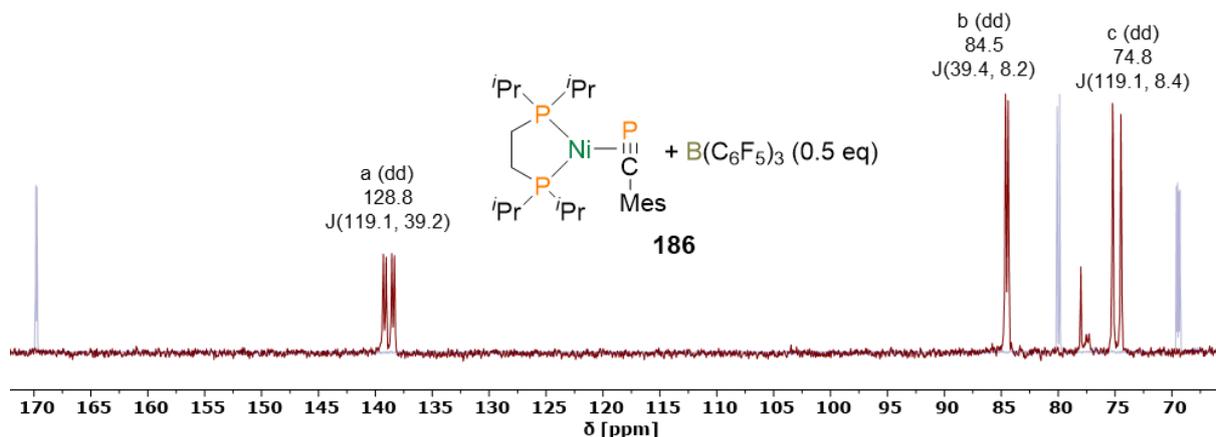
Figure 97. Superimposed ^{31}P{^{1}H} NMR spectra of [(dippe)Ni(MesCP)] (**142**, blue) and after the addition of 0.5 eq B(C$_6$F$_5$)$_3$ yielding **186** (red) in benzene-d$_6$.

Astonishingly, the reaction of the very similar [(dcpe)Ni(MesCP)] (**147**) with B(C$_6$F$_5$)$_3$ (1 eq) resulted in decomposition of the complex, whereas [(dcpe)Ni(TrippCP)] (**149**) cleanly reacted under instant color shift from yellow to red. The ^{31}P{^{1}H} signal of the phosphaalkyne phosphorus atom is only δ = 10.7 ppm upfield shifted compared to **149**, significantly less than for **186**. The highly broadened resonance rather meets the expectation for a boron atom coupled phosphorus atom (Figure 98). The dcpe signals are around δ = 4 ppm downfield shifted and appear as triplet and a doublet of doublets. The lager doublet is $J_{P,P}$ = 60.1 Hz wide, which is less than half the coupling constant found in **186** and the smallest doublet of this kind for the boron complex series. The broad ^{11}B signal was found at δ = -0.2 ppm. The addition of benzyl azide, to prove for the existence of the cyaphido complex by forming a triazaphosphole (explanation cf.2.1.5.2.4), resulted in decomposition.
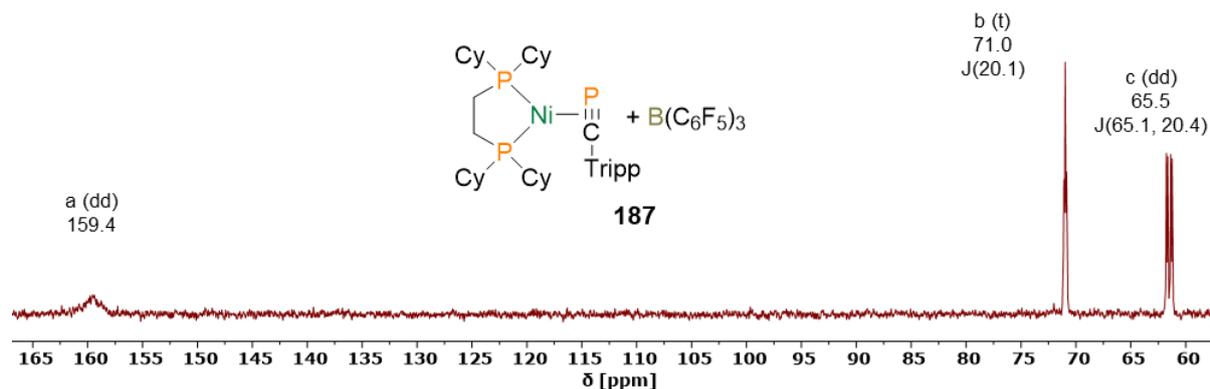
Figure 98. $^{31}P\{^1H\}$ NMR spectrum of [(dcpe)Ni(MesCP)] after the addition of 1 eq B(C$_6$F$_5$)$_3$ yielding **187** in benzene-d$_6$.

The analogous reaction with the small bite angle complex [(dcpm)Ni(TrippCP)] (**169**) showed a broad resonance with large upfield shift of δ = 56.3 ppm for the $^{31}P\{^1H\}$-phosphaalkyne signal and around δ = 7 ppm upfield shifted doublets ($J_{P,P}$ = 133.3 ,33.2 Hz) for the dcpm ligand in respect to the starting material.

The B(C$_6$F$_5$)$_3$ reaction with [(dcpe)Pd(MesCP)] (**185**) led to a broad doublet ($J_{P,P}$ = 219.0 Hz) for the assumed $^{31}P\{^1H\}$-phosphaalkyne signal without significant shift compared to **185**. The triplet and doublet of doublets resonances of the dcpe group are around $\delta(^{31}P\{^1H\})$ = 12 ppm shifted to the low field. The broad ^{11}B signal is located at δ = 0.4 ppm. The ^{19}F NMR showed three broad signals at δ = -129.23, -142.58 and -160.76 ppm for the pentafluorophenyl units.

Mixing the platinum complex [(dcpe)Pt(MesCP)] (**148**) with 0.5 eq B(C$_6$F$_5$)$_3$ resulted in a 1:1 ratio of the starting material and a new $^{31}P\{^1H\}$-upfield shifted boron adduct species (**190**). Further addition of 0.5 eq B(C$_6$F$_5$)$_3$ completed the conversion (Figure 99). Performing the synthesis with the corresponding C-CP cleavage product (**148σ**) surprisingly revealed equal $^{31}P\{^1H\}$ signals indicating the formation of the same boron adduct. The $^{31}P\{^1H\}$ phosphorus resonance (δ = 121.4 ppm) of the associated phosphaalkyne ligand is in between the signals found for the π- (δ = 140.0 ppm) and the σ-complex (δ = 96.6 ppm). The $^{31}P^{195}Pt$ coupling constants are only visible for the dcpe ligand and assigned to $^1J_{P,Pt}$ = 2783 and 3635 Hz, which is more in line with the π-complex. The ^{11}B spectrum showed one broad signal at δ = -5.7 ppm. The signals in the ^{19}F spectrum were unremarkable and appeared nearly unchanged in respect to B(C$_6$F$_5$)$_3$.
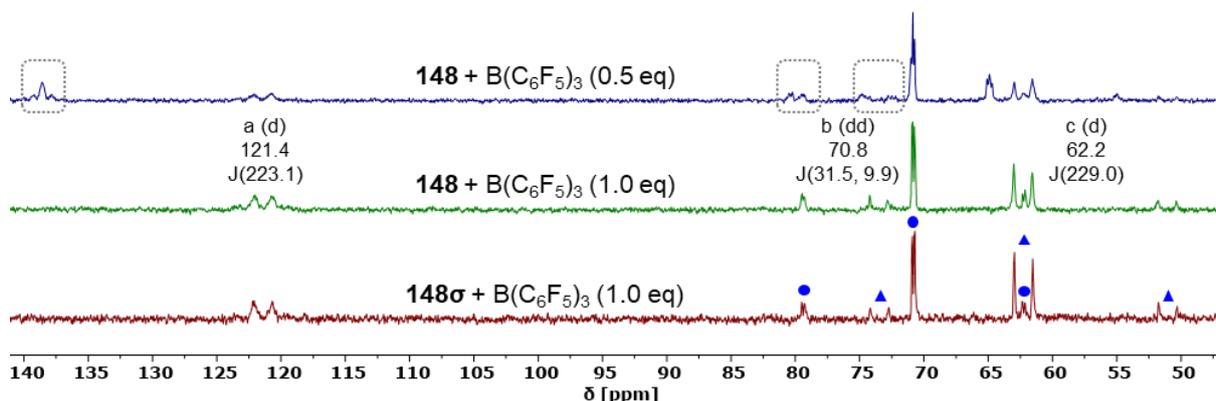
Figure 99. $^{31}P\{^1H\}$ NMR spectra of [(dcpe)Pt(MesCP)] (**148**) after the addition of 0.5 eq (blue) and 1.0 eq B(C$_6$F$_5$)$_3$ (green). $^{31}P\{^1H\}$ spectrum of [(dcpe)Pt(CP)(Mes)] (**148σ**) after the addition of 1.0 eq B(C$_6$F$_5$)$_3$ (red). The grey dashed boxes tag the remaining signals of the starting material (**148**). The blue cycles and triangles mark the ^{195}Pt satellites of the resulting boron adduct **190**.

Surprisingly, B(C$_6$F$_5$)$_3$ did not react with the σ-complex of [(dcpe)Pt(CP)(Tripp)] (**150σ**), however, the slowly generated π-complex [(dcpe)Pt(TrippCP)] (**150**) immediately formed the boron adduct (**191**), which showed $^{31}P\{^1H\}$ resonances at δ = 118.4 (br), 68.8 (dd) and 58.9 (d) ppm with $^{31}P^{195}Pt$ coupling constants of $^1J_{P,Pt}$ = 2861 and 3456 Hz for the dcpe ligand. The ^{11}B signal was assigned to δ = -4.2 ppm, whereas the ^{19}F spectrum did not change.

The addition of B(C$_6$F$_5$)$_3$ to the, neither thermally nor photochemically activatable, [(dcpe)Pt(Mes*CP)] (**153**) resulted in three new $^{31}P\{^1H\}$ signals at δ = 120.1 (d, br), 66.7 (dd) and 57.1 (dd) ppm with $^{31}P^{195}Pt$ coupling constants of $^1J_{P,Pt}$ = 2995 and 3334 Hz for the dcpe ligand. In contrast to the other two platinum-based boron adducts (**190**, **191**), the $^{31}P\{^1H\}$ resonance of the phosphaalkyne is a more distinct doublet with a much lower coupling constant of $J_{P,P}$ = 80.8 Hz.

The $^{31}P\{^1H\}$ signals of all synthesized boron adducts (Figure 96) are summarized in Table 11, together with the relevant shifts of the corresponding π- and σ-complexes. All phosphaalkyne phosphorus (P1) signals of the boron adducts, except for the palladium compound **189**, are δ($^{31}P\{^1H\}$) = 8 to 56 ppm upfield shifted in respect to the corresponding π-complex, even though, the platinum-based boron adducts **190** and **191** are downfield shifted with respect to their corresponding σ-complex. These results are unexpected for the presumed boron η^1-coordination to P1 of the π-complex. Normally, a slight downfield shift would be expected upon coordination of the boron adduct (Lewis acid), due to the electron density transfer from the P1 to the boron, leading to a de-shielding of the P1. Computational NMR predictions for the simplified version of [(dcpe)Pt(MesCP)] (**148**) confirm this consideration by a downfield shift of δ($^{31}P\{^1H\}$) = 5.2 and 5.4 ppm for the π- and σ-complexes (Figure 100). Except of the actual $^{31}P\{^1H\}$ shifts, there is further NMR information to evaluate the molecular configuration. Even though a distinct $^1J_{P,B}$ coupling constant is not visible for any of the boron adducts, the broadened P1 signals are in line with the estimated $^1J_{P,B}$ coupling.[396, 400, 420] The NMR pattern

of the $^{31}P\{^1H\}$ signals, the general presence of a $^2J_{P,P}$ coupling between diphosphine phosphorus nuclei, as well as the magnitude of the coupling are evidence for the formation of boron adducts of the π-complex instead of σ-complex. Furthermore, the $^1J_{P,Pt}$ constants of the boron adducts are much closer to those found in the π-complexes and the increase of the $^{31}P^{195}Pt$ coupling of the *trans* phosphorus (P2) is in line with the expectation of a decreased σ-donation from the phosphaalkyne phosphorus, due to the diminished electron density upon coordination to the boron. The increased $^1J_{P2,Pt}$ also indicates the formation of π-complex boron adducts.

Table 11. $^{31}P\{^1H\}$ signals of the boron adducts and the corresponding P1 shifts relative to the corresponding π- ($\Delta\pi$) and σ-complex ($\Delta\sigma$). P1 is in relationship with the phosphaalkyne phosphorus, while P2 (*cis* to P1) and P3 (*trans* to P1) are assigned to the diphosphine ligand.

| cmd	$^{31}P\{^1H\}$ P1 [ppm]	$J_{P,P}$ P1 [Hz]	$^{31}P\{^1H\}$ P2 [ppm]	$J_{P,P}$ P2 [Hz]	$^{31}P\{^1H\}$ P3 [ppm]	$J_{P,P}$ P3 [Hz]	$\Delta\pi$	$\Delta\sigma$
186	128.8	119.1, 39.2	84.5	39.4, 8.2	74.8	119.1, 8.4	-43.8	-
187	159.4	br	71.0	20.1	65.5	65.1, 20.4	-11.7	-
188	143.1	br	14.3	33.2	8.8	133.3	-56.3	-
189	99.8	219.0	72.4	29.6	66.7	219.6, 29.6	0.6	-
190	121.4	223.1	70.8	31.5, 9.9	62.2	229.0	-18.6	24.8
191	118.4	br	68.8	27.0, 13.6	58.9	194.5	-31.5	9.5
192	120.1	80.8	66.7	30.6, 21.2	57.1	82.4, 30.5	-7.9	-
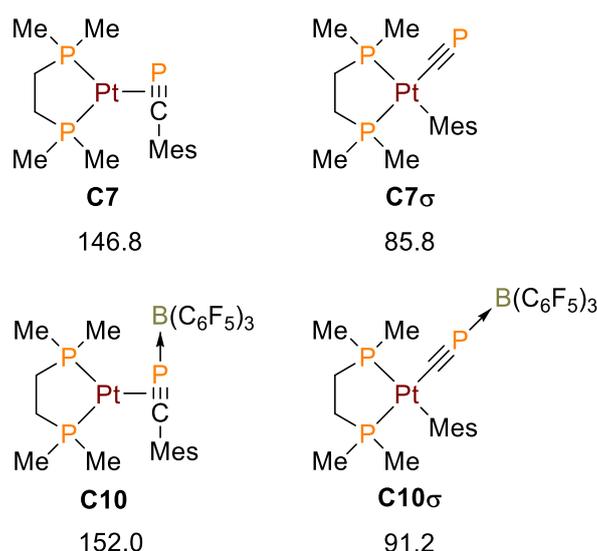
Figure 100. Structure of the predicted platinum complexes and their corresponding boron adducts. NMR shifts of the phosphaalkyne/cyaphido phosphorus (P1) in ppm.

Interestingly, the increase of the $^1J_{P,Pt}$ for the *trans* phosphorus (P3) and the decrease of the $^1J_{P,Pt}$ for the *cis* phosphorus (P2) in [(dcpe)Pt(R-CP)] (R = Mes, Tripp, Mes*) across the

corresponding π-complex is reduced along the line from MesCP ($\Delta^1 J_{Pt,P2}$ = 430 Hz, $\Delta^1 J_{Pt,P3}$ = -273 Hz), TrippCP (244 Hz, -185 Hz), to Mes*CP (56 Hz, -50 Hz). All crystallization attempts to finally verify the molecular structure were unsuccessful. Independent of the used solvent, concentrated solutions of the boron adducts resulted without exception in slow decomposition under the formation of a dark red oil, whose NMR analysis were inconclusive.

2.1.5.1.1.3 Lewis-acid tungsten adducts

In the next step, tungsten hexacarbonyl was selected to continue with the investigation on the Lewis acid coordination due to its superb crystallization ability, which should help to receive single crystals for a molecular structure determination. A colorless THF solution of [W(CO$_6$)] was irradiated with UV light (λ_{max} = 365 nm) for 2.5 h and several times flushed with argon to remove the liberated CO. Subsequently, one equivalent of the obtained strong bright yellow THF solution of [W(CO$_5$)(thf)] was added to a THF solution of π-[(dcpe)Pt(MesCP)] (**148**) and σ-[(dcpe)Pt(CP)(Mes)] (**148σ**), respectively, resulting in a dark yellow solution. Indeed, the ^{31}P{^{1}H} NMR spectra were identical in both cases, as previously already observed for the addition of B(C$_6$F$_5$)$_3$. In contrast to B(C$_6$F$_5$)$_3$, [W(CO$_5$)(thf)], typically also reacts with free MesCP and TrippCP to cyclization products (cf. 2.1.2.3.9, Scheme 52), however, no evidence for similar reactions were found. The phosphaalkyne phosphorus (P1) resonance ($\delta(^{31}$P{^{1}H}) = 86.3 ppm) of the new species **193** showed a large upfield shift of $\delta(^{31}$P{^{1}H}) = 53.7 ppm, whereas the dcpe signals ($\delta(^{31}$P{^{1}H}) = 71.7, 64.2 ppm) did not shift in respect to **148** (Figure 101). The ^{31}P{^{1}H} NMR pattern is very similar to the boron adducts, mainly due to similar ^{31}P^{31}P and ^{31}P^{195}Pt coupling constants, especially due to the large doublet of the phosphorus *trans* to the phosphaalkyne phosphorus. In contrast to most of the boron adducts, the P1 resonance stayed sharp and revealed the $^1 J_{P,Pt}$ and the $^1 J_{P,W}$ coupling. The tungsten satellites can be easily differentiated from the platinum satellites by the natural abundance of the elements (^{183}W = 14%, ^{195}Pt = 34%), leading to less intense signals for the tungsten satellites. Both satellites are depicted in the magnification of Figure 101. The inner ^{31}P^{183}W resonances are overlapping with each other, whereas the inner ^{31}P^{195}Pt resonances are hidden below the main signal. The ^{195}Pt{^{1}H} displays one resonance as a doublet of doublets of doublets at δ = -4578 ppm (**148**: -4582 ppm, **148σ**: -4463 ppm), which confirms the found ^{195}Pt satellites at $^1 J_{P,Pt}$ = 3330, 2860 and 376 Hz. The ^{1}H spectrum revealed the singlets of MesCP (**68**) at δ = 6.82 (*meta*-H), 2.29 (*para*-Me) and 2.12 ppm (*ortho*-Me). The resonances of the dcpe are not resolved individually but can be found between δ = 2.05 and 0.75 ppm. The ^{13}C{^{1}H} shows a very broad resonance at δ = 215.7 ppm, which is most likely the carbon signal of the C≡P unit (**148**: δ = 226.8 ppm).
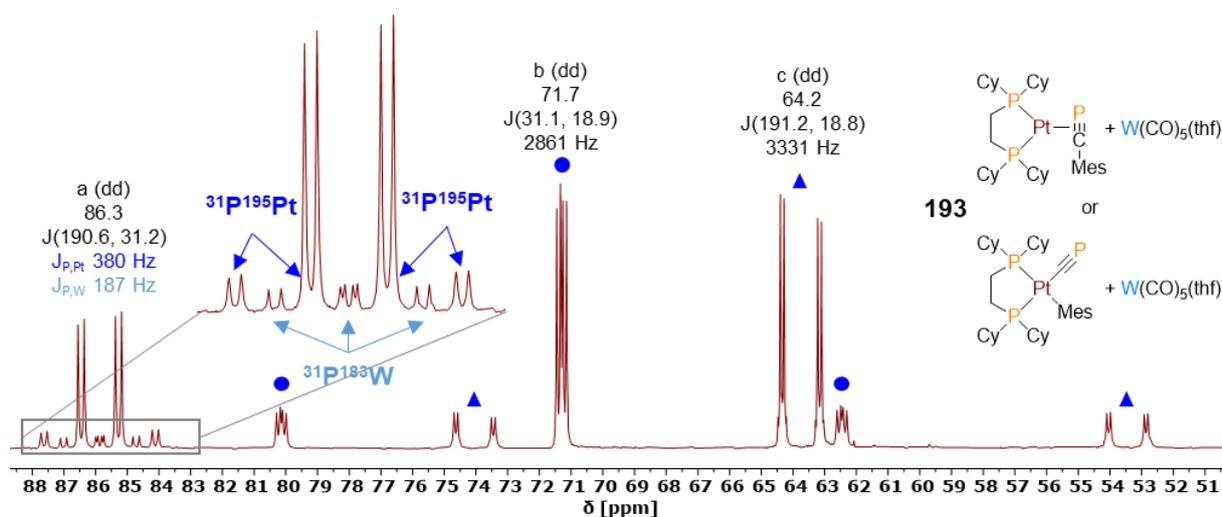
**Figure 101.** $^{31}P\{^1H\}$ NMR spectrum of [(dcpe)Pt(MesCP)] (**148**) or [(dcpe)Pt(CP)(Mes)] (**148σ**) after the addition of 1 eq [W(CO$_5$)(thf)] yielding **193** in tetrahydrofuran-d$_8$.

Compound **193** is stable, both as solid and in solution. Suitable crystals for single crystal diffraction could be collected by slow evaporation of a concentrated THF and toluene solution, which finally revealed the molecular configuration as π-complex (Figure 102). In comparison with **148** (cf. 2.1.3, Figure 63), the C≡P distance (**193**: 1.642(2), **148**: 1.66(1) Å) and the Pt1A-P1A bond length (**193**: 2.2847(5), **148**: 2.348(3) Å) are slightly shorter, whereas the Pt1A-C1A distance (**193**: 2.079(2), **148**: 2.046(8) Å) is marginally longer. The P1A-C1A-C4A angle (**193**: 149.4(2), **148**: 145.7(8)°) is closer to linearity and the P1A-Pt1A-P2A angle is expanded from 114.75(9) to 117.34(2)°, owing to the bulky tungsten moiety. In return, the C1A-Pt1A-P3A angle is narrower. All other bond lengths and angles are nearly identical.
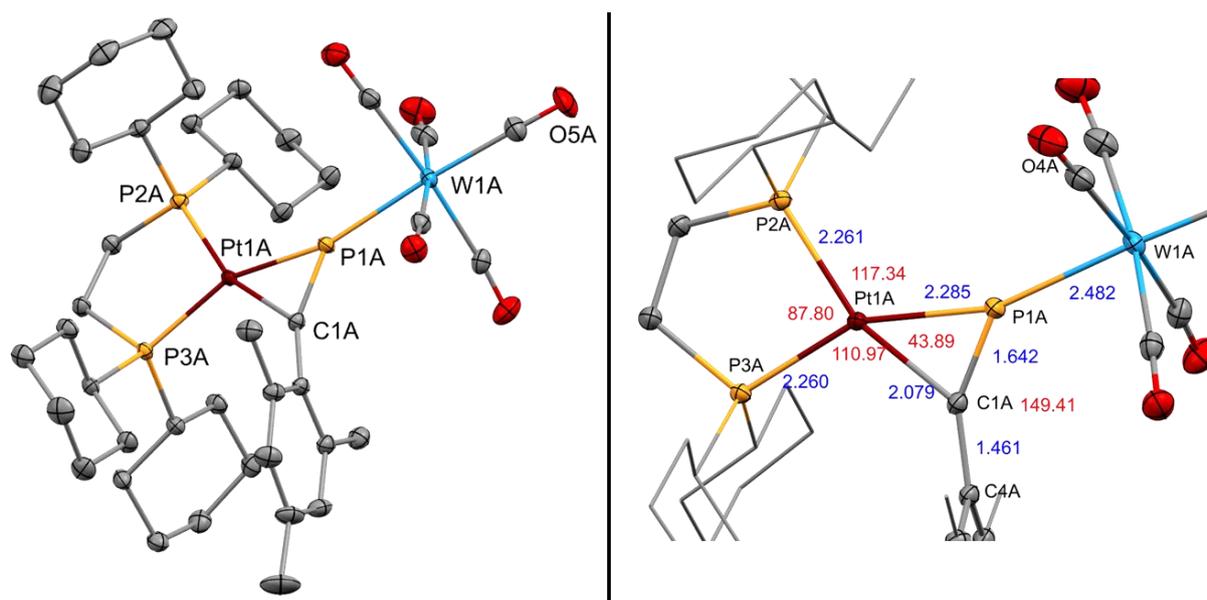
Figure 102. Molecular structure of [(dcpe)Pt(MesCP-W(CO)$_5$)] (**193**) in the crystal. Anisotropic displacement ellipsoids are shown at 50% probability level. Hydrogens and a second molecule of **193** in the asymmetric unit omitted for clarity. Selected bond lengths (Å) in blue and angles (°) in red.

Even though a respective mixture of π- and σ-complex **150/150σ**, **166/166σ** or **170/170σ**, was used for the reaction with [W(CO$_5$)(thf)], consistently one single product was obtained. With respect to the gathered information of **193** and on the basis of the ^{31}P{^{1}H} NMR spectroscopy results of the other products (Table 12), all tungsten complexes are considered as π-complexes (Figure 103). A comparison of **193** and **194** with the relevant boron adducts (**190**, **191**) reveal very similar ^{31}P^{195}Pt coupling constants and the tendency of a likewise reduction of the increased $^1J_{P2,Pt}$ and decreased $^1J_{P3,Pt}$ over the corresponding π-complex from MesCP ($\Delta^1J_{P2,Pt}$ = 126 Hz, $\Delta^1J_{P3,Pt}$ = -196 Hz) to Mes*CP ($\Delta^1J_{P2,Pt}$ = 94 Hz, $\Delta^1J_{P3,Pt}$ = -175 Hz). In addition, GOICOECHEA and YANG recently demonstrated, by means of the Lewis acids [W(CO$_5$)(thf)] and B(C$_6$F$_5$)$_3$, that electrophiles cannot coordinate to the phosphorus lone pair of the cyaphido complex [Au(IDipp)(C≡P)] (**1.35**, cf. 1.4.3.5) before a nucleophile had been coordinated to the π-system of the cyaphido ligand.[203] Taking all this into account, it is most likely that all synthesized boron adducts are coordination products of the π-complexes, exactly like the tungsten compounds.
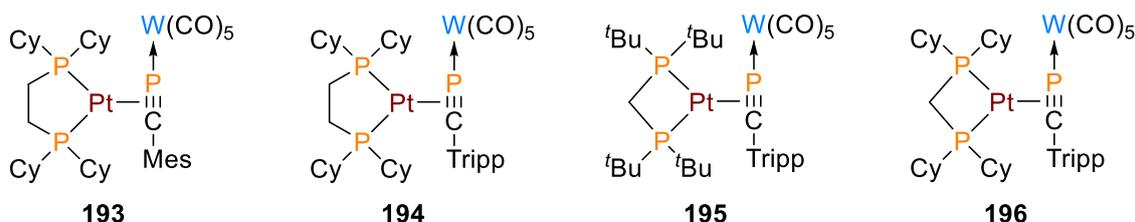
**Figure 103.** Products received from the reaction of **148/148σ**, **150/150σ**, **166/166σ** or **170/170σ** with [W(CO$_5$)(thf)].

Table 12. ^{31}P{^{1}H} signals of the [(P,P)Pt(aryl-C≡P-W(CO)$_5$] complexes. P1 is the phosphaalkyne phosphorus, while P2 (*cis* to P1) and P3 (*trans* to P1) are assigned to the diphosphine ligand. ^{a} suspected value.

cmd	^{31}P{^{1}H} P1 [ppm]	$J_{P,P}$ P1 [Hz]	^{31}P{^{1}H} P2 [ppm]	$J_{P,P}$ P2 [Hz]	^{31}P{^{1}H} P3 [ppm]	$J_{P,P}$ P3 [Hz]	^{195}P{^{1}H} Pt [ppm]	$J_{Pt,P}$ Pt [Hz]	$J_{W,P}$ W [Hz]
193	86.3	190.6, 31.2	71.7	31.1, 18.9	64.2	191.2, 18.8	-4578	376 2860 3330	187
194	88.2	187.3, 29.6	71.4	29.5, 17.7	62.5	187.6, 17.6	-4553	367 2867 3303	186
195	90.4	205.0, 24.6	16.5	22.9	13.3	205.0, 20.6	-	421 2466 2870	185
196	95.9	214.2, 21.2	-8.7	22.8	-11.2	213.9, 24.5	-	428 2392 2820	184
193a	97.5	174.8	70.9	32.5, 23.1	63.5	170.0, 21.7	-	530^a 2892 3238	-

In contrast to the boron complex **190**, [(dcpe)Pt(MesCP-W(CO)$_5$)] (**193**) could be partly transformed into a new species (**193a**, 16%) upon irradiation with violet light (λ_{max} = 405 nm)

for 5 h. Prolonged photolysis for two days increased the amount of **193a** to 21%, however, at the cost of considerable decomposition. Additionally, the reverse reaction occurred at room temperature, which rapidly reduced the quantity of **193a** to around 7% until it slowed significantly down, leaving around 3% of **193a** after one week. This behaver matches the previously discussed back reactions of most synthesized cyaphido complexes. The remarkable shift of the P1 signal from δ = 86.3 to 97.5 ppm in the $^{31}P\{^1H\}$ NMR (Figure 104) also indicates a significant change of the phosphorus surrounding, which might be caused by the formation of a cyaphido product. However, the mostly unchanged dcpe shifts, the general coupling pattern, which is still similar to **193**, and the fact that the boron complex **190** did not react on photolysis, argue against the formation of a cyaphido species. Instead, a further substitution of one or more carbonyl groups of the tungsten with THF under the irradiation process is assumed. Later, the liberated CO, which is trapped in the sealed vial, coordinated to the tungsten again, slowly completing the reverse reaction.
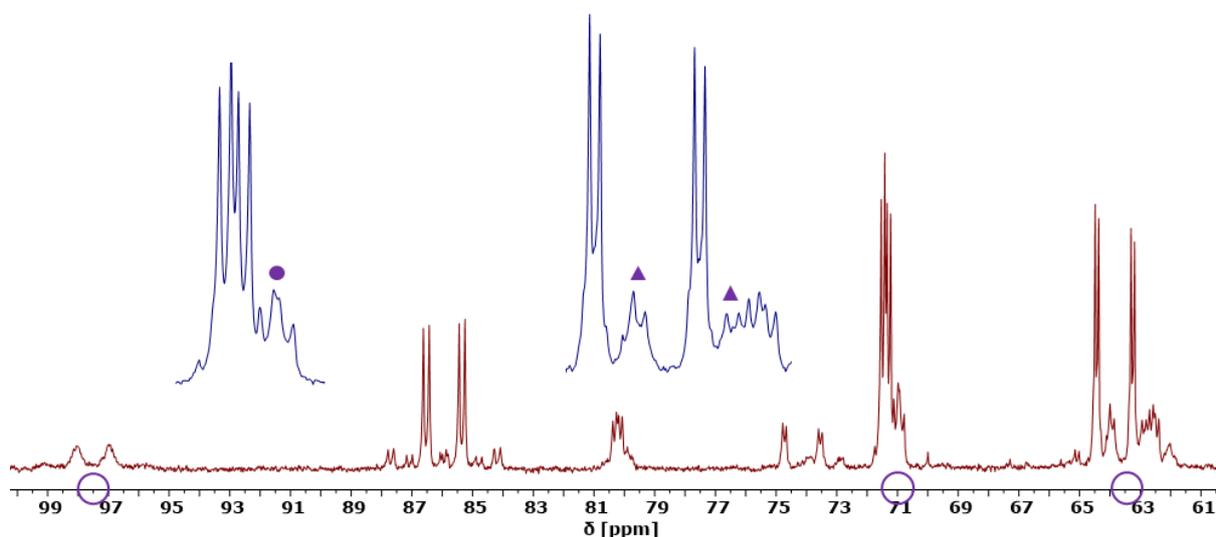

Figure 104. $^{31}P\{^1H\}$ NMR spectrum of [(dcpe)Pt(MesCP-W(CO)$_5$)] (**193**) after 5 h of irradiation with violet light, showing additional signals (purple rings, dots, triangles) of the new compound **193σ** tetrahydrofuran-d$_8$. Magnification of the dcpe signals represented in blue.

2.1.5.2 Consecutive reaction on the cyaphido moiety

#### 2.1.5.2.1 Additional complexation of the cyaphido ligand

Knowledge about the coordination chemistry of the cyaphido ligand is still very limited, even though, ANGELICI *et al.* and recently GOICOECHEA and YANG demonstrated the feasibility for platinum (**1.4a**, **1.6a**) and gold complexes (**1.35**), bearing an accessible cyaphido ligand. The Lewis-acid experiments already showed that ZnCl$_2$, which did not react, and [(W(CO$_5$)(thf)]], which only yielded π-complexes, are not suitable for the coordination. The addition of [(PPh$_3$)$_2$Pt(C$_2$H$_4$)] (**183**), [(acac)Rh(CO)$_2$] or [Re(CO)$_5$]$_2$ to [(dcpe)Pt(CP)(Tripp)] (**150σ**) showed

no reaction. $AuCl \cdot SMe_2$ and [(CO)AuCl] reacted at room temperature with [(dcpe)Pt(CP)(Mes)] (**148σ**) but did not yield a cyaphido complex. The reaction with [(CO)AuCl] mainly gave [(dcpe)PtCl_2] and undefined decomposition products, whereas the addition of $AuCl \cdot SMe_2$ resulted in shifted $^{31}P\{^1H\}$ signals for the dcpe ligand and three new singlets, which might result of the loss of the C≡P unit. The analysis of the $^{31}P\{^1H\}$ NMR spectra over time surprisingly revealed the rapid liberation of MesCP (**68**, $\delta = 0.5$ ppm) upon addition of $AuCl \cdot SMe_2$. Furthermore, a singlet at $\delta = 63.4$ ppm with ^{195}Pt satellites ($J_{P,Pt} = 3552$ Hz) appeared and the dcpe signals shifted to $\delta = 73.4$ ppm (d, $J_{P,P} = 2.7$ Hz, $J_{Pt,P} = 3080$ Hz) and $\delta = 66.0$ ppm (d, $J_{P,P} = 2.5$ Hz, $J_{P,Pt} = 3314$ Hz). In the course of the reaction, the signal of MesCP vanished, while two new signals at $\delta(^{31}P\{^1H\}) = 238.0$ and 234.4 ppm appeared. With the help of the ^{195}Pt satellites, all signals could most likely be assigned to a group of four compounds (Figure 105). The first compound is [(dcpe)PtCl_2][421] ($\delta(^{31}P\{^1H\}) = 63.4$ ppm), which was already observed as by-product of previous reactions. The next compound is described by the two dcpe phosphorus nuclei, which couple to each other as a doublet. That indicates an unsymmetrical molecule without further phosphorus atoms at least within a $^3J_{P,P}$. Considering the SMe_2 in the reaction solution might suggest the complex [(dcpe)Pt(SMe)(Me)]. However, the very similar [(dippe)Pt(SMe)(Me)][422-423] shows slightly different signals ($\delta(^{31}P\{^1H\}) = 66.6$ ppm, (s, $J_{P,Pt} = 1828$ Hz); $\delta(^{31}P\{^1H\}) = 64.2$, (s, $J_{P,Pt} = 2846$ Hz)). An unsymmetrical S,S bridged[424] complex could also be excluded. Furthermore, the large ^{195}Pt satellites of more than $J_{P,Pt} = 3000$ Hz eliminate methyl as ligand but argue for chloride, which suggests the literature unknown [(dcpe)Pt(SMe)(Cl)] (**G1**) as the best option. Originating from free MesCP (**68**) in the solution by reverse reaction of the C-CP cleavage, the MesCP could either coordinate to the gold atom or be attacked by anions like Mes⁻, Me⁻, Cl⁻, leading to phosphaalkenes. The closest matches in the literature are $Ph_2C=PMes$ ($\delta(^{31}P\{^1H\}) = 233$ ppm) and $Ph_2C=PCl$ ($\delta(^{31}P\{^1H\}) = 235$ ppm),[9] which makes the below suggested structures (**G2**, **G3**) plausible. However, these results are speculative and need further proof by ^1H NMR spectroscopy and mass spectrometry.
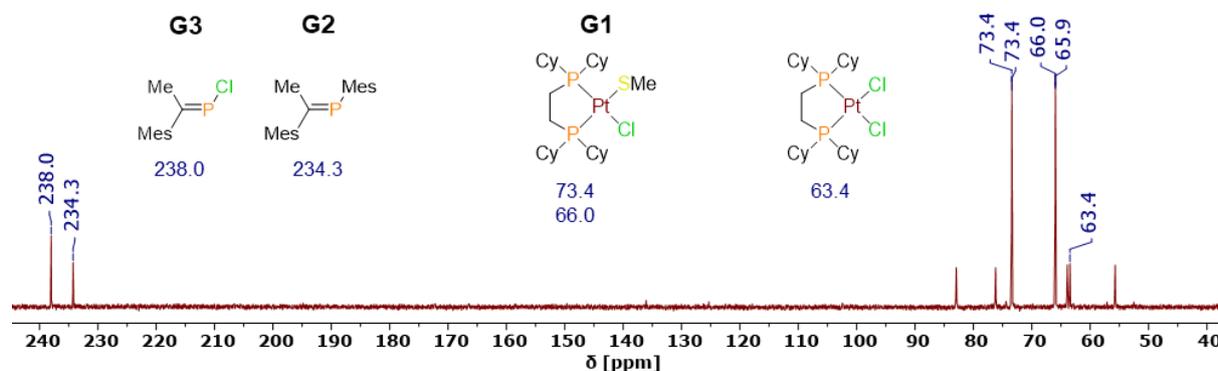
Figure 105. $^{31}P\{^1H\}$ NMR spectrum of a reaction mixture of [(dcpe)Pt(CP)(Mes)] (**148σ**) with $AuCl \cdot SMe_2$. Molecular structure suggestions assigned to the resonances.

The reaction of [(dcpe)Pt(CP)(Mes)] (**148σ**) with one equivalent [Cr(CO)$_3$(MeCN)$_3$] at room temperature in THF was more successful and showed an instant color change from yellow to deep red. The ^{31}P{^{1}H} NMR spectrum revealed a complete conversion to a new species (**197**) with a slightly downfield shifted signal for the C≡P unit to δ = 102.9 ppm (**148σ**: 96.6 ppm), which matches the expectation of a de-shielding of the phosphorus nucleus. The dcpe ligand resonances are upfield shifted to δ = 55.6 and 46.2 ppm, with respect to the starting material (δ = 60.2, 49.2 ppm). The ^{31}P^{31}P coupling constants are similarly small ($J_{P,P}$ = ≤ 14.4 Hz) as in **148σ**, which was observed for all examined platinum based cyaphido complexes. Even better results were exhibited by the ^{195}Pt satellites (Figure 106). With around $J_{P,Pt}$ = 300 Hz for the C≡P, $J_{P,Pt}$ = 1851 Hz for the *cis* and $J_{P,Pt}$ = 2046 Hz for the *trans* phosphorus atom (to C≡P), they are still in the area of **148σ** ($^{1,2}J_{P,Pt}$ = 338, 1654, 2164 Hz). All these figures indicate the presence of a cyaphido ligand. However, further investigations like infrared spectroscopy, mass spectrometry and single crystal diffraction should be performed to resolve the molecular structure and determinate the coordination mode (π or σ) of the chromium. Interestingly, the ^{31}P{^{1}H} spectrum showed additional resonances, especially a doublet of doublets at δ = 169.1 ppm and a doublet at δ = 152.9 ppm, whereas the signals of the π-complex **148** (around 10%), remaining after the irradiation, have almost vanished.
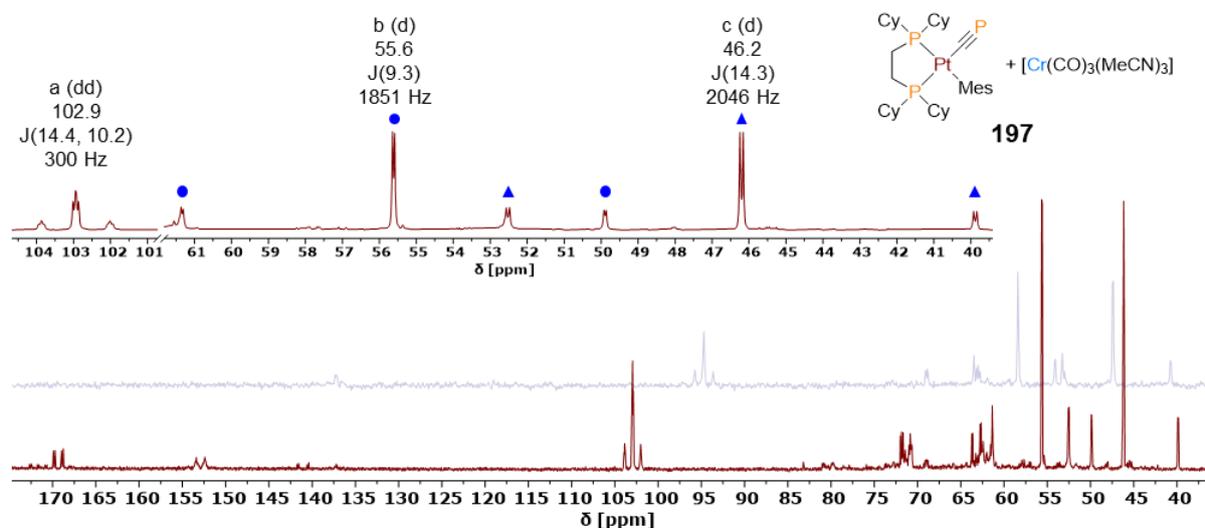

Figure 106. ^{31}P{^{1}H} NMR spectrum of a reaction mixture of [(dcpe)Pt(CP)(Mes)] (**148σ**) with [Cr(CO)$_3$(MeCN)$_3$] (red) in THF with magnification of the new resonances assigned to **197**. The blue cycles and triangles tag the corresponding ^{195}Pt satellites. The blue ghost NMR (background) shows the starting material mixture of around 90% (**148σ**) and 10% (**148**) to visualize the signal shift.

To investigate this further, a pure THF sample of the π-complex **148** was reacted with [Cr(CO)$_3$(MeCN)$_3$]. Indeed, the reaction produced mainly the previous spotted compound **198** with the characteristic large doublet of doublets ($J_{P,P}$ = 154.6, 32.7 Hz) at δ(^{31}P{^{1}H}) = 169.1 ppm for the phosphaalkyne phosphorus. The significant downfield shift and the large ^{195}Pt satellites of the dcpe ligand in comparison with **148**, as well as the large $J_{P,P}$, similar to the boron (**190**) and tungsten (**193**) adducts, indicate the coordination of the

chromium to the π-complex. As in the case of **197**, the molecular structure and the coordination mode (π or σ) are not clear yet and need further investigation. Even though, the coordination of multiple [Cr(CO)$_3$(MeCN)$_3$] units, one per coordination site, or the formation of a chromium bridged dimer cannot be excluded, they are unlikely due to the 1:1 stoichiometry between the starting material and [Cr(CO)$_3$(MeCN)$_3$].

In addition of the signals of **198**, three further resonances at δ(^{31}P{^{1}H}) = 152.9 ppm (d, $J_{P,P}$ = 178.0 Hz), 69.5 ppm (t, $J_{P,P}$ = 23.5 Hz) and 65.4 (dd, 179.4, $J_{P,P}$ = 24.4 Hz) can be allocated to another compound **199**. The pronounced doublet of doublets again suggests a π-complex, however further assumptions are hampered by the not-resolved ^{195}Pt satellites. Placing the results into the context set for the tungsten complexes (cf. **193a**), **199** could be the coordination complex of a substituted chromium compound variant, like the exchange of MeCN ligands with THF.
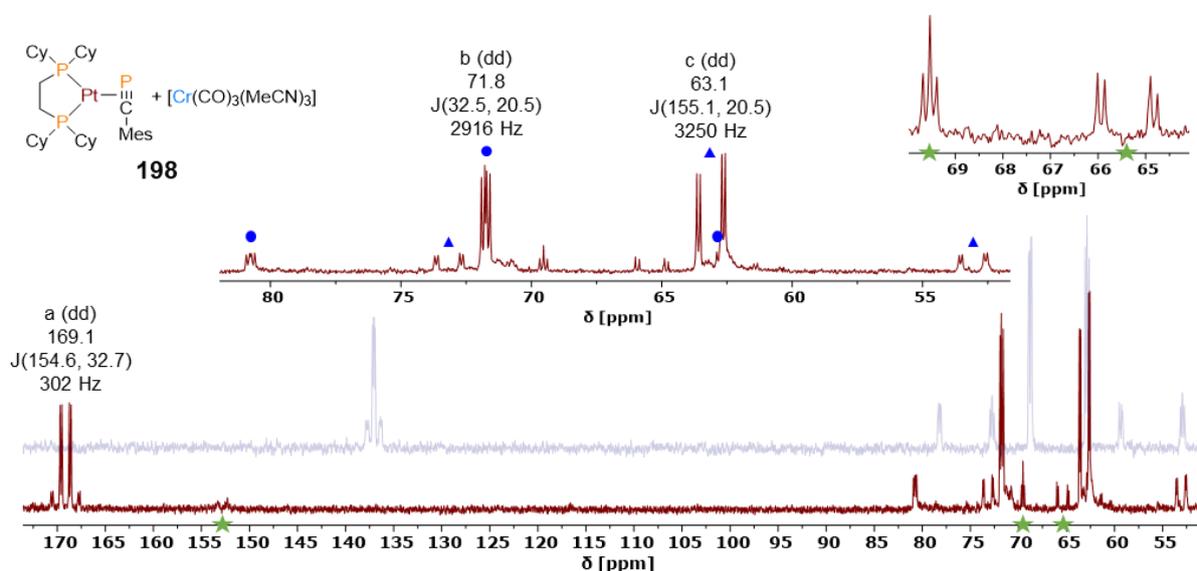
Figure 107. ^{31}P{^{1}H} NMR spectrum of [(dcpe)Pt(MesCP)] (**148**) with [Cr(CO)$_3$(MeCN)$_3$] (red) in THF with magnification of the new dcpe resonances assigned to **198** and **199** (green star).The blue cycles and triangles tag the corresponding ^{195}Pt satellites, whereas the green stars mark the resonances of **199**. The blue ghost NMR (background) shows the starting material (**148**) to visualize the signal shift.

2.1.5.2.2 Attempted cyaphido exchange with cyanides

Since the calculations for nickel carbonyl complexes (cf. 2.1.4.1) predict only a slightly higher bond strength to the nickel for the cyaphido versus the cyanido ligand, it was examined if the addition of a cyanide salt to a cyaphido complex could undergo a salt metathesis reaction, leading to the exchange of the C≡P$^-$ moiety with C≡N$^-$ or if the exchange can take place by initiation of the back reaction to the π-complex.

In a first attempt, [(dcpe)Pt(CP)(Mes)] (**148σ**) was dissolved in THF and added to an excess of solid sodium cyanide, which most probable did not react due to its insolubility in THF.

According to the literature, sodium cyanide is only soluble in few common solvents like H_2O, poorly in MeOH and ppm scale in DMF.[425-426] Since water and alcohols are not suitable for the cyaphido complexes, the reaction was repeated in a 1:1 mixture of THF and MeCN, DMSO or DMF. Only the DMF reaction mixture, heated to T = 85 °C for 2 days, showed traces of two additional resonances at $\delta(^{31}P\{^1H\})$ = 18.5 and 1.2 ppm and a high amount of liberated dcpe (**30**) ligand next to the reverse reaction to the π-complex in the $^{31}P\{^1H\}$ NMR spectrum. Surprisingly, the reaction of **148σ** with copper cyanide in a 1:1 mixture of THF and MeCN showed a rapid darkening of the yellow-orange solution and the participation of a red-brown solid. The $^{31}P\{^1H\}$ spectrum revealed a clean transformation by showing only three signals (**200**), a very broad one, typical for a copper-phosphorus coordination, at δ = 137.8 ppm, and two for the dcpe ligand at δ = 69.8 ppm (dd, $J_{P,P}$ = 35.8, 15.4 Hz, $J_{P,Pt}$ = 3035 Hz) and δ = 64.3 ppm (dd, $J_{P,P}$ = 35.4, 29.9 Hz, $J_{P,Pt}$ = 3252 Hz). Overall, the signal shifts and coupling constants are very close to the π-complex **148**. Based on the gained knowledge from the reaction of [W(CO)$_5$(thf)], the copper of CuCN probably coordinates to the phosphorus lone pair of the C≡P moiety of either **148σ** or **148**. It is conceivable that the coordination to **148σ** initiates the fast back reaction to the π-complex, which is presumable more thermodynamically stable. The formation of a cyanido-platinum complex can be excluded, due to the $^{31}P\{^1H\}$ signals and corresponding ^{195}Pt satellites. In the next approach, tetraethylammonium cyanide was used as cyanide source to improve the solubility in organic solvents. An excess of a MeCN solution of Et$_4$N(CN) was poured in a THF solution of **148σ** and stirred at room temperature for two weeks. Apart from the transformation of **148σ** into **148**, nearly identical $^{31}P\{^1H\}$ NMR signals (**201**, δ = 84.2 ppm (d, $J_{P,P}$ = 7.7 Hz), 17.5 ppm (d, $J_{P,P}$ = 36.6, 7.5 Hz), 1.6 ppm (d, $J_{P,P}$ = 36.6 Hz) and liberated dcpe as in the case of Na(CN), were detected. Switching to tetrabutylammonium cyanide, which is soluble in THF, yielded almost identical $^{31}P\{^1H\}$ NMR signals (**202**, δ = 83.0 ppm (d, $J_{P,P}$ = 6.3 Hz, $J_{P,Pt}$ = 410 Hz), 16.9 ppm (d, $J_{P,P}$ = 35.1, 6.3 Hz, $J_{P,Pt}$ = 1710 Hz), 1.3 ppm (d, $J_{P,P}$ = 35.3 Hz) in significant higher intensity, together with liberated dcpe and initial traces of non-reacted **148** within a week by consuming **148σ**. Most of the free dcpe could be removed by repetitive precipitation of a brown solid via dropwise addition of pentane after concentration of the THF solution. Analysis of the liquid phase by ^1H and ^{31}P NMR spectroscopy confirmed the presence of free dcpe. The $^{31}P\{^1H\}$ spectrum of the solid residue showed mainly signals of the new compound **202** and traces of **148**, which was slowly converted into two singlets at δ = 66.5 and 10.0 ppm (Figure 108). Even though all three phosphorus atoms of **202** are connected to each other in one structure, the doublet at δ = 1.3 ppm does not show any ^{195}Pt satellites, which may indicate that the dcpe ligand is only connected to the platinum center over one phosphorus. The ^{195}Pt satellites of the other phosphorus signals are still in line with a possible cyaphido ligand ($J_{P,Pt}$ = 410 Hz) and a phosphine ($J_{P,Pt}$ = 1710 Hz, one phosphorus atom of the dcpe) *trans* to the mesityl group.

Unfortunately, the ^{1}H NMR spectrum is populated with the signals of excessive Bu$_4$N(CN) and does not allow reliable conclusions, whereas the ^{195}Pt{^{1}H} spectrum shows one broad signal at δ = -4639 ppm.
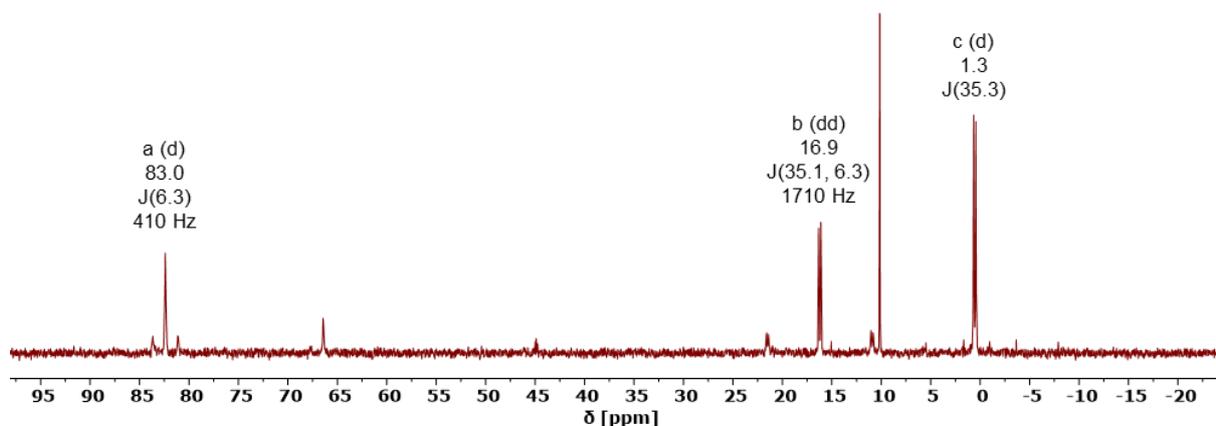
Figure 108. ^{31}P{^{1}H} NMR spectrum of **202** in tetrahydrofuran-d$_8$.

The hypothetical substitution of one dcpe phosphorus of **148σ** with C≡N$^-$ would rise the oxidation state of the platinum to +III, which requires presence of a strong reducing agent.[427-429] Furthermore, a resulting Pt(+III) complex is paramagnetic (15 valence electrons) and would not provide such a clear NMR spectrum. Numerous di- and trinuclear platinum complexes[430] and ring structures[431] can be excluded since the recorded ^{31}P{^{1}H} spectrum indicates an unsymmetrical structure. An assignment or even rough estimation of the structure is not possible, due to the lack of reliable data. Nevertheless, based on knowledge of the liberated dcpe, the literature known compound **2.36**[432] (Scheme 64) may serve as an inspiration for future investigations.
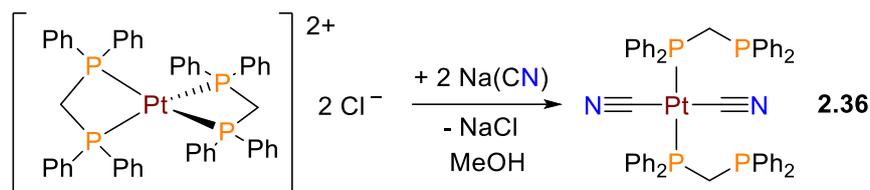
Scheme 64. Literature synthesis of *trans*-[(dppm)$_2$Pt(CN)$_2$] (**2.36**).

The analogous reaction between [(dippe)Pt(CP)(Mes)] (**143σ**) and Bu$_4$N(CN) delivers similar ^{31}P{^{1}H} NMR signals (**203**, δ = 84.2 ppm (d, $J_{P,P}$ = 6.8 Hz, $J_{P,Pt}$ = 410 Hz), 25.6 ppm (d, $J_{P,P}$ = 35.1, 6.8 Hz, $J_{P,Pt}$ = 1724 Hz), 9.7 ppm (d, $J_{P,P}$ = 35.5 Hz)). The signals δ(^{31}P{^{1}H}) = 25.6 and 9.7 ppm are in line with the proposed downfield shift of dippe (**8**), coordinated over one phosphorus. Surprisingly, the ^{31}P{^{1}H} resonances from the reaction of [(dcpe)Pt(CP)(Tripp)] (**150σ**) with Bu$_4$N(CN) diverge from **202** and **203**. Besides the signal of the liberated dcpe as an intense singlet at δ(^{31}P{^{1}H}) = 13.9 ppm, the ^{31}P{^{1}H} NMR spectrum showed two doublets (**204**, δ = 62.5 ppm (d, $J_{P,P}$ = 4.9 Hz, $J_{P,Pt}$ = 2885 Hz), 41.3 ppm (d, $J_{P,P}$ = 5.1 Hz, $J_{P,Pt}$ = 865 Hz), whose shifts are similar to the dcpe ligand of the starting material **143σ**

(δ = 60.9, $J_{P,Pt}$ = 2885 Hz, 48.6 ppm, $J_{P,Pt}$ = 865 Hz), but with significantly changed [31]Pt[195]Pt coupling constants. The fate of the cyaphido ligand is unknown, but several resonances with poor intensity suggest decomposition. The [195]Pt satellites of $J_{P,Pt}$ = 865 Hz are very uncommon and are too small for a typical $^1J_{P,Pt}$, but also too large for a $^2J_{P,Pt}$ coupling. While indirectly in the $^{31}P\{^1H\}$ visible, [195]Pt-[195]Pt couplings can be excluded by the too simple spin system.[430, 433-434] Insufficient isolation of **204** prevented further data collection.

2.1.5.2.3 Additions on the cyaphido ligand

Based on the reactivity of the C≡P triple bond, the cyaphido ligand should be capable to undergo numerous addition reaction like other phosphaalkynes (cf. 1.3.4). In the typical addition reaction of HCl to phosphaalkynes, the protons are added to the negatively polarized carbon atom, whereas the chlorides are attached to the positively polarized phosphorus atom.[6, 75] Indeed, stepwise addition of HCl (1 - 4 eq) to [(dcpe)Pt(CP)(Mes)] (**148σ**) in toluene at room temperature decolorized the yellow solution and yielded [(dcpe)PtCl$_2$] (**209**) as product, according to the $^{31}P\{^1H\}$ NMR spectra. Surprisingly, no other products could be identified at room temperature. However, four equivalents of HCl were necessary to consume all starting material **148σ**. Therefore, the reaction was repeated and monitored by low temperature $^{31}P\{^1H\}$ NMR spectroscopy, starting the reaction with four equivalents of HCl at T = -94 °C. The NMR spectra were taken at T = -90, -80, -60, -50, -30, 0 and +25 °C. The most relevant spectra are depicted as stacked illustration in Figure 109 and support the mechanism of the stepwise HCl addition to **148σ** (Scheme 65). Spectrum #2 showcases that the reaction took place even at T = -90 °C. All starting material **148σ** was already converted to different species, however, the dcpe ligand signals are broadened, due to the ongoing reaction and the generation of multiple similar products. Most prominent are the singlets at δ = 239.7 (br) and 191.3 ppm. The last one stayed sharp over the whole reaction sequence, which indicates that it is not part of any dcpe complex. Starting from -80 C a new broad singlet at δ = 175.3 ppm appeared, which got more distinct at higher temperatures. Furthermore, the signal of [(dcpe)PtCl$_2$] (**209**, δ = 64.8 ppm, $^1J_{P,Pt}$ = 3568 Hz)[421] together with two more dcpe based resonances at δ = 66.7 and 57.5 ppm ($J_{P,Pt}$ = 3792 Hz) appeared. Due to the substantial number of different dcpe compounds with additional [195]Pt satellites, not all signals could be assigned to a specific compound. Most species are present from T = -60 to -30 °C and got fully consumed at elevated temperatures. Reaching room temperature (#6), mostly the resonances of the product [(dcpe)PtCl$_2$] (**209**) and the always sharp singlet at δ = 191.3 ppm remained present.

The supposed mechanism (Scheme 65), the stepwise addition of HCl to the cyaphido ligand and the final cleavage of it and the mesityl group, is supported by sequential low-temperature NMR spectra analysis. All previously mentioned relevant resonances are visible in spectrum

#4 and will be in the following assigned to their assumed compounds. The first reaction step, the addition of one equivalent of HCl, is represented by the resonance at $\delta = 239.7$ ppm, a broad singlet with a $^{31}P^{195}Pt$ coupling constant of $J_{P,Pt} = 118$ Hz. The ^{31}P NMR signals of chlorinated phosphaalkenes usually appear in this area.[9] This is in good agreement with the postulated phosphaalkene complex **205**. The next addition of HCl would lead to compound **206**, represented by the doublet at $\delta = 173.3$ ppm (d, $^2J_{P,P} = 44.2$ Hz, $^1J_{P,Pt}$ = n.r.), in line with dichlorophosphines.[435] The third equivalent of HCl probably splits off dichloromethylphosphine (**208**), giving [(dcpe)Pt(Cl)(Mes)] (**207**). **208** shows a sharp singlet at $\delta = 191.3$ ppm,[436] whereas no dcpe signals could be assigned to **207** with certainty. However, several resonances are in the area of the similar literature known complex [(dcpe)Pt(Cl)(Ph)] $(\delta(^{31}P\{^1H\}) = 62.5, 52.5$ ppm).[437-438] In the final step, the fourth equivalent of HCl substitutes mesityl with another chloride, yielding [(dcpe)PtCl$_2$] (**209**)[421] and was ultimately proven by single crystal reflection of colorless crystals, obtained from a concentrated toluene solution. The alternative mechanism, the direct cleavage of HC≡P and stepwise addition of HCl, is not supported by the $^{31}P\{^1H\}$ NMR spectroscopic analysis, due to the lack of the signals for HC≡P ($\delta = -32.0$ ppm) and the expected intermediate H$_2$C=PCl ($\delta = 300.4$ ppm).
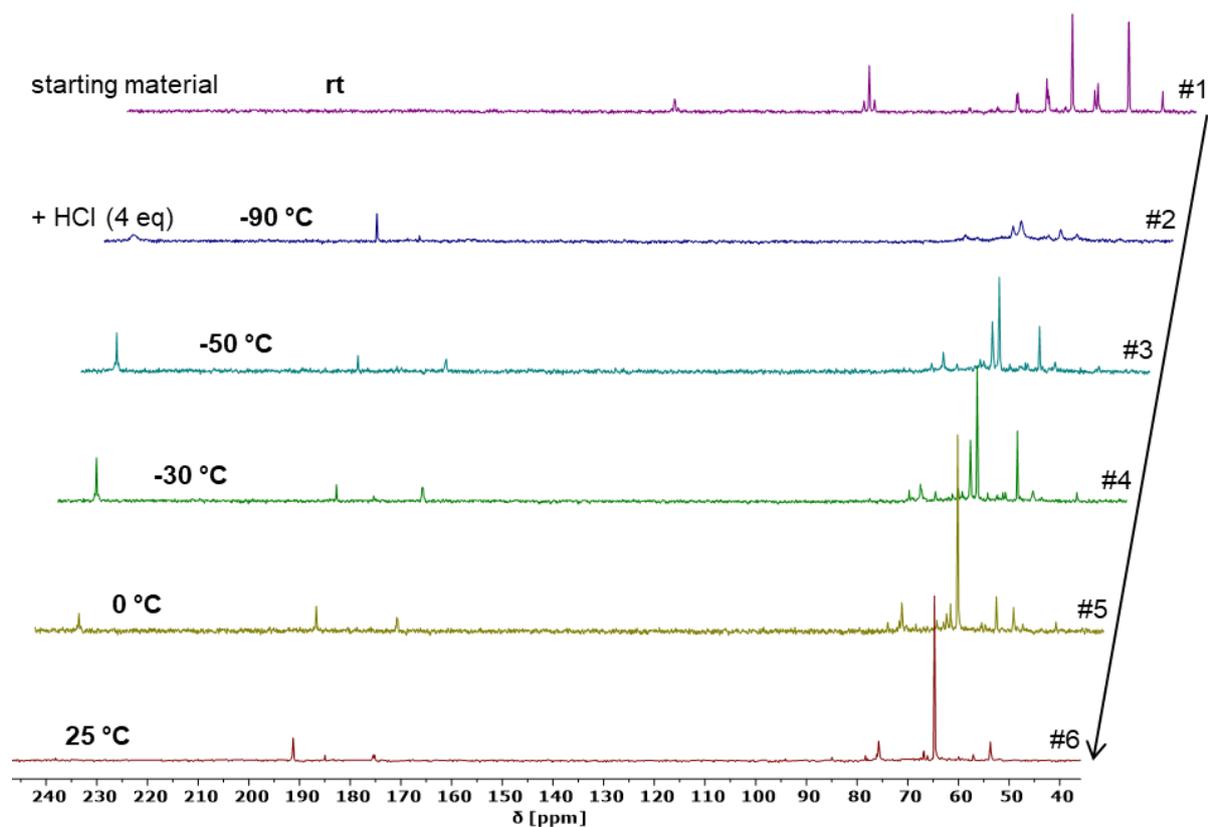
Figure 109. Stacked $^{31}P\{^1H\}$ NMR spectra of the reaction of [(dcpe)Pt(CP)(Mes)] (**148σ**) with HCl (4 eq) monitored over the course of different temperatures.
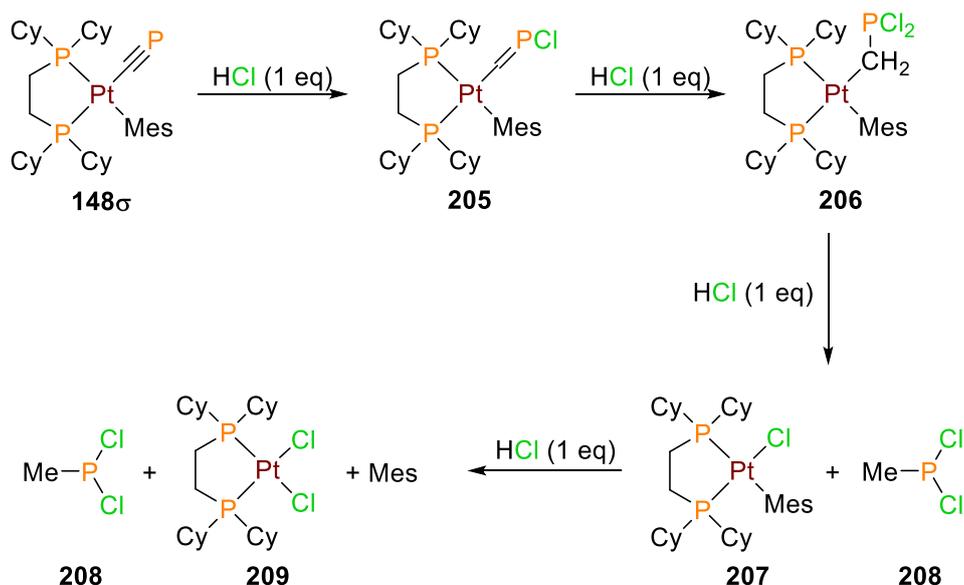
Scheme 65. Suggested reaction mechanism for the addition of [(dcpe)Pt(CP)(Mes)] (**148σ**) with HCl (4 eq).

In a first trial to protonate the cyaphido phosphorus atom of [(dcpe)Pt(CP)(Mes)] (**148σ**), one equivalent of the bulky super Brønsted acid H[Al(OTeF$_5$)$_4$][439] was added on top of a yellow mixture of [(dcpe)Pt(CP)(Mes)] (**148σ**, 90%) and [(dcpe)Pt(MesCP)] (**148**, 10%) in *ortho*-difluorobenzene at T = -30 °C in a J. Young NMR tube. The solution turned red on the interaction surface of the two layers. The blend of both solution layers resulted in a dark yellow-brown solution. The ^{31}P{^{1}H} NMR spectrum revealed three singlets. The main component is described by a singlet at $δ$ = 57.8 ppm with ^{195}Pt satellites of $J_{P,Pt}$ = 3921 Hz and does not fit the considered [(dcpe)PtH$_2$] nor [(dcpe)Pt($μ$-H)]$_2$.[440] The other two singlets are located at $δ$ = 78.4 ppm ($J_{P,Pt}$ = 3436 Hz) and $δ$ = 59.3 ppm ($J_{P,Pt}$ = 2188 Hz). None of these structures could be identified even by combining 1H, ^{13}C{^{1}H}, ^{19}F and ^{27}Al NMR experiments. Up to date, no further investigations in this regard were made, however, individual experiments with pure samples of [(dcpe)Pt(CP)(Tripp)] (**150σ**) and [(dcpe)Pt(TrippCP)] (**150**) are suggested to determine the origin of the found ^{31}P{^{1}H} signals.

Alternatively to protonation, the methylation of the cyaphido phosphorus was considered and already demonstrated on a additionally side-on coordinated cyaphido ligand by ANGELICI and co-workers (cf. 1.4.3.2).[204] The first attempts were carried out with strong alkylating Meerwein's salts, namely trimethyloxonium and triethyloxonium tetrafluoroborate. Depending on the solvent, both reagents either did not dissolve and showed no reactivity or caused the complete decomposition of starting material [(dcpe)Pt(CP)(Mes)] (**148σ**). Concluding Meerwein reagent as too strong, the more selective iodomethane was chosen instead. The reaction of one equivalent MeI with [(dcpe)Pt(CP)(Mes)] (**148σ**) at room temperature was monitored by ^{31}P{^{1}H} NMR, displaying a slow reaction with no further change after one day. Five new signals ($δ$ = 66.6, 62.3, 68.3, 46.5, 36.5 ppm) were counted, but the three signals of

the starting material remained the main component. Additional three equivalents of MeI were added to the reaction solution until all **148σ** was consumed, while the five new resonances sizably increased (Figure 110). The singlet at $δ = 66.6$ ppm ($^1J_{P,Pt} = 3362$ Hz) clearly belongs to [(dcpe)PtI$_2$] (**210**),[421, 438] which was later confirmed by single crystal reflection of a colorless crystal, obtained from a concentrated toluene reaction solution. The singlet at 36.5 without ^{195}Pt satellites is most likely methylated dcpe (**211**).[441-442] The two doublets (b1, b2) at $δ = 62.3$ ($J_{P,Pt} = 2050$ Hz) and $δ = 46.5$ ($J_{P,Pt} = 55$ Hz) ppm with a ^{31}P^{31}P coupling constant of around $J_{P,P} = 8.8$ Hz do not fit to [(dcpe)Pt(I)(Mes)][438] and could not be assigned to a compound. However, the ^{31}P^{195}Pt coupling constant of b2 is remarkable small, which might indicate a $^3J_{P,Pt}$ coupling.[34] The compound of the third singlet at 58.3 ($J_{P,Pt} = 3790$ Hz) should be symmetric, assuming it still contains the dcpe ligand. Any bridged platinum dimer or an arene complex (e.g. [{(dcpe)Pt($μ$-Mes)}$_2$][I$_2$])[443] would be a highly hypothetically guess, based on the ^{31}P{^{1}H} shift and ^{195}Pt satellites.
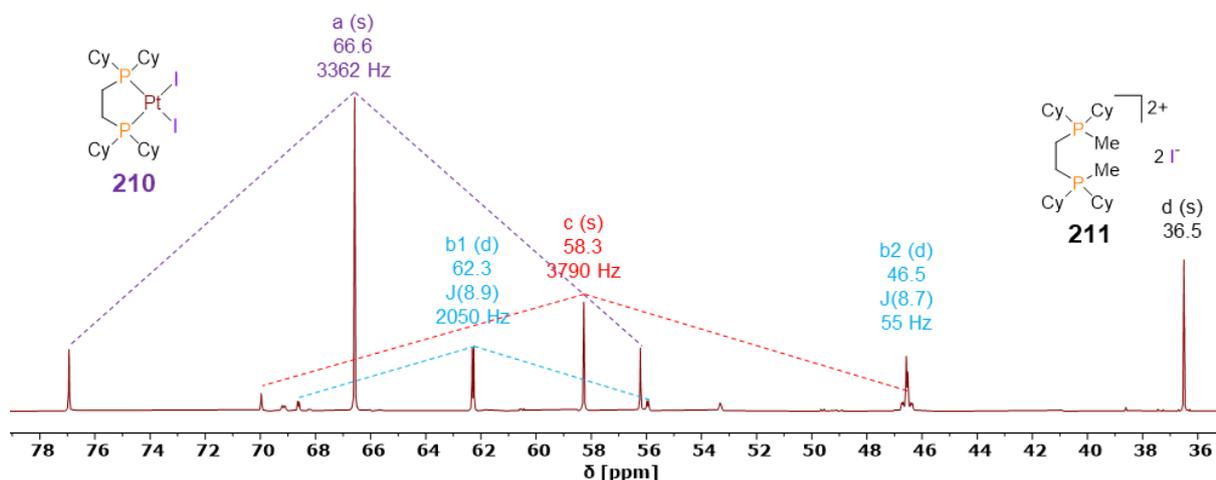

Figure 110. ^{31}P{^{1}H} NMR spectrum of the reaction of [(dcpe)Pt(CP)(Mes)] (**148σ**) with MeI (4 eq) with assignment of the ^{195}Pt satellites and compounds (**210**: approved by XRD, **211**: plausible by comparison with literature values).

The reaction was repeated with the more kinetically stabilized [(dcpe)Pt(CP)(Tripp)] (**150σ**) and one equivalent of MeI, which cleanly yielded [(dcpe)PtI$_2$] (**210**) as only product. The reaction sequence was even slower than for [(dcpe)Pt(CP)(Mes)] (**148σ**), reaching the end point at room temperature after about one week. The received ratio of 1:4 (**210:150σ**) suggests that four equivalents of MeI are required for full conversion, which could point to the same mechanism as for the reaction of [(dcpe)Pt(CP)(Mes)] (**148σ**) with HCl to [(dcpe)PtCl$_2$] (**209**). However, none of the expected intermediates (cf. Scheme 65 and replace HCl with MeI) could be monitored by ^{31}P{^{1}H} NMR spectroscopy. Even though, these intermediates do not last long enough to get detected, the final by-product ^{t}BuPI$_2$ ($δ(^{31}P{^{1}H})) = 168 ppm[444] ;cf. Scheme 65, analogy to **208**) should. Following the ^{31}P{^{1}H} spectra in chronological order, the impression is created that [(dcpe)Pt(CP)(Tripp)] (**150σ**) first undergoes the reverse reaction to [(dcpe)Pt(TrippCP)] (**150**) before reacting with MeI. Again, this result supports the assumption

that electrophiles cannot coordinate to the phosphorus lone pair of a cyaphido complex before a nucleophile had been coordinated to the π-system of the cyaphido ligand (cf. 1.4.3.5, 2.1.5.1.1.3). Another attempt with the bulkier ^{i}PrI together with **150σ** provided the same outcome.

2.1.5.2.4 Cycloaddition reactions at the cyaphido ligand

Phosphaalkynes are known to undergo different types of cycloaddition reactions (cf. 1.3.4, Scheme 5) due to their polarized triple bond. In the presence of electron donating transition metal MesCP is usually able to undergo a cyclodimerization process by attacking a second electron accepting MesCP to form a 1,3-diphosphacyclobutadiene. Therefore, it was analyzed if the triple bond of the cyaphido ligand is still able to perform cycloaddition reactions. Initially, MesCP (**68**) was added to a THF solution of [(dcpe)Pt(CP)(Mes)] (**148σ**). No reaction was observed, besides the slow decomposition of the mesitylphosphaalkyne and the reverse reaction of **148σ** to the π-complex **148** at elevated temperatures. Even the more reactive phosphaethynolate anion of NaOC≡P[51, 98] and the similar Ph$_3$SnP=C=O[214, 445] did not react with **148σ**. In following attempts, the possibility to undergo Diels-Alder reactions was investigated. Therefore, 2,3-dimethyl-1,3-butadiene or 2,3,4,5-tetraphenyl-2,4-cyclopentadien-1-one was added to **148σ** and heated to T = 120 °C. Only the reverse reaction to **148** was observed. Even the irradiation with UV light (λ_{max} = 365 nm, 100 W) to regenerate the σ-complex in small yields at elevated temperatures, just created **148σ**. A problem might be the required heat for the intermolecular cycloaddition reaction. Under these conditions, it most likely competes with the intramolecular reverse reaction, which proceeds faster. As already demonstrated, azides react reasonably fast in a "click" type reaction with phosphaalkynes at room temperature (cf. 2.1.2.3.9). Thus, different azides were probed to circumvent the issue with the omnipresent reverse reaction. Indeed, the new triazaphosphole (TAP) species **215** (Figure 111) was formed by the reaction of benzyl azide (BnN$_3$, **117**) with **148σ** in THF at room temperature. Upon addition of BnN$_3$ to the strong yellow THF solution of **148σ**, the solution brightens up to pale yellow and three new signals at δ = 202.9 (d, $^3J_{P,P}$ = 29.4 Hz, $^2J_{P,Pt}$ = 618 Hz), 59.5 (s, $^1J_{P,Pt}$ = 1801 Hz) and 49.6 (d, $^3J_{P,P}$ = 29.2 Hz, $^1J_{P,Pt}$ = 1985 Hz) ppm appeared in the ^{31}P{^{1}H} NMR spectrum, while the signals of **148σ** (δ = 96.6 (dd, $^3J_{P,P}$ = 17.7, 10.4 Hz, $^2J_{P,Pt}$ = 338 Hz), 60.2 (d, $^3J_{P,P}$ = 10.3 Hz, $^1J_{P,Pt}$ = 1654 Hz), 49.2 (d, $^3J_{P,P}$ = 17.8 Hz, $^1J_{P,Pt}$ = 2164 Hz) ppm) slowly decreased over a period of 6 h. The large downfield shift of the former cyaphido phosphorus in the ^{31}P{^{1}H} spectrum is prominent and in line with the predictions for the simplified molecule **C11** (δ(^{31}P) = 194.8 ppm) in respect to the increased de-shielding caused by the adjacent nitrogen atom.
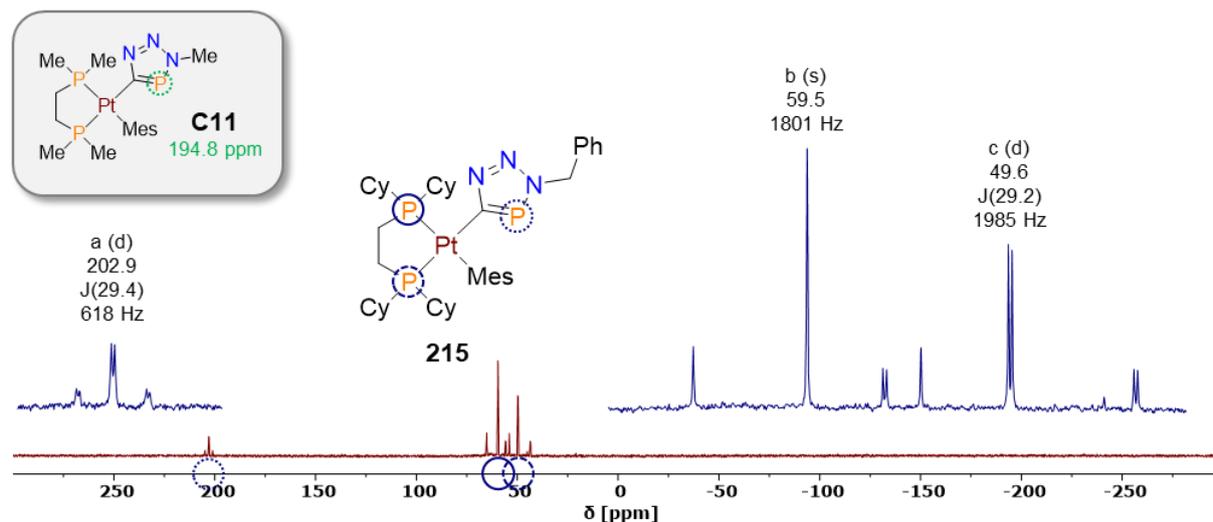
Figure 111. $^{31}P\{^1H\}$ NMR spectrum of [(dcpe)Pt(Mes)(TAP-Bn)] (**215**), magnification of the signals (blue) and the predicted $^{31}P\{^1H\}$ shift of the TAP phosphorus of the simplified structure **C11** (left box).

The ^1H NMR spectrum shows distinct resonances for the *meta*-protons of the mesityl unit ($\delta = 7.05$ ppm (s)), the phenyl group of the TAP ($\delta = 7.03$ ppm (m), 6.94 ppm (m)), the methylene bridge between the TAP and the phenyl with $^1H^{31}P$ coupling ($\delta = 5.35$ ppm (d, $^2J_{H,P} = 4.43$ Hz), the *ortho*-methyl groups ($\delta = 2.80$ ppm (s)) and para-methyl groups ($\delta = 2.35$ ppm (s)) of the mesityl. The ethylene bridge as well as the cyclohexyl groups of the dcpe ligand are not distinguishable and cumulated in a not resolved resonance from $\delta = 1.94$ to 0.86 ppm. If the same reaction is carried out at $T = 60$ °C or started with a 3:2 ratio of **148σ** to **148**, it resulted in the release of free TAP (**120**, $\delta(^{31}P\{^1H\}) = 177.8$ ppm; cf. 2.1.2.3.9, Figure 43) and a significant amount of by-product, which is represented by a singlet at $\delta = 66.4$ ppm with $J_{P,Pt} = 3501$ Hz in the $^{31}P\{^1H\}$ spectrum. Assuming that the by-product is caused by reaction with the π-complex **148**, a pure sample of **148** was reacted with BnN$_3$. Surprisingly, this very slow reaction did not yield the expected singlet and one equivalent of the azide was not enough to consume all starting material. Instead, three new $^{31}P\{^1H\}$ signals were detected, a singlet for the free TAP (**120**) and two independent doublets at $\delta = 60.0$ and 47.7 ppm with $^{31}P^{195}Pt$ coupling constants of $J_{P,Pt} = 3112$ Hz and 3333 Hz, respectively. The analog reaction with the nickel derivative **147** yielded only one singlet at $\delta = 46.9$ ppm, however, isolation attempts were not promising according to several additional signals found in the ^1H NMR spectrum.

After successful generation of the triazaphospholato platinum complex **215**, a full series of ten compounds was synthesized by a combination of the σ-complexes [(dippe)Pt(CP)(Mes)] (**143σ**), [(dippe)Pt(CP)(Tripp)] (**144σ**), [(dcpe)Pt(CP)(Mes)] (**148σ**), [(dcpe)Pt(CP)(Tripp)] (**150σ**) and [(dcpm)Pt(CP)(Tripp)] (**170σ**) together with the azides BnN$_3$ (**117**), MesN$_3$ (**118**), DippN$_3$ (**119**) and 2,6-bis(azidomethyl)pyridine. The resulted products are portrayed in Figure 112 and the corresponding $^{31}P\{^1H\}$ NMR signals are summarized in Table 13.

212 R = Bn
213 R = Dipp

214

215 R = Bn
216 R = Mes
217 R = Dipp

218

219 R = Bn
220 R = Dipp

221
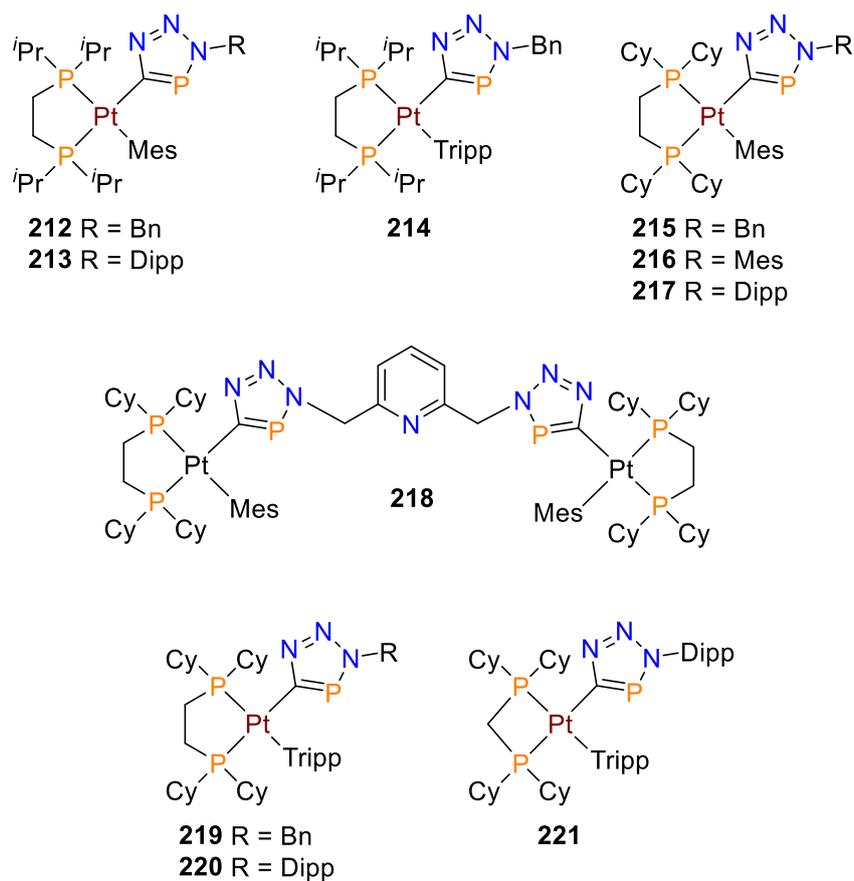
Figure 112. Overview of the synthesized triazaphospholato complexes.

Table 13. $^{31}P\{^1H\}$ signals of the [(P,P)Pt(aryl)(TAP-R] complexes **212** - **221**. P1 is the triazaphospholato phosphorus, while P2 (*cis* to P1) and P3 (*trans* to P1) are assigned to the diphosphine ligand.

cmd	$^{31}P\{^1H\}$ P1 [ppm]	$J_{P,P}$ P1 [Hz]	$^{31}P\{^1H\}$ P2 [ppm]	$J_{P,P}$ P2 [Hz]	$^{31}P\{^1H\}$ P3 [ppm]	$J_{P,P}$ P3 [Hz]	$^{195}Pt\{^1H\}$ Pt [ppm]	$J_{Pt,P}$ Pt [Hz]
212	205.1	28.2	67.7	-	58.2	28.6	-	611 1815 1998
213	212.2	27.5	66.9	3.8	58.2	27.4	-4501	592 1803 2025
214	208.8	30.0	64.0	-	54.9	29.8	-4495	571 1825 1994
215	202.9	29.4	59.5	-	49.6	29.2	-	618 1801 1985
216	205.9	28.8	60.1	-	50.8	28.7	-	608 1800 2014
217	211.0	28.3, 4.0	59.0	3.9	50.3	28.4	-4489	595 1801 2026
218	205.6	29.5	60.2	-	50.5	28.9	-	605 1805 2005
219	206.9	31.3	56.1	3.0	46.6	31.0	-	592 1802 2005

|								
220	218.6	28.3	58.9	-	48.3	28.4	-	575 1813 2008
221	210.6	29.8	-26.3	21.7	-35,6	26.5	-	609 1560 1656

The diphosphine phosphorus atom shifts and ^{31}P^{195}Pt coupling constants within the same diphosphine ligand type are notably similar and in good agreement with their respective starting material (σ-complex). All triazaphospholato phosphorus resonances are above $\delta(^{31}$P$) = 200$ ppm, more specifically, in the area of around $\delta(^{31}$P$) \approx 200$ to 220 ppm. The tendency of the largest downfield shift is given by the row of the azides (DippN$_3$ > MesN$_3$ > BnN$_3$) and the aryl ligand on the platinum (Tripp > Mes), resulting in the lowest shift for **215** ($\delta(^{31}$P$\{^1$H$\}) = 202.9$ ppm) and the highest for **220** ($\delta(^{31}$P$\{^1$H$\}) = 218.6$ ppm). Generally, the reaction rates are significantly decreased with increased steric demand of the azides or the aryl group of the σ-complex, meaning the reaction between BnN$_3$ (1 eq) and a mesityl containing σ-complex are completed within 6 to 12 h, whereas the reaction of MesN$_3$ or DippN$_3$ (1 eq) with a Tripp σ-complex can take up to a week at room temperature. Certainly, the gained flexibility by the methylene bridge in BnN$_3$ and 2,6-bis(azidomethyl)pyridine is the main reason for that. In consequence, it seems reasonable to combine BnN$_3$ (**117**) with [(dippe)Pt(CP)(Mes)] (**143σ**) or [(dcpe)Pt(CP)(Mes)] (**148σ**) to obtain mostly pure triazaphospholato-platinum-complex samples. Whereas this might be true in theory, only a mixture of π- and σ-complex could be used due to the limitation by the generation of the σ-complexes of this type. The logical alternative was the use of [(dcpe)Pt(CP)(Tripp)] (**150σ**), which can be obtained as pure substance. Unfortunately, the reaction with the σ-complex proceeded extremely slow, while, in contrast to **143σ** and **148σ**, the reaction with the π-complex (**150**), slowly forming via reverse reaction from **150σ**, is executed much faster and resulted a large amount of unknown by-product that decomposed rapidly. This can be avoided by a large excess of azide (10 - 20 eq) but at the costs of overall purity. An isolation by common laboratory techniques like solubility, recrystallization, sublimation or column chromatography were not successful or sufficient for any triazaphospholato platinum complex, synthesized in one of the discussed ways. Hence, all described azide-cyaphido-complex combinations (Figure 112) were necessary to find a suitable system to isolate one of the target compounds in reasonable yields for further characterization and final prove of identity. Generally, the best results were achieved with DippN$_3$ (**119**, 1 eq), even though a significant amount of by-product was generated, depending on the σ-complex type. The by-product was neither isolated nor characterized (Table 14), however, is proposed to occur from the reaction of DippN$_3$ with the π-complex or an intermediate at the formation of it. Assuming its origin from a Pt(0) species, like the π-complex, it could hypothetically be an side-on coordinated triazaphosphole complex.

This might be proven in the future by addition of an adequate triazaphosphole to [(dcpe)Pt(COD)] (**45**), but was not part of this work. The by-product **217a** from the reaction of [(dcpe)Pt(CP)(Mes)] (**148σ**) and DippN$_3$ (**119**) decomposed quickly in the reaction mixture at room temperature, forming the new species **217b**, which is described by a doublet of doublets in the ^{31}P{^{1}H} spectrum at (δ = 71.5 ppm ($J_{P,P}$ = 26.0, 14.4 Hz, $J_{P,Pt}$ = 2925 Hz). The signals of the corresponding phosphorus nuclei, indicated by the given coupling, could not be found.

Table 14. ^{31}P{^{1}H} signals of the by-products of **213**, **217**, **220** and **221**, labeled with an additional **a**. Not found (nf) signals of **213a**, due to low amount and resulting low NMR intensity. Compounds **213a** and **217a** are unstable in the reaction mixture at room temperature. **217a** apparently decompose into a new compound (**217b**, δ(^{31}P{^{1}H}) = 71.5 ppm (dd, $J_{P,P}$ = 26.0, 14.4 Hz, $J_{P,Pt}$ = 2925 Hz)).

cmd	^{31}P{^{1}H} P1 [ppm]	$J_{P,P}$ P1 [Hz]	^{31}P{^{1}H} P2 [ppm]	$J_{P,P}$ P2 [Hz]	^{31}P{^{1}H} P3 [ppm]	$J_{P,P}$ P3 [Hz]	$J_{Pt,P}$ Pt [Hz]
213a	nf	nf	61.7	17.4	59.2	6.5	2405 3631
217a	73.8	18.1, 7.9	56.5	18.0, 3.2	53.3	8.4, 3.3	400 2428 3632
220a	65.6	23.8, 6.0	51.6	22.9, 6.7	46.8	6.0	284 2431 3665
221a	66.1	12.8	-28.6	51.4, 12.9	-32.0	51.1, 12.9	351 1946 3240

After the effected decomposition of **217a** to **217b**, **217** was successfully isolated by extraction with pentane and filtration through a Whatman filter from the crude solid as pale-yellow solution. The identity of **217** could be validated by NMR spectroscopy (Figure 113), high resolution mass spectrometry, elemental analysis and ultimately by single crystal diffraction (Figure 114). The geometry, bond lengths and angles of the platinum center are nearly identical to **148σ** (Figure 79) with exception of the bond between platinum and the triazaphospholato carbon (Pt2-C49), which is slightly elongated from 1.974(2) to 2.043(5) Å. The bond lengths and angles within the triazaphospholato ligand itself are unremarkable and close to the values found in neutral 3,5-disubstituted 3*H*-1,2,3,4-triazaphosphole derivatives.[446] With that proof of the molecular structure, **217** is the first reported complex bearing an anionic triazaphospholato ligand. Furthermore, the crystallographic data confirmed the regioselective [3+2] cycloaddition reaction of an azide with the cyaphido ligand, which is in conformity with the reaction of phosphaalkynes with organic azides. In perspective of the isolobal relationship between a CH fragment and a trivalent phosphorus, this reaction is in analogy with the [3+2] cycloaddition reaction between metal-acetylides and azides.[447-450] Overall, this result demonstrated the possibility of consecutive reactions on the cyaphido moiety.
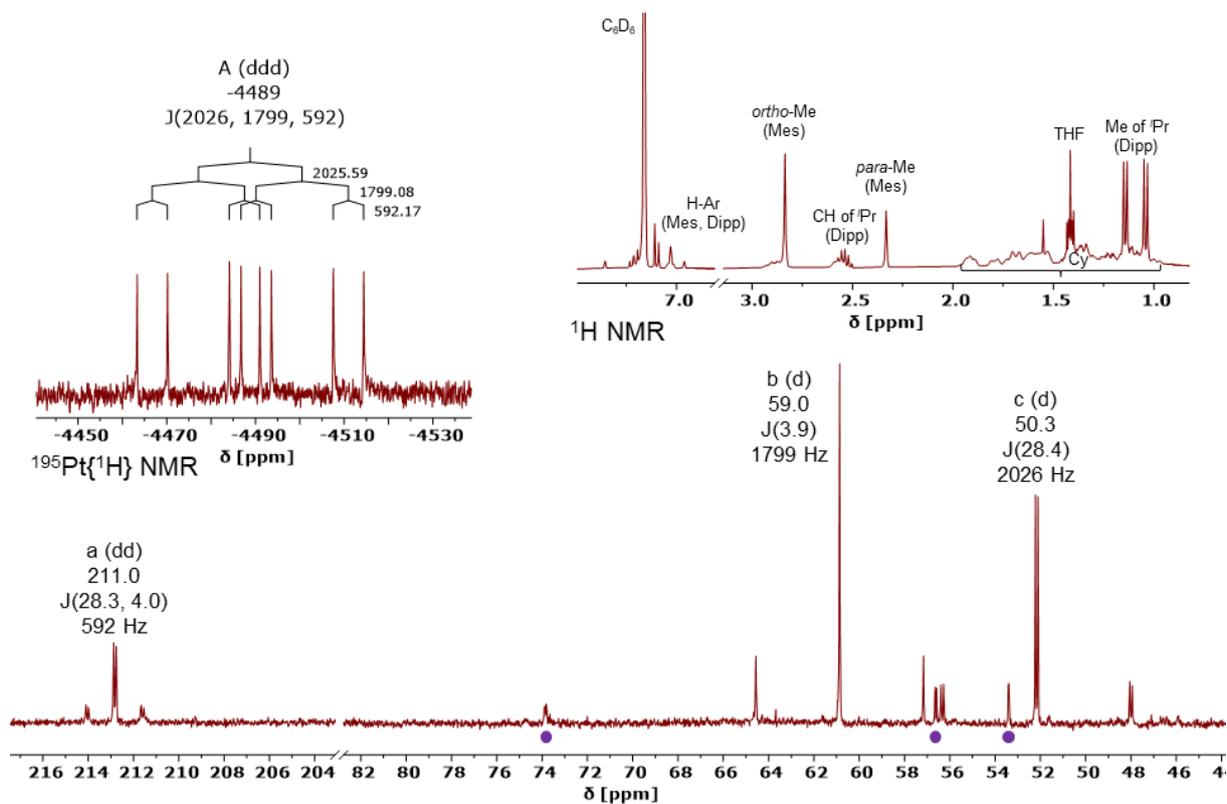
Figure 113. $^{31}P\{^1H\}$ and $^{195}Pt\{^1H\}$ (top left) NMR spectrum of [(dcpe)Pt(Mes)(TAP-Dipp)] (**217**) with around 14% by-product (**217a**, purple dots) in tetrahydrofuran. ^1H NMR spectrum (top right) of resolved crystals of **217** in benzene-d_6.
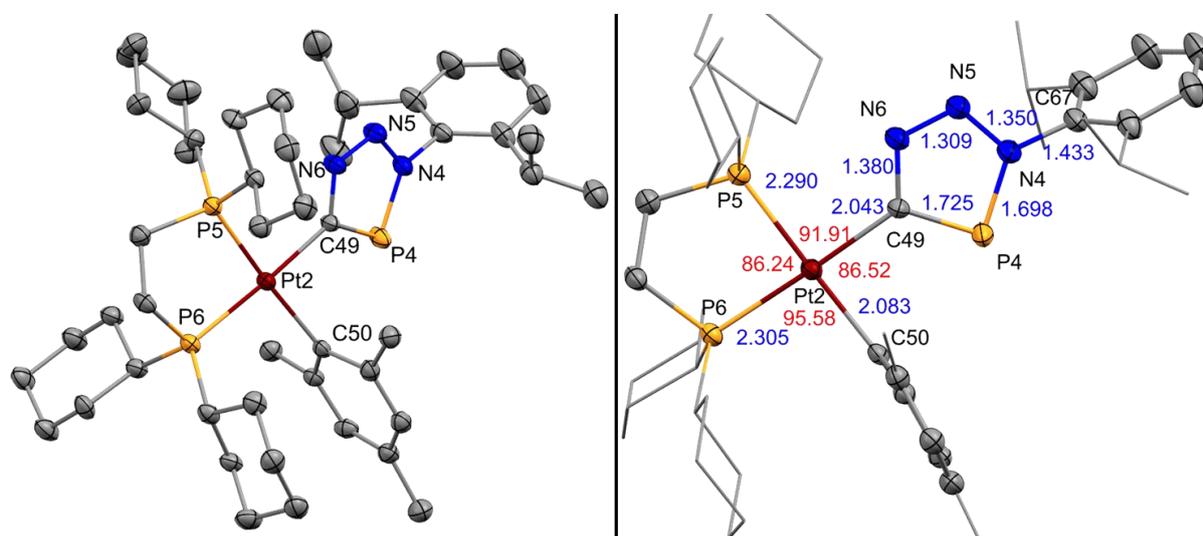
Figure 114. Molecular structure of [(dcpe)Pt(Mes)(TAP-Dipp)] (**217**) in the crystal. Anisotropic displacement ellipsoids are shown at 50% probability level. Hydrogens and second molecular structure in the asymmetric unit omitted for clarity. Selected bond lengths (Å) in blue and angles (°) in red.

2.2 Synthesis of cyaphido gold complexes by C≡P⁻ transfer

Independent of the recent progress in the synthesis of novel cyaphido transition metal complexes (cf. chapter 1.4.2), there is a demand for easy-to-use cyaphido transfer reagents like [Mg(^{Dipp}NacNac)(C≡P)(dioxane)][162] (**1.22a**, cf. 1.4.3.4) to avoid individual designed multistep syntheses to access novel cyaphido complexes. Ideally, those transfer reagents should be simple in the production and storable for a long time like the numerous cyanide salts[451] for the cyanido equivalents. Probably, sodium phosphaethynolate[49] (NaOC≡P, cf. 1.3.3) is still the most related phosphorus source, meeting those requirements, to date. Even though it transfers the phosphaethynolate anion, it can sometimes be considered as "phosphorus" transfer reagent.[452]

Following the endeavor in the search of a cyaphido transfer reagent, trimethylsilylphosphaalkyne[75, 77] (Me₃Si-CP, **53**, cf. 2.1.2.3.1) was selected as an accessible precursor for the release of C≡P⁻. Silyl groups are widely used as protection unit in the organic synthesis, especially as silyl ethers to preserve OH groups.[453-454] There is a broad variety of desilylation reagents, [455-456] the strongest are mostly fluoride reagents,[457] which serve as F⁻ source. The high reactivity of the fluoride ion is usually explained by the generation of the very strong silicon-fluorine bond, which has a typical dissociation energy of around 700 kJ·mol⁻¹.[458] As already stated (cf. chapter 1.3.2), phosphaalkynes and their reactivity are related to acetylenes. Several examples for the desilylation of acetylenes with fluoride reagents are known.[459-461] Furthermore, the famous synthesis of the first stable cyaphido complex by GRÜTZMACHER *et al.* (cf. 1.4.2.3) is also based on the silyl group cleavage to generate the C≡P moiety *in situ* directly on the metal core.[37] Hence, trimethylsilylphosphaalkyne seemed to be an excellent contender for the release and transfer of the cyaphide anion.

Although the desilylation of silylphosphaalkynes are evident and have already been successfully applied by the group of GRÜTZMACHER and CROSSLEY (cf. 1.4.2.3) in the coordination sphere of ruthenium and Me₃SiCP (**53**) is known since 1981, no further references were found. At the risk of retaking many non-documented failures, the desilylation of **53** and aspired C≡P⁻ release/transfer was step by step examined until exhibited signs of success. Before presenting the relevant results of the successful transfer, a very brief summary of the previous conduced reactions (Table 15) should illustrate the development process to avoid future iterations of the same reactions. A first attempt (**#1**) was carried out with TBAF (tetra-*n*-butylammonium fluoride) as F⁻ source in toluene. Indeed, the formation of fluorotrimethylsilane (Me₃SiF or TMS-F) was observed by ^{19}F NMR spectroscopy (δ = -178.3) in the brown solution, which indicates the split between the Me₃Si⁺ and C≡P⁻ unit. In principle, the naked cyaphide anion might be stabilized by the cation and, in consequence, associated with the ^{n}Bu₄N⁺. However, cycloaddition reactions of the highly reactive cyaphide anion with further cyaphides

could also lead to polymeric structures as known for not sterically shielded phosphaalkynes like HCP or MeCP (cf. 1.3.2, Figure 4). The negative charge might be compensated by the $^{n}Bu_4N^+$ ion or unpredictable side reactions. Surprisingly, the $^{31}P\{^{1}H\}$ NMR spectrum only showed one main signal, a singlet at $\delta = 10.1$ ppm. Nevertheless, identification of a potential C≡P species is not trivial, due to the lack of unequivocal proof techniques and especially the ^{31}P shifts vary widely. Usually, the C≡P group can be best identified by X-ray crystallography. Alternatively, a combination of NMR, infrared spectroscopy, mass spectrometry and chemical follow-up reaction are suitable. In some of the previous cyaphido complexes the mass of the C≡P⁻ anion could be found in the negative mass spectrum. For the reactions listed in Table 15 mostly ^{1}H, $^{13}C\{^{1}H\}$, ^{19}F and ^{31}P NMR spectroscopy were used, sometimes ESI-MS or APCI-MS and IR was realized in addition. Chemically, azides (BnN₃, DippN₃) were occasionally applied to force cycloaddition reactions, Me₃SiCl to regain Me₃SiCP by precipitation of a metal chloride salt or [W(CO)₅(thf)] to receive coordination products. Most of the reactions were performed in toluene-dioxane mixtures at $T = -78\,°C$ and allowed to warm to room temperature. If the solubility of the fluoride sources were insufficient, the reactions were repeated with MeCN or DCM as a solvent. For all concluded fluorination reaction Me₃SiF (#3, Ph₃SiF) was observed in the ^{19}F NMR spectra.

Table 15. Summary of the conducted Me₃SiCP (**53**) cleavage reaction with different fluoride sources (and second reagents). Only in #3 the bulkier Ph₃SiCP (**58**) was used. All reactions released Me₃SiF (#3, Ph₃SiF). The new $^{31}P\{^{1}H\}$ shifts of the unidentified products are listed. Abbreviations: TBAF = tetra-*n*-butylammonium fluoride, TBAT = tetra-*n*-butylammonium difluorotriphenylsilicate, 18C6 = 18-crown-6, DB18C6 = dibenzo-18-crown-6, Crypt-222 = [2.2.2]cryptand, phosphazenium Cl = tetrakis{[tris(dimethylamino)phosphoranyliden]amino}phosphonium chloride, I*i*Pr = 1,3-diisopropylimidazol-2-ylidene, IMe₄ = 1,3-dimethylimidazol-2-ylidene.

nr	F⁻ source	sec. reagent	new $^{31}P\{^{1}H\}$ main signals [ppm]
#1	TBAF	-	10.1 (s)
#2	TBAT	-	10.5 (s)
#3	TBAT	-	179.2(s), 67.2 (s), 7.6 (d)
#4	Ph₄PF	-	22.8 (s)
#5	Ph₃SnF	-	17.8 (br)
#6	$^{n}Bu_4N$ Ph₃SnF₂	-	15.1 (br)
#7	CsF	-	none
#8	CsF	18C6	273.2 (s), 10.2 (s)
#9	CsF	DB18C6	267.1 (s), 11.2 (s)
#10	CsF	Crypt-222	273.7 (s)
#11	KF	18C6	11.2 (s)
#12	KF	DB18C6	10.4 (s)
#13	KF	Crypt-222	264.8 (s)
#14	KF	phosphazenium Cl	28.7 (d), 24.7 (s), 22.1 (s)
#15	AgF	-	42.8 (d), 20.8 (s)
#16	AgF	18C6	42.5 (d), 21.7 (s)
#17	AgF	Mes*Br	34.8 (s)
#18	AgF	*t*BuCl	42.0 (d), 20.4 (s)
#19	AgF	IMe₄	265.1 (s), 7.7 (s), -26.2 (s)
#20	AgF	I*i*Pr	-24.5 (s)

#21	AuF$_3$	-	39.8 (s), 39.2 (br), 38.1 (dt)
#22	CsAuF$_4$	-	none
#23	Me$_4$N AuF$_4$	-	none

The identity of **#1** could not be resolved, however, the generation of Me$_3$SiF was a major indicator for the cleavage and motivation to continue this project. In a next attempt (**#2**), solid TBAT (tetra-*n*-butylammonium difluorotriphenylsilicate) was used as fluoride source, because it is more reliably water free than TBAF.[462] The red-brown reaction solution showed the same major ^{31}P{^{1}H} signals as for TBAF. Astonishingly, in a settled solution of **#2**, the two ^{31}P{^{1}H} signals 325.8 (d, $^2J_{P,P}$ = 31.8 Hz) and 314.9 (t, $^2J_{P,P}$ = 32.4 Hz) could be found, which are in excellent agreement with 3,5-bis(trimethylsilyl)-1,2,4-triphosphole. This might indicate the formation of an "P" source like in the reaction of CsF with MesCP (cf. 2.1.2.3.9). The reaction was repeated with the bulkier Ph$_3$SiCP (**58**, **#3**), but this time, there was no evidence for the formation of a 1,2,4-triphosphole. The next pursuits were aimed to find a suitable counter ion, which is able to stabilize the naked C≡P$^-$ anion. Further reactions of Me$_3$SiCP with Ph$_4$PF[463] (**#4**), Ph$_3$SnF[464] (**#5**), ^{n}Bu$_4$N Ph$_3$SnF$_2$[465-466] (**#6**) were unremarkable. The reaction with CsF (**#7** - **#10**) and KF (**#11** - **#13**) as an F$^-$ source, showed similar results as the reaction with TBAF or TABT, but often generated an additional singlet in the ^{31}P{^{1}H} spectrum between $δ$ = 265 - 273 ppm depending on the used solvent. A connection between these singlets was not revealed, however the existence of a C≡P species can be most likely excluded based on additional measurements and attempts of follow-up reactions. An exception to those outcomes was the reaction of KF together with the extremely bulky tetrakis{[tris(dimethylamino)-phosphoranyliden]amino}phosphonium chloride (**#14**). The intention was the reaction of the free potassium with the chloride of the phosphonium salt to provide the phosphonium ion as an adequate counter ion for the C≡P$^-$ anion after the initial fluorination of the TMS group. The observed ^{31}P{^{1}H} shifts were similar to Ph$_4$PF (**#4**). Potentially, better results might be obtained by exchanging the chloride of the phosphonium ion by fluoride.[467-468] This was not done, due to the expected low yields, the high price of the phosphonium chloride itself and the necessary time for the preparation of phosphonium chloride from scratch by multistep synthesis. The reactions with AgF (**#15** & **#16**) in toluene proceed fast, yielding first a red and upon warming to room temperature a brown solution with two resonances in the ^{31}P{^{1}H} NMR spectrum, a doublet at $δ$ = 42.8 ppm ($J_{P,F}$ = 994.5 Hz) and a singlet at $δ$ = 20.8 ppm. The coupling of the doublet is typical for a $^1J(^{31}P^{19}F)$.[469] The responding ^{19}F signal (ddd) is located at $δ$ = -69.0 ppm and the ^{31}P spectrum revealed additional signals at $δ$ = 42.2 ppm (ddt, J = 994.5, 577.8, 18.0 Hz) and $δ$ = 21.6 ppm (dt, J = 530.3, 18.1 Hz). The ^{1}H^{31}P HMBC NMR spectrum showed two cross-couplings in the aromatic region ($δ$ = 7.62, 6.23 ppm) and several very close signals in the aliphatic area at around $δ$ = 0.5 ppm. Over a longer period, the signals slightly changed their shifts and the coupling pattern, indicating ongoing reactions. Thus, no

further assignments have been made. Instead, the reaction was repeated with additional Mes*Br in the reaction solution (**#17**) with the goal to precipitate AgBr and force the direct C≡P⁻ anion transfer to receive Mes*CP (**76**). Indeed, the $^{31}P\{^1H\}$ spectrum showed only on signal at δ = 34.8 ppm, which is in agreement with the expected product. Further investigation of the product revealed that this signal only matches Mes*CP by accident and a second experiment with ^{t}BuCl (**#18**), which theoretically yields ^{t}BuCP, verified that. In two other reactions with AgF *N*-heterocyclic carbenes (**#19** & **#20**) were added to build a silver complex ([(NHC)Ag(CP)]) instead of a salt, which resulted in a blood red solution with yellow precipitation even at room temperature and changed NMR signals. Still, none of them could be assigned to a C≡P species. The reactions with other gold fluorination reagents (**#21** - **#23**) also did not lead to identifiable C≡P species.

Despite the lack of success, the direct transfer of the C≡P⁻ onto a transition metal complex seemed more promising. Ideally, the transition metal precursor should also act as a fluoride source for the fluoride-cyaphido exchange. Fortunately, BRAUN *et al.* very recently developed novel fluorido gold(I) complexes, which can also be used as a fluorination reagents.[470] First test reactions between [(IDipp)AuF] (**225-F**) and Me₃SiCP (**53**) were conducted.[471] The *N*-heterocyclic carbene IDipp (1,3-bis(2,6-diisopropylphenyl)imidazol-2-ylidene) was deliberately chosen, because it should result the already literature known cyaphido gold(I) complex **1.35** (cf. 1.4.3.4, Figure 17) upon successful reaction. Indeed, the reaction of **225-F** and **53** in DCM/toluene, performed in a PFA tube (perfluoroalkoxy), started at around *T* = -97 °C and warmed to room temperature, showed only one signal in the ^{31}P NMR spectrum at δ = 83.9 ppm (Figure 115), matching the literature value of δ = 84.1 ppm. The ^{19}F NMR of the yellow reaction mixture showed the release of Me₃SiF. Further NMR characterization were not obtained, due to the decomposition of [(IDipp)Au(CP)] (**1.35**) upon vacuum application to the reaction mixture to exchange the liquid with deuterated solvent, which was later achieved through other iterations. Nevertheless, this was clear evidence for the successful formation of **1.35**. For further investigations suitable [(NHC)AuF] complexes (**222-F** - **225-F**) were synthesized, starting with the addition of NHCs (IMe₄, I^{i}Pr, SIMes, IDipp) to AuCl · SMe₂ (Scheme 66). The halogen exchange for the [(NHC)AuCl] complexes (**222-Cl** - **225-Cl**) with sodium iodide, yielded the corresponding iodido complexes **222-I** - **225-I**. Together with a significant excess of AgF suspended in DCM, these were filled into a PFA tube and flame-sealed under vacuum for sonication in a water ultrasonic bath for around 1 h. After the opening of the PFA tube either under a strong stream of argon or in the glovebox, the liquid phase (DCM) was transferred with a filter cannula into a another PFA tube. The PFA tube containing the corresponding fluorido-complex-DCM solution (**222-F** - **225-F**) was frozen in liquid nitrogen, then the toluene solution of Me₃SiCP (**53**) was added on top. The complete frozen sample was again flame-sealed under vacuum, stored in a beaker until it was defrosted, before

it was shaken to blend the two solutions. The still sealed PFA tubes were slid into a regular NMR tube for the measurement of $^{31}P\{^1H\}$, ^{31}P and ^{19}F NMR spectra.
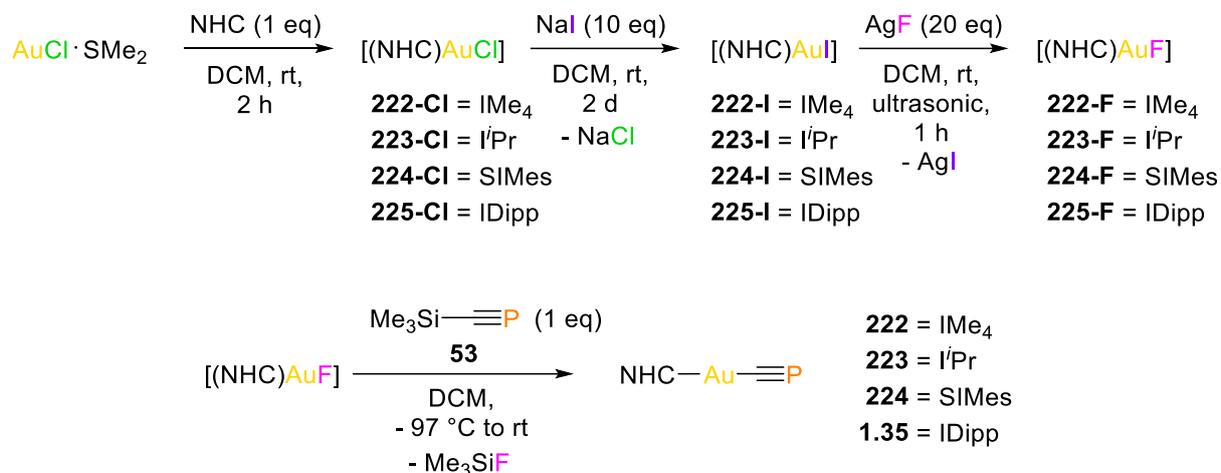

Scheme 66. Reaction route from AuCl · SMe2 to the cyaphido gold(I) complexes **222**, **224** and **1.35**. The final reaction towards **223** was not successful. I^{i}Pr = 1,3-diisopropylimidazol-2-ylidene, IMe$_4$ = 1,3-dimethylimidazol-2-ylidene, SIMes = 1,3-bis(2,4,6-trimethylphenyl)-4,5-dihydroimidazol-2-ylidene, IDipp = (1,3-bis(2,6-diisopropyl-phenyl)imidazol-2-ylidene.

All recorded ^{19}F spectra revealed the signal for Me$_3$SiF after the final reaction step. The yellow toluene-DCM-d_2 reaction solution of the potential [(IMe$_4$)Au(CP)] (**222**) showed exclusively one singlet at δ = 81.1 ppm in the ^{31}P spectrum (Figure 115). The ^1H spectrum revealed a singlet of δ = 3.76 ppm for the nitrogen methyl groups and a singlet of δ = 2.14 ppm for the backbone methyl units. The reaction towards [(I^{i}Pr)Au(CP)] (**223**) gave several $^{31}P\{^1H\}$ signals, but none of them in the area around δ = 80 ppm, which indicates decomposition out of unknown reason. The ^{31}P spectrum of the SIMes derivative displayed again exclusively one singlet at δ = 84.5 ppm (Figure 115). Several isolation efforts of the compounds **222**, **224** and **1.35** failed, due to decomposition under reduced pressure. To accomplish the full NMR characterization, the experiments must be performed in deuterated solvents. However, at the current state, Me$_3$SiCP (**53**) is produced as toluene solution. The fast decomposition of neat Me$_3$SiCP made it difficult to isolate it or to exchange the solvent. Frist endeavors showed that Me$_3$SiCP might be separated from a Me$_3$SiCP-tolunene solution if captured in a cooling trap by the right combination of vacuum and temperature. Alternatively, the new complexes might be crystallizable without previous isolation. Despite the lack of the current characterization, the successful cyaphido transfer between Me$_3$SiCP (**53**) and [(NHC)AuF] is most likely, due to the similarity ^{31}P signals among the new **222**, **224** compounds and the literature known complex [(IDipp)Au(CP)] (**1.35**).

A more direct approach to access the cyaphido gold(I) complexes **224**, by addition of Me$_3$SiCP (**53**) to [(NHC)AuCl], resulted in a yellow solution with a singlet at δ = 130 ppm in the $^{31}P\{^1H\}$ NMR. The reaction mixture was transferred into a PFA tube containing one equivalent of AgF. Upon sonication, the solution slowly turned dark yellow and a solid formed. Afterwards, no

^{31}P{^{1}H} signals could be detected anymore. Likewise ineffective was the replacement of the NHC species with triphenylphosphine at the last reaction step, following the same reaction route as for the NHC derivatives (Scheme 66). The failure can certainly be attributed to the fast decomposition of [(Ph$_3$P)AuF].[472] Switching to the stable [(BrettPhos)AuF] (BrettPhos = dicyclohexyl-[3,6-dimethoxy-2-[2,4,6-tri(propan-2-yl)phenyl]phenyl]phosphane), indeed, resulted in a signal pair of two doublets (δ = 74.4 ppm ($J_{P,P}$ = 13.3), 44.0 ppm ($J_{P,P}$ = 12.4)) in the ^{31}P{^{1}H} spectrum, which suggests the formation of [(BrettPhos)Au(CP)] (**226**, Figure 115).
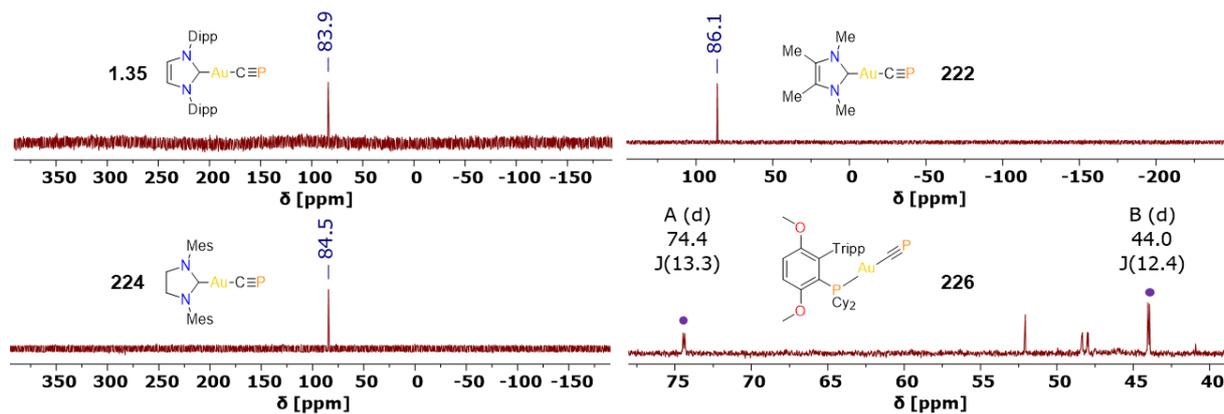
Figure 115. ^{31}P{^{1}H} NMR spectrum of the proposed structures [(IDipp)Au(CP)] (**1.35**, top left), [(IMe$_4$)Au(CP)] (**222**, top right), [(SIMes)Au(CP)] (**224**, bottom left) and [(BrettPhos)Au(CP)] (**226**, bottom right).

3   Conclusion and outlook

Since the discovery of H-C≡P by GIER in 1961, several small, labile derivatives have been synthesized before the preparation of the kinetically stabilized ^tBu-C≡P by BECKER *et al.* established phosphaalkynes as regular building block in the phosphorus chemistry in 1981. Today, various sterically stabilized phosphaalkynes are accessible by the hexamethyldisiloxane elimination route or the double elimination of HCl from a dichlorophosphine (Scheme 67). Alterations of this methods have been used to attain Me_3Si-C≡P (**53**), Ph_3Si-C≡P (**59**), Mes-C≡P (**68**), Mes*-C≡P (**76**) and the new representatives Tripp-C≡P (**81**) and Mdtbp-C≡P (**86**).
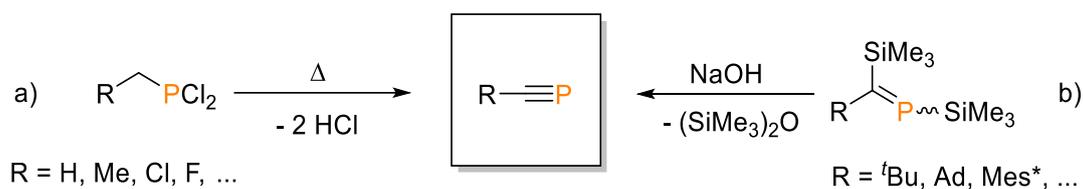
Scheme 67. Common synthesis of phosphaalkynes by double elimination of HCl from a dichlorophosphine (a) or hexamethyldisiloxane elimination of a phosphaalkene (b).

In a theoretical evaluation, the HOMO-LUMO gaps of all synthesized phosphaalkynes were compared with their corresponding acetylenes and nitriles, confirming the similarity in reactivity of phosphaalkynes and acetylenes by their HOMO orbitals. Furthermore, the electron density, electron localization and natural bond orbitals of phenylphosphaalkyne, phenylacetylene and benzonitrile were analyzed. The tendency to undergo cycloaddition reaction was validated for the arylphosphaalkynes by the generation of phosphinines, triazaphospholes, triphospholes and cyclodimers in the coordination sphere of tungsten and iron. Moreover, the obtained arylphosphaalkynes were used to create novel phosphaalkyne nickel, palladium and platinum complexes with variations of the bite angle size through the applied chelating diphosphine-co-ligands (Scheme 68). As precursor selected complexes were fully characterized by means of ^1H, $^{31}P\{^1H\}$, $^{13}C\{^1H\}$, $^{195}Pt\{^1H\}$ NMR and UV-Vis spectroscopy, EI mass spectrometry, elemental analysis and single crystal X-ray diffraction. The phosphaalkyne phosphorus in the platinum complexes has a typical $^{31}P\{^1H\}$ shift of $\delta = 125 - 150$ ppm for the ethylene (C_2) and $\delta = 155 - 165$ ppm for the methylene (C_1) bridged derivatives. The nickel complexes showed an average downfield shift of about $\delta \approx 30$ ppm, whereas the signals of palladium complexes appeared around $\delta \approx 40$ ppm upfield shifted. The $^{13}C\{^1H\}$ NMR shifts of the coordinated phosphaalkyne carbon atom are between $\delta = 220$ and 240 ppm. The $^{195}Pt\{^1H\}$ signals of the formal platinum(0) square-planar complexes are located at around $\delta \approx -4550$ ppm for the C_2 and at around $\delta \approx -4000$ ppm for the C_1 derivatives. The precursors were subject of photolysis experiments to receive novel cyaphido complexes.
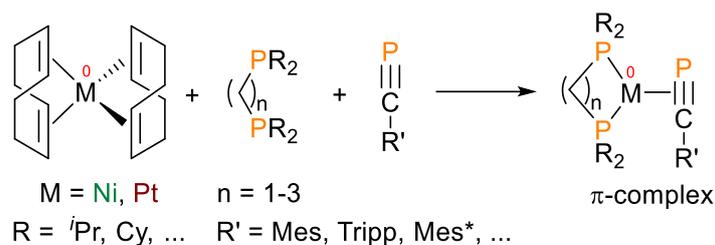
**Scheme 68.** General synthesis of arylphosphaalkynes complexes (π-complexes).

The elusive cyaphido ligand was discovered by ANGELICI and co-workers in 1992. GRÜTZMACHER *et al.* succeeded in the isolation of the first stable cyaphido complex 14 years later. However, cyaphido complexes are still very rare and the chemical potential of the cyaphido moiety is inhibited by steric shielding. Therefore, the general knowledge regarding its reactivity is limited. Theoretical studies were applied to receive deeper insights into the coordination modes of $C\equiv P^-$. Essentially, the cyaphide anion is a slightly better π-donor and a significant stronger π-acceptor than the cyanide anion. In contrast to cyanido, a terminally, via the carbon atom coordinated cyaphido ligand, will always favor a side-on over the end-on interaction via the phosphorus lone pair for the coordination with a second metal fragment. Inspired by the $C(sp)$-$C(sp^2)$ bond cleavage in diphenylacetylene by the photolysis of a platinum(0) complex, this concept was successfully transferred to the isolobal phosphaalkyne analogs, resulting in seven novel cyaphido complexes. The best conditions for the irradiation process are intense light at the lowest absorption band of the specific compound ($\lambda \approx 400$ nm), low temperatures ($T < 0\,°C$) and polar solvents (THF). The σ-donor capability of the diphosphine ligand and the π-acceptor properties of the *ortho*-substituted arylphosphaalkyne have a major impact on activation process, most likely due to the necessary MLCT from the platinum $5d_{x2-y2}$ into the antibonding π^* orbital of the phosphaalkyne. The best results were found for [(dcpe)Pt(TrippCP)] (**150**). Currently, the violet light ($\lambda_{max} = 405$ nm) induced C-C$\equiv$P bond scission and oxidative reaction ($Pt^0 \rightarrow Pt^{II}$) could only be accomplished for the C_2 and C_1 platinum complexes (Scheme 69). Even at $T = -20\,°C$, the thermally induced reverse reaction is present and aggravated the isolation and characterization of the cleavage products. The thermodynamical downhill reductive elimination could be successfully suppressed by narrowing the bite angle of the chelating diphosphine, resulting the C_1 analog [(dcpm)Pt(TrippCP)] (**170**). The cyaphido Pt(II) complexes were characterized by means of ^{1}H, ^{31}P$\{^1$H$\}$, ^{13}C$\{^1$H$\}$, ^{195}Pt$\{^1$H$\}$ NMR and IR spectroscopy. The typical chemical ^{31}P$\{^1$H$\}$ shift of the C$\equiv$P moiety in the cyaphido complexes is at $\delta = 100$ - 110 ppm, upfield shifted to the precursors. The ^{13}C$\{^1$H$\}$ shifts of the carbon atom are typically nearly identical to the phosphaalkyne complexes, meaning $\delta = 220$ - 240 ppm. The ^{195}Pt$\{^1$H$\}$ signals of the C_2 complexes are about $\delta \approx 100$ ppm (-4450 ppm) and the C_1 analogs around $\delta \approx 200$ ppm (-3800 ppm), downfield shifted in comparison with their precursors. The measured stretching vibrations of the C$\equiv$P unit were between $\tilde{v} = 1242$ and 1262 cm^{-1}. The molecular structure of

[(dcpe)Pt(CP)(Mes)] (**146σ**), [(dcpe)Pt(CP)(Tripp)] (**150σ**) and [(dcpm)Pt(CP)(Tripp)] (**170σ**) in the crystal ultimately confirmed the identity of the cyaphido ligand on the platinum core. The frontier molecular orbitals of the Pt(II)-cyaphido complex **170σ** show significant discrepancies from the literature known archetype [(dppe)$_4$Ru(CP)(X)] complexes. The cyaphido bears only a small ratio of the HOMO, but has a major contribution to the LUMO. The HOMO-1 and HOMO-3 are dominated by the $\pi_{C\equiv P}$ contribution, whereas the HOMO-6 possesses significant contribution of the phosphorus lone pair. These orbitals are highly relevant for consecutive reactions of the cyaphido ligand.
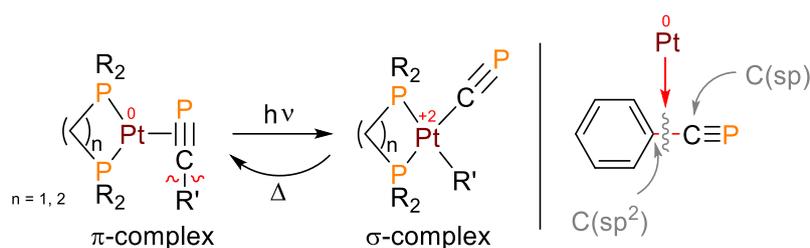
Scheme 69. Violet light (λ_{max} = 405 nm) induced C-CP cleavage reaction of arylphosphaalkynes Pt(0) complexes and thermal reverse reaction of the generated cyaphido Pt(II) complexes.

Only very recently, YANG and GOICOECHEA reported on the successive coordination behavior of an exclusively terminal bonded cyaphido ligand. The terminal cyaphido group highly favors a side-on coordination with a nucleophile as the first follow-up reaction, before allowing the attack on an electrophile via the phosphorus lone pair. Their observation is supported by the conducted consecutive reactions of the cyaphido Pt(II) complexes with the Lewis acids B(C$_6$F$_5$)$_3$ and [W(CO)$_5$(thf)], exclusively forming Lewis-acid adducts with the phosphaalkyne Pt(0) complexes, which were in most cases instantly *in situ* generated by the initiated reductive elimination of the cyaphido Pt(II) complexes. Moreover, the [3+2] cycloaddition of the cyaphido moiety with azides to novel triazaphospholato Pt(II) complexes clearly demonstrated the reactivity of the C≡P triple bond (Scheme 70). The registered ^{31}P{^{1}H} chemical shifts of the triazaphospholato ligand are around $\delta \approx$ 200 - 220 ppm, about $\delta \approx$ 30 ppm downfield shifted compared to their corresponding free triazaphospholes. The ^{195}Pt{^{1}H} signals of the C$_2$ derivatives are typically with around $\delta \approx$ -4500 ppm only δ = 50 ppm upfield shifted to the cyaphido precursors.
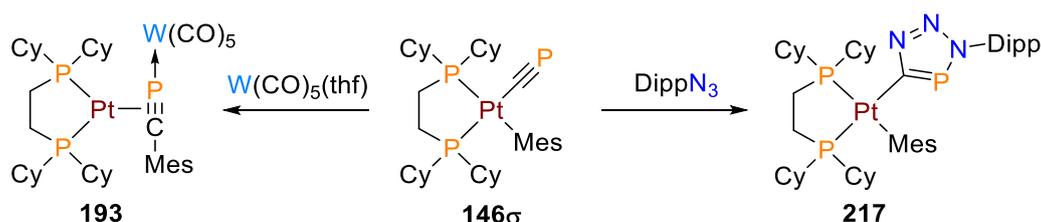
Scheme 70. Consecutive reactions of the cyaphido Pt(II) complexes with the Lewis acid [W(CO)$_5$(thf)] (left) and with the 2,6-diisopropylphenyl azide (right).

Parallel to the ambitions of this work of finding a simple way to transfer the cyaphido group, Goicoechea *et al.* demonstrated the first, highly polar cyaphido magnesium reagent to transfer the C≡P⁻ unit by salt metathesis protocol onto metal halides in 2021. Pursuing the idea of using the well-known Me₃Si-C≡P as cyaphide anion source, by cleaving the trimethylsilyl with an appropriate electrophilic fluorination reagent, led to three novel cyaphido gold(I) complexes (Scheme 71). The complexes were accessible by the generation of electron rich gold(I) fluoride precursors, which acts as F⁻ source and suitable complexation reagent for the liberated C≡P⁻ anion.
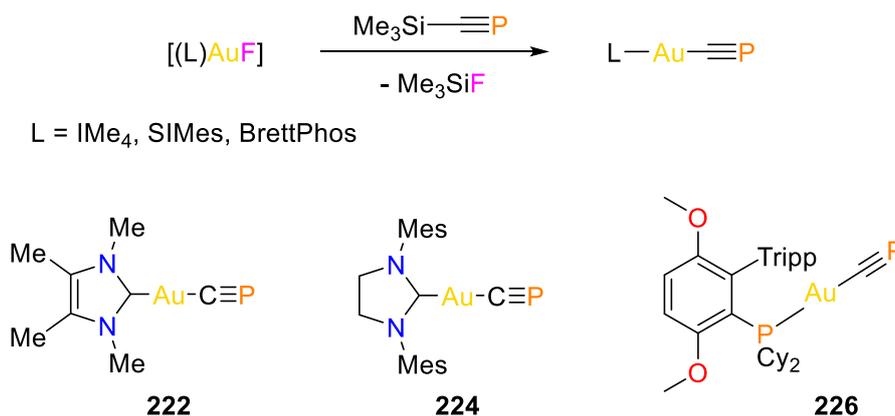
Scheme 71. C≡P⁻ anion transfer onto an electron rich gold fragment induced by the fluoride Me₃Si cleavage of Me₃Si-C≡P.

The overall results, creation of novel cyaphido Pt(II) complexes by photolysis of phosphaalkyne Pt(0) precursors, demonstration of consecutive reactions to obtain novel triazaphospholato Pt(II) complexes and the cyaphide anion transfer onto a gold(I) core, enrich the still limited cyaphido chemistry and surely assist the evolution and design of prospective cyaphido compounds.

This project was finished with great success, but not all issues has been fully covered yet. First, there is still room for the improvements of the electron donating ligands, namely the diphosphines. With the background of the P,N ligand experiments, the impact of an asymmetric (diphosphine) ligand on the side-on coordination of the phosphaalkyne would be interesting. Furthermore, it is still pending if a suitable hemilabile polydentate ligand might lead to catalytic reactions with the option to link several phosphaalkyne units together. The narrow bite angle greatly suppressed the reductive elimination, stabilizing the cyaphido system. This effect can potentially be further boosted by applying a more narrow R_2P-N-P_2 ligand or by substitution of the protons of the dcpm methylene backbone.[326] Apart from tweaking the diphosphine ligands, stronger *σ*-donating *N*-heterocyclic carbenes could be introduced.[241] Some initial experiments with bipyridine, to build up cleavable phosphaalkyne nickel complexes, showed promising findings,[243] however the products appeared to be unstable at room temperature. The arylphosphaalkynes possess even more potential for improvements. As demonstrated, small

changes in the substitution pattern (Mes to Tripp) showed huge effects on the backlight induced C-CP cleavage reaction. Particularly for the installment of electron-withdrawing groups in *ortho* position, an increased stability of the resulting cyaphido complexes is expected. The not yet isolated 2,4,6-tris(trifluoromethyl)phenylphosphaalkyne (**92**) is a promising candidate for this purpose and might be feasible by trapping at low temperatures or *in situ* reaction with [(dcpe)Pt(COD)]. Furthermore, alternative arylphosphaalkynes bearing EWGs are conceivable. Although, the recently carried out synthesis of cyaphido gold complexes by cleavage and transfer of the C≡P⁻ anion from the trimethylsilylphosphaalkyne still needs to be fully verified, first efforts to transfer this concept on silver and cooper have been started.[473-475] Another idea is to combine the two demonstrated cyaphido complex syntheses (Pt & Au) to skip the requirement of a Pt(0) species and avoid the photolysis to generate the cyaphido Pt(II) complexes (Scheme 72). Theoretically, this concept can also be applied to any other metal and grants access to novel cyaphido complexes.

Scheme 72. Theoretical reaction to obtain [(dcpe)Pt(CP)(Mes)] (**146σ**) without Pt(0) precursor and photolysis.

Many well-known nitrile and acetylene cleavage processes like direct methods,[247] catalytic cycles[244, 476] or specific designed cage molecules[252] provide additional inspiration for the phosphaalkynes scission due to the isolobal concept between phosphorus, nitrogen and methine. Another auspicious concept to get direct access to the cyaphide anion and generate either a cyaphide salt or transfer the C≡P⁻ unit onto metals is provided in Scheme 73.[477-478] The relevant reagent to adopt this process is the well-known Li or Na[P(SiMe₃)] salt, which can be easily prepared from P(SiMe₃)₃ and stored under inert atmosphere at room temperature.

Scheme 73. Theoretical concept to generate an *in situ* C≡P species for consecutive reactions (a), or a cyaphido manganese complex (b).

With the recently developed, innovative preparations of novel cyaphido complexes and the possibility even to transfer the high reactive cyaphide anion, the cyaphide ion will certainly

become a more common ligand and a new building block for cycloaddition reactions. Surely, the cyaphido chemistry has just being started into a prosper future.

4 Experimental section

*Note: Parts of the experimental section were already published in the supporting information of J. Am. Chem. Soc. **2021**, 143, 19365.[372]*

4.1 General remarks

All reactions were performed under an argon atmosphere in oven-dried glassware using modified Schlenk techniques or in an MBraun glovebox unless otherwise stated. The photoreactions were performed with either a single Blak-Ray B-100 AP 100 W Hg-Lamp (λ_{max} = 365 nm) or a setup of four Onforu 15 W blacklight LED arrays (λ_{max} = 405 nm). All common solvents and commercially available chemicals were used without further purification if not stated otherwise. Heptane and 1,5-cyclooctadiene were dried and stored over sieves. 1,2-Bis(diisopropylphosphino)ethane[328], bis(di-*tert*-butylphosphino)methane[315], bis(dicyclo-hexylphosphino)methane[315], bis(cyclooctadiene)platinum(0)[279], Ph$_4$PF[463] and ^{n}Bu$_4$N Ph$_3$SnF$_2$[466] were prepared according to literature procedures. P(TMS)$_3$ was synthesized according to common literature procedures by the technicians DORIAN REICH and MARKUS PESCHKE. Bis(cyclooctadiene)nickel(0) was purchased from ABCR. 1,2-Bis(dicyclohexyl-phosphino)ethane was bought from Acros Organics. All other chemicals were purchased from common retailers. All dry and deoxygenated solvents were prepared using standard techniques or were obtained from a MBraun solvent purification system. The ^{1}H, ^{13}C{^{1}H}, ^{31}P{^{1}H} and ^{195}Pt{^{1}H} NMR spectra were recorded on a JEOL ECA400/ECS400/ECZ600/ECP500/ECX400 or Bruker Avance700/Avance500/DPX400 spectrometer and all chemical shifts are reported relative to the residual resonance in the deuterated solvents. The ^{31}P NMR is calibrated against H$_3$PO$_4$ and ^{195}Pt NMR is calibrated against Na$_2$PtCl$_6$ as a standard. The EI-Mass spectrometry measurements were performed on a Waters Autospec Premier. Elemental analyses were performed on an Elementar Vario EL Cube. The UV-Vis measurements were performed on a Perkin Elmer Lambda 465. The IR vibrational spectra were measured on a Bruker Alpha FTIR spectrometer equipped with a diamond ATR in the solid state (pure powder) under an argon atmosphere. Low-temperature diffraction data were collected on Bruker-AXS X8 Kappa Duo diffractometers with *IµS* micro-sources, performing ϕ-and ω-scans. The structure data were collected using either a Photon 2 CPAD detector with Mo K_α radiation (λ = 0.71073 Å) or a Smart APEX2 CCD detector with Cu K_α radiation (λ = 1.54178 Å). The structures were solved by dual-space methods using SHELXT[479] and refined against F^2 on all data by full-matrix least squares with SHELXL-2017[480] following established refinement strategies[481]. The program Olex2[482] was used to aid in the refinement of the compound structures. All non-hydrogen atoms were refined anisotropically. All hydrogen atoms were included into the model at geometrically calculated positions and refined using a riding model. The isotropic displacement parameters of all

hydrogen atoms were fixed to 1.2 times the *U*-value of the atoms they are linked to (1.5 times for methyl groups). The collection and the refinement of the crystallographic data were assisted by NATHAN COLES and MANUELA WEBER. The crystallographic molecular structures were visualized with the program Mercury[483]. DFT Calculations were carried out with the ORCA 5.0.3 program suite[484-485] at the Curta[486], a general-purpose high-performance computer at the Free University of Berlin. Initial molecular structures were created in the program Avogadro[487] or were based on crystallographic data, if available. Initial geometries were optimized with the PBEh-3c method developed by Grimme and co-workers.[488-489] The single point calculations on the optimized organic structures were conducted with the B3LYP[490] functional with def2-TZVP[491] basis set and def2/J[492] auxiliary basis set. The cyaphido transition metal complexes were calculated by DANIEL FROST. To obtain more accurate results, the geometry of the complexes was further optimized with the ωB97xD-D3 functional[493] and a Triple-ζ-valence-basis set (def2-TZVP).[491] "Resolution of the identity" (RI) approximations were not employed since convergence problems were observed during the optimization step. Numerical or analytical frequency calculations were carried out to confirm the nature of stationary points found by geometry optimizations and to calculate standard Gibbs free energies ΔG_0 (p = 1 bar and T = 298 K). The absence of imaginary vibrational frequency modes indicated that the optimized structure is a local minimum, while one imaginary mode indicated a transition state. Standard convergence criteria were used for the geometry optimization (OPT) and the addition "tight" for SCF-calculations ("TIGHTSCF"). Final single point calculations on the optimized structures were conducted at the same level of theory. Additionally, for all calculations the empirical Van der Waals Correction (D3)[494-497] was used and solvent effects were taken into account with the Conductor-like-Polarizable-Continuum-Modell (CPCM)[498-501] for THF. Scalar relativistic effects were taken into account for platinum by means of Stuttgart effective core potential (ECP).[502] Molecular orbitals were visualized via the freely available program IBOView v20150427.[503-504] The nudged elastic band (NEB) method implemented in ORCA was used to obtain approximate transition states, followed by a saddle-point optimization ("OptTS"). To rationalize the photochemical behavior of the complexes and to get an estimate for the wavelength required to facilitate the photochemical C(sp)-C(sp²) bond activation, vertical excitation energies were calculated with an *ab initio* STEOM-DLPNO-CCSD non-parametrized method.[505] The STEOM-DLPNO-CCSD single point calculations were done with ORCA with the def2-TZVP basis set and a correlation fitting auxiliary basis set (def2-TZVP/C)[506] and the CPCM correction for THF on the geometries mentioned before. To improve accuracy, the "TIGHTPNO" truncation scheme defined by LIAKOS *et al.* was applied.[507] The structures used for the single point calculations had ωB97xD-D3/def2-TZVP quality. Additional TD-DFT calculations were performed at the ωB97xD-D3/def2-TZVP level of theory to evaluate the excitation energies for the complex **C7**, **C9**, **143**

and **170**. Overall the STEOM-DLPNO-CCSD method and the TD-DFT calculations show coherent excitation processes with defined and consistent differences in the excitation energies. The orca_plot module of the ORCA program suite was used to generate difference densities for the lowest energy transition and the plots were visualized via the UCSF Chimera 1.14 program package[505] and are presented together with the calculated UV-Vis spectra, which is visualized with ChemCraft.[508] NBO population analyses were carried out with the NBO 7.0 module[509] implemented in the ORCA program suite. The natural charges on atoms were calculated with the NPA. Intrinsic bond orbital (IBO) analysis[504] was conducted with the IBO module of ORCA and visualized by IBOView v20150427.[503] QTAIM analysis[510] was performed with the Multiwfn software (version 3.7)[511] using the wave functions (.wfn) generated at the B3LYP/def2-TZVP level of theory. ^{31}P NMR predictions were performed by ERIC YANG from the GOICOECHEA group in Oxford using optimized geometries obtained by the PBEh-3c composite method developed by Grimme and co-workers,[488] which uses a composite valence-double-zeta Gaussian AO basis set (def2-mSVP) for all atoms. The NMR shielding tensors were calculated using the Gauge Including Atomic Orbitals (GIAO) method,[512-514] and were carried out with the one-parameter hybrid Perdew-Burke-Ernzerhof (PBE0) functional,[515] using Jensen's segmented contracted pcsSeg-3 basis set for phosphorus,[516] and the composite def2-mSVP basis set for all other atoms. Relative chemical shifts were obtained using H_3PO_4 in water as a reference (δ = 0 ppm) and scaled using an empirical linear scaling method that has been previously shown to improve the accuracy of chemical shift predictions.[499, 517-522]

4.2 Syntheses

4.2.1 Preparation of bis(cycloocta-1,5-diene)platinum(0)

Dichloro(1,5-cyclooctadiene)platinum(II) (2)
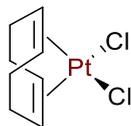
*Note: Working under air, no inert technique required. **2** was prepared by a slightly modified literature procedure.[284]*

1,5-cyclooctadiene (4.89 ml, 39.8 mmol, 3.30 eq) was added to a red solution of potassium tetrachloroplatinate(II) (**1**, 5.0 g, 12.0 mmol, 1.0 eq) in water (60 ml) and glacial acetic acid (80 ml). The red solution was heated to $T = 90\ °C$ for 1 h until the solution turned slightly pale yellow and a colorless precipitation has been formed. The warm solution was cooled down to $T = 0\ °C$ and filtrated through a pleated filter. The pale beige-colored residue was washed with water (3x 20 ml), ethanol (1x 10 ml) and diethyl ether (2x 20 ml). After drying *in vacuo*, a colorless powder (≥ 4.29 g, 11.5 mmol, 95%) was obtained.

¹H NMR (400 MHz, chloroform-d_1): $δ = 5.62$ (s, 2H, $J_{H,Pt} = 66$ Hz), 2.73 (m, 10H) ppm.

(1,3,5,7-cyclooctatetraene)dilithium (3)
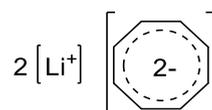
***3** was prepared according to the literature procedure.[285]*

Lithium flakes (1.00 g, 144 mmol, 4.16 eq) were added to a round-bottom Schlenk flask equipped with a large stirring bar. The lithium flakes were mechanically activated by stirring overnight. Diethyl ether (150 ml) and 1,3,5,7-cyclooctatetraene (COT, 3.87 ml, 34.6 mmol, 1.0 eq) were added and stirred at $T = 0\ °C$ for 16 h in the darkness. The formed precipitate was allowed to settle, an aliquot of the orange solution was removed with a syringe to check the molarity by titration*. The saturated orange solution of **3** usually has a concentration of ≥ 0.24 M and was directly used for reactions without further purifications and analytics.

*Titration against salicylaldehyde phenylhydrazone with two color changes from colorless/slightly yellow to strong yellow (1 eq) and from strong yellow to red (2 eq). Recommendation: Dropwise addition of product solution (1 ml) to a solution of salicylaldehyde phenylhydrazone (25 mg) in THF (10 ml).

Bis(cycloocta-1,5-diene)platinum(0) (4)
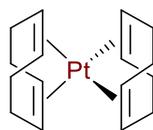
4 was prepared by a modified work up from the literature procedure.[279]

A diethyl ether solution of Li$_2$COT (**3**, 81.1 ml, 0.14 M, 1 eq) was added dropwise to a chilled suspension of [(COD)PtCl$_2$] (**2**, 4.06 g, 10.9 mmol, 1 eq) and COD (16 ml, 132 mmol, 12.2 eq) over a period of 5 min in the darkness. The temperature should not exceed T = -30 °C during the addition. The solvent (diethyl ether and COT) was removed *in vacuo* by maintaining around $T \approx 20$ °C by a water bath until complete dryness. The orange-brown residue was suspended and extracted with toluene (2x 50 ml) by syringe. The transferred dark brown suspension should rest until most of the non-soluble particles are settled. The dark liquid phase was directly transferred (transfer cannula) onto a solvent-free chromatography column packed with alumina of activity II and the column additionally washed with toluene (1x 40 ml, 1x 20 ml). The chromatographically purified pale yellow liquid phase was concentrated under reduced pressure until first colorless solid precipitated. The solid was first resolved by swiveling of the flask and then fully recrystallized/precipitated at T = -80 °C overnight. The solvent was removed with a syringe at T = -72 °C. The product was dried *in vacuo*, yielding a colorless powder (1.05 g, 2.55 mmol, 24%).

4.2.2 Preparation of chelating phosphines

1,2-bis(diisopropylphosphino)ethane (8)
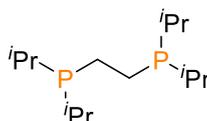
8 was prepared according to an adapted literature synthesis for 1,2-bis(diethylphosphino)-ethane.[327-328]

Magnesium flaks (3.14 g, 129 mmol, 6.0 eq) were added to a Schlenk flask equipped with a dropping funnel. The magnesium was mechanically activated by strong stirring with a stirring bar overnight, before diethyl ether (50 ml) was added. 2-Bromopropane (**5**, 12.2 ml, 129 mmol, 6.0 eq) mixed with diethyl ether (20 ml) was added dropwise to the refluxing magnesium suspension ($T_{\text{water bath}}$ = 45 °C) over a period of 45 min. After further refluxing for 4 h, a solution of 1,2-bis(dichlorophosphino)ethane (**7**, 3.26 ml, 21.6 mmol, 1 eq) in diethyl ether (20 ml) was added dropwise at T = -30 °C over a period of 30 min. After additional stirring at T = 0 °C for

30 min, the reaction mixture was quenched with degassed, saturated ammonium chloride solution. The organic phase was separated and collected with a separation funnel under inert conditions. The remaining water phase was washed with diethyl ether (2x 20 ml). The combined organic phase was dried with $MgSO_4$ and filtrated through a reverse frit. The solvent was removed from the filtrated under reduced pressure, yielding a pale-yellow oil. The crude product was purified by fractional distillation ($T = 58$ °C, $p = 4.5 \times 10^{-3}$ mbar, $T_{oil\ bath} = 89$ °C) as colorless, air sensitive oil (3.90 g, 14.9 mmol, 69%).

^{1}H NMR (400 MHz, benzene-d_6): δ = 1.64-1.57 (m, 8H, CH_2P, CHCH$_3$), 1.09-1.01 (m, 24H, CHCH_3) ppm.

^{31}P{^{1}H} NMR (162 MHz, benzene-d_6): δ = 8.9 (s) ppm.

1,2-bis(dicyclohexylphosphino)ethane (30)
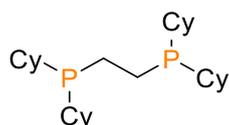
30 was purchased from Acros Organics.[327]

^{1}H NMR (400 MHz, tetrahydrofuran-d_8): δ = 1.86-1.75 (m, 16H), 1.73-1.69 (m, 4H), 1.59-1.56 (m, 4H), 1.51 (s, 4H), 1.38-1.18 (m, 20H) ppm.

^{31}P{^{1}H} NMR (162 MHz, tetrahydrofuran-d_8): δ = 0.9 (s) ppm.

Bis(di-*tert*-butylphosphino)methane (21)
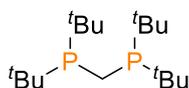
Preparation according the literature procedure of KARSCH.[329]

Bis(dichlorophosphino)methane (**9**, 5.00 g, 23 mmol, 3.12 ml, 1.0 eq) was added into a Schenk flask together with diethyl ether (60 ml). Tert-butyllithium (70.0 ml, 1.6 M in pentane, 0.11 mol, 4.9 eq) was added dropwise at $T = -40$ °C. After stirring at $T = 0$ °C for 16 h oxygen free water (100 ml) was added to the orange suspension. The water phase was separated and washed with pentane (22 ml). The combined organic phases were dried with $MgSO_4$, filtrated and the solvent was removed under reduced pressure. Fractional distillation ($T = 82-100$ °C, $p = 2.5 \times 10^{-2}$ mbar) purification provided a slightly yellow viscos liquid (1.26 g, 4.1 mmol, 10%; Lit.[329] 47%). The complete purification of the crude product failed.

^{1}H{^{31}P} NMR (400 MHz, dichloromethane-d_2): δ = 1.59 (s, 2H; CH$_2$), 1.19 (s, 36H, ^{t}Bu) ppm.

^{31}P{^{1}H} NMR (162 MHz, dichloromethane-d_2): δ = 22.8 (s) ppm.

Preparation according the literature procedure of HOFMANN.[315]

Step 1: ^{t}BuMgCl (**11**)

$$^t\text{Bu}-\text{MgCl}$$
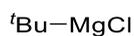
Magnesium flakes (25.0 mg, 1.0 mol, 1.1 eq) were added to a two-necked Schlenk flask equipped with a dropping funnel and mechanically activated by stirring overnight. After suspending of the magnesium with diethyl ether (100 ml), a solution of tert-butyl chloride (**10**, 100 ml, 0.92 mmol, 1.0 eq) in diethyl ether (100 ml) was added dropwise and stirred at T = 75 °C for 1 h. The grey suspension was filtrated through a reverse frit (P2), which was additionally washed with diethyl ether (50 ml), resulting the clear grey Grignard solution **11** (350 ml, 2.72 M in diethyl ether, 0.95 mol).The concentration of **11** was determined by titration against salicylaldehyde phenylhydrazone (505 mg, 2.4 mmol) in THF (20 ml).

Step 2: ^{t}Bu$_2$PCl (**12**)

$$^t\text{Bu}_2\text{PCl}$$

Phosphorus trichloride (37.0 ml, 0.42 mol, 1.0 eq) was added in a two-necked Schlenk flask equipped with a dropping funnel and diluted with diethyl ether (1 l). The Grignard solution **11** (350 ml, 2.72 M in diethyl ether, 0.95 mol) was added dropwise at T = -60 °C. The reaction mixture was first stirred at rt for 16 h and then at T = 75 °C for additional 2 h. The solid magnesium chloride was separated from the mixture by filtration though a reverse frit (P3 (8 cm diameter) filled with diatomaceous earth (5 cm) and washed with diethyl ether (420 ml). The solvent was removed *in vacuo* from the filtrate. The crude product was two times purified by fractional distillation (T = 28-38 °C, p = 1.0x10^{-1} mbar), yielding a colorless solution (11.5 ml, 52 mmol, 12%; Lit.[315] 60%).

^{1}H NMR (400 MHz, dichloromethane-d_2): δ = 1.21 (d, $^3J_{H,P}$ = 12.15 Hz, ^{t}Bu) ppm.

^{31}P{^{1}H} NMR (162 MHz, dichloromethane-d_2): δ = 144.5 (s) ppm.

Step 3: ^{t}Bu$_2$PCH$_3$ (**13**)

$$^t\text{Bu}_2\text{PCH}_3$$

Di-*tert*-butylchlorophosphine (**12**, 5.00 ml, 26 mmol, 1.0 eq) was added to a Schlenk flask equipped with a dropping funnel and diluted with pentane (20 ml). Methylllithium (22.0 ml, 1.6 M in diethyl ether, 35 mmol, 1.3 eq) was added dropwise at T = -78 °C and stirred at rt overnight. Oxygen free ammonium chloride solution (conc. 5%, 40 ml) was added to the reaction mixture. The water phase was separated and washed with pentane (2x 20 ml). The combined organic phases were dried with MgSO$_4$, filtrated and the solvent removed *in vacuo*, yielding a colorless liquid (4.07 ml, 21 mmol, 80%; Lit.[315] 96%).

^{1}H NMR (500 MHz, dichloromethane-d_2): δ = 1.06 (d, $^3J_{H,P}$ = 10.9 Hz; 18H, ^{t}Bu), 0.89 (d, $^2J_{H,P}$ = 4.1 Hz, 3H, CH$_3$) ppm.

^{31}P NMR (202 MHz, dichloromethane-d_2): δ = 11.7 (m) ppm.

Step 4: ^{t}Bu$_2$PCH$_2$Li (**14**)

$$^t\text{Bu}_2\text{PCH}_2\text{Li}$$

A *tert*-butyllithium solution (18.0 ml, 1.6 M in pentane, 29 mmol, 1.4 eq) was added into a Schlenk flask and the pentane was removed under reduced pressure. The resulting salt was dissolved in heptane (10 ml) and the solution of di-*tert*-butylmethylphosphine (**13**, 4.07 ml, 21 mmol, 1.0 eq) dissolved in heptane (10 ml) was added dropwise at rt. After stirring at T = 110 °C overnight, the colorless solid was separated from the orange suspension by filtration through a reverse frit and washed with pentene (2x 20 ml). The solvent was removed *in vacuo*, yielding a colorless solid (2.97 g, 18 mmol, 85%; Lit.[315] 90%).

^{1}H NMR (400 MHz, tetrahydrofuran-d_8): δ = 1.08 (d, $^2J_{H,P}$ = 12.7 Hz, 2H, CH$_2$), 0.99 (d, $^2J_{H,P}$ = 8.8 Hz, 18H, ^{t}Bu) ppm.

^{31}P{^{1}H} NMR (162 MHz, tetrahydrofuran-d_8): δ = 45.0 (s) ppm.

Step 5: $^tBu_2PCH_2P^tBu_2$ (**15**)
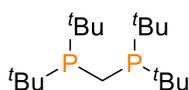
Di-*tert*-butylphosphinomethyllithium (**14**, 2.97 g, 18 mmol, 1.0 eq) was transferred to a Schlenk flask and suspended in THF (57 ml). Di-*tert*-butylchlorophosphine (**12**, 3.40 ml, 18 mmol, 1.0 eq) was added dropwise at T = -78 °C. The reaction mixture was stirred at rt overnight. After removing of the solvent *in vacuo*, the product was extracted with pentane (2x 25 ml). Oxygen free ammonium chloride solution (conc. 5%, 40 ml) was added to the pentane extract. The water phase was separated and washed with pentane (2x 30 ml). The combined organic phases were dried with $MgSO_4$, filtrated and the solvent removed under reduced pressure. The crude product was recrystallized at T = -21 °C in methanol (10 ml). The solvent was removed with a syringe at T = -30 °C. The remaining colorless crystals (3.06 g, 10 mmol, 65%; Lit.[315] 77%) were dried *in vacuo*.

^{1}H NMR (500 MHz, benzen-d_6): δ = 1.64 (s, 2H, CH_2), 1.22 (s, 36H, ^tBu) ppm.

^{13}C{^{1}H} NMR (215 MHz, benzene-d_6): δ = 32.7 (dd, $^3J_{C,P}$ = 12.5 Hz, $^1J_{C,P}$ = 10.4 Hz, CMe_3), 30.4 (t, $^2J_{C,P}$ = 8.3 Hz, CH_3), 13.3 (t, $^1J_{C,P}$ = 38.1 Hz, CH_2) ppm.

^{31}P{^{1}H} NMR (202 MHz, benzene-d_6): δ = 22.0 (s) ppm.

Bis(dicyclohexylphosphino)methan (21)
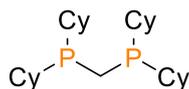
Preparation according the literature procedure of HOFMANN.[315]

Step 1: CyMgCl (**17**)

Cy−MgCl
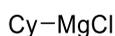
Magnesium flakes (32.6 mg, 1.34 mol, 1.1 eq) were added to a two-necked Schlenk flask equipped with a dropping funnel and mechanically activated by stirring overnight. After suspending of the magnesium with diethyl ether (150 ml), a solution of cyclohexyl chloride (**16**, 145 ml, 1.22 mmol, 1.0 eq) in diethyl ether (100 ml) was added dropwise and stirred at T = 75 °C for 3.5 h. The reaction mixture was diluted with diethyl ether (200 ml) and filtrated through a reverse frit (P2 (1 cm diameter) with diatomaceous earth (2 cm)), resulting the clear grey Grignard solution **17** (335 ml, 3.57 M in diethyl ether, 1.20 mol). The concentration of **17**

was determined by titration against salicylaldehyde phenylhydrazone (500 mg, 2.4 mmol) in THF (20 ml).

Step 2: Cy_2PCl (**18**)

$$Cy_2PCl$$

Phosphorus trichloride (45.0 ml, 0.52 mol, 1.0 eq) was added in a two-necked Schlenk flask equipped with a dropping funnel and diluted with diethyl ether (500 ml). The Grignard solution **17** (335 ml, 3.57 M in diethyl ether, 1.20 mol) was added dropwise at T = -60 °C in a period of 6 h. The reaction mixture was first stirred at rt overnight and then at T = 75 °C for additional 2 h. The solid magnesium chloride was separated from the mixture by filtration though a reverse frit (P3 (8 cm diameter) filled with diatomaceous earth (5 cm) and washed with diethyl ether (300 ml). The solvent was removed *in vacuo* from the filtrate. The crude product was purified by fractional distillation (T = 140 °C, p = 1.0×10^{-3} mbar), yielding a colorless solution (48.6 ml, 0.22 mmol, 43%; Lit.[315] 53%).

^{1}H NMR (400 MHz, dichloromethane-d_2): $δ$ = 1.90-1.75 (m, 10H, *ortho*-, *meta*-, *para*-CH_2), 1.75-1.68 (m, 2H, *ipso*-CH), 1.40-1.20 (m, 10H, *ortho'*-, *meta'*-, *para'*-CH_2) ppm.

^{31}P{^{1}H} NMR (162 MHz, dichloromethane-d_2): $δ$ = 129.2 (s) ppm.

Step 3: Cy_2PCH_3 (**19**)

$$Cy_2PCH_3$$

Dicyclohexylchlorophosphine (**18**, 12.0 ml, 56 mmol, 1.0 eq) was added to a Schlenk flask equipped with a dropping funnel and diluted with pentane (50 ml). Methyllithium (42.0 ml, 1.6 M in diethyl ether, 62 mmol, 1.2 eq) was added dropwise at T = -78 °C over a period of 30 min and stirred at rt overnight. The suspended lithium chloride was removed by filtration through a reverse frit (P3) and washed with pentane (3x 25 ml). The solvent was removed *in vacuo* from the filtrate, yielding a colorless viscos liquid (11.1 g, 52 mmol, 93%).

^{1}H NMR (500 MHz, dichloromethane-d_2): $δ$ = 1.84-1.70 (m, 8H, *ortho*-, *meta*-CH_2), 1.70-1.64 (m, 2H, *para*-CH_2), 1.43 (tq, $^2J_{H,P}$ = 11.9 Hz, $^3J_{H,H}$ = 3.1 Hz, $^3J_{H,H}$ = 3.0 Hz, 2H, *ipso*-CH_2), 1.35-1.18 (m, 8H, *ortho'*-, *meta'*-CH_2), 1.17-1.05 (m, 2H, *para'*-CH_2), 0.86 (d, $^2J_{H,P}$ = 2.8 Hz, 3H, PCH_3) ppm.

^{31}P{^{1}H} NMR (202 MHz, dichloromethane-d_2): $δ$ = -17.9 (s) ppm.

Step 4: Cy$_2$PCH$_2$Li (**20**)

$$\text{Cy}_2\text{PCH}_2\text{Li}$$

A tert-butyllithium solution (44.0 ml, 1.6 M in pentane, 70 mmol, 1.3 eq) was added into a Schlenk flask and the pentane was removed under reduced pressure. The resulting salt was dissolved in heptane (20 ml) and a solution of dicyclohexylmethylphosphine (**19**, 11.1 g, 52 mmol, 1.0 eq) dissolved in heptane (20 ml) was added dropwise at rt. After stirring at $T = 110\,°C$ overnight, the colorless solid was separated from the orange suspension by filtration through a reverse frit and washed with pentene (2x 20 ml). The solvent was removed *in vacuo*, yielding a colorless solid (10.9 g, 50 mmol, 95%).

^{1}H NMR (400 MHz, tetrahydrofuran-d_8): δ = -1.44 to -1.74 (m, 10H, *ortho*-, *meta*-, *para*-CH$_2$), -1.86 (tq, $^2J_{H,P}$ = 11.4 Hz, $^3J_{H,H}$ = 2.8 Hz, $^3J_{H,H}$ = 2.4 Hz, 2H, *ipso*-CH$_2$), -1.94 to -2.32 (m, 10H, *ortho*'-, *meta*', *para*'-CH$_2$), -2.48 (d, $^2J_{H,P}$ = 3.3 Hz, 2H, PCH$_2$) ppm.

^{31}P{^{1}H} NMR (162 MHz, tetrahydrofuran-d_8): δ = 12.1 (s) ppm.

Step 5: Cy$_2$PCH$_2$PCy$_2$ (**21**)
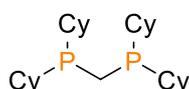
Dicyclohexylphosphinomethyllithium (**20**, 10.9 g, 50 mmol, 1.0 eq) was transferred to a Schlenk flask and suspended in THF (160 ml). Dicyclohexylchlorophosphine (**18**, 10.6 ml, 48 mmol, 1.0 eq) was added dropwise at $T = -78\,°C$. The reaction mixture was stirred at rt overnight. After removing of the solvent *in vacuo*, the product was extracted with pentane (2x 40 ml). Oxygen free ammonium chloride solution (conc. 5%, 50 ml) was added to the pentane extract. The water phase was separated and washed with pentane (2x 30 ml). The combined organic phases were dried with MgSO$_4$, filtrated and the solvent removed under reduced pressure. The crude product was recrystallized at $T = -21\,°C$ in a pentane-THF solution (49 ml, 1:1.3). The solvent was removed with a syringe at $T = -30\,°C$. The remaining colorless crystalline solid (11.9 g, 29 mmol, 59%; Lit.[315] 83%) was dried *in vacuo*.

^{1}H NMR (500 MHz, benzene-d_6): δ = 2.00-1.89 (m, 8H, *meta*-CH$_2$), 1.81-1.74 (m, 8H, *ortho*-CH$_2$), 1.69 (tt, $^3J_{H,H}$ = 11.9 Hz, $^3J_{H,H}$ = 3.0 Hz, 4H, *ipso*-CH$_2$), 1.66-1.61 (m, 4H, *para*-CH$_2$), 1.58 (s, 2H, PCH$_2$P) 1.52-1.34 (m, 8H, *ortho*'-CH$_2$), 1.31-1.15 (m, 12H, *meta*'-, *para*'-CH$_2$) ppm.

^{13}C{^{1}H} NMR (215 MHz, benzene-d_6): δ = 35.0 (t, $^1J_{C,P}$ = 5.4 Hz, *ipso*-C), 30.7 (t, $^2J_{C,P}$ = 8.0 Hz, *ortho*-C), 29.9 (t, $^3J_{C,P}$ = 6.0 Hz, *meta*-C), 27.9 (s, *para*-C), 13.8 (t, $^1J_{C,P}$ = 29.3 Hz, PCH$_2$P) ppm.

^{31}P{^{1}H} NMR (202 MHz, benzene-d_6): δ = -10.8 (s) ppm.

Bis(dicyclopentylphosphino)methane (24)
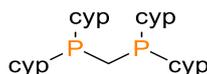
Modified preparation according the literature procedure of KARSCH.[329]

Step 1: cypMgCl (**23**)

$$cyp-MgCl$$
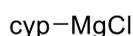
Magnesium flakes (3.83 mg, 0.16 mol, 1.1 eq) were added to Schlenk flask equipped with a dropping funnel and mechanically activated by stirring overnight. After suspending of the magnesium with diethyl ether (10 ml), a solution of cyclopentyl chloride (**22**, 15 ml, 0.14 mmol, 1.0 eq) in diethyl ether (10 ml) was added dropwise and stirred at $T = 75\ °C$ for 2 h. The reaction mixture filtrated through a reverse frit. The Grignard solution **23** was used for the next step without determination of the concentration. A full conversion was presumed.

Step 2: cyp$_2$PCH$_2$Pcyp$_2$ (**24**)
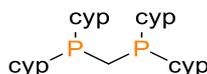
Bis(dichlorophosphino)methane (**9**, 5.00 g, 3.12 ml, 23 mmol, 1.0 eq) was transferred to a Schlenk flask and dissolved in diethyl ether (150 ml). The Grignard reagent **23** was added dropwise at $T = -30\ °C$ over a period of 2 h. The reaction mixture was diluted with diethyl ether (400 ml) stirred at rt overnight. Oxygen free ammonium chloride solution (conc. 5%, 300 ml). The water phase was separated and washed with diethyl ether (150 ml). The combined organic phases were dried with MgSO$_4$, filtrated and the solvent removed under reduced pressure. The crude product was recrystallized at $T = -80\ °C$ in diethyl ether (17.5 ml). The solvent was removed with a syringe at $T = -78\ °C$. The colorless solid was dried *in vacuo* and subsequently distilled ($T_{oil\ bath} = 180\ °C$, $p = 1\text{x}10^{-3}$ mbar), yielding a colorless liquid (1.85 g, 5.3 mmol, 23%). Around 50% by-products (measured by ^{31}P NMR) remained in the crude mixture. A complete purification of the crude product was not possible.

^{31}P NMR (202 MHz, benzene-*d$_6$*): $δ = -11.9$ (m) ppm.

Diisopropylphosphinodimethylamino)ethane (29)
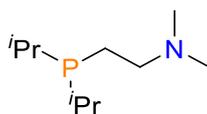
Preparation according the literature procedure of WERNER.[337]

Step 1: 2-chloro-*N,N*-dimethylethan-1-amine (**26**)
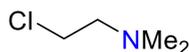
Potassium hydroxide (8.0 g, 143 mmol, 1.51 eq) was added to a two-necked Schlenk tube connected over a glass bridge with another Schlenk tube, which is cooled with liquid nitrogen bath. 2-chloro-*N,N*-dimethylethan-1-amine hydrochloride (**25**, 11.0 g, 94.7 mmol, 1.0 eq) was added to the potassium hydroxide. The reaction mixture was shaken several times within a total period of 5 min. The release product was transferred and trapped in the chilled flask by applying reduced pressure. The frozen product was directly used for the following reaction step after melting.

Step 2: ^{i}Pr$_2$PH (**28**)

^{i}Pr$_2$PH

A solution of chlorodiisopropylphosphine (**27**, 10.0 g, 65.8 mmol, 1.0 eq) in diethyl ether (50 ml) was added dropwise to a suspension of lithium aluminum hydride (3.77 g, 99.3 mmol, 1.51 eq) in diethyl ether (50 ml) at T = 0 °C over a period of 30 min. After additional stirring at T = 0 °C for 30 min the reaction mixture was allowed to warm to rt and the reaction progress monitored by ^{31}P NMR. The suspension was cooled to T = 0 °C and quenched with oxygen free water (40 ml). The organic phase was separated, dried with MgSO$_4$ and filtrated through a reverse frit filled with silica (5 cm). The solvent was removed in vacuo at T = -30 °C, yielding a colorless liquid.

^{1}H NMR (400 MHz, benzene-*d$_6$*): δ = 2.91 (dt, $^1J_{H,P}$ = 192.1 Hz, $^3J_{H,H}$ = 6.0 Hz, 1H, PH), 1.80 (m, 2H, PCH), 1.04 (m, 12H, CH$_3$) ppm.

^{31}P NMR (162 MHz, benzene-*d$_6$*): δ = -16.7 (d, $^1J_{P,H}$ = 192 Hz) ppm.

Step 3: ^{i}Pr$_2$PCH$_2$NMe$_2$ (**29**)
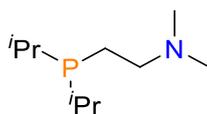
Diisopropylphosphine (**28**, 3.9 g, 33 mmol, 1.0 eq) diluted with THF (40 ml) was added in a two-necked Schlenk flask equipped with a reflux condenser. After addition of *n*-buthyllithium (14 ml, 2.5 M, 35 mmol) at $T = 0$ °C the reaction mixture was stirring at $T = 75$ °C for 30 min. A solution of 2-chloro-*N*,*N*-dimethylethan-1-amine (**26**, 3.7 ml, 33 mmol, 1 eq) in THF (10 ml) was added over a period of 1 h. After cooling to rt, an oxygen free, saturated solution of ammonium chloride (45 ml) was added. The organic layer was separated and the solvent removed by reduced pressure. The high viscous crude product was purified by fractional distillation ($T = 72$ °C, $p = 7$ mbar, $T_{oil\ bath} = 100$ °C), yielding a colorless jelly (3.95 g, 51%).

^{1}H NMR (400 MHz, benzene-d_6): δ = 2.47 (m, 2H, CH$_2$N), 2.13 (s, 6H, NCH$_3$), 1.57 (m, 2H, CH$_2$P), 1.57 (m, 2H, PCH), 1.06-0.98 (m, 12H, PCHCH_3) ppm.

^{31}P{^{1}H} NMR (162 MHz, benzene-d_6): δ = 0.3 (s) ppm.

4.2.3   Preparation of ancillary reagents

Lithium-bis(trimethylsilyl)phosphide bistetrahydrofuran (65)

LiP(SiMe$_3$)$_2$ · 2 THF
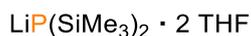
P(SiMe$_3$)$_3$ (**64**, 8.0 ml, 6.88 g, 27.5 mmol) was diluted in THF (50 ml) and transferred to a Schlenk flask equipped with a dropping funnel. Methyllithium (17.2 ml, 27.5 mmol, 1 eq, 1.6 M in diethyl ether) was added dropwise at $T = 0$ °C over a period of 30 min. After stirring at rt overnight the solvent was removed under reduced pressure, yielding a white powder (6.3 g, 24.7 mmol, 90%; LiP(SiMe$_3$)$_2$ · THF).[523]

Note: LiP(SiMe$_3$)$_2$ · 2 THF is a fluffy powder, additional or too long drying of the product under vacuum partly removes the coordinated THF and might yield the sticky LiP(SiMe$_3$)$_2$ · THF or even LiP(SiMe$_3$)$_2$ · n THF (n < 1), which shows less shifted ^{31}P signals around -237 ppm. However, dissolving any of those products in THF-d_8 should always result a ^{31}P shift of around -305 ppm.

^{1}H NMR (400 MHz, benzene-d_6): δ = 3.71 (THF), 1.34 (THF), 0.55 (s, 18H, Si(CH$_3$)$_3$) ppm.

^{31}P{^{1}H} NMR (162 MHz, benzene-d_6): δ = -296.3 (s) ppm.

Benzylazide (117)
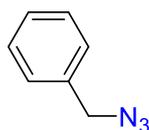
Note: Working under air, no inert technique required.

Benzyl bromide (3.47 ml, 5.0 g, 29.2 mmol, 1 eq) was added dropwise to a solution of sodium azide (2.85 g, 43.8 mmol, 1.5 eq) dissolved in DMSO (60 ml). After stirring at rt for 16 h, water (100 ml) was added to the slightly yellow solution. The product was extracted from the reaction mixture with diethyl ether (4x 100 ml). The diethyl ether phase was narrowed to 100 ml and washed with water (4x 100 ml), dried with $MgSO_4$ and the solvent removed *in vacuo*. The product (3.44 g, 88%) was obtained as colorless viscous liquid.

^{1}H NMR (400 MHz, chloroform-d_1): δ = 7.44 - 7.35 (m, 5H, ArH), 4.36 (s, 2H, CH_2) ppm.

[W(CO)5(thf)]

[W(CO)$_5$(thf)]

Tungsten hexacarbonyl (1.0 g, 2.84 mmol) was dissolved in 60 ml and irradiated with UV light (high-pressure Hg lamp, 100 W, λ_{max} = 365 nm) for 6 h. The reaction tube was purged with argon every 2 h to remove liberated CO gas. The yellow solution was concentrated to about 20 ml and stored at T = -20 °C.

Tricarbonylbis(cyclooctene)iron(0) (138)

(coe)$_2$Fe(CO)$_3$

138 was prepared according to an adapted literature synthesis.[383]

Iron pentacarbonyl (0.69 ml, 1.0 g, 5.1 mmol, 1 eq) and cyclooctene (6.62 ml, 5.6 g, 51.0 mmol, 10 eq) was diluted in 40 ml pentane. After degassing via freeze-pump-thaw, the solution was cooled to T = -72 °C and irradiated with UV light (high-pressure Hg lamp, 100 W, λ_{max} = 365 nm) for 3 h. The CO gas was removed by bubbling argon through the reaction mixture for around 5 min. The irradiation was continued for at T = -60 °C for 3 h. The reaction mixture was filtered through diatomaceous earth. The pentane was removed by reduced pressure from the yellow filtrate at T = -20 °C. The greenish cyclooctene solution was stored at T = -80 °C.

4.2.4 Preparation of phosphaalkynes

Trimethylsilylphosphaalkyne

$$Me_3Si \!\!-\!\!\!\equiv\!\! P$$
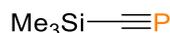
Prepared according to the literature synthesis.[77]

Step 1: ((trimethylsilyl)methyl)magnesium chloride (**51**)

$$Me_3Si \frown MgCl$$
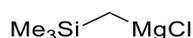
Magnesium flakes (12.9 mg, 530 mmol, 1.3 eq) were transferred to a three-necked Schlenk flask equipped with a reflux condenser and a dropping funnel. The magnesium was activated by stirring overnight with two pearls of iodine. After addition of diethyl ether (200 ml) to the activated magnesium, a solution of (**50**, chloromethyl)trimethylsilane (50.0 g, 408 mmol, 1 eq) in diethyl ether (50 ml) was added dropwise to the suspension at rt over a period of 1 h. After refluxing for 1 h, the mixture was allowed to cool down and settle.

Step 2: dichloro((trimethylsilyl)methyl)phosphine (**52**)

$$Me_3Si \frown PCl_2$$
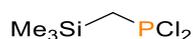
Phosphorus trichloride (35.7 ml, 56.0 g, 408 mmol, 1 eq) was added to Schlenk flask equipped with dropping funnel and diluted with diethyl ether (100 ml). The Grignard solution (**51**) was transferred to the funnel with a filter cannula and added dropwise to the solution at T = -72 °C within 1 h. Additional diethyl ether (800 ml) was added for stirring at rt overnight. Hydrogen chloride (150 ml, 2 M in diethyl ether) was added and the stirring was continued for 12 h. The suspension was filtrated through diatomaceous earth (reverse frit) to remove the MgCl$_2$. The solvent was *in vacuo* removed from the filtrate at T = 20 °C, yielding a slightly yellow liquid (35.8 g, 189 mmol, 46 5). *Note: The product is volatile under a strong vacuum. The removement of the solvent is completed if the solution stops bubbling.*

^{1}H NMR (400 MHz, dichloromethane-d_2): δ = 2.08 (d, $^2J_{H,P}$ = 15.4 Hz, 2H, CH$_2$P), 0.22 (s, 9H, Si(CH$_3$)$_3$) ppm.

^{31}P{^{1}H} NMR (162 MHz, dichloromethane-d_2): δ = 207.4 (s) ppm.

Step 3: trimethylsilylphosphaalkyne (**53**)

$$Me_3Si \!\!-\!\!\!\equiv\!\! P$$
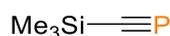
AgOTf (12.0 g, 46.5 mmol, 2.2 eq) was added to a solution of dichloro((trimethylsilyl)methyl)phosphine (**52**, 4.0 g, 21.2 mmol, 1.0 eq) in toluene (125 ml) at rt and stirred for 30 min in the darkness. Under strong stirring DABCO (5.22 g, 46.5 mmol, 2.2 eq) was added portion-wise to the suspension while maintaining rt with the help of a water bath. After stirring at rt for 1 h, the liquid phase was separated and collected via cooling trap (liquid nitrogen) and reduced pressure. The toluene solution of the product (0.09 M) was transferred to another flask and stored at T = -80 °C. The concentration and yield (1.31 g, 11.3 mmol, 53%) was defined by ^{31}P NMR against triphenylphosphine.[77]

^{31}P NMR (162 MHz, toluene): δ = 96.2 (s) ppm.

Triphenylsilylphosphaalkyne (58)

$$Ph_3Si\!-\!\!\equiv\!\!P$$
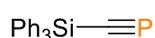
Step 1: (triphenylsilyl)methyl chloride (**55**)

$$Ph_3Si\diagup\diagdown Cl$$
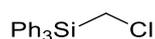
Bromobenzene (**54**, 2.87 ml, 4.23 g, 23 mmol, 1 eq) was added dropwise to a suspension of activated magnesium flakes (3.48 mg, 143 mmol, 6.23 eq) in THF (100 ml). After stirring at rt for 2 h, the solution was transferred to another flask via filter cannula. A solution of trichloro(chloromethyl)silane in THF (38 ml) was added dropwise to the Grignard solution at T = 0 °C. After refluxing for 24 h, the solution was hydrolyzed with saturated, aqueous ammonium chloride solution (77 ml) and diethyl ether (150 ml). The separated organic layer was dried over MgSO$_4$, filtrated and concentrated by rotary evaporation. The crude product was purified by column chromatography on silica with a hexane-DCM mixture (1:1) and recrystallized from ethanol, yielding a colorless solid (5.73 mg, 18.6 mmol, 81%).[524]

^{1}H NMR (400 MHz, chloroform-d_1): δ = 7.63-7.58 (m, 6H, Si(Ph$_3$)$_3$), 7.50-7.45 (m, 3H, Si(Ph$_3$)$_3$), 3.54 (s, 2H) ppm.

Step 2: ((triphenylsilyl)methyl)magnesium chloride (**56**)

$$Ph_3Si\diagup\diagdown MgCl$$
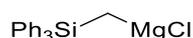
A solution of (triphenylsilyl)methyl chloride (**55**, 5.70 g, 18.6 mmol, 1 eq) in THF (22 ml) was added dropwise to a suspension of activated magnesium flakes (4.39 mg, 180 mmol, 9.78 eq) in THF (22 ml) at rt within 30 min. After stirring for 3 h, the mixture was allowed to settle.

Step 3: dichloro((triphenylsilyl)methyl)phosphine (**57**)

$$Ph_3Si \diagup PCl_2$$
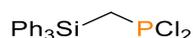
Phosphorus trichloride (4.84 ml, 7.60 g, 55.4 mmol, 3 eq)) was added to Schlenk flask equipped with dropping funnel and diluted with THF (44 ml). The Grignard solution (**56**) was transferred to the funnel with a filter cannula and added dropwise to the solution at T = -78 °C. After stirring the reaction mixture at rt overnight, the solvent was removed *in vacuo*. The crude product was extracted with toluene (88 ml) and filtrated through diatomaceous earth (reverse frit). The solvent was removed under reduced pressure, yielding a colorless solid (6.86 g, 18.3 mmol, 99%).

^{1}H NMR (400 MHz, benzene-d_6): δ = 7.43-7.38 (m, 6H, Si(Ph$_3$)$_3$), 7.14-7.02 (m, 9H, Si(Ph$_3$)$_3$), 2.53 (d, $^2J_{H,P}$ = 14.34 Hz, 2H, CH$_2$P) ppm.

^{31}P{^{1}H} NMR (162 MHz, benzene-d_6): δ = 199.4 (s) ppm.

Step 4: triphenylsilylphosphaalkyne (**58**)

$$Ph_3Si \equiv\!\!\!- P$$
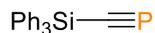
AgOTf (746 mg, 2.90 mmol, 2.2 eq) was added to a solution of dichloro((triphenylsilyl)methyl)phosphine (**57**, 495 mg, 1.32 mmol, 1.0 eq) in toluene (24 ml) at rt and stirred for 15 min in the darkness before DABCO (325 mg, 2.90 mmol, 2.2 eq) was added to the suspension. After stirring at rt for 1 h, the reaction mixture was filtrated through a diatomaceous earth plug with toluene and the solvent was removed under reduced pressure. The product (139 mg, 460 µmol, 35%) was obtained as a red-brown solid with a purity of around 50%.[37] *Note: Triphenylsilylphosphaalkyne is not stable in solid state. It is recommended to use it imminently after the synthesis as toluene solution.*

^{1}H NMR (400 MHz, dichloromethane-d_2): δ = 7.65-7.62 (m, 6H, Si(Ph$_3$)$_3$), 7.46-7.42 (m, 3H, Si(Ph$_3$)$_3$), 7.40-7.36 (m, 6H, Si(Ph$_3$)$_3$) ppm.

^{31}P{^{1}H} NMR (162 MHz, dichloromethane-d_2): δ = 112.4 (s) ppm.

2,4,6-trimethylphenylphosphaalkyne (68)
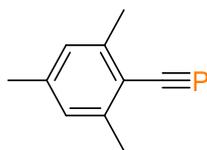
Mesitylphosphaalkyne (68) was prepared by a modified synthesis of trimethylsilylphosphaalkyne (58) of RUSSEL and co-workers.[77] There is another synthesis for 68 from REGITZ et al. which was not reproducible.[351]

Step 1: 2-(chloromethyl)-1,3,5-trimethylbenzene (**69**)
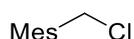
Note: Working under air, no inert technique required.

A mixture of mesitylene (100 g, 832 mmol, 1.0 eq), paraformaldehyde (26.2 g, 874 mmol, 1.05 eq) and hydrochloric acid (240 ml, 37%, 2.91 mol) in acetic acid (240 ml) was stirred and slowly heated over a period of 1.5 h to $T = 40$ °C. After cooling down to ambient temperature, the mixture was diluted with water (1.0 l) and DCM (200 ml) and the product was extracted with DCM (4x50 ml). The combined organic phases were washed with water (5x100 ml) and evaporated at $p = 11 - 12$ mbar ($T_{water\ bath} = 42$ °C). A colorless oil (134 g, 790 mmol, 95% yield) was obtained. After 15 - 18 hours at $T = +4$ °C the oil crystallized. The crystals were dissolved in *n*-pentane and transferred into a suitable round-bottom flask. The flask is swiveled in liquid nitrogen until the product precipitated as colorless crystals and the solvent was decanted off (repeated 3x). Finally, the product was collected by filtration from cold *n*-pentane and dried *in vacuo*. A white solid with a melting point of $T = 39$ °C is obtained. (95.9 g, 566 mmol, 68% yield)

¹H NMR (400 MHz, Chloroform-*d₁*): $\delta = 6.88$ (s, 2H, aryl-H), 4.66 (s, 2H, *ipso*-C*H₂*Cl), 2.40 (s, 6H, *ortho*-C*H₃*), 2.27 (s, 3H, *p*-C*H₃*) ppm.

Step 2: (2,4,6-trimethylbenzyl)zinc(II) chloride (**70**)
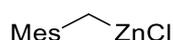
A suspension of zinc powder (9.85 g, 151 mmol, 2.0 eq) and DME (80 ml) was stirred at rt in a strong ultrasonic bath (ELMA Transsonic 310/H) for 30 min (*with increased particle size of the zinc longer activation times might be necessary*). 2,4,6-trimethylbenzyl chloride (12.7 g, 75.3 mmol, 1.0 eq) was dissolved in DME (15 ml) and added dropwise with a dropping funnel at $T = 10 - 12$ °C to the suspension. The reaction mixture was stirred for additional 2 h at

$T = 10\,°C$. It is important to maintain the temperature between $T = 10 - 12\,°C$ to avoid the formation of by-products. The reaction mixture was filtered through diatomaceous earth to remove any residual elemental zinc. A colorless to pale yellow solution was obtained. The organozinc reagent was then used without further purification in the subsequent step.

Step 3: dichloro(2,4,6-trimethylbenzyl)phosphane (**71**)
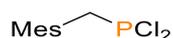
Phosphorus trichloride (3.66 g, 41.8 mmol, 2.0 eq) was added to a Schenk-flask prefilled with DME (50 ml). The (2,4,6-trimethylbenzyl)zinc(II) chloride (1.0 eq) solution from the above step was added dropwise *via* dropping funnel to the solution at $T = 0\,°C$. After completion of the addition, the reaction mixture was allowed to warm to ambient temperature and stirred overnight. The solvent was removed *in vacuo* and the residue was dissolved in DCM, forming a suspension. The suspension was filtered through silica. Removal of the solvent under reduced pressure gave a pale yellow oil. After a bulb-to-bulb distillation ($T_{\text{oil bath}} = 134\,°C$, $p = 6.0\text{x}10^{-2}$ mbar) a colorless oil was obtained. (3.69 g, 15.70 mmol, 75%)

^{1}H NMR (400 MHz, dichloromethane-d_2): $\delta = 6.61$ (s, 2H, aryl-H), 3.88 (d, 2H, *ipso*-CH_2PCl$_2$), 2.40 (s, 6H, *ortho*-CH_3), 2.27 (d, 3H, *para*-CH_3) ppm.

^{31}P{^{1}H} NMR (162 MHz, dichloromethane-d_2): $\delta = 185.8$ (s) ppm.

Step 4: 2,4,6-trimethylphenylphosphaalkyne (**68**)
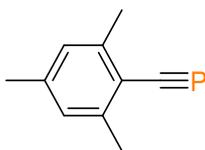
The following reaction should be performed in the absence of light to prevent the decomposition of AgOTf.

AgOTf (8.49 g, 33.0 mmol, 2.2 eq) was added to a toluene solution (150 ml) of **71** (3.53 g, 15.0 mmol, 1.0 eq) and stirred for 30 min at rt. After the addition of DABCO (3.71 g, 33.0 mmol, 2.2 eq) the reaction mixture was stirred for another hour, before it was filtered through diatomaceous earth to remove the AgCl$_2$. The toluene was removed from the slightly brown solution under reduced pressure. The residue was dissolved in *n*-pentane and purified by column chromatography, the product comes with the colorless *n*-pentane fraction, whereas the impurities stay on the silica. The *n*-pentane was removed under reduced pressure, yielding **3**

as a colorless liquid (1.34 g, 8.28 mmol, 55%). The product must be stored under T = -20 °C in the absence of light.

^{1}H NMR (400 MHz, dichloromethane-d_2): δ = 6.88 (s, 2H, aryl-H), 2.47 (s, 6H, *ortho*-CH_3), 2.28 (d, 3H, *para*-CH_3) ppm.

^{31}P NMR (162 MHz, dichloromethane-d_2): δ = 1.5 (s) ppm.

2,4,6-tri(isopropyl)phenylphosphaalkyne (81)
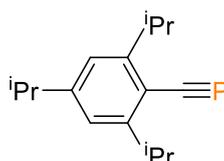
Note: In the meantime, another synthesis protocol with lower yields for 81 was published.[185]

Step 1: 2-(chloromethyl)-1,3,5-triisopropylbenzene (**78**)
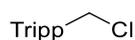
Note: Working under air, no inert technique required.

A mixture of 1,3,5-triisopropylbenzene (30 ml, 125 mmol, 1.0 eq), paraformaldehyde (19.3 g, 375 mmol, 3.0 eq) and hydrochloric acid (50 ml, 37%) in acetic acid (50 ml) was heated to T = 95 °C for 24 h with vigorous stirring, yielding a waxy colorless solid layer on the liquid surface which was chopped into small clumps with a spatula. The suspension was diluted with water (200 ml) and DCM (50 ml). The product was extracted with DCM (3x50 ml). The combined organic phases were washed with water (3x50 ml) and dried with MgSO$_4$. The solvent was removed *in vacuo* yielding a crude product mixture (about 40% starting material). The crude mixture was again mixed with the same amount of fresh paraformaldehyde (19.3 g, 375 mmol, 3.0 eq), hydrochloric acid (50 ml, 37%) and acetic acid (50 ml). After additional heating at T = 95 °C for 2 days the same work up procedure (DCM 3x50 ml, water 3x50 ml) was used to obtain a highly viscous, pale yellow oil. Vacuum distillation yielded two fractions (starting material: T = 72 °C, $T_{oil\ bath}$ = 115 °C, p = 1.0x10^{-3} mbar; product: T = 75 °C, $T_{oil\ bath}$ = 115-122 °C, p = 1.0x10^{-3} mbar). The second fraction contains the product as a highly viscous, colorless oil (**2a**, 26.3 g, 104 mmol, 83%), which solidifies over time.

^{1}H NMR (400 MHz, chloroform-d_1): δ = 6.94 (s, 2H, aryl-*H*), 4.66 (s, 2H, *ipso*-CH_2Cl), 3.22 (sept, $^3J_{H,H}$ = 6.85 Hz, 2H, *ortho*-CH(CH$_3$)$_2$), 2.79 (sept, $^3J_{H,H}$ = 6.91 Hz, 1H, *para*-CH(CH$_3$)$_2$), 1.20 (d, $^3J_{H,H}$ = 6.86 Hz, 12H, *ortho*-CH(CH_3)$_2$), 1.16 (d, $^3J_{H,H}$ = 6.89 Hz, 6H, *para*-CH(CH_3)$_2$) ppm.

Step 2: (2,4,6-triisopropylbenzyl)zinc(II) chloride (**79**)

$$\text{Tripp} \frown \text{ZnCl}$$
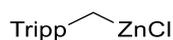
Due to the limited success of scaling up the following reaction, two sperate reactions were performed simultaneously and combined later.

Zinc powder (5.17 g, 79.1 mmol, 4.0 eq) was suspended in DME (20 ml) and stirred at rt for 2 h in a strong ultrasonic bath (ELMA Transsonic 310/H). After this time, additional DME (60 ml) and 2,4,6-triisopropylbenzyl chloride (5.0 ml, 19.0 mmol, 1.0 eq) were added. The reaction mixture was heated to $T = 75\ °C$ with stirring for 16 h. At this point the two reaction mixtures were combined and filtered through diatomaceous earth to remove any residual elemental zinc. A colorless to pale yellow solution was obtained. The organozinc reagent was then used without further purification in the subsequent step.

^{1}H NMR (400 MHz, tetrahydrofuran-d_8): $δ$ = 6.79 (s, 2H, aryl-H), 3.30 (sept, 2H, *ortho*-CH-Me), 2.74 (sept, 1H, *para*-CH-Me$_2$), 1.75 (s, 1H, *ipso*-CH$_2$Cl), 1.19 (d, 12H, *ortho*-CHCH_3), 1.17 (d, 6H, *para*-CHCH_3) ppm.

Step 3: dichloro(2,4,6-triisopropylbenzyl)phosphine (**80**)

$$\text{Tripp} \frown \text{PCl}_2$$
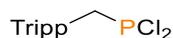
Phosphorus trichloride (17.3 ml, 27.2 g, 198 mmol, 5.0 eq) was diluted with DME (40 ml). The (2,4,6-triisopropylbenzyl)zinc(II) chloride (1.0 eq) solution from the above step was added dropwise *via* a dropping funnel to the solution at $T = 0\ °C$. After completion of the addition, the reaction mixture was allowed to warm to ambient temperature and stirred overnight. The solvent was removed *in vacuo* and the resulting residue was dissolved in DCM, forming a suspension. The suspension was filtered through silica. Removal of the solvent under reduced pressure yielded a pale-yellow solid (7.31 g, 22.9 mmol, 58%).

^{1}H NMR (400 MHz, dichloromethane-d_2): $δ$ = 7.06 (s, 2H, aryl-H), 3.95 (d, $^2J_{H,P}$ = 13.0 Hz, 2H, *ipso*-CH_2PCl$_2$), 3.30 (sept, $^3J_{H,H}$ = 6.81 Hz, 2H, *ortho*-CH(CH$_3$)$_2$), 2.88 (sept, $^3J_{H,H}$ = 6.79 Hz, 1H, *para*-CH(CH$_3$)$_2$), 1.25 (d, $^3J_{H,H}$ = 6.96 Hz, 12H, *para*-CH(CH_3)$_2$), 1.25 (d, $^3J_{H,H}$ = 6.77 Hz, 6H, *ortho*-CH(CH_3)$_2$) ppm.

^{13}C{^{1}H} NMR (101 MHz, dichloromethane-d_2): $δ$ = 149.1 (d, $^5J_{C,P}$ = 3.5 Hz), 148.6 (d, $^3J_{C,P}$ = 3.6 Hz), 123.5 (d, $^2J_{C,P}$ = 6.8 Hz), 122.3 (d, $^4J_{C,P}$ = 2.3 Hz), 43.1 (d, $^1J_{C,P}$ = 3.5 Hz), 34.8 (s), 30.9 (d, $^4J_{C,P}$ = 6.3 Hz), 24.4 (s), 24.3 (s) ppm.

^{31}P NMR (162 MHz, dichloromethane-d_2): $δ$ = 184.1 (t, $^2J_{P,H}$ = 12.96 Hz) ppm.

Step 4: 2,4,6-tri(isopropyl)phenylphosphaalkyne (**81**)
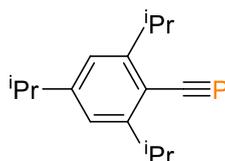
Four separate reactions were performed at once for the following synthesis. The reaction should be performed in the absence of light to prevent the decomposition of AgOTf.

AgOTf (2.54 g, 9.87 mmol, 2.1 eq) was added into a toluene solution (100 ml) of **80** (1.50 g, 4.70 mmol, 1.0 eq) and stirred for 30 min at rt. After the addition of 1,4-diazabicyclo[2.2.2]octane (DABCO, 1.11 g, 9.87 mmol, 2.1 eq) the reaction mixture was stirred at $T = 50\,°C$ for 1 h. All four reaction mixtures were combined and filtered through diatomaceous earth to remove the AgCl. The pale-yellow toluene solution was concentrated to about 200 ml and purified by column chromatography. The solvent was removed *in vacuo.* Vacuum distillation of the crude product (sec. fraction: $T = 50\,°C$, $T_{\text{oil bath}} = 90\,°C$, $p = 1.2\times10^{-3}$ mbar) yields a highly viscous colorless oil (1.72 g, 6.98 mmol, 37%), which is sensitive towards light. The product must be stored at $T = -20\,°C$ in the absence of light.

¹H NMR (700 MHz, benzene-*d₆*): $\delta = 7.00$ (s, 2H, aryl-*H*), 3.95 (sept, $^3J_{\text{H,H}} = 6.88$ Hz, 2H, *ortho*-C*H*(CH₃)₂), 2.69 (sept, $^3J_{\text{H,H}} = 6.94$ Hz, 1H, *para*-C*H*(CH₃)₂), 1.26 (d, $^3J_{\text{H,H}} = 7.02$ Hz, 12H, *para*-CH(C*H₃*)₂), 1.14 (d, $^3J_{\text{H,H}} = 7.00$ Hz, 6H, *ortho*-CH(C*H₃*)₂) ppm.

¹³C{¹H} NMR (176 MHz, benzene-*d₆*): $\delta = 163.5$ (d, $^1J_{\text{C,P}} = 46.0$ Hz), 153.9 (d, $J_{\text{C,P}} = 5.3$ Hz), 150.9 (d, $J_{\text{C,P}} = 6.1$ Hz), 125.7 (d, $^2J_{\text{C,P}} = 21.2$ Hz), 120.7 (s), 35.1 (s), 32.0 (s), 23.9 (s), 23.4 (s) ppm.

³¹P NMR (162 MHz, benzene-*d₆*): $\delta = 3.8$ (s) ppm.

2,4,6-tri-(*tert*-butyl)phenylphosphaalkyne (75)
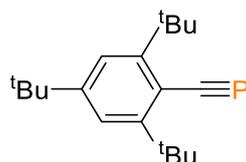
**75** *was prepared according to an adapted literature synthesis.*[79]

Step 1: 2-bromo-1,3,5-tri-*tert*-butylbenzene (**73**)

Mes*Br

Note: Working under air, no inert technique required.

1,3,5-tri-*tert*-butylbenzene (**72**, 16.0 g, 64.9 mmol, 1 eq) was added together with freshly distilled trimethyl phosphate (250 ml) to a two-necked Schlenk flask equipped with a reflux condenser and dropping funnel. The solution was heated to T = 55 °C before bromine (8.01 ml, 25.0 g, 156.5 mmol, 2.4 eq) was added dropwise. The reaction mixture was stirred at T = 100 °C for 48 h. The formed solid was collected by filtration, washed with water (50 ml) and acetone (2x 3 ml). After drying under reduced pressure, a colorless solid (13.7 g, 42.2 mmol, 65%) was obtained.[525]

^{1}H NMR (400 MHz, chloroform-*d₁*): δ = 7.43 (s, 2H, *meta*-H), 1.60 (s, 18H, *ortho*-[t]Bu), 1.33 (s, 9H, *para*-[t]Bu) ppm.

Step 2: 2,4,6-tri-*tert*-butylbenzoic acid (**74**)
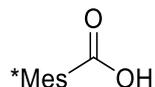
Note: Working under air, no inert technique required.

2-bromo-1,3,5-tri-*tert*-butylbenzene (**73**, 13.7 g, 42.2 mmol, 1 eq) was added together with diethyl ether (250 ml) to a two-necked Schlenk flask equipped with a reflux condenser and dropping funnel. After the dropwise addition of *n*-butyllithium (42.2 ml, 0.106 mmol, 2.5 M in hexane), the solution was refluxed for 1 h. The solution was allowed to cool down to rt before dry ice (around 80 mg) was added. The next day, aqueous HCl (100 ml, conc. 10%) was added to reaction mixture. The organic layer was separated and washed with water (3x 50 ml). The combined organic phases were dried with MgSO₄, filtrated and the solvent removed *in vacuo*. The residue was recrystallized from hexane, yielding a colorless solid (5.12 g, 17.6 mmol, 42%). The most common impurity is unreacted starting material which has good solubility in hexane, while the product is mostly insoluble in hexane.[526-527]

^{1}H NMR (400 MHz, chloroform-*d₁*): δ = 7.45 (s, 2H, *meta*-H), 1.49 (s, 18H, *ortho*-[t]Bu), 1.33 (s, 9H, *para*-[t]Bu) ppm.

Step 3: 2,4,6-tri-*tert*-butylbenzoyl chloride (**75**)

2,4,6-tri-*tert*-butylbenzoic acid (**75**, 3.00, 10.3 mmol, 1 eq) was dissolved in diethyl ether (100 ml). Freshly distilled thionyl chloride (2.25 ml, 3.69 g, 31 mmol, 3 eq) and some drops of

pyridine was added to the solution. The reaction mixture was stirred at rt for 24 h and filtrated through a reverse frit (P4). After removing of the solvent under reduced pressure, the product was obtained as colorless solid (3.06 g, 9.91 mmol, 96%).[526-527]

¹H NMR (400 MHz, chloroform-*d₁*): δ = 7.45 (s, 2H, *meta*-H), 1.50 (s, 18H, *ortho*-*t*Bu), 1.35 (s, 9H, *para*-*t*Bu) ppm.

¹³C{¹H} NMR (101 MHz, chloroform-*d₁*): δ = 174.0 (COCl), 152.1 (*para*-C), 144.5 (*ortho*-C), 133.4 (*ipso*-C), 123.2 (*meta*-C), 37.4 (*ortho*-C(CH₃)₃), 35.1 (*para*-C(CH₃)₃), 32.4 (*ortho*-C(*C*H₃)₃), 30.9 (*para*-C(*C*H₃)₃) ppm.

Step 4: 2,4,6-tri-(*tert*-butyl)phenylphosphaalkyne (**76**)
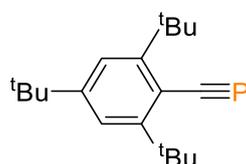
2,4,6-tri-tert-butylbenzoyl chloride (1.87 g, 6.07 mmol, 1 eq) was added to LiP(TMS)₂·THF (1.56 g, 6.07 mmol, 1 eq) in THF (50 ml) and stirred for 16 h at rt. The solvent was removed from the deep red reaction mixture under reduced pressure. The product was extracted from the residue with *n*-pentane and purified by column chromatography (the collection needs to be stopped when the yellow fraction reaches the bottom of the column). The *n*-pentane was removed under reduced pressure, yielding a colorless powder (543 mg, 1.88 mmol, 31%).[79]

¹H NMR (400 MHz, benzene-*d₆*): δ = 7.43 (s, 2H, aryl-H), 1.73 (s, 18H, *ortho*-*t*Bu), 1.24 (s, 9H, *para*-*t*Bu) ppm.

³¹P NMR (162 MHz, benzene-*d₆*): δ = 34.5 (s) ppm.

3,5-di-(*tert*-butyl)phenylphosphaalkyne (86)
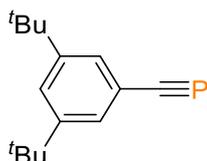
Step 1: 1-(bromomethyl)-3,5-di-*tert*-butylbenzene (**83**)
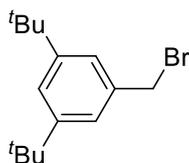
Note: Working under air, no inert technique required.

1,3-Di-*tert*-butyl-5-methylbenzene (**82**, 12.6 g, 61.7 mmol, 1 eq), *N*-bromsuccinimid (11.0 g, 61.7 mmol, 1 eq) and benzoylperoxide (0.45 g, 1.9 mmol, 0.03 eq) were suspended in chloroform (125 ml) and refluxed at $T = 75\,°C$ for 2 h. The yellow to orange solution was allowed to cool down to rt, leading to crash out of excessive *N*-bromsuccinimid. Addition of water (50 ml) to the solution dissolves the solid. Sodium thiosulfate was added to the mixture to quench traces of bromide. The organic layer was separated, washed with water (3x 40 ml) and dried with $MgSO_4$. The solvent was removed by rotary evaporation, yielding an orange oil (16.2 g, 57.2 mmol, 93%).[363-365]

^{1}H NMR (400 MHz, chloroform-d_1): δ = 7.37 (t, 1H, *para*-H), 7.24 (d, 2H, *ortho*-H), 4.50 (s, 2H, CH_2Br), 1.33 (s, 18H, ^tBu) ppm.

Step 2: (3,5-di-*tert*-butylbenzyl)zinc(II) bromide (**84**)
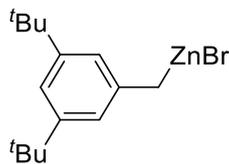
Zinc powder (1.85 g, 28.2 mmol, 4.0 eq) was suspended in DME (10 ml) and stirred at rt for 2 h by a strong ultrasonic bath (ELMA Transsonic 310/H). Then, additional DME (30 ml) and 1-(bromomethyl)-3,5-di-tert-butylbenzene (**83**, 2.0 g, 7.1 mmol, 1.0 eq) were added. The reaction mixture was conventionally stirred first at rt for 16 h then at $T = 75\,°C$ for 3 h. The reaction mixture was filtered through diatomaceous earth to remove any residual elemental zinc. A colorless to pale-yellow solution was obtained. The organozinc reagent was then used without further purification in the subsequent step.

The ^{1}H NMR revealed a mixture of starting material, unknown by-product (probably a DME-Zn complex) and product.

^{1}H NMR (400 MHz, benzene-d_6): δ = 7.16 (s, 1H, *para*-H), 7.08 (s, 2H, *ortho*-H), 2.26 (s, 2H, CH_2ZnBr), 1.31 (s, 18H, ^tBu) ppm.

Step 3: dibromo(3,5-di-*tert*-butylbenzyl)phosphine (**85**)
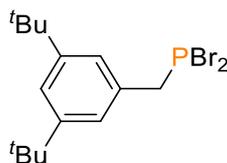
Phosphorus tribromide (2 ml, 5.73 g, 21.2 mmol, 3.0 eq) was diluted with DME (100 ml). The (3,5-di-*tert*-butylbenzyl)zinc(II) bromide (**84**, 1.0 eq) solution from the above step was added dropwise via a dropping funnel to the solution at T = 0 °C over a period of 1 h. After completion of the addition, the reaction mixture was allowed to warm to ambient temperature and stirred overnight. The solvent was removed *in vacuo* and the resulting residue was dissolved in DCM. The pale orange solution was filtered through silica. Removal of the solvent under reduced pressure yielded the pale-yellow product (5.16 g, 13.1 mmol, 67%).

^{1}H NMR (400 MHz, benzene-d_6): δ = 7.42 (d, $J_{H,H}$ = 1.89 Hz 1H, *para*-H), 6.98 (s, 2H, *meta*-H), 3.61 (d, $^2J_{H,P}$ = 17.52 Hz, CH$_2$P), 1.25 (s, 18H, ^{t}Bu) ppm.

^{31}P NMR (162 MHz, benzene-d_6): δ = 174.3 (t, $^2J_{P,H}$ = 18.3 Hz) ppm.

^{1}H NMR (600 MHz, dichloromethane-d_2): δ = 7.40 (s, 1H, *para*-H), 7.14 (s, 2H, *meta*-H), 4.08 (d, $^2J_{H,P}$ = 16.96 Hz, CH$_2$P), 1.33 (s, 18H, ^{t}Bu) ppm.

^{13}C{^{1}H} NMR (151 MHz, dichloromethane-d_2): δ = 151.9 (s, *meta*-C), 132.6 (d, $^2J_{C,P}$ = 10.0 Hz, *ipso*-C), 124.5 (d, $J_{C,P}$ = 5.9 Hz, *ortho*-C), 122.2 (d, $J_{C,P}$ = 3.6 Hz, *para*-C), 49.8 (d, $J_{C,P}$ = 49.9 Hz, CH$_2$P), 35.1 (s, C(CH$_3$)$_3$), 31.6 (s, C(CH_3)$_3$) ppm.

^{31}P{^{1}H} NMR (243 MHz, dichloromethane-d_2): δ = 175.2 (s) ppm.

Step 4: 3,5-di-(*tert*-butyl)phenylphosphaalkyne (**86**)
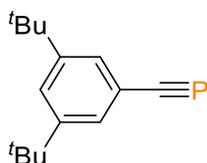
The reaction should be performed in the absence of light to prevent the decomposition of AgOTf.

AgOTf (2.15 g, 8.27 mmol, 2.2 eq) was added into a toluene solution (150 ml) of **85** (1.50 g, 3.81 mmol, 1.0 eq) and stirred for 30 min at rt. After the addition of 1,4-diazabicyclo[2.2.2]octane (DABCO, 0.94 g, 8.37 mmol, 2.2 eq) the reaction mixture was stirred at rt for 1 h. The reaction mixture was filtered through diatomaceous earth to remove the AgCl

and the solvent was removed by reduced pressure. The product was extracted with pentane and purified by column chromatography with pentane as eluent. The solvent was removed *in vacuo*, yielding a colorless solid (232 mg, 99.9 µmol, 26%), which is probably sensitive towards light and heat. The product must be stored at $T = -20\ °C$ in the absence of light.

^{1}H NMR (600 MHz, dichloromethane-d_2): $\delta = 7.47$ (s, 1H, *para*-H), 7.42 (s, 2H, *meta*-H), 1.30 (s, 18H, ^{t}Bu) ppm.

^{13}C{^{1}H} NMR (151 MHz, dichloromethane-d_2): $\delta = 168.8$ (d, $^1J_{C,P} = 46.9$ Hz, CP), 151.4 (s, *meta*-C), 129.0 (d, $^2J_{C,P} = 19.9$ Hz, *ipso*-C), 127.7 (d, $J_{C,P} = 8.2$ Hz, *ortho*-C), 124.9 (d, $J_{C,P} = 4.9$ Hz, *para*-C), 35.1 (s, $C(CH_3)_3$), 31.4 (s, $C(CH_3)_3$) ppm.

^{31}P NMR (243 MHz, dichloromethane-d_2): $\delta = -36.3$ (s) ppm.

*alternative unsuccessful attempt for **86** via Me$_3$SiOSiMe$_3$ elimination route*

Step 1: 3,5-di-*tert*-butylbenzoic acid (**87**)
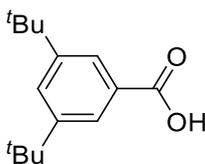
Note: Working under air, no inert technique required.

Potassium permanganate (24.2 g, 153 mmol, 2.48 eq) was portion-wise added over a period of 2 h to a mixture of 1,3-di-*tert*-butyl-5-methylbenzene (**82**, 12.6 g, 61.7 mmol, 1 eq), pyridine (33.9 ml, 420 mmol, 6.82 eq), potassium hydroxide (5.3 g, 94.0 mmol, 1.54 eq) and water (12 ml, 0.6 mmol, 0.01eq) at $T = 95\ °C$. After stirring at $T = 105\ °C$ overnight, the cold reaction mixture was filtrated and the residue in the filter was washed with aqueous KOH (2 N) and water. The filtrate was acidified with sulfuric acid and extracted with ether. The organic layer was separated, dried with MgSO$_4$, filtrated and concentrated to dryness by rotary evaporation. The residue was recrystallized from an ethanol-water solution, yielding a colorless solid (1.60 g, 6.8 mmol, 11%).[360-361]

Note: The product is water soluble, whereas the starting material is not.

^{1}H NMR (400 MHz, chloroform-d_1): $\delta = 7.99$ (d, $^3J_{H,H} = 1.94$ Hz, 2H, *ortho*-H), 7.69 (t, $^3J_{H,H} = 1.80$ Hz, 1H, *para* -H), 1.37 (s, 18H, ^{t}Bu) ppm.

^{13}C{^{1}H} NMR (101 MHz, chloroform-d_1): $\delta = 150.8$ (s, *meta*-C), 137.0 (*ipso*-C), 123.5 (s, o*rtho*-C), 119.5 (*para*-C), 34.9 (s, $C(CH_3)_3$), 31.7 (s, $C(CH_3)_3$) ppm.

Step 2: 3,5-di-*tert*-butylbenzoyl chloride (**88**)
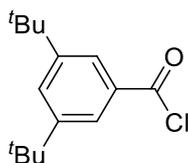
3,5-di-*tert*-butylbenzoic acid (**87**, 1.60 g, 6.83 mmol, 1 eq) was heated under reflux in an excess of thionyl chloride (20 ml) with some drops DMF (0.1 ml) for overnight. After removal of all solvents *in vacuo*, the colorless product was obtained in approximate quantitative yields and used without further purifications.[362]

^{1}H NMR (400 MHz, chloroform-*d$_1$*): δ = 7.97 (d, $^3J_{H,H}$ = 1.81 Hz, 2H, *ortho*-H), 7.79 (t, $^3J_{H,H}$ = 1.78 Hz, 1H, *para* -H), 1.37 (s, 18H, *^{t}Bu) ppm.

Step 3: 3,5-di-(*tert*-butyl)phenylphosphaalkyne (**86**)
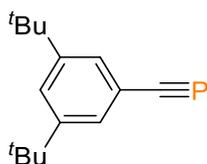
3,5-di-*tert*-butylbenzoyl chloride (**88**, 1 eq) was added to the solution of LiP(SiCH$_3$)$_2$ (1 eq) in THF at rt, T = 0 °C or T = -40 °C. The reaction mixture turned fist yellow and finally red while warming to rt. The ^{31}P NMR showed a triplet (J = 2.8 Hz) at 62 ppm. No product was formed and the observed species could not be identified.

3,5-di-*tert*-butylbenzoyl chloride (**88**, 1 eq) was added to the solution of P(SiCH$_3$)$_3$ (1 eq) in THF at rt, T = 0 °C or T = -40 °C. The reaction mixture turned yellow while reaching rt. The ^{31}P NMR showed two signals at 126 and 123 ppm, which probably indicated the formation of the two E-/Z-Isomers (see below). Addition of bases like NaOH to convert to the desired product failed. However, treating the reaction mixture with NaOH changed the color to red and yields the same ^{31}P signal as for the reaction with LiP(SiCH$_3$)$_2$.
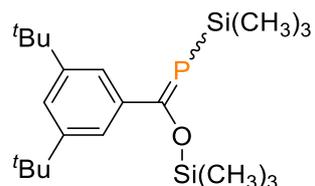
Performing both reactions in toluene instead of THF gave the same outcome.

2,4,6-tris(trifluoromethyl)phenylphosphaalkyne (92)
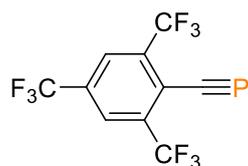
Step 1: 2,4,6-tris(trifluoromethyl)benzoic acid (**90**)
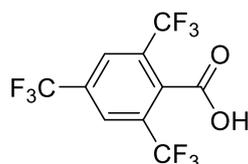
1,3,5-tris(trifluoromethyl)benzene (**89**, 5.00 g, 17.7 mmol, 1.0 eq) was diluted in diethyl ether (5 ml). After cooled to T = -10 °C, nBuLi (10.6 ml, 26.6 mmol, 1.5 eq) was added dropwise to the solution and stirred at T = -5 °C for 1 h. Subsequently, CO_2 was bubbled through the reaction mixture for 30 min by warming dry ice in a separate flask and transferring the gas through a pipe filled with $CaCl_2$ (10 cm) to the reaction flask. Aqueous HCl (5 ml, 6 M) was added to the reaction solution at T = 0 °C and stirred for around 10 min. The organic layer was separated and the water phase washed with ethyl acetate (3x 10 ml). The combined organic phases were dried with $NaSO_4$, filtrated and the solvent removed *in vacuo*. After washing of the residue with hexane, the product was obtained as colorless oil (1.82 g, 5.58 mmol, 32%).[366]

^{1}H NMR (400 MHz, chloroform-d_1): δ = 8.20 (s, 2H, *meta*-H) ppm.

^{19}F{^{1}H} NMR (377 MHz, chloroform-d_1): δ = 59.8 (s, 6F, *ortho*-CF$_3$), 63.4 (s, 3F, *para*-CF$_3$) ppm.

Step 2: 2,4,6-tris(trifluoromethyl)benzoyl chloride (**91**)
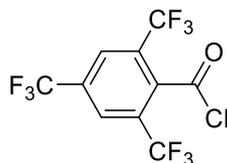
2,4,6-tris(trifluoromethyl)benzoic acid (**90**, 1.80 g, 5.51 mmol, 1.0 eq) was suspended in tetrachloromethane (3 ml) and cooled to T = 0 °C. Phosphorus pentachloride (1.43 g, 6.89 mmol, 1.25 eq) was added to the suspension. The reaction mixture was first stirred at T = 0 °C for 45 min, then at rt for 15 min and finally at T = 80 °C for 1 h. The tetrachloromethane was removed by applying static vacuum at T = 55 °C and collected in a

cooling trap with the purpose to reuse it. The product was obtained as a colorless, crystalline solid (1.09 g, 3.15 mmol, 57%).[528]

^{1}H NMR (400 MHz, dichloromethane-d_2): δ = 8.27 (s, 2H, *meta*-H) ppm.

^{19}F{^{1}H} NMR (377 MHz, dichloromethane-d_2): δ = 58.7 (s, 6F, *ortho*-CF$_3$), 63.9 (s, 3F, *para*-CF$_3$) ppm.

Step 3: 2,4,6-tris(trifluoromethyl)phenylphosphaalkyne (**92**)
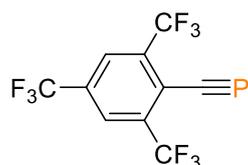
The 2,4,6-tris(trifluoromethyl)benzoyl chloride (**91**, 1 eq) was transferred to a Young NMR or Schlenk tube and dissolved in THF or toluene. The phosphorus source (LiP(SiCH$_3$)$_2$ or P(SiCH$_3$)$_3$) was added at T = -15, 0, rt, 50, 70 or 100 °C. The potential product was spotted by ^{31}P NMR at 94.5 ppm (nearly matching the calc. value 108.5 ppm), but not isolated. The best results were obtained with LiP(SiCH$_3$)$_2$ from T = -15 °C up to 50 °C.

*It is assumed that **92** can be extracted together with the solvent (like **53**) from the reaction mixture to the cooling trap under reduced pressure. However, all isolation attempts failed.*

1,4-bis(phosphaethynyl)durene (97)
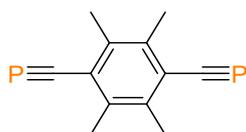
Step 1: 1,4-bis(chloromethyl)-2,3,5,6-tetramethylbenzene (**94**)
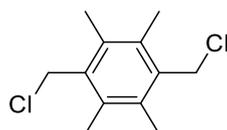
Note: Working under air, no inert technique required.

1,2,4,5-Tetramethylbenzene (Durene, **93**, 50.0 g, 372 mmol, 1 eq) was suspended in glacial acetic acid (150 ml) together with paraformaldehyde (33.6 g, 1.12 mol, 3 eq). After addition of aqueous HCl (conc. 37%, 149 ml, 1.79 mol, 4.8 eq), the suspension was stirred at T = 120 °C for 60 h. The resulting black solution was decanted from the colorless waxy solid. The

remaining waxy solid was crushed and mixed with the same amount of glacial acetic acid, paraformaldehyde and aqueous HCl. This time, additional zinc chloride (52.0 g, 382 mmol) was added as a catalyst. After stirring at $T = 120$ °C for 16 h, the reaction mixture was filtrated. The residue in the filter was washed with water until it became colorless. The solid was recrystallized from DCM (800 ml, $T = 40$ °C to -20 C), yielding thin colorless needles (81.7 g, 95%).

^{1}H NMR (400 MHz, benzene-d_6): δ = 4.28 (s, 4H, CH$_2$Cl), 1.99 (s, 12H, CH$_3$) ppm.

Step 2: 1,4-ClZnCH$_2$-2,3,5,6-tetramethylbenzene (**95**)
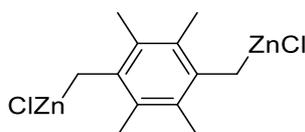
Note: The reaction was carried out at two different temperature, rt and $T = 75$ °C, with the same result. Hence, there is only one reaction described.

Zinc powder (5.66 g, 86.5 mmol, 8.0 eq) was suspended in DME (20 ml) and stirred/activated at rt by ultrasonication for 1 h. After addition of 1,4-bis(chloromethyl)-2,3,5,6-tetramethylbenzene (**94**, 2.50 g, 10.8 mmol, 1 eq) and DME (40 ml), the suspension was stirred for 16 h at $T = $ rt/75 °C. The reaction mixture was filtrated through diatomaceous earth to remove the excess of Zn and the precipitated colorless powder. The filtrate was used without further purification or isolation.

The same product was alternatively produced as LiCl adduct.

Zinc powder (2.83 g, 42.3 mmol, 4.0 eq) was suspended in DME (20 ml) and stirred/activated by ultrasonication for 16 h. After addition of DME (60 ml), Lithium chloride (1.83 g, 43.3 mmol, 4 eq) was added to the suspension and stirred for 10 min. 1,4-bis(chloromethyl)-2,3,5,6-tetramethylbenzene (**94**, 2.50 g, 10.8 mmol, 1 eq) was partly dissolved in toluene (80 ml) and portion-wise added to the reaction mixture. The zinc powder was slowly consumed over a period of 16 h, while colorless powder precipitated. The reaction mixture was filtrated through diatomaceous earth to remove the excess of Zn and the precipitated white powder. The filtrate was analyzed by ^{1}H NMR and used without further purification or isolation.

^{1}H NMR (400 MHz, benzene-d_6): δ = 3.06 (s, 4H, CH$_2$Cl), 1.99 (s, 12H, CH$_3$) ppm.

1,3,5-tris(phosphaethynyl)mesitylene (105)
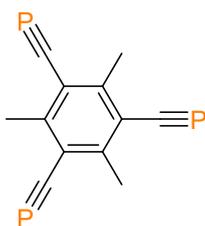
Step 1: 1,3,5-tris(chloromethyl)-2,4,6-trimethylbenzene (**98**)
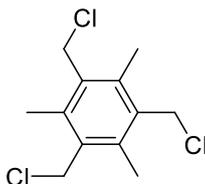
Note: Working under air, no inert technique required.

Mesitylene (**60**, 27.8 ml, 24.2 g, 201 mmol, 1 eq) was suspended in glacial acetic acid (120 ml) together with paraformaldehyde (24.2 g, 805 mol, 4 eq). After addition of aqueous HCl (conc. 37%, 120 ml) the solution was stirred at T = 30 °C for 72 h. The resulting pale-yellow solution was decanted from the colorless waxy solid. The remaining waxy solid was crushed and mixed with the same amount of glacial acetic acid, paraformaldehyde and aqueous HCl. These steps were repeated three times until the ^{1}H NMR only shows the product compound. The reaction mixture was filtrated and the residue in the filter was washed with water (3x 100 ml) and pentane (2x 20 ml). Drying of the solid *in vacuo* yielded a colorless powder (48.0 g, 181 mmol, 90%).

^{1}H NMR (400 MHz, chloroform-d_1): δ = 4.67 (s, 3H, Ar-H), 2.49 (s, 2H, CH$_2$), 2.40 (s, 4H, CH$_2$) ppm.

Step 2: 1,3,5-tris(iodomethyl)-2,4,6-trimethylbenzene (**99**)
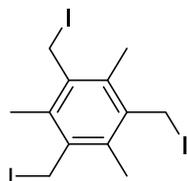
1,3,5-tris(chloromethyl)-2,4,6-trimethylbenzene (**98**, 5.0 g, 18.8 mmol, 1 eq) was mixed with sodium iodide (11.3 g, 75.3 mmol, 4 eq) in acetone (188 ml) and stirred at rt for 16 h. The suspension was filtrated and the solvent was removed from the filtrate by rotary evaporation. The residue was dissolved in ethyl acetate (100 ml) and washed with water (2x 50 ml). The organic phase was dried with MgSO$_4$, filtrated and the solvent removed under reduced

pressure. The crude product was purified by column chromatography (hexane: ethyl acetate, 1:1), yielding a slightly yellow solid (1.03 g, 1.91 mmol, 10%).

¹H NMR (400 MHz, chloroform-*d₁*): δ = 4.44 (s, 3H, Ar-H), 2.29 (s, 2H, CH_2), 2.28 (s, 4H, CH_2) ppm.

Step 3: 1,3,5-XMCH$_2$-2,4,6-trimethylbenzene (**100 - 103**)

100 M = Mg, X = Cl
101 M = Mg, X = I
102 M = Zn, X = Cl
103 M = Zn, X = I
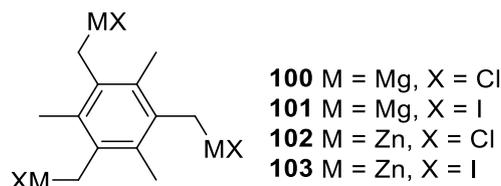
Either **98** (2.5 g, 9.41 mmol, 1 eq) or **99** (500 mg, 926 µmol, 1 eq) was added to a suspension of either activated magnesium (9 eq) (by stirring) or activated zinc (9 eq) (by ultrasonication) in DME (100 ml for **98**, 20 ml for **99**) at rt. The reaction mixture was heated to reflux for 24 h. After cooling to rt, the suspension was filtrated through diatomaceous earth and the filtrate was directly used for the next step without further purification or analysis.

Step 4: ((2,4,6-trimethylbenzene-1,3,5-triyl)tris(methylene))tris(dichlorophosphane) (**104**)
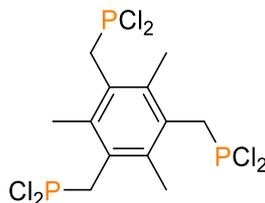
100 - 103 were treated with PCl₃, however only in the case of **101** relevant ³¹P signals could be observed and is described here.

Phosphorus trichloride (1.91 g, 13.9 mmol, 15 eq) was diluted with DME (6 ml) and cooled to T = 0 °C. The Grignard solution (**101**) was added dropwise to the solution. After completed addition, the reaction mixture was heated to reflux for 24 h. The solvent was removed at rt under reduced pressure. The residue was dissolved in toluene (3 ml) and analyzed by ³¹P NMR. The four signals were observed, two of them (183.0, 182.9 ppm) might fit to the expected signal for the product (calc. 184.5 ppm). The solvent was removed, the residue dissolved in pentane and filtrated through silica. Further analysis of the liquid did not show any ³¹P signals.

³¹P NMR (162 MHz, toluene): δ = 183.0 (s), 182.9 (s), 176.9 (s, PI₃), -9.7 (s) ppm.

4.2.5 Preparation of phosphinines

2-mesitylphosphinine (110)
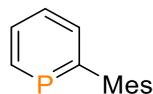
Mesitylphosphaalkyne (**68**, 30 mg, 165 µmol, 1 eq) was added together with 2-pyrone (60 ml, excess) to a Young NMR tube filled with toluene (1 ml) and heated to T = 100 °C for 3 days. The solvent was removed *in vacuo* and the product extracted with pentane from the red residue. The pentane phase was filtered through a silica plug (glass pipette). The solvent was removed under reduced pressure and the colorless residue was dissolved in benzene-d_6.

^{1}H NMR (400 MHz, benzene-d_6): $δ$ = 8.71-8.59 (m, 1H, $J_{H,P}$ = 38.22 Hz, Ar-H), 7.44-7.14 (m, 3H, $J_{H,P}$ = 58.77 Hz, $J_{H,P}$ = 18.08 Hz, Ar-H), 6.86 (sept, 2H, Ar-H), 2.10 (s, 3H, CH$_3$), 2.04 (s, 6H, CH$_3$) ppm.

^{31}P NMR (162 MHz, benzene-d_6): $δ$ = 208.9 (br) ppm.

2-bromo-6-mesitylphosphinine (111) & 3-bromo-2-mesitylphosphinine (111a)

Mesitylphosphaalkyne (**68**, 42 mg, 231 µmol, 1 eq) was added together with 3-bromopyrone (excess) to a Young NMR tube filled with toluene (1 ml) and heated to T = 100 °C for 2 days. The solvent was removed *in vacuo* and the product extracted with pentane from the red residue. The pentane phase was filtered through a silica plug (glass pipette). The solvent was removed by reduced pressure and the colorless residue was dissolved in benzene-d_6.

^{1}H NMR (400 MHz, benzene-d_6): $δ$ = 8.43-8.31 (m, 1H, $J_{H,P}$ = 38.79 Hz, Ar-H), 7.68-7.55 (m, 2H, Ar-H), 7.06-6.95 (m, 2H, Ar-H), 6.85 (br, 3H, Ar-H), 6.78 (br, 2H, Ar-H), 6.78-6.72 (m, 1H, Ar-H), 2.02 (s, 6H, CH$_3$), 1.92 (s, 12H, CH$_3$) ppm (signals for a mixture of **111** & **111a**).

^{31}P NMR (162 MHz, benzene-d_6): $δ$ = 221.8 (d (br), $J_{P,H}$ = 37.1 Hz, **111a**), 208.3 (br, **111**) ppm.

2-(triphenylsilyl)phosphinine (112)
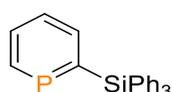
Triphenylsilylphosphaalkyne (**58**, 72 mg, 238 µmol, 2.86 eq) was stirred together with 2-pyrone (8 mg, 83.3 µmol, 1.0 eq) in diglyme (5 ml) at T = 130 °C for 16 h. The reaction mixture was purified by column chromatography (silica, eluent hexane/ethyl acetate (1:1)).

^{31}P{^{1}H} NMR (162 MHz, toluene): δ = 239.6 (s) ppm.

2-(triphenylsilyl)phosphinine (114)
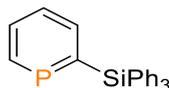
Triphenylsilylphosphaalkyne (**58**, 64 mg, 210 µmol, 4.0 eq) was stirred together with 2-pyrone (10 mg, 52.6 µmol, 1.0 eq) in diglyme (5 ml) at T = 130 °C for 16 h. The reaction mixture was purified by column chromatography (silica, eluent hexane/ethyl acetate (1:1)).

^{31}P{^{1}H} NMR (162 MHz, toluene): δ = 237.4 (s) ppm.

4.2.6   Preparation of triazaphospholes

5-mesityl-3-phenyl-3*H*-1,2,3,4-triazaphosphole (120)
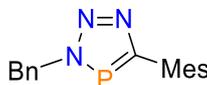
Mesitylphosphaalkyne (**68**, 0.86 ml of 0.144 m in THF, 20 mg, 123 µmol, 1 eq) was added together with benzylazide (**117**, 0.33 ml of 0.376 m in THF 16.4 mg, 124 µmol, 1 eq) to a Young NMR tube filled with THF (1 ml). After 2 days at rt the THF solution was concentrated by reduced pressure and pentane was added dropwise until colorless solid precipitated. The solid was washed with pentane, dried *in vacuo* and dissolved in THF-d$_8$.

^{1}H NMR (400 MHz, tetrahydrofuran-*d$_8$*): δ = 7.40-7.28 (m, 5H, Ar-H of Ph), 6.93 (s, 2H, Ar-H of Mes), 5.87 (dd, J = 6.79, 3.18 Hz, 2H, CH$_2$), 2.28 (s, 3H, *para*-CH$_3$ of Mes), 2.05 (s, 6H, *ortho*-CH$_3$ of Mes) ppm.

^{13}C{^{1}H} NMR (151 MHz, tetrahydrofuran-*d$_8$*): δ = 128.8 (d, $^{1}J_{C,P}$ = 24.4 Hz, CP), 129.8 (s, 2C, Ar-C of Mes), 129.4, 129.2 (s, 5C, Ar-C of Ph), 56.7 (d, $^{1}J_{C,P}$ = 12.4 Hz, CH$_2$), 21.6 (s, 2C, *ortho*-CH$_3$), 21.3 (s, *para*-CH$_3$) ppm.

**^{31}P{^{1}H} NMR (162 MHz, tetrahydrofuran-*d$_8$*)**: δ = 177.4 (s) ppm.

3,5-Dimesityl-3*H*-1,2,3,4-triazaphosphol (121)
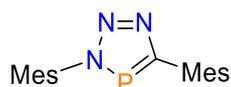
Mesitylphosphaalkyne (**68**, 30 mg, 185 µmol, 1 eq) was added together with mesitylazide (**118**, 30 mg, 185 µmol, 1 eq) to a Young NMR tube filled with toluene (1 ml). After 3 days at rt the solvent was removed by reduced pressure and the residue washed with pentane (3x 4 ml), yielding a colorless solid.

¹H NMR (400 MHz, dichloromethane-*d₂*): δ = 7.07 (s, 2H, Ar-H), 7.02 (s, 2H, Ar-H), 2.39 (s, 3H, *para*-CH₃), 2.35 (s, 6H, *ortho*-CH₃), 2.15 (s, 3H, *para*-CH₃), 2.01 (s, 6H, *ortho*-CH₃) ppm.

¹³C{¹H} NMR (151 MHz, dichloromethane-*d₂*): δ = 182.3 (d, $^1J_{C,P}$ = 51.1 Hz, CP), 140.0, 138.8, 137.4, 137.3, 136.2 (d, $J_{C,P}$ = 6.9 Hz), 135.3 (d, J_{CP} = 1.6 Hz), 129.5, 128.9, 21.3, 21.2, 21.2, 17.6. ppm.

³¹P NMR (162 MHz, dichloromethane-*d₂*): δ = 182.8 (s) ppm.

3-phenyl-5-triisopropylphenyl-3*H*-1,2,3,4-triazaphosphole (122)
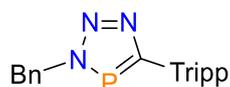
TrippCP (**81**, 1 eq) and benzylazide (**117**, excess) were added to a Young NMR tube filled with benzene-d₆ (1 ml). After succeeded reaction at rt overnight, the NMR spectra were measured. The product was not isolated.

¹H NMR (400 MHz, tetrahydrofuran-*d₈*): δ = 7.21 (s, 2H, Ar-H of Tripp), 7.08-6.96 (m, 5H, Ar-H of Ph), 5.29 (d, J = 6.56 Hz, 2H, CH₂), 3.23 (sept, $^3J_{H,H}$ = 6.86 Hz, 1H, *para*-C*H*(CH₃)₂), 2.9 (sept, $^3J_{H,H}$ = 6.96 Hz, 2H, *ortho*-C*H*(CH₃)₂), 1.19 (d, $^3J_{H,H}$ = 6.88 Hz, 12H, *para*-CH(C*H₃*)₂), 1.14 (d, $^3J_{H,H}$ = 7.08 Hz, 6H, *ortho*-CH(C*H₃*)₂) ppm.

³¹P{¹H} NMR (162 MHz, benzene-*d₆*): δ = 179.4 (s) ppm.

3-mesityl-5-triisopropylphenyl-3*H*-1,2,3,4-triazaphosphole
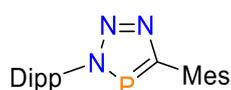
TrippCP (**68**, 1 eq) and 2,6-diisopropylphenylazide (**119**, 1 eq) were added to a Young NMR tube filled with THF (1 ml). After succeeded reaction at rt overnight, the NMR spectra were measured. The product was not isolated.

^{31}P{^{1}H} **NMR (162 MHz, tetrahydrofuran)**: δ = 185.3 (s) ppm.

3-(2,6-diisopropylphenyl)-5-triisopropylphenyl-3*H*-1,2,3,4-triazaphosphole (123)
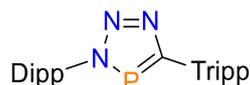
TrippCP (**81**, 1 eq) and 2,6-diisopropylphenylazide (**119**, excess) were added to a Young NMR tube filled with THF (1 ml). After succeeded reaction at rt overnight, the NMR spectra were measured. The product was not isolated.

^{31}P{^{1}H} **NMR (162 MHz, tetrahydrofuran)**: δ = 187.5 (s) ppm.

5-((3,5-di-*tert*-butyl)phenyl)-3-triisopropylphenyl-3*H*-1,2,3,4-triazaphosphole (124)
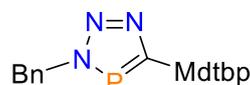
MdtbpCP (**86**, 1 eq) and benzylazide (**117**, excess) were added to a Young NMR tube filled with THF (1 ml). After succeeded reaction at rt overnight, the NMR spectra were measured. The product was not isolated.

^{31}P{^{1}H} **NMR (162 MHz, tetrahydrofuran)**: δ = 172.1 (s) ppm.

5-((3,5-di-*tert*-butyl)phenyl)-3-triisopropylphenyl-3*H*-1,2,3,4-triazaphosphole (124)
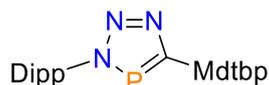
MdtbpCP (**86**, 1 eq) and 2,6-diisopropylphenylazide (**119**, excess) were added to a Young NMR tube filled with THF (1 ml). After succeeded reaction at rt overnight, the NMR spectra were measured. The product was not isolated.

^{31}P{^{1}H} **NMR (162 MHz, tetrahydrofuran)**: δ = 178.5 (s) ppm.

4.2.7 Preparation of 1,2,4-triphospholes

Cesium 3,5-mesityl-1,2,4-triphospholide
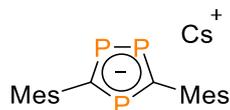
Method A: 2,4,6-trimethylbenzoyl chloride (**63**, 0.23 ml, 250 mg, 1.37 mmol, 1 eq) and P(SiMe$_3$)$_3$ (**64**, 0.40 ml, 343 mg, 1.40 mmol, 1 eq) were added to a suspension of CsF (478 mg, 2.3 eq) in 1,4-dioxane (7 ml) and stirred at $T = 90\ °C$ for 20 days. After 15 days the strong yellow suspension turned red.

Method B: Mesitylphosphaalkyne (**68**, 0.5 ml of 0.244 M in toluene, 20 mg, 123 µmol, 1 eq) and P(SiMe$_3$)$_3$ (**64**, 0.035 ml, 31 mg, 123 µmol, 1 eq) were added to a suspension of CsF (43.1 mg, 2.3 eq) in 1,4-dioxane (2 ml) and stirred at $T = 90\ °C$ for 5 days. The solvent was removed *in vacuo* and the red residue was washed with a THF-pentane (1:8) solution (3x 1 ml). Removing the solvent under reduced pressure yielded an orange-red powder.

^{1}H NMR (400 MHz, tetrahydrofuran-d_8): δ = 6.74 (s, 4H, *meta*-CH), 2.17 (s, 6H, CH$_3$), 2.12 (s, 12H, CH$_3$) ppm.

^{13}C{^{1}H} NMR (151 MHz, tetrahydrofuran-d_8): δ = 190.6 (m, C$_{heterocycle}$), 145.2 (m, *ipso*-C), 137.4 (*ortho*-C), 132.8 (s, *para*-C), 127.8 (s, *meta*-CH), 22.9 (s, CH$_3$), 21.3 (s, CH$_3$) ppm.

^{31}P{^{1}H} NMR (162 MHz, tetrahydrofuran-d_8): δ = 264.8 (d, $^2J_{P,P}$ = 38.0 Hz, 2P), 256.6 (d, $^2J_{P,P}$ = 37.9 Hz, 2P) ppm.

4.2.8 Cyclooligomerization reactions of phosphaalkynes on metal(0) precursors

[{η^4-1,3-(Mes)$_2$P$_2$}W(CO)$_3$] (136)
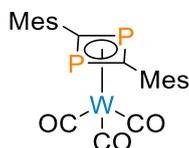
Mesitylphosphaalkyne (**68**, 0.32 ml of 0.252 M in THF, 10 mg, 62.0 µmol, 2.0 eq) was added at rt to a THF (2 ml))solution of [W(CO$_5$)(thf)] (0.6 ml of 0.102 M in THF). The strong yellow solution turned immediately red. After two weeks at rt the sample was heated to $T = 65\ °C$ for 10 days.

^{31}P NMR (202 MHz, tetrahydrofuran): δ = 57.7 (s) ppm.

## [{η^4-1,3-(Tripp)$_2$P$_2$}W(CO)$_3$] (137)
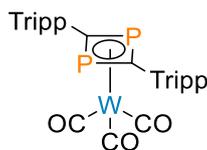
TrippCP (**81**, 0.75 ml of 0.213 M in THF, 39 mg, 122 µmol, 2.0 eq) was added at rt to a THF (3 ml) solution of [W(CO$_5$)(thf)] (1.19 ml of 0.102 M in THF). The strong yellow solution turned immediately dark red. After two weeks at rt the sample was heated to T = 65 °C for 10 days.

^{31}P NMR (202 MHz, tetrahydrofuran): δ = 69.1 (s) ppm.

[{η^4-1,3-(Mes)$_2$P$_2$}Fe(CO)$_3$] (140)
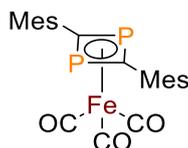

Mesitylphosphaalkyne (**68**, 1.0 ml of 0.251 M in THF, 40.7 mg, 251 µmol, 2.5 eq) was added at T = -40 °C to a solution of [Fe(CO$_3$)(coe)$_2$] (1.6 ml of 0.06 M in pentane). The green reaction mixture was stirred at T = -20 °C for 2 h until it was allowed to warm to rt. The solvent was removed *in vacuo* and the solid residue was sublimed at T = 140 °C at p = 1x10^{-3} mbar. The orange solid was dissolved in THF. Slow evaporation of the solvent yielded orange crystals suitable for XRD measurement and compared with the crystals found in the database (CCDC: 234605, CSD: OBOBEN).

^{1}H NMR (600 MHz, tetrahydrofuran-d_8): δ = 6.51 (s, 4H, *meta*-CH), 2.31 (s, 12H, *ortho*-CH$_3$), 1.96 (s, 6H, *para*-CH$_3$) ppm.

^{31}P NMR (202 MHz, tetrahydrofuran-d_8): δ = 76.9 (s) ppm.

[{η^4-1,3-(Tripp)$_2$P$_2$}Fe(CO)$_3$] (141)
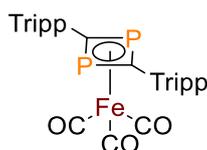
TrippCP (**81**, 0.96 ml of 0.193 M in THF, 45.6 mg, 185 µmol, 2.5 eq) was added at T = -50 °C to a solution of [Fe(CO$_3$)(coe)$_2$] (1.16 ml of 0.06 M in pentane). The green reaction mixture was stirred at T = -50 °C for 2 h until it was very slowly allowed to warm to rt. The solvent was

removed *in vacuo* and the solid residue was sublimed at $T = 50 - 180\ °C$ at $p = 1\times10^{-3}$ mbar. The red solid was dissolved in THF.

^{31}P NMR (162 MHz, tetrahydrofuran): $\delta = 109.1$ (s, crude product) ppm.

### 4.2.9   Preparation of phosphaalkyne platinum(0) complexes

General synthesis for the *π*-complexes
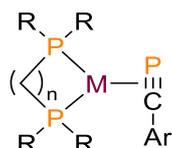
The reactions to produce the *π*-complexes were performed in an argon filled glovebox equipped with a freezer ($T = -25\ °C$). Ni(COD)$_2$ or Pt(COD)$_2$ (10-50 mg, 1 eq) was added into a scintillation vial and dissolved in THF (2-8 ml) with vigorous stirring. Addition of a (di)phosphine solution (0.2 M in THF, 1 eq) results in a significant color change to yellow/orange after several seconds. The reaction mixture was stirred at rt for at least 30 minutes. The formation of the [((di)phosphine)M(COD)] can be monitored by ^{31}P{^{1}H} NMR spectroscopy. Once complete conversion is achieved, the reaction mixture was cooled to $T = -25\ °C$. A chilled solution of phosphaalkyne (0.2 M in THF, $T = -25\ °C$, 1 eq) was added dropwise to the reaction mixture over 5 - 10 min. The reaction solution was allowed to warm to rt and stirred overnight. The solvent was removed under reduced pressure, yielding the product as yellow to red powders (quantitative conversion by NMR).

If necessary, the Pt complexes can be filtered through a Whatman glass paper filter, whereas the Ni complexes can be filtered through diatomaceous earth to remove any polymeric particles from the phosphaalkyne excess. Traces of dippe or dcype can be removed by washing with *n*-pentane.

[(dippe)Ni(MesCP)] (142)
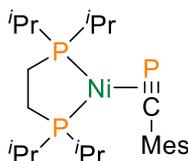
^{1}H NMR (600 MHz, tetrahydrofuran-d_8): $\delta = 6.71$ (s, 2H, *meta-H*-Mes), 2.18 (s, 3H, *para*-CH_3-Mes), 2.21 (ddt, $^2J_{H,P} = 14.5$ Hz, $^3J_{H,H} = 7.23$ Hz, $J = 3.01$ Hz, 2H, P-CH), 1.98 (s, 6H, *ortho*-CH_3-Mes), 1.92 (ddt, $^2J_{H,P} = 14.0$ Hz, $^3J_{H,H} = 6.94$ Hz, $J = 2.96$ Hz, 2H, P-CH), 1.69 (m, 4H, P-

CH_2), 1.27 (ddt, $^3J_{H,P}$ = 14.8 Hz, $^3J_{H,H}$ = 6.86 Hz, J = 2.78 Hz, 6H, CH_3 of ^{i}Pr), 1.11 (ddt, $^3J_{H,P}$ = 12.9 Hz, $^3J_{H,H}$ = 6.72 Hz, J = 2.79 Hz, 6H, CH_3 of ^{i}Pr), 0.98 (ddt, $^3J_{H,P}$ = 12.6 Hz, $^3J_{H,H}$ = 6.54 Hz, J = 2.75 Hz, 6H, CH_3 of ^{i}Pr), 0.77 (ddt, $^3J_{H,P}$ = 14.9 Hz, $^3J_{H,H}$ = 6.92 Hz, J = 2.77 Hz, 6H, CH_3 of ^{i}Pr) ppm.

^{13}C{^{1}H} NMR (151 MHz, tetrahydrofuran-d_8): δ = 231.8 (dd, J = 80.1, 32.5, 4.7 Hz, CP), 149.7 (app. t, J = 6.7 Hz, Mes), 132.1 (Mes), 128.9 (Mes), 128.2 (Mes), 26.3 (ddd, J = 32.3, 17.1, 4.0 Hz), 22.7 (app. t, J = 20.4 Hz), 22.49, 22.45 (app. t, J = 17.8 Hz), 21.3, 20.1 (d, J = 5.0 Hz), 19.5, 19.4 (d, J = 6.9 Hz), 18.9 ppm.

^{31}P{^{1}H} NMR (243 MHz, tetrahydrofuran-d_8): δ = 172.6 (d, $^2J_{P,P}$ = 16.4 Hz, CP), 82.2 (d, $^2J_{P,P}$ = 33.9 Hz, dippe), 71.8 (dd, $^2J_{P,P}$ = 33.9, 16.5 Hz, dippe) ppm.

HRMS (EI pos): m/z calc. for [$C_{24}H_{43}NiP_3$]: 482.1931; found: 482.1937

Elemental analysis for $C_{24}H_{43}NiP_3$: calc.: C: 59.65%, H: 8.97%; found: C: 59.67%, H: 8.99%

[(dippe)Pt(MesCP)] (143)
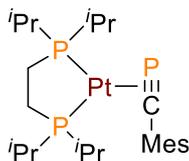
^{1}H NMR (600 MHz, tetrahydrofuran-d_8): δ = 6.76 (s, 2H, *meta*-H-Mes), 2.27 (s, 3H, *para*-CH_3-Mes), 2.22 (dq, $^2J_{H,P}$ = 14.2 Hz, $^3J_{H,H}$ = 7.16 Hz, 2H, P-CH), 2.03 (s, 6H, *ortho*-CH_3-Mes), 1.99 (dq, $^2J_{H,P}$ = 14.3 Hz, $^3J_{H,H}$ = 6.84 Hz, 2H, P-CH), 1.67 (m, 4H, P-CH_2), 1.25 (dd, $^3J_{H,P}$ = 15.7 Hz, $^2J_{H,H}$ = 7.03 Hz, 6H, CH_3 of ^{i}Pr), 1.08 (dd, $^3J_{H,P}$ = 13.9 Hz, $^2J_{H,H}$ = 7.04 Hz, 6H, CH_3 of ^{i}Pr), 0.93 (dd, $^3J_{H,P}$ = 13.7 Hz, $^2J_{H,H}$ = 6.89 Hz, 6H, CH_3 of ^{i}Pr), 0.74 (dd, $^3J_{H,P}$ = 16.0 Hz, $^2J_{H,H}$ = 7.17 Hz, 6H, CH_3 of ^{i}Pr) ppm.

^{13}C{^{1}H} NMR (151 MHz, tetrahydrofuran-d_8): δ = 232.7 (ddd, J = 83.1, 59.1, 8.7 Hz, CP), 148.9 (br. d, J = 7.2 Hz, Mes), 132.9 (Mes), 129.6 (Mes), 127.9 (Mes), 26.6 (ddd, J = 38.5, 22.1 3.6 Hz), 24.8 (ddd, J = 48.4, 26.6, 14.8 Hz), 21.9, 21.2, 20.2 (d, J = 5.5 Hz), 19.4, 18.9 (d, J = 6.1 Hz), 18.5 ppm.

^{31}P{^{1}H} NMR (243 MHz, tetrahydrofuran-d_8): δ = 140.5 (dd, $^2J_{P,P}$ = 29.2, 15.7 Hz, $^1J_{P,Pt}$ = 234 Hz, CP), 82.9 (dd, $^2J_{P,P}$ = 37.2, 15.7 Hz, $^1J_{P,Pt}$ = 3056 Hz, dippe), 74.0 (dd, $^2J_{P,P}$ = 37.1, 29.1 Hz, $^1J_{P,Pt}$ = 3211 Hz, dippe) ppm.

^{195}Pt{^{1}H} NMR (86 MHz, tetrahydrofuran-d_8): δ = -4611 (ddd, $^1J_{Pt,P}$ = 3211, 3056, 234 Hz) ppm.

**HRMS (EI pos)**: m/z calc. for [$C_{24}H_{43}P_3Pt$]: 619.2226; found: 619.2203

Elemental analysis for $C_{24}H_{43}P_3Pt$: calc.: C: 46.52%, H: 7.00%; found: C: 46.76%, H: 7.04%

[(dippe)Pt(TrippCP)] (144)
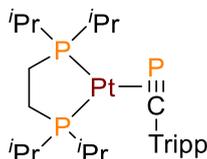
$^{31}P\{^1H\}$ NMR (162 MHz, tetrahydrofuran): δ = 145.8 (dd, $^2J_{P,P}$ = 28.7, 17.7 Hz, $^1J_{P,Pt}$ = 229 Hz, C*P*), 79.5 (dd, $^2J_{P,P}$ = 36.5, 16.7 Hz, $^1J_{P,Pt}$ = 3044 Hz, dippe), 70.7 (dd, $^2J_{P,P}$ = 36.5, 28.2 Hz, $^1J_{P,Pt}$ = 3213 Hz, dippe) ppm.

## [(dippe)Ni(Mes*CP)] (145)
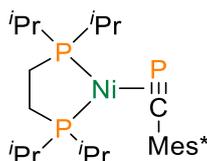
^1H NMR (600 MHz, tetrahydrofuran-d_8): δ = 7.17 (s, 2H, *meta-H*-Mes*), 2.24 (dq, $^2J_{H,P}$ = 14.3 Hz, $^3J_{H,H}$ = 7.21 Hz, 2H, P-C*H*), 1.91 (dq, $^2J_{H,P}$ = 13.9 Hz, $^3J_{H,H}$ = 6.95 Hz, 2H, P-C*H*), 1.62 (m, 4H, P-C*H*$_2$), 1.42 (s, 9H, *para*-C*H*$_3$-Mes*), 1.29 (s, 18H, *ortho*-C*H*$_3$-Mes*), 1.26 (dd, $^3J_{H,P}$ = 15.0 Hz, $^2J_{H,H}$ = 7.38 Hz, 6H, C*H*$_3$ of ^{i}Pr), 1.10 (dd, $^3J_{H,P}$ = 12.6 Hz, $^2J_{H,H}$ = 6.76 Hz, 6H, C*H*$_3$ of ^{i}Pr), 0.91 (dd, $^3J_{H,P}$ = 12.1 Hz, $^2J_{H,H}$ = 6.71 Hz, 6H, C*H*$_3$ of ^{i}Pr), 0.71 (dd, $^3J_{H,P}$ = 14.6 Hz, $^2J_{H,H}$ = 7.22 Hz, 6H, C*H*$_3$ of ^{i}Pr) ppm.

$^{13}C\{^1H\}$ NMR (151 MHz, tetrahydrofuran-d_8): δ = 238.5 (dd, J = 71.9, 35.2 Hz, *C*P), 150.6 (app. t, J = 6.8 Hz, Mes*), 143.9 (Mes*), 140.8 (Mes*), 121.1 (Mes*), 38.3, 35.4, 32.9, 26.4 (dd, J = 17.9, 3.4), 22.1 (app. t, J = 16.2 Hz), 21.9 (app. t, J = 20.9 Hz), 20.1 (d, J = 3.9 Hz), 20.0 (d, J = 5.9 Hz), 19.4, 18.6 ppm.

$^{31}P\{^1H\}$ NMR (243 MHz, tetrahydrofuran-d_8): δ = 156.3 (d, $^2J_{P,P}$ = 14.8 Hz, C*P*), 80.1 (d, $^2J_{P,P}$ = 37.8 Hz, dippe), 60.5 (dd, $^2J_{P,P}$ = 37.8, 14.8 Hz, dippe) ppm.

HRMS (EI pos): m/z calc. for [$C_{33}H_{61}NiP_3$]: 608.3340; found: 608.3325

Elemental analysis for $C_{33}H_{61}NiP_3$: calc.: C: 65.03%, H: 10.09%; found: C: 63.53%, H: 9.61%

[(dippe)Pt(Mes*CP)] (146)
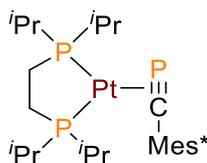
¹H NMR (600 MHz, tetrahydrofuran-d_8): δ = 7.23 (s, 2H, *meta-H*-Mes*), 2.22 (dq, $^2J_{H,P}$ = 14.0 Hz, $^3J_{H,H}$ = 6.99 Hz, 2H, P-C*H*), 1.96 (dq, $^2J_{H,P}$ = 14.1 Hz, $^3J_{H,H}$ = 7.23 Hz, 2H, P-C*H*), 1.62 (m, 4H, P-C*H₂*), 1.42 (s, 9H, *para*-C*H₃*-Mes*), 1.30 (s, 18H, *ortho*-C*H₃*-Mes*), 1.25 (dd, $^3J_{H,P}$ = 15.7 Hz, $^2J_{H,H}$ = 7.05 Hz, 6H, C*H₃* of ^{i}Pr), 1.07 (dd, $^3J_{H,P}$ = 14.0 Hz, $^2J_{H,H}$ = 7.00 Hz, 6H, C*H₃* of ^{i}Pr), 0.89 (dd, $^3J_{H,P}$ = 13.2 Hz, $^2J_{H,H}$ = 6.97 Hz, 6H, C*H₃* of ^{i}Pr), 0.66 (dd, $^3J_{H,P}$ = 15.9 Hz, $^2J_{H,H}$ = 7.15 Hz, 6H, C*H₃* of ^{i}Pr) ppm.

¹³C{¹H} NMR (151 MHz, tetrahydrofuran-d_8): δ = 232.7 (m, *C*P), 150.6 (br. m, Mes*), 144.7 (Mes*), 141.9 (Mes*), 121.8 (Mes*), 38.4, 35.2, 32.9, 26.7 (dd, J = 23.1, 3.2), 24.6 (dd, J = 25.7, 13.0 Hz), 23.9 (dd, J = 26.9, 15.7 Hz), 20.0 (d, J = 4.8 Hz), 19.32, 19.26 (d, J = 5.9 Hz), 18.1 ppm.

³¹P{¹H} NMR (243 MHz, tetrahydrofuran-d_8): δ = 126.5 (dd, $^2J_{P,P}$ = 28.8, 18.7 Hz, $^1J_{P,Pt}$ = 167 Hz, C*P*), 78.0 (dd, $^2J_{P,P}$ = 39.0, 18.7 Hz, $^1J_{P,Pt}$ = 3036 Hz, dippe), 65.5 (dd, $^2J_{P,P}$ = 39.0, 28.8 Hz, $^1J_{P,Pt}$ = 3283 Hz, dippe) ppm.

¹⁹⁵Pt{¹H} NMR (86 MHz, tetrahydrofuran-d_8): δ = -4576 (ddd, $^1J_{Pt,P}$ = 3283, 3036, 167 Hz) ppm.

HRMS (EI pos): m/z calc. for [$C_{33}H_{61}P_3Pt$]: 745.3634; found: 745.3694

Elemental analysis for $C_{33}H_{61}P_3Pt$: calc.: C: 53.14%, H: 8.24%; found: C: 50.74%, H: 7.62%

[(dcpe)Ni(MesCP)] (147)
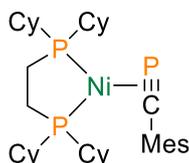
¹H NMR (400 MHz, tetrahydrofuran-d_8): δ = 6.75 (s, 2H, *meta-H*-Mes), 2.20 (s, 3H, *para*-C*H₃*-Mes), 1.99 (s, 6H, *ortho*-C*H₃*-Mes), 1.79-0.69 (m, 48H, P-C*H*, P-C*H₂*, Cy) ppm.

³¹P{¹H} NMR (162 MHz, tetrahydrofuran-d_8): δ = 169.6 (d, $^2J_{P,P}$ = 16.9 Hz, C*P*), 70.4 (d, $^2J_{P,P}$ = 35.6 Hz, dcpe), 62.2 (dd, $^2J_{P,P}$ = 35.6, 16.4 Hz, dcpe) ppm.

[(dcpe)Pt(MesCP)] (148)
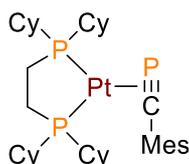
^{1}H NMR (600 MHz, tetrahydrofuran-d_8): $δ$ = 6.78 (s, 2H, *meta*-*H*-Mes), 2.29 (s, 3H, *para*-C*H$_3$*-Mes), 2.06 (s, 6H, *ortho*-C*H$_3$*-Mes), 1.97-0.73 (m, 48H, P-C*H*, P-C*H$_2$*, Cy) ppm.

^{13}C{^{1}H} NMR (151 MHz, tetrahydrofuran-d_8): $δ$ = 226.8 (m, *C*P), 148.9 (br. d, J = 6.7 Hz, Mes), 132.9 (Mes), 129.7 (Mes), 127.9 (Mes), 36.6 (dd, J = 22.9, 3.4 Hz), 36.0 (dd, J = 21.4, 3.6 Hz), 30.6 (d, J = 4.1 Hz), 30.0, 29.1, 28.9 (d, J = 4.8 Hz), 28.0 (app. dq, J = 29.5, 10.5 Hz), 27.4, 27.1, 26.6, 24.6 (m), 22.0, 21.2 ppm.

^{31}P{^{1}H} NMR (243 MHz, tetrahydrofuran-d_8): $δ$ = 140.0 (dd, $^2J_{P,P}$ = 29.5, 15.6 Hz, $^1J_{P,Pt}$ = 230 Hz, C*P*), 71.7 (dd, $^2J_{P,P}$ = 37.8, 14.5 Hz, $^1J_{P,Pt}$ = 3056 Hz, dcpe), 65.8 (dd, $^2J_{P,P}$ = 37.7, 29.4 Hz, $^1J_{P,Pt}$ = 3205 Hz, dcpe) ppm.

^{195}Pt{^{1}H} NMR (86 MHz, tetrahydrofuran-d_8): $δ$ = -4582 (ddd, $^1J_{Pt,P}$ = 3205, 3056, 230 Hz) ppm.

HRMS (EI pos): m/z calc. for [$C_{36}H_{59}P_3Pt$]: 779.3478; found: 779.3465

Elemental analysis for $C_{36}H_{59}P_3Pt$: calc.: C: 55.44%, H: 7.63%; found: C: 55.83%, H: 7.79%

[(dcpe)Ni(TrippCP)] (149)
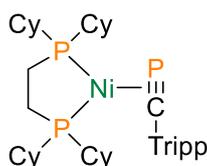
^{31}P{^{1}H} NMR (162 MHz, tetrahydrofuran): $δ$ = 171.1 (d, $^2J_{P,P}$ = 16.8 Hz, C*P*), 67.1 (d, $^2J_{P,P}$ = 32.6 Hz, dcpe), 59.6 (dd, $^2J_{P,P}$ = 32.7, 15.8 Hz, dcpe) ppm.

[(dcpe)Pt(TrippCP)] (150)
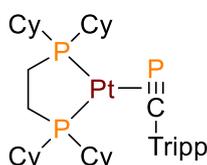
¹H NMR (600 MHz, tetrahydrofuran-*d₈*): δ = 6.94 (s, 2H, *meta*-*H*-Tripp), 3.21 (sept, $^3J_{H,H}$ = 6.87 Hz, 2H, *ortho*-C*H*-Tripp), 2.86 (sept, $^3J_{H,H}$ = 6.90 Hz, 1H, *para*-C*H*-Tripp), 1.20-1.38 (d, $^3J_{H,H}$ ~ 6.9 Hz, 18H, *ortho*&*para*-C*H₃*-Tripp), 2.05-0.76 (m, 48H, P-C*H*, P-C*H₂*, Cy) ppm.

¹³C{¹H} NMR (151 MHz, tetrahydrofuran-*d₈*): δ = 225.5 (ddd, J = 80.8, 59.5, 8.1 Hz, *C*P), 147.2 (br. d, J = 6.2 Hz, Tripp), 144.9 (Tripp), 141.0 (Tripp), 119.7 (Tripp), 36.9 (dd, J = 22.8, 3.0 Hz), 36.1 (dd, J = 20.7, 3.5 Hz), 35.5, 30.4 (d, J = 4.5 Hz), 30.1, 30.0, 29.6 (d, J = 4.0 Hz), 28.0 (m), 27.5, 27.0, 25.0 (dd, J = 27.4, 15.6 Hz), 24.4 (m) ppm.

³¹P{¹H} NMR (243 MHz, tetrahydrofuran-*d₈*): δ = 146.9 (dd, $^2J_{P,P}$ = 29.1, 17.5 Hz, $^1J_{P,Pt}$ = 217 Hz, C*P*), 69.2 (dd, $^2J_{P,P}$ = 35.4, 16.7 Hz, $^1J_{P,Pt}$ = 3046 Hz, dcpe), 64.2 (dd, $^2J_{P,P}$ = 35.4, 29.1 Hz, $^1J_{P,Pt}$ = 3212 Hz, dcpe) ppm.

¹⁹⁵Pt{¹H} NMR (86 MHz, tetrahydrofuran-*d₈*): δ = -4578 (ddd, $^1J_{Pt,P}$ = 3212, 3046, 217 Hz) ppm

HRMS (EI pos): m/z calc. for [$C_{42}H_{71}P_3Pt$]: 863.4417; found: 863.4429

Elemental analysis for $C_{42}H_{71}P_3Pt$: calc.: C: 58.38%, H: 8.28%; found: C: 58.42%, H: 8.42%

[(dcpe)Ni(MdtbpCP)] (151)
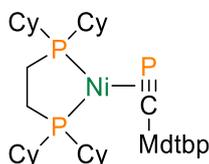
Might be unstable, no signal for C≡P phosphorus (calculated 177.2 ppm) found.

³¹P{¹H} NMR (162 MHz, tetrahydrofuran): δ = 58.9.1 (d, $^2J_{P,P}$ = 39.6 Hz, dcpe), 58.7 (s), 50.6 (dd, $^2J_{P,P}$ = 39.6, 14.6 Hz, dcpe) ppm.

[(dcpe)Pt(MdtbpCP)] (152)
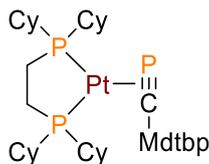
¹H NMR (700 MHz, tetrahydrofuran-*d₈*): δ = 7.42 (s, 1H, *para*-H), 7.23 (s, 2H, *meta*-H), 2.12-1.05 (m, 48H, P-C*H*, P-C*H₂*, Cy) ppm.

^{13}C{^{1}H} NMR (176 MHz, tetrahydrofuran-d_8): δ = 232.3 (m, C*P*), 150.3, 129.5, 124.4, 120.6, 37.4, 36.7, 35.6, 34.7, 32.4, 31.6, 30.5, 30.0, 29.6, 29.0, 28.4, 28.0, 27.7, 27.4, 27.1 ppm.

^{31}P{^{1}H} NMR (162 MHz, tetrahydrofuran-d_8): δ = 137.3 (dd, $^2J_{P,P}$ = 31.0, 19.7 Hz, $^1J_{P,Pt}$ = 204 Hz, C*P*), 69.6 (dd, $^2J_{P,P}$ = 33.4, 19.4 Hz, $^1J_{P,Pt}$ = 2937 Hz, dcpe), 64.3 (t, $^2J_{P,P}$ = 31.8 Hz, $^1J_{P,Pt}$ = 3178 Hz, dcpe) ppm.

[(dcpe)Pt(Mes*CP)] (153)
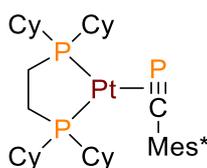
^{31}P{^{1}H} NMR (162 MHz, tetrahydrofuran): δ = 128.0 (dd, $^2J_{P,P}$ = 28.8, 18.8 Hz, $^1J_{P,Pt}$ = 166 Hz, C*P*), 67.4 (dd, $^2J_{P,P}$ = 39.3, 18.8 Hz, $^1J_{P,Pt}$ = 2045 Hz, dcpe), 58.9 (dd, $^2J_{P,P}$ = 29.2, 28.1 Hz, $^1J_{P,Pt}$ = 3278 Hz, dcpe) ppm.

[(dcpe)Ni(Ph$_3$SiCP)] (156)
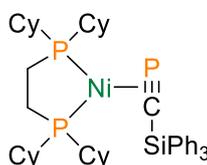
Area of the C≡P phosphorus signal (calculated 322.7 ppm) not scanned.

^{31}P{^{1}H} NMR (162 MHz, toluene): δ = 75.4.1 (d, $^2J_{P,P}$ = 29.3 Hz, dcpe), 66.0 (dd, $^2J_{P,P}$ = 29.3, 18.5 Hz, dcpe) ppm.

[(dcpe)Ni(TritylCP)] (158)
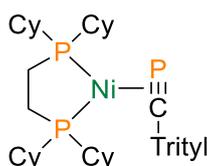
^{1}H NMR (400 MHz, tetrahydrofuran-d_8): δ = 7.42-7.41 & 7.15-7.06 (m, 15H, Ar-H), 2.12-1.05 (m, 48H, P-C*H*, P-C*H$_2$*, Cy) ppm.

³¹P{¹H} NMR (162 MHz, tetrahydrofuran-*d₈*): δ = 148.9 (d, $^2J_{P,P}$ = 15.0 Hz, C*P*), 71.9 (dd, $^2J_{P,P}$ = 27.4, 11.5 Hz, dcpe), 56.4 (dd, $^2J_{P,P}$ = 28.9, 16.9 Hz, dcpe) ppm.

[(dippdmae)Ni(MesCP)] (159)
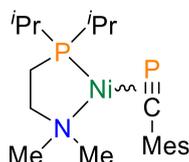
³¹P{¹H} NMR (162 MHz, tetrahydrofuran-*d₈*): δ = 165.7 (m, C*P*), 39.2 (m, dippdmae) ppm. Note: broad multiplets ³¹P{¹H} signals due to *cis-trans* isomerism.

[dippdmae)Pt(MesCP)] (160)
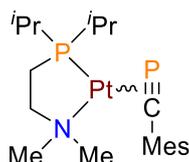
¹H NMR (400 MHz, tetrahydrofuran-*d₈*): δ = 6.76 (s, 2H, *meta-H*-Mes), 2.24 (s, 3H, *para*-C*H₃*-Mes), 2.42-1.91 (P-C*H*, P-C*H₂*), 2.02 (s, 6H, *ortho*-C*H₃*-Mes), 1.28-1.17 (m, 6H, C*H₃* of *ⁱ*Pr), 1.05-0.99 (m, 6H, C*H₃* of *ⁱ*Pr) ppm.

³¹P{¹H} NMR (162 MHz, tetrahydrofuran-*d₈*): δ = 112.3 (t, $^2J_{P,P}$ = 18.5 Hz, $^1J_{P,Pt}$ = 195 Hz, C*P*), 32.6 (dd, $^2J_{P,P}$ = 24.7, 20.4 Hz, $^1J_{P,Pt}$ = 3556 Hz, dippdmae), 30.6 (dd, $^2J_{P,P}$ = 24.6, 16.7 Hz, $^1J_{P,Pt}$ = 3362 Hz, dippdmae) ppm. Note: two ³¹P{¹H} signals due to *cis-trans* isomerism.

[dippdmae)Ni(Mes*CP)] (161)
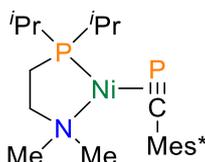
¹H NMR (400 MHz, tetrahydrofuran-*d₈*): δ = 7.15 (s, 2H, *meta-H*-Mes*), 2.33 (dq, $^2J_{H,P}$ = 16.1 Hz, $^3J_{H,H}$ = 6.75 Hz, 2H, P-C*H*), 2.05 (hept, $^3J_{H,H}$ = 7.16 Hz, 2H, P-C*H*), 1.57 (m, 4H, P-C*H₂*), 1.55 (s, 18H, *ortho*-C*H₃*-Mes*), 1.28 (s, 9H, *para*-C*H₃*-Mes*), 1.25 (dd, $^3J_{H,P}$ = 15.0 Hz, $^2J_{H,H}$ = 7.18 Hz, 6H, C*H₃* of *ⁱ*Pr), 1.16 (dd, $^3J_{H,P}$ = 12.9 Hz, $^2J_{H,H}$ = 6.97 Hz, 6H, C*H₃* of *ⁱ*Pr) ppm.

31P{1H} NMR (162 MHz, tetrahydrofuran-d_8): δ = 159.4 (d, $^2J_{P,P}$ = 11.2 Hz, C*P*), 57.7 (dd, $^2J_{P,P}$ = 11.0 Hz, dippdmae) ppm.

[dippdmae)Pt(Mes*CP)] (162)
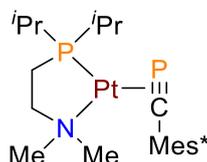
1H NMR (400 MHz, tetrahydrofuran-d_8): δ = 7.28 (s, 2H, *meta-H*-Mes*), 2.33 (s), 2.12 (s), 1.53 (s), 1.45 (s), 1.38 (s), 1.32 (s), 1.30 (s), 1.25-0.98 (C*H₃* of *i*Pr) ppm. Note: full assignment not possible, due to decomposition products.

31P{1H} NMR (162 MHz, tetrahydrofuran-d_8): δ = 101.3 (br, $^1J_{P,Pt}$ = 118 Hz, C*P*), 63.3 (d, $^2J_{P,P}$ = 6.5 Hz, $^1J_{P,Pt}$ = 3878 Hz, dippdmae) ppm.

General synthesis for the C₁ π-complexes

In derogation of the common procedure, all phosphaalkyne complexes bearing a methylene bridged diphosphine need additional cooling and reaction time, updating the procedure to:

Ni(COD)₂ (**36**) or Pt(COD)₂ (**4**, 10-50 mg, 1 eq) was added into a scintillation vial and dissolved in THF (2-8 ml) with vigorous stirring and cooled to *T* = -25 °C. Chilled diphosphine solution (0.2 M in THF, 1 eq, *T* = -25 °C) was added and slowly allowed to warm to rt. The reaction mixture was stirred at rt for at least 3 h. The reaction mixture was cooled to *T* = -25 °C and a chilled solution of phosphaalkyne (0.2 M in THF, *T* = -25 °C, 1 eq) was added dropwise to the usually strong orange/red colored reaction mixture over 15 min. The reaction solution was allowed to warm to rt and stirred overnight. The solvent was removed under reduced pressure, yielding the product as dark orange (Ni) or red (Pt) powder.

[(dtbpm)Ni(TrippCP)] (165)
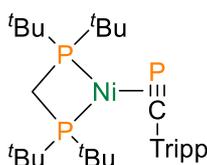
31P{1H} NMR (162 MHz, tetrahydrofuran-d_8): δ = 195.9 (d, $^2J_{P,P}$ = 21.3 Hz, C*P*), 48.3 (d, $^2J_{P,P}$ = 89.3 Hz, dtbpm), 41.3 (dd, $^2J_{P,P}$ = 89.1, 21.4 Hz, dtbpm) ppm.

[(dtbpm)Pt(TrippCP)] (166)
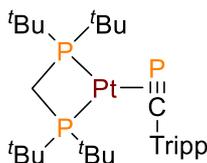
¹H NMR (700 MHz, tetrahydrofuran-*d₈*): δ = 6.88 (s, 2H, *meta-H*-Tripp), 3.85 (t, $^2J_{H,P}$ = 7.3 Hz, P-C*H₂*-P), 3.23 (sept, $^3J_{H,H}$ = 6.89 Hz, 2H, *ortho*-C*H*-Tripp), 2.81 (sept, $^3J_{H,H}$ = 6.89 Hz, 1H, *para*-C*H*-Tripp), 1.46 (d, $^3J_{H,P}$ = 15.7 Hz, 18H, *ᵗBu*), 1.21 (s, $^3J_{H,H}$ = 6.95 Hz, 12H, *ortho*-C*H₃*-Tripp), 1.19 (d, $^3J_{H,P}$ = 12.7 Hz, 18H, *ᵗBu*),1.13 (s, $^3J_{H,H}$ = 6.83 Hz, 6H, *para*-C*H₃*-Tripp) ppm.

¹³C{¹H} NMR (176 MHz, tetrahydrofuran-*d₈*): δ = 221.5 (m, *C*P), 146.3 (d, *J* = 6.5 Hz, Tripp), 144.9 (d, *J* = 3.0 Hz, Tripp), 140.7 (br, Tripp), 119.4 (Tripp), 40.1 (t, *J* = 13.4 Hz), 35.7 (d, *J* = 10.7 Hz), 35.4 (d, *J* = 9.9 Hz), 34.9 (d, *J* = 10.2 Hz), 31.4 (d, *J* = 7.2 Hz), 31.2 (d, *J* = 6.8 Hz), 30.3 (d, *J* = 9.2 Hz) ppm.

³¹P{¹H} NMR (202 MHz, tetrahydrofuran-*d₈*): δ = 155.8 (dd, $^2J_{P,P}$ = 33.7, 16.7 Hz, $^1J_{P,Pt}$ = 220 Hz, C*P*), 29.4 (dd, $^2J_{P,P}$ = 58.6, 33.3 Hz, $^1J_{P,Pt}$ = 2626 Hz, dtbpm), 25.1 (dd, $^2J_{P,P}$ = 58.7, 16.3 Hz, $^1J_{P,Pt}$ = 2683 Hz, dtbpm) ppm.

[(dcpm)Ni(MesCP)] (167)
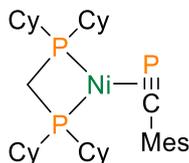
³¹P{¹H} NMR (162 MHz, tetrahydrofuran-*d₈*): δ = 192.3 (d, $^2J_{P,P}$ = 20.4 Hz, C*P*), 22.0 (d, $^2J_{P,P}$ = 49.1 Hz, dcpm), 16.9 (dd, $^2J_{P,P}$ = 50.3, 21.7 Hz, dcpm) ppm.

[(dcpm)Ni(TrippCP)] (169)
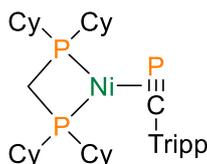
¹H NMR (700 MHz, tetrahydrofuran-*d₈*): δ = 6.89 (s, 2H, *meta-H*-Tripp), 3.31 (sept, $^3J_{H,H}$ = 6.81 Hz, 2H, *ortho*-C*H*-Tripp), 2.80 (sept, $^3J_{H,H}$ = 6.75 Hz, 1H, *para*-C*H*-Tripp), 2.54 (t, $^2J_{H,P}$ =

7.3 Hz, P-CH_2-P), 1.23 (d, $^3J_{H,H}$ = 6.95 Hz, 6H, *para*-CH_3-Tripp), 1.13 (d, $^3J_{H,H}$ = 6.86 Hz, 12H, *ortho*-CH_3-Tripp), 2.05-0.79 (m, 46H, P-CH, Cy) ppm.

^{13}C{^{1}H} NMR (176 MHz, tetrahydrofuran-d_8): δ = 229.2 (m, CP), 147.8 (Tripp), 144.3 (d, J = 2.6 Hz, Tripp), 140.2 (d, J = 3.6 Hz, Tripp), 119.8 (Tripp), 36.3 (dd, J = 10.3, 4.5 Hz), 36.0 (dd, J = 11.4, 4.5 Hz), 35.6 (m), 31.3-24.1 (multiple signals for Cy) ppm.

^{31}P{^{1}H} NMR (202 MHz, tetrahydrofuran-d_8): δ = 199.4 (d, $^2J_{P,P}$ = 21.3 Hz, CP), 22.1 (d, $^2J_{P,P}$ = 48.1 Hz, dcpm), 16.1 (dd, $^2J_{P,P}$ = 48.6, 20.8 Hz, dcpm) ppm.

[(dcpm)Pt(TrippCP)] (170)
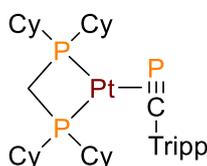
Pt(COD)$_2$ (**4**, 50 mg, 122 µmol, 1 eq) was added into a scintillation vial, dissolved in THF (8 ml) under vigorous stirring and cooled to T = -25 °C. Chilled dcpe (**30**, 600 µl of 0.2 M in THF, 122 µmol, 1 eq, T = -25 °C) was added and allowed to warm to rt. After 3 h the deep red reaction solution was again cooled to T = -25 °C and a chilled solution of TrippCP (**81**, 600 µl of 0.2 M in THF, 122 µmol, 1 eq, T = -25 °C) was added dropwise to the reaction mixture over 5 - 10 min. The solution brightened slightly during this time and was allowed to warm to rt overnight with stirring. The solvent was removed under reduced pressure, yielding the product as a red powder (quantitative conversion by NMR).

^{1}H NMR (700 MHz, tetrahydrofuran-d_8): δ = 6.89 (s, 2H, *meta*-H-Tripp), 3.36 (t, $^2J_{H,P}$ = 4.5 Hz, P-CH_2-P), 3.35 (sept, $^3J_{H,H}$ = 7.06 Hz, 2H, *ortho*-CH-Tripp), 2.84 (sept, $^3J_{H,H}$ = 6.95 Hz, 1H, *para*-CH-Tripp), 1.24 (d, $^3J_{H,H}$ = 6.99 Hz, 6H, *para*-CH_3-Tripp), 1.10 (d, $^3J_{H,H}$ = 6.97 Hz, 12H, *ortho*-CH_3-Tripp), 2.08-0.87 (m, 46H, P-CH, Cy) ppm.

^{13}C{^{1}H} NMR (176 MHz, tetrahydrofuran-d_8): δ = 224.5 (m, CP), 146.6 (d, J = 7.2 Hz, Tripp), 144.9 (d, J = 2.7 Hz, Tripp), 140.9 (d, J = 4.3 Hz, Tripp), 119.5 (Tripp), 35.9 (app. t, J = 9.5 Hz), 35.6 (dd, J = 10.7, 8.2 Hz), 35.4, 33.7 (m), 30.6 (d, J = 2.7 Hz), 30.5 (d, J = 3.8 Hz), 30.2, 29.8 (d, J = 5.3 Hz), 29.3, 28.2 (dd, J = 29.7, 11.2 Hz), 27.9 (dd, J = 17.4, 11.2 Hz), 27.3, 27.0, 25.2, 24.1 ppm.

^{31}P{^{1}H} NMR (242 MHz, tetrahydrofuran-d_8): δ = 163.8 (dd, $^2J_{P,P}$ = 36.1, 17.7 Hz, $^1J_{P,Pt}$ = 224 Hz, CP), 1.4 (t, $^2J_{P,P}$ = 12.5 Hz, $^1J_{P,Pt}$ = 2543 Hz, dcpm), -0.4 (dd, $^2J_{P,P}$ = 35.7, 9.7 Hz, $^1J_{P,Pt}$ = 2654 Hz, dcpm) ppm.

^{195}Pt{^{1}H} NMR (86 MHz, tetrahydrofuran-d_8): δ = -3991 (ddd, $^1J_{Pt,P}$ = 2657, 2546, 224 Hz) ppm

HRMS (EI pos): m/z calc. for [C$_{41}$H$_{69}$P$_3$Pt]: 849.4260; found: 849.4259

Elemental analysis for C$_{41}$H$_{69}$P$_3$Pt: calc.: C: 57.93%, H: 8.18%; found: C: 56.72%, H: 7.90%

[(dippp)Ni(MesCP)] (172)
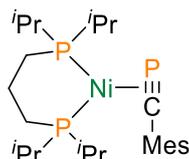
^{1}H NMR (400 MHz, tetrahydrofuran-d_8): δ = 6.70 (s, 2H, *meta*-*H*-Mes), 2.17 (s, 3H, *para*-CH_3-Mes), 2.18 (m, 2H, P-C*H*), 1.98 (s, 6H, *ortho*-CH_3-Mes), 1.95 (pent, $^3J_{H,H}$ = 7.09 Hz, 2H, P-C*H*), 1.72 (m, 4H, P-CH_2), 1.28 (dd, $^3J_{H,P}$ = 14.7 Hz, $^3J_{H,H}$ = 7.12 Hz, 6H, CH_3 of ^{i}Pr), 1.14 (dd, $^3J_{H,P}$ = 12.6 Hz, $^3J_{H,H}$ = 6.96 Hz, 6H, CH_3 of ^{i}Pr), 1.01 (dd, $^3J_{H,P}$ = 12.5 Hz, $^3J_{H,H}$ = 6.92 Hz, 6H, CH_3 of ^{i}Pr), 0.83 (dd, $^3J_{H,P}$ = 14.7 Hz, $^3J_{H,H}$ = 7.20 Hz, 6H, CH_3 of ^{i}Pr) ppm.

^{31}P{^{1}H} NMR (162 MHz, tetrahydrofuran-d_8): δ = 164.9 (dd, $^2J_{P,P}$ = 13.2, 6.2 Hz, C*P*), 30.4 (d, $^2J_{P,P}$ = 5.6 Hz, dippp), 28.7 (d, $^2J_{P,P}$ = 13.0 Hz, dippp) ppm.

[(dcpp)Ni(MesCP)] (173)
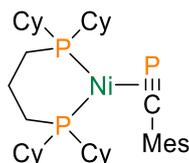
^{1}H NMR (400 MHz, tetrahydrofuran-d_8): δ = 6.74 (s, 2H, *meta*-*H*-Mes), 2.29 (s, 3H, *para*-CH_3-Mes), 2.00 (s, 6H, *ortho*-CH_3-Mes), 2.09-0.84 (m, 48H, P-C*H*, P-CH_2, Cy) ppm.

^{31}P{^{1}H} NMR (162 MHz, tetrahydrofuran-d_8): δ = 164.4 (dd, $^2J_{P,P}$ = 13.8, 5.7 Hz, C*P*), 22.4 (d, $^2J_{P,P}$ = 4.7 Hz, dcpp), 22.2 (d, $^2J_{P,P}$ = 13.2 Hz, dcpp) ppm.

[(dcpp)Pt(MesCP)] (174)
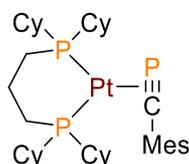
¹H NMR (400 MHz, benzene-*d₆*): δ = 6.93 (s, 2H, *meta-H*-Mes), 2.38 (s, 6H, *ortho*-C*H₃*-Mes), 2.31 (s, 3H, *para*-C*H₃*-Mes), 2.22-0.90 (m, 48H, P-C*H*, P-C*H₂*, Cy) ppm.

³¹P{¹H} NMR (162 MHz, benzene-*d₆*): δ = 126.0 (dd, $^2J_{P,P}$ = 24.8, 17.3 Hz, $^1J_{P,Pt}$ = 221 Hz, C*P*), 19.4 (d, $^2J_{P,P}$ = 23.8 Hz, $^1J_{P,Pt}$ = 3305 Hz, dcpp), 17.9 (d, $^2J_{P,P}$ = 15.6 Hz, $^1J_{P,Pt}$ = 3119 Hz, dcpp) ppm.

[(dppp)Ni(MesCP)] (175)
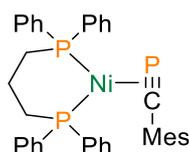
³¹P{¹H} NMR (162 MHz, tetrahydrofuran): δ = 151.4 (s, C*P*), 19.2 (s, dppp), 18.0 (s, dppp) ppm.

[(dppf)Ni(MesCP)] (176)
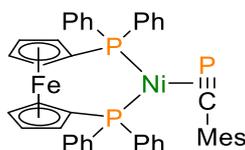
¹H NMR (400 MHz, tetrahydrofuran-*d₈*): δ = 7.88- 6.95 (four distinct muliplets 7.88, 7.41, 7.17, 6.95, 20H, Ph), 6.29 (s, 2H, *meta-H*-Mes), 4.46 (q, $^3J_{H,H}$ = 1.99 Hz, 2H, Fc), 4.34 (t, $^3J_{H,H}$ = 1.88 Hz, 2H, Fc), 4.14 (t, $^3J_{H,H}$ = 1.83 Hz, 2H, Fc), 3.82 (q, $^3J_{H,H}$ = 1.86 Hz, 2H, Fc), 2.31 (s, 6H, *ortho*-C*H₃*-Mes), 2.10 (s, 3H, *para*-C*H₃*-Mes) ppm.

³¹P{¹H} NMR (162 MHz, tetrahydrofuran-*d₈*): δ = 149.7 (d, $^2J_{P,P}$ = 15.2 Hz, C*P*), 28.9 (dd, $^2J_{P,P}$ = 15.6, 4.8 Hz, dppf), 27.8 (d, $^2J_{P,P}$ = 4.8 Hz, dppf) ppm.

[(2-(4,6-diphenylphosphinin-2-yl)pyridine)Ni(MesCP)] (177)
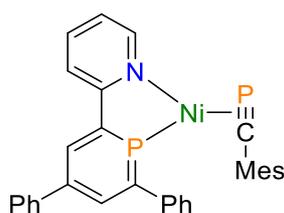
³¹P{¹H} NMR (162 MHz, tetrahydrofuran): δ = 231.1 (s, C*P*), 184.7 (s, phosphinine) ppm.

General synthesis for the non-chelated π-complexes

Ethylenebis(triphenylphosphine)platinum(0) (**183**, 40-170 mg, 1 eq) was added into a scintillation vial and dissolved in THF (4-15 ml) under vigorous stirring. Phosphaalkyne solution (0.2 M in THF, 1 eq) was added stirred at rt for 1 h. The solvent was removed under reduced pressure, yielding a red powder.

[(PPh₃)₂Pt(MesCP)] (178)
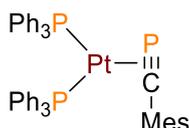
³¹P{¹H} NMR (162 MHz, tetrahydrofuran): δ = 96.9 (dd, $^2J_{P,P}$ = 23.9, 12.1 Hz, $^1J_{P,Pt}$ = 165 Hz, CP), 29.2 (t, $^2J_{P,P}$ = 23.4 Hz, $^1J_{P,Pt}$ = 3700 Hz, PPh₃), 25.1 (dd, $^2J_{P,P}$ = 23.1, 11.7 Hz, $^1J_{P,Pt}$ = 3454 Hz, PPh₃) ppm.

[(PPh₃)₂Pt(TrippCP)] (179)
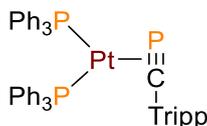
³¹P{¹H} NMR (162 MHz, tetrahydrofuran): δ = 105.9 (dd, $^2J_{P,P}$ = 24.0, 13.1 Hz, $^1J_{P,Pt}$ = 145 Hz, CP), 29.0 (t, $^2J_{P,P}$ = 23.7 Hz, $^1J_{P,Pt}$ = 3725 Hz, PPh₃), 23.4 (dd, $^2J_{P,P}$ = 23.7, 12.3 Hz, $^1J_{P,Pt}$ = 3424 Hz, PPh₃) ppm.

[(PPh₃)₂Pt(MdtbpCP)] (180)
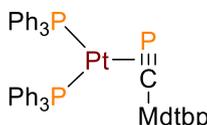
³¹P{¹H} NMR (162 MHz, tetrahydrofuran): δ = 111.6 (dd, $^2J_{P,P}$ = 26.3, 14.5 Hz, $^1J_{P,Pt}$ = 108 Hz, CP), 32.6 (t, $^2J_{P,P}$ = 24.8 Hz, $^1J_{P,Pt}$ = 3566 Hz, PPh₃), 25.7 (dd, $^2J_{P,P}$ = 23.7, 13.1 Hz, $^1J_{P,Pt}$ = 3262 Hz, PPh₃) ppm.

[(dippe)Pd(MesCP)] (184)
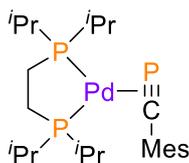
Pd(PPh$_3$)$_4$ (100 mg, 86.5 µmol, 1 eq) was added into a scintillation vial and dissolved in THF (6 ml). Addition of dippe (**8**, 450 µl of 0.191 M in THF, 86.5 µmol, 1 eq) brightened up the orange solution. After 15 min a solution of MesCP (**68**, 350 µl of 0.244 M in THF, 86.5 µmol, 1 eq) was added to the reaction mixture. The solution turned intense orange and was stirred at rt overnight. The solvent was removed under reduced pressure, yielding the product as an orange powder (quantitative conversion by NMR).

^{1}H NMR (400 MHz, benzene-d_6): δ = 6.94 (s, 2H, *meta-H*-Mes), 2.43 (s, 6H, *ortho*-CH_3-Mes), 2.28 (s, 3H, *para*-CH_3-Mes), 1.81 (dq, $^2J_{H,P}$ = 14.3 Hz, $^3J_{H,H}$ = 7.13 Hz, 2H, P-CH), 1.66 (dq, $^2J_{H,P}$ = 14.3 Hz, $^3J_{H,H}$ = 7.05 Hz, 2H, P-CH), 1.20 (m, 4H, P-CH_2), 1.14 (dd, $^3J_{H,P}$ = 15.8 Hz, $^3J_{H,H}$ = 7.06 Hz, 6H, CH_3 of ^{i}Pr), 0.89 (dd, $^3J_{H,P}$ = 13.3 Hz, $^3J_{H,H}$ = 6.99 Hz, 6H, CH_3 of ^{i}Pr), 0.77 (ddt, $^3J_{H,P}$ = 12.8 Hz, $^3J_{H,H}$ = 6.87 Hz, 6H, CH_3 of ^{i}Pr), 0.73 (ddt, $^3J_{H,P}$ = 14.5 Hz, $^3J_{H,H}$ = 7.02 Hz 6H, CH_3 of ^{i}Pr) ppm.

^{31}P{^{1}H} NMR (162 MHz, benzene-d_6): δ = 97.2 (t, $^2J_{P,P}$ = 18.8 Hz, CP), 71.1 (t, $^2J_{P,P}$ = 15.8 Hz, dippe), 60.1 (dd, $^2J_{P,P}$ = 20.9, 15.4 Hz, dippe) ppm.

[(dcpe)Pd(MesCP)] (185)
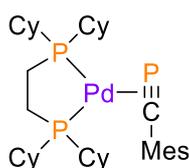
Pd$_2$(dba)$_3$ (50 mg, 55 µmol, 1 eq) and dcpe (**30**, 109 µmol, 2 eq) was added into a scintillation vial and dissolved in THF (6 ml). After stirring for 15 min a solution of MesCP (**68**, 770 µl of 0.143 M in THF, 109 µmol, 1 eq) was added to the dark yellow reaction mixture. The solution turned light green and back to yellow after stirred at rt overnight. The solvent was removed under reduced pressure, yielding the product as an orange powder (quantitative conversion by NMR). The dba was removed by washing with hot hexane under significant loss of product.

^{1}H NMR (400 MHz, tetrahydrofuran-d_8): δ = 6.76 (s, 2H, *meta-H*-Mes), 2.23 (s, 3H, *para*-CH_3-Mes), 2.07 (s, 6H, *ortho*-CH_3-Mes), 1.89-0.63 (m, 48H, P-CH, P-CH_2, Cy) ppm.

^{31}P{^{1}H} NMR (162 MHz, tetrahydrofuran-*d$_8$*): δ = 99.2 (dd, $^2J_{P,P}$ = 22.6, 16.5 Hz, C*P*), 61.0 (t, $^2J_{P,P}$ = 15.5 Hz, dcpe), 53.1 (dd, $^2J_{P,P}$ = 22.4, 15.0 Hz, dcpe) ppm.

4.2.10 Preparation of cyaphido platinum(II) complexes

General setup for the irradiation of the Pt complexes

The π-Pt complex (**143**, **144**, **148**, **150**, **152**, **166**, **170**, 24.4 - 122 µmol) was dissolved in THF (1-5 ml) and either transferred into in a J. Youngs NMR tube or in a thin Schlenk tube equipped with a magnetic stirring bar and placed in the middle of a setup of four 15 W violet light LED array (λ_{max} = 405 nm) with a distance to the tube of about 5 cm. The irradiation was performed at rt (lower temperature favors the formation of σ-Pt complex). Depending on the used π-Pt complex the reaction time varies from 1.5 to 18 h.

Remarks

In the following, the typical conversion ratio at rt is given as percentage for the σ-Pt complex for each complex. According to NMR studies there are no side-products, all unreacted π-Pt complex stays unchanged in solution. The oxidative addition reaction (irradiation) and reductive elimination (thermal back reaction) can be repeated several times without showing any side-products in the NMR spectrum for a pure sample.

With the exception for the conversion of **166** and **170** (both directions). These systems release dtbpm (**15** for **166**) or dcypm (**21** for **170**) and probably also TrippCP (**76**), which undergoes further unspecific side reactions upon irradiation.

The determination of the kinetics for the thermal back reaction by ^{1}H and ^{31}P NMR spectroscopic studies show insufficient results, due to a large deviation for the reaction time. Most samples of **148σ** show full back reaction to **148** in less than a 1 h (THF, T = 60 °C), whereas other samples only show 20% conversion under the same conditions. It is assumed that elemental platinum nanoparticles, which might be released by the synthesis of the compound in different amounts, catalyze the back reaction and lead to the unpredictable results for the kinetics.

[(dippe)Pt(Mes)(CP)] (143σ)
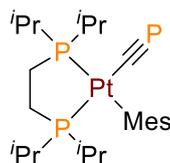
Irradiation time of 1.5 h gives about 70% conversion.

^{1}H NMR (700 MHz, tetrahydrofuran-d_8): δ = 6.55 (s, 2H, *meta*-*H*-Mes), 2.43 (s, 6H, *ortho*-CH_3-Mes), 2.11 (s, 3H, *para*-CH_3-Mes), 2.68 (dq, $^{2}J_{H,P}$ = 16.4 Hz, $^{3}J_{H,H}$ = 7.11 Hz, 2H, P-C*H*), 2.12 (dq, $^{2}J_{H,P}$ = 15.8 Hz, $^{3}J_{H,H}$ = 7.03 Hz, 2H, P-C*H*), 1.75 (m, 4H, P-CH_2), 1.45 (dd, $^{3}J_{H,P}$ = 16.1 Hz, $^{2}J_{H,H}$ = 7.17 Hz, 6H, CH_3 of ^{i}Pr), 1.22 (dd, $^{3}J_{H,P}$ = 13.5 Hz, $^{2}J_{H,H}$ = 7.06 Hz, 6H, CH_3 of ^{i}Pr), 1.07 (dd, $^{3}J_{H,P}$ = 13.8 Hz, $^{2}J_{H,H}$ = 6.97 Hz, 6H, CH_3 of ^{i}Pr), 0.89 (dd, $^{3}J_{H,P}$ = 15.1 Hz, $^{2}J_{H,H}$ = 7.20 Hz, 6H, CH_3 of ^{i}Pr) ppm.

^{13}C{^{1}H} NMR (176 MHz, tetrahydrofuran-d_8): δ = 232.7 (app. dt, J = 114.3, 10.5 Hz, *C*P), 153.9 (dd, J = 102.4, 8.64 Hz, *ipso*-*C*-Mes), 143.5 (Mes), 131.3 (Mes), 128.0 (Mes), 27.4 (d, J = 3.6 Hz), 25.9, 22.7, 19.4, 19.1 (d, J = 2.6 Hz), 18.9, 18.0 ppm.

^{31}P{^{1}H} NMR (162 MHz, tetrahydrofuran-d_8): δ = 99.0 (dd, $^{3}J_{P,P}$ = 18.2, 10.07 Hz, $^{2}J_{P,Pt}$ = 340 Hz, C*P*), 68.9 (d, $^{2,3}J_{P,P}$ = 10.7 Hz, $^{1}J_{P,Pt}$ = 1653 Hz, dippe), 57.9 (d, $^{2,3}J_{P,P}$ = 18.0 Hz, $^{1}J_{P,Pt}$ = 2169 Hz, dippe) ppm.

^{195}Pt{^{1}H} NMR (86 MHz, tetrahydrofuran-d_8): δ = -4476 (ddd, $^{1,2}J_{Pt,P}$ = 2169, 1653, 340 Hz) ppm.

IR: $\tilde{\nu}$ = 1242 (C≡P) cm^{-1}.

[(dippe)Pt(Tripp)(CP)] (144σ)
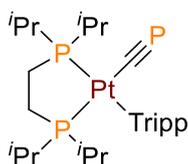
Irradiation time of 4.5 h gives about 83% conversion.

^{31}P{^{1}H} NMR (162 MHz, tetrahydrofuran): δ = 107.5 (dd, $^{3}J_{P,P}$ = 17.2, 11.9 Hz, $^{2}J_{P,Pt}$ = 335 Hz, C*P*), 66.1 (d, $^{2,3}J_{P,P}$ = 11.1 Hz, $^{1}J_{P,Pt}$ = 1639 Hz, dippe), 54.4 (d, $^{2,3}J_{P,P}$ = 17.1 Hz, $^{1}J_{P,Pt}$ = 2153 Hz, dippe) ppm.

[(dcype)Pt(Mes)(CP)] (148σ)
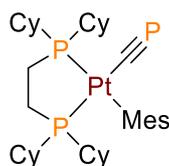
Irradiation time of 1.5 h leads to about 80% conversion.

^{1}H NMR (400 MHz, tetrahydrofuran-d_8): δ = 6.78 (s, 2H, *meta*-*H*-Mes), 2.45 (s, 6H, *ortho*-C*H*$_3$-Mes), 2.13 (s, 3H, *para*-C*H*$_3$-Mes), 2.33-0.69 (m, 24H, P-C*H*, P-C*H*$_2$, Cy) ppm.

^{31}P{^{1}H} NMR (162 MHz, tetrahydrofuran-d_8): δ = 96.6 (dd, $^3J_{P,P}$ = 17.7, 10.4 Hz, $^2J_{P,Pt}$ = 338 Hz, C*P*), 60.2 (d, $^{2,3}J_{P,P}$ = 10.3 Hz, $^1J_{P,Pt}$ = 1654 Hz, dcpe), 49.2 (d, $^{2,3}J_{P,P}$ = 17.8 Hz, $^1J_{P,Pt}$ = 2164 Hz, dcpe) ppm.

^{195}Pt{^{1}H} NMR (86 MHz, tetrahydrofuran-d_8): δ = -4463 (ddd, $^{1,2}J_{Pt,P}$ = 2164, 1654, 338 Hz) ppm.

IR: $\tilde{\nu}$ = 1259 (C≡P) cm^{-1}.

[(dcpe)Pt(Tripp)(CP)] (150σ)
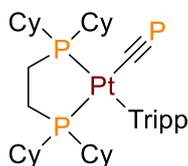
Irradiation time of 3 h leads to full conversion.

^{1}H NMR (600 MHz, tetrahydrofuran-d_8): δ = 6.75 (s, 2H, *meta*-*H*-Tripp), 3.71 (sept, $^3J_{H,H}$ = 6.78 Hz, 2H, *ortho*-C*H*-Tripp), 2.74 (sept, $^3J_{H,H}$ = 6.90 Hz, 1H, *para*-C*H*-Tripp), 1.20-1.38 (dd, J = 18.33, 6.77 Hz, d, $^3J_{H,H}$ = 6.90 Hz, 18H, *ortho*&*para*-C*H*$_3$-Tripp), 2.33-0.67 (m, 24H, P-C*H*, P-C*H*$_2$, Cy) ppm.

^{13}C{^{1}H} NMR (151 MHz, tetrahydrofuran-d_8): δ = 225.5 (d, J = 117.8 Hz, *C*P), 155.0, 152.3 (dd, J = 102.0, 8.7 Hz, Tripp), 144.1 (Tripp), 120.5 (Tripp), 37.2, 34.8 (d, J = 25.6 Hz), 34.3 (d, J = 26.9 Hz), 30.3, 29.9 (d, J = 5.9 Hz), 29.1, 27.8 (d, J = 10.0 Hz), 27.5 (d, J = 16.6 Hz), 26.8, 24.2, 23.3 (dt, J = 27.4, 13.7 Hz), 22.6 (dd, 25.0, 10.4 Hz) ppm.

^{31}P{^{1}H} NMR (162 MHz, tetrahydrofuran-d_8): δ = 108.9 (dd, $^3J_{P,P}$ = 18.2, 10.7 Hz, $^2J_{P,Pt}$ = 331 Hz, C*P*), 60.9 (d, $^{2,3}J_{P,P}$ = 10.6 Hz, $^1J_{P,Pt}$ = 1647 Hz, dcpe), 48.6 (d, $^{2,3}J_{P,P}$ = 17.5 Hz, $^1J_{P,Pt}$ = 2145 Hz, dcpe) ppm.

^{195}Pt{^{1}H} NMR (86 MHz, tetrahydrofuran-d_8): δ = -4393 (ddd, $^{1,2}J_{Pt,P}$ = 2145, 1647, 331 Hz) ppm.

IR: $\tilde{\nu}$ = 1260 (C≡P) cm^{-1}.

[(dcpe)Pt(Mdtbp)(CP)] (152σ)
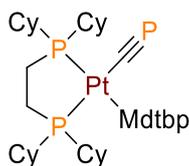
Irradiation time about 36 h leads to about 80% conversion and several by-products.

^{31}P{^{1}H} NMR (162 MHz, tetrahydrofuran-d_8): δ = 90.2 (dd, $^3J_{P,P}$ = 18.6, 10.0 Hz, $^2J_{P,Pt}$ = 348 Hz, C*P*), 58.1 (d, $^{2,3}J_{P,P}$ = 9.5 Hz, $^1J_{P,Pt}$ = 1590 Hz, dcpe), 49.5 (d, $^{2,3}J_{P,P}$ = 18.4 Hz, $^1J_{P,Pt}$ = 2169 Hz, dcpe) ppm.

[(dtbpm)Pt(Tripp)(CP)] (166σ)
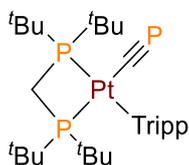
Irradiation time of 18 h leads to about 70% conversion.

^{31}P{^{1}H} NMR (162 MHz, tetrahydrofuran-d_8): δ = 104.9 (t, $^3J_{P,P}$ = 13.2 Hz, $^2J_{P,Pt}$ = 360 Hz, C*P*), -7.6 (t, $^{2,3}J_{P,P}$ = 9.0 Hz, $^1J_{P,Pt}$ = 1333 Hz, dtbpm), -11.1 (dd, $^{2,3}J_{P,P}$ = 14.6, 6.9 Hz, $^1J_{P,Pt}$ = 1761 Hz, dtbpm) ppm.

[(dcpm)Pt(Tripp)(CP)] (170σ)
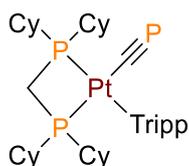
Irradiation time of 18 h leads to about 95% conversion.

¹H NMR (700 MHz, tetrahydrofuran-*d₈*): δ = 6.67 (s, 2H, *meta*-*H*-Tripp), 3.23 (sept, $^3J_{H,H}$ = 6.79 Hz, 2H, *ortho*-C*H*-Tripp), 3.23 (t, $^2J_{H,P}$ = 8.7 Hz, 2H, P-C*H₂*-P), 2.71 (sept, $^3J_{H,H}$ = 6.90 Hz, 1H, *para*-C*H*-Tripp), 1.34 (dd, *J* = 22.43, 6.84 Hz, 6H, *para*-C*H₃*-Tripp), 1.19 (dd, *J* = 15.58, 6.83 Hz, 12H, *ortho*-C*H₃*-Tripp), 2.08-0.87 (m, 20H, P-C*H*, Cy) ppm.

¹³C{¹H} NMR (176 MHz, tetrahydrofuran-*d₈*): δ = 222.7 (app. d, *J* = 122.1 Hz, *C*P), 151.3 (Tripp), 151.8 (dd, *J* = 110.4, 5.1 Hz, Tripp), 143.6 (Tripp), 119.9 (Tripp), 37.6 (d, *J* = 3.4 Hz), 36.2 (dd, *J* = 15.1, 4.4 Hz), 35.2, 34.9 (dd, *J* = 15.8, 5.3 Hz), 29.9 (d, *J* = 6.1 Hz), 29.3, 28.2 (d, *J* = 3.5 Hz), 28.1 (d, *J* = 2.2 Hz), 28.0, 27.9, 27.7 (d, *J* = 10.5 Hz), 27.2 (*J* = 4.4 Hz), 26.8, 24.4 ppm.

³¹P{¹H} NMR (162 MHz, tetrahydrofuran-*d₈*): δ = 110.5 (dd, $^3J_{P,P}$ = 18.8, 11.2 Hz, $^2J_{P,Pt}$ = 345 Hz, C*P*), -29.1 (dd, $^{2,3}J_{P,P}$ = 30.2, 10.2 Hz, $^1J_{P,Pt}$ = 1343 Hz, dcpm), -38.2 (dd, $^{2,3}J_{P,P}$ = 30.2, 18.5 Hz, $^1J_{P,Pt}$ = 1824 Hz, dcpm) ppm.

¹⁹⁵Pt{¹H} NMR (86 MHz, tetrahydrofuran-*d₈*): δ = -3792 (ddd, $^{1,2}J_{Pt,P}$ = 1824, 1343, 345 Hz) ppm.

IR: $\tilde{\nu}$ = 1262 (C$\equiv$P) cm^{-1}.

4.2.11 Consecutive reactions

4.2.11.1 Lewis-acid adducts

General synthesis for the boron adducts
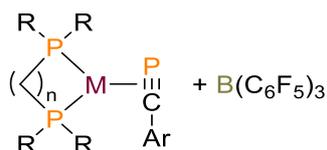
The boron adducts were synthesized in an argon filled glovebox. The appropriate π-complex [(P,P)M(R-C≡P)] (10-200 mg, 1 eq) was added into a scintillation vial and dissolved in toluene (2-20 ml) with vigorous stirring, yielding a yellow or orange solution. Addition of a colorless B(C₆F₅)₃ solution (toluene, 1 eq) results in a significant color change to red after several seconds at room temperature. The reaction solutions were directly analyzed by NMR spectroscopy, showing a quantitative conversion. Occasionally, the solvent was exchanged by removal under reduced pressure and redissolving of the red solid in the adequate deuterated solvent.

[(dippe)Ni(MesCP)] + B(C₆F₅)₃ (186)
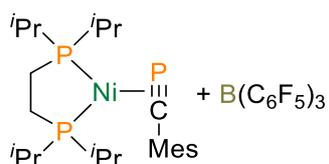
Diverging from the general synthesis only 0.5 eq of B(C₆F₅)₃ was used.

¹¹B NMR (128 MHz, toluene): δ = -11.7 (br) ppm.

¹⁹F NMR (176 MHz, toluene): δ = -130.62 (s), -135.11 (s), -165.66 (m) ppm.

³¹P{¹H} NMR (162 MHz, toluene): δ = 128.8 (dd, $J_{P,P}$ = 119.1, 39.2 Hz, CP), 84.5 (dd, $J_{P,P}$ = 39.4, 8.2 Hz, dippe), 74.8 (dd, $J_{P,P}$ = 119.1, 8.4 Hz, dippe) ppm.

[(dcpe)Ni(TrippCP)] + B(C₆F₅)₃ (187)
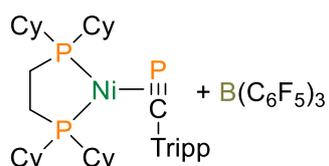
¹¹B NMR (128 MHz, toluene): δ = -0.2 (br) ppm.

³¹P{¹H} NMR (162 MHz, toluene): δ = 159.4 (br, CP), 71.0 (t, $J_{P,P}$ = 20.1, dcpe), 65.1 (dd, $J_{P,P}$ = 65.1, 20.4 Hz, dcpe) ppm.

[(dcpm)Ni(TrippCP)] + B(C₆F₅)₃ (188)
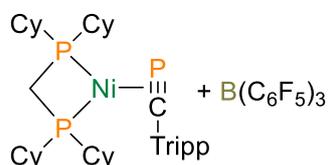
³¹P{¹H} NMR (162 MHz, toluene-*d₆*): δ = 143.1 (br, CP), 14.3 (d, $J_{P,P}$ = 33.2 Hz, dcpm), 8.8 (d, $J_{P,P}$ = 133.3 Hz, dcpm) ppm.

[(dcpe)Pd(MesCP)] + B(C₆F₅)₃ (189)
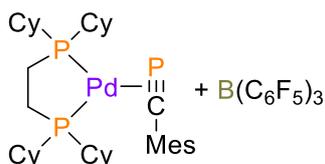
¹¹B NMR (128 MHz, toluene): δ = 0.4 (br) ppm.

¹⁹F NMR (176 MHz, toluene): δ = -129.23 (br), -142.58 (br), -160.76 (br) ppm.

³¹P{¹H} NMR (162 MHz, toluene): δ = 99.8 (d, $J_{P,P}$ = 219.0, C*P*), 72.4 (t, $J_{P,P}$ = 29.6 Hz, dcpe), 66.7 (dd, $J_{P,P}$ = 219.6, 29.6 Hz, dcpe) ppm.

[(dcpe)Pt(MesCP)] + B(C₆F₅)₃ (190)
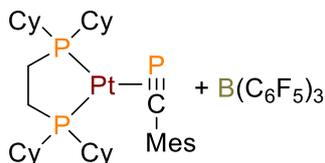
¹¹B NMR (128 MHz, toluene): δ = -5.7 (br) ppm.

¹⁹F NMR (176 MHz, toluene): δ = -128.88 (d, 22.38 Hz), -142.04 (t, 21.27), -160.23 (td, 23.31, 9.31 Hz) ppm.

³¹P{¹H} NMR (162 MHz, toluene): δ = 121.4 (d, $J_{P,P}$ = 223.1 Hz, C*P*), 70.8 (dd, $J_{P,P}$ = 31.5, 9.9 Hz, $J_{P,Pt}$ = 2783 Hz, dcpe), 62.2 (d, $J_{P,P}$ = 229.0 Hz, $J_{P,Pt}$ = 3635 Hz, dcpe) ppm.

[(dcpe)Pt(TrippCP)] + B(C₆F₅)₃ (191)
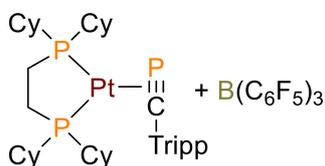
¹¹B NMR (128 MHz, toluene): δ = -4.2 (br) ppm.

¹⁹F NMR (176 MHz, toluene): δ = -128.93 (br), -157.21 (br), -163.86 (s) ppm.

³¹P{¹H} NMR (162 MHz, toluene): δ = 118.4 (br, C*P*), 68.8 (dd, $J_{P,P}$ = 27.0, 13.6 Hz, $J_{P,Pt}$ = 2861 Hz, dcpe), 58.9 (d, $J_{P,P}$ = 194.5 Hz, $J_{P,Pt}$ = 3456 Hz, dcpe) ppm.

[(dcpe)Pt(Mes*CP)] + B(C$_6$F$_5$)$_3$ (192)
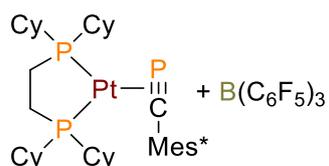
^{11}B NMR (128 MHz, toluene): δ = -2.94 (br) ppm.

^{31}P{^{1}H} NMR (162 MHz, toluene): δ = 120.1 (d, $J_{P,P}$ = 80.8 Hz, C*P*), 66.7 (dd, $J_{P,P}$ = 30.6, 21.2 Hz, $J_{P,Pt}$ = 2995 Hz, dcpe), 57.1 (dd, $J_{P,P}$ = 82.4, 30.5 Hz, $J_{P,Pt}$ = 3334 Hz, dcpe) ppm.

General synthesis for the tungsten adducts
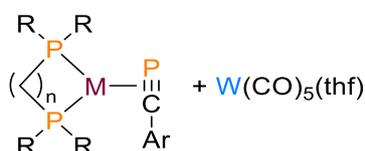
The tungsten adducts were synthesized using the Schlenk line technique. The appropriate π-complex [(P,P)M(CP)(R)] (25-150 mg, 1 eq) was added into a Schlenk tube and dissolved in THF (5-15 ml) with vigorous stirring, yielding an orange or red solution. [W(CO)$_6$] (1.0 g, 2.84 mmol) was dissolved in THF (20 ml) and irradiated with a mercury high pressure lamp (λ_{max} = 365 nm) for 2.5 h. The resulting strong yellow [W(CO)$_5$(thf)] solution (1 eq, 0.142 M in THF) was added to the cyaphido complex solution at rt, resulting in a noticeable color shift from bright to dark yellow. The solvent was removed under reduced pressure, yielding a yellow powder.

[(dcpe)Pt(MesCP-W(CO$_5$)] (193)
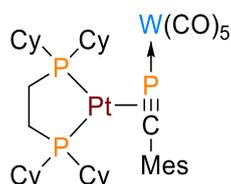
^{1}H NMR (600 MHz, tetrahydrofuran-d_8): δ = 6.82 (s, 2H, *meta*-*H*-Mes), 2.29 (s, 3H, *para*-C*H*$_3$-Mes), 2.12 (s, 6H, *ortho*-C*H*$_3$-Mes), 2.05-0.75 (m, 48H, P-C*H*, P-C*H*$_2$, Cy) ppm.

^{13}C{^{1}H} NMR (151 MHz, tetrahydrofuran-d_8): δ = 215.7 (m, C*P*), 202.8 (d, J = 27.6 Hz, *trans*-CO), 197.8 (d, $J_{C,W}$ = 128.9 Hz, *trans*-CO),145.7 (Mes), 134.1 (Mes), 130.1 (Mes), 128.3 (Mes),

36.9 (d, J = 25.7 Hz), 36.6 (d, J = 25.7 Hz), 30.8, 30.2, 29.1, 28.9, 28.1 (d, J = 10.7 Hz), 27.7 (m), 26.9, 25.9 (m), 24.5 (ddd, 42.8, 29.2, 12.7), 21.8, 21.2 ppm.

^{31}P{^{1}H} NMR (162 MHz, tetrahydrofuran-d_8): δ = 86.3 (dd, $^2J_{P,P}$ = 190.6, 31.2 Hz, $^1J_{P,Pt}$ = 380 Hz, $^1J_{P,W}$ = 187 Hz, CP), 71.7 (dd, $^2J_{P,P}$ = 31.1, 18.9 Hz, $^1J_{P,Pt}$ = 2861 Hz, dcpe), 64.2 (dd, $^2J_{P,P}$ = 191.2, 18.2 Hz, $^1J_{P,Pt}$ = 3331 Hz, dcpe) ppm.

^{195}Pt{^{1}H} NMR (86 MHz, tetrahydrofuran-d_8): δ = -4578 (ddd, $^1J_{Pt,P}$ = 3330, 2860, 376 Hz) ppm.

Photolysis of [(dcpe)Pt(MesCP-W(CO$_5$)] (193a)

193 was irradiated at rt by a setup of four 15 W violet light LED array (λ_{max} = 405 nm) with a distance to the J. Youngs NMR tube of about 5 cm for 2.5 h, yielding around 16% of the new compound **193a**. Extended irradiation for 2 days gave around 21% of **193a**. Fast back reaction to **193** prevent isolation and further characterization of **193a**.

^{31}P{^{1}H} NMR (162 MHz, tetrahydrofuran-d_8): δ = 97.5 (d, $^2J_{P,P}$ = 174.8 Hz, $^1J_{P,Pt}$ = approx. 530 Hz, CP), 70.9 (dd, $^2J_{P,P}$ = 32.9, 23.1 Hz, $^1J_{P,Pt}$ = 2892 Hz, dcpe), 63.5 (dd, $^2J_{P,P}$ = 170.0, 21.7 Hz, $^1J_{P,Pt}$ = 3238 Hz, dcpe) ppm.

[(dcpe)Pt(TrippCP-W(CO$_5$)] (194)
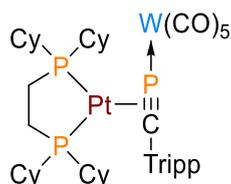
^{31}P{^{1}H} NMR (162 MHz, tetrahydrofuran-d_8): δ = 88.2 (dd, $^2J_{P,P}$ = 187.3, 29.6 Hz, $^1J_{P,Pt}$ = 369 Hz, $^1J_{P,W}$ = 186 Hz, CP), 71.4 (dd, $^2J_{P,P}$ = 29.5, 17.7 Hz, $^1J_{P,Pt}$ = 2871 Hz, dcpe), 62.5 (dd, $^2J_{P,P}$ = 187.6, 17.6 Hz, $^1J_{P,Pt}$ = 3306 Hz, dcpe) ppm.

^{195}Pt{^{1}H} NMR (86 MHz, tetrahydrofuran-d_8): δ = -4553 (ddd, $^1J_{Pt,P}$ = 3302, 2867, 367 Hz) ppm.

[(dtbpm)Pt(TrippCP-W(CO$_5$)] (195)
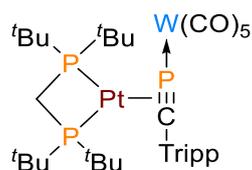
^{31}P{^{1}H} NMR (162 MHz, tetrahydrofuran): δ = 90.4 (dd, $^2J_{P,P}$ = 205.0, 24.6 Hz, $^1J_{P,Pt}$ = 421 Hz, $^1J_{P,W}$ = 185 Hz, C*P*), 16.5 (t, $^2J_{P,P}$ = 22.9 Hz, $^1J_{P,Pt}$ = 2466 Hz, dtbpm), 13.3 (dd, $^2J_{P,P}$ = 205.0, 20.6 Hz, $^1J_{P,Pt}$ = 2870 Hz, dtbpm) ppm.

[(dcpm)Pt(TrippCP-W(CO$_5$)] (196)
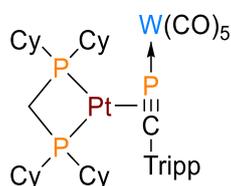
^{31}P{^{1}H} NMR (162 MHz, tetrahydrofuran): δ = 95.9 (dd, $^2J_{P,P}$ = 214.2, 21.2 Hz, $^1J_{P,Pt}$ = 428 Hz, $^1J_{P,W}$ = 184 Hz, C*P*), -8.7 (t, $^2J_{P,P}$ = 22.8 Hz, $^1J_{P,Pt}$ = 2392 Hz, dcpm), -11.2 (dd, $^2J_{P,P}$ = 213.9, 24.5 Hz, $^1J_{P,Pt}$ = 2820 Hz, dcpm) ppm.

4.2.11.2 Complexation of C≡P

[(dcpe)Pt(CP)(Mes)] + [Cr(CO)$_3$(MeCN)$_3$] (197)
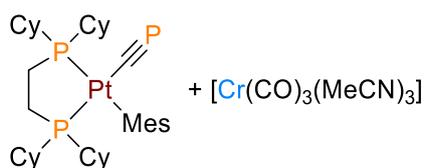
[(dcpe)Pt(CP)(Mes)] (**148σ**, 11 mg, 14 µmol, 1 eq) dissolved in 1.0 ml was added to J. Young NMR tube filled with [Cr(CO)3(MeCN)3] (3.7 mg, 14 µmol, 1 eq) at rt and shook for around 30 seconds, accompanied by a color change from orange to deep red.

^{31}P{^{1}H} NMR (162 MHz, tetrahydrofuran-*d$_8$*): δ = 102.9 (dd, $J_{P,P}$ = 14.4, 10.2 Hz, $J_{P,Pt}$ = 300 Hz, C*P*), 55.6 (d, $J_{P,P}$ = 9.3 Hz, $J_{P,Pt}$ = 1851 Hz, dcpe), 46.2 (d, $J_{P,P}$ = 14.3 Hz, $J_{P,Pt}$ = 2046 Hz, dcpe) ppm.

[(dcpe)Pt(MesCP)] + [Cr(CO)₃(MeCN)₃] (198)
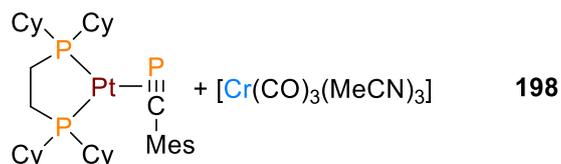
[(dcpe)Pt(CP)(Mes)] (**148**, 11 mg, 14 µmol, 1 eq) dissolved in 1.0 ml was added to J. Young NMR tube filled with [Cr(CO)3(MeCN)3] (3.7 mg, 14 µmol, 1 eq) at rt and shook for around 30 seconds, accompanied by a color change from orange to red.

³¹P{¹H} NMR (162 MHz, tetrahydrofuran-d_8): δ = 169.1 (dd, $J_{P,P}$ = 154.6, 32.7 Hz, $J_{P,Pt}$ = 302 Hz, CP), 71.8 (dd, $J_{P,P}$ = 32.5, 20.5 Hz, $J_{P,Pt}$ = 2916 Hz, dcpe), 63.1 (dd, $J_{P,P}$ = 155.1, 20.5 Hz, $J_{P,Pt}$ = 3250 Hz, dcpe) ppm.

[(dcpe)Pt(MesCP)] + [Cr(CO)₃(MeCN)₃] (199)

Both reactions **197**, **198** generated small amounts of the unknown by-product **199**.

³¹P{¹H} NMR (162 MHz, tetrahydrofuran-d_8): δ = 152.9 (d, $J_{P,P}$ = 178.0 Hz, CP), 69.5 (t, $J_{P,P}$ = 23.5 Hz, dcpe), 65.4 (dd, $J_{P,P}$ = 179.4, 24.4 Hz, dcpe) ppm.

4.2.11.3 Cyaphido replacement tryouts

General synthesis for the attempted cyaphido exchange with cyanido
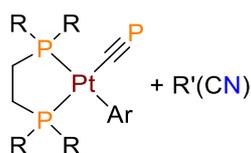
A high excess of the relevant cyanide salt was added into a Schlenk tube and dissolved (Bu₄(CN) in THF) or suspended (Et₄(CN) or Cu(CN) in MeCN). The appropriate π-complex [(P,P)M(CP)(R)] (10-25 mg, 1 eq) was separately dissolved in THF (2-5 ml) and the resulting orange solution transferred to the cyanide salt. The reaction mixture was stirred at room temperature for 1 week. The NMR samples were directly taken from the reaction mixture.

[(dcpe)Pt(CP)(Mes)] + [Cu(CN)] (200)
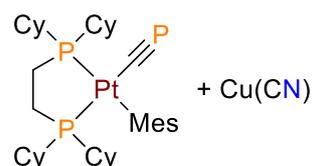
^{31}P{^{1}H} **NMR (162 MHz, tetrahydrofuran/acetonitrile)**: δ = 137.8 (br, C*P*), 69.8 (dd, $J_{P,P}$ = 32.8, 15.4 Hz, $J_{P,Pt}$ = 3035 Hz, dcpe), 64.3 (dd, $J_{P,P}$ = 35.4, 29.9 Hz, $J_{P,Pt}$ = 3252 Hz, dcpe) ppm.

[(dcpe)Pt(CP)(Mes)] + [Et$_4$N(CN)] (201)
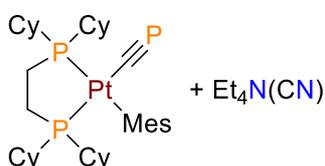
^{31}P{^{1}H} **NMR (162 MHz, tetrahydrofuran/acetonitrile)**: δ = 84.2 (d, $J_{P,P}$ = 7.7 Hz), 17.5 (dd, $J_{P,P}$ = 36.6, 7.5 Hz), 1.6 (d, $J_{P,P}$ = 36.1 Hz) ppm.

[(dcpe)Pt(CP)(Mes)] + [Bu$_4$N(CN)] (202)
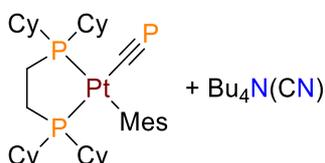
The purity of the crude product was improved by repetitive precipitation (5x) from THF under dropwise addition of pentane.

^{31}P{^{1}H} **NMR (162 MHz, tetrahydrofuran-*d$_8$*)**: δ = 83.0 (d, $J_{P,P}$ = 6.3 Hz, $J_{P,Pt}$ = 410 Hz), 16.9 (dd, $J_{P,P}$ = 35.1, 6.3 Hz, $J_{P,Pt}$ = 1710 Hz), 1.3 (d, $J_{P,P}$ = 35.3 Hz) ppm.

[(dippe)Pt(CP)(Mes)] + [Bu$_4$N(CN)] (203)
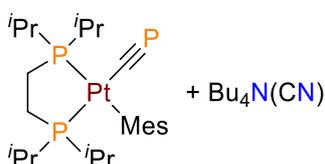
31P{1H} NMR (162 MHz, tetrahydrofuran-*d₈*): δ = 84.4 (d, $J_{P,P}$ = 6.8 Hz, $J_{P,Pt}$ = 410 Hz), 25.6 (dd, $J_{P,P}$ = 35.1, 6.8 Hz, $J_{P,Pt}$ = 1724 Hz), 9.7 (d, $J_{P,P}$ = 35.5 Hz) ppm.

[(dcpe)Pt(CP)(Tripp)] + [Bu₄N(CN)] (204)
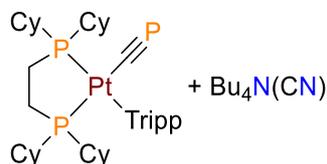
31P{1H} NMR (162 MHz, tetrahydrofuran-*d₈*): δ = 62.5 (d, $J_{P,P}$ = 4.9 Hz, $J_{P,Pt}$ = 2885 Hz), 41.3 (d, $J_{P,P}$ = 5.1 Hz, $J_{P,Pt}$ = 865 Hz) ppm.

4.2.11.4 Addition reactions on cyaphido

[(dcpe)PtCl] (209)
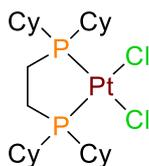
[(dcpe)Pt(CP)(Mes)] (**148σ**, 13.2 mg, 1 eq, 17 µmol) was added in a J. Young NMR tube and dissolved in toluene (1 ml). HCl (2 N in Et₂O, 34 µl, 4 eq) was added at T = -78 °C with a Hamilton syringe. The yellow solution turned colorless upon warming to rt, while a colorless solid precipitated. Removing of the solvent under reduced pressure and washing the residue with pentane yielded a colorless powder.

31P{1H} NMR (162 MHz, toluene): δ = 64.8 (s, $^1J_{P,Pt}$ = 3568 Hz).

[(dcpe)PtCl] (210)
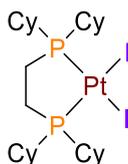
[(dcpe)Pt(CP)(Mes)] (**148σ**, 15.8 mg, 1 eq, 20 µmol) or [(dcpe)Pt(CP)(Tripp)] (**150σ**, 1 eq) was added in Schlenk tube and dissolved in THF (3 ml). MeI or *i*PrI (excess, 5 eq) was added at rt with a Hamilton syringe. The yellow solution brightens up after several days, while a colorless

solid precipitated. Removing of the solvent under reduced pressure and washing the residue with pentane yielded colorless flakes.

^{31}P{^{1}H} NMR (162 MHz, tetrahydrofuran-d_8): δ = 66.6 (s, $^1J_{P,Pt}$ = 3362 Hz).

4.2.11.5 Cycloaddition of azides on the cyaphido unit

General synthesis for the triazaphosphole complexes
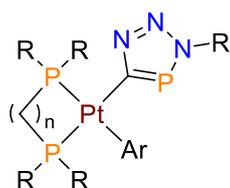
A azide solution (around 0.3 M in THF, 150 µmol, 1 eq) was added to a cyaphido complex ([(P,P)Pt(CP)(Ar)], 150 µmol, 1 eq) dissolved in THF (20 ml) and stirred at rt up to 1 week. The solvent was removed *in vacuo.* The crude product was resolved in a suitable solvent for NMR measurements. Caution: Due to very slow reaction rates of the Tripp cyaphido derivatives with bulky azides like MesN$_3$ or DippN$_3$, up to 10 eq of azide are required to prevent side reactions and attain the best possible results. Temperatures above T = 25 °C should be avoided to prevent profuse formation of π-complex by the reverse reaction of the cyaphido complex.

[(dippe)Pt(Mes)(TAP-Bn)] (212)
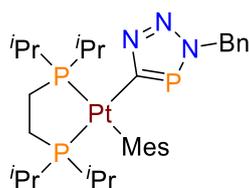
^{31}P{^{1}H} NMR (162 MHz, tetrahydrofuran-d_8): δ = 205.1 (d, $^3J_{P,P}$ = 28.1 Hz, $^2J_{P,Pt}$ = 611 Hz, C*P*), 67.7 (s, $^1J_{P,Pt}$ = 1815 Hz, dippe), 58.2 (d, $^3J_{P,P}$ = 28.6 Hz, $^1J_{P,Pt}$ = 1998 Hz, dippe) ppm.

[(dippe)Pt(Mes)(TAP-Dipp)] (213)
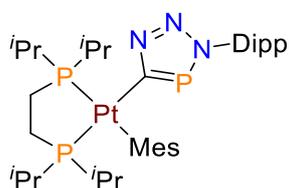
^{31}P{^{1}H} NMR (162 MHz, tetrahydrofuran-d_8): δ = 212.2 (d, $^3J_{P,P}$ = 27.5 Hz, $^2J_{P,Pt}$ = 594 Hz, C*P*), 66.9 (d, $J_{P,P}$ = 3.8 Hz, $^1J_{P,Pt}$ = 1800 Hz, dippe), 58.2 (d, $^3J_{P,P}$ = 27.4 Hz, $^1J_{P,Pt}$ = 2024 Hz, dippe) ppm.

^{195}Pt{^{1}H} NMR (86 MHz, tetrahydrofuran-d_8): δ = -4501 (ddd, $^{2,1}J_{Pt,P}$ = 2025, 1803, 592 Hz) ppm.

[(dippe)Pt(Tripp)(TAP-Bn)] (214)
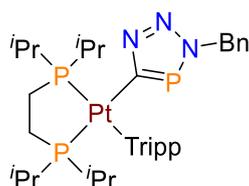
^{31}P{^{1}H} NMR (162 MHz, tetrahydrofuran-d_8): δ = 208.8 (d, $^3J_{P,P}$ = 30.0 Hz, $^2J_{P,Pt}$ = 572 Hz, C*P*), 64.0 (s, $^1J_{P,Pt}$ = 1825 Hz, dippe), 54.9 (d, $^3J_{P,P}$ = 29.8 Hz, $^1J_{P,Pt}$ = 1994 Hz, dippe) ppm.

^{195}Pt{^{1}H} NMR (86 MHz, tetrahydrofuran-d_8): δ = -4495 (ddd, $^{2,1}J_{Pt,P}$ = 1994, 1825, 571 Hz) ppm.

[(dcpe)Pt(Mes)(TAP-Bn)] (215)
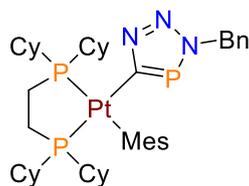
^{1}H NMR (400 MHz, benzene-d_6): δ = 7.04 (m, Ar), 6.94 (m, Ar), 5.34 (d, $^2J_{H,P}$ = 4.44 Hz, 2H, TAP-C*H$_2$*-Bn), 2.80 (s, 6H, *ortho*-C*H$_3$*-Mes), 2.36 (s, 3H, *para*-C*H$_3$*-Mes), 1.91-0.91 (m, 24H, P-C*H$_2$*, Cy) ppm.

^{31}P{^{1}H} NMR (162 MHz, tetrahydrofuran): δ = 202.9 (d, $^3J_{P,P}$ = 29.4 Hz, $^2J_{P,Pt}$ = 618 Hz, C*P*), 59.5 (s, $^1J_{P,Pt}$ = 1801 Hz, dcpe), 49.6 (d, $^3J_{P,P}$ = 29.2 Hz, $^1J_{P,Pt}$ = 1985 Hz, dcpe) ppm.

[(dcpe)Pt(Mes)(TAP-Bn)] (216)
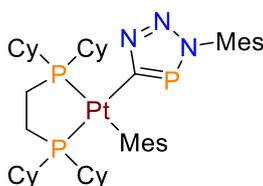
^{31}P{^{1}H} NMR (162 MHz, tetrahydrofuran): δ = 205.9 (d, $^3J_{P,P}$ = 28.8 Hz, $^2J_{P,Pt}$ = 608 Hz, C*P*), 60.1 (s, $^1J_{P,Pt}$ = 1800 Hz, dcpe), 50.8 (d, $^3J_{P,P}$ = 28.7 Hz, $^1J_{P,Pt}$ = 2014 Hz, dcpe) ppm.

[(dcpe)Pt(Mes)(TAP-Dipp)] (217)
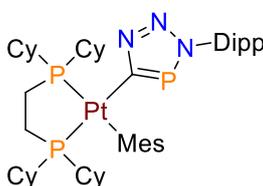
A solution of 2,6-diisopropylphenyl azide (320 µl of 0.379 M in THF, 122 µmol, 1 eq) was added to a yellow mixture of [(dcpe)Pt(MesCP)] (**148**) and [(dcpe)Pt(CP)(Mes)] (**148σ**) (ratio 1:4, 95 mg, 122 µmol, 1 eq) in THF (20 ml) and stirred at rt overnight. The solvent was removed *in vacuo* yielding a dark brown solid. The pale-yellow product could be obtained by extraction and filtration from *n*-pentane.

^{1}H NMR (400 MHz, benzene-*d$_6$*): δ = 7.11 (s, Ar), 7.09 (s, Ar), 7.03 (s, Ar), 2.84 (s, 6H, *ortho*-C*H$_3$*-Mes), 2.54 (sept, *J* = 6.92 Hz, 2H, C*H* of ^{i}Pr), 2.33 (s, 3H, *para*-C*H$_3$*-Mes), 1.14 (d, $^2J_{H,H}$ = 6.82 Hz, 6H, C*H$_3$* of ^{i}Pr), 1.04 (d, $^2J_{H,H}$ = 6.90 Hz, 6H, C*H$_3$* of ^{i}Pr), 1.97-0.97 (m, 24H, P-C*H$_2$*, Cy) ppm.

^{31}P{^{1}H} NMR (162 MHz, tetrahydrofuran): δ = 211.0 (dd, $^3J_{P,P}$ = 28.3, 4.0 Hz, $^2J_{P,Pt}$ = 592 Hz, C*P*), 59.0 (d, $^{2,3}J_{P,P}$ = 3.9 Hz, $^1J_{P,Pt}$ = 1799 Hz, dcpe), 50.3 (d, $^{2,3}J_{P,P}$ = 28.4 Hz, $^1J_{P,Pt}$ = 2026 Hz, dcpe) ppm.

^{195}Pt{^{1}H} NMR (86 MHz, tetrahydrofuran): δ = -4489 (ddd, $^{2,1}J_{Pt,P}$ = 2026, 1799, 592 Hz) ppm.

HRMS (EI pos): m/z calc. for [$C_{48}H_{76}N_3P_3Pt$]: 821.3570; found: 821.3606

Elemental analysis for $C_{48}H_{76}N_3P_3Pt$: calc.: C: 58.64%, H: 7.79%, N: 4.27%; found: C: 56.30%, H: 7.91%, N: 4.02%.

[{(dcpe)Pt(Mes)(TAP)}₂-*o*-methylpyridine)] (218)
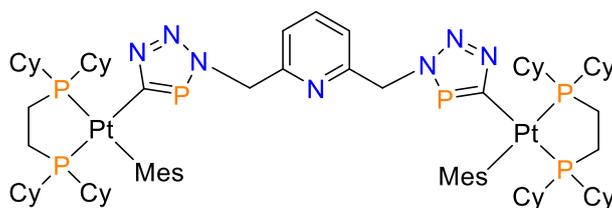
¹H NMR (400 MHz, tetrahydrofuran-*d₈*): δ = 7.55 (t, $^3J_{H,H}$ = 7.75 Hz, 2H, *para*-H-py), 7.18 (d, $^3J_{H,H}$ = 7.60 Hz, 2H, *ortho*-H-py), 6.59 (s, 4H, *meta*-H-Mes), 5.70 (d, $^2J_{H,P}$ = 4.41 Hz, 4H, TAP-C*H₂*-py), 2.36 (s, 12H, *ortho*-C*H₃*-Mes), 2.13 (s, 6H, *para*-C*H₃*-Mes), 1.24-0.86 (m, 48H, P-C*H₂*, Cy) ppm.

³¹P{¹H} NMR (162 MHz, tetrahydrofuran-*d₈*): δ = 205.6 (d, $^3J_{P,P}$ = 29.5 Hz, $^2J_{P,Pt}$ = 605 Hz, C*P*), 60.2 (s, $^1J_{P,Pt}$ = 1805 Hz, dcpe), 50.5 (d, $^3J_{P,P}$ = 28.9 Hz, $^1J_{P,Pt}$ = 2005 Hz, dcpe) ppm.

[(dcpe)Pt(Tripp)(TAP-Bn)] (219)
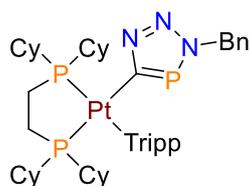
³¹P{¹H} NMR (162 MHz, tetrahydrofuran): δ = 206.9 (d, $^3J_{P,P}$ = 31.3 Hz, $^2J_{P,Pt}$ = 592 Hz, C*P*), 56.1 (d, $J_{P,P}$ = 3.0 Hz, $^1J_{P,Pt}$ = 1802 Hz, dcpe), 46.6 (d, $^3J_{P,P}$ = 31.0 Hz, $^1J_{P,Pt}$ = 1990 Hz, dcpe) ppm.

[(dcpe)Pt(Tripp)(TAP-Dipp)] (220)
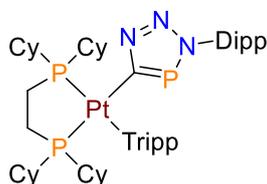
³¹P{¹H} NMR (162 MHz, tetrahydrofuran): δ = 218.6 (d, $^3J_{P,P}$ = 28.3 Hz, $^2J_{P,Pt}$ = 575 Hz, C*P*), 58.9 (s, $^1J_{P,Pt}$ = 1813 Hz, dcpe), 48.3 (d, $^3J_{P,P}$ = 28.4 Hz, $^1J_{P,Pt}$ = 2008 Hz, dcpe) ppm.

[(dcpm)Pt(Tripp)(TAP-Dipp)] (221)
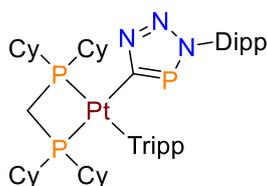
^{31}**P{^{1}H} NMR (162 MHz, tetrahydrofuran)**: δ = 210.6 (d, $^3J_{P,P}$ = 29.8 Hz, $^2J_{P,Pt}$ = 609 Hz, C*P*), -26.3 (d, $J_{P,P}$ = 21.7 Hz, $^1J_{P,Pt}$ = 1560 Hz, dcpm), -36.6 (t, $J_{P,P}$ = 26.5 Hz, $^1J_{P,Pt}$ = 1656 Hz, dcpm) ppm.

4.2.12 Preparation of cyaphido gold(I) complexes

General synthesis for the cyaphido gold(+1) complexes
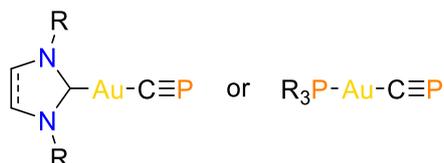
Note: The first 3 steps for the synthesis of the [(L)Au(F)] complexes were performed analogously to a literature protocol.[470]

[(L)Au(Cl)]

AuCl · SMe$_2$ (300 mg, 1.02 µmol, 1 eq) and the appropriate NHC or Phosphine (1.02 µmol, 1 eq) were dissolved in DCM (10 ml) and stirred for 2 h at rt. All volatiles were removed *in vacuo*. The residue was washed with pentane (2x 2 ml) and dried, yielding a colorless powder.

[(L)Au(I)]

NaI (10 eq) and [(L)Au(Cl)] (1 eq) were suspended in DCM (10 ml) and stirred at rt for 2 days. After filtration of the reaction mixture, the filtrate was concentrated under reduce pressure until a colorless solid precipitated. Pentane (5 ml) was added and the formed colorless solid was collected by filtration and dried.

[(L)Au(F)]

[(L)Au(I)] (70 µmol, 1 eq) and AgF (1.4 mmol, 20 eq) were added to a PFA tube and suspended in DCM (0.5 ml). The PFA tube sample was first frozen in liquid nitrogen and then flame-sealed under vacuum. The sealed sample was sonicated in an ultrasonic bath for 1 h. After opening the PFA tube under a stream of argon, the liquid phase was transferred by a filtration cannula into another PFA tube and again frozen in liquid nitrogen. A toluene solution of Me$_3$SiCP

(0.11 M in toluene, 1 eq) was added on top of the frozen DCM solution of [(L)Au(F)]. The sample was completely frozen in liquid nitrogen and flame-sealed under vacuum. The closed PFA tube was stored in a beaker at rt until it was fully defrosted. The sample was shaken several times to blend the two phases. The PFA tube containing a yellow solution was slid into a regular NMR tube to run the NMR measurements.

$$AuCl \cdot SMe_2 \xrightarrow[\substack{DCM, rt, \\ 2\ h}]{L\ (1\ eq)} [LAuCl] \xrightarrow[\substack{DCM, rt, \\ 2\ d \\ -\ NaCl}]{NaI\ (10\ eq)} [LAuI] \xrightarrow[\substack{DCM, rt, \\ ultrasonic, \\ 1\ h \\ -\ AgI}]{AgF\ (20\ eq)} [LAuF] \xrightarrow[\substack{DCM, \\ -97\ °C\ to\ rt \\ -\ Me_3SiF}]{Me_3Si-\!\!\equiv\!\!P\ (1\ eq)} L-Au-\!\!\equiv\!\!P$$

L = NHC, PR$_3$
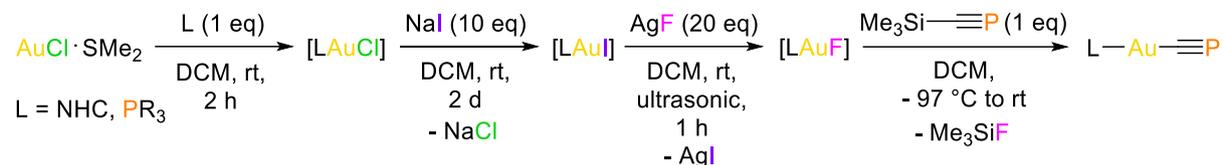
[(IMe$_4$)Au(CP)] (222)
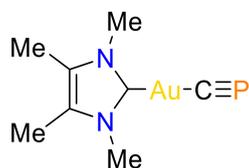
^{31}P{^{1}H} NMR (162 MHz, toluene/DCM-d_2): δ = 86.1 (s) ppm.

[(SIMes)Au(CP)] (224)
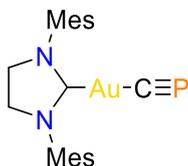
^{31}P{^{1}H} NMR (162 MHz, toluene/DCM-d_2): δ = 84.5 (s) ppm.

[(IDipp)Au(CP)] (1.35)
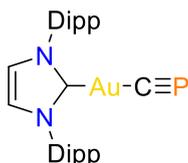
^{31}P{^{1}H} NMR (162 MHz, toluene/DCM-d_2): δ = 83.9 (s) ppm.

[(BrettPhos)Au(CP)] (226)
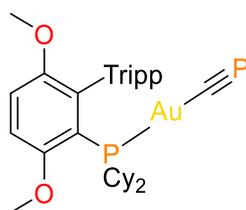
^{31}P{^{1}H} NMR (162 MHz, toluene/DCM-d_2): δ = 74.4 (d, $^3J_{P,P}$ = 13.3 Hz, C*P*), 44.0 (d, $^3J_{P,P}$ = 12.4 Hz, BrettPhos) ppm.

5 Appendix

5.1 Calculated ^{31}P NMR shifts

Calculated ^{31}P shifts of the phosphaalkyne, cyaphido or triazaphospholato phosphorus nuclei. [a] C≡P group was not complete planar to the benzene ring, [b] the BMe$_3$ group detached during the calculations and was too far away for a proper dative coordination to the phosphorus.

cpd number **81**	**76**	**86**	**92**
calc. [ppm] 11.5	32.3	-28.1	108.5[a]

C1	**C2**	**C3**	**C4**	**C5**
183.8	300.9	322.7	145.7	177.2

C6	**C7**	**C8**
108	146.8	267.5

C4σ	**C5**σ	**C6**σ	**C7**σ
194.4	171.6	125	85.8

C10	**C10**σ	**C11**
152.0	91.2[b]	194.8

C12

240.8

C12σ

165.9

C13

180.1
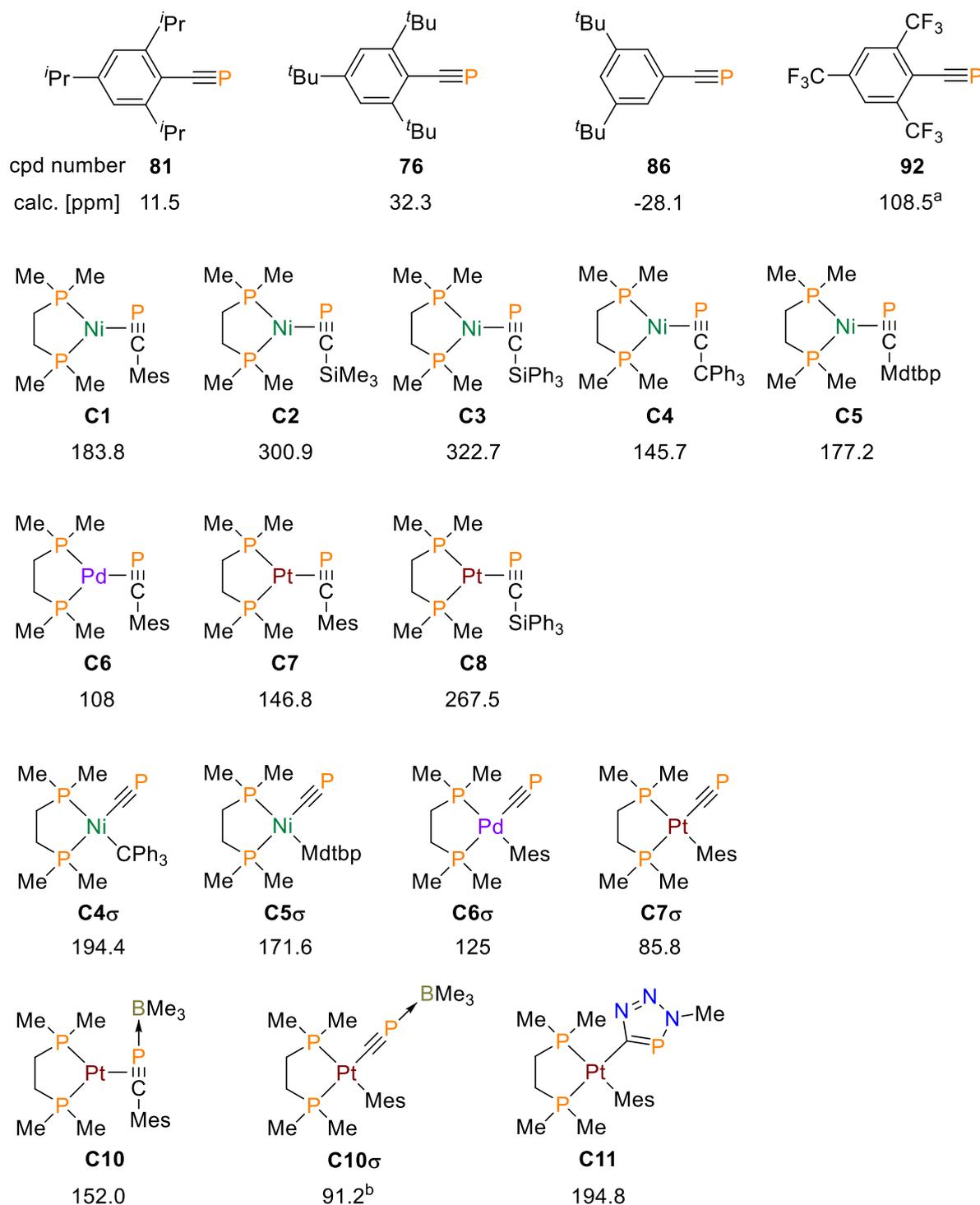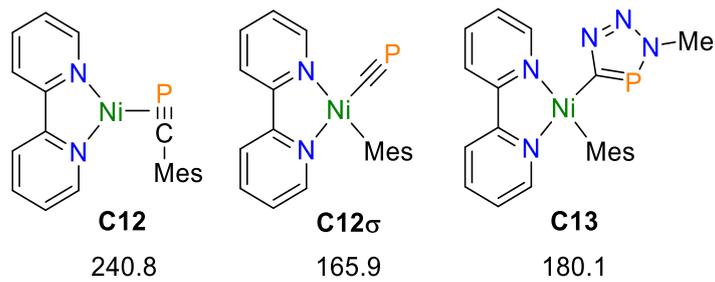
5.2 ^{31}P shift comparison of the σ-/π-complex systems

Overview over the ^{31}P{^{1}H}, ^{195}P{^{1}H} NMR signals of the relevant π-complexes (green), which were successful converted into the corresponding σ-complexes (red).

compounds	nr	^{31}P{^{1}H} P1 [ppm]	$J_{P,P}$ P1 [Hz]	$J_{P,Pt}$ P1 [Hz]	^{31}P{^{1}H} P2 [ppm]	$J_{P,P}$ P2 [Hz]	$J_{P,Pt}$ P2 [Hz]	^{31}P{^{1}H} P3 [ppm]	$J_{P,P}$ P3 [Hz]	$J_{P,Pt}$ P3 [Hz]	^{195}Pt{^{1}H} Pt1 [ppm]
[(dippe)Pt(CP)(Mes)]	**143σ**	99.0	18.2, 10.7	340	68.9	10.7	1653	57.9	18.0	2169	-4476
[(dippe)Pt(CP)(Tripp)]	**144σ**	107.5	17.2, 11.9	335	66.1	11.1	1639	54.4	17.1	2153	
[(dcpe)Pt(CP)(Mes)]	**148σ**	96.6	17.7, 10.4	338	60.2	10.3	1654	49.2	17.8	2164	-4463
[(dcpe)Pt(CP)(Tripp)]	**150σ**	108.9	18.2, 10.7	331	60.9	10.6	1647	48.6	17.5	2145	-4393
[(dcpe)Pt(CP)(Mdtbp)]	**152σ**	90.2	18.6, 10.0	348	58.1	9.5	1590	49.5	18.4	2169	
[(dtbpm)Pt(CP)(Tripp)]	**166σ**	104.9	13.2	360	-7.6	9.0	1333	-11.1	14.6, 6.9	1761	
[(dcpm)Pt(CP)(Tripp)]	**170σ**	110.5	18.8, 11.2	345	-29.1	30.2, 10.2	1343	-38.2	30.2, 18.5	1824	-3792
[(dippe)Pt(MesCP)]	**143**	140.5	29.2, 15.7	234	82.9	37.2, 15.7	3056	74.0	37.1, 29.1	3211	-4611
[(dippe)Pt(TrippCP)]	**144**	145.8	28.7, 17.2	229	79.5	36.5, 16.7	3044	70.7	36.5, 28.2	3213	
[(dcpe)Pt(MesCP)]	**148**	140.0	29.5, 15.6	230	71.7	37.8, 14.5	3056	65.8	37.7, 29.4	3205	-4582
[(dcpe)Pt(TrippCP)]	**150**	149.9	29.1, 17.5	217	69.2	35.4, 16.7	3046	64.2	35.4, 29.1	3212	-4578
[(dcpe)Pt(MdtbpCP)]	**152**	137.3	31.0, 19.7	204	69.6	33.4, 19.4	2937	64.3	31.8	3178	
[(dtbpm)Pt(TrippCP)]	**166**	155.8	33.7, 16.7	220	29.4	58.6, 33.3	2626	25.1	58.7, 16.3	2683	
[(dcpm)Pt(TrippCP)]	**170**	163.8	36.1, 17.7	224	1.4	17.1, 9.3	2543	-0.4	35.7, 9.7	2654	-3991

5.3 UV-Vis spectra

All UV-Vis spectra were recorded in THF. All *π*-complex sample and **150σ** are pure. The *σ*-complex sample **143σ** contain at least 30% of the corresponding *π*-complex.
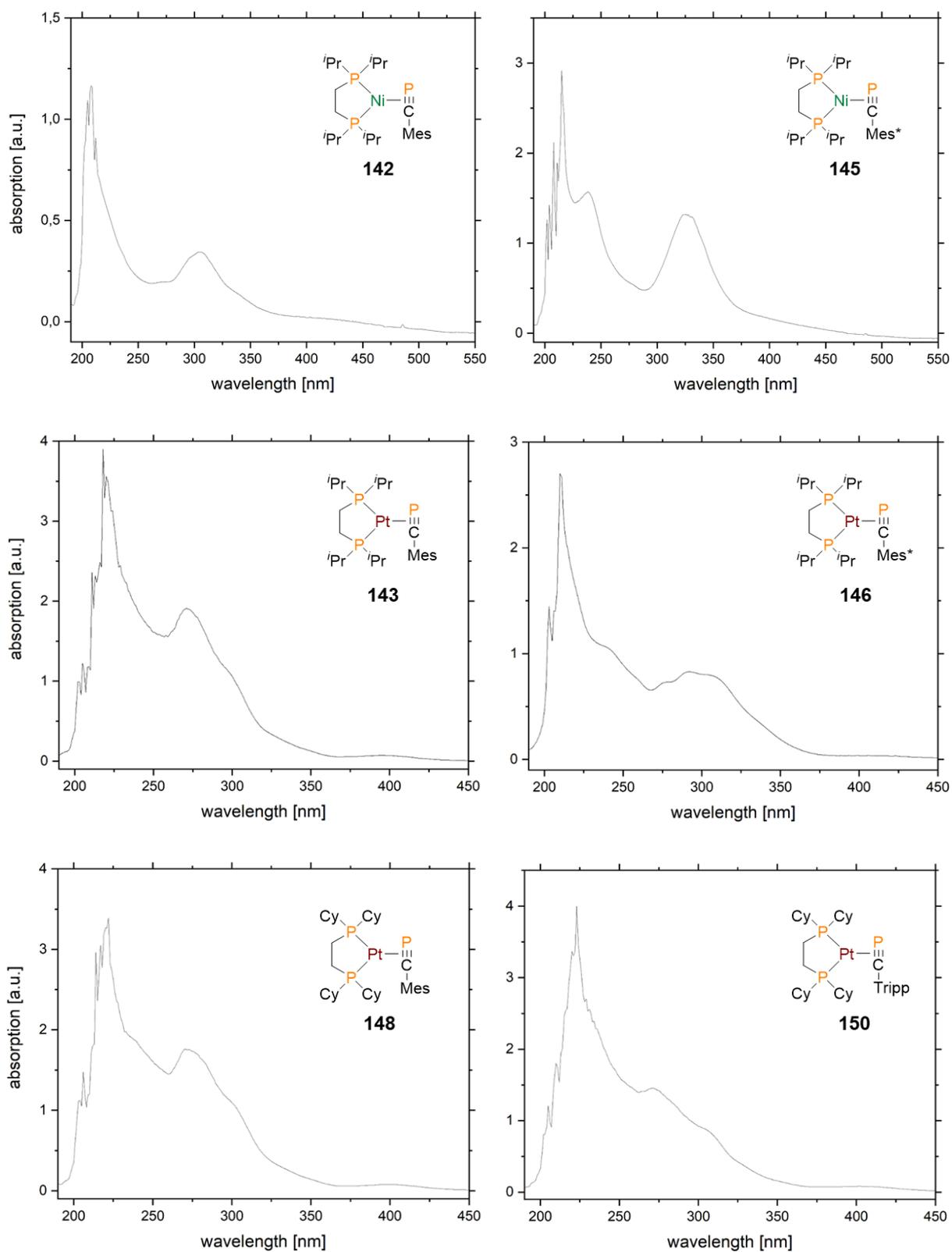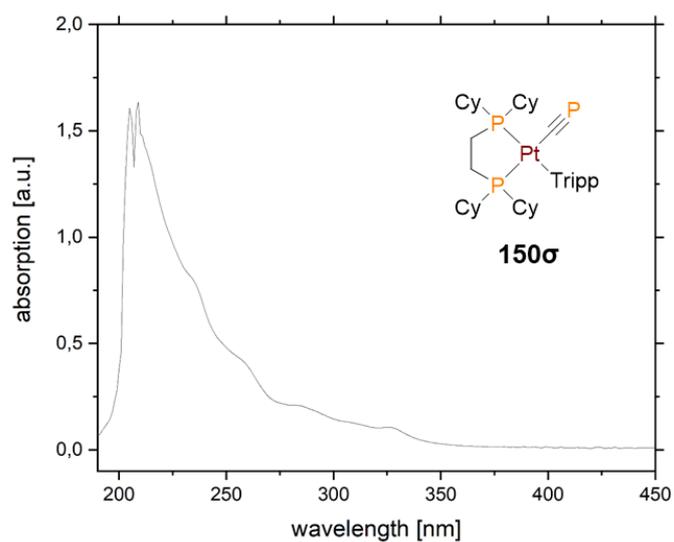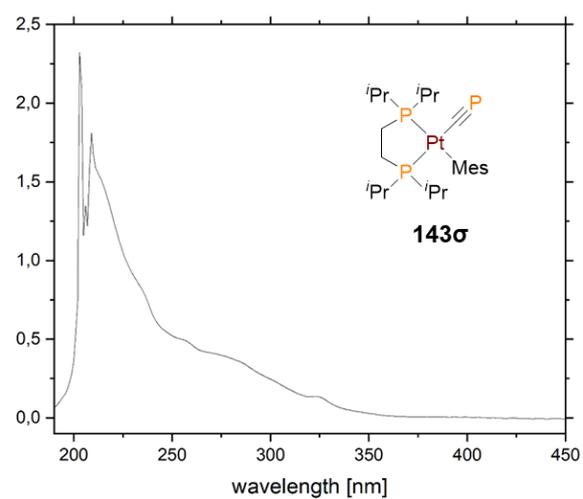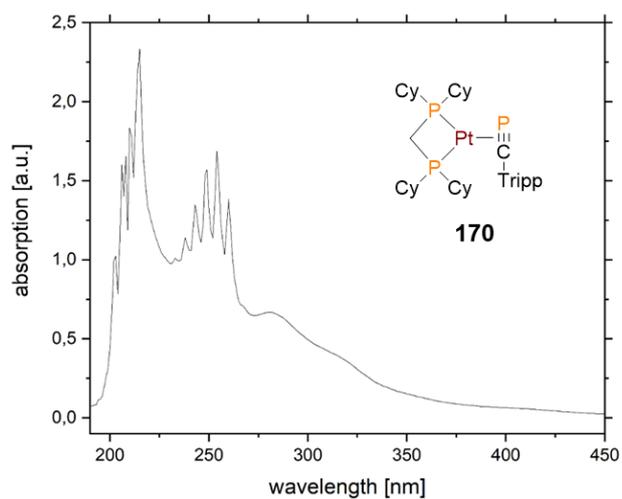
5.4 Infrared spectra

All IR spectra were recorded from the product powders.
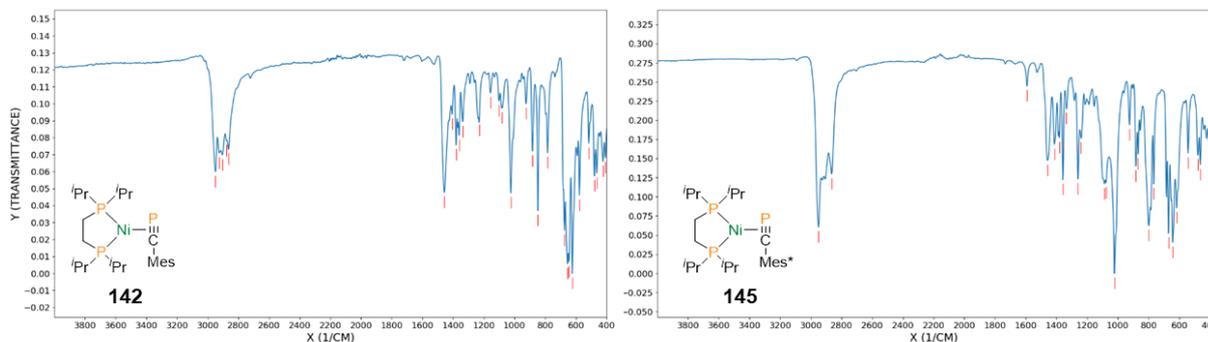
IR (**142**) = 2949 (m), 2925 (m), 2904 (m), 2878 (w), 2864 (m), 1458 (s), 1407 (w), 1381 (m), 1360 (w), 1338 (w), 1230 (w), 1156 (w), 1101 (w), 1083 (w), 1024 (s), 924 (w), 883 (m), 848 (vs), 785 (m), 675 (vs), 655 (vs), 647 (vs), 624 (vs), 577 (s), 516 (m), 479 (s), 465 (m), 424 (m), 408 (m) cm^{-1}; IR (**145**) = 2949 (vs), 2864 (m), 1591 (vw), 1458 (m), 1413 (m), 1381 (w), 1358 (s), 1336 (w), 1260 (s), 1240 (w), 1087 (s), 1077 (s), 1022 (vs), 924 (w), 883 (m), 869 (m), 800 (vs), 767 (s), 671 (vs), 642 (vs), 618 (vs), 543 (m), 479 (m), 463 (m) cm^{-1}.
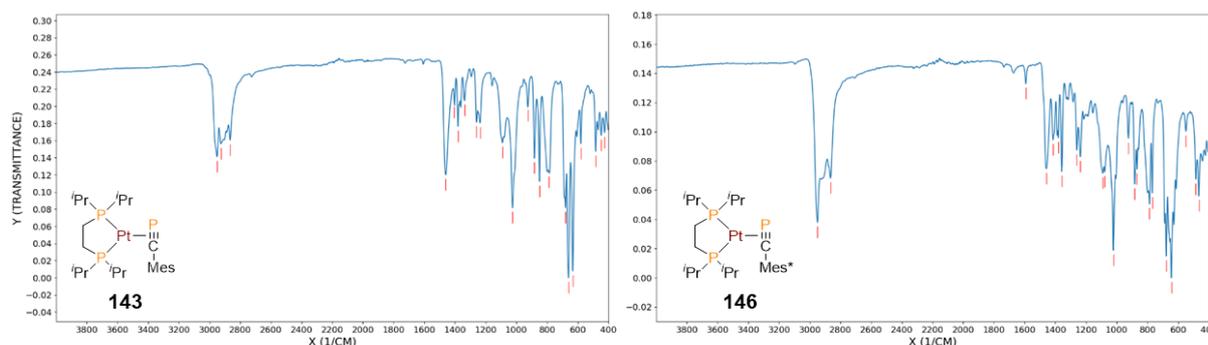
IR (**143**) = 2951 (m), 2925 (w), 2866 (w), 1460 (m), 1405 (w), 1381 (w), 1338 (w), 1260 (w), 1236 (w), 1091 (w), 1026 (s), 924 (w), 883 (m), 851 (s), 787 (m), 681 (s), 661 (vs), 632 (vs), 579 (w), 483 (m), 449 (w), 426 (w) cm^{-1}; IR (**146**) = 2949 (vs), 2864 (m), 1593 (vw), 1458 (m), 1415 (w), 1381 (w), 1358 (m), 1260 (m), 1238 (m), 1091 (m), 1079 (m), 1022 (vs), 924 (w), 883 (s), 869 (m), 787 (s), 769 (s), 677 (vs), 645 (vs), 551 (w), 485 (s), 465 (s) cm^{-1}.
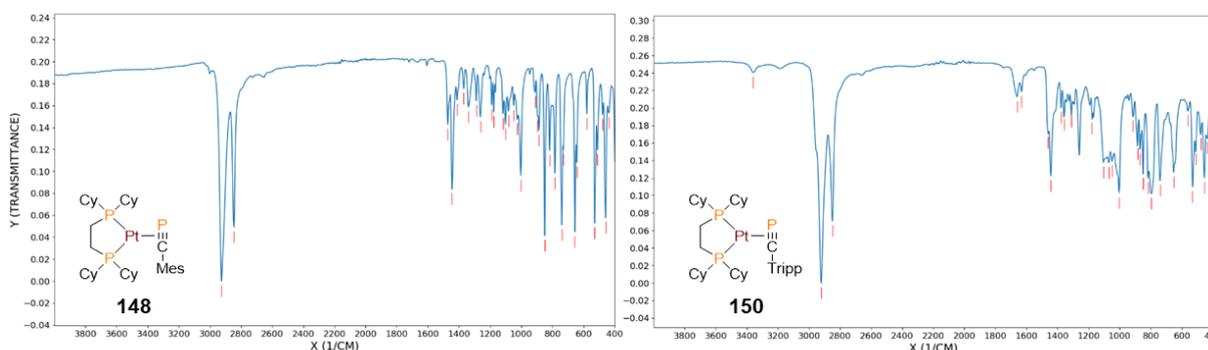
IR (**148**) = 2927 (vs), 2845 (vs), 1473 (w), 1446 (s), 1413 (w), 1371 (vw), 1340 (w), 1289 (w), 1263 (w), 1189 (w), 1177 (w), 1118 (w), 1101 (w), 1083 (w), 1048 (w), 1026 (w), 1003 (m), 912 (w), 895 (w), 887 (w), 851 (vs), 818 (m), 785 (m), 740 (vs), 730 (m), 657 (vs), 645 (m), 579 (w), 530 (vs), 512 (m), 479 (w), 459 (vs), 439 (w) cm^{-1}; IR (**150**) = 3359 (vw), 2921 (vs), 2849 (vs), 1660 (w), 1632 (vw), 1462 (w), 1444 (m), 1377 (w), 1356 (w), 1309 (w), 1179 (w), 1105 (m), 1071 (m), 1050 (m), 1003 (s), 916 (w), 885 (w), 871 (m), 851 (m), 818 (m), 797 (s), 740 (m), 653 (m), 561 (w), 532 (s), 510 (m), 479 (w), 455 (m), 439 (w) cm^{-1}.

IR (**170**) = 2921 (vs), 2849 (vs), 1446 (s), 1377 (w), 1356 (w), 1293 (w), 1260 (w), 1175 (w), 1105 (w), 1071 (m), 1001 (m), 916 (w), 885 (m), 871 (m), 848 (s), 812 (m), 751 (m), 673 (w), 510 (m), 498 (m), 459 (m) cm^{-1}; IR (**143σ** & **143**; ratio 3:2) = 2951 (m), 2923 (m), 2868 (m), 1458 (s), 1383 (w), 1362 (w), 1318 (m), 1242 (w), 1158 (w), 1093 (w), 1075 (w), 1028 (s), 926 (w), 883 (m), 846 (s), 789 (m), 714 (w), 683 (vs), 663 (vs), 632 (vs), 581 (w), 487 (m), 467 (w), 449 (w) cm^{-1}.

IR (**148σ** & **148**; ratio 1:3) = 2922 (vs), 2846 (vs), 1445 (vs), 1342 (w), 1319 (w), 1258 (s), 1178 (m), 1069 (vs), 1002 (vs), 912 (m), 887 (m), 851 (vs), 809 (vs), 739 (vs), 713 (m), 656 (vs), 580 (m), 530 (vs), 512 (s), 458 (s) cm^{-1}; IR (**150σ**) = 2955 (m), 2923 (vs), 2849 (vs), 1444 (m), 1418 (w), 1377 (w), 1356 (w), 1311 (m), 1260 (w), 1179 (w), 1097 (m), 1069 (m), 1050 (m), 1018 (m), 1003 (m), 916 (w), 887 (w), 869 (w), 851 (m), 818 (m), 791 (s), 751 (m), 738 (s), 663 (s), 649 (w), 534 (vs), 512 (w), 481 (w), 455 (w), 434 (w) cm^{-1}.

IR (**170σ** & **170**; ratio 1:3) = 2921 (vs), 2849 (vs), 1444 (s), 1377 (w), 1356 (w), 1316 (w), 1293 (w), 1260 (w), 1175 (w), 1105 (w), 1069 (s), 1001 (m), 914 (w), 885 (m), 871 (m), 848 (s), 812 (m), 751 (s), 669 (m), 510 (s) cm^{-1}.

5.5 X-ray crystallographic data

Identification code	15a	21a	68
Empirical formula	$C_{30}H_{66}NiO_5P_4$	$C_{25}H_{52}O_5P_2$	$C_{19}H_{29}P$
Formula weight	689.41	494.60	288.39
Temperature/K	100(2)	100.0	100(2)
Crystal system	monoclinic	monoclinic	monoclinic
Space group	$P2_1/c$	$C2/c$	$P2_1/n$
a/Å	10.8186(2)	23.6897(12)	9.9060(5)
b/Å	16.1898(3)	9.0331(5)	11.0122(6)
c/Å	10.9735(2)	14.7140(8)	16.4158(10)
α/°	90	90	90
β/°	109.0245(7)	118.372(2)	96.201(2)
γ/°	90	90	90
Volume/Å³	1817.04(6)	2770.5(3)	1780.27(17)
Z	2	4	4
ρ_{calc}g/cm³	1.260	1.186	1.076
μ/mm⁻¹	0.744	1.669	0.145
F(000)	748.0	1088.0	632.0
Crystal size/mm³	0.65 × 0.443 × 0.276	0.46 × 0.13 × 0.07	0.23 × 0.21 × 0.06
Radiation	MoKα (λ = 0.71073)	CuKα (λ = 1.54178)	MoKα (λ = 0.71073)
2Θ range for data collection/°	4.664 to 51.542	8.484 to 136.714	4.462 to 52.846
Index ranges	-13 ≤ h ≤ 13, -19 ≤ k ≤ 19, -11 ≤ l ≤ 13	-28 ≤ h ≤ 28, -10 ≤ k ≤ 10, -17 ≤ l ≤ 17	-11 ≤ h ≤ 12, -12 ≤ k ≤ 13, -20 ≤ l ≤ 20
Reflections collected	28836	19587	14604
Independent reflections	3333 [R_{int} = 0.0297, R_{sigma} = 0.0142]	2523 [R_{int} = 0.0720, R_{sigma} = 0.0329]	3670 [R_{int} = 0.0393, R_{sigma} = 0.0334]
Data/restraints/parameters	3333/1/195	2523/0/158	3670/0/190
Goodness-of-fit on F²	1.045	1.176	1.036
Final R indexes [I>=2σ (I)]	R_1 = 0.0310, wR_2 = 0.0771	R_1 = 0.0614, wR_2 = 0.1652	R_1 = 0.0404, wR_2 = 0.0984
Final R indexes [all data]	R_1 = 0.0333, wR_2 = 0.0791	R_1 = 0.0626, wR_2 = 0.1661	R_1 = 0.0543, wR_2 = 0.1059
Largest diff. peak/hole / e Å⁻³	0.81/-0.84	0.74/-0.71	0.25/-0.34

Identification code	76	98	142
Empirical formula	$C_{10}H_{11}P$	$C_{12}H_{15}Cl_3$	$C_{24}H_{43}NiP_3$
Formula weight	162.16	265.59	483.20
Temperature/K	100.03	100(2)	100(2)
Crystal system	trigonal	triclinic	monoclinic
Space group	$P3_121$	$P-1$	$P2_1/n$
a/Å	13.6923(5)	9.2057(2)	8.8988(2)
b/Å	13.6923(5)	9.25070(10)	15.9373(3)
c/Å	8.4916(4)	9.2732(2)	18.6658(4)
α/°	90	118.1877(5)	90
β/°	90	102.0372(6)	93.4571(7)
γ/°	120	108.0117(5)	90
Volume/Å³	1378.71(12)	599.78(2)	2642.42(10)
Z	6	2	4
ρ_{calc}g/cm³	1.172	1.471	1.215
μ/mm⁻¹	2.083	0.727	0.924
F(000)	516.0	276.0	1040.0
Crystal size/mm³	0.275 × 0.177 × 0.149	0.38 × 0.26 × 0.15	0.35 × 0.28 × 0.26
Radiation	CuKα (λ = 1.54178)	MoKα (λ = 0.71073)	MoKα (λ = 0.71073)
2Θ range for data collection/°	7.454 to 149.274	5.136 to 52.898	4.96 to 52.83
Index ranges	-17 ≤ h ≤ 17, -17 ≤ k ≤ 17, -10 ≤ l ≤ 10	-11 ≤ h ≤ 11, -11 ≤ k ≤ 10, -11 ≤ l ≤ 11	-11 ≤ h ≤ 11, -19 ≤ k ≤ 18, -23 ≤ l ≤ 23

Reflections collected	22267	10159	28809
Independent reflections	1896 [R_{int} = 0.0442, R_{sigma} = 0.0214]	2473 [R_{int} = 0.0246, R_{sigma} = 0.0206]	5409 [R_{int} = 0.0356, R_{sigma} = 0.0261]
Data/restraints/parameters	1896/0/110	2473/0/139	5409/0/264
Goodness-of-fit on F^2	1.140	1.085	1.042
Final R indexes [I>=2σ (I)]	R_1 = 0.0297, wR_2 = 0.0749	R_1 = 0.0253, wR_2 = 0.0708	R_1 = 0.0296, wR_2 = 0.0704
Final R indexes [all data]	R_1 = 0.0299, wR_2 = 0.0751	R_1 = 0.0278, wR_2 = 0.0723	R_1 = 0.0369, wR_2 = 0.0738
Largest diff. peak/hole / e Å^{-3}	0.16/-0.35	0.34/-0.38	0.68/-0.33

Identification code	143	145	146
Empirical formula	$C_{24}H_{43}P_3Pt$	$C_{33}H_{61}NiP_3$	$C_{33}H_{61}P_3Pt$
Formula weight	619.58	609.43	745.81
Temperature/K	100(2)	103.7	150.0
Crystal system	monoclinic	monoclinic	monoclinic
Space group	P2$_1$/c	P2$_1$/c	P2$_1$/c
a/Å	14.7712(12)	9.5405(9)	9.5083(2)
b/Å	10.6893(9)	19.7858(17)	20.1797(4)
c/Å	17.2098(14)	18.5102(16)	18.6164(4)
α/°	90	90	90
β/°	103.831(3)	94.075(4)	93.9650(10)
γ/°	90	90	90
Volume/Å^3	2638.5(4)	3485.3(5)	3563.47(13)
Z	4	4	4
ρ$_{calc}$g/cm^3	1.560	1.161	1.390
μ/mm^{-1}	5.508	0.714	4.091
F(000)	1240.0	1328.0	1528.0
Crystal size/mm^3	0.179 × 0.101 × 0.072	0.362 × 0.193 × 0.18	0.26 × 0.24 × 0.13
Radiation	MoKα (λ = 0.71073)	MoKα (λ = 0.71073)	MoKα (λ = 0.71073)
2Θ range for data collection/°	4.524 to 61.134	4.28 to 61.26	4.294 to 61.076
Index ranges	-21 ≤ h ≤ 21, -15 ≤ k ≤ 15, -24 ≤ l ≤ 24	-13 ≤ h ≤ 13, -28 ≤ k ≤ 28, -26 ≤ l ≤ 26	-13 ≤ h ≤ 13, -28 ≤ k ≤ 28, -26 ≤ l ≤ 26
Reflections collected	130431	129982	92693
Independent reflections	8082 [R_{int} = 0.0867, R_{sigma} = 0.0357]	10717 [R_{int} = 0.0649, R_{sigma} = 0.0292]	10872 [R_{int} = 0.0456, R_{sigma} = 0.0244]
Data/restraints/parameters	8082/706/454	10717/0/351	10872/0/351
Goodness-of-fit on F^2	1.061	1.099	1.083
Final R indexes [I>=2σ (I)]	R_1 = 0.0316, wR_2 = 0.0477	R_1 = 0.0338, wR_2 = 0.0707	R_1 = 0.0198, wR_2 = 0.0378
Final R indexes [all data]	R_1 = 0.0503, wR_2 = 0.0516	R_1 = 0.0514, wR_2 = 0.0810	R_1 = 0.0268, wR_2 = 0.0406
Largest diff. peak/hole / e Å^{-3}	1.02/-1.31	0.47/-0.45	0.53/-1.00

Identification code	148	148σ	150σ
Empirical formula	$C_{36}H_{59}P_3Pt$	$C_{36}H_{59}P_3Pt$	$C_{42}H_{71}P_3Pt$
Formula weight	779.83	779.83	863.98
Temperature/K	100	100	100.1
Crystal system	monoclinic	monoclinic	monoclinic
Space group	P2$_1$/c	P2$_1$/c	P2$_1$/c
a/Å	12.4228(5)	12.4228(5)	9.6079(10)
b/Å	19.6106(8)	19.6106(8)	10.3645(12)
c/Å	16.7798(6)	16.7798(6)	41.187(5)
α/°	90	90	90
β/°	109.785(2)	109.785(2)	95.772(3)
γ/°	90	90	90

Volume/Å^3	3846.6(3)	3846.6(3)	4080.6(8)
Z	4	4	4
ρ_{calc}g/cm^3	1.347	1.347	1.406
μ/mm^{-1}	3.794	3.794	3.584
F(000)	1592.0	1592.0	1784.0
Crystal size/mm^3	0.319 × 0.176 × 0.134	0.319 × 0.176 × 0.134	0.416 × 0.239 × 0.14
Radiation	MoKα (λ = 0.71073)	MoKα (λ = 0.71073)	MoKα (λ = 0.71073)
2Θ range for data collection/°	4.126 to 66.352	4.126 to 66.352	4.054 to 39.398
Index ranges	-19 ≤ h ≤ 19, -29 ≤ k ≤ 30, -25 ≤ l ≤ 25	-19 ≤ h ≤ 19, -29 ≤ k ≤ 30, -25 ≤ l ≤ 25	-8 ≤ h ≤ 9, -9 ≤ k ≤ 9, -39 ≤ l ≤ 39
Reflections collected	252429	252429	12574
Independent reflections	14667 [R_{int} = 0.0526, R_{sigma} = 0.0216]	14667 [R_{int} = 0.0526, R_{sigma} = 0.0216]	3586 [R_{int} = 0.1912, R_{sigma} = 0.1611]
Data/restraints/parameters	14667/0/364	14667/0/364	3586/69/431
Goodness-of-fit on F^2	1.046	1.045	1.038
Final R indexes [I>=2σ (I)]	R_1 = 0.0215, wR_2 = 0.0475	R_1 = 0.0215, wR_2 = 0.0475	R_1 = 0.0737, wR_2 = 0.1202
Final R indexes [all data]	R_1 = 0.0281, wR_2 = 0.0496	R_1 = 0.0281, wR_2 = 0.0495	R_1 = 0.1205, wR_2 = 0.1372
Largest diff. peak/hole / e Å^{-3}	1.07/-1.04	1.07/-1.05	0.76/-1.17

Identification code	170	170σ	173
Empirical formula	C$_{41}$H$_{69}$P$_3$Pt	C$_{47}$H$_{75}$P$_3$Pt	C$_{37}$H$_{61}$NiP$_3$
Formula weight	849.96	926.99	657.47
Temperature/K	100.0	100(2)	104(2)
Crystal system	triclinic	triclinic	monoclinic
Space group	P-1	P-1	P2$_1$/c
a/Å	9.8039(6)	10.3444(6)	14.9581(14)
b/Å	10.8351(6)	10.9595(6)	14.3777(15)
c/Å	19.2710(9)	20.5526(12)	18.3190(18)
α/°	95.226(2)	97.560(2)	90
β/°	103.502(2)	102.594(2)	112.463(3)
γ/°	90.307(2)	91.958(2)	90
Volume/Å^3	1981.48(19)	2249.4(2)	3640.8(6)
Z	2	2	4
ρ_{calc}g/cm^3	1.425	1.369	1.199
μ/mm^{-1}	3.689	3.255	0.688
F(000)	876.0	959.0	1424.0
Crystal size/mm^3	0.333 × 0.225 × 0.174	0.295 × 0.245 × 0.18	0.24 × 0.14 × 0.06
Radiation	MoKα (λ = 0.71073)	MoKα (λ = 0.71073)	MoKα (λ = 0.71073)
2Θ range for data collection/°	4.178 to 61.2	4.102 to 66.282	4.584 to 54.97
Index ranges	-14 ≤ h ≤ 14, -15 ≤ k ≤ 15, -27 ≤ l ≤ 27	-15 ≤ h ≤ 15, -16 ≤ k ≤ 16, -31 ≤ l ≤ 31	-19 ≤ h ≤ 17, -18 ≤ k ≤ 18, -22 ≤ l ≤ 23
Reflections collected	145642	206434	51651
Independent reflections	12159 [R_{int} = 0.0500, R_{sigma} = 0.0225]	17129 [R_{int} = 0.0353, R_{sigma} = 0.0169]	8345 [R_{int} = 0.1586, R_{sigma} = 0.0934]
Data/restraints/parameters	12159/129/484	17129/3171/776	8345/0/370
Goodness-of-fit on F^2	1.090	1.098	1.019
Final R indexes [I>=2σ (I)]	R_1 = 0.0246, wR_2 = 0.0474	R_1 = 0.0156, wR_2 = 0.0349	R_1 = 0.0565, wR_2 = 0.1066
Final R indexes [all data]	R_1 = 0.0291, wR_2 = 0.0492	R_1 = 0.0174, wR_2 = 0.0354	R_1 = 0.0996, wR_2 = 0.1197
Largest diff. peak/hole / e Å^{-3}	0.84/-1.62	0.81/-0.68	0.65/-0.71

Identification code	193	217
Empirical formula	$C_{41}H_{59}O_5P_3PtW$	$C_{48}H_{76}N_3P_3Pt$
Formula weight	1103.73	983.11
Temperature/K	100.0	100(2)
Crystal system	triclinic	triclinic
Space group	P-1	P-1
a/Å	14.9175(19)	10.4289(9)
b/Å	15.1712(17)	22.9059(18)
c/Å	21.539(3)	23.3221(19)
α/°	72.114(4)	117.801(3)
β/°	73.565(5)	90.224(3)
γ/°	70.030(4)	102.743(3)
Volume/Å³	4272.8(9)	4769.9(7)
Z	4	4
ρ_{calc}g/cm³	1.716	1.369
μ/mm⁻¹	6.113	3.077
F(000)	2168.0	2032.0
Crystal size/mm³	0.176 × 0.152 × 0.011	0.5 × 0.43 × 0.24
Radiation	MoKα (λ = 0.71073)	MoKα (λ = 0.71073)
2Θ range for data collection/°	3.91 to 61.106	3.646 to 63.344
Index ranges	-21 ≤ h ≤ 21, -21 ≤ k ≤ 21, -30 ≤ l ≤ 30	-15 ≤ h ≤ 15, -32 ≤ k ≤ 33, -34 ≤ l ≤ 34
Reflections collected	645735	247848
Independent reflections	26142 [R_{int} = 0.0540, R_{sigma} = 0.0169]	32009 [R_{int} = 0.0684, R_{sigma} = 0.0411]
Data/restraints/parameters	26142/0/925	32009/0/1006
Goodness-of-fit on F^2	1.062	1.098
Final R indexes [I>=2σ (I)]	R_1 = 0.0170, wR_2 = 0.0363	R_1 = 0.0505, wR_2 = 0.1177
Final R indexes [all data]	R_1 = 0.0222, wR_2 = 0.0388	R_1 = 0.0588, wR_2 = 0.1280
Largest diff. peak/hole / e Å⁻³	0.88/-1.14	3.98/-4.39

6 List of abbreviation

18C6	18-crown-6
2.2.2-crypt	[2.2.2]Cryptand, 4,7,13,16,21,24-Hexaoxa-1,10-diazabicyclo[8.8.8]hexacosane
acac	acetylacetonate anion
A_E	electrophilic additions
A_N	nucleophilic additions
Bn	benzyl
bpy	2,2′-bipyridine
BrettPhos	dicyclohexyl-[3,6-dimethoxy-2-[2,4,6-tri(propan-2-yl)phenyl]phenyl]phosphane
calc.	calculated
COD	1,5-cyclooctadiene
coe	cyclooctene
COT	cycloocta-1,3,5,7-tetraene
dcp.	decomposition
cpd	compound
DABCO	1,4-diazabicyclo[2.2.2]octane
DB18C6	dibenzo-18-crown-6
DBU	1,8-Diazabicyclo[5.4.0]undec-7-ene
DCM	dichloromethane
Dcpe	1,2-bis(dicyclohexylphosphino)ethane
Dcpm	bis(dicyclohexylphosphino)methane
dcpp	1,3-bis(dicyclohexylphosphino)propane
dcppm	bis(dicyclopentylphosphino)methane
DFT	density-functional theory
Dipp	2,6-di(isopropyl)phenyl
Dippdmae	(diisopropylphosphinodimethylamino)ethane
Dippe	1,2-bis(diisopropylphosphino)ethane
DippNacNac	CH{C(CH3)N-(Dipp)}2
dippp	1,3-bis(diisopropylphosphino)propane
DippPDI	diisopropylphenyl)imidazol-2-ylidene
DME	1,2-dimethoxyethane
DMF	dimethylformamide
dmpe	1,2-bis(dimethylphosphino)ethane)

dmpm	1,2-bis(dimethylphosphino)methane
DMSO	dimethyl sulfoxide
dppe	1,2-bis(diphenylphosphino)ethane
dppf	bis(diphenylphosphino)ferrocene
dppp	1,3-bis(diphenylphosphino)propane
dtbpe	1,2-bis(tetra-butylphosphino)ethane
dtbpm	bis(di-tert-butylphosphino)methane
durene(CP)$_2$	1,4-bis(phosphaethynyl)durene
EDD	electron-density distribution
EDG	electron-releasing group
EI	electron impact ionization
ELT	electron localization function
EN	electronegativity
eq	equivalent
ESI	electrospray Ionization
EWG	electron-withdrawing group
exp.	experimental
HOMO	highest occupied molecular orbital
HRMS	high resolution mass spectrometry
IDipp	1,3-bis(2,6-diisopropylphenyl)imidazol-2-ylidene
I^{i}Pr	1,3-diisopropylimidazol-2-ylidene
ILCT	intra-ligand charge transfer
IMe$_4$	1,3-dimethylimidazol-2-ylidene
IMes	1,3-dimesitylimidazol-2-ylidene
IR	infrared (spectrophotometry)
LLCT	ligand-to-ligand charge transfer
LUMO	lowest occupied molecular orbital
Mdtbp	(3,5-di-tert-butyl)phenyl, (3,5-di-tert-butyl)benzene
MEP	molecular electrostatic potential
Mes	mesityl, mesitylene
Mes*	1,3,5-tri-tert-butylphenyl, 1,3,5-tri-tert-butylbenzene (supermesitylene)
Mes^t(CP)$_3$	1,3,5-tris(phosphaethynyl)mesitylene
MLCT	metal-to-ligand charge transfer
MO	molecular orbital

MS	mass spectrometry
NacNac	*β*-diketiminate ligand
NBO	natural bond orbital
nf	not found
NHC	*N*-heterocyclic carbenes
NMR	nuclear magnetic resonance (spectroscopy)
NPA	natural population analysis
n.r.	not resolved
OTf	trifluoromethanesulfonate (triflate)
PBA	Prussian Blue analog
P,N	(P,N), chelating phosphine-amine ligand
P,P	(P,P), chelating diphosphine ligand
ppm	parts per million
rt	room temperature
SIMes	1,3-bis(2,4,6-trimethylphenyl)-4,5-dihydroimidazol-2-ylidene
TAP	triazaphosphole
TBAF	tetra-*n*-butylammonium fluoride
TBAT	tetra-*n*-butylammonium difluorotriphenylsilicate
TD-DFT	time-dependent density-functional theory
THF	tetrahydrofuran
TMS	trimethylsilyl
Tripp	(2,4,6-triisopropyl)phenyl, (2,4,6-triisopropyl)benzene
Ttfmp	(2,4,6-tris(trifluoromethyl)phenyl, (2,4,6-tris(trifluoromethyl)benzene
UV	ultraviolet (light)
UV-Vis	UV–visible spectrophotometry
XRD	X-ray diffraction

7 References

[1]   A. Michaelis, L. Gleichmann, *Ber. Dtsch. Chem. Ges.* **1882**, *15*, 801-804.
[2]   G. Wittig, M. Rieber, *Justus Liebigs Ann. Chem.* **1949**, *562*, 177-186.
[3]   D. E. C. Corbridge, *Phosphorus - Chemistry, Biochemistry and Technology, Vol. Sixth Edition*, CRC Press, **2013**, 1-22.
[4]   A. Kraszewski, J. Stawinski, *Pure Appl. Chem.* **2007**, *79*, 2217-2227.
[5]   W. H. Powell, *Pure Appl. Chem.* **1984**, *56*, 769-778.
[6]   T. E. Gier, *J. Am. Chem. Soc.* **1961**, *83*, 1769-1770.
[7]   A. B. Burg, W. Mahler, *J. Am. Chem. Soc.* **1961**, *83*, 2388-2389.
[8]   P. Floch, *Coordination Chemistry Reviews* **2006**, *250*, 627-681.
[9]   R. Appel, F. Knoll, I. Ruppert, *Angew. Chem.* **1981**, *93*, 771-784.
[10]   L. N. Markovski, V. D. Romanenko, *Tetrahedron* **1989**, *45*, 6019-6090.
[11]   M. Regitz, *Chem. Rev.* **1990**, *90*, 191-213.
[12]   M. Regitz, P. Binger, *Angew. Chem. Int. Ed. Engl.* **1988**, *27*, 1484-1508.
[13]   J. F. Nixon, *Coord. Chem. Rev.* **1995**, *145*, 201-258.
[14]   C. Muller, D. Vogt, *Dalton Trans* **2007**, 5505-5523.
[15]   C. Müller, D. Vogt, *C. R. Chim.* **2010**, *13*, 1127-1143.
[16]   C. Müller, L. E. E. Broeckx, I. de Krom, J. J. M. Weemers, *Eur. J. Inorg. Chem.* **2012**, *2013*, 187-202.
[17]   N. T. Coles, A. Sofie Abels, J. Leitl, R. Wolf, H. Grützmacher, C. Müller, *Coord. Chem. Rev.* **2021**, *433*, 213729.
[18]   J. A. W. Sklorz, C. Müller, *Eur. J. Inorg. Chem.* **2015**, *2016*, 595-606.
[19]   F. Mathey, *J. Organomet. Chem.* **1994**, *475*, 25-30.
[20]   U. Schmidt, *Angew. Chem. Int. Ed. Engl.* **1975**, *14*, 523-528.
[21]   F. Mathey, *Angew. Chem. Int. Ed. Engl.* **1987**, *26*, 275-286.
[22]   K. Dimroth, P. Hoffmann, *Angew. Chem. Int. Ed. Engl.* **1964**, *3*, 384-384.
[23]   R. Allmann, *Angew. Chem. Int. Ed. Engl.* **1965**, *4*, 150-151.
[24]   G. Märkl, *Angew. Chem.* **1966**, *78*, 907-908.
[25]   A. J. Ashe, *J. Am. Chem. Soc.* **1971**, *93*, 3293-3295.
[26]   E. Niecke, W. Flick, *Angew. Chem. Int. Ed. Engl.* **1973**, *12*, 585-586.
[27]   G. Recker, *Z. anorg. allg. Chem.* **1976**, *423*, 242-254.
[28]   A. Schmidpeter, J. Luber, H. Tautz, *Angew. Chem.* **1977**, *89*, 554-555.
[29]   M. Yoshifuji, I. Shima, N. Inamoto, K. Hirotsu, T. Higuchi, *J. Am. Chem. Soc.* **1981**, *103*, 4587-4589.
[30]   G. Becker, G. Gresser, W. Uhl, *Z. Naturforsch. B* **1981**, *36*, 16-19.
[31]   R. Appel, J. Peters, A. Westerhaus, *Angew. Chem.* **1982**, *94*, 76-77.
[32]   A. H. Cowley, N. C. Norman, S. Quashie, *J. Am. Chem. Soc.* **1984**, *106*, 5007-5008.
[33]   P. Le Floch, D. Carmichael, L. Ricard, F. Mathey, *J. Am. Chem. Soc.* **1991**, *113*, 667-669.
[34]   H. Jun, R. J. Angelici, *Organometallics* **1994**, *13*, 2454-2460.
[35]   N. C. Zanetti, R. R. Schrock, W. M. Davis, *Angew. Chem. Int. Ed. Engl.* **1995**, *34*, 2044-2046.
[36]   C. E. Laplaza, W. M. Davis, C. C. Cummins, *Angew. Chem. Int. Ed. Engl.* **1995**, *34*, 2042-2044.
[37]   J. G. Cordaro, D. Stein, H. Ruegger, H. Grutzmacher, *Angew. Chem. Int. Ed. Engl.* **2006**, *45*, 6159-6162.
[38]   R. J. P. Corriu, J. P. Dutheil, G. F. Lanneau, *J. Am. Chem. Soc.* **1984**, *106*, 1060-1065.
[39]   G. F. Lanneau, *Phosphorus Sulfur Silicon Relat. Elem.* **1986**, *27*, 43-54.
[40]   R. J. P. Corriu, G. F. Lanneau, D. Leclercq, *Tetrahedron* **1989**, *45*, 1959-1974.
[41]   K. B. Dillon, F. Mathey, J. F. Nixon, *The Carbon Copy: From Organophosphorus to Phospha-organic Chemistry*, John Wiley & Sons, New York, **1998**.
[42]   W. M. Haynes, D. R. Lide, T. J. Bruno, *CRC Handbook of Chemistry and Physics, Vol. 97*, CRC Press, Boca Raton, **2016**.
[43]   F. Mathey, *Angew Chem Int Ed Engl* **2003**, *42*, 1578-1604.

[44] T. Gorlich, P. Coburger, E. Yang, J. Goicoechea, H. Grutzmacher, C. Muller, *Angew. Chem. Int. Ed. Engl.* **2023**.

[45] R. Appel, F. Knoll, I. Ruppert, *Angew. Chem. Int. Ed. Engl.* **1981**, *20*, 731-744.

[46] J. F. Nixon, *Chem. Rev.* **1988**, *88*, 1327-1362.

[47] R. Appel, F. Knoll, *Adv. Inorg. Chem. - Double Bonds Between Phosphorus and Carbon, Vol. 33*, **1989,** 259-361.

[48] L. Weber, *Eur. J. Inorg. Chem.* **2000**, *2000*, 2425-2441.

[49] J. M. Goicoechea, H. Grutzmacher, *Angew. Chem. Int. Ed. Engl.* **2018**, *57*, 16968-16994.

[50] W. Shober, Bush, F. Spanutius, William, *Early Publications of the Leihigh Faculty* **1894**, 229-232.

[51] F. F. Puschmann, D. Stein, D. Heift, C. Hendriksen, Z. A. Gal, H. F. Grutzmacher, H. Grutzmacher, *Angew. Chem. Int. Ed. Engl.* **2011**, *50*, 8420-8423.

[52] G. Becker, W. Schwarz, N. Seidler, M. Westerhausen, *Z. anorg. allg. Chem.* **1992**, *612*, 72-82.

[53] G. Herzberg, *Nature* **1930**, *126*, 131-132.

[54] R. S. Mulliken, *J. Am. Chem. Soc.* **1950**, *72*, 4493-4503.

[55] K. S. Pitzer, *J. Am. Chem. Soc.* **1948**, *70*, 2140-2145.

[56] M. J. Hopkinson, H. W. Kroto, J. F. Nixon, N. P. C. Simmons, *J. Chem. Soc., Chem. Commun.* **1976**, 513-515.

[57] M. J. Hopkinson, H. W. Kroto, J. F. Nixon, N. P. C. Simmons, *Chem. Phys. Lett.* **1976**, *42*, 460-461.

[58] H. W. Kroto, J. F. Nixon, N. P. C. Simmons, *J. Mol. Spectrosc.* **1979**, *77*, 270-285.

[59] R. S. Ram, P. F. Bernath, *J. Mol. Spectrosc.* **1987**, *122*, 275-281.

[60] M. Guelin, J. Cernicharo, G. Paubert, B. E. Turner, *Astron. Astrophys.* **1990**, *230*, L9-L11.

[61] M. Agundez, J. Cernicharo, M. Guelin, *Astrophys. J.* **2007**, *662*, L91-L94.

[62] P. Pyykkö, Y. Zhao, *Mol. Phys.* **1990**, *70*, 701-714.

[63] H. Jun, V. G. Young, R. J. Angelici, *J. Am. Chem. Soc.* **1992**, *114*, 10064-10065.

[64] P. Jutzi, *Angew. Chem.* **1975**, *87*, 269-283.

[65] P. Jutzi, *Chem. unserer Zeit* **1981**, *15*, 149-154.

[66] B. Pellerin, J.-M. Denis, J. Perrocheau, R. Carrie, *Tetrahedron Lett.* **1986**, *27*, 5723-5726.

[67] T. A. Cooper, H. W. Kroto, J. F. Nixon, O. Ohashi, *J. Chem. Soc., Chem. Commun.* **1980**, 333-334.

[68] E. P. O. Fuchs, M. Hermesdorf, W. Schnurr, W. Rösch, H. Heydt, M. Regitz, P. Binger, *J. Organomet. Chem.* **1988**, *338*, 329-340.

[69] H. Eshtiagh-Hosseini, H. W. Kroto, J. F. Nixon, S. Brownstein, J. R. Morton, K. F. Preston, *J. Chem. Soc., Chem. Commun.* **1979,** 653-654.

[70] J. C. T. R. B. S. Laurent, T. A. Cooper, H. W. Kroto, J. F. Nixon, O. Ohashi, K. Ohno, *J. Mol. Struct.* **1982**, *79*, 215-220.

[71] M. C. Durrant, H. W. Kroto, D. McNaughton, J. F. Nixon, *J. Mol. Spectrosc.* **1985**, *109*, 8-14.

[72] P. L. Arnold, F. G. N. Cloke, J. F. Nixon, *Chem. Commun.* **1998**, 797-798.

[73] G. Hierlmeier, R. Wolf, *Angew. Chem. Int. Ed. Engl.* **2021**, *60*, 6435-6440.

[74] D. W. N. Wilson, D. D. L. Jones, C. D. Smith, M. Mehta, C. Jones, J. M. Goicoechea, *Dalton Trans* **2022**, *51*, 898-903.

[75] R. Appel, A. Westerhaus, *Tetrahedron Lett.* **1981**, *22*, 2159-2160.

[76] W. Fiedler, O. Lober, U. Bergstrasser, M. Regitz, *Eur. J. Org. Chem.* **1999**, *1999*, 363-371.

[77] S. M. Mansell, M. Green, R. J. Kilby, M. Murray, C. A. Russell, *C. R. Chim.* **2010**, *13*, 1073-1081.

[78] T. Allspach, M. Regitz, G. Becker, W. Becker, *Synthesis* **1986**, *1986*, 31-36.

[79] G. Märkl, H. Sejpka, *Tetrahedron Lett.* **1986**, *27*, 171-174.

[80] J. G. Cordaro, D. Stein, H. Grutzmacher, *J. Am. Chem. Soc.* **2006**, *128*, 14962-14971.

[81]   A. Chirila, R. Wolf, J. Chris Slootweg, K. Lammertsma, *Coord. Chem. Rev.* **2014**, *270-271*, 57-74.
[82]   A. Mack, M. Regitz, *Chem. Ber.* **1997**, *130*, 823-834.
[83]   A. C. Gaumont, J. M. Denis, *Chem. Rev.* **1994**, *94*, 1413-1439.
[84]   M. Regitz, *J. Heterocycl. Chem.* **1994**, *31*, 663-677.
[85]   E. A. Ishmaeva, I. I. Patsanovskii, *Russ. Chem. Rev.* **1985**, *54*, 243-248.
[86]   M. Z. Bani-Fwaz, *J. Coord. Chem.* **2020**, *73*, 887-916.
[87]   M. Regitz, *Bull. Soc. Chim. Belg.* **1992**, *101*, 359-379.
[88]   G. Becker, M. Böhringer, R. Gleiter, K. H. Pfeifer, J. Grobe, D. L. Van, M. Hegemann, *Chem. Ber.* **1994**, *127*, 1041-1045.
[89]   A. N. Chernega, G. N. Koidan, A. P. Marchenko, A. A. Korkin, *Heteroat. Chem* **1993**, *4*, 365-368.
[90]   L. Ermolaeva, A. Ionkin, *Heteroat. Chem* **1992**, *3*, 435-438.
[91]   J. Grobe, D. Le Van, M. Hegemann, B. Krebs, M. Läge, *Angew. Chem. Int. Ed. Engl.* **1992**, *31*, 95-96.
[92]   J. Grobe, D. Le Van, M. Hegemann, B. Krebs, M. Läge, *Heteroat. Chem* **1994**, *5*, 337-341.
[93]   J. Grobe, D. L. Van, M. Hegemann, B. Krebs, M. Läge, *Chem. Ber.* **1993**, *126*, 63-65.
[94]   J. Grobe, D. L. Van, B. Lüth, M. Hegemann, *Chem. Ber.* **1990**, *123*, 2317-2320.
[95]   E. Niecke, R. Streubel, M. Nieger, D. Stalke, *Angew. Chem.* **1989**, *101*, 1708-1710.
[96]   D. Bourissou, P. Le Floch, F. Mathey, G. Bertrand, *C.R. Acad. Sci., Ser. IIc: Chim.* **1999**, *2*, 351-357.
[97]   U. Fleischer, H. Grützmacher, U. Krüger, *J. Chem. Soc., Chem. Commun.* **1991**, 302-303.
[98]   X. Chen, S. Alidori, F. F. Puschmann, G. Santiso-Quinones, Z. Benko, Z. Li, G. Becker, H. F. Grutzmacher, H. Grutzmacher, *Angew. Chem. Int. Ed. Engl.* **2014**, *53*, 1641-1645.
[99]   G. Becker, K. Hübler, *Z. anorg. allg. Chem.* **1994**, *620*, 405-417.
[100]   F. Tambornino, A. Hinz, R. Köppe, J. M. Goicoechea, *Angew. Chem.* **2018**, *130*, 8362-8366.
[101]   A. R. Jupp, M. B. Geeson, J. E. McGrady, J. M. Goicoechea, *Eur. J. Inorg. Chem.* **2016**, *2016*, 639-648.
[102]   G. L. Hou, B. Chen, W. J. Transue, Z. Yang, H. Grutzmacher, M. Driess, C. C. Cummins, W. T. Borden, X. B. Wang, *J. Am. Chem. Soc.* **2017**, *139*, 8922-8930.
[103]   W.-G. Veek, *doctoral thesis* **1997**, Technische Universität Kaiserslautern.
[104]   M. Brym, C. Jones, *Dalton Trans* **2003**, 3665-3667.
[105]   F. Brodkorb, M. Brym, C. Jones, C. Schulten, *J. Organomet. Chem.* **2006**, *691*, 1025-1029.
[106]   H. Jun, V. G. Young, R. J. Angelici, *J. Am. Chem. Soc.* **1991**, *113*, 9379-9380.
[107]   L. Weber, I. Schumann, T. Schmidt, H. G. Stammler, B. Neumann, *Z. anorg. allg. Chem.* **1993**, *619*, 1759-1764.
[108]   L. Weber, *Eur. J. Inorg. Chem.* **2003**, *2003*, 1843-1856.
[109]   C. C. Cummins, *Angew. Chem. Int. Ed. Engl.* **2006**, *45*, 862-870.
[110]   J. C. Duchamp, M. Pakulski, A. H. Cowley, K. W. Zilm, *J. Am. Chem. Soc.* **1990**, *112*, 6803-6809.
[111]   K. Jayasuriya, *J. Mol. Struc.-THEOCHEM* **1992**, *257*, 405-415.
[112]   M. Y. Antipin, A. N. Chernega, K. A. Lysenko, Y. T. Struchkov, J. F. Nixon, *J. Chem. Soc., Chem. Commun.* **1995**, 505-506.
[113]   M. F. Lucas, M. C. Michelini, N. Russo, E. Sicilia, *J Chem Theory Comput* **2008**, *4*, 397-403.
[114]   K. Jayasuriya, *Int. J. Quantum Chem* **1992**, *44*, 327-336.
[115]   K. Jayasuriya, *J. Mol. Struc.-THEOCHEM* **1992**, *256*, 17-27.
[116]   K. Hübler, P. Schwerdtfeger, *Inorg. Chem.* **1999**, *38*, 157-164.
[117]   A. Modelli, J. F. Nixon, G. K. B. Clentsmith, *Chem. Phys. Lett.* **2002**, *366*, 122-127.
[118]   J. C. T. R. B.-S. Laurent, M. A. King, H. W. Kroto, J. F. Nixon, R. J. Suffolk, *J. Chem. Soc., Dalton Trans.* **1983**, 755-759.

[119] S. M. Bachrach, *J. Comput. Chem.* **1989**, *10*, 392-406.
[120] R. Appel, G. Maier, H. P. Reisenauer, A. Westerhaus, *Angew. Chem.* **1981**, *93*, 215-215.
[121] J. C. T. R. B.-S. Laurent, P. B. Hitchcock, H. W. Kroto, J. F. Nixon, *J. Chem. Soc., Chem. Commun.* **1981**, 1141-1143.
[122] P. Binger, R. Milczarek, R. Mynott, C. Krüger, Y. H. Tsay, E. Raabe, M. Regitz, *Chem. Ber.* **1988**, *121*, 637-645.
[123] P. Binger, R. Milczarek, R. Mynott, M. Regitz, W. Rösch, *Angew. Chem. Int. Ed. Engl.* **1986**, *25*, 644-645.
[124] D. Böhm, F. Knoch, S. Kummer, U. Schmidt, U. Zenneck, *Angew. Chem.* **1995**, *107*, 251-254.
[125] P. B. Hitchcock, M. J. Maah, J. F. Nixon, *J. Chem. Soc., Chem. Commun.* **1986**, 737-738.
[126] P. S. Kramkowski, Manfred, *Eur. J. Inorg. Chem.* **2000**, *2000*, 1869-1876.
[127] R. Wolf, J. C. Slootweg, A. W. Ehlers, F. Hartl, B. de Bruin, M. Lutz, A. L. Spek, K. Lammertsma, *Angew. Chem. Int. Ed. Engl.* **2009**, *48*, 3104-3107.
[128] S. I. Al-Resayes, S. I. Klein, H. W. Kroto, M. F. Meidine, J. F. Nixon, *J. Chem. Soc., Chem. Commun.* **1983**, 930-932.
[129] G. Brauers, M. Green, C. Jones, J. F. Nixon, *J. Chem. Soc., Chem. Commun.* **1995**, 1125-1126.
[130] R. A. Sanguramath, N. S. Townsend, J. M. Lynam, C. A. Russell, *Eur. J. Inorg. Chem.* **2013**, *2014*, 1783-1787.
[131] C. Jones, C. Schulten, A. Stasch, *Dalton Trans* **2006**, 3733-3735.
[132] A. D. D. Burrows, Alk, M. Green, J. C. Jeffery, C. Jones, J. M. Lynam, M. T. Nguyen, *Angew. Chem. Int. Ed. Engl.* **2001**, *40*, 3221-3224.
[133] D. Himmel, M. Seitz, M. Scheer, *Z. Anorg. Allg. Chem.* **2004**, *630*, 1220-1228.
[134] P. Kramkowski, M. Scheer, G. Baum, *J. Organomet. Chem.* **1998**, *553*, 511-516.
[135] E.-M. Rummel, P. Mastrorilli, S. Todisco, M. Latronico, G. Baláse, A. V. Virovets, M. Scheer, *Angew. Chem.* **2016**, *128*, 13495-13499.
[136] D. W. N. Wilson, N. H. Rees, J. M. Goicoechea, *Organometallics* **2019**, *38*, 4601-4606.
[137] P. B. Hitchcock, M. Amélia, N. D. A. Lemos, M. F. Meidine, J. F. Nixon, A. J. L. Pombeiro, *J. Organomet. Chem.* **1991**, *402*, C23-C26.
[138] M. F. Meidine, M. Amélia N. D. A.Lemos, A. J. L. Pombeiro, J. F. Nixon, P. B. Hitchcock, *J. Chem. Soc., Dalton Trans.* **1998**, 3319-3324.
[139] S. M. Mansell, M. Green, C. A. Russell, *Dalton Trans* **2012**, *41*, 14360-14368.
[140] P. B. Hitchcock, J. A. Johnson, M. A. N. D. A. Lemos, M. F. Meidine, J. F. Nixon, A. J. L. Pombeiro, *J. Chem. Soc., Chem. Commun.* **1992**, 645-646.
[141] C. Jones, C. Schulten, A. Stasch, *Eur. J. Inorg. Chem.* **2008**, *2008*, 1555-1558.
[142] R. B. Bedford, A. F. Hill, J. D. E. T. Wilton-Ely, M. D. Francis, C. Jones, *Inorg. Chem.* **1997**, *36*, 5142-5144.
[143] T. Gröer, G. Baum, M. Scheer, *Organometallics* **1998**, *17*, 5916-5919.
[144] P. B. Hitchcock, M. J. Maah, J. F. Nixon, J. A. Zora, G. J. Leigh, M. A. Bakar, *Angew. Chem. Int. Ed. Engl.* **1987**, *26*, 474-475.
[145] A. J. L. Pombeiro, *J. Organomet. Chem.* **2001**, *632*, 215-226.
[146] D. Carmichael, S. I. Al-Resayes, J. F. Nixon, *J. Organomet. Chem.* **1993**, *453*, 207-210.
[147] P. Binger, B. Biedenbach, A. T. Herrmann, F. Langhauser, P. Betz, R. Goddard, C. Krüger, *Chem. Ber.* **1990**, *123*, 1617-1623.
[148] G. Becker, W. A. Herrmann, W. Kalcher, G. W. Kriechbaum, C. Pahl, C. T. Wagner, M. L. Ziegler, *Angew. Chem. Int. Ed. Engl.* **1983**, *22*, 413-414.
[149] S. I. Al-Resayes, P. B. Hitchcock, M. F. Meidine, J. F. Nixon, *J. Chem. Soc., Chem. Commun.* **1984**, 1080-1082.
[150] R. Bartsch, J. F. Nixon, N. Sarjudeen, *J. Organomet. Chem.* **1985**, *294*, 267-272.
[151] J. C. T. R. Burckett-St. Laurent, P. B. Hitchcock, H. W. Kroto, M. F. Meidine, J. F. Nixon, *J. Organomet. Chem.* **1982**, *238*, C82-C84.

[152]   M. F. Meidine, J. F. Nixon, R. Mathieu, *J. Organomet. Chem.* **1986**, *314*, 307-310.

[153]   D. Seyferth, J. S. Merola, R. S. Henderson, *Organometallics* **1982**, *1*, 859-866.

[154]   J. C. T. R. Burckett-St.Laurent, H. W. Kroto, J. F. Nixon, K. Ohno, *J. Mol. Spectrosc.* **1982**, *92*, 158-161.

[155]   W. Rösch, U. Hees, M. Regitz, *Chem. Ber.* **1987**, *120*, 1645-1652.

[156]   R. Suter, Z. Benko, M. Bispinghoff, H. Grutzmacher, *Angew. Chem. Int. Ed. Engl.* **2017**, *56*, 11226-11231.

[157]   J.-C. Guillemin, T. Janati, J.-M. Denis, *J. Chem. Soc., Chem. Commun.* **1992**, 415-416.

[158]   J. C. Guillemin, T. Janati, J. M. Denis, *J. Org. Chem.* **2001**, *66*, 7864-7868.

[159]   W. J. Transue, J. Yang, M. Nava, I. V. Sergeyev, T. J. Barnum, M. C. McCarthy, C. C. Cummins, *J. Am. Chem. Soc.* **2018**, *140*, 17985-17991.

[160]   W. J. Transue, A. Velian, M. Nava, M. A. Martin-Drumel, C. C. Womack, J. Jiang, G. L. Hou, X. B. Wang, M. C. McCarthy, R. W. Field, C. C. Cummins, *J. Am. Chem. Soc.* **2016**, *138*, 6731-6734.

[161]   A. S. Ionkin, W. J. Marshall, B. M. Fish, L. A. Howe, *Organometallics* **2010**, *29*, 4154-4158.

[162]   D. W. N. Wilson, S. J. Urwin, E. S. Yang, J. M. Goicoechea, *J. Am. Chem. Soc.* **2021**, *143*, 10367-10373.

[163]   K. K. Laali, B. Geissler, M. Regitz, J. J. Houser, *J. Org. Chem.* **1995**, *60*, 6362-6367.

[164]   A. M. Arif, A. R. Barron, A. H. Cowley, S. W. Hall, *J. Chem. Soc., Chem. Commun.* **1988**, 171-172.

[165]   O. Wagner, M. Ehle, M. Regitz, *Angew. Chem. Int. Ed. Engl.* **1989**, *28*, 225-226.

[166]   A. Schäfer, M. Weidenbruch, W. Saak, S. Pohl, *Angew. Chem.* **1987**, *99*, 806-807.

[167]   A. H. Cowley, S. W. Hall, C. M. Nunn, J. M. Power, *J. Chem. Soc., Chem. Commun.* **1988**, 753-754.

[168]   L. L. Liu, J. Zhou, L. L. Cao, D. W. Stephan, *J. Am. Chem. Soc.* **2019**, *141*, 16971-16982.

[169]   A. H. Cowley, S. W. Hall, C. M. Nunn, J. M. Power, *Angew. Chem. Int. Ed. Engl.* **1988**, *27*, 838-839.

[170]   M. Weidenbruch, S. Olthoff, K. Peters, H. G. von Schnering, *Chem. Commun.* **1997**, 1433-1434.

[171]   W. Rösch, T. Facklam, M. Regitz, *Tetrahedron* **1987**, *43*, 3247-3256.

[172]   H. C. Kolb, M. G. Finn, K. B. Sharpless, *Angew. Chem. Int. Ed. Engl.* **2001**, *40*, 2004-2021.

[173]   R. Huisgen, *Proc. Chem. Soc.* **1961**, 357-369.

[174]   V. V. Rostovtsev, L. G. Green, V. V. Fokin, K. B. Sharpless, *Angew. Chem. Int. Ed. Engl.* **2002**, *41*, 2596-2599.

[175]   C. W. Tornoe, C. Christensen, M. Meldal, *J. Org. Chem.* **2002**, *67*, 3057-3064.

[176]   B. C. Boren, S. Narayan, L. K. Rasmussen, L. Zhang, H. Zhao, Z. Lin, G. Jia, V. V. Fokin, *J. Am. Chem. Soc.* **2008**, *130*, 8923-8930.

[177]   W. Liang, K. Nakajima, K. Sakata, Y. Nishibayashi, *Angew. Chem. Int. Ed. Engl.* **2019**, *58*, 1168-1173.

[178]   W. Rösch, M. Regitz, *Z. Naturforsch. B* **1986**, *41*, 931-934.

[179]   G. Märkl, G. Y. Jin, E. Silbereisen, *Angew. Chem. Int. Ed. Engl.* **1982**, *21*, 370-371.

[180]   T. Wettling, J. Schneider, O. Wagner, C. G. Kreiter, M. Regitz, *Angew. Chem. Int. Ed. Engl.* **1989**, *28*, 1013-1014.

[181]   V. Caliman, P. B. Hitchcock, J. F. Nixon, M. Hofmann, P. Von Ragué Schleyer, *Angew. Chem.* **1994**, *106*, 2284-2286.

[182]   G. Hierlmeier, P. Coburger, M. Bodensteiner, R. Wolf, *Angew. Chem. Int. Ed. Engl.* **2019**, *58*, 16918-16922.

[183]   T. Wettling, G. Wolmershäuser, P. Binger, M. Regitz, *J. Chem. Soc., Chem. Commun.* **1990**, 1541-1543.

[184]   K. Nakajima, W. Liang, Y. Nishibayashi, *Org. Lett.* **2016**, *18*, 5006-5009.

[185]   T. Gläsel, H. Jiao, M. Hapke, *ACS Catalysis* **2021**, *11*, 13434-13444.

[186] G. Becker, W. Becker, R. Knebl, H. Schmidt, U. Weeber, M. Westerhausen, *Nova Acta Leopold* **1985**, *59*, 55.

[187] G. Becker, W. Becker, R. Knebl, H. Schmidt, U. Hildenbrand, M. Westerhausen, *Phosphorus Sulfur Silicon Relat. Elem.* **1987**, *30*, 349-352.

[188] M. T. Nguyen, T.-K. Ha, *J. Mol. Struc.-THEOCHEM* **1986**, *139*, 145-152.

[189] M. T. Nguyen, L. Landuyt, L. G. Vanquickenborne, *J. Org. Chem.* **1993**, *58*, 2817-2821.

[190] S. Creve, M. T. Nguyen, L. G. Vanquickenborne, *Eur. J. Inorg. Chem.* **1999**, *1999*, 1281-1289.

[191] M. Hofmann, P. V. Schleyer, M. Regitz, *Eur. J. Org. Chem.* **1999**, *1999*, 3291-3303.

[192] E. Kurita, Y. Tomonaga, S. Matsumoto, K. Ohno, H. Matsuura, *J. Mol. Struc.-THEOCHEM* **2003**, *639*, 53-67.

[193] C. Beck, R. Schinke, J. Koput, *J. Chem. Phys.* **2000**, *112*, 8446-8457.

[194] V. F. Kalasinsky, S. Pechsiri, *J. Raman Spectrosc.* **1985**, *16*, 190-192.

[195] J. K. Tyler, *J. Chem. Phys.* **1964**, *40*, 1170-1171.

[196] J. W. C. Johns, J. M. R. Stone, G. Winnewisser, *J. Mol. Spectrosc.* **1971**, *38*, 437-440.

[197] O. Mó, M. Yáñez, J.-C. Guillemin, E. H. Riague, J.-F. Gal, P.-C. Maria, C. Dubin Poliart, *Chem. Eur. J.* **2002**, *8*, 4919-4924.

[198] P. Dréan, J. Demaison, L. Poteau, J. M. Denis, *J. Mol. Spectrosc.* **1996**, *176*, 139-145.

[199] S. P. Anderson, H. Goldwhite, D. Ko, A. Letsou, F. Esparza, *J. Chem. Soc., Chem. Commun.* **1975**, 744-745.

[200] G. Pascoli, H. Lavendy, *J. Phys. Chem. A* **1999**, *103*, 3518-3524.

[201] P. Botschwina, *Chem. Phys. Lett.* **1985**, *114*, 58-62.

[202] M. F. C. Ladd, *J. Chem. Soc., Dalton Trans.* **1977**, 220-223.

[203] E. S. Yang, J. M. Goicoechea, *Angew. Chem. Int. Ed. Engl.* **2022**, *61*, e202206783.

[204] W. V. Konze, V. G. Young, R. J. Angelici, *Organometallics* **1999**, *18*, 258-267.

[205] K. Dehnicke, *Angew. Chem.* **1976**, *88*, 774-774.

[206] W. P. Fehlhammer, M. Fritz, *Chem. Rev.* **1993**, *93*, 1243-1280.

[207] M. Finze, E. Bernhardt, H. Willner, C. W. Lehmann, *Angew. Chem. Int. Ed. Engl.* **2004**, *43*, 4160-4163.

[208] A. Ehlers, J. G. Cordaro, D. Stein, H. Grutzmacher, *Angew. Chem. Int. Ed. Engl.* **2007**, *46*, 7878-7881.

[209] N. Trathen, M. C. Leech, I. R. Crossley, V. K. Greenacre, S. M. Roe, *Dalton Trans* **2014**, *43*, 9004-9007.

[210] M. C. Leech, I. R. Crossley, *Dalton Trans* **2018**, *47*, 4428-4432.

[211] S. K. Furfari, M. C. Leech, N. Trathen, M. C. Levis, I. R. Crossley, *Dalton Trans* **2019**, *48*, 8131-8143.

[212] L. D. Field, A. M. Magill, T. K. Shearer, S. J. Dalgarno, P. Turner, *Organometallics* **2007**, *26*, 4776-4780.

[213] C. J. Hoerger, F. W. Heinemann, E. Louyriac, L. Maron, H. Grützmacher, K. Meyer, *Organometallics* **2017**, *36*, 4351-4354.

[214] D. Heift, Z. Benko, H. Grutzmacher, *Dalton Trans* **2014**, *43*, 5920-5928.

[215] S. P. Green, C. Jones, A. Stasch, *Science* **2007**, *318*, 1754-1757.

[216] M. H. Chisholm, K. Choojun, J. C. Gallucci, P. M. Wambua, *Chem. Sci.* **2012**, *3*.

[217] R. Appel, F. Knoll, *Adv. Inorg. Chem.* **1989**, *33*, 259-361.

[218] D. Touchard, S. Guesmi, L. Le Pichon, A. Daridor, P. H. Dixneuf, *Inorg. Chim. Acta* **1998**, *280*, 118-124.

[219] M. C. Levis, K. G. Pearce, I. R. Crossley, *Inorg. Chem.* **2019**, *58*, 14800-14807.

[220] S. Gaillard, A. M. Slawin, S. P. Nolan, *Chem Commun (Camb)* **2010**, *46*, 2742-2744.

[221] E. Gail, S. Gos, R. Kulzer, J. Lorösch, A. Rubo, M. Sauer, R. Kellens, J. Reddy, N. Steier, W. Hasenpusch, *Ullmann's encycl. ind. chem., Vol. 40*, 7th ed., Wiley-VCH, **2011**, 673-704.

[222] S. F. Rach, F. E. Kuhn, *Chem Rev* **2009**, *109*, 2061-2080.

[223] B. M. Chadwick, A. G. Sharpe, *Adv. Inorg. Chem. and Radiochemistry* **1966**, *8*, 83-178.

[224] K. R. Dunbar, R. A. Heintz, *Progress in Inorganic Chemistry - Chemistry of transition metal cyanide compounds, Vol. 45*, Wiley and Sons, New York, **1997**, 283-392.

[225] M. Shatruk, C. Avendano, K. R. Dunbar, *Progress in Inorganic Chemistry - Cyanide-bridged complexes of transition metals: A molecular magnetism perspective*, **2009**, 153-334.

[226] P. Rigo, A. Turco, *Coord. Chem. Rev.* **1974**, *13*, 133-172.

[227] T. P. Hanusa, *Encyclopedia Of Inorganic And Bioinorganic Chemistry - Cyanide Complexes of the Transition Metals*, 1st ed., John Wiley & Sons, New York, **2011**.

[228] W. P. Griffith, *Quarterly Reviews, Chemical Society - Cyanide Complexes of the Transition Metals* **1962**, *16*, 188-207.

[229] A. L. Lougheed, *Prometheus* **1989**, *7*, 61-74.

[230] J. S. Macathure, *J. Soc. Chem. Ind.* **1890**, *9*, 267-305.

[231] E. S. Koumousi, R. Jeon Ie, Q. Gao, P. Dechambenoit, D. N. Woodruff, P. Merzeau, L. Buisson, X. Jia, D. Li, F. Volatron, C. Mathoniere, R. Clerac, *J. Am. Chem. Soc.* **2014**, *136*, 15461-15464.

[232] S. Ferlay, T. Mallah, R. Ouahès, P. Veillet, M. Verdaguer, *Nature* **1995**, *378*, 701-703.

[233] J. R. Jiménez, J. Glatz, A. Benchohra, G. Gontard, L. M. Chamoreau, J. F. Meunier, A. Bousseksou, R. Lescouëzec, *Angew. Chem.* **2020**, *132*, 8166-8170.

[234] A. L. Casalnuovo, R. J. McKinney, C. A. Tolman, *Encyclopedia of Inorganic Chemistry - Hydrocyanation by Homogeneous Catalysis, Vol. 10*, John Wiley & Sons, New York, **2006**.

[235] P. R. Sruthi, S. Anas, *J. Polym. Sci.* **2020**, *58*, 1039-1061.

[236] E. L. Muetterties, D. H. Gerlach, A. R. Kane, G. W. Parshall, J. P. Jesson, *J. Am. Chem. Soc.* **1971**, *93*, 3543-3544.

[237] G. W. Parshall, *J. Am. Chem. Soc.* **1974**, *96*, 2360-2366.

[238] Y. Nakao, *Chem Rev* **2021**, *121*, 327-344.

[239] G. Favero, A. Morvillo, A. Turco, *J. Organomet. Chem.* **1983**, *241*, 251-257.

[240] A. Morvillo, A. Turco, *J. Organomet. Chem.* **1981**, *208*, 103-113.

[241] T. Schaub, C. Doring, U. Radius, *Dalton Trans* **2007**, 1993-2002.

[242] J. Wilting, C. Müller, A. C. Hewat, D. D. Ellis, D. M. Tooke, A. L. Spek, D. Vogt, *Organometallics* **2004**, *24*, 13-15.

[243] M. Abla, T. Yamamoto, *J. Organomet. Chem.* **1997**, *532*, 267-270.

[244] Y. Nakao, S. Oda, T. Hiyama, *J. Am. Chem. Soc.* **2004**, *126*, 13904-13905.

[245] D. Churchill, J. H. Shin, T. Hascall, J. M. Hahn, B. M. Bridgewater, G. Parkin, *Organometallics* **1999**, *18*, 2403-2406.

[246] H. Nakazawa, M. Itazaki, K. Kamata, K. Ueda, *Chem Asian J* **2007**, *2*, 882-888.

[247] X. Li, H. Sun, F. Yu, U. Flörke, H.-F. Klein, *Organometallics* **2006**, *25*, 4695-4697.

[248] M. R. Grochowski, J. Morris, W. W. Brennessel, W. D. Jones, *Organometallics* **2011**, *30*, 5604-5610.

[249] L. Munjanja, C. Torres-López, W. W. Brennessel, W. D. Jones, *Organometallics* **2016**, *35*, 2010-2013.

[250] Y. Nishihara, M. Miyasaka, Y. Inoue, T. Yamaguchi, M. Kojima, K. Takagi, *Organometallics* **2007**, *26*, 4054-4060.

[251] D. A. Clarke, M. M. Hunt, R. D. W. Kemmitt, *J. Organomet. Chem.* **1979**, *175*, 303-313.

[252] T. Lu, X. Zhuang, Y. Li, S. Chen, *J. Am. Chem. Soc.* **2004**, *126*, 4760-4761.

[253] D. S. O. Marlin, Marilyn M., P. K. Mascharak, *Angew. Chem. Int. Ed. Engl.* **2001**, *40*, 4752-4754.

[254] J. J. Garcia, W. D. Jones, *Organometallics* **2000**, *19*, 5544-5545.

[255] C. Müller, R. J. Lachicotte, W. D. Jones, *Organometallics* **2002**, *21*, 1975-1981.

[256] N. M. Brunkan, D. M. Brestensky, W. D. Jones, *J. Am. Chem. Soc.* **2004**, *126*, 3627-3641.

[257] J. J. García, A. Arévalo, N. M. Brunkan, W. D. Jones, *Organometallics* **2004**, *23*, 3997-4002.

[258]   T. A. Ateşin, T. Li, S. Lachaize, J. J. García, W. D. Jones, *Organometallics* **2008**, *27*, 3811-3817.
[259]   T. A. Atesin, T. Li, S. Lachaize, W. W. Brennessel, J. J. Garcia, W. D. Jones, *J. Am. Chem. Soc.* **2007**, *129*, 7562-7569.
[260]   B. D. Swartz, N. M. Reinartz, W. W. Brennessel, J. J. Garcia, W. D. Jones, *J. Am. Chem. Soc.* **2008**, *130*, 8548-8554.
[261]   T. Li, J. J. García, W. W. Brennessel, W. D. Jones, *Organometallics* **2010**, *29*, 2430-2445.
[262]   W. Jones, B. Swartz, W. Brennessel, *Synlett* **2018**, *29*, 747-753.
[263]   C. Muller, C. N. Iverson, R. J. Lachicotte, W. D. Jones, *J. Am. Chem. Soc.* **2001**, *123*, 9718-9719.
[264]   C. Müller, R. J. Lachicotte, W. D. Jones, *Organometallics* **2002**, *21*, 1118-1123.
[265]   A. Gunay, W. D. Jones, *J. Am. Chem. Soc.* **2007**, *129*, 8729-8735.
[266]   A. Gunay, C. Müller, R. J. Lachicotte, W. W. Brennessel, W. D. Jones, *Organometallics* **2009**, *28*, 6524-6530.
[267]   A. Gunay, W. W. Brennessel, W. D. Jones, *Organometallics* **2015**, *34*, 2233-2239.
[268]   C. Müller, R. J. Lachicotte, W. D. Jones, *Organometallics* **2002**, *21*, 1190-1196.
[269]   B. D. Swartz, W. W. Brennessel, W. D. Jones, *Organometallics* **2011**, *30*, 1523-1529.
[270]   E. Clot, M. Besora, F. Maseras, C. Megret, O. Eisenstein, B. Oelckers, R. N. Perutz, *Chem Commun (Camb)* **2003**, 490-491.
[271]   L. Abis, A. Sen, J. Halpern, *J. Am. Chem. Soc.* **1978**, *100*, 2915-2916.
[272]   H. Petzold, T. Weisheit, H. Gorls, H. Breitzke, G. Buntkowsky, D. Escudero, L. Gonzalez, W. Weigand, *Dalton Trans* **2008**, 1979-1981.
[273]   D. Escudero, M. Assmann, A. Pospiech, W. Weigand, L. Gonzalez, *Phys. Chem. Chem. Phys.* **2009**, *11*, 4593-4600.
[274]   D. Escudero, T. Weisheit, W. Weigand, L. Gonzalez, *Dalton Trans* **2010**, *39*, 9505-9513.
[275]   T. Weisheit, D. Escudero, H. Petzold, H. Gorls, L. Gonzalez, W. Weigand, *Dalton Trans* **2010**, *39*, 9493-9504.
[276]   B. Bogdanovic, M. Kroner, G. Wilke, *Justus Liebigs Ann Chem* **1966**, *699*, 1-23.
[277]   D. J. Krysan, P. B. Mackenzie, *J. Org. Chem.* **1990**, *55*, 4229-4230.
[278]   M. Green, J. A. K. Howard, J. L. Spencer, F. G. A. Stone, *J. Chem. Soc., Chem. Commun.* **1975**, 449-451.
[279]   M. Green, J. A. K. Howard, J. L. Spencer, F. G. A. Stone, *J. Chem. Soc., Dalton Trans.* **1977**, 271-277.
[280]   G. E. Herberich, B. Heßner, *Z. Naturforsch. B* **1979**, *34*, 638-639.
[281]   S. Ogoshi, M. Morita, K. Inoue, H. Kurosawa, *J. Organomet. Chem.* **2004**, *689*, 662-665.
[282]   D. Walther, K. Heubach, L. Böttcher, H. Schreer, H. Görls, *Z. anorg. allg. Chem.* **2002**, *628*, 20-30.
[283]   D. B. Dell'Amico, L. Labella, F. Marchetti, S. Samaritani, *J. Organomet. Chem.* **2011**, *696*, 1349-1354.
[284]   J. X. McDermott, J. F. White, G. M. Whitesides, *J. Am. Chem. Soc.* **1976**, *98*, 6521-6528.
[285]   J. L. Spencer, S. D. Ittel, M. A. Crushing Jr., *Inorganic Syntheses, Vol. XIX*, John Wiley & Sons, New York, **1979**, 214.
[286]   J. Gottfriedsen, A. Miloslavina, F. T. Edelmann, *Tetrahedron Lett.* **2004**, *45*, 3583-3584.
[287]   S. Majumder, A. L. Odom, *Tetrahedron Lett.* **2008**, *49*, 1771-1772.
[288]   L. H. Simons, J. J. Lagowski, *Tetrahedron Lett.* **2002**, *43*, 1771-1773.
[289]   A. Werner, *Z. Anorg. Allg. Chem.* **1893**, *3*, 267-330.
[290]   C. Janiak, H.-J. Meyer, D. Gudat, P. Kurz, E. Riedel, H.-J. Meyer, *Riedel Moderne Anorganische Chemie, Vol. 5*, De Gruyter, Berlin, **2018**.
[291]   E. I. Musina, A. S. Balueva, A. A. Karasik, *Organophosphorus Chemisty - Phosphines: preparation, reactivity and applications, Vol. 48*, **2019**, 1-63.
[292]   M. P. Mitoraj, A. Michalak, *Inorg. Chem.* **2010**, *49*, 578-582.

[293]   N. S. Antonova, J. J. Carbó, J. M. Poblet, *Organometallics* **2009**, *28*, 4283-4287.
[294]   A. Pascariu, S. Iliescu, A. Popa, G. Ilia, *J. Organomet. Chem.* **2009**, *694*, 3982-4000.
[295]   K. Issleib, D. W. Müller, *Chem. Ber.* **1959**, *92*, 3175-3182.
[296]   F. A. Cotton, B. Hong, *Progress in Inorganic Chemistry - P*olydentate Phosphines: Their Syntheses, Structural Aspects, and Selected Applications, Vol. 40, John Wiley & Sons, New York, **1992**.
[297]   C. Flener Lovitt, G. Frenking, G. S. Girolami, *Organometallics* **2012**, *31*, 4122-4132.
[298]   C. A. Tolman, *Chem. Rev.* **1977**, *77*, 313-348.
[299]   M. N. Birkholz, Z. Freixa, P. W. van Leeuwen, *Chem. Soc. Rev.* **2009**, *38*, 1099-1118.
[300]   Z. Freixa, P. W. N. M. van Leeuwen, *Dalton Trans.* **2003**, 1890-1901.
[301]   W. J. van Zeist, R. Visser, F. M. Bickelhaupt, *Chemistry* **2009**, *15*, 6112-6115.
[302]   J. A. Gillespie, D. L. Dodds, P. C. Kamer, *Dalton Trans* **2010**, *39*, 2751-2764.
[303]   C. P. Casey, G. T. Whiteker, *Isr. J. Chem.* **1990**, *30*, 299-304.
[304]   M. Iwamoto, S. Yuguchi, *J. Org. Chem.* **1966**, *31*, 4290-4291.
[305]   M. Portnoy, D. Milstein, *Organometallics* **1993**, *12*, 1655-1664.
[306]   P. Dierkes, P. W. N. M. van Leeuwen, *J. Chem. Soc., Dalton Trans.* **1999**, 1519-1530.
[307]   S. Sakaki, B. Biswas, M. Sugimoto, *J. Chem. Soc., Dalton Trans.* **1997**, 803-810.
[308]   F. M. Bickelhaupt, K. N. Houk, *Angew. Chem. Int. Ed. Engl.* **2017**, *56*, 10070-10086.
[309]   I. Fernandez, F. M. Bickelhaupt, *Chem. Soc. Rev.* **2014**, *43*, 4953-4967.
[310]   W. J. van Zeist, F. M. Bickelhaupt, *Dalton Trans* **2011**, *40*, 3028-3038.
[311]   S. D. Pike, I. Pernik, R. Theron, J. S. McIndoe, A. S. Weller, *J. Organomet. Chem.* **2015**, *784*, 75-83.
[312]   R. M. Beesley, C. K. Ingold, J. F. Thorpe, *J. Chem. Soc., Trans.* **1915**, *107*, 1080-1106.
[313]   M. E. Jung, G. Piizzi, *Chem Rev* **2005**, *105*, 1735-1766.
[314]   J. C. Sarker, A. K. Raha, S. Ghosh, G. Hogarth, S. E. Kabir, M. G. Richmond, *J. Organomet. Chem.* **2014**, *750*, 49-58.
[315]   F. Eisenträger, A. Göthlich, I. Gruber, H. Heiss, C. A. Kiener, C. Krüger, J. Ulrich Notheis, F. Rominger, G. Scherhag, M. Schultz, B. F. Straub, M. A. O. Volland, P. Hofmann, *New J. Chem.* **2003**, *27*, 540-550.
[316]   P. Hofmann, H. Heiß, G. Müller, *Z. Naturforsch. B* **1987**, *42*, 395-409.
[317]   A. B. Chaplin, A. S. Weller, *Inorg. Chem.* **2010**, *49*, 1111-1121.
[318]   M.-D. Su, S.-Y. Chu, *Inorg. Chem.* **1998**, *37*, 3400-3406.
[319]   J. C. Jeffrey, T. B. Rauchfuss, *Inorg. Chem.* **1979**, *18*, 2658-2666.
[320]   W.-H. Zhang, S. W. Chien, T. S. A. Hor, *Coord. Chem. Rev.* **2011**, *255*, 1991-2024.
[321]   P. W. van Leeuwen, P. C. Kamer, J. N. Reek, P. Dierkes, *Chem Rev* **2000**, *100*, 2741-2770.
[322]   A. Jutand, A. Mosleh, *J. Org. Chem.* **1997**, *62*, 261-274.
[323]   J. M. Brown, P. J. Guiry, *Inorg. Chim. Acta* **1994**, *220*, 249-259.
[324]   I. Albers, E. Álvarez, J. Cámpora, C. M. Maya, P. Palma, L. J. Sánchez, E. Passaglia, *J. Organomet. Chem.* **2004**, *689*, 833-839.
[325]   A. L. Clevenger, R. M. Stolley, N. D. Staudaher, N. Al, A. L. Rheingold, R. T. Vanderlinden, J. Louie, *Organometallics* **2018**, *37*, 3259-3268.
[326]   S. M. Mansell, *Dalton Trans* **2017**, *46*, 15157-15174.
[327]   R. J. Burt, J. Chatt, W. Hussain, G. J. Leigh, *J. Organomet. Chem.* **1979**, *182*, 203-206.
[328]   M. D. Fryzuk, T. Jones, F. W. B. Einstein, *Organometallics* **1984**, *3*, 185-191.
[329]   H. H. Karsch, *Z. Naturforsch. B* **1983**, *38*, 1027-1030.
[330]   H. H. Karsch, H. Schmidbaur, *Z. Naturforsch. B* **1977**, *32*, 762-767.
[331]   M. F. Lappert, J. B. Pedley, B. T. Wilkins, O. Stelzer, E. Unger, *J. Chem. Soc., Dalton Trans.* **1975**, 1207-1214.
[332]   K. Issleib, W. Seidel, *Chem. Ber.* **1959**, *92*, 2681-2694.
[333]   M. Fild, O. Stelzer, R. Schmutzler, G. Doak, *Inorganic Syntheses, Vol. 14*, **1973**, 4-9.
[334]   N. Boback, *bachelor thesis* **2020**, Freie Universität Berlin.
[335]   F. R. Jensen, C. H. Bushweller, *J. Am. Chem. Soc.* **1969**, *91*, 3223-3225.

[336]   J. Otto, *bachelor thesis* **2019**, Freie Universität Berlin.

[337]   H. Werner, A. Hampp, K. Peters, E. M. Peters, L. Walz, H. G. v. Schnering, *Z. Naturforsch. B* **1990**, *45*, 1548-1558.

[338]   K. Zhu, P. D. Achord, X. Zhang, K. Krogh-Jespersen, A. S. Goldman, *J. Am. Chem. Soc.* **2004**, *126*, 13044-13053.

[339]   K. Timmer, D. H. M. W. Thewissen, J. W. Marsman, *Recl. Trav. Chim. Pays-Bas* **1988**, *107*, 248-255.

[340]   M. S. Blais, J. C. W. Chien, M. D. Rausch, *Organometallics* **1998**, *17*, 3775-3783.

[341]   C. R. Lee, M. Hubert, C. N. Van Dau, D. Peter, A. M. Krstulovic, *Analyst* **2000**, *125*, 1255-1259.

[342]   B. Cohen, E. R. Van Artsdalen, J. Harris, *J. Am. Chem. Soc.* **1948**, *70*, 281-285.

[343]   C. Golumbic, J. S. Fruton, M. A. X. Bergmann, *J. Org. Chem.* **1946**, *11*, 518-535.

[344]   W. Bonrath, K. R. Pörschke, G. Wilke, K. Angermund, C. Krüger, *Angew. Chem. Int. Ed. Engl.* **1988**, *27*, 833-835.

[345]   F. Schager, K.-J. Haack, R. Mynott, A. Rufińska, K.-R. Pörschke, *Organometallics* **1998**, *17*, 807-814.

[346]   H. C. Clark, P. N. Kapoor, I. J. McMahon, *J. Organomet. Chem.* **1984**, *265*, 107-115.

[347]   J. A. Davies, R. J. Staples, *Polyhedron* **1991**, *10*, 899-908.

[348]   N. Simhai, C. N. Iverson, B. L. Edelbach, W. D. Jones, *Organometallics* **2001**, *20*, 2759-2766.

[349]   P. Hofmann, H. Heiss, P. Neiteler, G. Müller, J. Lachmann, *Angew. Chem. Int. Ed. Engl.* **1990**, *29*, 880-882.

[350]   J. J. Eisch, C. A. Kovacs, P. Chobe, *J. Org. Chem.* **1989**, *54*, 1275-1284.

[351]   A. Mack, E. Pierron, T. Allspach, U. Bergsträßer, M. Regitz, *Synthesis* **1998**, *1998*, 1305-1313.

[352]   M. G. Blanc, *Bull. Soc. Chim. Fr.* **1923**, *33*, 313.

[353]   L. I. Belen'kii, Y. B. Vol'kenshtein, I. B. Karmanova, *Russ. Chem. Rev.* **1977**, *46*, 891-903.

[354]   W. Samstag, J. W. Engels, *Angew. Chem. Int. Ed. Engl.* **1992**, *31*, 1386-1388.

[355]   C. Elschenbroich, *Organometallics*, 3 ed., Wiley-VCH, Weinheim, **2006**.

[356]   K. S. Suslick, S. J. Doktycz, *J. Am. Chem. Soc.* **1989**, *111*, 2342-2344.

[357]   S. Petriček, A. Demšar, *Polyhedron* **2010**, *29*, 3329-3334.

[358]   O. Mummenhoff, *internship in the working group C. Müller* **2021**, Freie Universität Berlin.

[359]   E. D. Hughes, C. K. Ingold, *J. Chem. Soc. Faraday Trans.* **1941**, *37*, 657-685.

[360]   I. Katsumi, H. Kondo, K. Yamashita, T. Hidaka, K. Hosoe, T. Yamashita, K. Watanabe, *Chem Pharm Bull (Tokyo)* **1986**, *34*, 121-129.

[361]   J. Y. C. Lim, N. Yuntawattana, P. D. Beer, C. K. Williams, *Angew. Chem.* **2019**, *131*, 6068-6072.

[362]   E. M. Igumnova, E. Mishchenko, T. Haug, H. M. Blencke, J. U. E. Sollid, E. G. A. Fredheim, S. Lauksund, K. Stensvag, M. B. Strom, *Bioorg. Med. Chem.* **2016**, *24*, 5884-5894.

[363]   D. Fournier, D. Poirier, *Eur. J. Med. Chem.* **2011**, *46*, 4227-4237.

[364]   T. Furuyama, M. Asai, N. Kobayashi, *Chem Commun (Camb)* **2014**, *50*, 15101-15104.

[365]   F. M. Jradi, D. O'Neil, X. Kang, J. Wong, P. Szymanski, T. C. Parker, H. L. Anderson, M. A. El-Sayed, S. R. Marder, *Chem. Mater.* **2015**, *27*, 6305-6313.

[366]   G. E. Carr, R. D. Chambers, T. F. Holmes, D. G. Parker, *J. Organomet. Chem.* **1987**, *325*, 13-23.

[367]   A. Metzger, *doctoral thesis* **2010**, Ludwig-Maximilians-Universität (Munich).

[368]   S. H. Eltamany, H. Hopf, *Tetrahedron Lett.* **1980**, *21*, 4901-4904.

[369]   H. Finkelstein, *Ber. Dtsch. Chem. Ges.* **1910**, *43*, 1528-1532.

[370]   K. G. Pearce, I. R. Crossley, *J. Org. Chem.* **2020**, *85*, 14697-14707.

[371]   K. G. Pearce, V. Simenok, I. R. Crossley, *Dalton Trans* **2020**, *49*, 5482-5492.

[372]   T. Gorlich, D. S. Frost, N. Boback, N. T. Coles, B. Dittrich, P. Muller, W. D. Jones, C. Muller, *J. Am. Chem. Soc.* **2021**, *143*, 19365-19373.

[373] D. Cremer, E. Kraka, *Angew. Chem. Int. Ed. Engl.* **1984**, *23*, 627-628.

[374] M. H. Habicht, F. Wossidlo, M. Weber, C. Muller, *Chemistry* **2016**, *22*, 12877-12883.

[375] M. H. Habicht, F. Wossidlo, T. Bens, E. A. Pidko, C. Muller, *Chemistry* **2018**, *24*, 944-952.

[376] S. Giese, *doctoral thesis* **2020**, Freie Universität Berlin.

[377] S. Giese, D. Buzsaki, L. Nyulaszi, C. Muller, *Chem Commun (Camb)* **2019**, *55*, 13812-13815.

[378] W. Rösch, M. Regitz, *Angew. Chem. Int. Ed. Engl.* **1984**, *23*, 900-901.

[379] A. S. Ionkin, W. J. Marshall, B. M. Fish, A. A. Marchione, L. A. Howe, F. Davidson, C. N. McEwen, *Eur. J. Inorg. Chem.* **2008**, *2008*, 2386-2390.

[380] A. S. Ionkin, W. J. Marshall, B. M. Fish, A. A. Marchione, L. A. Howe, F. Davidson, C. N. McEwen, *Organometallics* **2008**, *27*, 5118-5121.

[381] A. S. Ionkin, W. J. Marshall, B. M. Fish, M. F. Schiffhauer, F. Davidson, C. N. McEwen, *Organometallics* **2009**, *28*, 2410-2416.

[382] A. Petrov, *doctoral thesis* **2022**, Freie Universität Berlin.

[383] H. Fleckner, F. W. Grevels, D. Hess, *J. Am. Chem. Soc.* **1984**, *106*, 2027-2032.

[384] P. Binger, B. Biedenbach, R. Schneider, M. Regitz, *Synthesis* **1989**, *1989*, 960-961.

[385] J. R. L. Priqueler, I. S. Butler, F. D. Rochon, *Appl. Spectrosc. Rev.* **2006**, *41*, 185-226.

[386] A. Pidcock, R. E. Richards, L. M. Venanzi, *J. Chem. Soc. A* **1966**, *0*, 1707-1710.

[387] F. H. Allen, A. Pidcock, *J. Chem. Soc. A: Inorganic, Physical, Theoretical* **1968**, 2700-2704.

[388] F. H. Allen, A. Pidcock, C. R. Waterhouse, *J. Chem. Soc. A: Inorganic, Physical, Theoretical* **1970**, 2087-2093.

[389] T. G. Appleton, H. C. Clark, L. E. Manzer, *Coord. Chem. Rev.* **1973**, *10*, 335-422.

[390] F. R. Hartley, *Chem. Soc. Rev.* **1973**, *2*, 163-179.

[391] P. L. Goggin, R. J. Goodfellow, S. R. Haddock, B. F. Taylor, I. R. H. Marshall, *J. Chem. Soc., Dalton Trans.* **1976**, 459-467.

[392] J. Soulié, J. Y. Lallemand, R. C. Rao, *Org. Magn. Reson.* **1979**, *12*, 67-70.

[393] L. Bemi, H. C. Clark, J. A. Davies, C. A. Fyfe, R. E. Wasylishen, *J. Am. Chem. Soc.* **1982**, *104*, 438-445.

[394] R. K. Harris, I. J. McNaught, P. Reams, K. J. Packer, *Magn. Reson. Chem.* **1991**, *29*, S60-S72.

[395] W. P. Power, R. E. Wasylishen, *Inorg. Chem.* **1992**, *31*, 2176-2183.

[396] J. F. Nixon, A. Pidcock, *Annu. Rep. NMR Spectrosc.* **1969**, *2*, 345-422.

[397] F. B. Ogilvie, J. M. Jenkins, J. G. Verkade, *J. Am. Chem. Soc.* **1969**, *92*, 1916-1923.

[398] R. D. Bertrand, F. B. Ogilvie, J. G. Verkade, *J. Am. Chem. Soc.* **1970**, *92*, 1908-1915.

[399] E. G. Finer, R. K. Harris, *Prog. Nucl. Magn. Reson. Spectrosc.* **1970**, *6*, 61-118.

[400] J. G. Verkade, *Coord. Chem. Rev.* **1972**, *9*, 1-106.

[401] J. Hu, R. Lin, J. H. K. Yip, K.-Y. Wong, D.-L. Ma, J. J. Vittal, *Organometallics* **2007**, *26*, 6533-6543.

[402] H. Arii, M. Takahashi, H. Takahashi, K. Mochida, T. Kawashima, *Chem. Lett.* **2012**, *41*, 1538-1540.

[403] E. O. Greaves, C. J. L. Lock, P. M. Maitlis, *Can. J. Chem.* **1968**, *46*, 3879-3891.

[404] J. O. Glanville, J. M. Stewart, S. O. Grim, *J. Organomet. Chem.* **1967**, *7*, P9-P10.

[405] K. Zhang, J. Hu, K. C. Chan, K. Y. Wong, J. H. K. Yip, *Eur. J. Inorg. Chem.* **2007**, *2007*, 384-393.

[406] T. Gathy, O. Riant, D. Peeters, T. Leyssens, *J. Organomet. Chem.* **2011**, *696*, 3425-3430.

[407] E. Lindner, R. Fawzi, H. A. Mayer, K. Eichele, W. Hiller, *Organometallics* **1992**, *11*, 1033-1043.

[408] J. Chatt, R. Mason, D. W. Meek, *J. Am. Chem. Soc.* **1975**, *97*, 3826-3827.

[409] R. K. Harris, E. D. Becker, S. M. Cabral de Menezes, R. Goodfellow, P. Granger, *Pure Appl. Chem.* **2001**, *73*, 1795-1818.

[410] P. Coburger, *personal communication* **2022**.

[411] T. A. K. Al-Allaf, G. Butler, C. Eaborn, A. Pidcock, *J. Organomet. Chem.* **1980**, *188*, 335-343.

[412] B. Dittrich, *IUCrJ* **2021**, *8*, 305-318.

[413] B. Dittrich, S. Chan, S. Wiggin, J. S. Stevens, E. Pidcock, *CrystEngComm* **2020**, *22*, 7420-7431.

[414] C. A. Tolman, W. C. Seidel, J. D. Druliner, P. J. Domaille, *Organometallics* **1984**, *3*, 33-38.

[415] R. J. McKinney, W. A. Nugent, *Organometallics* **1989**, *8*, 2871-2875.

[416] Y. Nakao, A. Yada, S. Ebata, T. Hiyama, *J. Am. Chem. Soc.* **2007**, *129*, 2428-2429.

[417] A. Yada, S. Ebata, H. Idei, D. Zhang, Y. Nakao, T. Hiyama, *Bull. Chem. Soc. Jpn.* **2010**, *83*, 1170-1184.

[418] A. Acosta-Ramírez, M. Muñoz-Hernández, W. D. Jones, J. J. García, *J. Organomet. Chem.* **2006**, *691*, 3895-3901.

[419] J. Huang, C. M. Haar, S. P. Nolan, J. E. Marcone, K. G. Moloy, *Organometallics* **1999**, *18*, 297-299.

[420] R. W. Rudolph, C. W. Schultz, *J. Am. Chem. Soc.* **1971**, *93*, 6821-6822.

[421] M. Hackett, G. M. Whitesides, *J. Am. Chem. Soc.* **1988**, *110*, 1449-1462.

[422] S. Kundu, W. W. Brennessel, W. D. Jones, *Organometallics* **2011**, *30*, 5147-5154.

[423] S. Kundu, B. E. R. Snyder, A. P. Walsh, W. W. Brennessel, W. D. Jones, *Polyhedron* **2013**, *58*, 99-105.

[424] R. Mas-Balleste, M. Capdevila, P. A. Champkin, W. Clegg, R. A. Coxall, A. Lledos, C. Megret, P. Gonzalez-Duarte, *Inorg. Chem.* **2002**, *41*, 3218-3229.

[425] H.-S. Kwak, S.-H. Ri, S.-O. Pak, J.-H. Ri, S.-H. Jong, *Sep. Sci. Technol.* **2019**, *56*, 107-116.

[426] M. J. Blandamer, J. Burgess, A. J. Duffield, *J. Chem. Soc., Dalton Trans.* **1980**, 1-6.

[427] C. M. Che, W. P. Schaefer, H. B. Gray, M. K. Dickson, P. B. Stein, D. M. Roundhill, *J. Am. Chem. Soc.* **1982**, *104*, 4253-4255.

[428] R. Usón, J. Forniés, M. Tomás, B. Menjón, K. Sünkel, R. Bau, *J. Chem. Soc., Chem. Commun.* **1984**, *0*, 751-752.

[429] T. V. O'Halloran, S. J. Lippard, *Isr. J. Chem.* **1985**, *25*, 130-137.

[430] R. J. Puddephatt, *J. Organomet. Chem.* **2017**, *849-850*, 268-278.

[431] B. H. Xia, C. M. Che, D. L. Phillips, K. H. Leung, K. K. Cheung, *Inorg. Chem.* **2002**, *41*, 3866-3875.

[432] F. S. M. Hassan, D. P. Markham, P. G. Pringle, B. L. Shaw, *J. Chem. Soc., Dalton Trans.* **1985**, 279-283.

[433] P. Braunstein, G. E. Herberich, M. Neuschütz, M. U. Schmidt, *J. Organomet. Chem.* **1999**, *580*, 66-71.

[434] Anna L. Bandini, G. Banditelli, M. Manassero, A. Albinati, D. Colognesi, J. Eckert, *Eur. J. Inorg. Chem.* **2003**, *2003*, 3958-3967.

[435] K. Moedritzer, L. Maier, L. C. D. Groenweghe, *J. Chem. Eng. Data* **1962**, *7*, 307-310.

[436] L. D. Quin, M. D. Gordon, S. O. Lee, *Org. Magn. Reson.* **1974**, *6*, 503-507.

[437] M. Hackett, J. A. Ibers, G. M. Whitesides, *J. Am. Chem. Soc.* **1988**, *110*, 1436-1448.

[438] J. A. Davies, R. J. Staples, *Polyhedron* **1991**, *10*, 909-917.

[439] A. Wiesner, T. W. Gries, S. Steinhauer, H. Beckers, S. Riedel, *Angew. Chem. Int. Ed. Engl.* **2017**, *56*, 8263-8266.

[440] H. C. Clark, M. J. H. Smith, *J. Am. Chem. Soc.* **1986**, *108*, 3829-3830.

[441] C. Lichtenberg, M. Elfferding, J. Sundermeyer, *Eur. J. Inorg. Chem.* **2010**, *2010*, 3117-3124.

[442] S. S. Lau, W. Wu, P. E. Fanwick, R. A. Walton, *Polyhedron* **1997**, *16*, 3649-3654.

[443] W. V. Konze, B. L. Scott, G. J. Kubas, *J. Am. Chem. Soc.* **2002**, *124*, 12550-12556.

[444] V. D. Romanenko, V. I. Tovstenko, L. N. Markovski, *Synthesis* **1980**, *1980*, 823-825.

[445] D. Heift, Z. Benko, H. Grutzmacher, *Chemistry* **2014**, *20*, 11326-11330.

[446] J. A. Sklorz, S. Hoof, N. Rades, N. De Rycke, L. Konczol, D. Szieberth, M. Weber, J. Wiecko, L. Nyulaszi, M. Hissler, C. Muller, *Chemistry* **2015**, *21*, 11096-11109.

[447] T. J. Del Castillo, S. Sarkar, K. A. Abboud, A. S. Veige, *Dalton Trans* **2011**, *40*, 8140-8144.

[448] Y.-H. Lo, T.-H. Wang, C.-Y. Lee, Y.-H. Feng, *Organometallics* **2012**, *31*, 6887-6899.

[449] L. Casarrubios, M. C. de la Torre, M. A. Sierra, *Chemistry* **2013**, *19*, 3534-3541.

[450]   C. C. Beto, E. D. Holt, Y. Yang, I. Ghiviriga, K. S. Schanze, A. S. Veige, *Chem Commun (Camb)* **2017**, *53*, 9934-9937.

[451]   E. Gail, S. Gos, R. Kulzer, J. Lorösch, A. Rubo, M. Sauer, R. Kellens, J. Reddy, N. Steier, W. Hasenpusch, *Cyano Compounds, Inorganic, Vol. 10*, Wiley-VCH Verlag GmbH & Co. KGaA, Weinheim, **2011**.

[452]   A. M. Tondreau, Z. Benkő, J. R. Harmer, H. Grützmacher, *Chem. Sci.* **2014**, *5*, 1545-1554.

[453]   R. D. Crouch, *Tetrahedron* **2013**, *69*, 2383-2417.

[454]   T. D. Nelson, R. D. Crouch, *Synthesis* **1996**, *1996*, 1031-1069.

[455]   J. R. Gold, L. H. Sommer, F. C. Whitmore, *J. Am. Chem. Soc.* **1948**, *70*, 2874-2876.

[456]   C. Eaborn, *J. Organomet. Chem.* **1975**, *100*, 43-57.

[457]   M. N. Bakola-Christianopoulou, *Appl. Organomet. Chem.* **2001**, *15*, 889-900.

[458]   V. Gouverneur, B. Greedy, *Chemistry* **2002**, *8*, 766-772.

[459]   J. S. Capani, Jr., J. E. Cochran, J. C. Liang, *J. Org. Chem.* **2019**, *84*, 9378-9384.

[460]   A. B. Holmes, C. L. D. Jennings-White, A. H. Schulthess, B. Akinde, D. R. M. Walton, *J. Chem. Soc., Chem. Commun.* **1979**, 840-842.

[461]   S. Kim, B. Kim, J. In, *Synthesis* **2009**, *2009*, 1963-1968.

[462]   Y. Kaburagi, Y. Kishi, *Org. Lett.* **2007**, *9*, 723-726.

[463]   S. J. Brown, J. H. Clark, D. J. Macquarrie, *J. Chem. Soc., Dalton Trans.* **1988**, 277-280.

[464]   J. Beckmann, D. Dakternieks, A. Duthie, C. Mitchell, F. Ribot, J. B. d'Espinose de la Caillerie, B. Revel, *Appl. Organomet. Chem.* **2004**, *18*, 353-358.

[465]   M. Gingras, *Tetrahedron Lett.* **1991**, *32*, 7381-7384.

[466]   M. Gingras, Y. M. Chabre, J. M. Raimundo, *Synthesis* **2006**, *2006*, 182-185.

[467]   R. Schwesinger, R. Link, G. Thiele, H. Rotter, D. Honert, H.-H. Limbach, F. Männle, *Angew. Chem. Int. Ed. Engl.* **1991**, *30*, 1372-1375.

[468]   R. Schwesinger, R. Link, P. Wenzl, S. Kossek, *Chemistry* **2005**, *12*, 438-445.

[469]   J. F. Nixon, R. Schmutzler, *Spectrochim. Acta* **1964**, *20*, 1835-1842.

[470]   S. G. Rachor, R. Muller, P. Wittwer, M. Kaupp, T. Braun, *Inorg. Chem.* **2022**, *61*, 357-367.

[471]   S. Rachor, *laboratory cooperation* **2022**, Freie Universität Berlin / Humboldt-Universität zu Berlin.

[472]   T. Mathieson, A. Schier, H. Schmidbaur, *Z. Naturforsch. B* **2000**, *55*, 1000-1004.

[473]   C. M. Wyss, B. K. Tate, J. Bacsa, M. Wieliczko, J. P. Sadighi, *Polyhedron* **2014**, *84*, 87-95.

[474]   H. M. J. Wang, I. J. B. Lin, *Organometallics* **1998**, *17*, 972-975.

[475]   L. Messori, L. Marchetti, L. Massai, F. Scaletti, A. Guerri, I. Landini, S. Nobili, G. Perrone, E. Mini, P. Leoni, M. Pasquali, C. Gabbiani, *Inorg. Chem.* **2014**, *53*, 2396-2403.

[476]   H. Nakazawa, M. Itazaki, K. Kamata, K. Ueda, *Chem.: Asian J.* **2007**, *2*, 882-888.

[477]   M. Moll, H. Behrens, P. Merbach, K.-H. Trümmer, G. Thiele, K. Wittmann, *Z. Naturforsch. B* **1986**, *41*, 606-616.

[478]   M. Xu, B. Kooij, T. Wang, J. H. Lin, Z. W. Qu, S. Grimme, D. W. Stephan, *Angew. Chem. Int. Ed. Engl.* **2021**, *60*, 16965-16969.

[479]   G. M. Sheldrick, *Acta Crystallogr A* **2008**, *64*, 112-122.

[480]   G. M. Sheldrick, *Acta Crystallogr C Struct Chem* **2015**, *71*, 3-8.

[481]   P. Müller, *Crystallogr. Rev.* **2009**, *15*, 57-83.

[482]   O. V. Dolomanov, L. J. Bourhis, R. J. Gildea, J. A. K. Howard, H. Puschmann, *J. Appl. Crystallogr.* **2009**, *42*, 339-341.

[483]   C. F. Macrae, I. Sovago, S. J. Cottrell, P. T. A. Galek, P. McCabe, E. Pidcock, M. Platings, G. P. Shields, J. S. Stevens, M. Towler, P. A. Wood, *J. Appl. Crystallogr.* **2020**, *53*, 226-235.

[484]   F. Neese, *Wiley Interdiscip. Rev. Comput. Mol. Sci.* **2011**, *2*, 73-78.

[485]   F. Neese, F. Wennmohs, U. Becker, C. Riplinger, *J. Chem. Phys.* **2020**, *152*, 224108.

[486]   L. Bennett, B. Melchers, B. Proppe, *Curta: A General-purpose High-Performance Computer at ZEDAT* **2020**, Freie Universität Berlin.

[487] Avogadro: an open-source molecular builder and visualization tool. Version 1.2.0. modified version with extended ORCA support, http://avogadro.openmolecules.net/ and https://orcaforum.cec.mpg.de.

[488] S. Grimme, J. G. Brandenburg, C. Bannwarth, A. Hansen, *J. Chem. Phys.* **2015**, *143*, 054107.

[489] R. Sure, J. G. Brandenburg, S. Grimme, *ChemistryOpen* **2016**, *5*, 94-109.

[490] A. D. Becke, *J. Chem. Phys.* **1993**, *98*, 5648-5652.

[491] F. Weigend, R. Ahlrichs, *Phys. Chem. Chem. Phys.* **2005**, *7*, 3297-3305.

[492] F. Weigend, *Phys. Chem. Chem. Phys.* **2006**, *8*, 1057-1065.

[493] J. D. Chai, M. Head-Gordon, *Phys. Chem. Chem. Phys.* **2008**, *10*, 6615-6620.

[494] S. Grimme, S. Ehrlich, L. Goerigk, *J. Comput. Chem.* **2011**, *32*, 1456-1465.

[495] S. Grimme, J. Antony, S. Ehrlich, H. Krieg, *J. Chem. Phys.* **2010**, *132*, 154104.

[496] S. Grimme, *J. Comput. Chem.* **2006**, *27*, 1787-1799.

[497] S. Grimme, *J. Comput. Chem.* **2004**, *25*, 1463-1473.

[498] A. Klamt, G. Schüürmann, *J. Chem. Soc., Perkin Trans. 2* **1993**, 799-805.

[499] V. Barone, M. Cossi, *J. Phys. Chem. A* **1998**, *102*, 1995-2001.

[500] J. Andzelm, C. Kölmel, A. Klamt, *J. Chem. Phys.* **1995**, *103*, 9312-9320.

[501] Y. Takano, K. N. Houk, *J Chem Theory Comput* **2005**, *1*, 70-77.

[502] D. Andrae, U. Huermann, M. Dolg, H. Stoll, H. Preu, *Theor. Chem. Acc.* **1990**, *77*, 123-141.

[503] G. Knizia, J. E. Klein, *Angew. Chem. Int. Ed. Engl.* **2015**, *54*, 5518-5522.

[504] G. Knizia, *J Chem Theory Comput* **2013**, *9*, 4834-4843.

[505] E. F. Pettersen, T. D. Goddard, C. C. Huang, G. S. Couch, D. M. Greenblatt, E. C. Meng, T. E. Ferrin, *J. Comput. Chem.* **2004**, *25*, 1605-1612.

[506] A. Hellweg, C. Hättig, S. Höfener, W. Klopper, *Theor. Chem. Acc.* **2007**, *117*, 587-597.

[507] D. G. Liakos, M. Sparta, M. K. Kesharwani, J. M. Martin, F. Neese, *J Chem Theory Comput* **2015**, *11*, 1525-1539.

[508] Chemcraft - graphical software for visualization of quantum chemistry computations. https://www.chemcraftprog.com.

[509] E. D. Glendening, F. Weinhold, *Chem. Phys. Lett.* **2018**, *711*, 23-26.

[510] R. F. W. Bader, *Acc. Chem. Res.* **1985**, *18*, 9-15.

[511] T. Lu, F. Chen, *J. Comput. Chem.* **2012**, *33*, 580-592.

[512] F. London, *J. phys. Radium* **1937**, *8*, 397-409.

[513] W. J. Hehre, R. Ditchfield, J. A. Pople, *J. Chem. Phys.* **1972**, *56*, 2257-2261.

[514] T. Helgaker, M. Jaszunski, K. Ruud, *Chem Rev* **1999**, *99*, 293-352.

[515] C. Adamo, V. Barone, *J. Chem. Phys.* **1999**, *110*, 6158-6170.

[516] F. Jensen, *J Chem Theory Comput* **2015**, *11*, 132-138.

[517] I. A. Konstantinov, L. J. Broadbelt, *J. Phys. Chem. A* **2011**, *115*, 12364-12372.

[518] A. E. Aliev, D. Courtier-Murias, S. Zhou, *J. Mol. Struc.-THEOCHEM* **2009**, *893*, 1-5.

[519] R. Jain, T. Bally, P. R. Rablen, *J. Org. Chem.* **2009**, *74*, 4017-4023.

[520] P. R. Rablen, S. A. Pearlman, J. Finkbiner, *J. Phys. Chem. A* **1999**, *103*, 7357-7363.

[521] S. K. Latypov, F. M. Polyancev, D. G. Yakhvarov, O. G. Sinyashin, *Phys. Chem. Chem. Phys.* **2015**, *17*, 6976-6987.

[522] D. M. York, M. Karplus, *J. Phys. Chem. A* **1999**, *103*, 11060-11079.

[523] F. Uhlig, S. Gremler, M. Dargatz, M. Scheer, E. Herrmann, *Z. anorg. allg. Chem.* **1991**, *606*, 105-108.

[524] J. J. Eisch, C. S. Chiu, *Heteroat. Chem* **1994**, *5*, 265-274.

[525] D. E. Pearson, M. G. Frazer, V. S. Frazer, L. C. Washburn, *Synthesis* **1976**, *1976*, 621-623.

[526] H. A. Staab, D. Lauer, *Chem. Ber.* **1968**, *101*, 864-878.

[527] S. R. Ditto, R. J. Card, P. D. Davis, D. C. Neckers, *J. Org. Chem.* **1979**, *44*, 894-896.

[528] J.-T. Ahlemann, H. W. Roesky, M. Noltemeyer, H.-G. Schmidt, L. N. Markovsky, Y. G. Shermolovich, *J. Fluorine Chem.* **1998**, *87*, 87-90.